CHARACTERISATION OF THE EVOLVING PROPERTIES OF FRICTION STIR SPOT ALUMINIUM AND COPPER WELDS

by

Mukuna Patrick, Mubiayi

A thesis submitted in fulfilment of the requirements for the degree of

Doctor Philosophiae: Mechanical Engineering Science

Submitted to the

Faculty of Engineering and the Built Environment

University of Johannesburg

Johannesburg,

South Africa

2015

Supervisor: Prof. E.T. Akinlabi

DECLARATION

I, Mukuna Patrick Mubiayi, hereby declare that this thesis, which I herewith submit for the research qualification **DOCTOR PHILOSOPHIAE IN MECHANICAL ENGINEERING** to the University of Johannesburg, department of Mechanical Engineering Science, is my own work; and it has not previously been submitted by me to any other institution.

DEDICATION

This work is dedicated to my lovely wife, Sandra Mwadi Tshibangu, and our little angel, Tiffany Nsuaya Mukuna, whom I love and treasure so much.

ACKNOWLEDGEMENTS

I am grateful to the many people who have contributed, in one way or another, to the achievement of this thesis.

First and above all, I want to thank the Almighty God, for His unconditional love. He made it possible for me to do all things through Jesus Christ, who strengthens me during hard times.

I am sincerely grateful to Professor E.T. Akinlabi, my supervisor, for everything she has done to bring this research work to a happy conclusion. Her contribution to the achievement of this thesis is beyond calculation.

I would like to thank the University Research Committee (URC) from the University of Johannesburg for the financial assistance.

I would like to express my appreciation to Mr Brown Riaan at NMMU (Nelson Mandela Metropolitan University) for operating the friction stir welding platform.
I also appreciate the assistance of Mr Tshepo Ntsoane from NECSA (Nuclear Energy Corporation of South Africa) for his assistance with the XRD and the residual stress analyses.

It remains for me to thank my parents, seniors, brothers, sisters, friends and colleagues who have contributed financially, as well as morally to the accomplishment of this task.

I think of:

- My parents, Professor Robert Mukuna Tshimpela and Marie Louise Nsuaya Mubiayi for their financial support and endless love.
- My mother-in-law, Marie Jeanne Mwadi, and my late father-in-law Daniel Tshibangu, who could not be here to enjoy this success with us. May his soul rest in peace.
- My spiritual mentor, Father Terry Mutesha Mwando.
- All my brothers (Michel, Emile, Serge, Tonny and Kastro Mukuna), brothers-in-law (Patrick, Christian, Cola, Alain, Yannick and Martin Tshibangu) and sisters-in-law (Angelique, Henriette, Cynthia and Regina Tshibangu) for their encouragement.

- Dr Kimberly Battle for always encouraging me during my studies.
- Ms Nomsa Baloyi for her assistance in the Extraction Metallurgy Laboratory at the University of Johannesburg.
- Dr Mamookho Elizabeth Makhatha for her encouragement.
- My friends and all my colleagues from MAMS research group for being there for me.

ABSTRACT

Dissimilar metal joining techniques are necessary for the manufacturing of a number of structures and parts in the industries. Aluminium and copper are widely used in engineering structures, due to their unique performances, such as higher electrical conductivity, heat conductivity, corrosion resistance and mechanical properties even if they have considerable differences in their melting points. Among the aims for future years in the automotive industry is the development and implementation of new technologies, including a broad application of friction stir spot welding (FSSW) of similar and dissimilar materials.

Friction stir spot welding (FSSW) is a variant of friction stir welding (FSW) for spot welding applications. Joining aluminium and copper to meet the requirements from the electrical industry have been conducted by using different joining techniques, such as ultrasonic welding, friction welding and laser welding. However, the major challenge with these techniques is the occurrence of brittle intermetallic compounds in the joint zone. FSSW has been successfully used to join aluminium and copper by a few researchers; but more research is needed to investigate the evolving properties of FSSW between copper and aluminium.

The current research project joined 3 mm thick AA1060 and C11000, by using friction stir spot welding (FSSW), and by using different tool geometries namely a flat pin/flat shoulder and a conical pin/concave shoulder and different process parameters, in order to fill the gap in the literature in this field of study. Limited research results exist on friction stir spot welding between aluminium and copper. However, the successful joining of these two materials has the potential for many applications in the industry. The spot welds were produced and characterised through optical microscopy, and by scanning electron microscopy for the microstructural evolution; while the chemical and phase identification were analysed using energy dispersive spectroscopy and X-ray diffraction, respectively.

Furthermore, tensile testing, microhardness profiling, residual stress analysis, electrical resistivity and statistical analysis were also conducted. This was done to investigate the relationship between the process parameters, the tool geometry and the produced welds. The real time forces acting during the welding process were monitored and analysed. It was observed that the maximum forge

forces recorded showed that there was an increase with the increase of the shoulder plunge depth; whereas a decrease was noticed, when the rotational speed was increased for the flat pin/flat shoulder tool. The same was also noticed for the conical pin/concave shoulder employed, which is due to the generation of the different heat input during the welding process.

The possibility of the formation of intermetallic compounds in the welds was analysed using the X-ray diffraction and energy dispersive spectroscopy. Furthermore, microhardness measurements and lap-shear tensile and electrical resistivity analyses were also conducted, in order to correlate the investigations on the produced spot welded samples, and to allow for a detailed evaluation of the quality of the spot welds.

The microstructure of the spot welds produced at different processing parameters was studied. A copper ring (hook) was present in all the spot welds; and it was found that the length increases with the shoulder plunge depth; while the spot welds produced at 1200 rpm for the two tool geometries exhibited a decrease and a slight increment in the length of the copper ring using a flat pin/flat shoulder and conical pin/ concave shoulder, respectively. The copper penetrating into the aluminium created an interlocking which helped the two plates to adhere to each other during the tensile testing procedure.

The mapping of a region of the keyhole and copper ring of the spot weld showed different microstructures with copper particles and fragments in the Aluminium matrix. A good material mixing was achieved in most of the spot welds produced. Furthermore, the mapping of the SZ of the welds showed the different distribution of the copper particles in the aluminium matrix.

The X-ray diffraction analyses using a 2 mm collimator revealed low peaks for the presence of the Al_2Cu and Cu_3Al intermetallic compounds in the joints produced, when using a conical pin/concave shoulder at 800 rpm (1 mm shoulder plunge depth) and 1200 rpm (0.5 mm shoulder plunge depth). A further XRD analysis was performed in three different locations of the spot weld samples, namely: the stir zone (SZ), the thermo-mechanically affected zone (TMAZ) and the heat-affected zone (HAZ) was conducted using a 0.8 mm collimator.

The most common intermetallic compounds formed in the spot weld samples were Al_4Cu_9, $Al Cu_3$, Al_2Cu_3 and Al_2Cu, which also showed low peaks. Moreover, the energy dispersive spectroscopy (EDS) analysis also revealed low peaks for the presence of intermetallic compounds in the keyhole and interfacial regions of the welds, which correlated to the X- ray diffraction analyses.

High failure loads of 5225 N and 4844 N were achieved using a flat pin/flat shoulder produced at 800 rpm, 1 mm shoulder plunge depth and 1200 rpm, and 1 mm shoulder plunge depth, respectively. It was observed that by increasing the shoulder plunge depth, high strength welds were obtained. Additionally, the two highest failure loads obtained using a conical pin/concave shoulder were 2991 N and 4606 N, respectively; where the parameters used were 800 rpm, 0.5 mm pin plunge depth and 1200 rpm, and 1 mm shoulder plunge depth, respectively.

Furthermore, higher microhardness values were obtained in the stir zone for all the welds, which correlated to the intermetallics formed at the interface. There was no apparent trend linking the process parameters and the tool geometries to the microhardness profiles obtained. The electrical resistivity results revealed comparatively high values for all the spot welds compared to the parent materials; while the electrical resistivity of the spot welds produced at 800 rpm, and a 1 mm shoulder plunge depth using a conical pin and concave shoulder exhibited lower values when compared to those of the parent materials.

The residual stresses were measured in the stir zone and on the copper ring; and the results showed that the residual stresses were compressive. The maximum residual stress of -116.8 MPa was found on the copper ring of the welds produced at 800 rpm, 0.5 mm shoulder plunge depth, using a flat pin and a flat shoulder tool. The probability distribution function (PDF) of the microhardness results revealed that the process parameters and the tool geometries have a significant effect on the distribution of the microhardness values in the different locations of the produced spot welds.
The knowledge generated in this research work has contributed towards the understanding of different properties exhibited by the friction stir spot joining between aluminium and copper.

TABLE OF CONTENTS

ABBREVIATIONS

Al	Aluminium
BM	Base material
BSE	Backscattered Electron
Cu	Copper
EDS	Energy-Dispersive X-ray Spectroscopy
FSW	Friction Stir Welding
FSSW	Friction Stir Spot Welding
HAZ	heat-affected zone
HV	Vicker's hardness
kN	Kilo-Newton
SEM	Scanning Electron Microscope
SZ	stir zone
TMAZ	thermo-mechanically affected zone
rpm	Revolutions per minute
OM	Optical Microscope
WEDM	Wire Electrical Discharge Machining
XRD	X-Ray Diffraction

LIST OF FIGURES

LIST OF TABLES

LIST OF PUBLICATIONS

1. M.P. Mubiayi, E.T Akinlabi, "**Evolving properties of friction stir spot welds between AA1060 and commercially pure copper C11000**" Manuscript submitted to the Transactions of Nonferrous Metals Society of China, Manuscript ID: TNMSC-2015-0985 (Paper accepted for publication).
2. M.P. Mubiayi, E.T Akinlabi "**Characterization of the intermetallic compounds in aluminium and copper friction stir spot welds**". Manuscript submitted and accepted for oral presentation at the upcoming ICMPC2016 conference. Paper ID: 244.
3. M.P Mubiayi, E.T Akinlabi "**Friction Stir Spot Welding between Copper and Aluminium: microstructural Evolution**". Proceedings of the International MultiConference of Engineers and Computer Scientists 2015 Vol II, IMECS 2015, March 18 - 20, 2015, Hong Kong (ISBN: 978-988-19253-9-8, ISSN: 2078-0958 (Print); ISSN: 2078-0966 (Online)).
4. M.P Mubiayi and Esther T. Akinlabi, "**Friction Stir Spot Welding of Dissimilar Materials: An Overview**" Lecture Notes in Engineering and Computer Science, Proceedings of The World Congress on Engineering and Computer Science 2014, WCECS 2014, 22-24 October, 2014, San Francisco, USA, pp 1089-1094. (ISBN: 978-988-19252-0-6).
5. M.P Mubiayi, E.T Akinlabi "**Friction Stir Welding of dissimilar materials between Aluminium Alloys and Copper -An overview**" Lecture Notes in Engineering and Computer Science, Proceedings of The World Congress on Engineering the World (WCE) 2013,July 3-5, London, UK (ISSN:2078-0966, ISBN: 978-988-19252-9-9).
6. M.P Mubiayi, E.T Akinlabi "**Friction stir welding of dissimilar materials : An overview**" paper presented at ICAMAME 2013: International Conference on Aerospace, Mechanical, Automotive and Materials Engineering (WASET), Johannesburg, South Africa, April 29-30, 2013, (ISSN:1307-6892), published in International Journal of Mechanical, Aerospace, Industrial and Mechatronics Engineering Vol:7 No:4, 2013.
7. M.P. Mubiayi, E.T Akinlabi "An overview on Friction Stir Spot Welding of dissimilar materials". **Book chapter** in the Transactions on Engineering Technologies 2014, IAENG,

Springer, (ISBN 978-94-017-7235-8, ISBN 978-94-017-7236-5 (eBook), DOI 10.1007/978-94-017-7236-5).

8. M.P Mubiayi, E.T Akinlabi "**microstructural Evolution of Friction Stir Spot Welding between Copper and Aluminium"** manuscript submitted and accepted as a **Book chapter** to be published in the Transactions on Engineering Technologies book (Springer 2016).
9. M.P. Mubiayi, E.T Akinlabi, "**Residual stresses and microstructure in friction stir spot dissimilar welding between aluminium and copper**" Manuscript submitted to the Advanced Engineering Materials journal (Under review).
10. M.P Mubiayi, E.T Akinlabi, "**Characterization of the evolving microstructures and intermetallic compounds in aluminium and copper friction stir spot welds**" (Peer reviewed poster), Light Metals Technology (LMT) conference, 27-29 July 2015, Port Elizabeth, South Africa.

GLOSSARY OF TERMS

A

Alloy – A substance having metallic properties and being composed of two or more chemical elements, of which at least one is a metal.

Alloying element – The alloying element is an element added to and remaining in the metal, which changes its structure and properties.

B

Backing plate – A layer of material that is placed below the joint interfaces of the materials to be welded. It provides a surface to oppose the vertical downward force on the material; and it protects the machine bed.

Bending stress – If a beam is subjected to a bending moment, the fibres in the upper part are extended; and those in the lower part are compressed. Tensile and compressive stresses are thereby induced, which vary from zero at the neutral axis of the beam, to a maximum at the outer fibres. These stresses are called bending stresses.

Breaking load – the load at which fracture occurs.

Brittleness – the tendency of a material to fracture without first undergoing significant plastic deformation.

Brittle fracture – rapid fracture preceded by little or no plastic deformation.

C

Clamping System – Is the device used to hold, locate and prevent the workpiece from moving during the large forces involved in the FSW process.

Coalescence –the merging of two or more materials (metals) into one.

D

Defect - A discontinuity or discontinuities that accumulate to render a weld or part thereof unable to meet the minimum acceptance standards or criteria of the design specifications.

Deformation – Is a change in the form of a body due to stress, heat, or other causes.

Diffraction – the scattering of electrons by any crystalline material, through discrete angles, and depending only on the lattice spacing of the material and the velocity of the electrons.

Ductility – the ability of a material to deform plastically before fracture.

Dwell time – the period of time after the rotating tool has been plunged into the work, and for which it remains stationary, generating frictional heat and plasticizing the materials, before commencing the traverse along the joint (seconds).

E

EDM (Electrical discharge machining) – This is a manufacturing process whereby a desired shape is obtained using electrical discharges (sparks).

Elastic region – a material is said to be stressed within the elastic region, when the working stress does not exceed the elastic limit.

Elastic deformation – This is the deformation of the material that is recovered when force is applied to it.

Elastic limit – This is the greatest stress, which a material is capable of sustaining without any permanent strain remaining upon complete release of the stress.

Elongation – the increase in gauge length of a body subjected to a tension force, referenced to a gauge length of a body. Usually expressed as a percentage of the original gauge length.

Elongation (%) – the total percent increase in the gauge length of a specimen after a tensile test.

Engineering strain – this is a dimensionless value that is the change in length (ΔL) per unit length of the original linear dimension (Lo) along the loading axis of the specimen; that is $e = \Delta L$, Lo the amount that a material deforms per unit length in a tensile test.

Equilibrium – a state of dynamic balance between the opposing actions, reactions, or velocities of a reversible process.

Etchant –a chemical solution used to etch a metal to reveal the structural details.

Etching – subjecting the surface of a metal to preferential chemical or electrolytic attack to reveal the structural details for metallographic subsequent examination.

Extrusion – the process whereby a material is shaped by force or squeezed through a die or nozzle.

F

Filler Metal – Metal added in making a welded, brazed, or soldered joint.

Force control – A mode in the friction stir welding process, in which a known force from previous welds is added to other input process parameters, in order to produce a weld.

Fusion – The melting together of filler metal and base metal, or of base metal only, which results in coalescence.

Fusion welding – Any welding process that uses fusion of the base metal to make the weld.

Friction – The force required to cause one body in contact with another to begin to move.

Friction stir welding and friction stir spot welding – This is a process developed at The Welding Institute (TWI) that utilizes local friction heating to produce continuous solid-state seams. It allows butt and lap joints to be made, without the use of filler metals. The solid-state low distortion welds produced are achieved with relatively low costs, using simple and energy-efficient mechanical equipment.

G

Grain – An individual crystallite in metals.

Grain growth – This is a phenomenon, which occurs when the temperature of a metal is raised; the grains begin to grow and their size may eventually exceed the original grain size.

Grain size – A measure of the areas or volumes of grains in a polycrystalline metal or alloy, usually expressed as an average when the individual sizes are fairly uniform. Grain size is reported in terms of the number of grains per unit area or volume, the average diameter, or as a number derived from the area measurements.

Grain boundary – An interface separating two grains, whereby the orientation of the lattice changes from that of one grain to that of the other. When the orientation change is very small, the boundary is sometimes referred to as a sub-boundary structure.

Grinding – removing material from the surface of a work piece by using a grinding wheel or abrasive grinding papers.

H

Hardness – This is a term used for describing the resistance of a material to plastic deformation.

Hardness test – This measures the resistance of a material to penetration by a sharp object.

Hardening – Increasing the hardness by means of a suitable treatment.

Heat-Affected Zone – The portion of the base metal which has not been melted, but whose mechanical properties have been altered by the heat of welding or cutting.

Homogeneous – The chemical composition and the physical state of any physical small portion, and one, which is the same as that of any other portion.

Hot working – A deformation under conditions that result in recrystallization.

I

Indentation hardness – This is the hardness, as evaluated from the measurements of an area of an indentation, made by pressing a specified indenter into the surface of a material under specified static loading conditions.

Intensity (X-rays) – The energy per unit time of a beam per unit area, which is perpendicular to the direction of propagation.

Interfacial region – A weld joint boundary of the workpieces indicating the positions of the pin and shoulder diameters during the welding process.

Intermetallic compounds – These are any solid materials, composed of two or more metal atoms in a definite proportion, which have a definite structure, which differ from those of its constituent metals.

J

Joint efficiency – The ratio of the strength of a joint to the strength of the base metal, expressed as a percentage.

K

Keyhole – This is an exit hole, which is left behind by the friction stir spot welding process after the weld has been done.

L

Lap Joint – A welded joint in which two overlapping metal parts are joined by means of a fillet, plug or slot weld.

M

Macrograph – A graphic reproduction of a prepared surface of a specimen at a magnification not exceeding 25x.

Macrostructure – The structure of metals, as revealed by macroscopic examination of the etched surface of a polished specimen.

Magnification – The ratio between the length of a line in the image plane to the length of a line on the imaged material.

Mechanical properties – These are the properties of a material that reveal its elastic or inelastic behaviour, when a force is applied, indicating the suitable mechanical applications.

Microstructure – The structure of a prepared surface of a metal, as revealed by a microscope at a particular magnification.

O

Oxidation – the addition of Oxygen to a compound.

P

Parameter – The minimum and maximum parameters that would describe the operating range of a variable.

Parent material – This is the sheet-metal plate in its 'as manufactured form', as supplied.

Plastic deformation – this is the distortion of material continuously and permanently in any direction. The deformation that remains or would remain permanent after the release of the stress that caused it.

Polished surface – This is a surface that reflects a large proportion of the incident light in a peculiar manner.

Position control – This is a mode in FSW, in which the machine automatically adjusts the forces acting during the welding process.

Plunge depth – This is the maximum depth that the tool shoulder penetrates into the weld plates.

Plunge force – During the plunging stage of the tool pin in FSW, the vertical force in the direction of the Z-axis movement is normally referred to as the plunging force.

R

Recrystallisation – This is a change from one crystal structure to another, such as that occurring upon heating and/or cooling through a critical temperature.

Residual stress – This is the stress in a body, which is at rest, in equilibrium, and at a uniform temperature in the absence of any external force.

Retreating side – The retreating side of the tool is where the local direction of the weld surface, due to tool rotation and the direction of the traverse, are in the opposite direction.

Rolling direction – This refers to the direction in which the billet was rolled during the sheet-metal plate manufacture.

Rotational speed – The tool rotation speed is the rate of angular rotation (usually specified in rpm) of the tool around its rotational axis.

S

Scanning Electron Microscope – An electron microscope, in which the image is formed by a beam operating simultaneously with an electron probe scanning the object.

Side flash – In FSW, this is a build-up of weld material, normally on the retreating side of the rotating tool, which has a 'peel-like' effect; this is termed the side flash.

Solid-phase – A physically homogeneous and distinct portion of a material system in the solid state.

Spindle speed – This is also referred to as the rotational speed; and it is the speed of the work holding device (chuck), measured in revolutions per minute.

Spindle torque – This is the spindle torque required to rotate the FSW tool, when plunging it into and traversing through the work piece along the joint (Nm).

Stress – This is the load applied to a piece of material; and it tends to cause deformation, which is resisted by the internal forces set up within the materials, which are referred to as stresses. The intensity of the stress is estimated as the force acting on the unit area of the cross-section, namely: as Newtons per square metre, or as Pascals.

T

Tensile strength – This is the maximum tensile stress, which a material is capable of sustaining. Tensile strength is calculated from the maximum load during a tension test carried out to rupture, and from the original cross-sectional area of the specimen.

Tensile test – This measures the response of a material to a slowly applied axial force. The yield strength, tensile strength, modulus of elasticity and ductility are thereby obtained.

Tool displacement – This refers to the offset of the tool at a certain distance from the weld centre line.

Tool shoulder – This refers to that part of the welding tool, which rotates, and is normally disk-shaped.

Tool pin – This refers to that part of the tool that rotates in contact with the surface of the work piece.

Tool plunge – This is the process of forcing the tool into the material at the start of the weld.

Tool tilt angle – The angle, at which the FSW tool is positioned relative to the work piece surface; that is, when zero tilt tools are positioned perpendicular to the work piece surface (degrees).

Traverse speed – This is also referred to as the feed rate; it is the speed at which the rotating FSW tool is translated along the joint line (mm/min).

V

Vickers hardness number – This is a number related to the applied load and the surface area of the permanent impression made by a square-based pyramid diamond indenter.

Void – This is the space that exists between the particles or grains. Normally, in welding, voids are associated with defects.

U

Unaffected material – This refers to the bulk of material, which is not affected by either heat or deformation, during the welding process.

W

Welding – This is the process of joining, in which the materials are enabled to form metallurgical bonds under the combined action of heat and pressure.

Weld nugget or stir zone – This refers to the recrystallized central area of the joint interface.

Welding speed – This is also known as the traverse speed; this is the speed (usually specified in mm/min) of the tool traversing along the work piece per specified time.

Work piece – The component to be welded.

Worm holes – This refers to a defect in a FS weld, usually on the advancing side of the rotating tool, due to the lack of mixing and re-bonding of the plasticized material.

CHAPTER ONE:

1 INTRODUCTION

1.1 Introduction

Friction stir welding (FSW) is a solid–state joining technique invented and patented by The Welding Institute (TWI) in 1991 for butt and lap welding of ferrous and non–ferrous metals and plastics. FSW is a continuous process that involves plunging a portion of a specially shaped rotating tool between the butting faces of the joint. The relative motion between the tool and the substrate generates frictional heat that creates a plasticized region around the immersed portion of the tool [1].

Prior to the development of FSW, conventional fusion welding processes were used to join similar and dissimilar materials. Aluminium and copper are difficult to weld with conventional welding processes, due to their high reflectivity and thermal conductivity. Brittle intermetallic phases develop in the joint zone; since copper and aluminium are not very soluble in one another in the solid state. These intermetallic phases lower the toughness of the weld, and lead to cracks during and after welding [2].

Friction stir spot welding (FSSW) is a variant of FSW for spot welding applications, as shown in Figure 1-1. The process consists of plunging a non-consumable rotating tool into the workpieces to be joined. Upon reaching the desired plunge depth, the rotating tool is held in that position for a desired time. This is also referred to as dwell period. Subsequently, the rotating tool is retracted from the welded joint, leaving behind a friction stir spot weld. As with traditional resistance spot welding, FSSW is limited to lap joint configurations [3].

Friction stir welding and friction stir spot welding processes use a non-consumable rotating tool consisting of a pin extending below a shoulder that is forced into the adjacent mating edges of the

work pieces. The heat input, the forging action, and the stirring action of the tool induces a plastic flow in the material, forming a solid state weld.

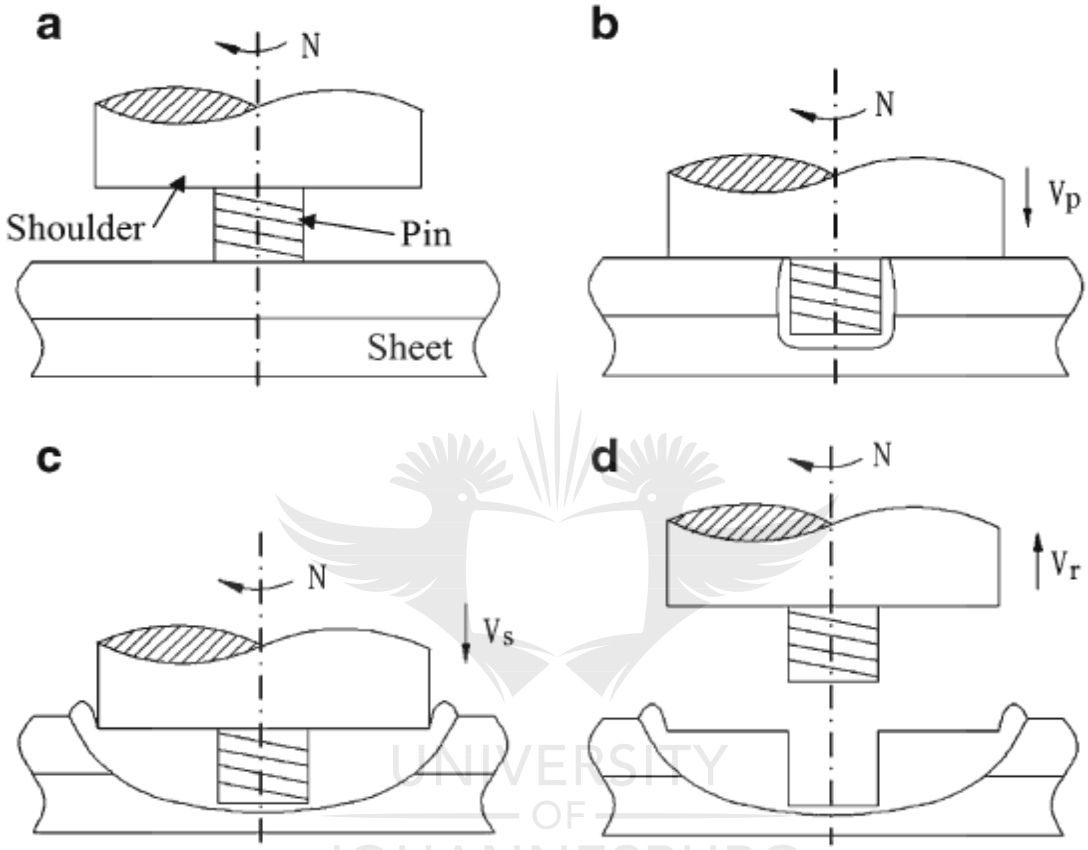

Figure 1-1 Illustration of friction stir spot welding process: (a) the pin comes in contact with the surface of the upper work piece; (b) the pin stirs in the workpieces; (c) the shoulder participates in the welding; (d) and finally, the tool is drawn out [4].

Nevertheless, FSW of aluminium to copper remains not yet fully researched; because, in addition to the different melting temperatures of the materials, the high chemical affinity of both base materials promotes the formation of brittle intermetallic Al/Cu phases. This still requires extensive research [5] [6] [7]. Furthermore, there are limited studies on FSSW, especially the FSSW of copper to aluminium. Heideman *et al.* [8], conducted metallurgical analyses of AA6061-T6 with

an average hardness of 58 HRB and oxygen-free pure copper, using the friction stir spot welding process. Özdemir *et al.* [9] investigated the effect of pin penetration depth on the mechanical properties of the FSS Welded AA1050 and pure copper. Shiraly *et al.* [10] conducted a study on the FSSW of Al/Cu composite produced by the accumulative roll-bonding process using AA1050 and pure copper as the parent materials.

Aluminium alloys are widely used to produce aerospace components with high specific strength. However, when traditional welding processes are applied to these alloys, they often prove to be disadvantageous. And this discourages the use of such welded components [11].

Furthermore, the aluminium-to-copper welding is increasingly used in some practical applications, such as heat transfer equipment, wiring and aesthetical applications [7].

1.2 Justification of the study

The welding quality of FSW is determined by material properties, tool design and the synthesised effect of the process parameters. The proper description of welding quality, the selection of the control variables characterising the process conditions, and the relation between the control variables and the process parameters must be established [12].

The contact between the shouldered regions of the tool with the work pieces generates significant frictional heat, as well as preventing plasticised material from being expelled from the weld. The tool is moved relatively along the joint line, forcing the plasticized material to coalesce behind the tool to form a solid–phase joint [1].

The forces in action during FSW are significant; and a proper fixture design is critical to the success of the weld. The axial force applied to the welding tool, keeping it embedded in the work piece, is commonly from 20kN to 60kN [13]. Consistent axial force is required to produce a good weld microstructure; but with constant weld parameters, the axial force can vary significantly during welding, producing welds with inconsistent tensile strength values [14].

Recently, Akinlabi *and* Akinlabi [15] reported that the advancing force, the vertical force, the torque and the heat input to the welds increase; as the shoulder diameter increases during friction stir welding of aluminium alloy and copper. They also indicated that the shoulder diameter influences the widths of the interfacial regions in the welds, such as the stir zone (SZ) and the thermo-mechanically affected zone (TMAZ).

It is then important to choose the right tool geometry and process parameters to produce sound welds.

An adequate tool-pin length was suggested for stirring up the oxide layers in the welds, in order to prevent any potential flaws [12]. A tool pin with a profiled surface was generally used to facilitate a downward auguring effect. This can be described as the tool gripping the plasticised material, and then pulling it in a downward direction [12].

Akinlabi [16] indicated that at a constant rotational speed, the high heat input condition is achieved at the lowest feed rate; while the weld produced at the highest feed rate is considered to have a low heat input. Furthermore, the intermediate heat input condition in the weld was achieved at a medium feed rate during the friction stir welding of aluminium alloy and pure copper. Heideman *et al.* [8] reported that the rotational speed, as well as the pin length have an effect on the Friction Stir Spot Welds with the rotational speed having the most significant effect; and this increases with any increase of the rotational speed.

Özdemir *et al.* [9], also concluded that hardness increases at the bottom region of the pin hole due to the heat input introduced by the rotating pin. Furthermore, they stated [9] that as the plunge depth increases and the grain size decreases, these cause a higher hardness.

Many emerging applications in power generation and the chemical, petrochemical, nuclear, aerospace and industries, and manufacturing led to the development of FSW for similar and dissimilar materials. It is consequently important to also generate more information on the FSSW of similar and dissimilar materials.

In the open literature, the joining of 1060 pure aluminium to C11000 pure copper of 3 mm using friction stir spot welding process is non-existent.

This project is focused on the friction stir spot welding, using different two-tool geometry and process parameters in regard to the material flow, microstructural evolution, as well as the mechanical and electrical properties, in order to produce sound Friction Stir Spot Welds between AA1060 to C11000.

Most studies on the material characterisation of aluminium and copper materials using FSSW focus on the chemical analyses and the mechanical testing [8], [9]. Furthermore, the investigation on the effect of material flow linked to the tool geometry, using different FSSW welding parameters, is of high importance especially in industry. On the other hand, the correlation between tool geometry, mechanical, microstructure and electrical properties is also important to the industries. Therefore, the use of the right tool geometry and process parameters in regard to producing sound Friction Stir Spot Welds between AA1060 and C11000 would add value to the body of knowledge in the field of FSSW, to enable the process to be applied industrially. Additionally, Babu *et al.* [17] concluded that the FSSW process can outperform riveting process.

The aim of this work is to explore the possibilities of extending the application of friction stir spot welding between aluminium and copper through an in-depth characterisation of the produced welds. In other words, the deeper fundamental understanding of the different properties of the produced welds when using friction stir spot welding would generate a platform that may be expected to extend the usage of FSSW technique to join aluminum and copper, which could be used in various industries, including the electrical and manufacturing industries.

1.3 Problem Statement

Friction stir welding has advantages compared to fusion welding processes. Problems, such as solidification cracking, porosity and liquation cracking are eliminated when using FSW because of its solid-state nature [18]. Friction stir welding and friction stir spot welding processes display the presence of deformations and microstructural differences in the weld zone, including the nugget zone (NZ), the thermo- mechanically affected zone (TMAZ) and the true heat- affected zone (HAZ). Moreover, in order to extend the use of FSSW in the South African industries, this

project will focus on generating data on the characterisation of friction stir spot welding between AA1060 to pure copper (C11000) using different tool geometry and process parameters.

Kahl *and* Osikowish [19] reported that copper and aluminium alloys are the preferred materials for electrical conductors. They also stated that there is an increase in joining technologies that are capable of producing dissimilar aluminium to copper joints, with good mechanical and electrical properties.

Therefore, weld parameters, such as rotational speed and the dwell time will also be studied, in order to understand the evolving properties of FSSW sound welds, which may be used in the manufacturing sector. On the other hand, the resulting weld integrity will have to be fully analysed.

1.4 Objectives

The use of the right tool geometry and welding parameters using experimental results should provide a good insight into the possible applications of FSSW in South African industries, especially in the manufacturing sector. The aim of this project is to choose and characterise sound produced Friction Stir Spot welds of AA1060 to C11000 using two different tool geometry and process parameters. The produced spot welds could be used in electrical and power generation industries (i.e. busbars). Furthermore, it is necessary to comply with a high quality weld in relation to mechanical, electrical and microstructural properties, and the welding parameters, in order to reduce any possible defects during FSSW. In addition, this research project will have the following sub-objectives:

- To investigate the effect of tool geometries on the friction stir spot welding of AA1060 pure aluminium to pure copper C11000.

- To investigate the effect of process parameters and tool geometry on the formation of intermetallic compounds, and their impact on the mechanical and electrical properties of the welds.

- To investigate the effect of process parameters and tool geometry on the residual stresses

- To investigate the effect of process parameters and tool geometry on the formation of the Cu rings.

1.5 Research methodology

A comprehensive literature study was conducted, in order to become familiar with past and recent FSW and FSSW processes. The literature survey was conducted to include information, such as the tool material to FSW and FSSW alloys of aluminium and copper, the availability of both materials, in addition to the experimental equipment needed to effectively carry out the characterization of the weld properties. The type of joint to be used in this study is lap joints. The materials used in the current project are aluminium alloys (AA1060) and pure copper (C11000) due to their good electrical conductivity. The welds were produced at the Nelson Mandela Metropolitan University (NMMU) using a FSW machine (MTS PDS I-Stir); and the material characterisation of the welds were conducted at the University of Johannesburg laboratories, and at the Nuclear Energy Corporation of South Africa (NECSA).

FSSW was performed on AA1060 and pure copper (C11000); additionally, various studies will be undertaken, including microstructural evolution, chemical analysis and mechanical characterisation. The effect of welding parameters will be investigated. The following analyses will be conducted to characterise the welds:

1.5.1 Microstructure investigation and chemical analyses

In the literature, the results can be found, showing a lack of unanimity concerning the structural and morphological characterisation of dissimilar welds [7]. The knowledge on the microstructure of similar and dissimilar materials is of importance. The following microstructural characterisation and chemical analyses were used in this project. These analyses included:

Optical microscope and scanning electron microscopy combined with energy-dispersive X-ray spectroscopy (SEM/EDS). These analyses were carried out on the spot welds to investigate the microstructural evolution, as well as the mapping and intermetallic population characteristics.

X-ray diffraction (XRD) was used in the project to determine the presence of intermetallic compounds (new phases) and their possible compositions. Furthermore, the X-ray diffraction technique was used to measure the residual stresses in the produced welds. The residual stresses

were measured in the stir zone (SZ) and on the copper ring to investigate the effects of process parameters and tool geometries.

1.5.2 Mechanical and electrical testing

Mechanical testing evaluation was carried out to characterise and analyse the welded parts: such as tensile shear test and microhardness; and these tests were performed on the welded spots.

The tensile shear testing was conducted to measure and compare the strength and the ductility of the spot welded samples using different tool geometries and process parameters.
The microhardness testing was carried out to investigate the effect of the presence of precipitates on the welded zone compared with the base material. Furthermore, the residual stresses were also measured using the X-ray diffraction method.

The electrical resistivity was also measured, in order to investigate the effect of the welding parameters on the electrical resistivity of the welds.

1.6 Delimitation

The current research project will focus on joining AA1060 and commercially pure copper C11000 using the friction stir spot welding process. Furthermore, only plates of 3 mm thickness of the two quoted metals were to be used.

1.7 Significance of the Research

Within the university, this project will add value in the research field of FSSW; since it is to the best of our knowledge the first project on friction stir spot welding using different tool geometries and process parameters to successfully join 3 mm thick AA1060 to copper C11000 plates. In general, the project should yield accurate information on FSSW tool shape, dimensions and process parameters during FSSW between aluminium and copper. This could expand the use of the FSSW process in the manufacturing sector in South Africa in particular, and in Africa in general. The latter could be an alternative solution to the resistance spot welding (RSW) technique and riveting.

1.8 Outline of the thesis

An introduction, justification, problem statement, objectives, research methodology, delimitation and significance of the study are all presented in **Chapter 1**.

Chapter 2 (Literature review): This chapter presents the basic concepts and discussions on the previous studies in the field of friction stir welding and friction stir spot welding of similar and dissimilar materials. Furthermore, it also presents a critical review on friction stir spot welding between aluminium and copper.

Chapter 3 (Methodology): All the experimental and analytical procedures used in this study are explained in this chapter.

Chapter 4 (Results and Discussion): The findings from the experimental and analytical procedures of the study are presented and discussed in this chapter.

Chapter 5 (Conclusions and recommendations): Conclusions are drawn on the basis of the results and the discussion presented in **Chapter 4**. Recommendations for future work are also laid out in this chapter.

References: All literature sources quoted in the dissertation appear at the end of each relevant chapter.

Appendix section: To be found in this section, are some of the selected analyses and the relevant data.

CHAPTER TWO

2 LITERATURE REVIEW

2.1 Introduction

This chapter focuses on the literature related to friction stir spot welding (FSSW) and friction stir welding (FSW). The factors affecting the friction stir spot welding process will be outlined, in addition to any previous studies conducted on FSSW and FSW between aluminium and aluminium, as well as aluminium to other materials, and aluminium to copper, will be summarised. Furthermore, a critical literature review will be conducted on FSSW between aluminium and copper.

2.2 Solid state welding

Solid-state welding is the process whereby joining is produced at temperatures beneath the melting point of the parent metal without the usage of any filler metal. Examples of solid state welding processes include friction welding, friction stir welding (FSW), spot welding and resistance welding. In the cited solid state welding, there are fewer defects; because the metals do not reach their melting temperatures [20].

2.3 Metallurgy of Aluminium-Copper system

The high metallurgical reactivity and affinity between aluminium and copper leads to the formation of hard and brittle intermetallic compounds in two zones, namely: the joint interface and the stir zone [104]. Copper and aluminium are the equilibrium solid phases of the Al-Cu system, and the terminal Face Centred Cubic (FCC) solid solutions; copper (Cu) is usually designated α; hereafter, the low-temperature ordered phase based on the FCC structure is designated α_2; β represents the disordered Body Centred Cubic (BCC) solid solution; β_1, the ordered BCC phase, which occurs in its metastable form; and β_0, a high-temperature phase; (iii) ε_1 and ε_2 comprise those phases of indefinite structure; (iv) phases with structures based on γ brass, γ_0, γ_1 and δ; and

(v) the equiatomic phases, η_1 and η_2, and near-equi-atomic phases, ζ_1 and ζ_2, with structures related to the η structures; and (vi) θ, and metastable transition phases θ' and θ", formed from supersaturated (Al) before the {θ + (Al)} equilibrium is reached. The solubility of aluminium in copper is 19.7 atomic percentage of aluminium; and the solubility decreases below the peritectoid temperature [105]. The Al/Cu phase diagram is presented in Figure 2-1.

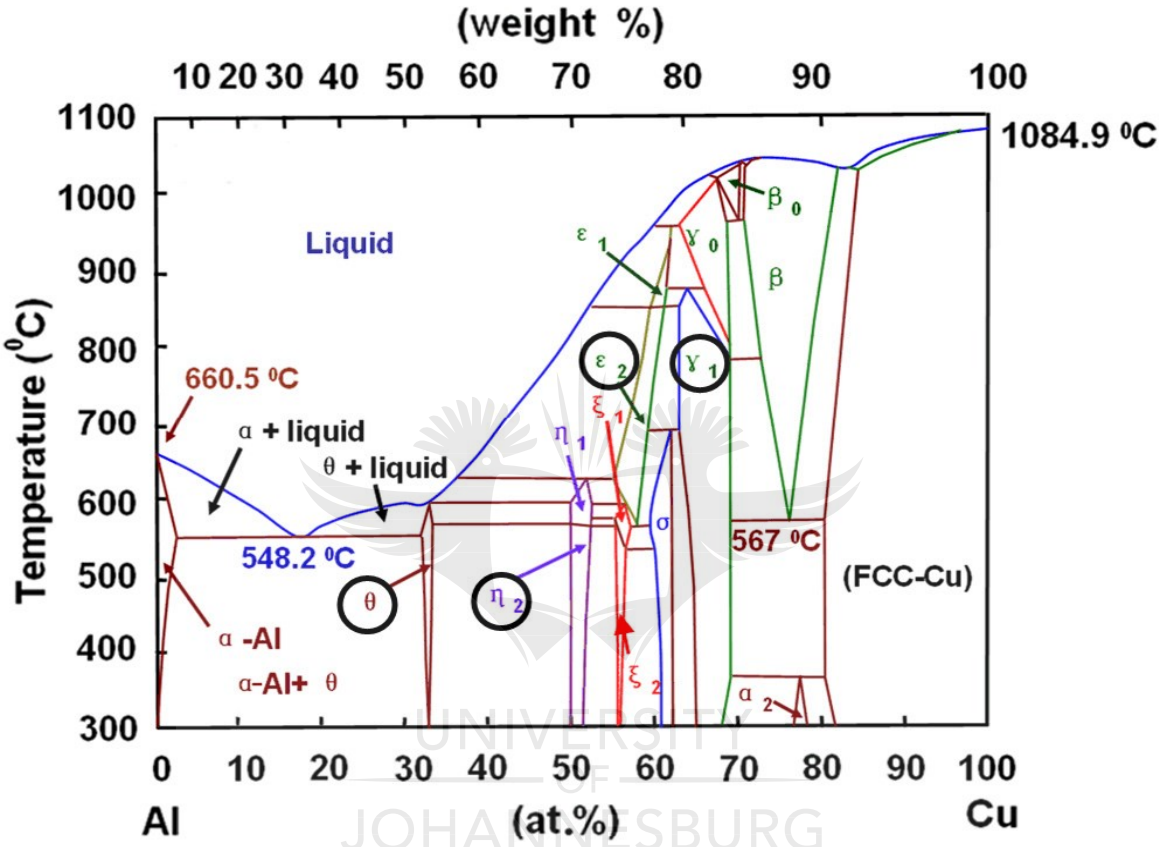

Figure 2-1 Binary diagram of Al–Cu [150]

Table 2.1 depicts a list of the common intermetallic compounds, their atomic percentages and weight composition [cited by Akinlabi 2010]. The weight percentage compositions found in Table 2.1 were calculated based on the chemical formulas of the intermetallic compounds, according to Akinlabi [105].

Table 2.1: Al-Cu Intermetallic compounds and their properties [cited by Akinlabi (2010)] [105]

Phase	Composition, atomic %Cu	Composition weight %Cu	Chemical formula	Temperature at which they are formed (°C)
(Al)	0 to 2.48	0	Al	0
θ	31.9 to 33.0	54	Al_2Cu	550
η_1	49.8 to 52.4	70	AlCu	591
η_2	49.8 to 52.3	70	AlCu	591
ζ_1	55.2 to 59.8	76	Al_3Cu_4	624
ζ_2	55.2 to 56.3	76	Al_3Cu_4	624
δ	59.3 to 61.9	78	Al_2Cu_3	700
γ_0	59.8 to 69	84	Al_4Cu_9	950
γ_1	62.5 to 69	84	Al_4Cu_9	950
β_0	67.6 to 70.2	88	$AlCu_3$	1048
β	70.6 to 82.0	88	$AlCu_3$	1048
Cu	80.3 to 100	89 to 100	Cu	1083

2.4 Residual stress measurement

Residual stresses can be defined as the stresses that persist within a material or body after manufacture and material processing in the absence of any external forces or thermal gradients. They can also be produced by service loading, leading to inhomogeneous plastic deformation in the part or sample. Consequently, residual stresses are not caused by loads (forces or moments) [21].

There are different reasons for the residual stresses, which can be possibly classified as:

- Differential plastic flow
- Differential cooling rates
- Phase transformations with volume changes, etc.

Residual stresses occur in various manufactured structures and components. Many investigations have been conducted to study this phenomenon and its effect on the mechanical properties of these components [21]. Different methods have been developed to measure the residual stress for different types of components, in order to obtain reliable evaluation. These methods include: non-destructive, semi-destructive and destructive methods, as depicted in Figure 2-2.

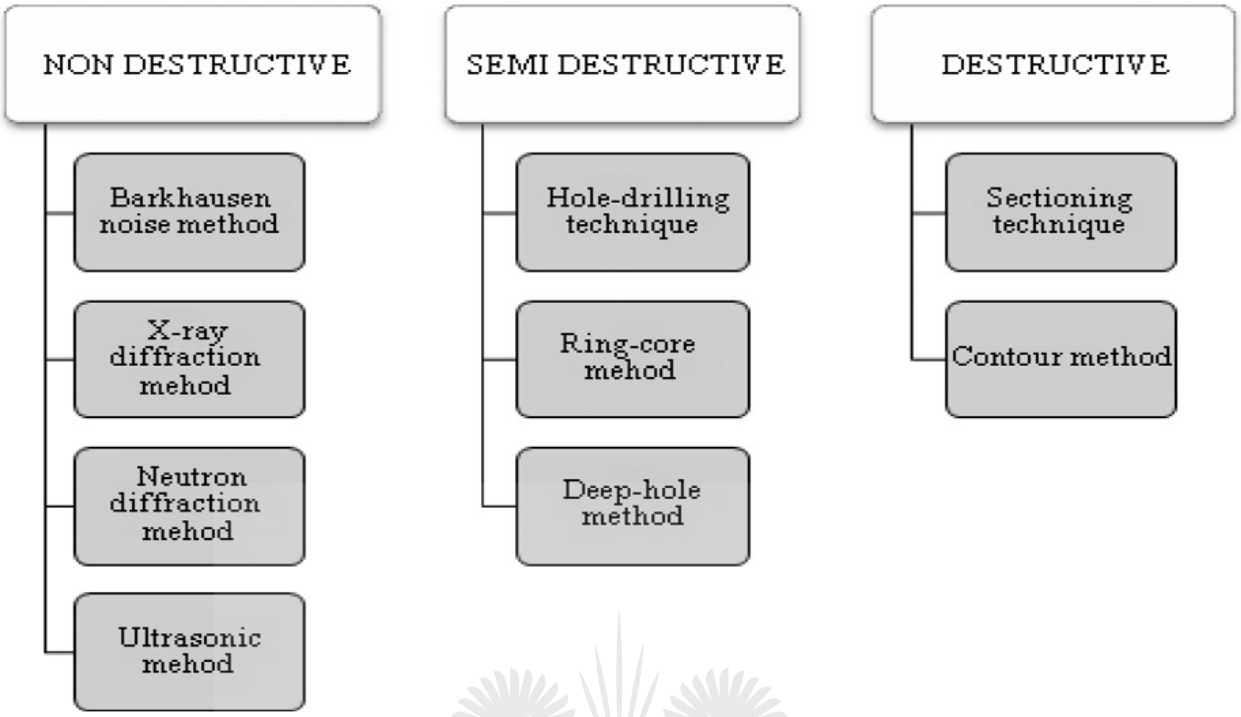

Figure 2-2 Residual stresses measurements methods [21]

2.4.1 Methods used to measure residual stresses

During the past years, many methods for measuring residual stresses have been developed. These include hole drilling, X-ray diffraction, synchrotron diffraction, neutron diffraction, curvature layer removal, Magnetic, ultrasonic and Raman. Table 2.2 shows a summary conducted by Lombard [22] on the different methods for residual stress measurements. The table also shows the principal advantages and limitations of the cited methods.

Table 2.2: Summary of various measurement techniques and their characteristics to determine residual stresses [22]

Method	Principle, advantages and limitations	Resolution, penetration and sampling volume	Material type
Hole Drilling	This method measures in plane stresses from distortion caused by stress relaxation in plates using rosettes. Many sources of error arise due to the shape and dimensions of the hole, surface conditions and non orthogonal hole drilling. The size of the rosette and hole-to-hole interference limits spatial resolution. Yielding can occur during hole drilling close to the surface of the sample, and this will lead to inaccurate measurements. Strain can be measured up to a depth equal to the diameter of the drilled hole.	Resolution 50-100 μm depth increment Penetration Equal to Hole diameter Sampling size 1-2 mm in diameter 1-2 mm deep	Metals Plastics Ceramics
X-ray Diffraction	The shifts in the position of Bragg peaks, caused by elastic strain induced in a sample, is used to determine strain. Grains are therefore considered as atomic strain gauges. This method requires (i) layer removal for depth measurements by using, for example, electro polishing techniques; (ii) the need to deduce principal stress directions (or measure 6 components of strain tensor); (iii) suitable lattice planes to be chosen; and (iv) The $\sin^2\Psi$ technique to be applied and does not require d_o measurements. Limitations include : the whole specimen must fit inside the diffractometer when measurements are taken; errors can arise from rough surfaces, e.g. welds; only near surface information can be measured; and this method is sensitive to surface preparation.	Resolution 20 μm depth 1 mm wide Penetration 5 μm - Ti 50 μm - Al 1 mm layers Sampling size 0.1-1 mm^2 0.05-0.1 mm	Metals Ceramics
Synchrotron Diffraction	This technique is discussed in detail in sections 5.6 to 5.10. Synchrotron X-ray advantages include: (i) 10^{12} times brighter than laboratory X-ray source. 20-300 keV beam with small wavelength ≈ 0.3 Å; (ii) Much higher penetration	Resolution 20 μm lateral 1 mm in-line Penetration >500 μm 20 mm – Al Sampling	Metals Ceramics

	depths (>20 mm in Al) than laboratory X-rays; (iii) Narrow beam and small sampling volume; (iv) Fast measurements ~ 20s per data point; and (v) low scattering angles ~ 10-20° depending on (h k l) planes investigated; and (vi) Standard diffraction techniques being used with synchrotron X-ray measurements. One limitation is that the gauge volume has an elongated diamond shape that could make strain measurements in certain directions not feasible due to long paths lengths into the material. This technique is best applied to thin plates.	size 0.1 mm^3	
Neutron Diffraction	Neutrons are scattered by an electron cloud or nuclei. Constructive interference leads to the generation of intensity peaks from Bragg reflected planes. Time of flight of the reflected beam is used to determine strain. Major advantages are: (i) high penetration depths of ~100 mm in Al and ~ 25 mm in steel; (ii) high spatial resolution – can measure to within 0.2 mm of surface; (iii) narrow beam (slits); (iv) full 3-d strain maps via strain scanning of specimen at the same time can be obtained; (v) automated translation and rotation of a specimen; (vi) strain measurements during fatigue, bending or tensile testing (that is in service measurements) can be taken; and (vii) time of flight measurements can be taken to obtain strains from different phases present in the same sample at the same time. This is possible because different hkl reflections will take different amounts of time to reach the detector.	Resolution 500 µm Penetration 100 mm – Al 25 mm – Fe 4 mm - Ti Sampling size >1 mm^3	Metals Ceramics

	The only limitation is that this technique is more expensive than Synchrotron X-ray radiation and highly qualified scientists are required to take strain measurements.		
Curvature Layer Removal	Measures in plane stresses by changes in curvature of a strip coated on the sample. The accuracy is limited by the minimum measurable curvature. Near surface stresses cannot be measured with this technique.	Resolution Variable Penetration Not applicable Sampling size Not applicable	All
Magnetic	Ferromagnetic properties are sensitive to the internal stress state in the sample. The magnetic domains closely aligned with stress are strained. The stress-induced magnetic anisotropy leads to the rotation of the magnetic field away from the applied direction. A sensor coil can monitor these small rotations. When no rotation is observed, principal stress axis and the magnetic axis are aligned. This technique is sensitive to the micro structural and chemistry changes in the sample. No universal or agreed method of data interpretation is available.	Resolution 1 mm Penetration 20-300 μm Sampling size >2 mm^2	Ferro-magnetic
Ultrasonic	The velocity of ultrasonic waves are sensitive to stress in materials. The changes in speed provide a measure of the average stress along the wave path through the material. Measurements are affected by microstructural changes in the sample. Difficulties arise in separating multi-axial stresses.	Resolution 5 mm Penetration >100 mm Sampling size 1-400 mm^2	Metals Ceramics
Raman	Laser light causes atomic bonds to vibrate in certain liquid and solid materials. This gives characteristic fluorescence luminescence lines of wavelength and intensity. Raman lines shift with changes in hydrostatic stress. This is a surface technique for samples that are not optically transparent.	Resolution 0.5 μm Penetration Surface Sampling size -	Ceramics Polymers Silicon carbide Alumina-zirconia Epoxy Sapphire Fibre composites

In the current research work, the X-ray diffraction method, which is a non-destructive method, is used.

2.5 Friction stir welding (FSW)

Friction stir welding (FSW) is a solid–state joining technique invented and patented by The Welding Institute (TWI) in 1991 for butt and lap welding of ferrous and non–ferrous metals and plastics. FSW is a continuous process that involves plunging a portion of a specially shaped rotating tool between the butting faces of the joint. The relative motion between the tool and the substrate generates frictional heat; and this creates a plasticized region around the immersed portion of the tool [1].

The friction stir welding process uses a non-consumable rotating tool consisting of a pin extending below a shoulder that is forced into the adjacent mating edges of the workpieces [23], as illustrated in Figure 2-3.

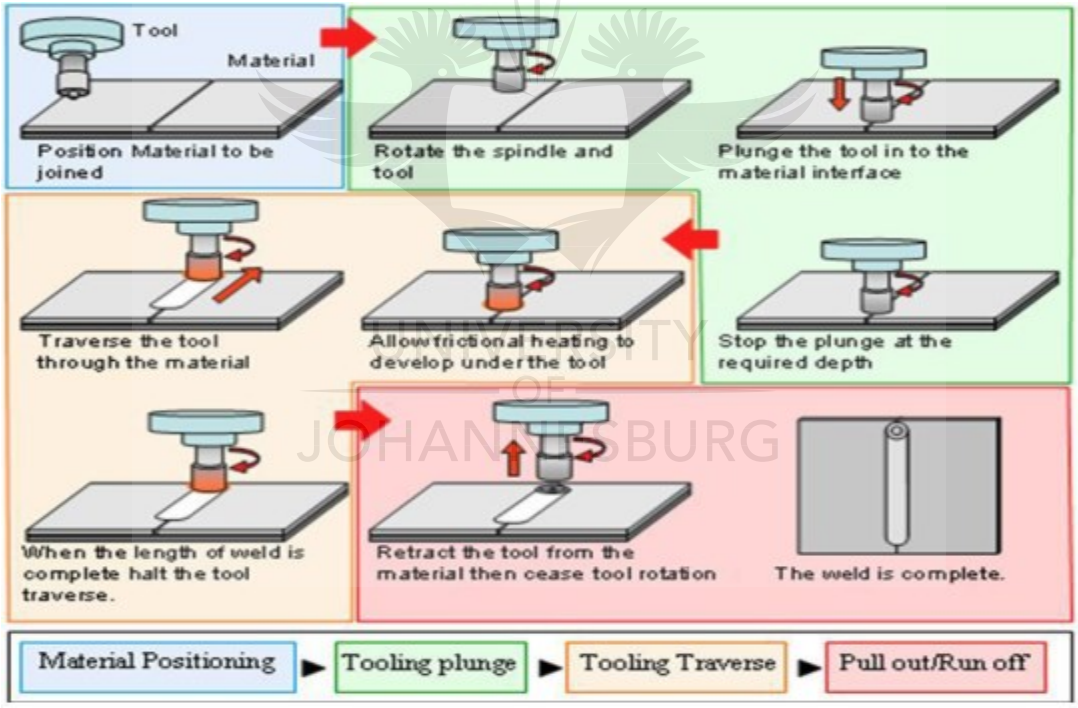

Figure 2-3 The friction stir welding process [24]

It was realised early in the development of FSW that the tool's design is critical in producing sound welds [25].

A basic and conventional design for a FSW tool is shown in Figure 2-4. FSW tools follow the same basic trends in terms of their shapes and geometries. They generally comprise three generic features, including: a shoulder, a probe also known as a pin, and any external features on the probe.

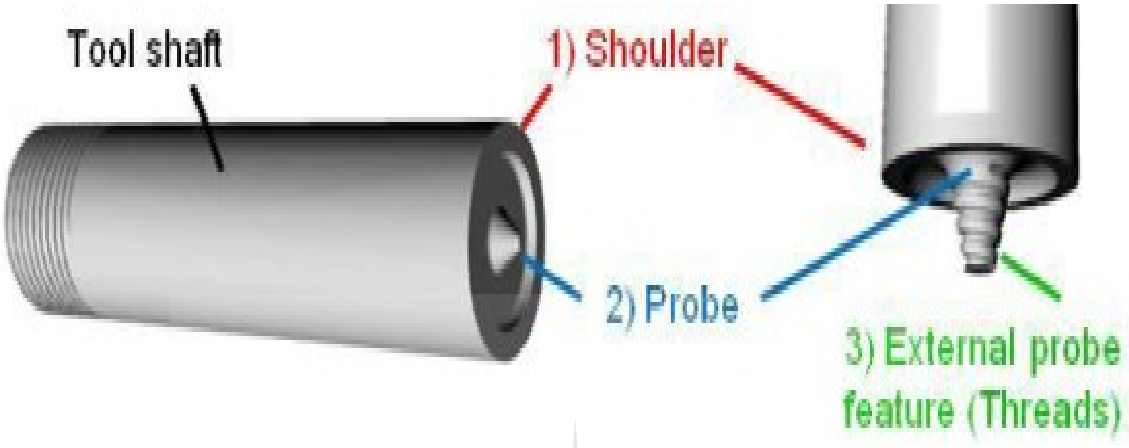

Figure 2-4 A Schematic View of a FSW Tool [24]

2.6 Friction stir spot welding (FSSW)

Friction stir spot welding (FSSW) is a variant of FSW for spot welding applications. A non-consumable rotating tool is plunged into the workpieces to be joined. Upon reaching the desired plunge depth, the rotating tool is held in that position for a pre-determined finite time (sometimes referred to as the dwell period). Subsequently, the rotating tool is retracted from the welded joint, leaving behind a friction stir spot weld. During FSSW, tool penetration and the dwell period essentially determine the heat generation, the material plasticisation around the pin, the weld geometry and therefore the mechanical properties of the welded joint [3]. A schematic illustration of the FSSW process is shown in Figure 2-5.

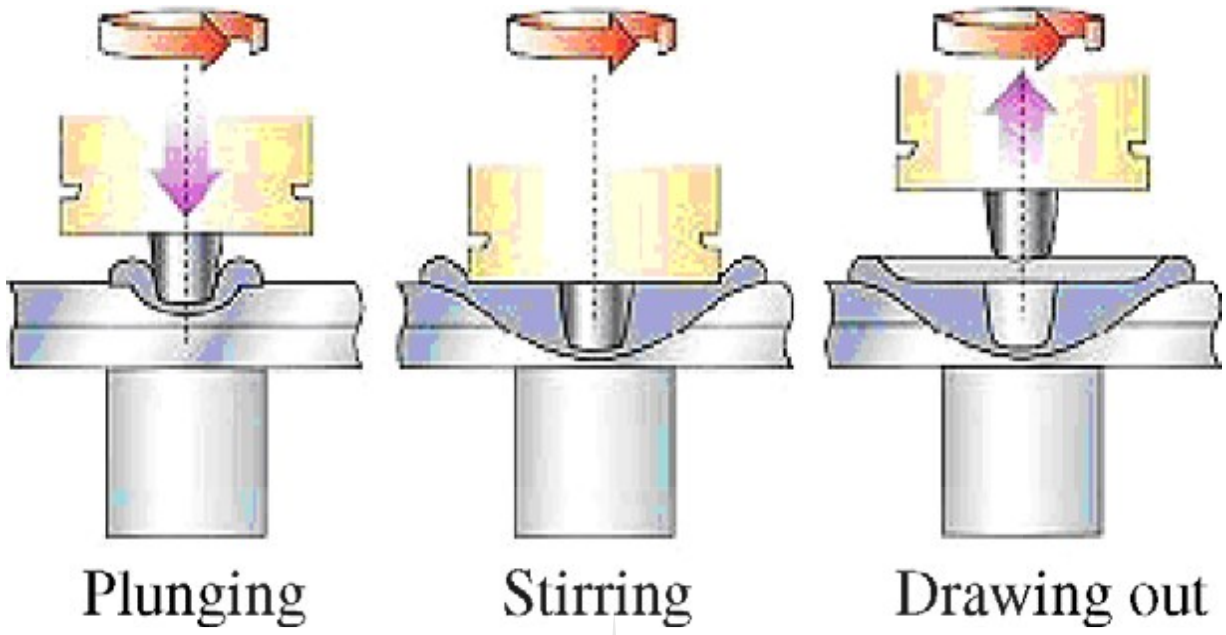

Figure 2-5 Schematic illustration of friction stir spot welding process [26]

The FSSW process uses a tool, similar to the FSW tool [24]. The shoulder generates the bulk of the frictional or deformational heat; whereas the pin assists in the material flow between the workpieces [3]. Besides the tool, the other parameters involved in FSSW are: the tool rotation speed; the tool plunge depth and the dwell period. These parameters determine the strength and finish of the weld joints [3].

2.6.1 Heat input during friction stir spot welding

During FSW, the tool moves over the base metal, stirring, deforming, and mixing it. The parent material, the anvil and the tool increase in temperature due to the influence of the tool on the parent material. This variation in temperature is a clear indication of the heat generation caused by frictional contact that takes place during the welding process [27]. In FSSW welding, the heat input is calculated by integrating the torque curve, and then using the equation 2.1 [28]:

$$U = \frac{2\pi}{60}\omega\int_{t_0}^{t_s} T dt \qquad 2.1$$

Where,

ω: Tool rotation speed

T: Torque

And t_0 and t_1 are the tool contact and withdrawal times

U: Heat input

However, this is only an estimate of the heat input. Yang et al. [29] used a similar equation to estimate the weld heat input, taking into consideration the heat input from the contribution of the tool plunge depth to the heat input, as depicted in Equations 2.2 and 2.3, respectively. Equation 2.4 shows the total heat input. The Equation 2.1 was used for all the heat input calculation in the current research work.

$$Q_{\Omega} = \int_0^t M_z \left(\frac{2\pi\Omega}{60} \right) dt \qquad 2.2$$

$$Q_f = \int_0^t F_z \, v_z \, dt \qquad 2.3$$

$$Q = Q_{\Omega} + Q_F = \left(\frac{2\pi\Omega}{60} \right) \int_0^t M_z \, dt + v_z \int_0^t F_z \, dt \qquad 2.4$$

Where:

Q : Total heat input

Q_{Ω} : heat input due to the contribution of the rotational speed

Q_F : heat input due to the contribution of the tool plunge

Ω : Rotational speed

M : Torque

F: Axial force

t: Time

2.6.2 Welding Parameters and tools

Even though FSSW has given thus far high quality spot welds, the suitable execution of the process and the control of a number of parameters is required, in order to get good quality joints. Process parameters, such as the rotational speed, the dwell time, and the plunge depth are of importance; and these factors will all be investigated in the current research work.

On the other hand, the FSW tool is considered to be the heart of the welding process, which has two primary parts, namely: the shoulder and the pin. These heat the workpiece material by friction. The shoulder part of the tool frictionally heats a portion of the workpiece; and it induces the axial downward force for welding consolidation.

Three types of shoulder end surfaces are normally used: the flat, the convex, and the concave shoulder end. Shoulder end surfaces can also have features, like scrolls, ridges, knurling, grooves and concentric circles, in order to increase the weld quality and the material mixing [30]. The different shapes of the tool pin and the shoulder are depicted in the Figures 2-6 and 2-7, respectively [30].

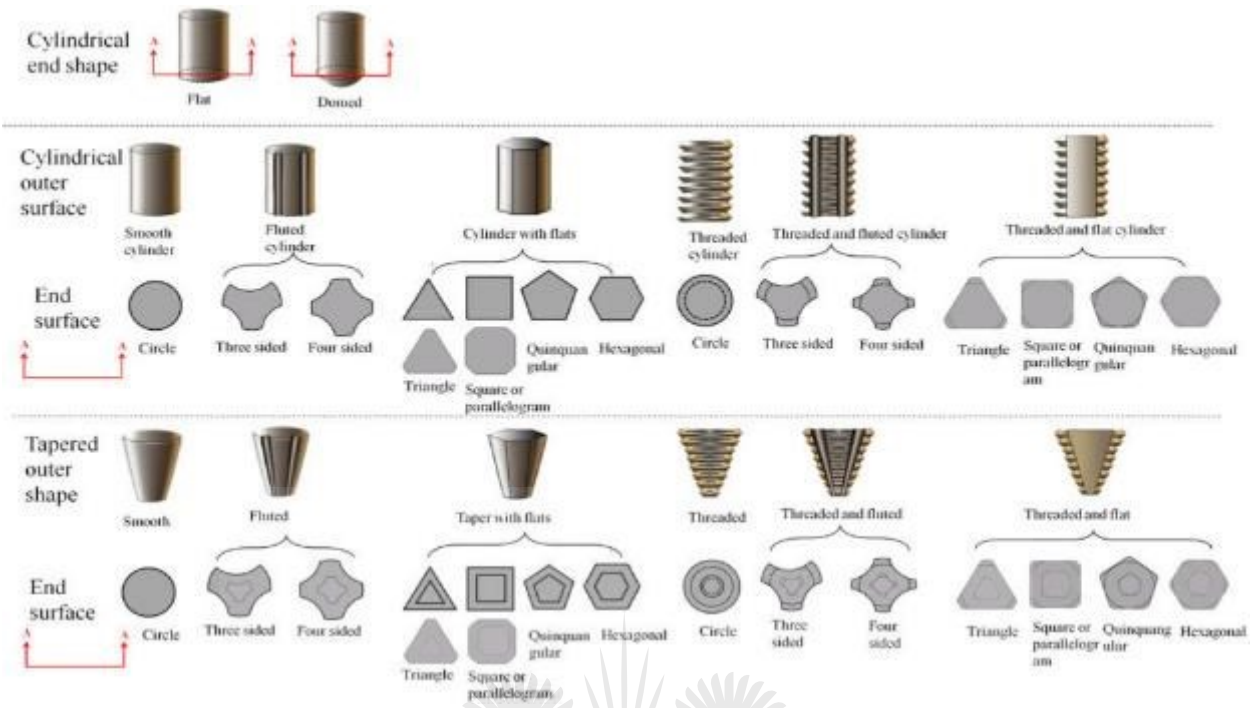

Figure 2-6 The different shapes of the tool pin [30]

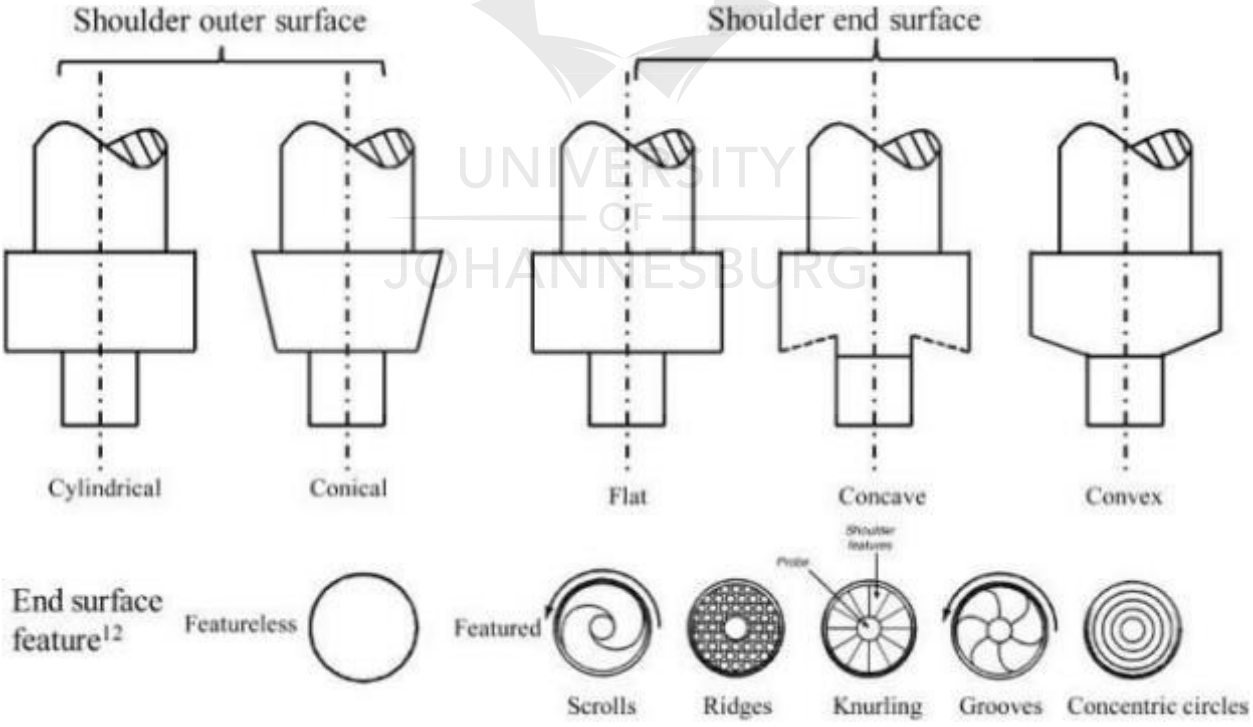

Figure 2-7 Tool shoulder geometries [30]

A review of the previous research work done in the field of FSW and FSSW, using different process parameters, such as the rotational speed, the traverse speed, the plunge depth, the dwell time, as well as the tool geometries, is conducted and summarised in the paragraphs to follow. The effects of the cited parameters and the different tool geometries are outlined.

2.6.3 Microstructural regions of FSSW

A nomenclature is required to accurately describe the different microstructure regions present after the FSSW of the workpieces. The cross section of the spot weld shows the five characteristics regions, as shown in Figure 2-8:

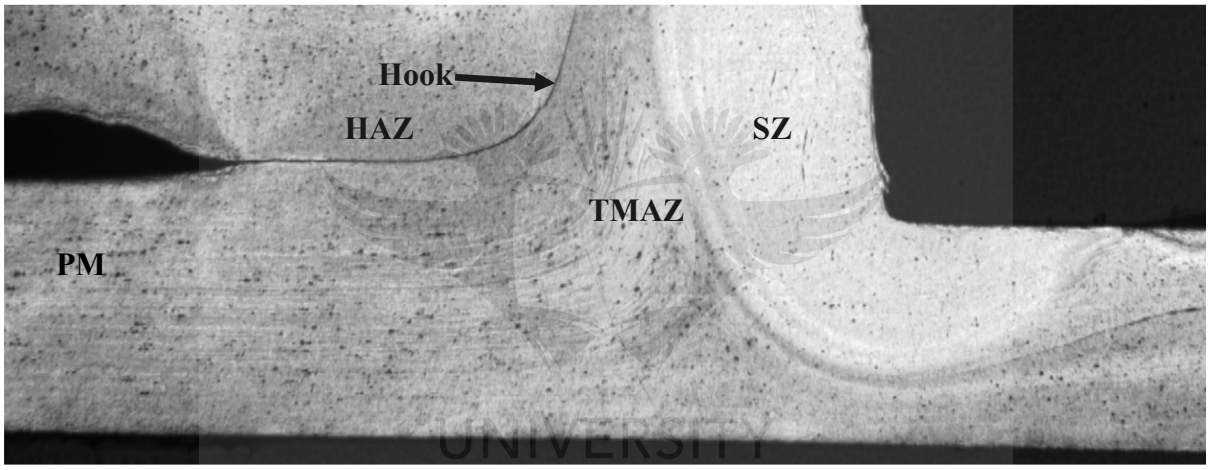

Figure 2-8 Cross-sectional appearance of a typical friction stir spot weld [3]

Parent material (**PM**): this is the material that is remote from the weld region that has not been deformed. However, it may have experienced thermal cycling from the weld. This is not affected by the heat in terms of the microstructure or mechanical properties.

Heat affected zone (**HAZ**): This region lies closer to the weld-centre; and it has experienced a thermal cycle during welding, which has modified the microstructure and/or the mechanical properties. However, there is no plastic deformation in this region.

The thermo-mechanically affected zone (**TMAZ**): In this region, the tool has plastically deformed the material. In some materials, it is possible to obtain significant plastic strain without

recrystallization in this region. There is a distinct boundary between the recrystallized zone and the TMAZ.

The stir zone (**SZ**): This is the fully recrystallized region that is in the immediate vicinity of the tool pin. The grains within the stir zone are roughly equiaxed; and they are frequently of an order of magnitude smaller than the grains in the parent material.

Hook: This is a characteristic feature of the friction stir spot welds in the lap configuration. It is the formation of a geometrical defect originating at the interface of the two welded sheets, sometimes called a 'hook'. Metallic materials often have a thin oxide film present on the surface. During welding, a hook is formed, because of the upward bending of the sheet interface due to the tool penetration into the bottom sheet. The oxide film is broken up into particles by the stirring of the tool. The particles could be dispersed into the weld region, thus causing partial or complete metallurgical bonding of the overlapped sheets in the weld region. The presence of the hook diminishes the integrity of the spot welds; since the failure (crack propagation) of the weld joint can occur along the hook, when the weld is subjected to any external loading [31].

2.7 Overview on Friction Stir Welding (FSW) and Friction Stir Spot Welding (FSSW)

This section illustrates an overview of FSW and FSSW of similar and dissimilar materials. Researchers have conducted and published reviews on the friction stir welding process [32-35] [108].

2.7.1 FSW materials combinations of the research studies and characterisation

2.7.1.1 FSW of dissimilar aluminium alloys

FSW between dissimilar aluminium alloys has been successfully researched; and the available literature can be found in the web of science. This section depicts some of the published results on FSW between the various aluminium alloys.

Li *and* Shen [36] successfully conducted lap joints of dissimilar AA6063 to AA5052 aluminium alloys, using a tool designed from quench hardening $W_9Mo_3Cr_4V$ with some geometric improvements. Furthermore, they placed the two overlap plates of AA5052 on the retreating side, which improved the joint integrity of the weld. They demonstrated that improving the degree of

mixing of the dissimilar Al alloys and promoting the material plastic deformation in the weld-zone during the FSW contributed to obtaining high-quality lap joints. The influence of the high temperature plastic behaviour on the friction stir weldability of two aluminium alloys (AA5083-H111/ AA6082-T6) is very popular in welding construction. This was conducted by Leitão *et al.* [37].

They found that the AA6082 aluminium alloy displayed good weldability in FSW; whereas the AA5083 alloy had a steady flow behaviour at increased temperatures; but a very poor weldability was registered under the same welding conditions of the AA6082-T6 alloy. Also, Guo *et al.* [38] investigated the microstructure and mechanical properties of AA1100-B4C MMC and AA6063 alloy. They found that all the dissimilar welds produced under the welding conditions investigated were stronger than the Al-B4C MMC base materials and demonstrated 100% joint efficiencies (UTS).

The material side of the welds or the use of a 0.8 mm offset did not have any significant impact on the tensile properties of the joined assembly even when varying the welding speed. Guo *et al.* [38] analysed the Mg concentration and B4C particle distribution. The results indicated a good material mixing and seamless bonding around the interface between the Al-B4C MMC and the AA6063 alloy during FSW.

Koilraj *et al.* [39] optimised the FSW process with respect to the tensile strength of the welds and the optimum settings. Furthermore, the optimum values of the rotational speed, the transverse speed, and D/d ratio are 700 rpm, 15 mm/min and 3, respectively. In addition, they concluded that the cylindrical threaded pin tool profile was the best among all the other tool profiles considered. Palanivel *et al.* [40] examined the influence of the tool rotational speed and the pin profile on the microstructure and tensile strength of the dissimilar friction stir welded aluminium alloys AA5083-H111 and AA6351-T6. The welds were fabricated by using straight tool profiles without any defects; while the tapered tool profiles caused a tunnel defect at the bottom of the joints under the experimental considered conditions.

Furthermore, three different regions, namely: the unmixed region, the mechanically mixed region and the mixed flow region were observed in the weld zone, as demonstrated in Figure 2-9 [40].

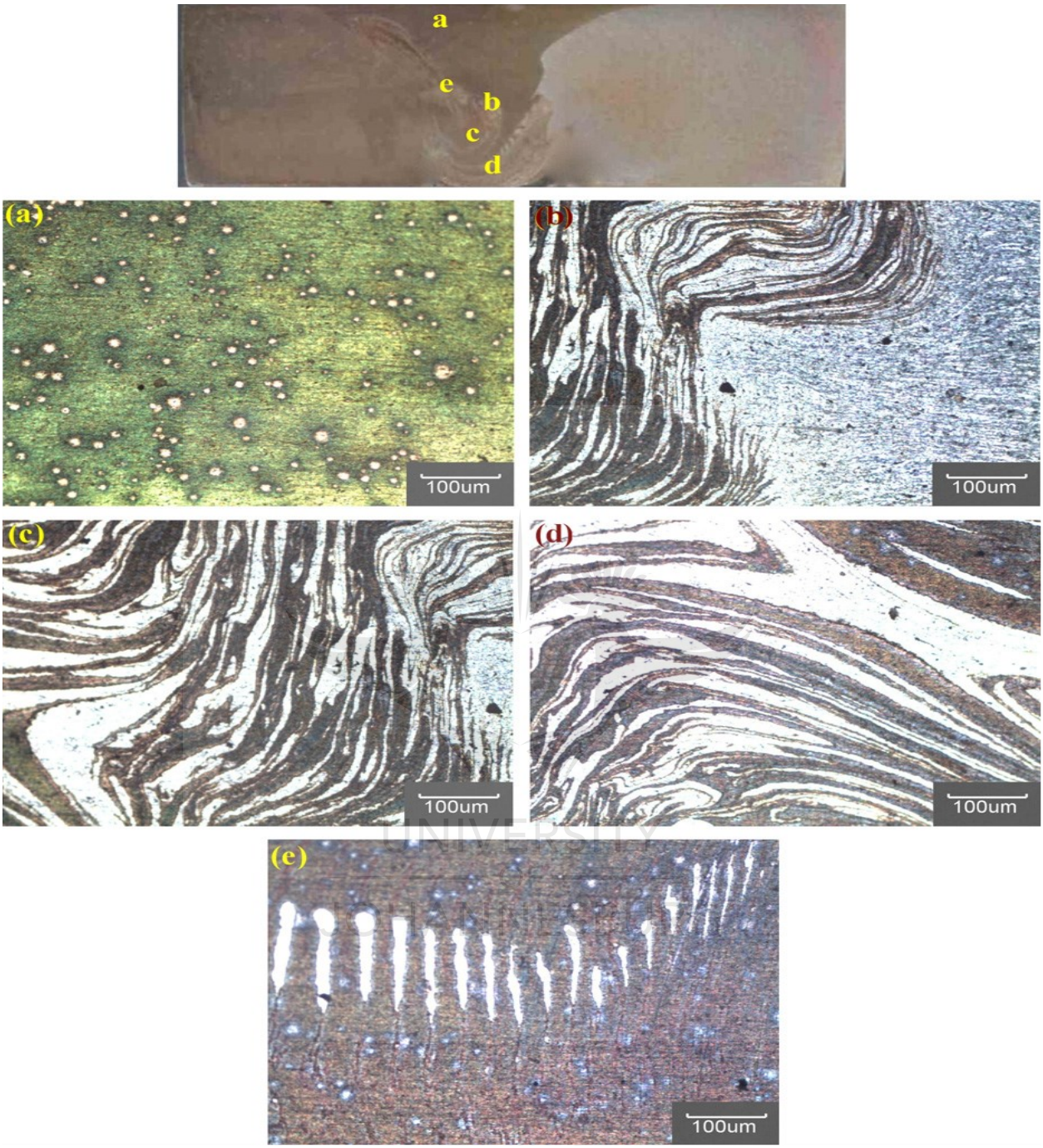

Figure 2-9 Microstructure of various regions in the weld zone, as marked in the macrostructure using SS (Straight Square) tool pin profile at 950 rpm: (a) unmixed region; (b–d) mixed flow region; and (e) mechanically mixed region [40]

Furthermore, Palanivel *et al.* [41] joined AA5083-H111 and AA6351-T6, using a tool rotational speed of 950 rpm and a straight square pin profile, which resulted in the highest tensile strength of 273 MPa. Moreover, the variation in the tensile strength of the dissimilar joints was attributed to the material flow behaviour, the loss of cold work in the HAZ of AA5083, the dissolution and the over aging of the precipitates of AA6351, as well as the formation of macroscopic defects in the weld zone. Da Silva *et al.* [42] investigated the mechanical properties and the microstructural features, as well as the material flow characteristics in dissimilar 2024-T3 and 7075-T6 FSW joints. The welds were produced at a fixed feed rate (254 mm/min) varying the rotation speed in three levels (400, 1000 and 2000 rpm).

Da Silva *et al.* [42] clearly stated that the typical microstructural features of FSW welds, such as SZ, TMAZ and HAZ regions were seen. A sharp transition from the HAZ / TMAZ to the SZ has been observed in the advancing side; while in the retreating side, such a transition is more gradual. They found that the minimum hardness value of the naturally aged samples in the HAZ at the retreating side was about 88% of 2024-T3 base material. The microhardness profile of the 1000 rpm friction stir welding condition performed at the mid-thickness line, as well as at 1 mm above and below the mid-thickness line, is shown in Figure 2-10.

Furthermore, 96% of the efficiency in terms of tensile strength was achieved using a 1000 rpm rotational speed. Fracture of the weld specimens occurred in the HAZ on the retreating side (2024-T3).

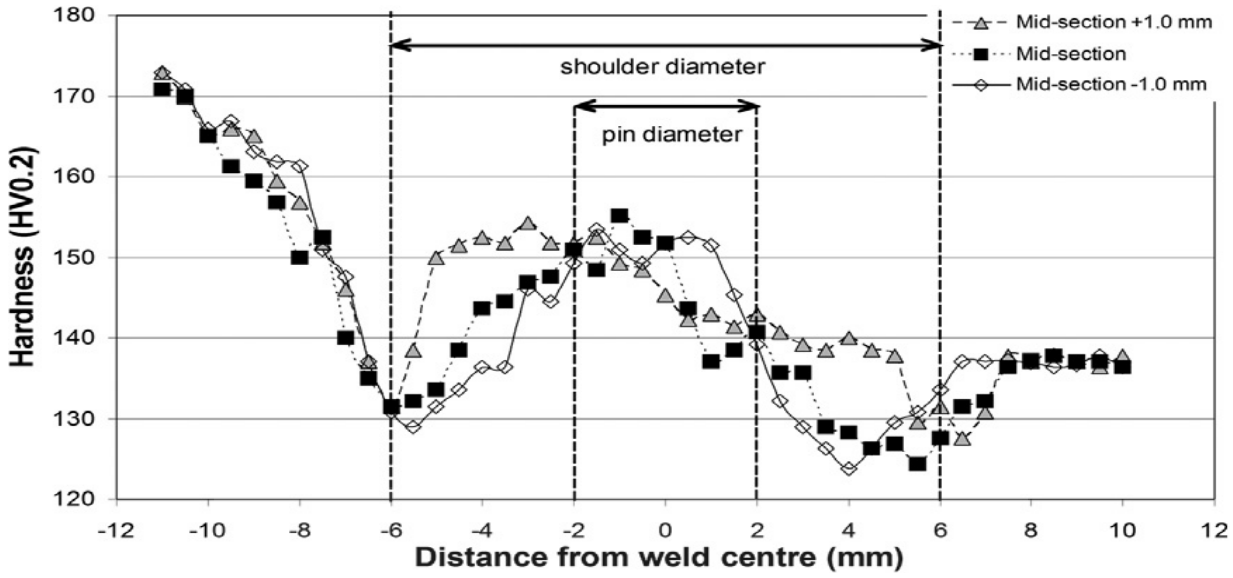

Figure 2-10 Microhardness distributions of FSW cross-sections joints performed at mid-thickness, as well as at 1 mm below and above the mid-thickness line. Condition: 1000 rpm [42]

Aval *et al.* [43] investigated the microstructures and mechanical properties in similar and dissimilar friction stir welding of AA5086-O and AA6061-T6, by using a thermo-mechanical model and experimental observations. They concluded that the hardness in AA5086 side mainly depends on recrystallization and the generation of fine grains in the weld nugget; whereas the hardness in the AA6061 side varies with the size, the volume fraction and the distribution of precipitates in the weld line and in the adjacent heat affected zone, as well as during the ageing period after welding. Aval *et al.* [43] further observed grain refinement in the stirred zone for all their samples. However, the finer grain size distribution is achieved within the AA6061 side; where the higher strain rates are produced.

Shen *et al.* [44] in their investigation on microstructures and electrochemical behaviours of the friction stir welding dissimilar welds observed that the microstructure of the FSW weld consists of finer grains in comparison with that of the parent material. Furthermore, intense plastic deformation and frictional heating during welding resulted in the generation of a dynamically recrystallized fine grained microstructure within the stirred zone. Tran *et al.* [45] investigated the behaviour of friction stir spot welding between AA 5754-O and AA 7075-T6. They showed that, under cyclic loading conditions, the micrographs show that the 5754/7075 and 7075/5754 welds

in cross-tension specimens mainly failed from the fatigue crack along the interfacial surface, and from the fracture surface through the upper sheet material [45]. Jun *et al.* [46] investigated the residual strains in dissimilar friction welds. The research was conducted using the Eigen strain Reconstruction Method in FSW between AA5083 and AA6082-T3. They further observed that full-field residual stress–strain distributions can be reconstructed relatively easily, based on the limited experimental data sets, using a transparent and straight forward FE modelling framework.

Another study was conducted by Ghosh *et al.* [47]. They joined A356 and 6061 aluminium alloys using FSW under different tool rotation and traversing speeds. They found that the interface microstructure within the weld nugget is dominated by the retreating side alloy as the signature of Si rich particle distribution; and this was evident for all the samples produced. They further observed that welds fabricated at the lowest tool rotational and traversing speed exhibited superior mechanical properties, when compared to the remaining welds produced. Sundaram *et al.* [48] friction stir welded AA2024-T6 and AA5083-H321, using five different pin profiles developed successfully, and which were suitable for the dissimilar FS welding of aluminium alloys. They further observed that increasing the tool rotational speed or welding speed led to an increase in the tensile strength; and that it reaches a maximum value, and then decreases.

Additionally, the increase in the tool axial force led to the increase in the tensile strength of the dissimilar FS welded joints. The tensile strength decreases after it has attained a maximum value.

Muruganandam *et al.* [49] in FS Welding of dissimilar 2024 and 7075 aluminium alloys, investigated the microstructures; and their results revealed that the process led to recrystallised grain structure and precipitates distribution. Moreira *et al.* [50] produced friction stir butt welds of AA6082-T6 with AA6061-T6. The welds exhibited intermediate properties; and the tensile tests failures occurred near the weld edge line where a minimum hardness value was observed. Furthermore, microstructural changes induced by the friction stir welding process were clearly identified.

Leitao *et al.* [51] used AA5182- H111 and AA6016-T4 sheet samples and joined them using FSW. Welds between both alloys exhibited a hardness variation consistent with the microstructural evolution across the TMAZ; and no significant decrease in the hardness was observed for the welds. Furthermore, their strength efficiency was about 90%. However, its ductility seriously

decreases relative to the base materials, due to the heterogeneous characteristics of these welds. Cavaliere *et al.* [52] studied the mechanical and microstructural behaviour of FSW between AA6082 and AA2024. They noticed that the vertical force increased as the travel speed for all the produced joints increases.

They also achieved the best tensile and fatigue properties for the joints with the AA6082 on the advancing side, and those which were welded with an advancing speed of 115 mm/min. Leitão *et al.* [53] joined AA 5182-H111 and AA 6016-T4 using the friction stir welding process. They found in the dissimilar welds that the presence of small defects at the weld root of the dissimilar welds induced the rupture of some of the blanks during the formability tests.

Hatamleh *and* DeWald [54] joined AA 2195 and AA 7075 and investigated the peening effect on the residual stresses of the produced welds. The results showed that the surface residual stresses resulting from shot peening on both AA 2195 and AA 7075 were higher compared to the laser peening, due to the high amount of cold work conducted on the surface from the shot peening. Furthermore, high values of tensile stresses were noticed in the mid-thickness on the laser peened samples.

Recent studies on the friction stir welding of dissimilar aluminium and its alloys have been reviewed; and a comprehensive summary of the results is presented. The section below summarises the FSW between Aluminium and magnesium alloys.

2.7.1.2 FSW between aluminium and magnesium alloys

Mofid *et al.* [55] studied the effect of water cooling during the friction stir welding of AA 5083 and AZ31C. They observed that the formation of intermetallic compounds in the stir zone of dissimilar welds significantly affects the mechanical properties of the welds. They suggested the use of submerged friction stir welding under water, which resulted in lower peak temperatures; and because of the lower heat input, the formation of intermetallic compounds was limited. This was compared with the air welded specimen, which had a relatively larger volume fraction of intermetallic compound, higher peak temperatures in the stir zone, and significantly higher hardness in the weld centre [55]. Malarvizhi *and* Balasubramanian [56] also investigated the influence of tool shoulder diameter to the pale thickness ratio on the stir zone formation and the

tensile properties of FS welded AA6061 and AZ31B. It was found that the joints produced when using a shoulder diameter of 21 mm (3.5 times the plate thickness) exhibited superior tensile properties compared with their counterparts (Figure 2-11).

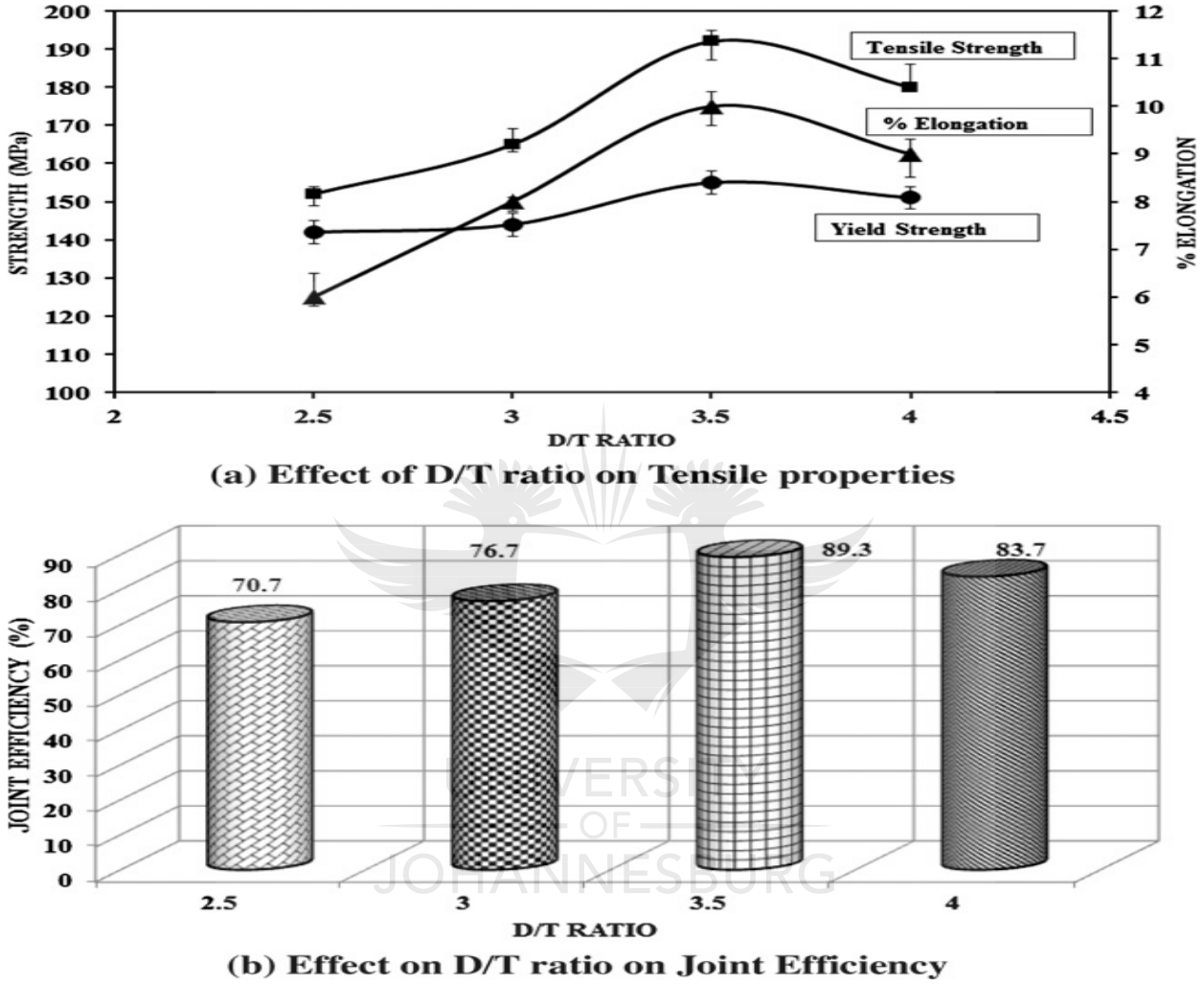

(a) Effect of D/T ratio on Tensile properties

(b) Effect on D/T ratio on Joint Efficiency

Figure 2-11 Effect of shoulder diameter on tensile properties [56]

Furthermore, Malarvizhi *and* Balasubramanian [56] found that the complex intercalated microstructures in the weld zone, with swirls and vortices, were indicative of the flow pattern of the dissimilar metals. Simoncini *and* Forcellese [57] investigated the effect of friction stir welding parameters and the tool configuration on the micro- and macro-mechanical properties of similar and dissimilar welds using AA5754 and AZ31 thin sheets. They used two different tool configurations with and without a pin. The results showed that the pinless tool leads to the obtaining of higher values of the ultimate tensile strength and ductility compared with the welds

made with a tool pin. The microstructure of the cross-section showed that the bonded interface is clearly evident. Venkateswaran *and* Reynolds [58] performed FSW on AA 6063-T5 and AZ31B-H24 and analysed the factors affecting the resulting weld properties. The nugget grain size on both the Al and Mg sides monotonically increased, as the tool rotational speed increases. Furthermore, the transverse tensile test results are correlated to several interface features, including the actual interface length, the extent of interpenetration between the aluminium and magnesium base metals, the maximum intermetallic layer thickness, and the area fraction of micro-void coalescence on the tensile fracture surfaces [58]. Sharifitabar *and* Nami [59] investigated the microstructures and hardness profiles across the interface of friction stir welded joints between monolithic AA 2024-T4 and Al/Mg_2Si metal matrix cast composite (MMC).

The results showed that there was a complicated pattern of material flow in the stir zone, especially in the sample welded in two passes. Furthermore, in the sample welded using one pass, it was found that the hardness increased from the base metal to the stir zone on the MMC side. Nevertheless, the hardness variation in the sample welded in two passes was complicated; and there was an alternative decrease and increase in the hardness value at the joint interface. The hardness variation across the joint interface between 2024 AA and Al/Mg_2Si MMC, using one and two passes is depicted in Figure 2-12.

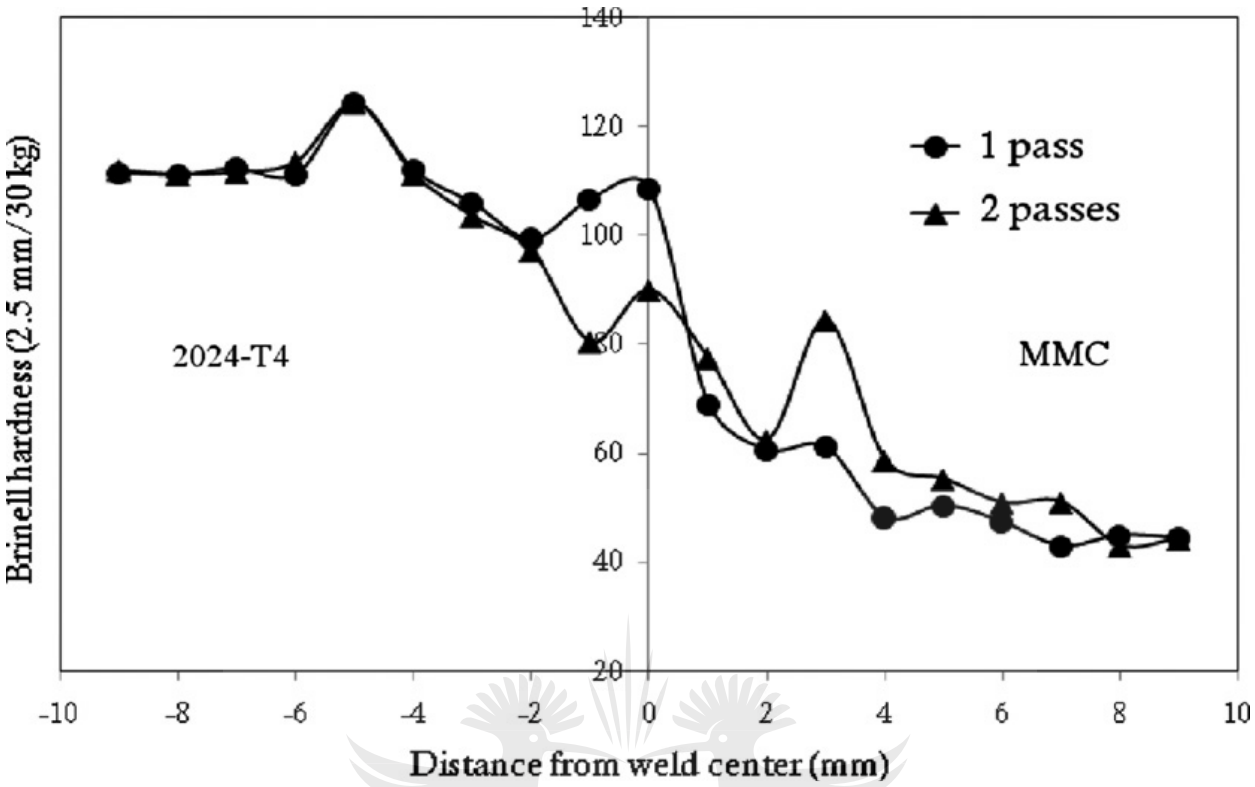

Figure 2-12 Variation of hardness across the joint interface between 2024 AA and Al/Mg_2Si MMC in samples welded in one and two passes correspondingly [59]

Yong *et al.* [60] investigated FSW between AA 5052 and AZ31 Mg alloy; they produced sound welds at a rotational speed of 600 rpm and a welding speed of 40 mm/min. The microstructure of the base metal was replaced by equiaxed and fine grains in the stir zone. Furthermore, at the top of the stir zone, 5052 and AZ31 alloys were simply bonded; while an onion ring structure, which consisted of aluminium bands and magnesium bands was formed at the bottom of the stir zone. Figure 2-13 depicts the microstructure of the three weld zones and the parent materials.

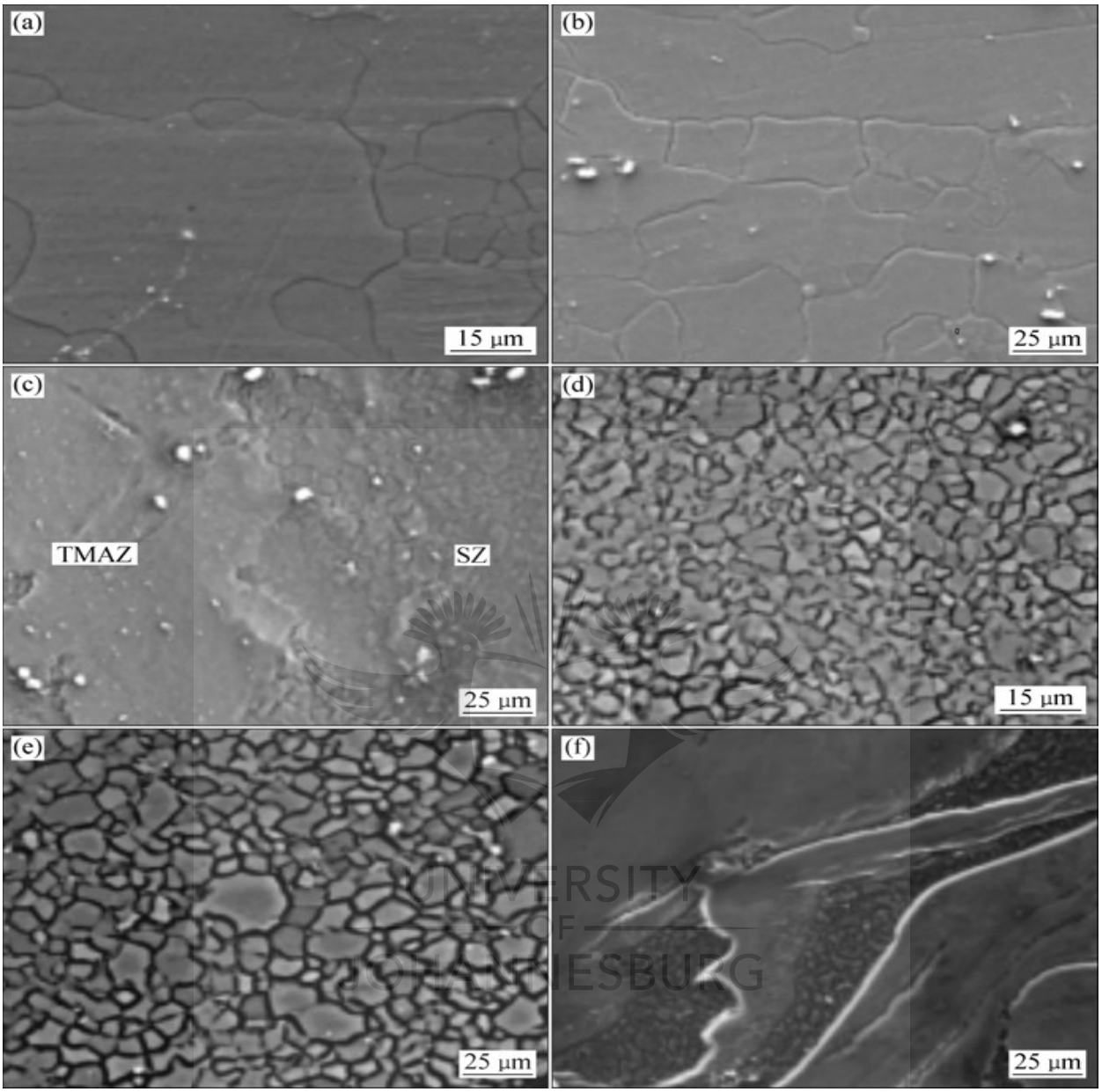

Figure 2-13 Scanning electron microscope images of AZ31 in different regions, (a) BM; (b) HAZ; (c) Interface of TMAZ/SZ; (d) SZ in Mg side; (e) SZ in Al side; (f) Intercalated microstructure [60]

In addition, Yong *et al.* [60] found that the microhardness profiles presented uneven distributions; and the maximum value of the microhardness in the stir zone was twice as high as that of that of the base materials [60]. Liu *et al.* [61] characterized the galvanic corrosion of a dissimilar friction stir welded 2024-T3 Al/AZ31B-H24. The Mg joint was prepared by using a water-based and a non-water-based polishing solution. It was shown that the water-based polishing solution induced

more easily the galvanic corrosion attack than the non-water-based polishing solution during the polishing process. Furthermore, they attributed the low microhardness value in the corroded region to the formation of a porous magnesium hydroxide layer with microcracks. Kostka *et al.* [62] characterised the microstructure of the interface between AA6040 and AZ31 joined by friction stir welding. The results showed that the intermetallic compound layer has a thickness of about 1 μm and consists mainly of a fine-grained $Al_{12}Mg_{17}$ phase. Figure 2-14 shows the TEM images where intermetallics are present.

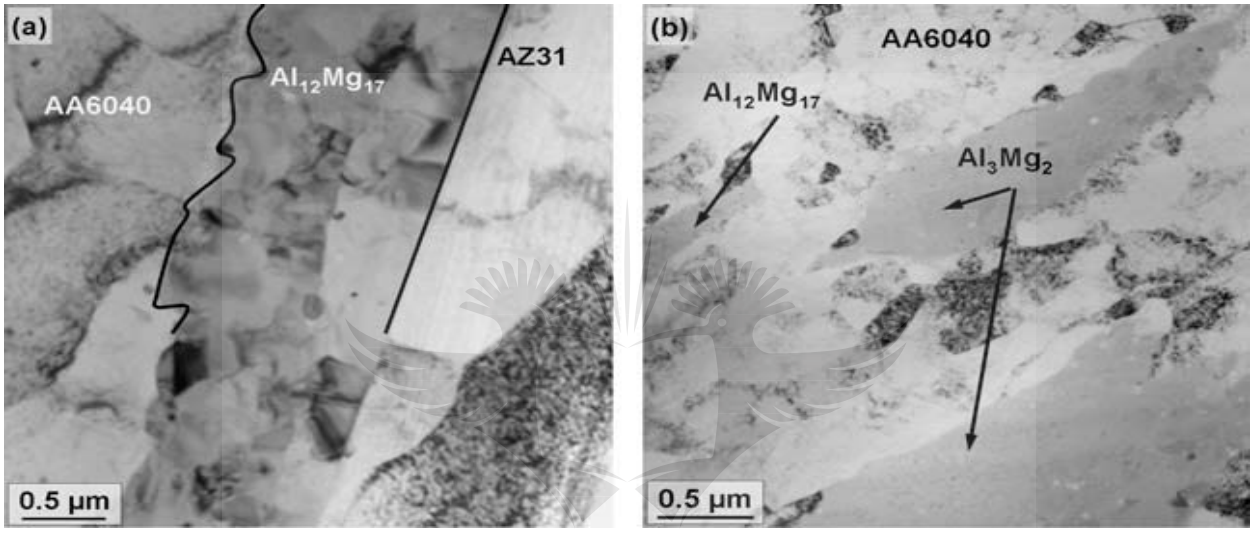

Figure 2-14 TEM micrograph of the interface region showing, (a) fine-grained $Al_{12}Mg_{17}$ intermetallic compound and (b) small nano size grained inclusions of the Al_3Mg_2 phase adjacent to the $Al_{12}Mg_{17}$. [62]

A review on the FSW between aluminium and magnesium alloys has been presented. However, all the authors reported the formation of intermetallic compounds, which are detrimental to the joint integrity. There is, therefore, a need for more research to reduce the formed intermetallics in the welds; as this would offer these dissimilar joints some opportunities for industrial applications.

2.7.1.3 FSW between aluminium alloys and steel

In this section, the research studies on FSW between aluminium and steel are reviewed.

AA 6111-T4 and DC04 low carbon steel sheets were friction stir welded by Chen *et al.* [63]. They successfully produced high quality friction spot welds between thin Al and steel automotive sheet

metal within a weld time of one second, which is the target time desired by industry. Ogura *et al.* [64] used AA3003/SUS304 and friction stir welded them in lap joints. The results showed that the strength in the centre region and on the advancing side was greater than that on the retreating side. Coelho *et al.* [65] investigated the mechanical properties and their relation to microstructure of AA6181-T4 and DP600 and HC260LA HSS plates by FSW.

The results showed that across all the weld regions on the Al alloy side (BM-HAZ-TMAZ-SZ), strong differences in the grain size distribution and shape occurred. Figure 2-15 shows the EDS mapping of the produced welds, where the distribution of Al, Fe and Zn can be seen.

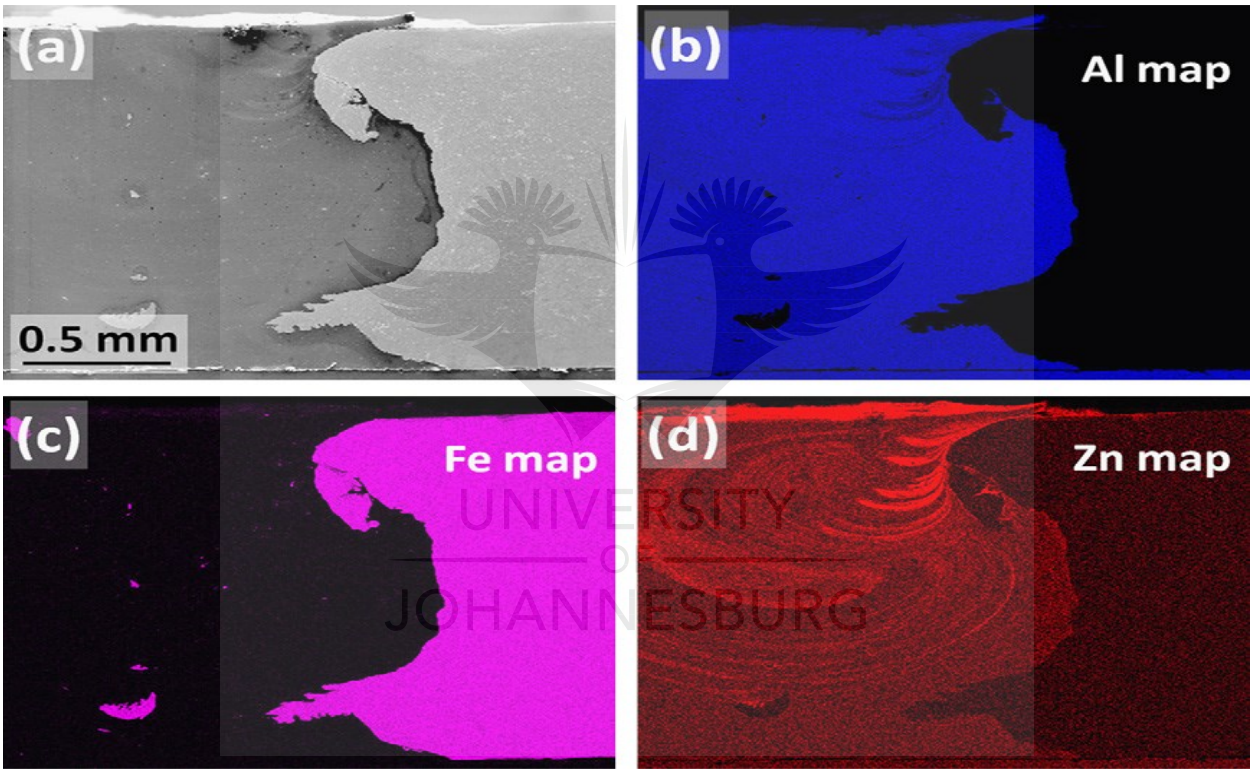

Figure 2-15 EDS mapping of element distributions: (a) The analysed region; (b) Aluminium (Al) distribution in blue; (c) Iron (Fe) distribution in pink; and (d) Zinc (Zn) distribution, highlighting the vortex-like structure on the advancing side in red[65]

Bang *et al.* [66] used hybrid FSW (HFSW) welding to join Al6061-T6 aluminium alloy and STS304 stainless steel. Their results showed that the maximum tensile strengths obtained at the weld were 93% of the aluminium alloy base metal for HFSW and 78% for FSW. Furthermore, fracture patterns of the crack propagation of HFS welds exhibit an entirely ductile fracture mode,

showing dimples on the fracture surface, and a locally brittle fracture mode with cleavage facets, which are hardly accompanied by plastic deformation [66]. Mashiko *et al.* [67] investigated the joint interface of friction stir welding between SUS304 and A6063 using an HTS-SQUID gradiometer. Large voids were observed on the joint interface by the conditions with excessive heating. Furthermore, the hardness test on the SUS boards near the interfaces, the SUS jointed with 200 mm/min, which caused excess heating, was considerably softer than the matrix [67]. Tanaka *et al.* [68] FS welded mild steel to A7075-T6 and investigated the joint strength. They found that the joint strength increased with any reduction in the thickness of the intermetallic compound at the weld interface, as shown in Figure 2-16.

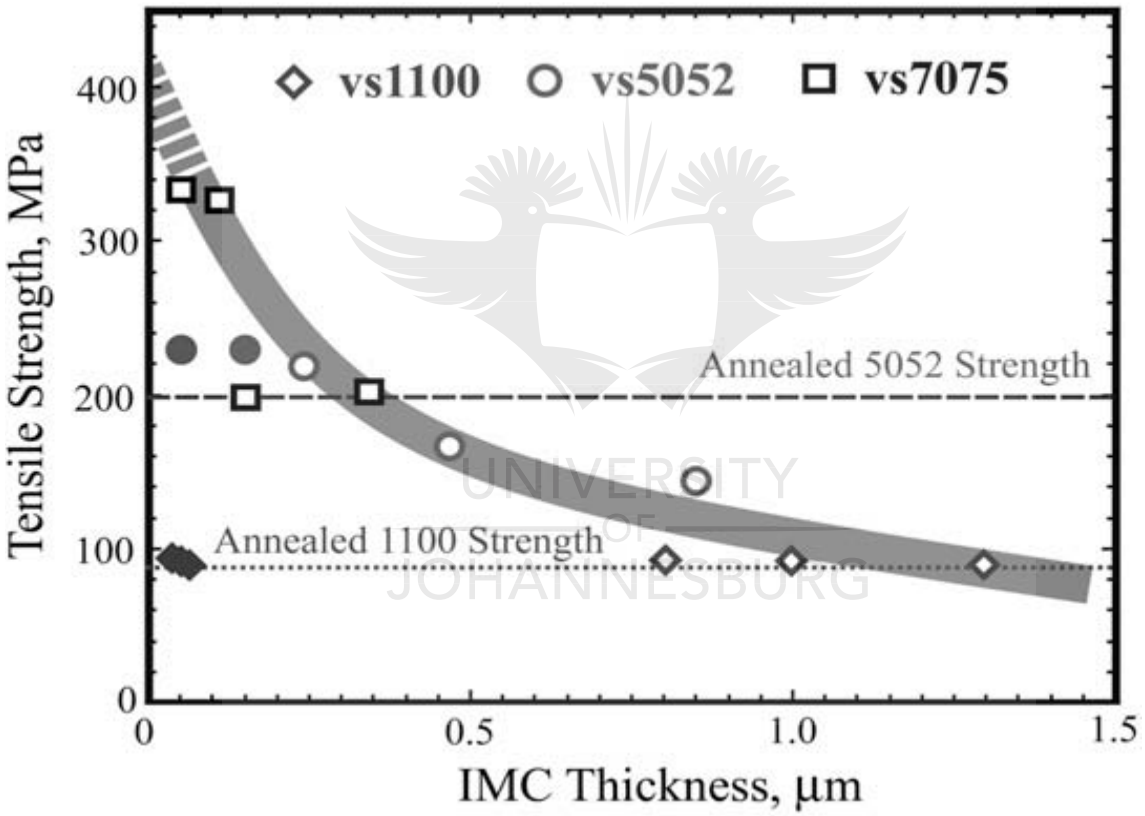

Figure 2-16 Effect of the intermetallics' thickness and the joint tensile strength for aluminium alloy to steel welds [68]

Uematsu *et al.* [69] welded A6061 and low-carbon steel sheets, SPCC by means of a friction stir spot welding (FSSW). The results showed that the high tensile-shear strength of the dissimilar welds was achieved by a newly designed scroll grooved tool without a probe.

It is challenging to weld aluminium and its alloys to steel using conventional welding techniques, due to the differences in their properties; but the studies reviewed above showed that Al and steel can be successfully joined by using the FSW process. Research on FSW between aluminium and titanium alloys are summarised in the section below.

2.7.1.4 FSW between Aluminium and Titanium alloys

Yu-hua *et al.* [70] friction stir welded TC1 Ti alloy and LF6 Al alloy plates. They obtained an excellent surface appearance; furthermore, the interface macrograph of the lap joint cross sections at different parameters significantly changed. They further noticed that at the welding speed of 60 mm/min and the tool rotation rate of 1500 rpm, the interfacial zone of the lap joint can be divided into three kinds of layers. When the welding speed increases to 150 mm/min, groove-like crack occurs on the interface. Yu-hua *et al.* [70] showed that the microhardness of the lap joint presents an uneven distribution; the maximum value of hardness reaches HV 502 in the middle of the stir zone.

Wei *et al.* [71] welded AA 1060 sheets and Ti–6Al–4V sheets, using the FSW lap process by employing the cutting pin of a rotary burr tool. They showed that there are many titanium scrapings distributed in the aluminium near the interface, as shown in Figure 2-17.

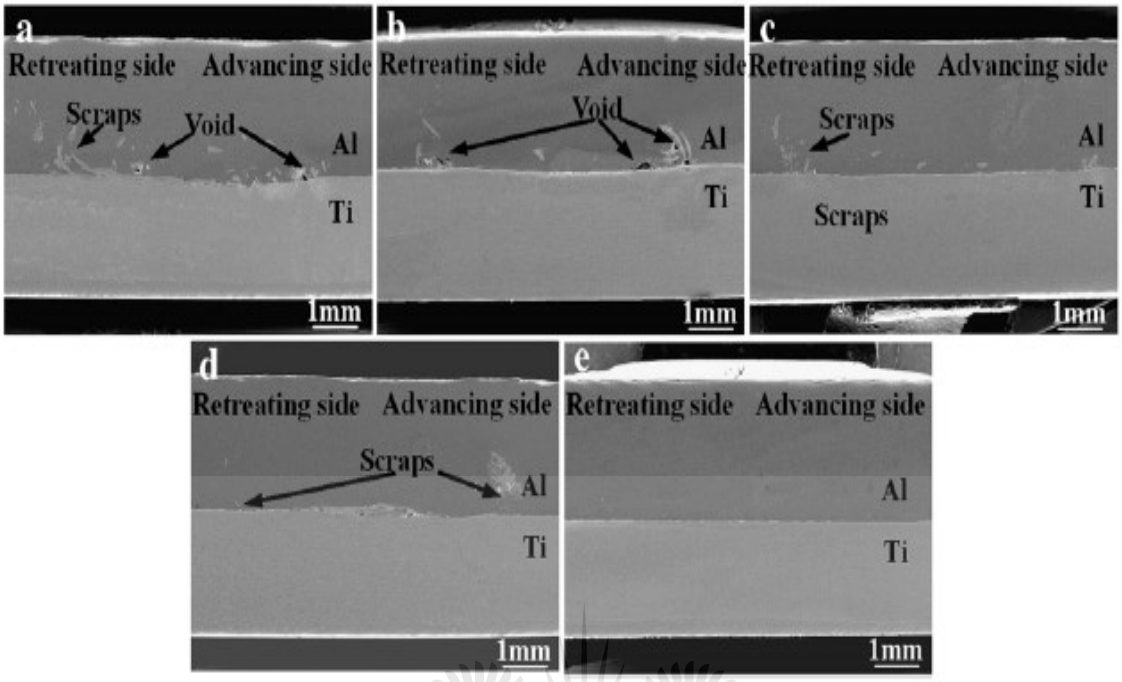

Figure 2-17 Joint interface between Aluminium and Titanium, where the Titanium scrapings are distributed in the aluminium [71]

In addition, a swirl-like structure with lighter and darker parts was observed in the SEM micrograph of the interface region [71]. Aonuma *and* Nakata [72] studied the effect of calcium on intermetallic compound layer between Mg–Al alloy and titanium. They found that calcium added in Mg–Al alloy reacted with aluminium to make Al_2Ca compound and this decreased the solid-solution aluminium in the matrix of the Mg–Al–Ca alloy. Furthermore, this suppressed the formation of the Ti–Al intermetallic compound layer at the joint interface. Aonuma *and* Nakata [72] showed that the suppression of the Ti–Al intermetallic compound layer at the joint interface resulted in the higher tensile strength of the dissimilar joint with titanium plate, in comparison with the Mg–Al alloy containing the same aluminium alloy.

Chen *and* Nakata [73] friction stir welded ADC12 cast aluminium alloy to pure titanium sheet. They observed the formation of a transient phase ($TiAl_3$) at the joining interface by an Al–Ti diffusion reaction. Furthermore, Chen *and* Nakata [73] observed that the formation of $TiAl_3$ is strongly dependent on welding speeds (heat inputs) during FSW; and this therefore affects the mechanical properties of such joints. Dressler *et al.* [74] investigated the feasibility of friction stir

welding between TiAl6V4 and AA2024-T3 and the properties of the produced joints. Furthermore, Dressler *et al.* [74] shifted the tool pin centre towards the aluminium plates; and they observed that the resulting microstructure is characteristic of a conventional friction stir weld. The microhardness profile of the welds (Figure 2-18) was high, when the indenter hit a titanium particle. They also found high hardness values in the stir zone [74].

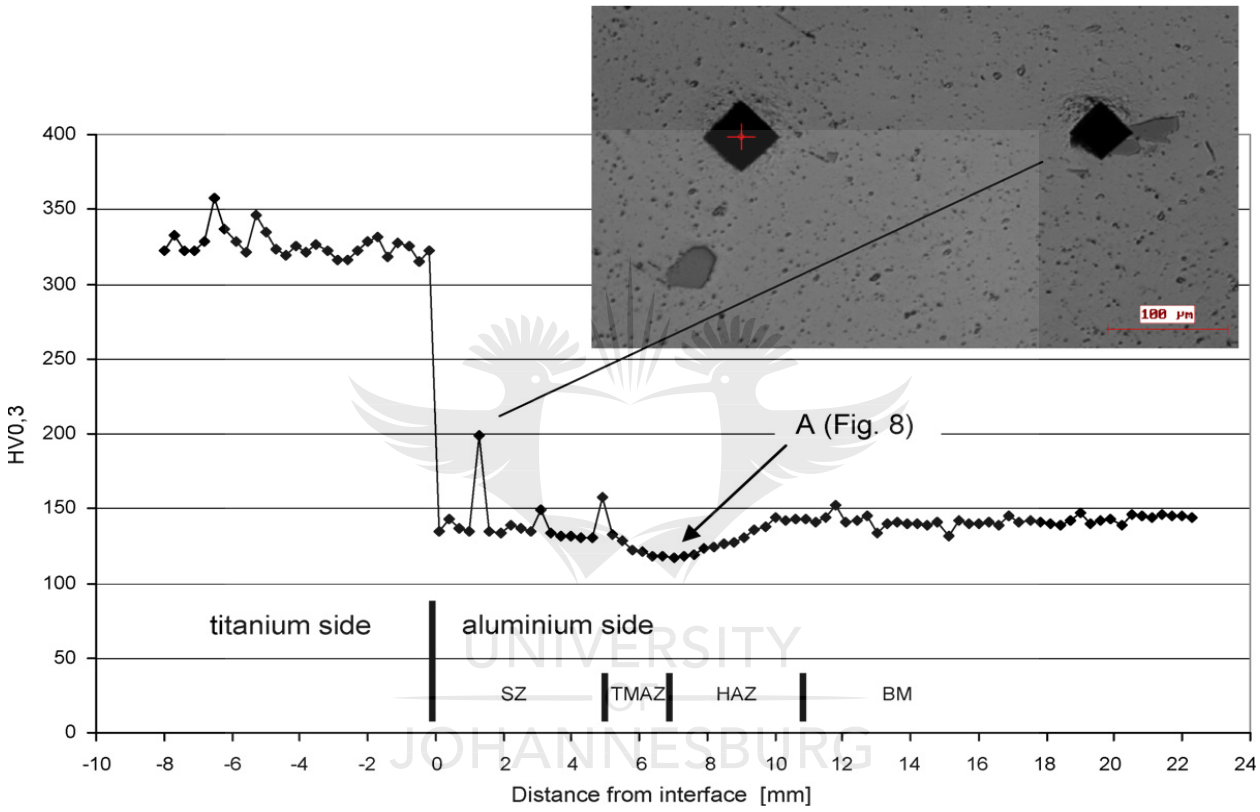

Figure 2-18 Friction stir welding of Titanium to aluminium alloys might have many applications in aerospace and industries; therefore, the development of this technique is of major importance [74]

2.7.1.5 Residual stress measurement of Friction Stir Welds

Pfeiffer *et al.* [75], measured the residual stress in FSW of two different types of components. AA 2219 T87 and AA 2219 T851 as the plate and the ring, respectively. The residual stresses were determined using X-ray diffraction. The spot diameters were 1 mm in the case of the plate and 2 mm in the case of the ring segment. CuKα radiation with an effective penetration depth of 37 µm

was used to determine the lattice strains from the diffraction line positions of the {422} - lattice planes. Calculation of the stresses was performed based on the $\sin^2 \psi$ –technique.

Substantial compressive stresses of ~70 MPa developed in the longitudinal direction at both sides of the remaining specimen, due to cutting. In the transverse direction, the smaller tensile stresses of ~30 MPa were created. Meanwhile, the stresses at the top and root side of the specimen were similar. It may therefore be concluded that no significant bending occurs due to cutting. These stress components are included in the results of the subsequent residual stress measurements for the removed specimens, as shown in Figure 2-19.

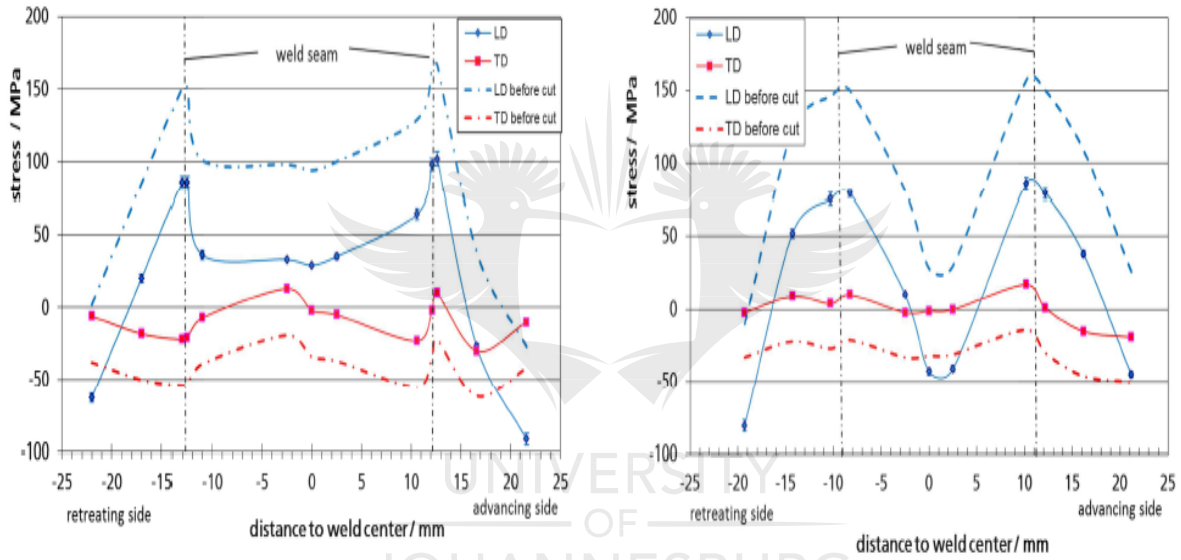

Figure 2-19 The distribution of surface residual stresses at the weld crown side (left) and the weld root side (right) of the specimen cut from the plate. Dashed lines denote the residual stress distribution before cutting. LD = longitudinal direction, TD = transverse direction [75]

Furthermore, only small stresses of up to 20 MPa were generated when cutting the circumferential cylinder weld. At the inner side of the ring (the weld root) all the stress components are compressive; whereas at the outer side (the weld crown), the transverse components tend to be tensile. These stress components are included in the results of the subsequent residual stress measurements on the part cut out of the cylinder. The transverse residual stresses are small and generally compressive. The residual stress distribution measured in the weld nugget at the outer

surface of the ring-segment (weld crown) indicates a reduction of tensile residual stresses already within the nugget near the fusion line. The transverse residual stress components tend to be more compressive near the fusion line and in the weld centre, as depicted if Figure 2-20.

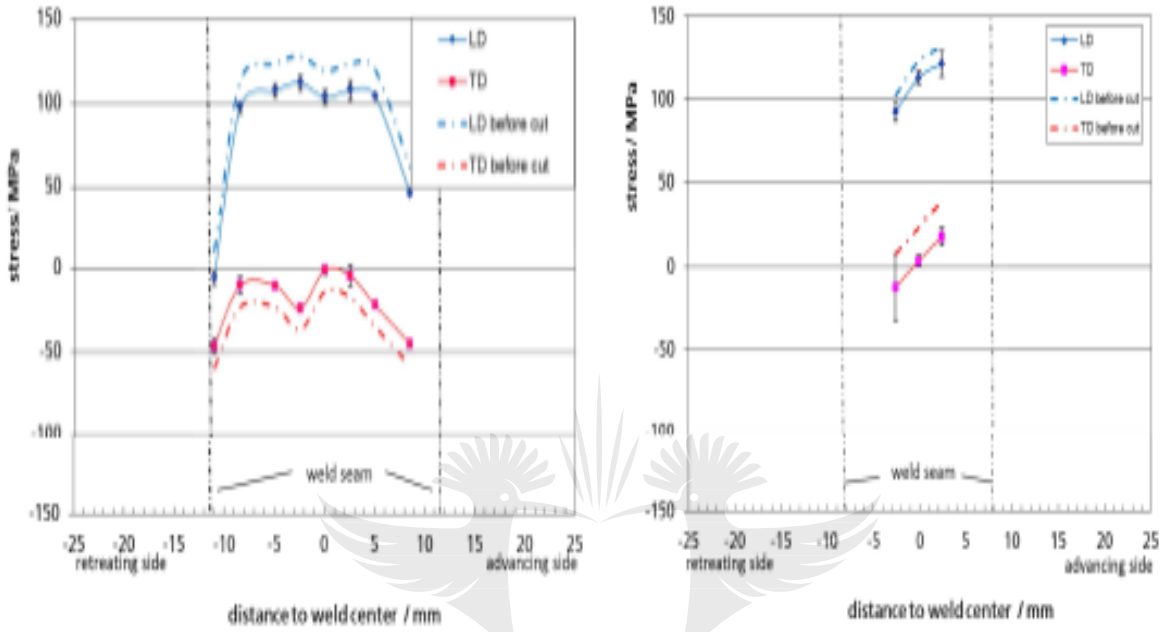

Figure 2-20 The distribution of surface residual stresses at the outer side of the ring segment (weld crown, left), and at the inner side of the ring segment (weld root, right), determined by XRD. Measurements outside the weld metal failed due to strong texture effects. Dashed lines indicate the residual stress distribution before cutting. LD = longitudinal direction, TD = transverse direction [75]

This is in contrast with the results for the FSW plates, in which the highest tensile residual stresses were found in the region around the fusion line, with lower residual stresses occurring in the weld centre [75].

Bach *et al.* [76] reported measurements of residual stress in FSW of AA 2024 T3 using Neutron diffraction. Two test specimens were used in the experiments. These were named as the welded plate and hammer peened plate. The variation of the transverse residual stress component (α_x) in the transverse (x) direction of both specimens is shown in Figure 2-21.

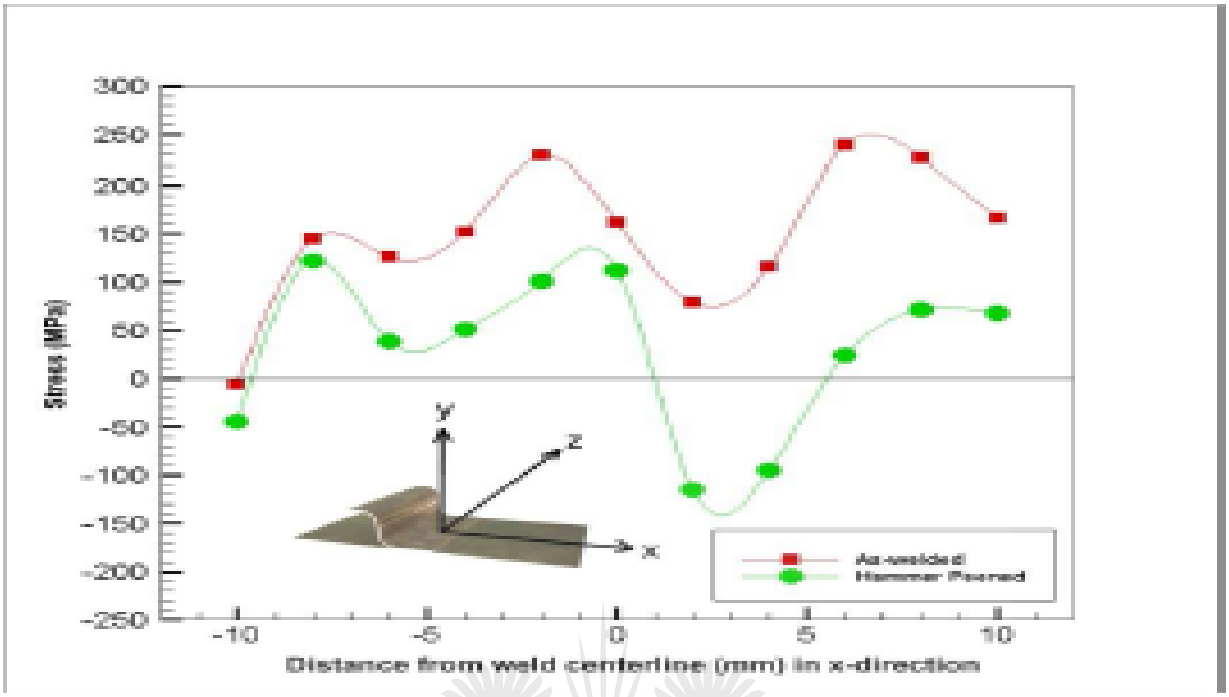

Figure 2-21 Traverse stress component (α_x) in the transverse (x) direction [76]

The as-welded stresses are greater than those in the hammer peened specimen at every slit depth. The maximum tensile stress in the as-welded plate was 239 MPa at a distance of x = 6 mm to the right of the weld centreline; whereas in the hammer peened specimen, the maximum tensile residual stress was 122 MPa at x = -8 mm to the left of the weld centreline. Comparing point by point across the weld in the transverse direction, the effects of hammer peening reduced the tensile residual stresses at every single point, and in most cases caused the stress to change from tension to compression [76].

Fratini *et al.* [77] determined the residual stress intensity factor K_{Ires} by the cut-compliance method and the residual stress distribution was calculated from the K_{Ires} data with an integral inverse solution based on the Schindler weight function. The AA 2024-T351 plates were friction stir welded. The results showed that that K_{Ires} profile for FSW decreases up to a minimum at ~9 mm away from the welding centreline; then, it rises to a positive maximum near the retreating side (R.S.). Weld residual stresses are tensile in the weld, with the external regions being subjected to compressive residual stress; however, this residual stress field did not warp the welded plate out of plane. Although, the residual stress maximum occurred in the advancing side zone (A.S.), the distribution was quite symmetrical, as shown in Figure 2-22 [77].

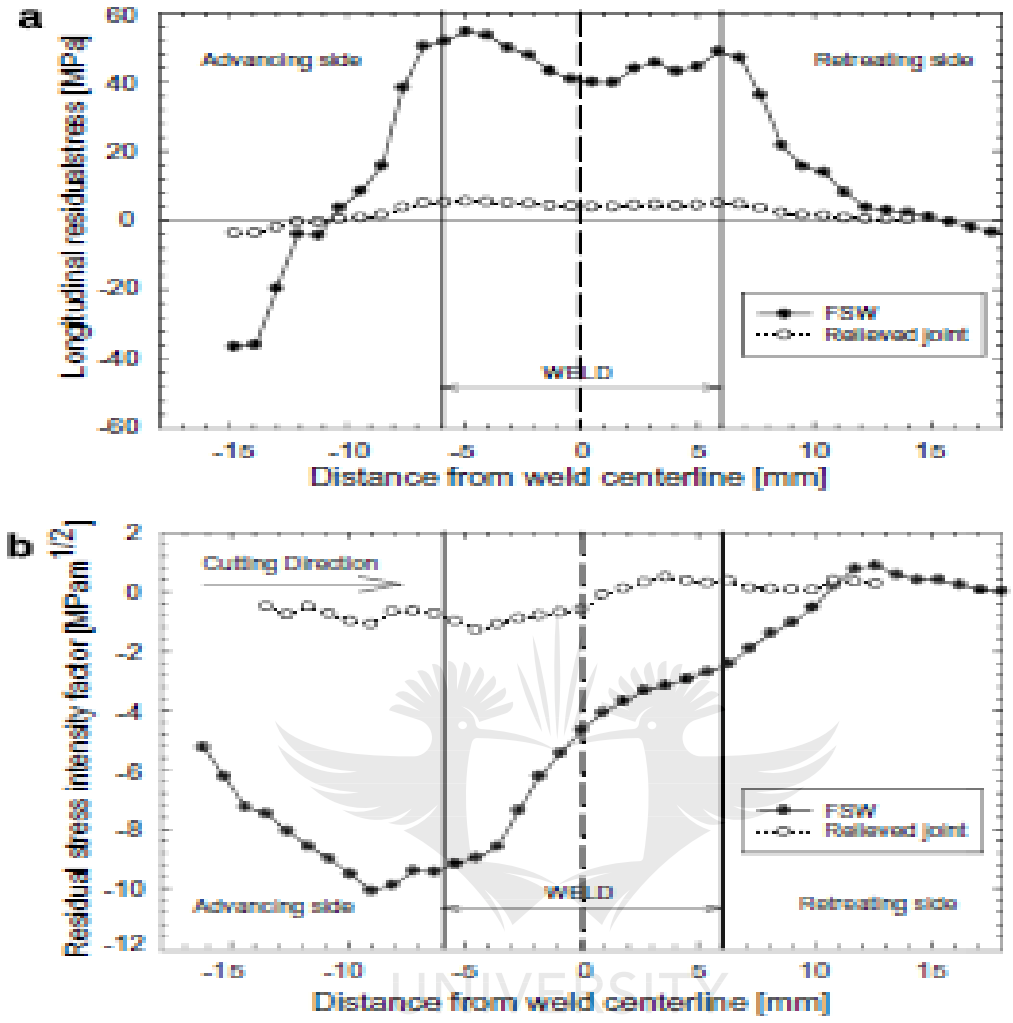

Figure 2-22(a) Longitudinal residual stress and (b) residual stress intensity factor, K_{Ires} , obtained with the cut-compliance method for FSW and the relieved joints [77]

Furthermore, they recorded a significant reduction in residual stress, up to 90% for the FSW joint after mechanical relief and a very low distribution of K_{Ires} was found; hence, they assumed that there should be very little influence of residual stress on the FCGR (Fatigue Crack Growth Propagation) in the stress relieved specimens. They concluded that the observed residual stress patterns are typical, not only of friction stir welds, but of most welds in general.

Ma *et al.* [78] Friction stir welded AA 2195-T8 plates and measured the residual stress, using Neutron diffraction. In order to investigate the influence of the sample dimensions on residual stress profiles, three samples of different sizes were used. The samples were named C (T) for the

cracks perpendicular to the weld, and ESE (T) for the cracks parallel to the weld. Figures 2-23 (a) and (b) show the X-direction stresses parallel and the Y-direction perpendicular to the weld, respectively. The X-direction stresses have a double peak tensile residual stress field of similar form in all three specimens. The maximum tensile residual stress parallel to the weld ranged from 120 MPa, for the largest sample, to 47 MPa in the smallest. Remote from the weld line at the notch tip, the minimum stress value varied from about -130 MPa to -20 MPa compression values for the largest and smallest samples. On the other hand, the Y-direction stresses did not change over the scan line as much as in the X direction; and this was roughly zero (±10 MPa) at the weld line.

At the notch tip, the residual Y stresses measured -50 MPa compression in the biggest sample, and -20 MPa in the other two samples. Around the notch tip, the residual stresses were always negative for all three sizes: both parallel to, and perpendicular to, the weld.

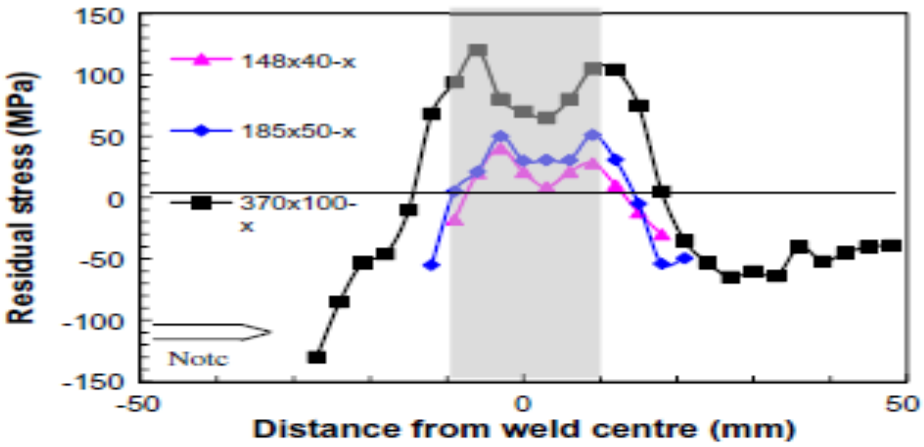

(a) Residual stress parallel to weld direction for 3 sizes of ESET samples

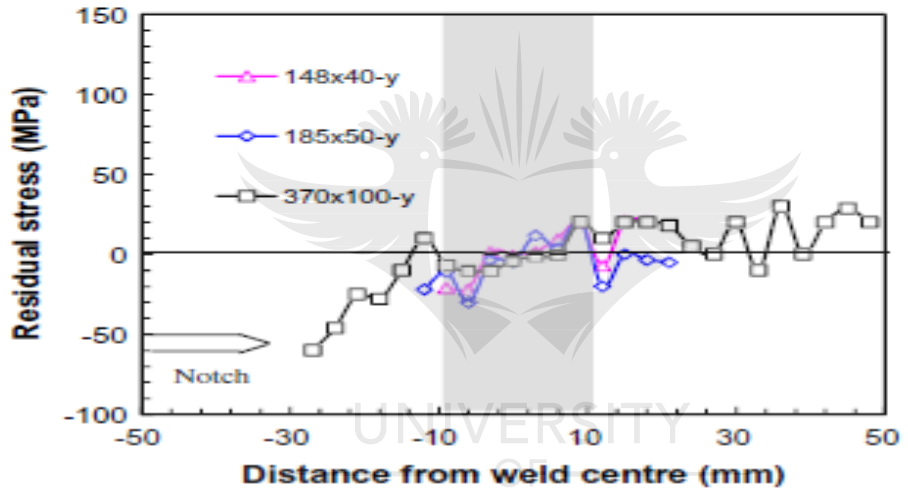

(b) Residual stress perpendicular to weld direction in 3 sizes of ESET samples

Figure 2-23 The residual stress profiles in ESE (T) samples. The shaded area shows the extent of the weld nugget region [78]

The residual stress profiles in three sizes C (T) test samples were also investigated. All three C (T) sample sizes showed a double peak in stress, similar to those found in the ESE (T) samples. The maximum residual stress parallel to the weld varied from 110 MPa for the largest sample to 95 MPa for the intermediate to 82 MPa, for the smallest. Furthermore, the residual stresses perpendicular to the weld at this location along the weld line were small, the same as in the ESE (T) samples, with a mean value of about 25 MPa tension, the sample size having little systematic effect (Figure 2-24).

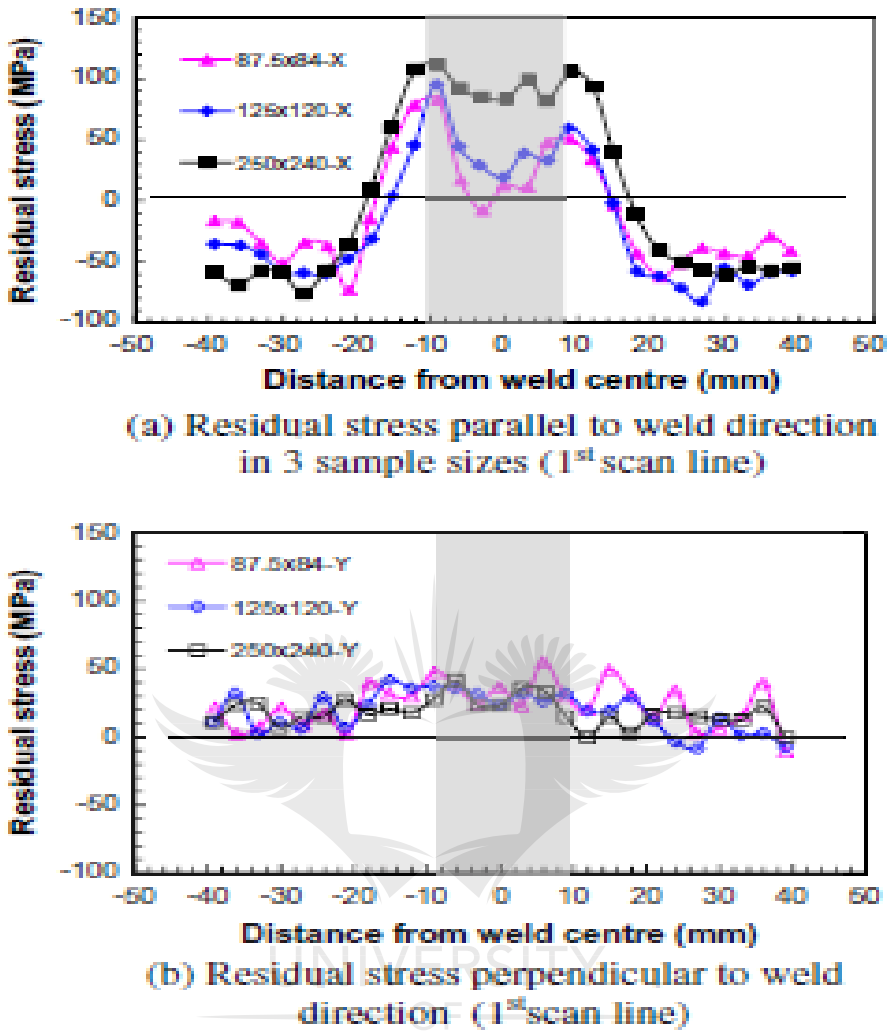

Figure 2-24 The residual stress profiles across the weld (1st scan line) in three sizes of C (T) samples. The shaded area shows the extent of the weld nugget region [78]

Ni *et al.* [79] friction stir welded AA2009 composite reinforced with 17 vol. % SiCp. The X-ray diffraction method was used to measure the residual stress of the FSW joints. The results indicated that tensile residual stresses in the weld, with a peak value of about 54 MPa in the weld centre. Furthermore, the tensile residual stresses decreased from the centreline to both the retracting side and the advancing side; and they reached about -70 MPa in the heat affected zone. At higher stress amplitudes of above ~ 150 MPa, the parent material showed longer fatigue lives than the FSW joint; but the difference decreased as the stress amplitudes decreased. Both the parent material and the FSW joints showed an equivalent fatigue life at lower stress amplitudes of below ~150 MPa

[79]. Steuwer *et al.* [80] carried out studies on the effect of the tool traverse and rotation speeds on the residual stresses by using a synchrotron X-ray method. The parent materials used were AA5083 non-aged hardenable and age-hardenable AA6082 friction stir welds. They found that, the region around the weld line was characterized by significant tensile residual stress fields, which are balanced by compressive stresses in the base material. On the other hand, the rotation speed of the tool has been found to have a substantially greater influence than the transverse speed on the properties and the residual stresses in the welds, mostly on the AA5083 side where the location of the peak stress moves from the stir zone to beyond the edge of the tool shoulder.

Furthermore, the changes in the residual stress are related to the microstructural and hardness changes. In particular, the larger stresses under the weld tool on the AA5083 side compared to the AA6082 side are related to a transient reduction in yield stress due to dissolution of the hardening precipitates during the welding prior to the natural ageing after welding [80].

Altenkirch *et al.* [81] used a synchrotron X-ray diffraction to measure the residual stress distribution in the Friction Stir Welds of AA7449. They investigated the effect of tensioning on the residual stresses. The results showed that by modifying the stress accumulation path, the application of a tensioning stress reduced the tensile magnitude of the final residual weld stresses [81].

Lombard *et al.* [82], investigated the effect of the varying welding parameters on the residual stresses profiles in Friction Stir Welds of AA5083-H321 using a synchrotron X-ray diffraction method. The results (Figure 2-25) showed that the residual stresses were generally tensile in the weld region, with balancing compressive stresses in the parent material. Furthermore, they concluded that the width of the tensile stress region and the maximum value of the tensile residual stress exhibited a linear dependency, with heat input being calculated by using the different welding process parameters. The heat input appeared to be dominated by the feed rate; and they suggested that the changes in the rotation speed are compensated for by changes in the measured torque.

Those changes in the heat input directly affected the shape of the residual stress profiles, with more heat input per unit length producing broader residual stress profiles, with lower maxima. The feed

rate dominance is supported by a good correlation between the maximum longitudinal residual stress and the feed rate [82].

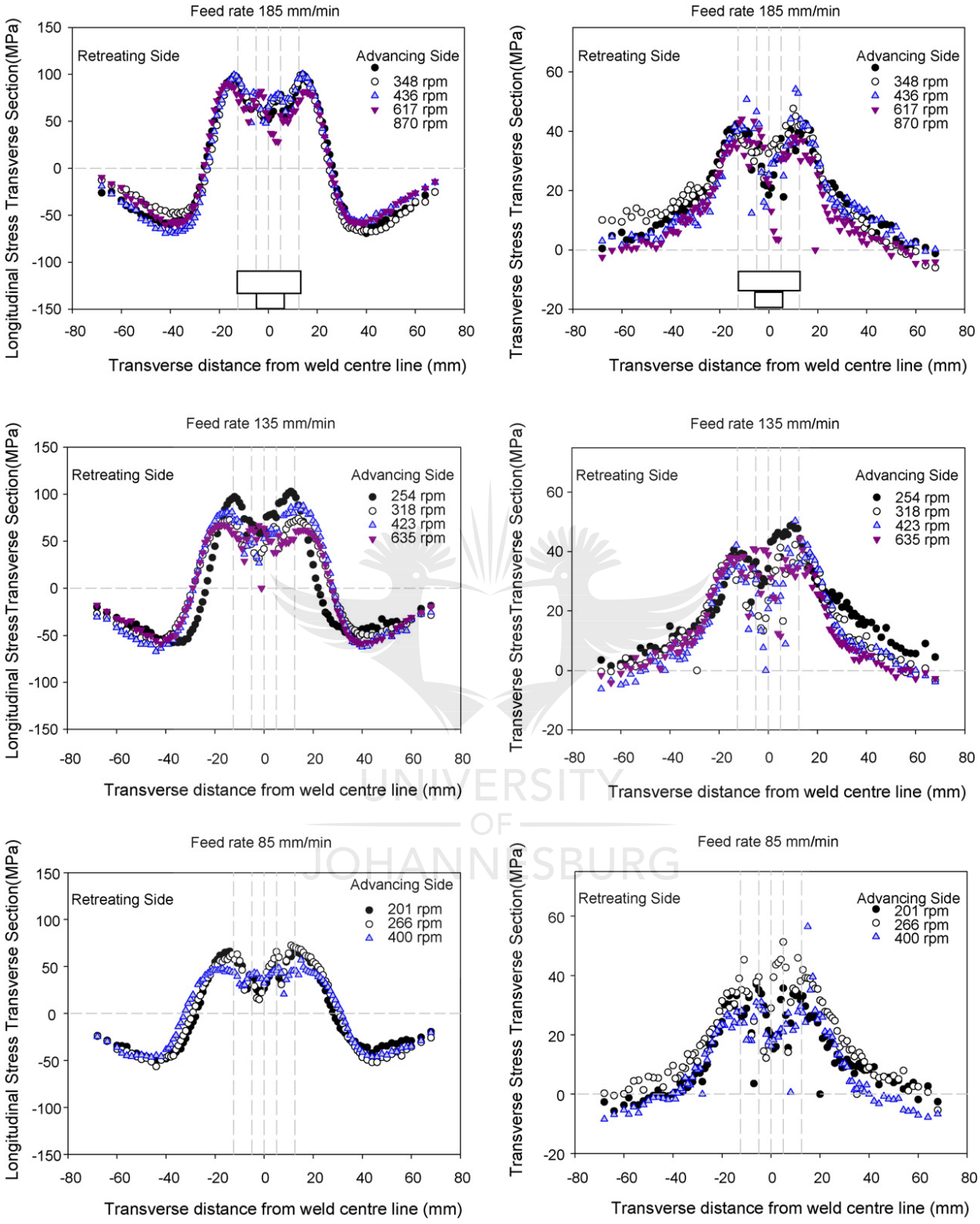

Figure 2-25 The longitudinal (left) and transverse (right) residual stress distributions for all the welds, grouped according to decreasing feed rate [82]

Peel *et al.* [83] used synchrotron X-rays method to measure the residual stress in the Friction stir welds of AA5083 sheet. The results showed that the peak longitudinal stresses increased as the traverse speed increases. They attributed the increase to steeper thermal gradients during welding and the reduced time for stress relaxation to occur. Furthermore, the tensile stresses appear to be limited to the softened weld zone resulting in a narrowing of the tensile region (and the peak stresses) as the traverse speed increases [83]. Figure 2-26 depicts the measured longitudinal and transverse residual stresses.

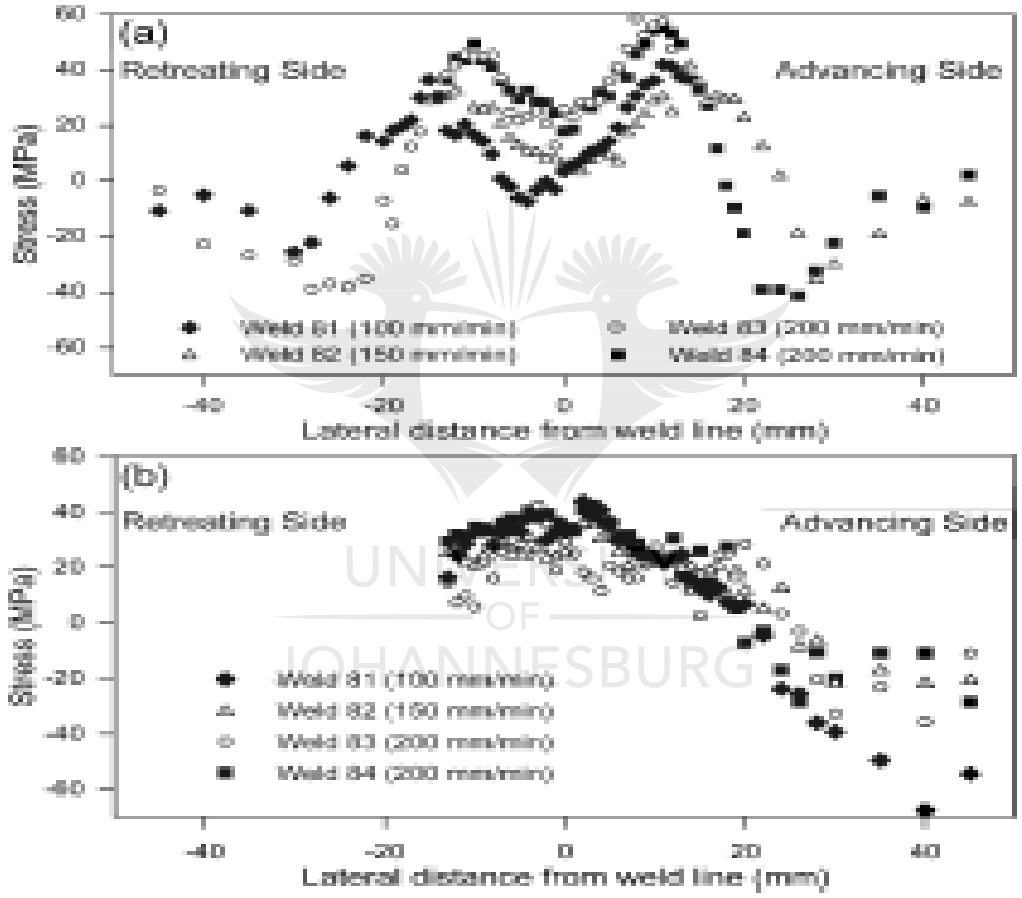

Figure 2-26 Longitudinal (a) and transverse residual stresses (b) as a function of lateral distance from the weld line for each weld as measured by the $\sin^2\psi$ method [83]

Prime *et al.* [84], friction stir welded AA7050-T7451 and AA2024-T351. The residual stresses were measured using the neutron diffraction method; and these researchers concluded that even in friction stir welding of thick, dissimilar, high-strength aluminium alloys, very low residual stresses are attained. The peak stresses of about 43 MPa were less than 20% of the material yield strength. They further said that, such low stresses are virtually unachievable in fusion welding. Even at those low magnitudes, the residual stresses affect fatigue behaviour and the measurement of fatigue properties; and therefore, they need to be addressed [84].

Residual stress investigations were conducted by Linton and Ripley [85] using neutron diffraction. The material used was AA7075-T651 rolled; and in the solution, it was heat-treated and artificially aged via stress relief after heat treatment. The results showed that at all the locations across the weld zone, the highest values of residual stress were recorded in the longitudinal direction; and the lowest values were recorded in the normal direction. For the freshly made weld, all the stress profiles displayed a peak in residual stress in the weld nugget, and a minimum value in the HAZ, just beyond the edge of the tool shoulder [85].

Furthermore, a slightly higher level of stress was recorded on the advancing side of the weld joint [85]. They concluded that, it is important that predictions of anticipated performance and integrity, with regard to resistance to fatigue cracking, should take into consideration the residual stress profiles in aged FSWs, rather than those present in the as-welded samples. This is particularly important for the FSW HAZ, where the as-welded compressive residual stresses become tensile with time [85].

2.7.2 Friction Stir Welding between aluminium and copper Alloys

2.7.2.1 Microstructural evolution and X-Ray Diffraction analyses

The development of laboratory work on the friction stir welding of dissimilar materials should provide a good insight into their possible industrial applications, and therefore, enhance industrial development. Liu *et al.* [86] observed while welding copper (T2) to AA 5A06 that the distribution between the copper (Cu) and aluminium (Al) has an evident boundary; and the material in the stir zone shows obvious plastic combination of both materials. Furthermore, they also observed clearly an onion ring structure in the stir zone, indicating good material flow. Additionally, they indicated

that the metal Cu and Al close to the copper side in the weld nugget (WN) zone showed a lamellar alternating structure characteristic [86]. However, a mixed structure characteristic of Cu and Al existed on the aluminium side of the weld nugget (WN) zone. The stir action of the tool, the frictional heat and the heat conductivity of Cu and Al could have induced the different structures on both sides in the weld nugget zone (Figure 2-27).

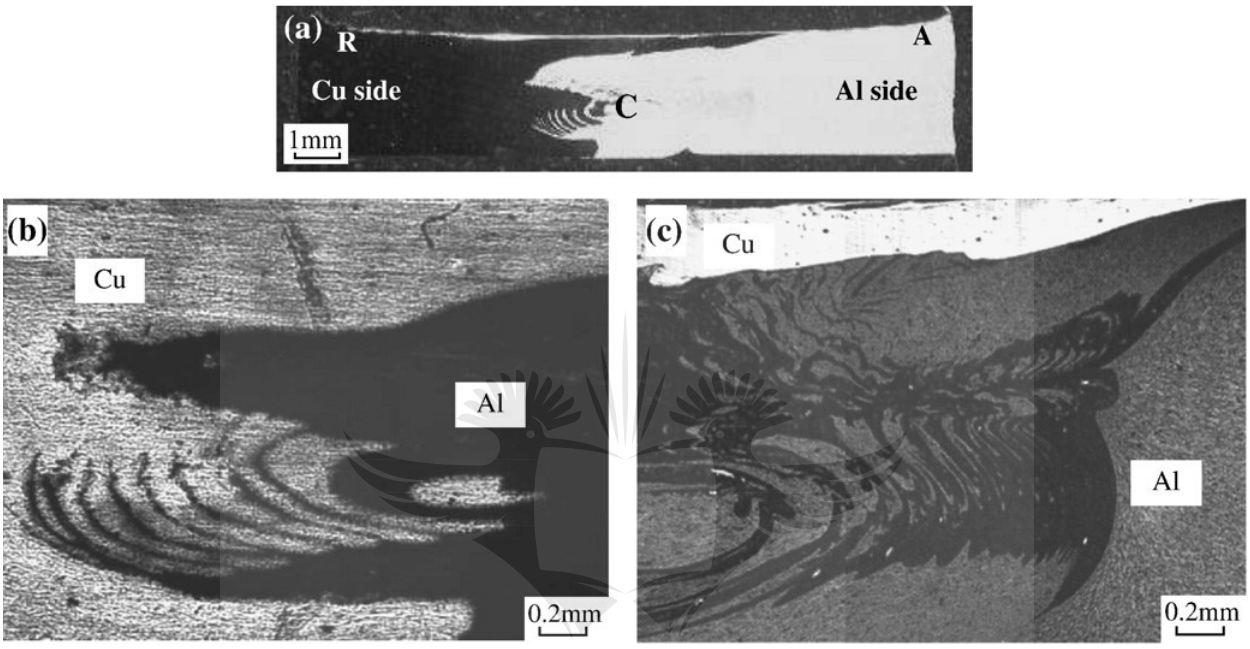

Figure 2-27 The microstructure in stir zone of friction stir weld for Cu/Al dissimilar materials. (a) Image of a cross section of friction stir weld; (b) Microstructure of Cu side in the weld nugget zone; (c) Microstructure of the Al side in the weld nugget zone [86]

The X-ray diffraction (XRD) analysis showed that there were no new Cu–Al intermetallics in the weld nugget zone. Consequently, the structure of the weld nugget zone was largely a plastic diffusion combination of Cu and Al [86].

However, Xue *et al.* [87] successfully welded AA1060 and 99.9% pure commercial copper (annealed). Then, they conducted an XRD analysis; and their results revealed the existence of distinct characteristic diffraction peaks of Al_2Cu and Al_4Cu_9. Hence, they stated that the Al_2Cu and Al_4Cu_9 were generated around the larger Cu particles; and for the smaller Cu particles, most of the copper was transformed into these two intermetallics (IMCs). However, the microstructures of the nugget zone consisted of a mixture of the aluminium matrix and Cu particles. The

distribution of the Cu particles with irregular shapes and various sizes was inhomogeneous in the nugget zone; and a particle-rich zone was formed near the bottom of the weld [87]. Furthermore, they examined the presence of the particles in the aluminium matrix of the nugget zone; and they attributed these to the stirring action of the tool pin that worn out the Cu pieces from the bulk copper, breaking up and scattering them during the FSW process [87].

AA5083 and commercially pure copper were joined using FSW by Bisadi *et al.* [88]. They observed that a very low welding temperature leads to some defects, like channels that showed up at a region near the sheets interface, especially in the Cu sheet (Figure 2-28).

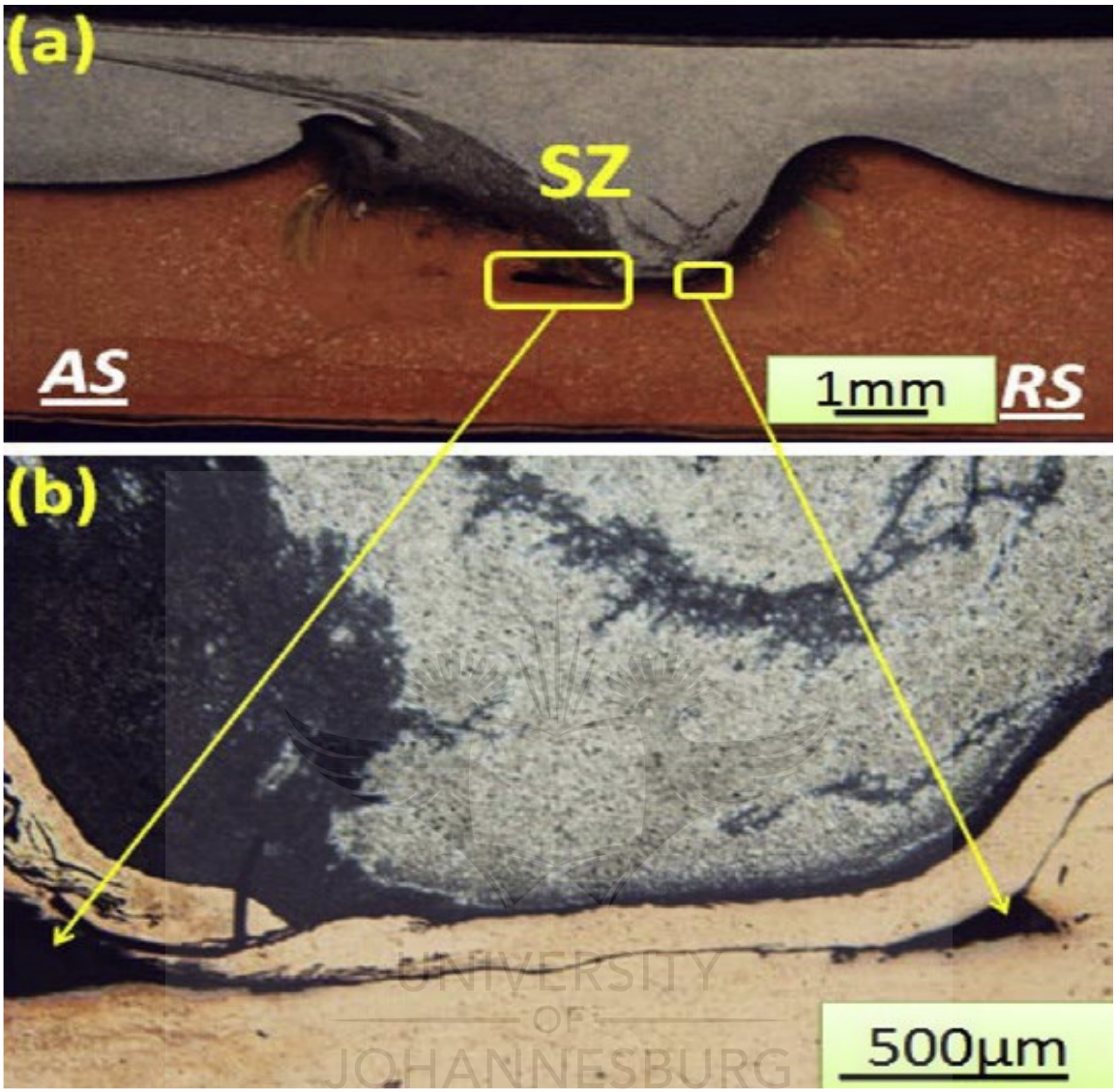

Figure 2-28 (a) Macrostructure; and (b) some channel defects on the sheet interfaces in the weld produced with 600 rpm and 32 mm/min [88]

Also, an extremely high process temperature leads to some cavities appearing at the interface of the diffused aluminium particles and the copper sheet material. Additionally, they found that increasing the process temperature reportedly leads to higher amounts of copper particles diffusing into the aluminium sheet. An increase in the intermetallic compositions and a number of micro cracks were observed.

On the other hand, Xue *et al.* [89] welded AA 1060 aluminium to commercially pure copper. They identified many defects in the nugget zone at the lower rotation speed of 400 rpm considered; whereas at higher rotation speeds of 800 and 1000 rpm, good metallurgical bonding between the Cu pieces and the Al matrix was achieved. Furthermore, a large volume defect was observed when the soft Al plate was placed at the advancing side. They attributed that to the hard copper bulk material, which was hard to transport to the advancing side during the FS welding [89]. Esmaeili *et al.* [90] joined AA 1050 and 70% Cu–30% Zn brass. The results showed that the structure of the sound joint at the nugget zone of aluminium is made up of a composite structure, consisting of intermetallics and brass particles, mainly at the upper region of the weld cross section. Furthermore, a multilayer intermetallic compound was formed at the interface at rotational speeds of higher than 450 rpm.

This layer was mainly composed of CuZn, $CuAl_2$ and Cu_9Al_4. The distribution, shape and size of the particles were irregular and inhomogeneous in the nugget zone of the aluminium [90].

Ouyang *et al.* [6] also conducted dissimilar FS welds using AA 6061(T6) to copper. They demonstrated that the direct FSW of AA 6061 to copper had been difficult, due to the brittle nature of the intermetallic compounds formed in the weld nugget. Moreover, the mechanically mixed region in the dissimilar AA 6061 to copper weld consisted mainly of several intermetallic compounds such as $CuAl_2$, CuAl, and Cu_9Al_4, together with small amounts of α-Al and a face-centred cubic solid solution of Al in Cu [6].

Abdollah-Zadeh *et al.* [91] friction stir welded AA 1060 to commercially pure copper. They observed intermetallic compounds of Al_4Cu_9, AlCu and Al_2Cu near the Al/Cu interface, where the crack can be initiated and propagated preferentially during the tensile tests. They also observed that higher rotational speeds increased the amount of intermetallic compounds formed at the aluminium/copper interface; while low rotational speed resulted in imperfect joints.

Saeid *et al.* [92] stated that the interface in the central region moved considerably into the bottom plate, while joining 1060 aluminium alloy to commercially pure copper. The vertical transport of the interface is attributed to the ring-vortex flow of materials created by the tool pin threads [92]. At higher welding speeds, less vertical transport of the interface was observed on the retreating side [92].

Akinlabi *et al.* [93] investigated the microstructure of the joint interface of AA 5754 and C11000 copper welds. The mixing of both materials was observed as leading to good metallurgical bonding at the joint interface. The aluminium rich region was black/silver; while the golden yellow region showed copper rich regions. Furthermore, Akinlabi *et al.* [94] observed a thickness reduction in the joint interface; but good mixing was achieved in the weld produced at a constant rotational speed of 600 rpm and feed rates of 50 and 150 mm/min. They attributed the reduction in thickness at the joint interfacial regions to heavy flash observed during the welding process [94]. In addition, a good material mixing was achieved in welds produced at lower feed rate due to the high heat generated; while the welds produced at high feed rates resulted in wormhole defect formation [94].

On the other hand, Galvao *et al.* [73] [95] observed that increasing the heat input, by performing welds under higher ω/v ratio, resulted in the formation of mixed material zones with increasing dimension and homogeneity. Furthermore [73] [95], the morphology of the mixing zones and the type and amount of the intermetallic phases, which they found to result from a thermo mechanically induced solid state process, are also strongly dependent on the welding parameters.

Galvao *et al.* [96] friction stir welded oxygen free copper with a high phosphorous content (Cu-DHP, R240) and AA 5083-H111. They observed that the welds performed with the aluminium placed at the advancing side of the tool were morphologically very irregular, being significantly thinner and exhibiting flash formation, due to the expulsion of the aluminium from the weld area. Furthermore, the aluminium, which is expelled, gave rise to the flash displayed for the welds performed with aluminium at the advancing side [96].

It was observed that when the aluminium plate is located at the retreating side of the tool, the material was dragged by the shoulder to the advancing side, where the harder copper plate was located [96]. In the FSW of dissimilar metals, the pin offset is a very important factor. Agarwal *et al.* [97] joined AA 6063 and 99.9% commercially pure copper using FSW. They observed that, as the pin offset is increased, there is improper mixing of the Al-Cu metals; and this resulted in the tunnelling defect.

Ratnesh *et al.* [98] observed that there were different microstructure features in the different zones. At the weld centre line, a mixed region of aluminium and copper was found. Small particles of

aluminium and copper were distributed in the opposite side by the stirring forces of the tool. The thermo mechanically affected zone (TMAZ) is clearly obtained in the copper; but it was not found in the aluminium. Thus, in both the metals, the heat affected zone (HAZ) was not clearly defined [98].

Ratnesh *and* Pravin [99] successfully joined AA 6061 and copper by FSW. They produced sound joints by shifting the centre line of the tool towards the copper plate on the advancing side. The presence of a ‘‘transition zone’’ was observed by Guerra *et al.* [100], while friction stir welding thick AA 6061 plates with a thin high purity copper foil. This transition zone was found to be about twice as thick on the retreating side, as it was on the advancing side. They believed that the material in this zone rotates; but its velocity decreases from the rotational velocity of the pin at the inner edge of the transition zone to zero at its outer edge [100].

Xue *et al.* [101] joined 1060 aluminium alloy and commercially pure copper with success through friction stir lap welds. They found that the nugget zone consisted of pure Al material; and a composite structure in the upper and the lower parts, respectively. They found that the Al/Cu interface was characterised by a thin, continuous and uniform intermetallic layer, producing a good interface bonding, as shown in Figure 2-29. Furthermore, good metallurgical bonding was achieved between the Al matrix and the Cu particles in the composite structure, due to the formation of a small number of intermetallics [101].

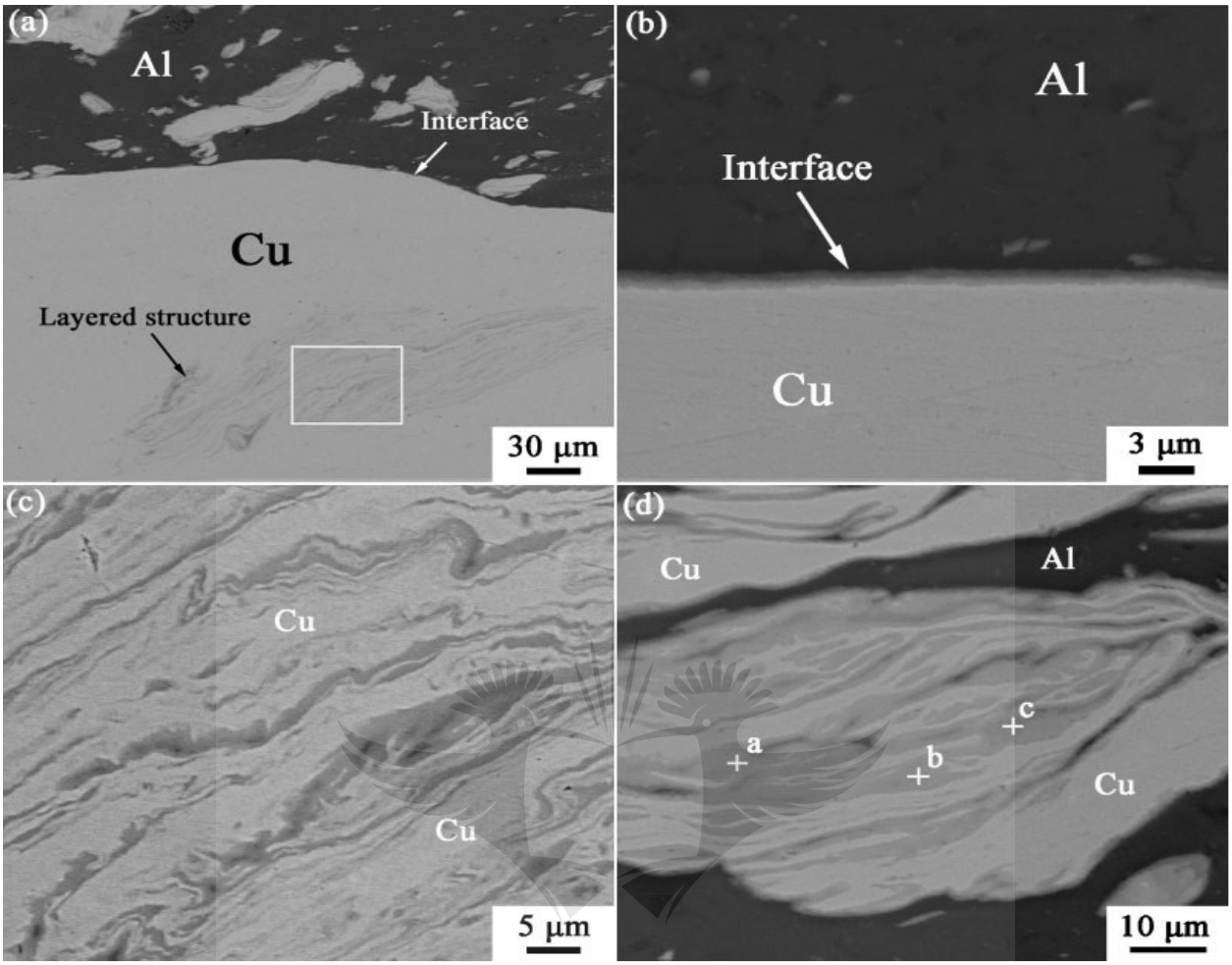

Figure 2-29 Backscattered electron images of Al/Cu joint: (a) The interface between the nugget zone and the Cu bulk; (b) magnified view of Al/Cu interface; (c) magnified view of layered structure in Cu bulk, as shown by the rectangle in (a); (d) layered structures in the nugget zone [101]

Akinlabi *et al.* [102] observed that the joint interfaces were characterised by mixed layers of aluminium and copper, as evident in the microstructures resulting from the heat input into the welds by the stirring action of the tool during the FSW process, as shown in Figure 2-30. Furthermore, they observed that the percentage decrease in the grain sizes increases towards the stir zones of the welds.

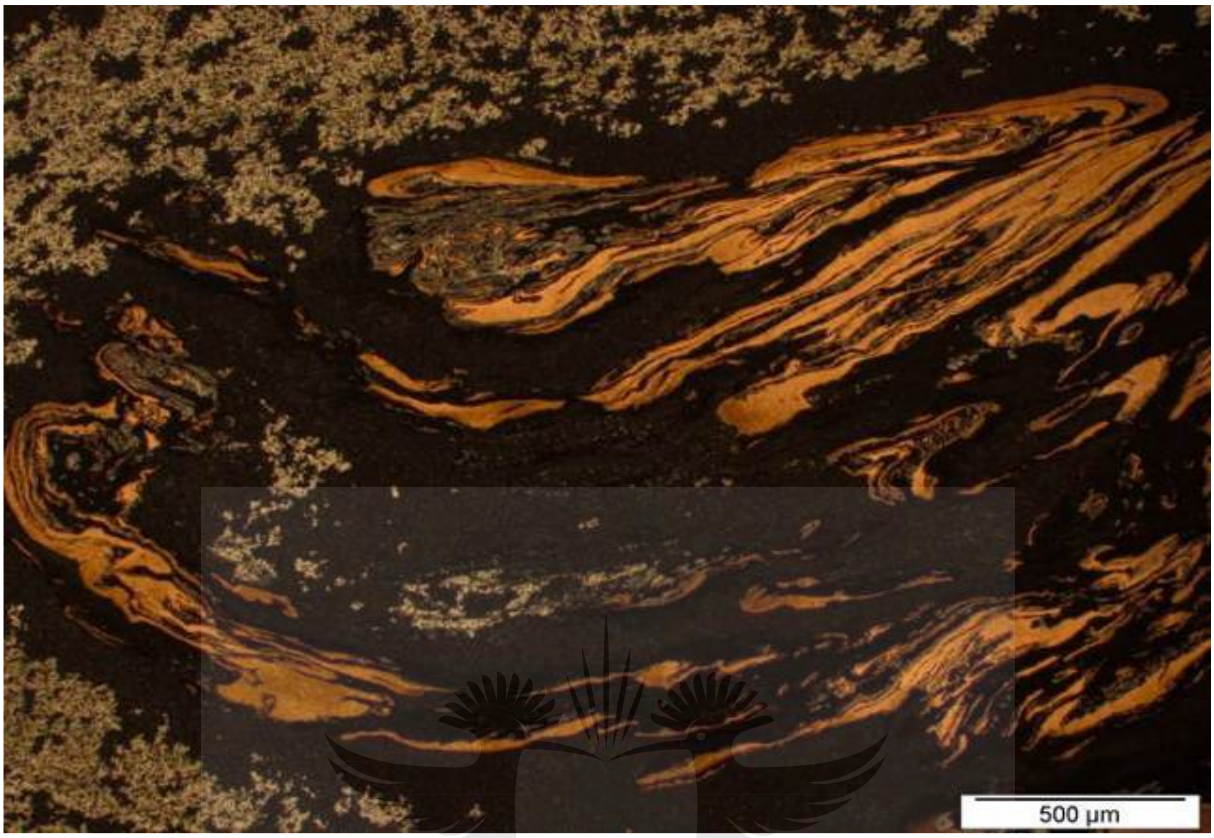

Figure 2-30 Microstructure of the friction stir weld produced at 600 rpm and 150 mm/min using a 15 mm shoulder diameter tool [102]

Li *et al.* [103] used pure copper and AA 1350; and they successfully joined them using FSW with the pin offset technique. They found that both copper and aluminium are greatly refined after FSW when compared with the base materials. No intermetallic compound was found, according to the XRD results. Esmaeili *et al.* [104] friction stir welded brass to AA 1050 at different rotation speeds. At low rotation speeds, and due to the low levels of heat input, no detectable intermetallic compound was observed.

As the rotation speeds increases, the gradual formation of intermetallics is initiated at the interface. Additionally, the increase in the rotational speed resulted in the thickening and development of intermetallic layers.

Akinlabi [105] conducted XRD analysis on AA 5754 and C11000 FSW welds. This revealed the formation of intermetallic compounds at the joint interfaces, including Al_2Cu and Al_4Cu_9, although their concentrations in the welds were very low.

Galvao *et al.* [7] observed that the aluminium to copper dissimilar welds displayed poor surface quality and thickness reduction mainly on those welds done with the aluminium in the advancing side. The results were compared with the FSW of similar materials welds, which nevertheless displayed good surface appearance with low flash and thickness reduction [7]. Avettand-Fenoe *et al.* [106] observed Al_2Cu and c1-Al_4Cu_9 phases in the dissimilar AA 6082 (T6) to copper friction stir welds. Their formation was essentially governed by both the thermo mechanical history and the local mixing of the chemical species.

Most recently, Al-Roubaiy *et al*. [107] conducted a study on the friction stir welding (FSW) between aluminium and copper, using experimental work by offsetting the pin to the aluminium side and controlling the parameters. Furthermore, a theoretical modelling was also used to correlate the experiments. They used 5083-H116 aluminium alloy and pure copper as the parent materials. The results showed that it is almost impossible to obtain a high quality Al-Cu direct joint without offsetting the pin in the softer material, which is Aluminium. The SEM/EDS observations revealed a steep drop in the diffusion rate of the Al across the interface; however, Cu and Mg had a little change in concentration through the interface [107].

Furthermore, Muthu and Jayabalan [108], friction stir welded AA1100-H14 aluminium and pure copper, by varying the tool travel speed; while the other parameters were kept constant. The XRD analysis revealed the presence of intermetallic compounds, namely: AlCu, Al_2Cu and Al_4Cu_9, as shown in Figure 2-31 [108].

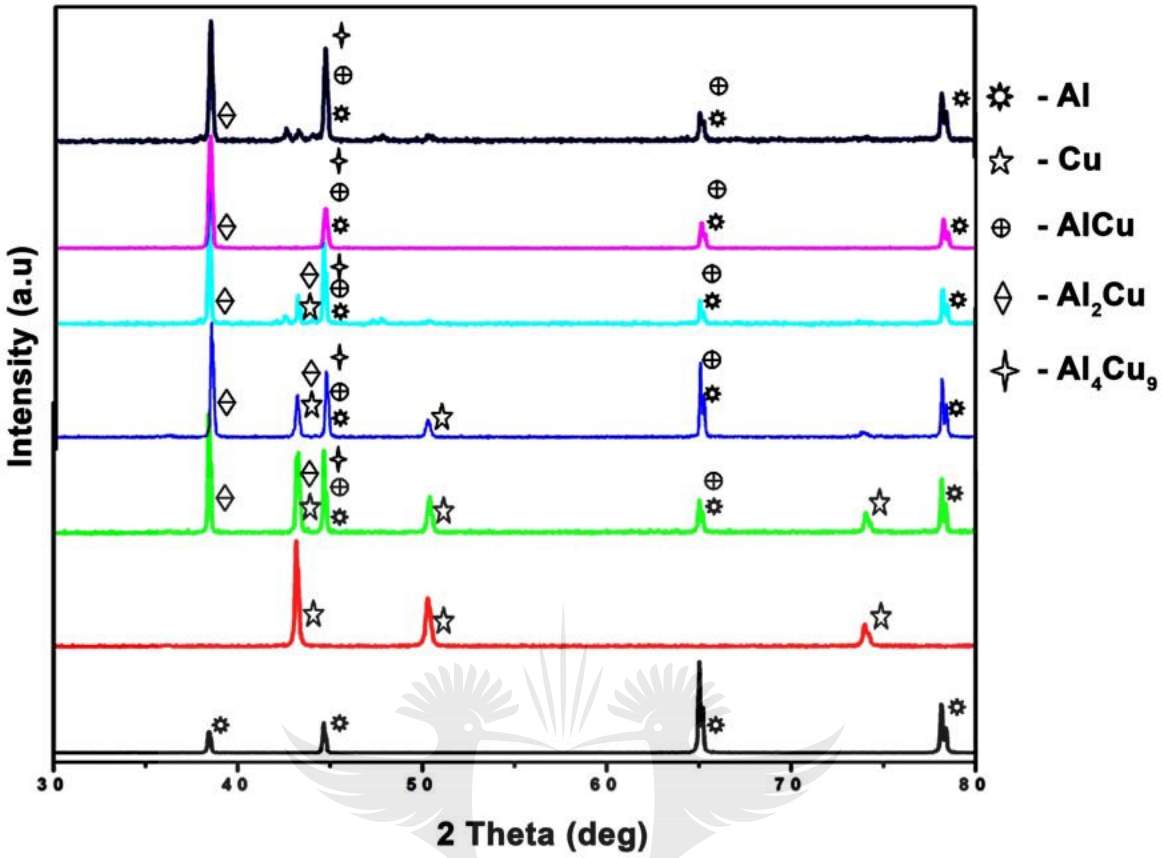

Figure 2-31 XRD spectrums revealing the presence of intermetallic compounds [108]

Recent research efforts on the microstructural evolution and XRD analyses have been reviewed. It may be summarised that in the FSW of aluminium to copper; placing the copper plate, which has a higher melting temperature at the advancing side yielded welds with good integrities. However, we noticed that most of the studies conducted showed the presence of intermetallic compounds while friction stir welding of aluminium and copper. Further analyses of these newly formed phases need to be conducted, in order to fully understand their impact on the welds. Optimisation of the processing parameters to reduce the formation of the intermetallic compounds at the joint interface also needs to be investigated.

2.7.2.2 Mechanical characterisation

The knowledge of the mechanical properties of the dissimilar friction stir welds between aluminium and copper is of importance, in order to enhance their usefulness in the industries.

Research has found that the maximum Ultimate Tensile Strength achieved in FSwelds of aluminium and copper was about 296 MPa; and this was obtained when the tool rotational speed was 950 rpm, and the travel speed was 150 mm/min [86]. Akinlabi [16] also measured the tensile test using different welding parameters. The results showed that the welds produced had Weld joint efficiencies of between 73% and 86%; and this might well be acceptable for design purposes.

Galvao *et al.* [7] stated that the welding conditions, specifically the rotational speeds and the traverse speeds that result in obtaining welds with good surface appearance do not necessarily lead to the production of sound dissimilar welds.

Furthermore, Esmaeili *et al.* [104] observed that the mechanical behaviour of joints is influenced as the rotational speed increases. They reported that the tensile strength of the weld produced increases, due to the formation of a narrow interfacial intermetallic layer and a lamellar composite structure within the stir zone. Then, the tensile strength decreases, due to the disappearance of a composite structure and the formation of defects in the stir zone [104]. The thickness of the interfacial intermetallic compound formation increases with an increase in the rotational speed. This results in the reduction of the tensile strength of the welds produced [104].

Li *et al.* [103] observed that the microhardness values measured are higher on the copper side of the nugget zone than it is on the aluminium side. This could be expected, as the UTS of copper is higher than that of the aluminium. Additionally, they found that the hardness at the bottom of the nugget is generally higher than it is in other regions, due to the stirring action of the tool pin leading to recrystallized grains. The UTS and the percentage elongation of the dissimilar joints were 152 MPa and 6.3%, respectively. However, the dissimilar joints failed in a ductile-brittle mixed fracture mode [103].

Akinlabi *and* Akinlabi [102] observed that there is an increase in the microhardness values at the joint interfaces of the welds, resulting from strain hardening due to the stirring of the tool pin and the shoulder previously occupied by these regions during the welding process; while the high peaks are due to the presence of intermetallics compounds occurring at the joint interface, as depicted in Figure 2-32.

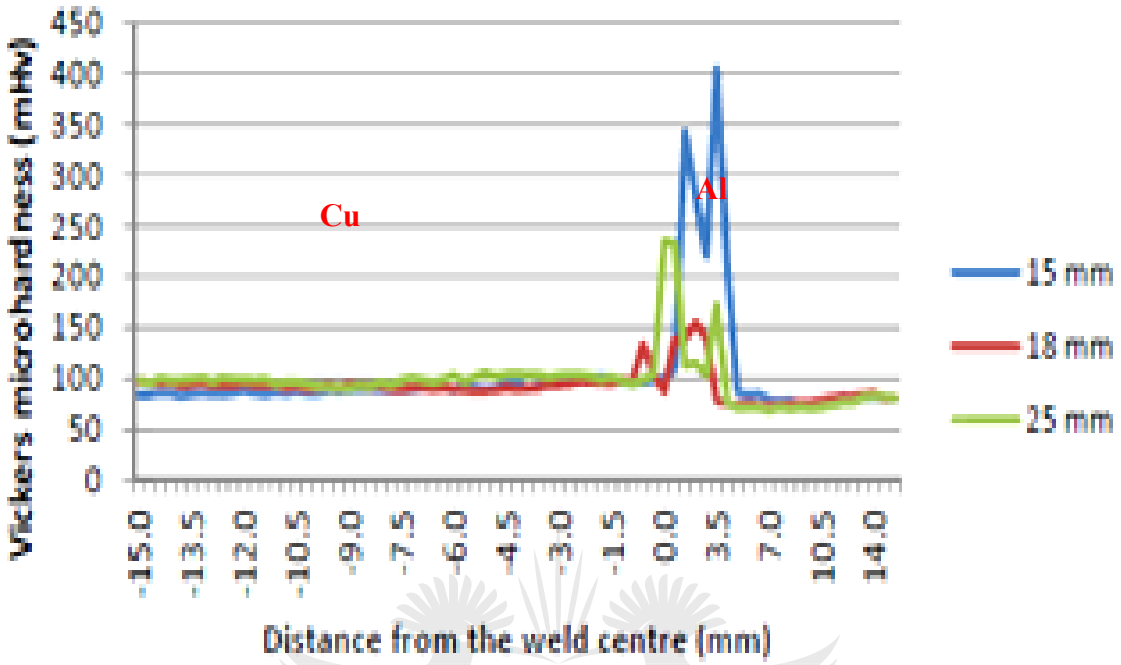

Figure 2-32 Vickers microhardness of welds produced at 600 rpm and 150 mm/min with the 15, 18 and 25 mm shoulder diameter tools [102]

However, Xue *et al.* [101] demonstrated that the FSW lap Al/Cu joints failed in the HAZ of the Al side; while the tensile shear load reached up to 2680 N when the Al plate was fixed on the advancing side. The hardness increased clearly in the layered structure, due to the strengthening effect of the Al/Cu intermetallics, which were mainly composed of Al_4Cu_9 phases [101].

The study conducted by Xue *et al.* [87] found that the large tensile specimen of the Al–Cu joint fractured at the HAZ of the Al side with a 13% elongation. The ultimate tensile strength (UTS) and the yield strength were ~90% and ~80% of the Al base material, respectively, and slightly lower than those of the Al base material, due to the annealing softening during the FSW process; while the mini-specimen fractured at the particles-rich zone (PRZ); and the UTS was about 210 MPa, which was considerably higher than in the Al BM [87].

Bisadi *et al.* [88] found that the maximum hardness values were measured on the copper side of the joint at the weld SZ, because of its fine grain size. In addition, in spite of the grain size

reductions, the hardness values of the joint aluminium side SZ were considerably lower than those of the aluminium base material. This could be due to the production of micro voids in this area.

Moreover, intermetallic compounds were detected mostly in the brittle fracture areas; and all the ultimate tensile stresses decreased when increasing the process temperature [88]. Poor tensile properties were achieved at the very large pin offsets and/or low rotation rates by Xue *et al.* [89], which they suggested could be due to the insufficient reaction between the Cu bulk / pieces and the Al matrix. Furthermore, good tensile properties were achieved in the FSW Al–Cu joints produced at higher rotation rates and proper pin offsets of 2 and 2.5 mm, due to the sufficient reaction [89].

The results from the work of Esmaeili *et al.* [90] indicated that the optimum ultimate strength of the sound joint was achieved from a proper material flow and metallurgical bonding through a narrow intermetallic layer at the interface, in addition to crack detection by the occurrence of lamellar composite structure (onion rings) in the stir zone [90].

Ouyang *et al.* [6] specifically found that different microhardness levels ranging from 136 to 760 $HV_{0.2}$ were produced in the weld nugget, corresponding to various microstructures, intermetallics and material flow patterns.

Ratnesh *et al.* [98] found that in the horizontal hardness profiles, the values were found to be about 110 HV and 106 HV for copper and for the aluminium base metals, respectively. The hardness values were stable for both metals in the HAZ; and they had a tendency to increase in the nugget zone; and this could be attributed to the formation of intermetallic compounds, as shown in Figure 2-33. The average tensile properties of the friction stir weld joints of Cu/Al varied from 138.7 MPa to 135.5 MPa [98].

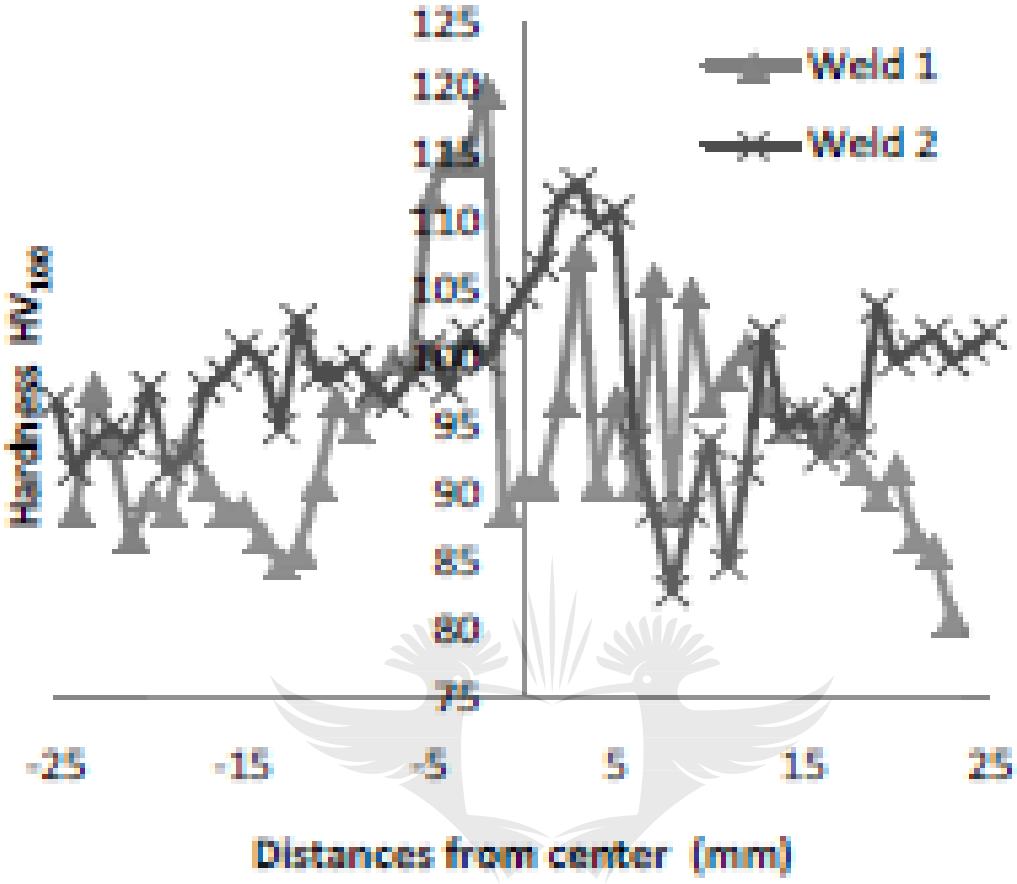

Figure 2-33 Microhardness profiles taken horizontally along the centre line of different friction stir welds [98]

Shukla *and* Shah [99] found that the maximum tensile strength of Al/Cu joint was low (62.2 MPa); and it was assumed that this was mainly due to the presence of intermetallic compounds. The increase in the rotational speed resulted in lower tensile strength, largely due to the increase in the amount of the intermetallic compounds formed at the Al/Cu interface [99]. Furthermore, in the stir zone, the hardness was slightly higher than those of the base metals. This was also taken to be due to the formation of hard and brittle intermetallic compounds of $CuAl_2$, CuAl and Cu_9Al_4 in the stir zone [99].

Saeid *et al.* [92] achieved maximum tensile shear strength of the lap joint between aluminium and copper, through FSW at a welding speed of 95 mm/min. Due to the formation of many microcracks

in the dark area at the welding speeds of 30 and 60 mm/min, the tolerable tensile shear was lower than that of 95 mm/min. While at higher welding speeds of 118 and 190 mm/min, the cavity defects were produced; and again the tensile shear strength decreased when compared with 95 mm/min [92]. The effect of the tool translational speed on the tensile shear strength is shown in Figure 2-34 [92].

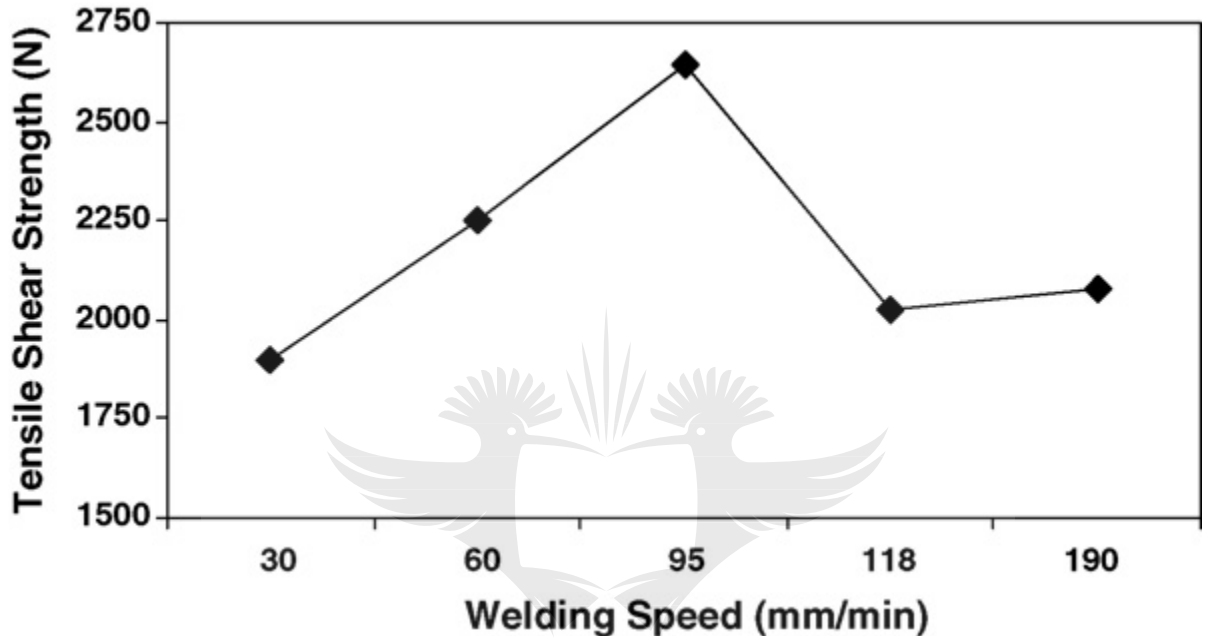

Figure 2-34 Effect of the tool translational speed on the tensile shear strength [92]

A maximum tensile strength was obtained at a rotational speed of 710 rpm, with a feed rate of 69 mm/min, and a pin offset of 0.2 mm. Furthermore, they identified experimentally and theoretically that the heat dissipation in the Cu side was higher than that in the Al side. This was further supported by a good agreement between the experiment and the modelling [107].

Muthu *and* Jayabalan [108], observed that the tool travel speed of 80 mm/min produced higher tensile strength and the joint efficiency of 113 MPa and 70.62 %, respectively. This was attributed to the formation of a defect free stir zone, and to the formation of a nano scale intermetallic layer at the joint interface [108].

In addition to the tensile testing and microhardness, Akinlabi *et al.* [93] measured the electrical resistivity of the welds. The results ranged between 0.087 and 0.1 μΩ. It was observed that the welds with the highest electrical resistivity of 0,101 μΩ were measured in those welds produced with high heat inputs.

In most of the above reviewed research outputs, friction stir welding could be an option in the future; and it could be the most used joining technique of dissimilar materials. However, more research needs to be done to improve the mechanical properties of the welds.

2.7.2.3 FSW tools used for aluminium and copper

In most of the research work conducted on FSW between aluminium and copper, the tool geometry and design are not generally fully disclosed, which could be due to proprietary reasons. Although tool geometry is a very important factor for producing sound welds, Rai *et al.* [109] conducted a review on FSW tools; but they did not provide much information on the FSW tools used for the joining of aluminium and copper in particular. Nevertheless, few researchers disclosed the tools used in their studies to friction stir weld aluminium to copper. Akinlabi *et al.* [105] successfully welded 5754 aluminium alloy and C11000 copper by employing the threaded pin and concave shoulder tool machined from H13 tool steel and hardened to 52 HRC.

Abdollah-Zadeh *et al.* [91] joined aluminium alloy 1060 rolled plate to commercially pure copper with thicknesses of 4 and 3 mm, using a SPK quenched and tempered tool steel, which had a shoulder diameter of 15 mm with a threaded pin of 5 mm diameter and was 6.5 mm long. Galvão *et al.* [96] used conical and scrolled shoulder tools to weld oxygen-free copper with a high phosphorous content (Cu-DHP, R 240) and AA 5083-H111.

Esmaeili *et al.* [90] used a hot working alloy steel tool, hardened to 45 HRC to weld AA 1050 to brass (CuZn30). The cited tool used was composed of a 15 mm diameter shoulder and a tapered slotted pin [90]. Saeid *et al.* [92] produced a weld between rolled plates of 1060 aluminium alloy and commercially pure copper, by using a quenched and tempered tool steel. The tool had a 15 mm diameter shoulder and a left-hand threaded pin (φ5mm×6.5 mm).

Li et *al.* [103] used a tool with a concave shoulder and a cone-threaded pin of 16 mm in diameter and 5.2 mm in diameter, respectively. The tool pin was 2.75 mm in length; and it was used to weld pure copper and AA 1350.

Agarwal *et al.* [97] used a tool made of AISI H13 tool steel and high speed steel (HSS), which had a shoulder of 18 mm and was 15 mm in diameter; and the tool pin was 7 mm in diameter and 3.7 mm pin length [97]. The above cited tool was used to weld AA 6063 to commercially pure copper plates. Guerra *et al.* [100] successfully joined AA 6061 with a thin high purity copper one-piece pin and shoulder from D2 tool steel heat treated to HRC62. The nib was 6.3 mm diameter and 5.8 mm long with standard 0.25/20 right-hand thread, and a 19 mm diameter shoulder.

FSW tools are of importance in the successful joining of similar and dissimilar materials; because such tools produce the thermo mechanical deformation and workpiece frictional heating necessary for friction stirring. Therefore, it is necessary to further improve the FSW tool geometry especially for dissimilar materials in order to produce high quality welds.

2.7.3 Friction Stir Spot Welding (FSSW) of similar and dissimilar materials

Friction stir spot welding has made some progress in various industries globally. This section outlines the past and current state of friction stir spot welding (FSSW) between similar and dissimilar materials. It is anticipated that the summarised findings should provide a good insight into the behaviour of different materials when joined by using the friction stir welding process.

2.7.3.1 FSSW between Aluminium alloys

Uematsu *et al.* [110], joined T4 treated 6061 using a double-acting tool consisting of an outer flat shoulder and an inner retractable probe, which could re-fill the probe hole. The microstructures of the weld zone were classified into MZ (mixed zone) and SZ, where fine equiaxed grains were observed due to the dynamic recrystallisation during FSSW process. They further found that the tensile strength of the joint was improved by the re-filling process; because the effective cross-sectional area of the nugget was increased [110].

Merzoug *et al.* [26], conducted experiments on AA6060-T5 using a tool steel of the type X210

CR 12 and the rotational speed of the tool ranged from 1000 to 2000 rpm. The tensile tests made it possible to establish the sample with (1000 rpm and 16 mm/min) has a good quality weld, (5 kN to 16 mm/min and 1000 rpm) when compared with values like 1.98 kN for 25 mm/min and 2000 rpm. The microhardness approached the maximum value; while they were moving away from the melting zone.

Zhang *et al.* [111] spot welded AA 5052-H112 of 1mm thickness. They concluded that softening occurs in the welds. A minimum hardness of 19.2 HV, which equals to 45.7% that of the BM, is measured in the HAZ. In addition, hardness in the TMAZ and SZ improves, due to the recrystallization. This causes the hardness distribution to exhibit a W-shaped appearance [111].The joints' strength decreases with increasing the tool rotational speed; while it is almost independent of the given tool dwell times [111].

Shen *et al.* [112] used AA 7075-T6 plates of 2 mm thickness; and the rotational speeds and the dwell time were varied, which were 1500, 1750 and 2000 rpm, and 3, 4 and 5 s, respectively. They investigated the microstructure and the mechanical properties of refill FSSW of AA7075-T6. The keyhole of the weld was refilled successfully; the microstructure of the weld exhibited variations in the grain sizes in the width and the thickness directions, as depicted in Figure 2-35 [112].

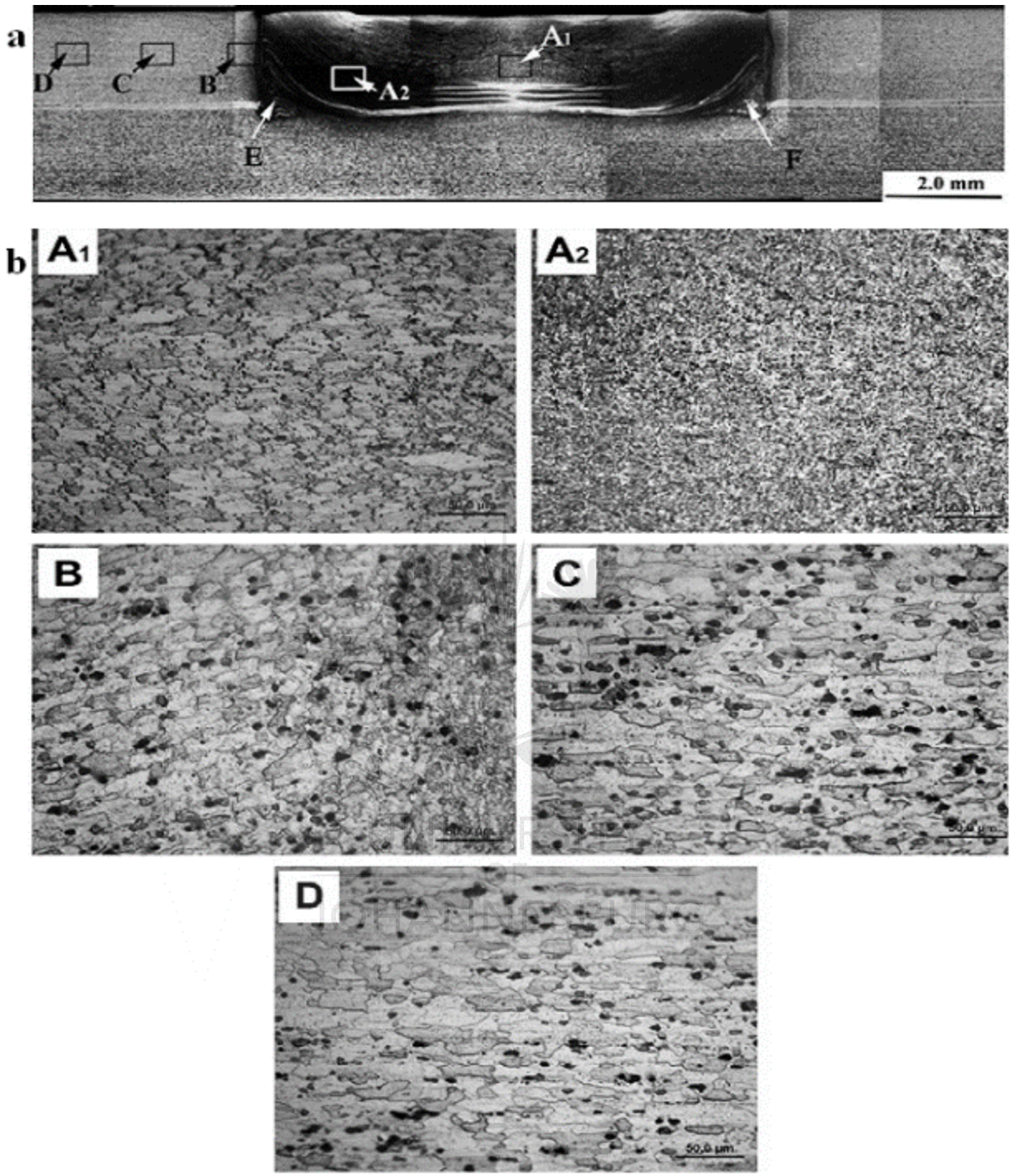

Figure 2-35 Microstructures on longitudinal section of RFSSW joint made at welding condition of the rotational speed of 1200 rpm and dwell time of 4 s: (a) cross section of the weld zone; (b) magnified views of the regions A1-D marked in a, respectively [112]

Additionally, they observed, defects associated with the material flow, such as hook, voids, bonding ligament and incomplete refill [112]. The hardness profile of the weld exhibited a W-shaped appearance in the macroscopic level. They attributed the change in hardness to the comprehensive effects of several factors, in which the precipitation state plays a decisive role.
Shen *et al.* [113], joined 6061-T4 aluminium alloy sheets with 2 mm thickness using a high-speed steel tool (JIS,SKD61), the shoulder diameter of which was 10 mm with a concave profile. A preferable appearance of the joint was obtained at higher rotational speed and longer duration time.

The microstructures of the weld were divided into four regions: BM, HAZ, TMAZ and SZ. It was found that there existed dynamic recrystallisation and dissolution of the precipitates in the weld. The hook geometries varied significantly, depending on the rotational speed and the duration time. The formation of the hook was attributed to the insufficient pressure vertical to the tool, the amount of material extruded upward, and the effective weld width increase with increasing rotational speed and duration time [113]. Furthermore, the Vickers hardness profile of the sheets showed a W-shaped or an upside down V-shaped appearance. The minimum hardness reached 46.7 HV in the periphery of the HAZ and TMAZ and different variation laws of Vickers hardness in each region of the weld were attributed to the comprehensive effects of the strain-hardening, the dissolution of the strengthening phase and the variation in the grain sizes.

The tensile/shear strength increases with the increasing rotational speed at any given duration of time. However, under a given rotational speed, the differences in tensile/shear strength among three duration times were found to be rather small. The tool rotational speed plays a determining role in the tensile/shear strength [113].

Tozaki *et al.* [114], joined AA6061-T4 sheets with 2mm thickness, using different probe lengths of 3.7, 3.1 and 2.4mm with a shoulder diameter of 10 mm. The probes were made of high-speed steel (Japanese Industrial Standard (JIS), SKD61) and had a standard metric M3.5 left-hand thread. A constant tool plunge rate of 20 mm/min and a shoulder plunge depth of 0.2mm below the upper plate surface were applied. Furthermore, the tool rotational speeds and the tool holding times were also varied. These were 2000, 2500 and 3000 rpm, and 0.2, 1 and 3 s, respectively. They observed that, the microstructures of the welds varied significantly, depending on the probe length, the tool rotational speed and the tool holding time; while the tensile shear strength increased with increasing probe length [114].

Badarinarayan *et al.* [31], joined annealed AA 5083 sheets with two different thicknesses of 1.64 and 1.24mm. The tool shoulder diameter was 12 mm with a concave profile; and the pin length was 1.6mm. The two different pin geometries were a conventional cylindrical and triangular pin. They concluded that the tool pin geometry significantly affects the hook. In the FSSW-C (cylindrical pin) weld, the hook runs gradually upward; and then it bypasses the stir zone and points downward towards the weld bottom. In the FSSW-T (triangular pin) weld, the hook was directed upwards towards the stir zone; and it ended with a very short plateau.

Mitlin *et al.* [115] spot welded Alcan AA 6111-T4sheets, using a flat shoulder pin made from H13 steel. The parameter that varied was the pin plunge depth, which ranged from 1.6 to 1.9 mm, in 0.1mm increments. The aluminium was fully recrystallized in the partially metallurgically and bonded region, in the fully metallurgically bonded region, and under the pin. The material under the shoulder had a significantly larger grain size than that under the pin, as well as a different texture; whereas the material under the shoulder had a significantly larger grain size than that under the pin, as well as a different texture [115].

Wang *and* Lee [116] spot welded AA6061-T6 with a thickness of 1mm. They found in their experimental results that under lap-shear loading conditions, the failure was initiated near the SZ in the middle part of the nugget; and the failure propagated along the circumference of the nugget to its final fracture. The location of the initial necking/shear failure was near the possible original notch tip; and the failures of the Friction Stir Spot Welds were fractured through the TMAZ near the weld nuggets [116]. Furthermore, the hardness initially decreases upon approaching the boundary between the base metal and the HAZ; and it then drops sharply to a minimum in the TMAZ.

After passing the TMAZ, the hardness gradually increases up to the SZ hardness [116].
Buffa *et al.* [117], used AA6082-T6 aluminium alloy, 1.5mm in thickness. They used a H13 steel quenched at 1020 ^{O}C, characterized by 52 HRC hardness. The shoulder was 15mm in diameter and a 40^{o} conical pin was adopted, with a major diameter of 7mm and a minor diameter of 2.2mm;

while the pin height was 2.6mm. They used a variation of the FSSW process and successfully produced the welds.

Wang *et al.* [118] joined commercially pure AA1050-H18 sheets with a 300µm thickness. The experimental results suggest that under lap-shear loading conditions, the failure is initiated near the SZ in the middle part of the nugget and the failure propagates along the circumference of the nugget to the point of final fracture. The location of the initial necking/shear failure is near the possibly original notch tip; and the failures of the Friction Stir Spot microwelds were fractured through the TMAZ near the weld nuggets.

Yuan *et al.* [119], spot welded 1mm thick AA6016-T4 sheets using two tools. A CP tool, which is a conventional tool with a centre pin; it has a concave shoulder with a 10.0mm diameter and a 1.5mm long step spiral pin with a root diameter of 4.5mm and a tip diameter of 3.0mm. The OC tool is the off-centre feature tool with the same concave shoulder shape and diameter, and three off-centre 0.8mm long hemispherical pin features. Both tools were machined from Densimet tungsten alloy. The results indicated that tool rotation speed and the plunge depth profoundly influenced the lap-shear separation loads [119].

Both of these tools exhibited a maximum weld separation load of about 3.3kN at 0.2mm shoulder-penetration depth; different tool rotation speeds, 1500rpm for the CP tool and 2500rpm for the OC tool [119].

Jeon *et al.* [120], used friction stir spot welding process to join, 3-mm-thick 5052-H32 and 6061-T6 aluminium alloy sheets. The z-force and the torque histories, as a function of tool displacement, vary significantly during the FSSW process. The force and torque histories during the FSSW process can be distinguished by different stages, based on the contact phenomena between the tool and the joined sheets. The shapes of the z-force histories are somewhat different for the selected material combinations, while the torque histories have quite similar shapes. The differences in the z-force histories for the different material combinations may be explained on the basis of the different mechanical behaviours of the aluminium alloys at various elevated temperatures [120].

Thoppul *and* Gibson [121] used AA6111-T4 to produced spot welds. From the microstructural studies, it is clear that increasing processing time increases both the tool depth of penetration and the bonding area between the lap joints.

Gerlich *et al.* [122] joined AA2014 T351, by using a tool with a shoulder diameter of 10 mm, a pin diameter of 4 mm, and a pin length of 2.2 mm. The tool was made of H13 steel with a hardness value of 46–48 HRC and a simple threaded pin profile. The plunge rate during all the spot welding trials was 2.5 mm/s; while the specified tool penetration depth was 2.2 mm. They found that the calculated strain rate during the spot welding decreases from 1600 to 0.6 s^{-1}, when the tool rotational speed increases from 750 to 3000 rpm. The low strain rate values were associated with tool slippage, resulting from the spontaneous melting of the S phase particles at temperatures ≥ 490 ^{o}C. Additionally, in contrast, when a low tool rotational speed is used during Spot Welding (750 rpm), the temperature never reaches 490 ^{o}C; and the calculated strain rate is 1600 s^{-1} [122].

Su *et al.* [123], investigated the friction stir spot welding of 5754 and Al 6111 sheets, using a tool having a smooth pin with or without a dwell period and spot welds made using a threaded tool without the application of a dwell period. They did not observe dissimilar intermixing in the spot welds made when using a tool with a smooth pin with or without the application of a dwell period, and in spot welds made using a threaded tool without the application of a dwell period. They further proposed that dissimilar intermixing during the dwell period in spot welding results from the incorporation of upper (Al 5754) and lower (Al 6111) sheet materials at the top of the thread on the rotating pin [123].

Babu *et al.* [17] welded 3mm thick AA2014-T4 and T6 conditions both with and without Alclad layers to investigate the effects of tool geometry and welding process parameters on joint formation. A good correlation between the process parameters, the bond width, the hook height, the joint strength, and the fracture mode was observed. They further found that the presence of Alclad layers and the base metal temper condition has no major effect on the joint formation and the joint strength [17].

Pathak *et al.* [124], joined AA5754 sheets, using tools with circular and tapered pins, considering different tool rotational speeds, plunge depths, and dwell times. Symmetric temperature profiles have been observed near the sheet-tool interface during spot welding using tools with circular and tapered pins at different rotational speeds. The peak temperature increases with any increase in the tool rotational speed and the dwell time. Tool geometry also affects the temperature distribution; as under similar conditions, tools with a circular pin generate more heat than tools with a tapered pin. The lap shear test with welded samples shows the influence of tool rotational speed, plunge depth, and dwell time.

The common observation for both the tools is that lap shear load increases with the increase in the said parameters [124].

2.7.3.2 FSSW between Aluminium and Magnesium

The FSSW process has been successfully used to Friction Stir Spot Weld aluminium to magnesium; and this process is used especially in the automotive and aerospace industries.

Suhuddin *et al.* [125] successfully joined Al alloy AA5754 to Mg alloy AZ31. Their microstructure analyses showed that the grain structure development in the stir zone was affected by grain boundary diffusion, interfacial diffusion and dynamic recrystallisation, which resulted in fine equiaxed grains of $Al_{12}Mg_{17}$ in the weld centre. Whereas the hardness profile of the Mg/Mg similar weld exhibited a W-shaped appearance, the lower hardness values appeared in the TMAZ and HAZ to be comprised of both Mg/Mg and Al/Al similar welds.

In the Al/Mg dissimilar weld, a characteristic interfacial layer consisting of intermetallic compounds (IMC) $Al_{12}Mg_{17}$ and Al_3Mg_2 was observed. Both Mg/Mg and Al/Al similar welds had significantly higher lap shear strength, failure energy and fatigue life than the Al/Mg dissimilar welds. While the Al/Al weld displayed a slightly lower lap shear strength than the Mg/Mg weld, the Al/Al weld had a higher failure energy and fatigue life [125].

Chowdhury *et al.* [126], used the FSSW process to spot weld Commercial AZ31B-H24 Mg and AA5754 with a thickness of 2 mm. They used a tool made from H13 tool steel, which had diameters of 13 mm for the scrolled shoulder and 5 mm for the left-hand threaded pin. A pin length

of 2.8 mm, a tool rotational rate of 2000 rpm, a tool plunge rate of 3 mm/s, a tool removal rate of 15 mm/s, a shoulder-plunge depth of 0.2 mm and a dwell time of 2 s was used. There was a presence of intermetallic compounds ($Al_{12}Mg_{17}$ and Al_3Mg_2). The microhardness profile of the Mg/Mg weld exhibited a W-shaped appearance, where the hardness gradually increased towards the keyhole direction [126].

Chowdhury *et al.* [127] conducted a study on the FSSW of Commercial AZ31B-H24 Mg and AA5754-O Al alloy sheets with a thickness of 2 mm, which were selected for FSSW. They observed a distinctive interfacial layer consisting of $Al_{12}Mg_{17}$ and Al_3Mg_2 intermetallic compounds in the Friction Stir Spot Welded dissimilar Al/Mg and Mg/Al adhesive joints. Furthermore, they stated that in comparison with the Al/Mg weld without adhesive, the extent of forming the intermetallic compounds decreased in the dissimilar adhesive joints. They also observed a much higher hardness, with values in between HV90 and 125, in the stir zone of Al/Mg and Mg/Al adhesive welds due to the presence of the intermetallic compound layer [127].

It was also observed that both Mg/Al and Al/Mg adhesive welds had significantly higher lap shear strength and failure energy than the Al/Mg dissimilar weld without adhesive [127].

Choi *et al.* [128], Friction Stir Spot joined 6K21 Al alloy and AZ31 Mg alloy with a tool made of general tool steel (SKD11) and composed of a shank, a shoulder, and a pin. The shoulder diameter, the pin diameter, the pin height and the weld tilt angle of the tool were 13.5 mm, 9.5 mm, 0.5 mm and 0, respectively. The results demonstrated the formation of IMCs in the interface between the Al and Mg alloy joint. These IMCs were revealed as Al_3Mg_2, formed on the Al substrate, and $Al_{12}Mg_{17}$, formed on the Mg substrate. In addition, the thickness of the intermetallic compounds layer increases with increasing tool rotation speed and duration time, and has a significant effect on the strengths of the joints.

The heavy thickness of the intermetallic compounds layer seriously deteriorates the mechanical properties of the joints. The maximum tensile shear fracture load of the Al and Mg alloy joint was about 1.6 kN; however, the load value decreased with an increase of the tool rotation speed and the duration time, owing to the cracks in the IMCs [128]. The microstructure in the Al and Mg alloy joint is shown Figure 2-36 [128]**.**

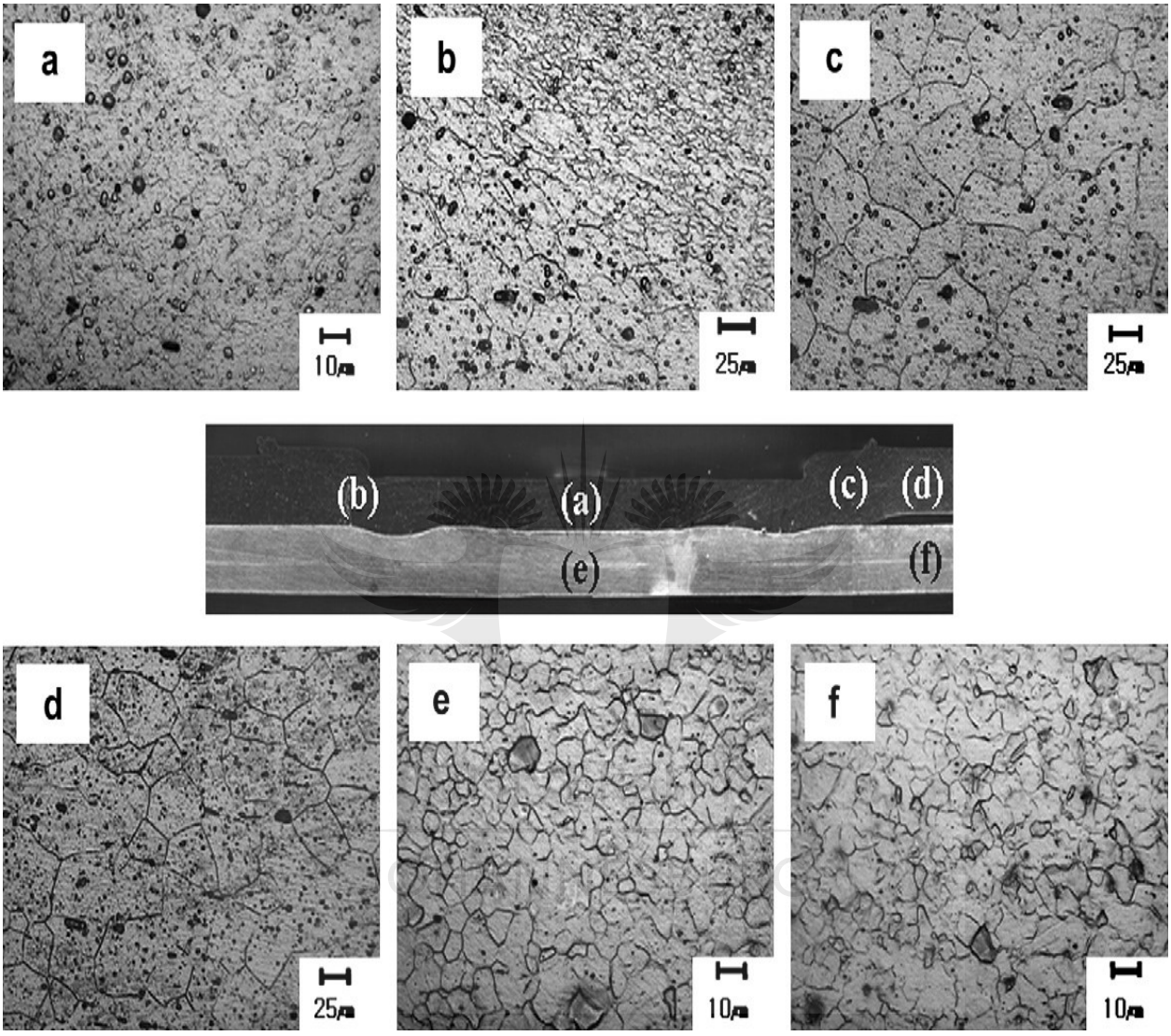

Figure 2-36 Microstructures in Al and Mg alloy joint at 1050 rpm-5 s: (a) stir zone (SZ); (b) thermal and mechanical affected zone (TMAZ); (c) the heat affected zone (HAZ); (d) base metal (BM) in the Al alloy; (e) below SZ, and (f) BM in Mg alloy [128]

Gerlich *et al.* [129] employed a 1.5 mm thick AZ91D, Al 6061-T6 and Al 5754- H12 and 1.3 mm thick Al 6111-T4. The plunge rate during FS spot welding ranged from 0.1 to 10 mm/s with the penetration depth controllable to 0.1 mm. The tool used to produce the spot welds was an H13 steel tool, which had a hardness of 46–48 HRc, a shoulder diameter of 10 mm, a pin diameter of 4

mm and a pin length of 2.2 mm. They found that the highest temperatures during the FS spot welding of Al 6111 and AZ91 base materials were close to the solidus temperatures of each base material and corresponded with 0.94*Ts* (Al 6111) and 0.99 Ts (AZ91). Where Ts is the solidus temperature of the material in degrees Kelvin [129].

2.7.3.3 FSSW between Aluminium and Steel

Chen *et al.* [130], welded 1 mm thick 6111-T4 Al and DC04 low-carbon steel sheet. The tool had an 11 mm diameter steel shoulder, with a scroll profile to improve the flow of the material, and a tapered 3 mm diameter WC 1 mm long probe. The radius of the probes orbital path was 2.5 mm; and this produced a swept area of 8 mm diameter on the steel surface. They produced high-quality friction spot welds between thin Al and steel automotive sheet within a weld time of one second, which is the desired target time by many industries.

Sun *et al.* [131], used a concave-shaped shoulder geometry tool with a diameter of 12 mm and a probe with a diameter of 4 mm to FSSW, a 1 mm thick commercial 6061 Al alloy, and a mild steel. They observed no obvious intermetallic compound layer along the Al/Fe interface after producing the welds. Furthermore, they observed that the shear tensile failure load can reach a maximum value of 3607 N. The probe length has little effect on the weld properties, which indicates that the tool life can be significantly extended by this new spot welding technique [131].

Figure 2-37 shows the electron backscattered diffraction (EBSD) map along the Al/Fe joint interface of the sample, when using a pin length of 1.0 mm in the first step [131].

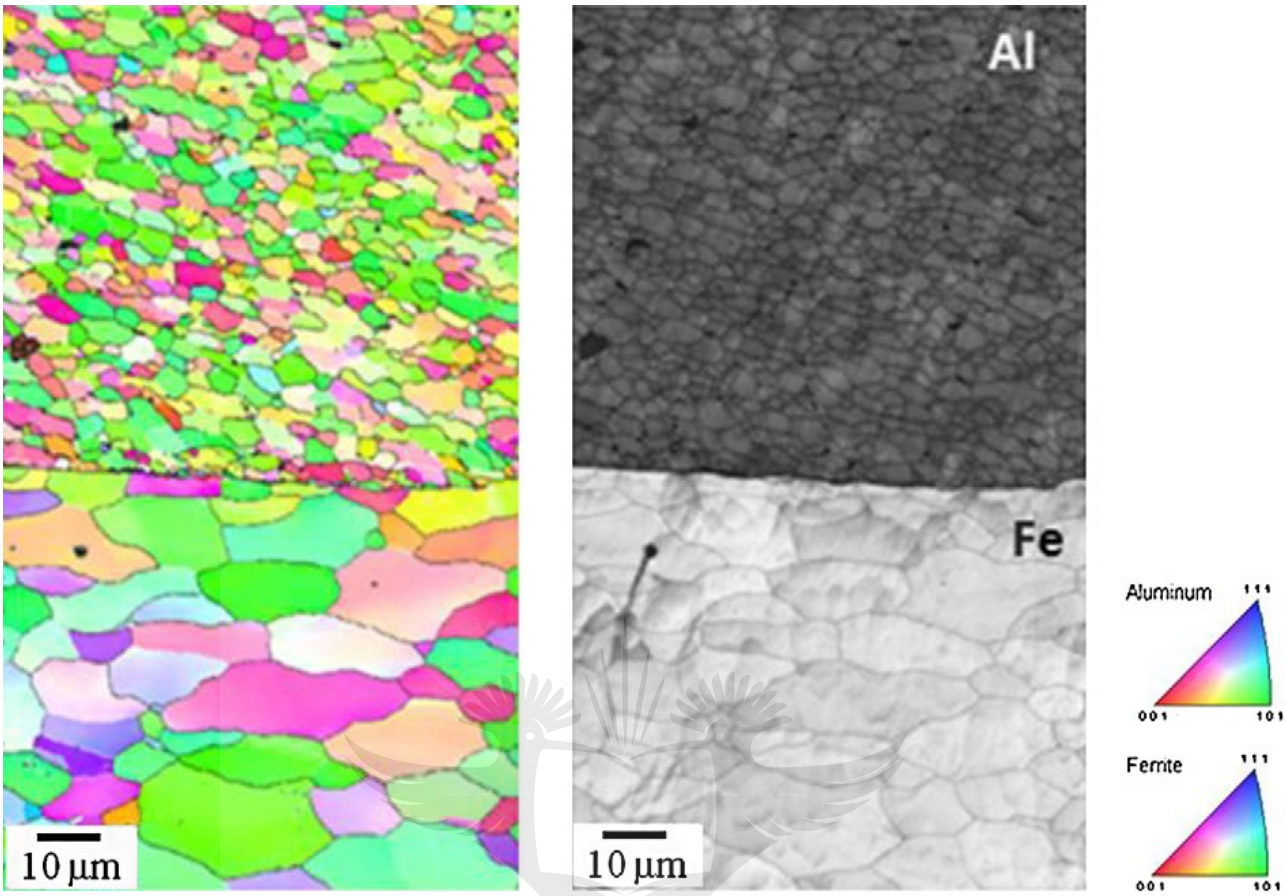

Figure 2-37 The electron backscattered diffraction (EBSD) map showing the microstructure along the Al/Fe joint interface [131]

Bozzi *et al.* [132], joined AA 6016 (1,2 mm thick) to a galvanized IF-steel sheet (2.0 mm thick) using a tool machined into tungsten rhenium alloy (W25Re). The intermetallic compounds layer thickness increases with the rotational speed and the penetration depth. They also noticed that the IMC layer seems to be necessary to improve the weld strength; but if the IMC layer is too thick, cracks initiate; and they propagate easily through the brittle IMC tangles [132].

Figner *et al.* [133], Friction Stir Spot Welded HX340 LAD sheets of steel of 1 mm thickness and aluminium AA5754-H111 of 2 mm thickness. They observed that by using the proper selection of spindle speed and dwell time, the strength of the spot weld can be improved significantly. Thus, a maximum load in the shear tension test of 8.4 kN per spot can be achieved; while by increasing

the dwell time, the number of intermetallic phases (IMP) increases; and they break off, causing a drop in strength [133].

2.7.3.4 FSSW between Aluminium alloys and Copper

Efforts have been made to produce friction stir spot welds between aluminium and copper. Ozdemir *et al.* [9] , Heideman *et al* [8] and Shiraly *et al.* [10] have both successfully friction stir spot welded a 3 mm thick AA1050 to pure copper, 1.5 mm thick AA6061 – T6 to oxygen free pure copper and AA1050 foil, 500µm thick to pure copper, 100 µm to produce a 2.3 mm thick multilayer sample, respectively. It was noticed that, while conducting an investigation into the existing literature on FSSW between aluminium and copper, that there were not many published results available; therefore, it is of importance that more research be conducted to optimise the process to enable it to be used as an alternative to riveting and resistance spot welding.

Ozdemir *et al.* [9] produced Friction Stir Spot welds using three different plunge depths, namely: 2.8, 4 mm and 5 mm, using a tool with a shoulder diameter of 20 mm and a pin with a diameter of 5 mm. Furthermore, the spot welds were produced using 1600 rpm rotation speed with 10 seconds hold time [9]. They produced spot welds with no macroscopic defects; and the grains on the copper side close to the Al/Cu interface were finer than those of the copper base metal. The difference in grain size was attributed to the effect of rotating pin which deformed the grains close to Al/Cu interface and the recrystallization of grains in the stir zone of the copper metal due to heat input [9].

Furthermore, the EDS analyses conducted revealed the formation of hard and brittle intermetallic compounds of AlCu, Al_2Cu and Al_4Cu_9 formed at the interface [9], as clearly shown in Figure 2-38.

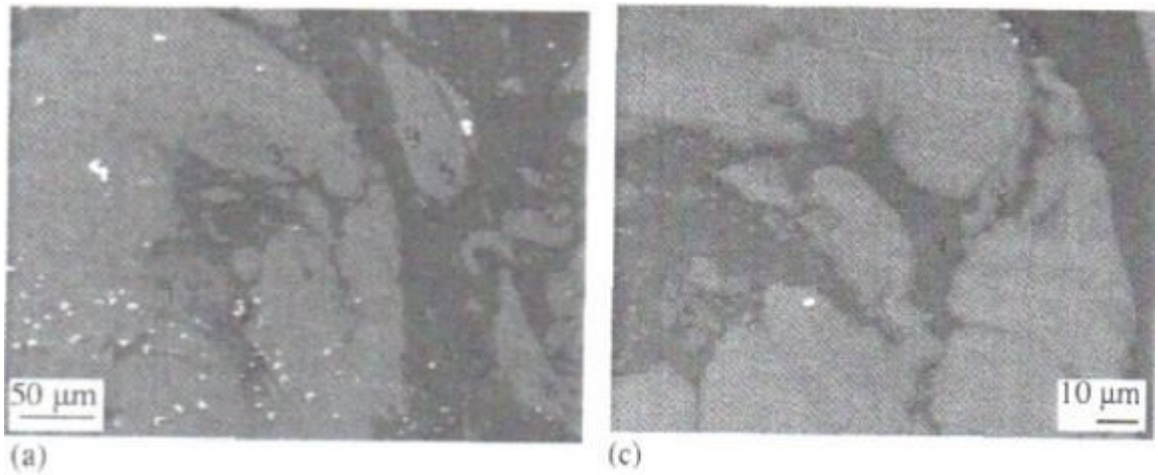

Elements	Points (for Figure 10a)					
	1	2	3	4	5	6
Al	67	46	4	98	46	43
Cu	33	54	96	2	54	57
	Points (for Figure 10c)					
	1	2	3	4	5	6
Al	66	66	80	96	42	98
Cu	34	34	20	4	58	2

Figure 2-38 SEM and EDS results, showing the presence of intermetallic compounds in the weld interface [9]

The tensile shear test results showed that 2.8 mm plunge depth produced poor results; whereas a 4mm plunge depth showed the highest values of shear tensile test compared to the 5mm. This was suspected to be due to the penetration of Cu into Al in a more diffused way [9]. Ozdemir *et al.* [9] also indicated that the hardness increases at the bottom region of the pin hole (in the Cu material) due to the heat input introduced by the rotating pin (Figure 2-39). Furthermore, they stated that as the plunge depth increases and the grain size decreases, which cause higher hardness at the Cu side for the 5 mm plunge depth; and due to the more diffuse and selective penetration of Cu into Al for the 5mm plunge depth, higher hardness values were obtained on the Al side [9].

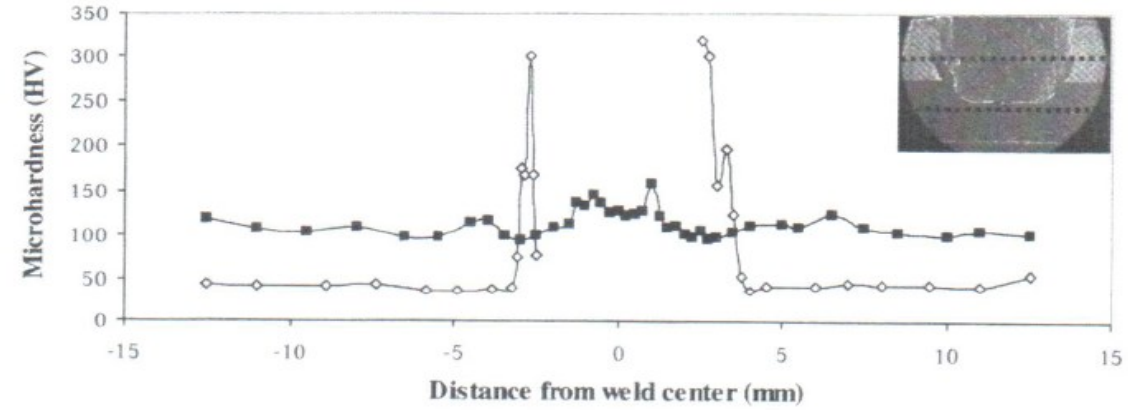

(a)

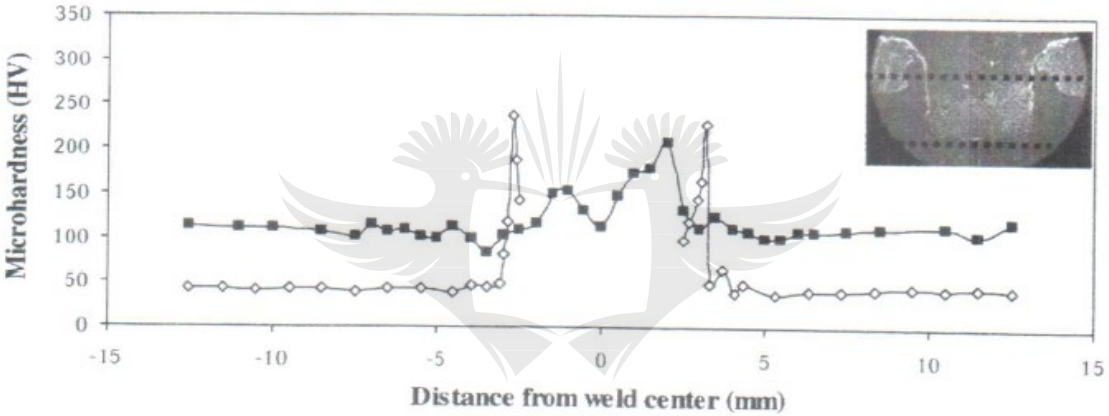

(b)

Figure 2-39 Microhardness results using 4mm (a) and 5 mm (b) plunge depths [9]

On the other hand, Heideman *et al.* [8] conducted a metallurgical analysis of AA 6061-T6 to oxygen-free Cu using the friction stir spot welding process. The tool used was a threaded pin design using a pre-hardened H13 tool steel with a shoulder of 10 mm, pin diameter of 4 mm and a thread pitch of 0.7mm. Two different plunge depths were used: 0.0 and 0.13 mm; and two different weld times of 3 and 6 seconds were utilised [8]. They used a rotation speed varying from 1000 to 2000 rpm. Furthermore, they indicated that, the rotation speed, the plunge depth and the tool length were the primary factors affecting the welds strength as shown in Table 2.3.

Table 2.3: The tensile strength of the spot welds using different rotational speeds, plunge depths and weld times [8]

Pin length, mm	Rotation speed, rev min^{-1}	Plunge depth, mm	Weld time, s	Average weld strength, N
1·83	1000	0·00	3	343
2·60	1000	0·00	3	552
1·83	2000	0·00	3	661
2·60	2000	0·00	3	1844
1·83	1000	0·13	3	531
2·60	1000	0·13	3	783
1·83	2000	0·13	3	1372
2·60	2000	0·13	3	2080
1·83	1000	0·00	6	535
2·60	1000	0·00	6	910
1·83	2000	0·00	6	742
2·60	2000	0·00	6	1964
1·83	1000	0·13	6	762
2·60	1000	0·13	6	431
1·83	2000	0·13	6	1694
2·60	2000	0·13	6	1734

The presence of an intermetallic interface was not observed in the strong welds; they were only in the form of small particles that do not connect along the bond line to become most detrimental to the weld quality [8], as shown in Figure 2-40.

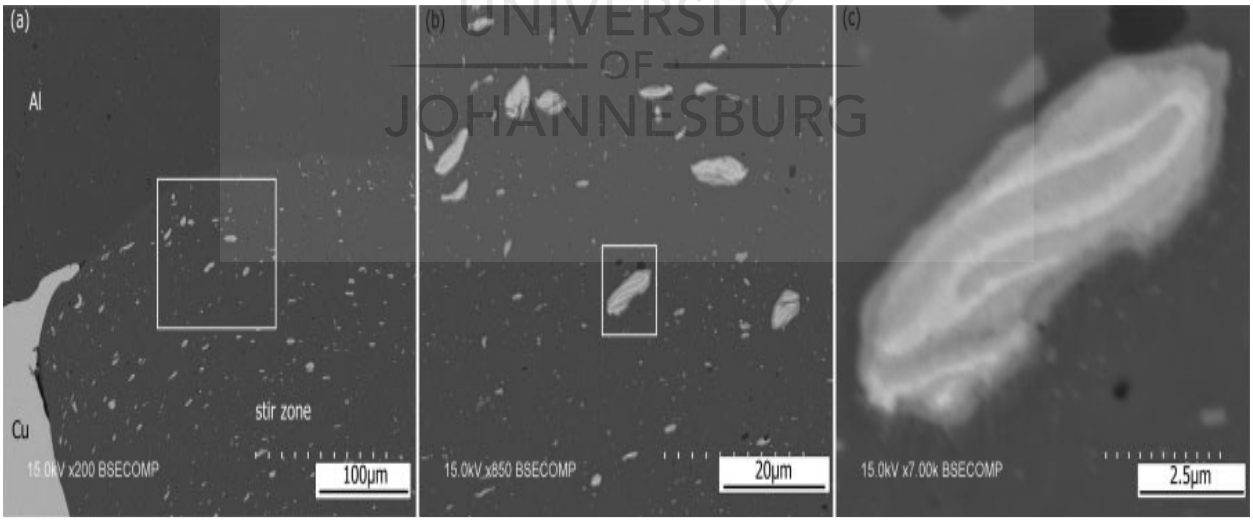

Figure 2-40 SEM images of intermetallic compounds [8]

Shiraly *et al.* [10] performed a FSSW of Al/Cu composite produced by accumulative roll-bonding process, using a triangular pin with no features (Figure 2-41).

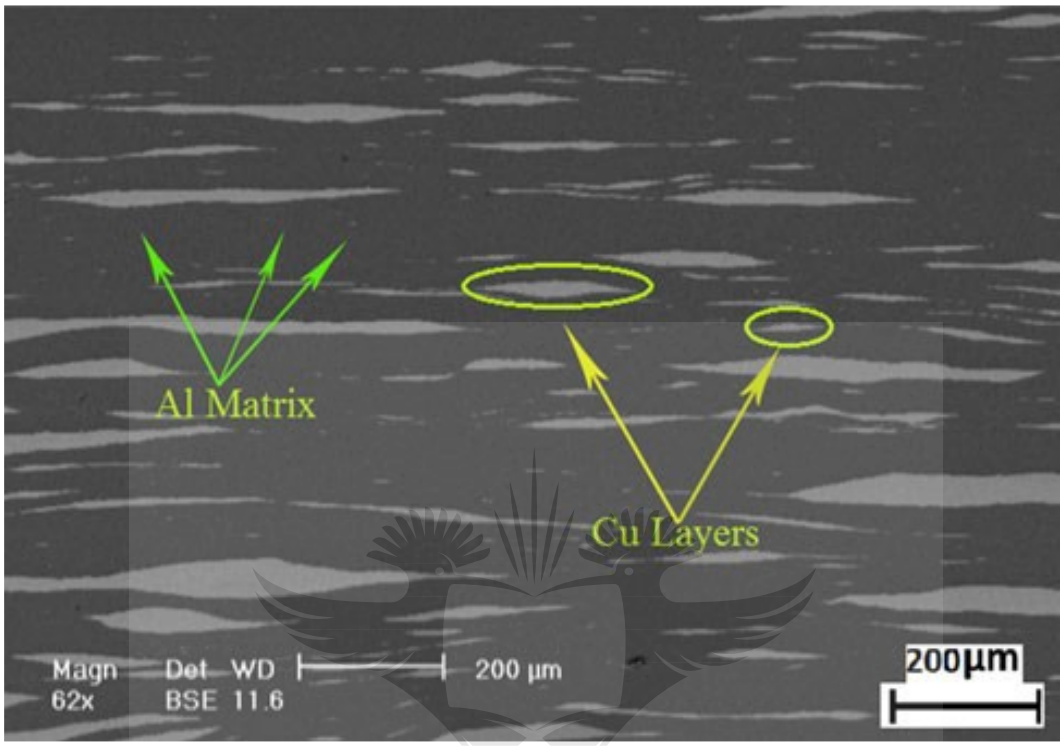

Figure 2-41 Cross-sectional SEM micrograph of Al/Cu composite produced using the accumulative roll bonding (ARB) process [10]

They found that the weld made at a lower tool rotation rate was not bonded; this was due to no intermixing between the upper and lower sheets. Furthermore, the maximum shear failure load increased with the increasing tool rotation rate, which can be attributed to the increasing area and effective length of the stir zone (SZ), as shown in Figure 2-42.

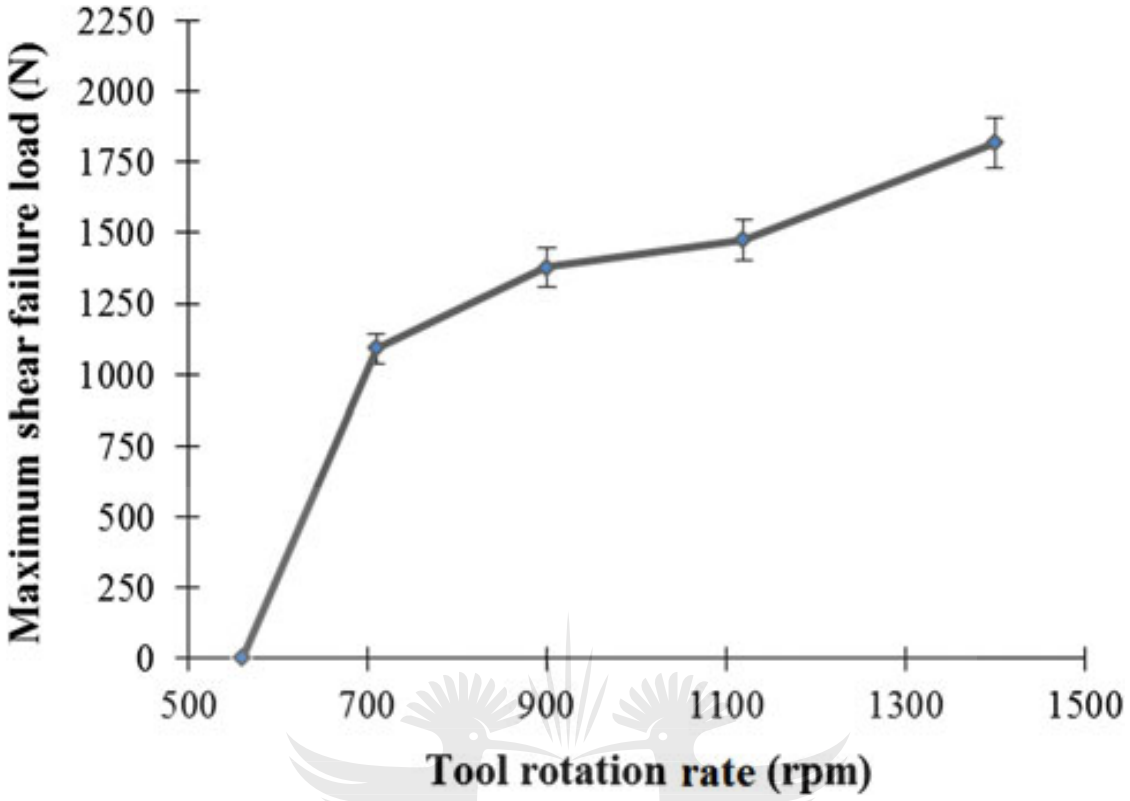

Figure 2-42 Effect of rotation rate on the maximum shear failure load [10]

The experimental interpretations showed the presence of the intermetallic compounds (Al_2Cu and $AlCu_3$) in the stir zone (SZ). The presence of the intermetallic compounds and the material crushing increased the hardness in the stir zone, as depicted in Figure 2-43 and Figure 2-44, for the intermetallic compounds and the hardness, respectively [10].

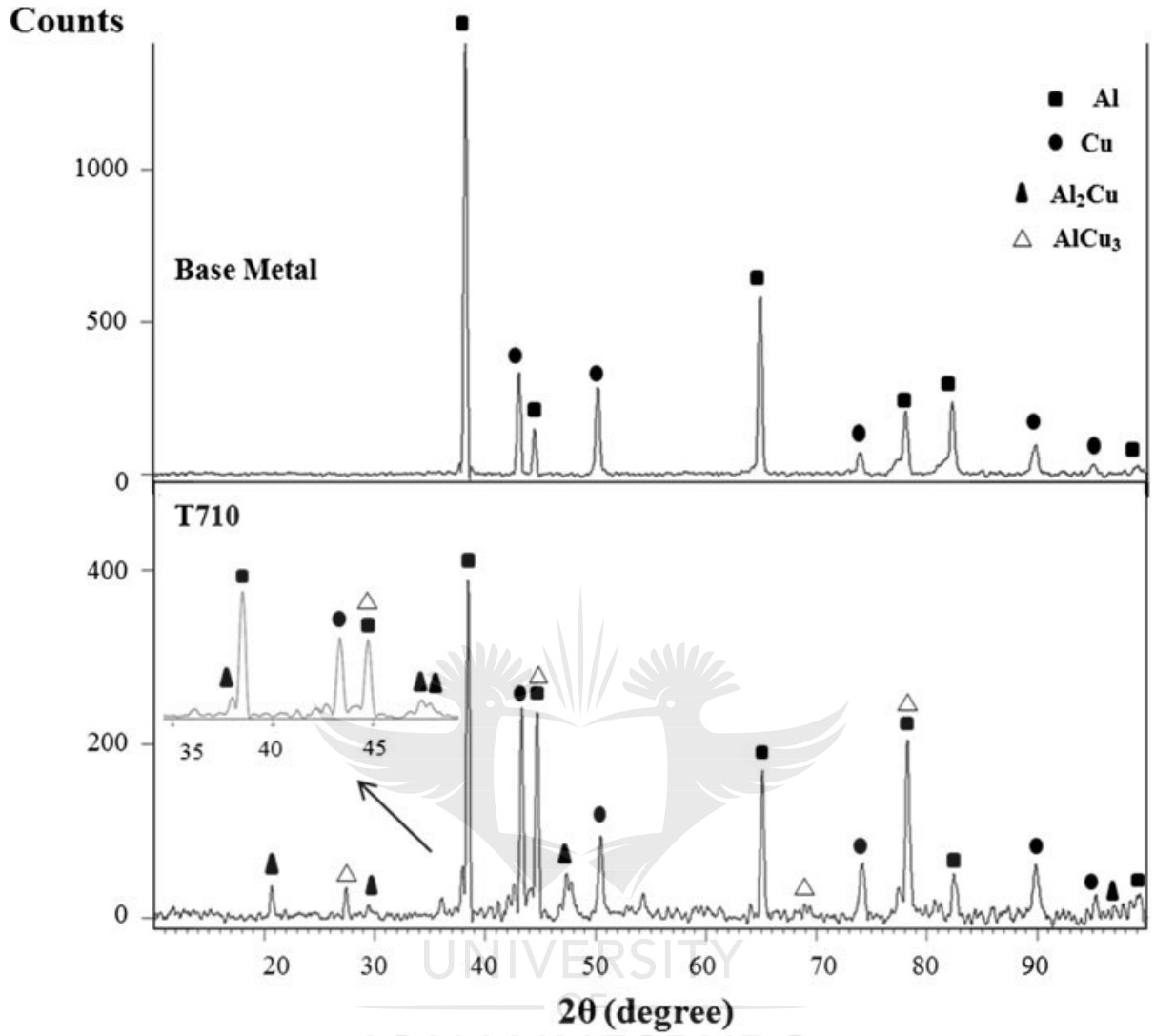

Figure 2-43 X-Ray Diffraction patterns of the parent material and the stir zone for sample T710 [10]

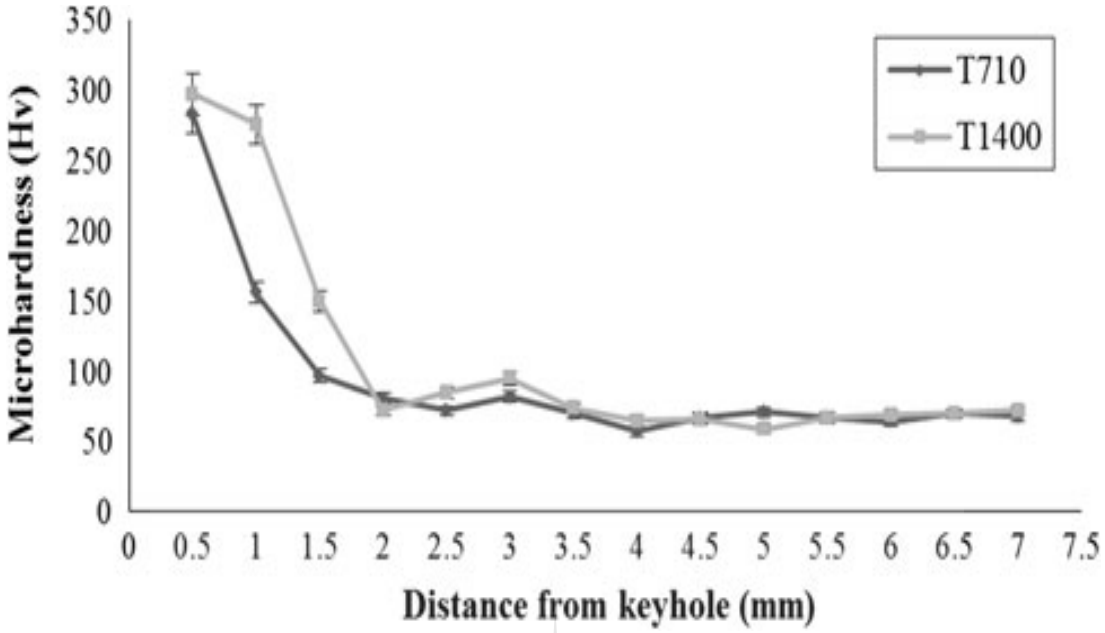

Figure 2-44 Microhardness profiles for sample T710 and T1400 [10]

2.8 Summary

A literature review has been conducted on the background of the FSW and FSSW processes. It shows that not much importance has been shown on producing FSSW welds between aluminium and copper, which could be an alternative solution to riveting and Resistance Spot Welding. In this study, we have focused on the usage of the FSSW method by using different tool geometries and process parameters to produce spot welds between AA1060 and C11000. Furthermore, the related review of the literature to the current study has been successfully conducted and published. The next chapter will present the research methodology.

CHAPTER THREE

3 METHODOLOGY

3.1 Introduction

With a basic understanding of the process of friction stir welding (FSW) and friction stir spot welding (FSSW), a design for the experimental approach was carried out, in order to get a better understanding of the effect of the tool geometry and the process parameters on the friction stir spot welds of AA1060 to C11000. Tools with different geometries were designed and machined to produce spot welds. Furthermore, a detailed experimental procedure and the methods of analysis used in this research will be discussed in this chapter.

The flow sheet summarising the different steps of the experimental procedures is displayed in Figure 3-1.

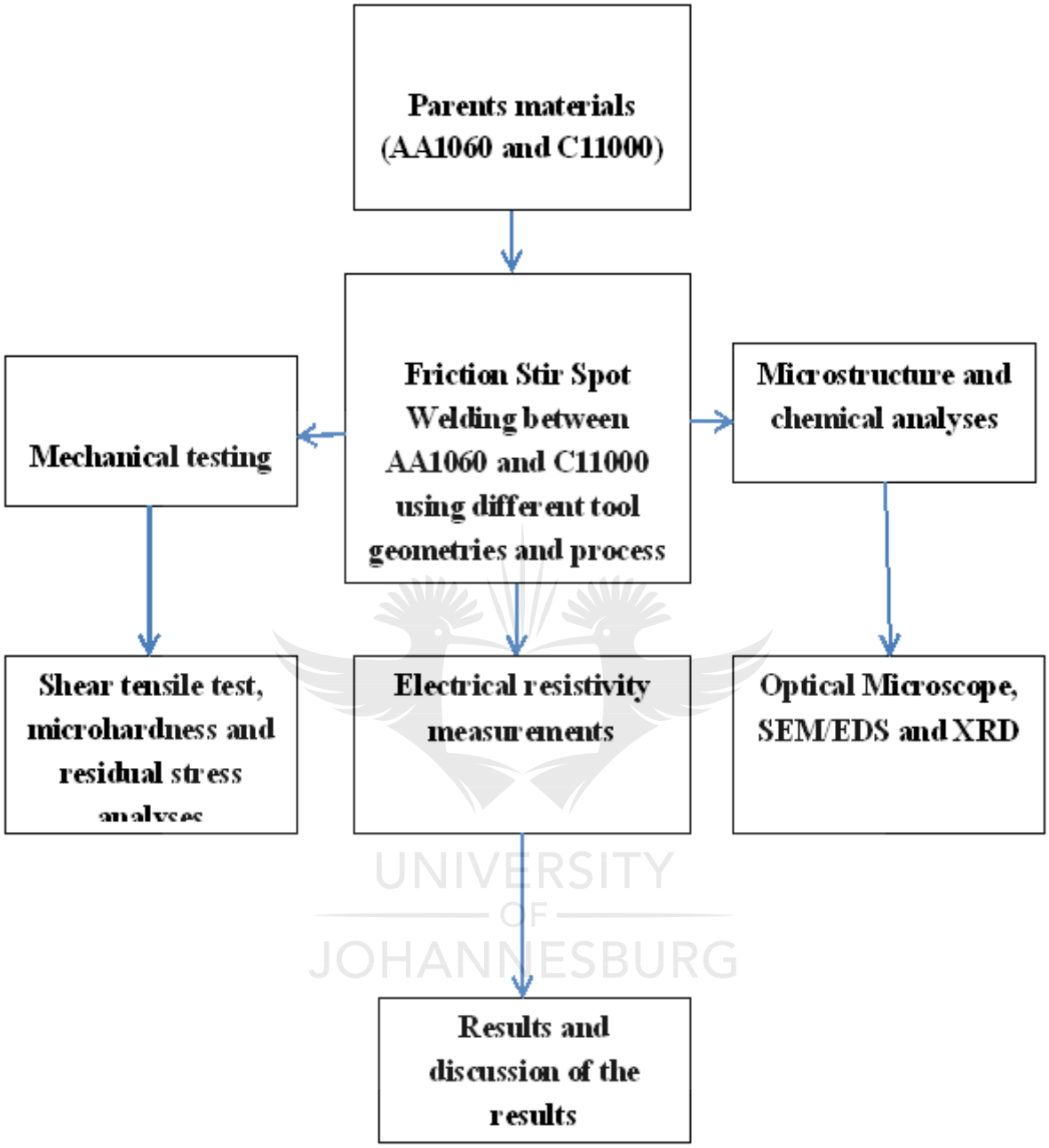

Figure 3-1 A summary of the experimental procedures used for the project

3.2 Experimental procedures

3.2.1 Parent materials

The parent materials used in the research work are AA 1060 aluminium alloy and C11000 copper. The dimensions of the test coupon for each plate are 600 x 120x 3 mm^3. The weld configuration used in this study is lap-joint welding. The sheets were welded in a 30 mm overlap configuration. The chemical composition of the two parent materials was determined, using a spectrometer (Q4 TASMAN). Emery paper was used to remove the oxide layer; and the plates were then washed with ethanol. Tables 3.1 and 3.2 show the chemical composition of AA1060 and C11000, respectively. Additionally, X-ray fluorescence spectrometer (XRF) analyses were conducted on the parent materials by using a Rigaku ZSX Primus II with SQX analysis software. The results can be seen in Appendix A.

Table 3.1: The chemical composition of AA1060 (in wt %)

Element	Si	Fe	Ga	Others	Al
Obtained	0.058	0.481	0.011	0.05	Balance

Table 3.2: The chemical composition of C11000 (in wt %)

Element	Zn	Pb	Ni	Al	Co	B	Sb	Nb	Others	Cu
Obtained	0.137	<0.1	0.02	0.023	0.012	0.077	0.036	0.043	<0.492	Balance

3.2.2 FSSW tools

The tools were machined to fit the FSW machine (MTS PDS I-Stir) at the Nelson Mandela Metropolitan University (NMMU), as shown in Figure 3-2. The tool material is H13 tool steel hardened to 50-52 HRC. The tool pin length and the diameter were kept constant at 4 mm and 5mm respectively; while the shoulder diameters were varied. The 20 mm diameter shoulder produced spot welds that were not characterised in the current research work; because most of the

produced welds failed during the cutting stage. The choice of the pin length was motivated by the fact that the pin length cannot be equal to the total thickness of the base materials. The tool geometry and dimensions are presented in Table 3.3; and the two tool features used in this project are shown in Figure 3-3.

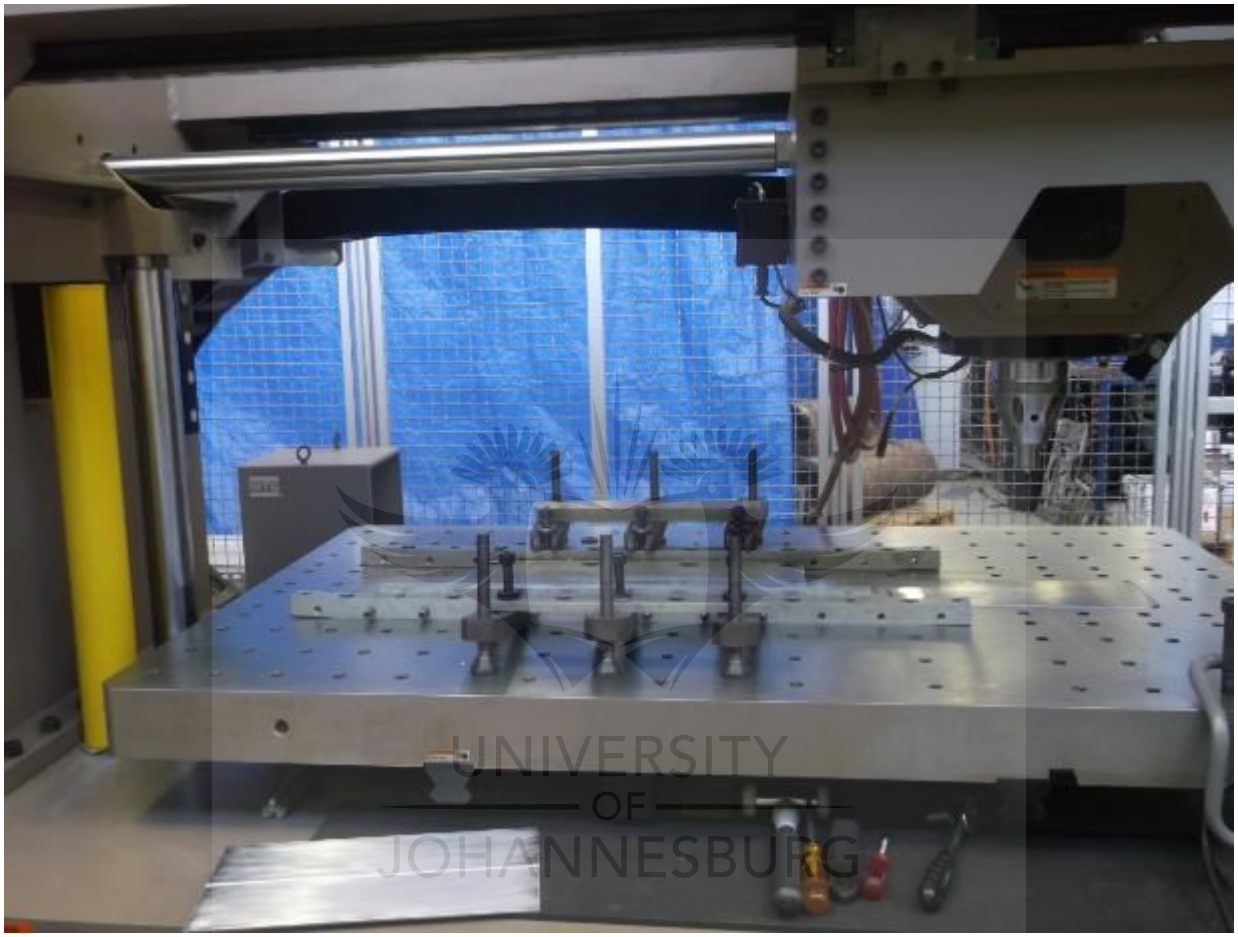

Figure 3-2 MTS PDS I-Stir FSW machine used to produce the Friction Stir Spot Welds

Table 3.3: FSSW Tool designs, dimensions and features

	Pin ϕ (mm)	Pin length (mm)	Shoulder ϕ (mm)	Features
Design A	**5**	**4**	**15**	Flat pin and shoulder (FPS)
	5	4	20	
Design B	**5**	**4**	**15**	Conical pin and concave shoulder (CCS)
	5	4	20	

Figure 3-3 The FSSW tool used in this project: (A) ϕ 5 mm, pin length 4.0 mm and ϕ 15.0 mm shoulder diameter of the Conical pin and concave shoulder (left) and ϕ 5 mm, pin length 4.0 mm and ϕ 15.0 mm Conical pin and concave shoulder (right). (B) ϕ 5 mm, pin length 4.0 mm and ϕ 15.0 mm shoulder diameter of the Conical pin and concave shoulder

3.2.3 Process parameters

The variables that mostly influenced the outcome of the FSSW process are identified as: the rotational speed, the plunge depth, the dwell time and the tool geometry; and these will be investigated. The dwell time of 10 seconds was considered for the current research work. Furthermore, the dwell time was optimised during the preliminary work at 10 seconds; and this was used for the final weld matrix. The rotational speed, the shoulder diameter and the shoulder plunge depth were varied for each of the designed tools.

In addition, the axial forces and the torques were recorded and correlated to the tool geometry and the process parameters. Two different rotational speeds were used in this investigation, namely, 800 and 1200 rpm. The shoulder plunge depths were 0.5 and 1.0 mm for each designed tool. Prior to the production of the final weld matrix, preliminary welds using different rotational speeds and tool designs were conducted and the results were analysed. It was noticed that almost all of the spot welds produced using 20 mm shoulder diameter tools failed; a picture of the failed spot welds is shown in Figure 3-4.

Figure 3-4 Failed spot welds produced using 20 mm shoulder diameter tools

Thus, the optimised rotational speeds and the chosen tool geometry were used to produce the final spot welds. A summary of the final design of the experiment is presented in Table 3.4. Emery papers were used to remove the oxide layer on the plates; and the plates were then washed with

ethanol. Furthermore, the total number of spot welds produced in this study are shown in Appendix B. In the open literature [8] [9] for lap weld configuration, the aluminium plates are put on top of the copper plates. This could be due to their differences in mechanical properties such as melting point. Xue *et al*. [101], stated that the change in the relative location of the aluminium plates would result in different mechanical properties because the deformation and fracture occurred at the aluminium plate side due to its lower strength than the copper plate. Therefore, in the current work the aluminium was put on top of the copper plate.

Table 3.4: Friction stir spot welding (FSSW) parameters and tool geometries

Shoulder plunge depth (mm)	Experiments	Tool rotational speed (rpm)	Shoulder diameter (mm)	
0.5	1	800	15	
0.5	2	**1200**	**15**	Flat pin and shoulder (FPS)
1	3	800	15	
1	4	**1200**	**15**	
0.5	5	800	15	
0.5	6	**1200**	**15**	Conical pin and concave shoulder (CCS)
1	7	800	15	
1	8	**1200**	**15**	

Figure 3-5: This illustrates the backing plate and the clamping system prior to the friction stir spot welding process. The backing plate used in this project was a mild steel plate bolted to the welding bed.

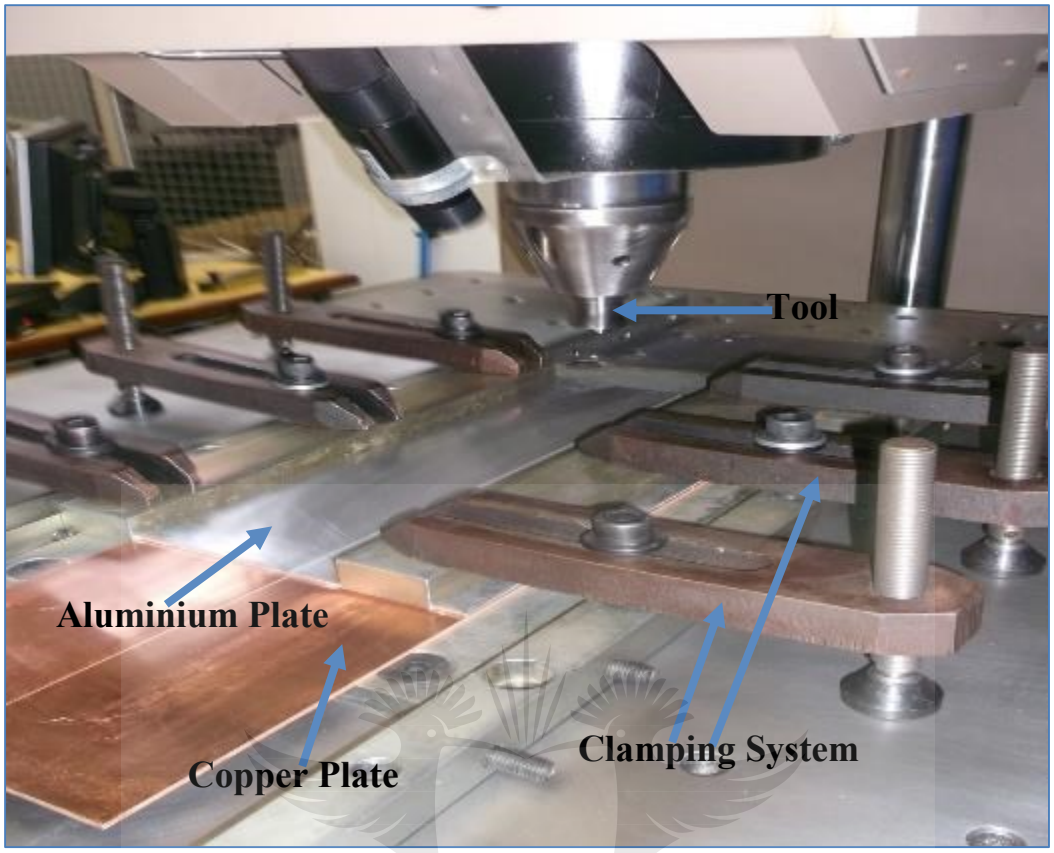

Figure 3-5 Showing the backing plate, the tool holder, the tool, the aluminium plate, copper plate and the clamping system

3.2.4 Experimental techniques

3.2.4.1 X-Ray Diffraction (XRD)

X-ray diffraction (XRD) analyses were conducted for the qualitative analyses (phase identification) of the possible intermetallic compounds and their possible composition. To run the analyses using XRD, spot welds samples were sectioned by using wire electrical discharge machining (WEDM), grinded and polished. The samples were examined using a D8 Advance diffractometer with a Cu tube; the recording range was 15º to 120º, a step size of 0.04º using a 2 mm collimator. Furthermore, an X-ray diffractometer Rigaku Ultima IV equipped with PDXL analytical software with Cu (K α) was also used to confirm the phase identification of the parent materials. The 2 theta scan was from 5º to 90º at 0.02 º per step (the results can be found in Appendix C). Additionally, intermetallic compound analyses were carried out in the SZ, TMAZ and in the HAZ of the samples. A D8 Discover diffractometer with Cu tube using a recording

range from 10 º to 125 º, with a step size of 0.04 º was used. A 0.8 mm collimator was used for a reliable identification of the phases at different locations of the spot weld. An EVA software program was used to process the diffraction pattern results obtained; and these were compared with the PDF ICCD 2007 (Powder Diffraction Files from the International Centre for Diffraction).

3.2.4.2 Optical Microscopy

To carry out this experiment, spot welds were sectioned using wire electrical discharge machining (WEDM), grinded and polished, and then mounted in polyfast thermoplastic cold mounting resin. The samples were prepared by using a standard metallographic procedure [134][135] and ASTM standard E3-11 [136]. Furthermore, iron III nitrate ($Fe(NO_3)_3$) added suspension was also used in the final polishing step (it helped to remove the copper scratches). The surface appearance of the spot welds was analysed using an Olympus BX51M microscope. A solution of $FeCl_3$ (10g) + HCl (6 ml) + Ethanol (C_2H_5OH) (20 ml) + H_2O (80 ml) was used to etch the copper side of the spot welds; while the aluminium side was etched with H_2O (190 ml) + HNO_3 (5 ml) + HCl (10 ml) + HF (2 ml).

3.2.4.3 Scanning Electron Microscopy (SEM) coupled with Energy Dispersive X-ray Spectroscopy (EDS)

Morphological and qualitative analyses of the spot welds were performed using SEM/EDS. The SEM provided information on the surface appearance; while the EDS provided information on their chemistry. A TESCAN equipped with an Oxford instrument was used to analyse the samples. The spot welds samples were cut by using wire electrical discharge machining (WEDM), grinded and polished, mounted and prepared, using the ASTM standard metallographic procedure [134] [135]. The samples were then inserted in the instrument and subjected to an electron beam under a vacuum. In order to obtain micrographs of the samples. The SEM instrument is coupled with EDS. The X-ray detector of the EDS measures the number of emitted X-rays in opposition to their energy.

The energy of the X-ray is characteristic of the element from which the X-ray was emitted. A spectrum of the energy in opposition to the relative counts of the detected X-rays will be obtained and evaluated for qualitative and quantitative determinations of the chemical elements present

[137]. The chemical composition analysis of the spot and selected surface of the spot welded samples was then determined using EDS.

3.2.4.4 Microhardness analysis

A Vickers microhardness test was conducted on the parent materials and the spot welded samples. The samples were prepared, according to the ASTM standard E384-11$^{\varepsilon 1}$ [138]. For the hardness test, a Vickers microhardness Diamond pyramid indenter Emco Test DuraScan tester was used (Appendix D). The measurements were made along the cross sections of the spot welds with a load of 100g and a dwell time of 10 seconds. The microhardness trend was measured across the weld in intervals of 0.5 mm, using the screw gauge attached to the Dura hardness tester. The standard recommended test method for Vickers microhardness of metallic samples is a 1 to 120 kgf load; and the chosen 100g to be used for this research study was based on the literature sources [7] [139][124].

The Vickers microhardness profiles were measured from the stir zone in the middle of the copper ring and in the bottom plate (copper), as shown in Figure 3-6.

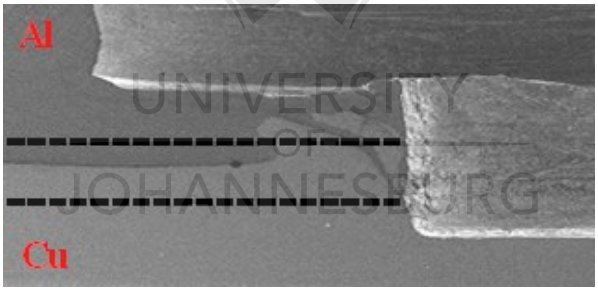

Figure 3-6 Representation of the spot weld with dashed lines illustrating the location of the microhardness profile measurements

3.2.4.5 Shear Tensile Testing

Lap shear tensile tests were applied, in order to determine the shear tension strength of the weld samples. The geometry of the tensile samples (a), as well as the shear tensile specimens used in the current research (b) are shown in Figure 3-7; and the tensile test machine plus the FSSW specimen can be found in Appendix E. The lap shear testing was performed, using an Instron

screw-driven tensile machine (Model 1195, 5500R) with 100 kN load cell and with a crosshead speed of 3 mm /min.

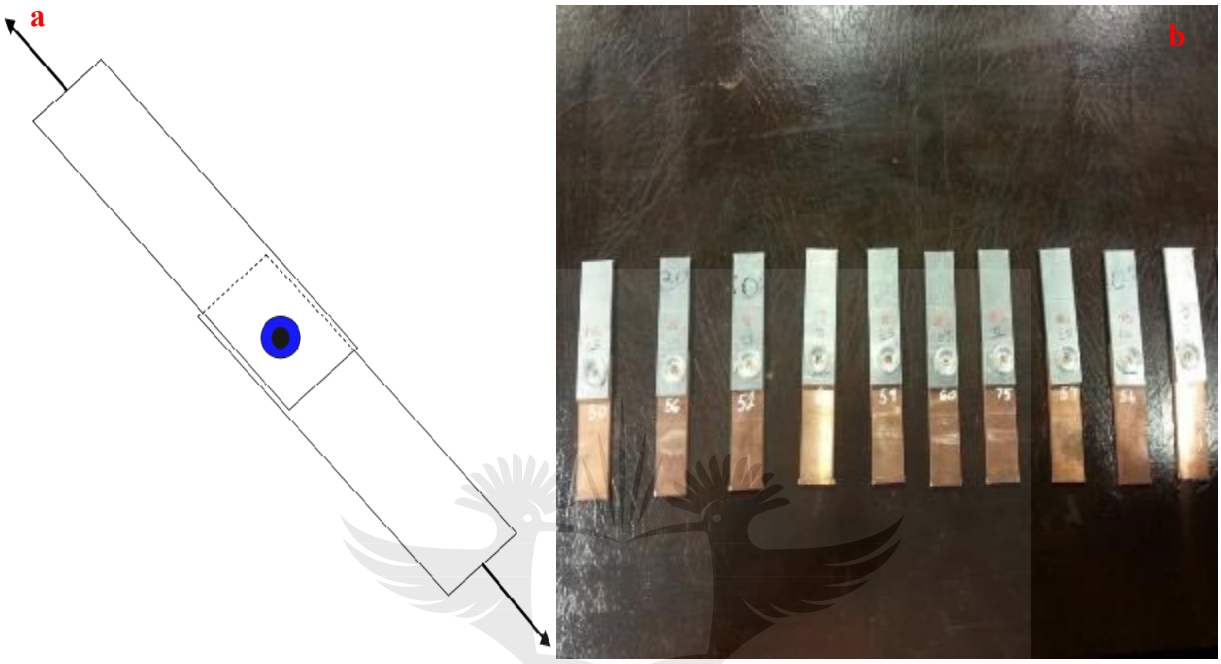

Figure 3-7 Geometry of the lap shear tensile sample (a) [139] and specimens used in the current study (b)

3.2.4.6 Electrical Resistivity determination

The electrical resistivity of the joint was determined, according to the method used by Akinlabi [105]. This was done by means of a calculation derived from the measurement of the electrical resistance values across the welds. The weld samples were prepared; and a Four-Point probe meter was used to measure the electrical resistance. The electrical resistance of the samples was measured, in accordance with the ASTM standard cited by Akinlabi [105]. The Four-Point probe meter consists of two probes carrying the current, with the other two probes sensing the voltage, as shown in Figure 3-8.

Figure 3-8 Experimental set-up for electrical resistance measurement

3.2.4.7 Residual stress measurements

The residual stress distribution in the Friction Stir Spot Welded plates were measured by using the non-destructive X-ray diffraction (XRD) technique. The technique employs interplanar spacing in the material, which serves as a strain gauge [140]. The principle involves monitoring of the selected Bragg peak(s) for different tilt angles for each azimuth angle. Using appropriate elastic constants, the measured strain can be converted to the corresponding residual stress. The residual stress investigations were taken in the SZ and the copper ring area. This was conducted, in order to investigate the effect of the presence of the copper ring extruded upward from the lower copper plate into the aluminium plate.

The commonly used $\sin^2\psi$-method was used in the current research study for the determination of the surface residual stresses. The analyses were conducted by using a Bruker D8 Discover diffractometer equipped with ¼ Eulearin cradle mounted on a θ-2θ goniometer. Probing was done using Cu K_α radiation (with 8 keV energy). The primary optics included a 0.8 mm collimator, as

well as a graphite monochromator. The sample alignment was done using a laser and video alignment system. A diffracted beam was collected using a 2D Vantec 500 detector. The detector was positioned where this coincided with one of the peaks used for the strain measurement. The sample detector distance was 20 cm, corresponding to a range of 32.7 ^{o} (2θ); and the measurement time per step ranged from 300 to 400 seconds.

The measurements were performed with the detector positioned at 136^{o} (2θ). In order to have the full stress tensor, the measurements were carried out at six azimuth angles i.e. ϕ and ϕ +180° (0°, 45°, 90°, 180°, 225°, 270°), with the latter allowing measurements at negative tilt angles. For each azimuth angle, a set of eight tilt angles (at 10° increments from 0° to 70°) were acquired. The data thus produced were analysed using a LEPTOS version 6.02 software from BRUKER AXS. The analysis was done using the 331 (136.5) Cu reflections. The picture of the BRUKER D8 Discover diffractometer used in this research study for the measurement of the residual stress is found in Appendix F.

3.3 Summary

Some preliminary investigations have been conducted on the parent materials. A design of the experiments was used, in order to set up the experiments to be conducted. The weld configuration is a lap joint and the aluminium was placed on top; while the copper was at the bottom. The next chapter will present and discuss the results generated when using the experimental set-up.

CHAPTER FOUR

4 RESULTS AND DISCUSSIONS

4.1 Introduction

This chapter covers the results and discussion of the analyses conducted on Friction Stir Welds produced using different process parameters and tools. The analyses included microstructure characterisation using the optical microscope (OM), the scanning electron microscope (SEM), chemical analysis and phase identification using energy dispersive spectroscopy (EDS), and X-ray diffraction (XRD), respectively. Mechanical analyses, such as the shear tensile test and microhardness were also conducted. Additionally, the electrical resistivity and the residual stress test were measured, using a four point probe and X-ray diffraction method, respectively. Statistical analyses were also done.

4.2 Forge forces generated during friction stir spot welds of copper and aluminium

During the friction stir spot welding process, a large axial load is experienced by the welding tool, due to the mechanical interaction with the workpieces. Forge forces were measured during the production of all the samples; and Figures 4-1 a and b show the forge force curves for the spot welds, using a Flat Pin and Shoulder (FPS) produced at 800 rpm (a) 1200 rpm (b) and 0.5 mm shoulder plunge depth, respectively. The rest of the forge force curve figures, using the different process parameters and tool geometries are found in Appendix G.

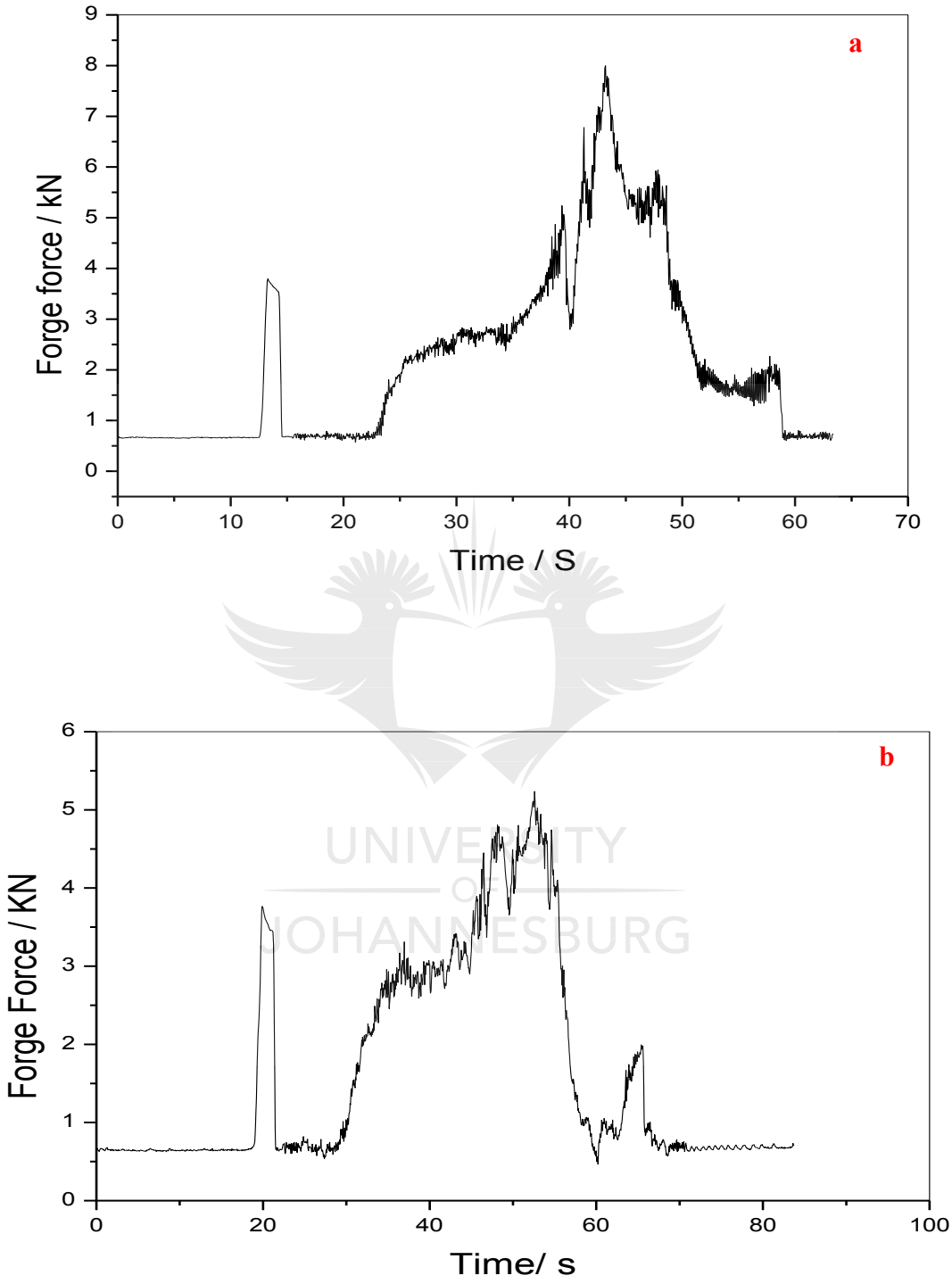

Figure 4-1 Forge forces curves using a flat pin and flat shoulder, (a) 800 rpm and 0.5 mm shoulder plunge depth, (b) 1200 rpm and 0.5 mm shoulder plunge depth

In the recorded curves showing the forge force versus time, it can be observed that for all the different process parameter combinations, the forge force increases during the first few seconds, and only slightly after 10 seconds, which can be attributed to when the tool touched the aluminium plates. Since the aluminium used in the current investigation is soft, the forge force quickly decreases when the aluminium is plasticised eventually reaching a forge force of less than 1 kN. The forge force starts to increase again after few seconds; and thereafter it increases quickly, which is assumed to be when the pin touches the copper plate; and it further increases when the shoulder touches the top plate (aluminium) until the shoulder reaches the targeted depth. The forge force reaches a maximum forge force; and then the force decreases until the tool is withdrawn from the plates. Table 4.1 and Table 4.2 show the experimental results of the maximum forge forces generated using a flat pin/flat shoulder and conical pin /concave shoulder tool, respectively.

Additionally, Figure 4-2 depicts the highest forge force obtained using the same process parameters and tool geometries. The real time curves are ideal; and they are a true reflection of the reaction forces during the welding process.

Table 4.1: Maximum forge forces generated during FSSW between Al/Cu using a flat pin and flat shoulder

Rotational speed (rpm)	Shoulder plunge depth (mm)	Max forge force (kN)
800	0.5	6.40
800	0.5	7.99
800	0.5	7.99
800	1	8.38
800	1	7.84
800	1	8.71
1200	0.5	5.24
1200	0.5	5.65
1200	0.5	6.47
1200	1	5.81
1200	1	5.81
1200	1	5.97

Table 4.2: Maximum forge forces generated during FSSW between Al/Cu using a conical pin and concave shoulder

Rotational speed (rpm)	Shoulder plunge depth (mm)	Max forge force (kN)
800	0.5	8.70
800	0.5	8.38
800	0.5	7.77
800	1	8.78
800	1	9.26
800	1	8.92
1200	0.5	6.53
1200	0.5	5.95
1200	0.5	6.42
1200	1	8.18
1200	1	7.34
1200	1	8.83

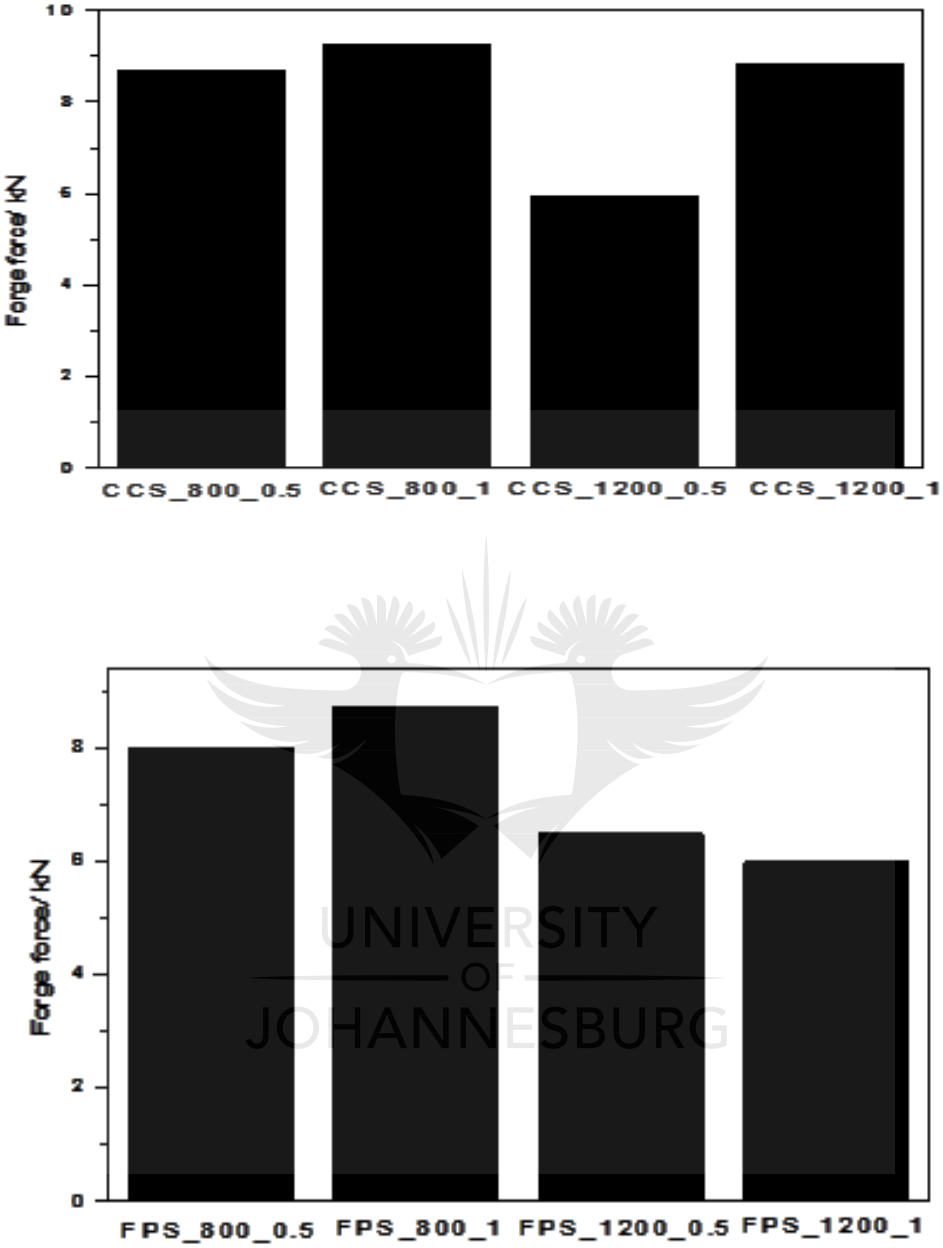

Figure 4-2 Maximum forge forces obtained for the different spot welds produced

It was noticed that the maximum forge force obtained increases with an increase in the plunge depth, except for the spot welds produced using 1200 rpm and a flat pin and flat shoulder. This is a clear indication that the shoulder plunge depth affects the forge forces. This can be attributed to

the effect of the tool pin depth in the copper plate (bottom plate), which has different properties compared to the top plate (aluminium). The maximum forge forces measured are the range between 5.24 and 9.26 kN; while the spot weld produced using a conical pin and a concave shoulder tool required higher forge forces than those produced with a flat pin and flat shoulder tool. The highest forge force of 9.26 kN was obtained with the conical pin and the concave shoulder tool at 800 rpm and a shoulder plunge depth of 1 mm.

4.3 Heat input analyses during friction stir spot welds of copper and aluminium

The torque was measured for all the welds produced, using different process parameters and tool geometries to enable the calculation of the energy heat input. The equation 2.1 was used to calculate the energy heat input. Figure 4-3 shows the torques variation and their fit for the spot weld produced at 800 rpm, 0.5 shoulder plunge depth using a flat pin and flat shoulder (a) and a conical pin and concave shoulder (b). Furthermore, Figure 4.4 depicts the corresponding residuals of the torques for the friction stir spot welds mentioned in Figure 4.3. The rest of the torque curves and their corresponding fits and the residuals can be found in Appendix H.

A Matlab 2014 software program was used to calculate the energy heat input. The equation below was generated using Matlab; and the energy heat input was then calculated.

T (t)= a0 + a1*cos(t*w) + b1*sin(t*w) + a2*cos(2*t*w) + b2*sin(2*t*w) + a3*cos(3*t*w) + b3*sin(3*t*w) + a4*cos(4*t*w) + b4*sin(4*t*w) + a5*cos(5*t*w) + b5*sin(5*t*w) + a6*cos(6*t*w) + b6*sin(6*t*w) + a7*cos(7*t*w) + b7*sin(7*t*w) + a8*cos(8*t*w) + b8*sin(8*t*w) 4.1

The Equation 4.1 was subtracted from Equation 2.1; and the integral (Equation 2.1) was then solved. A similar trend was observed with the forge force curves discussed in the previous section (4.2). This was also seen with the variations in the torque values.

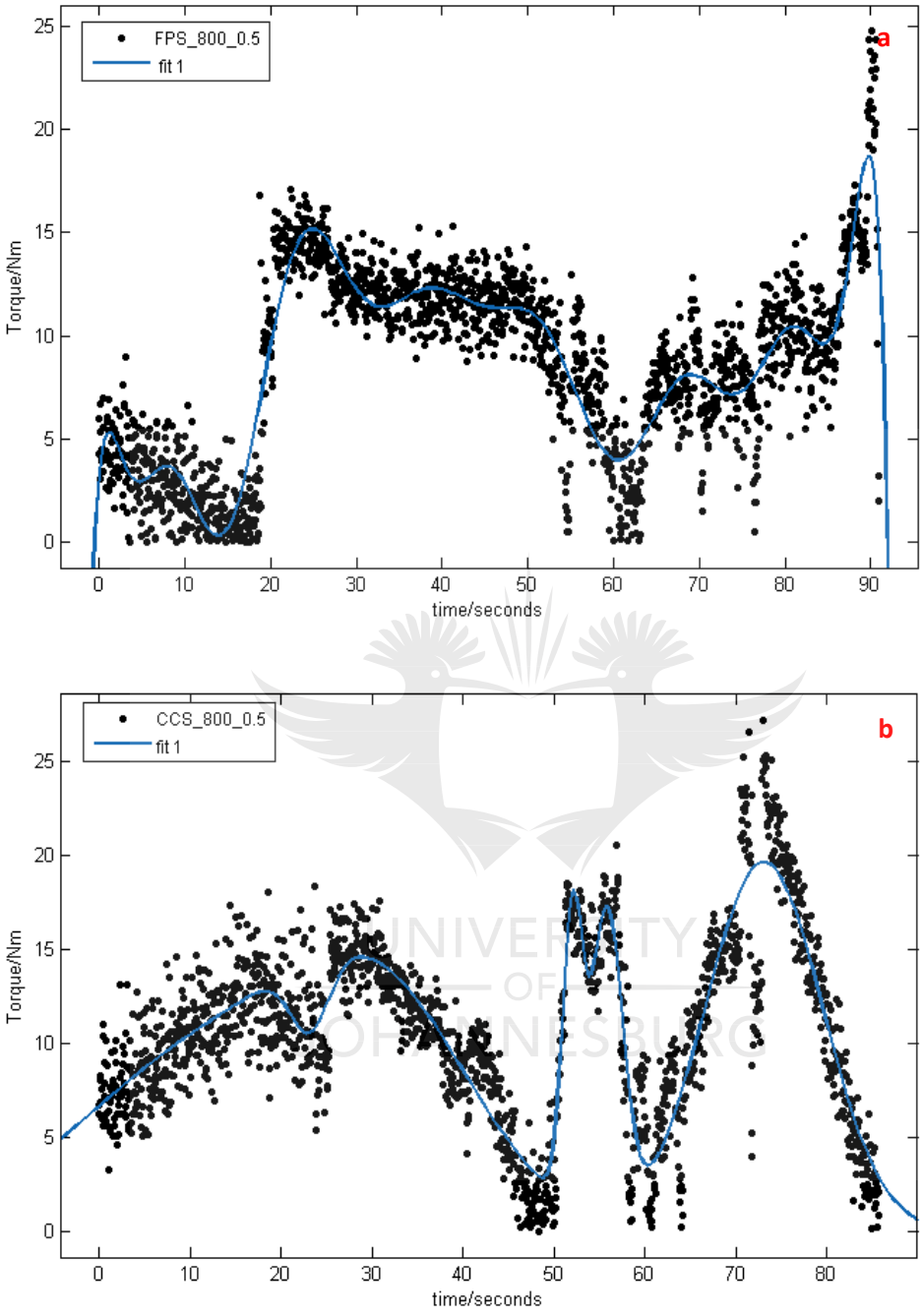

Figure 4-3 Torque variation versus time for the spot weld produced at 800 rpm, 0.5 shoulder plunge depth using a flat pin and flat shoulder tool (a) and a conical pin and concave shoulder (b)

It was observed that the torque increases with the variation of the shoulder plunge depth, except for the spot weld produced at 1200 rpm when using a flat pin and a flat shoulder tool. This was also observed on the maximum forge force presented in the previous section (4.2). The maximum recorded torques varied between 24.36 and 28.01 Nm for the spot weld produced at 800 rpm, 0.5 shoulder plunge depth and 800 rpm, 1 mm shoulder plunge depth using a flat pin/flat shoulder and conical pin and concave shoulder, respectively.

Furthermore, the residuals versus the fit value graphs of the torque generated for the samples produced at 800 rpm, 0.5 mm shoulder plunge depth using a flat pin/flat shoulder and conical pin and concave shoulder are shown in Figures 4-4 (a) and (b).

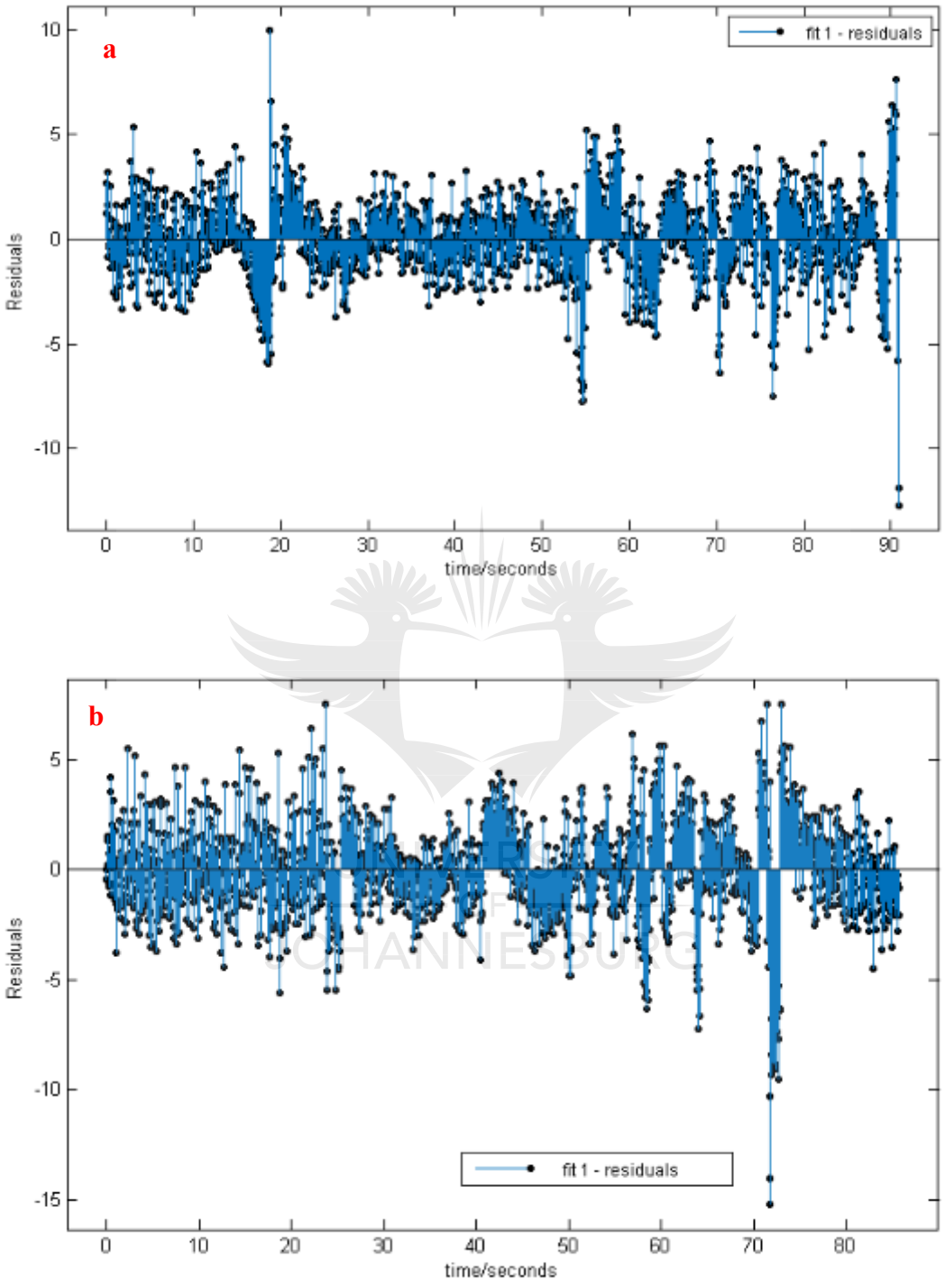

Figure 4-4 Corresponding residuals for the torque variation versus time for the spot weld produced at 800 rpm, 0.5 shoulder plunge depth using a flat pin and flat shoulder tool (a) and a conical pin and concave shoulder (b)

The residuals are approximations of the experimental error obtained by subtracting the observed responses from the predicted responses; and their constant changes, as depicted in the graphs, show their adequacy to predict the values of the torques in an acceptable way. It can be seen that there are fluctuations in all the residuals values. The R^2 and adjusted R^2values of the torques are depicted in Tables 4.3 and 4.4. It can be seen that the R^2 and adjusted R^2values of the torques are in the range of 80% for most of the produced spot welds, which shows a good correlation between the predicted values and the observed values. The calculated weld energy heat inputs are also presented in Table 4.5 and Table 4.6. The lowest and highest weld energy heat input of 45939 and 112770 J were obtained respectively for the spot welds produced at 800 rpm, 0.5 mm shoulder plunge depth and 1200 rpm, 0.5 mm shoulder plunge depth both using a flat pin and flat shoulder tool. The weld energy heat input varies with the variation of all the parameters.

Table 4.3: R^2 and adjusted R^2 of the torques for the welds produced using different process parameters and a flat pin and flat shoulder tool

Rotational speed (rpm)	Shoulder plunge depth (mm)	R^2	R^2 adjusted
800	0.5	0.8151	0.8133
800	0.5	0.7051	0.7011
800	0.5	0.8369	0.8341
800	1	0.8649	0.8629
800	1	0.7084	0.705
800	1	0.8003	0.7966
1200	0.5	0.7841	0.7815
1200	0.5	0.8732	0.8717
1200	0.5	0.8682	0.8666
1200	1	0.8037	0.8016
1200	1	0.8697	0.8683
1200	1	0.871	0.8696

Table 4.4: R^2 and adjusted R^2 of the torques for the welds produced using different process parameters and a conical pin and concave shoulder tool

Rotational speed (rpm)	Shoulder plunge depth (mm)	R^2	R^2 adjusted
800	0.5	0.7902	0.7881
800	0.5	0.8231	0.8203
800	0.5	0.7987	0.7962
800	1	0.8196	0.8172
800	1	0.7885	0.785
800	1	0.8399	0.8369
1200	0.5	0.7342	0.7311
1200	0.5	0.8528	0.851
1200	0.5	0.8304	0.828
1200	1	0.855	0.8529
1200	1	0.8589	0.8566
1200	1	0.8117	0.8083

Table 4.5: Maximum torque and weld energy heat input generated during FSSW between Al/Cu using a flat pin and flat shoulder

Rotational speed (rpm)	Shoulder plunge depth (mm)	Max torque (Nm)	Weld energy heat input (J)
800	0.5	24.36	45939
800	0.5	25.12	66852
800	0.5	25.09	56869
800	1	27.05	62645
800	1	26.58	68896
800	1	26.19	64974
1200	0.5	25.60	98016
1200	0.5	26.97	112770
1200	0.5	25.58	97862
1200	1	25.15	97733
1200	1	24.97	100430
1200	1	25.37	95362

Table 4.6: Maximum torque and weld energy heat input generated during FSSW between Al/Cu using a conical pin and concave shoulder

Rotational speed (rpm)	Shoulder plunge depth (mm)	Max torque (Nm)	Weld energy heat input (J)
800	0.5	27.17	77951
800	0.5	26.68	56580
800	0.5	25.60	79544
800	1	28.01	62873
800	1	27	62240
800	1	24.69	53422
1200	0.5	25.21	80134
1200	0.5	25.85	90539
1200	0.5	25.98	96148
1200	1	26.4	111080
1200	1	27.46	91911
1200	1	25.50	78561

Figure 4-5 presents the maximum recorded torques values using different process parameters and tool geometries. It was observed that the maximum torques increase with the increase of the shoulder plunge depth of the tool, except for the spot weld produced at 1200 rpm using a flat pin and flat shoulder tool, where a decrease was observed. Higher torques values were observed for the spot welds produced using a conical pin and concave shoulder tool compared to the welds produced using a flat pin and a flat shoulder tool.

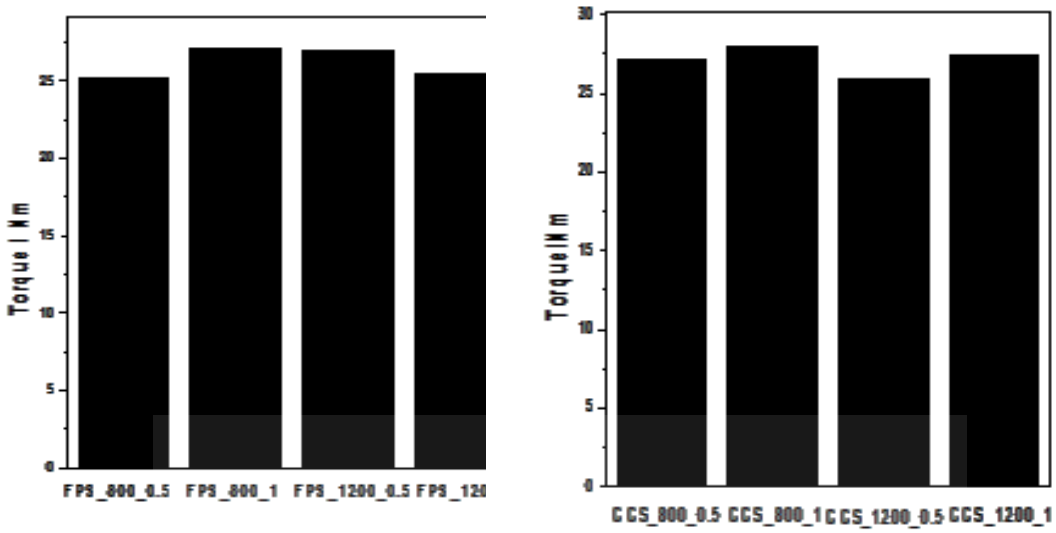

Figure 4-5 Maximum torques recorded for the different welds

4.4 Microstructural evolution

Figure 4-6 shows the top and the bottom of the spot welds produced at different process parameters and using different tool geometries.

Figure 4-6 Spot welds produced using different process parameters and tool geometries

Figure 4-7 and Figure 4-8 show the macroscopic appearances of the cross-section of the welds produced using different process parameters and the different tools geometries employed.

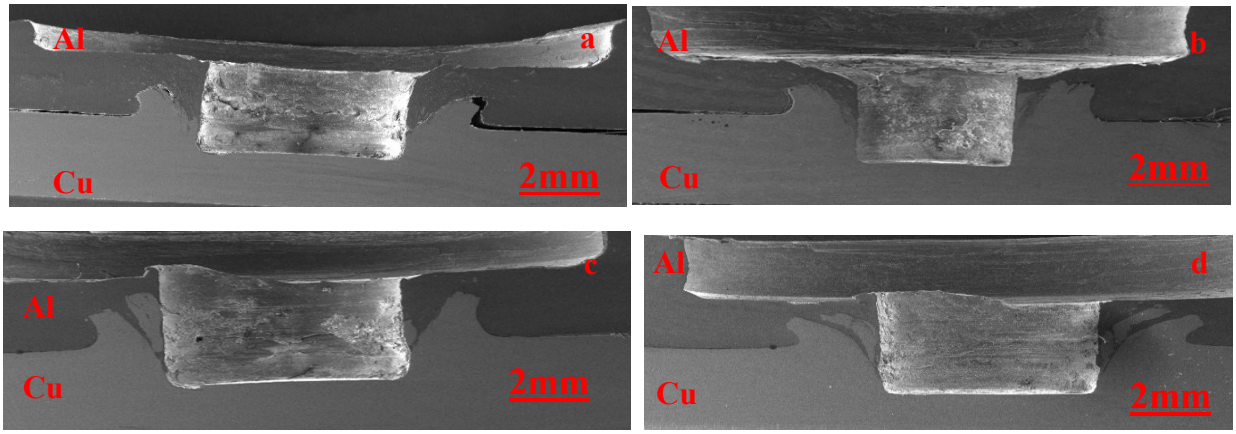

Figure 4-7 Micrographs of the cross sections of friction stir spot welds produced by using a flat pin and shoulder tool (a: FPS_800_0.5, b: FPS_800_1, c: FPS_1200_0.5 and d: FPS_1200_1)

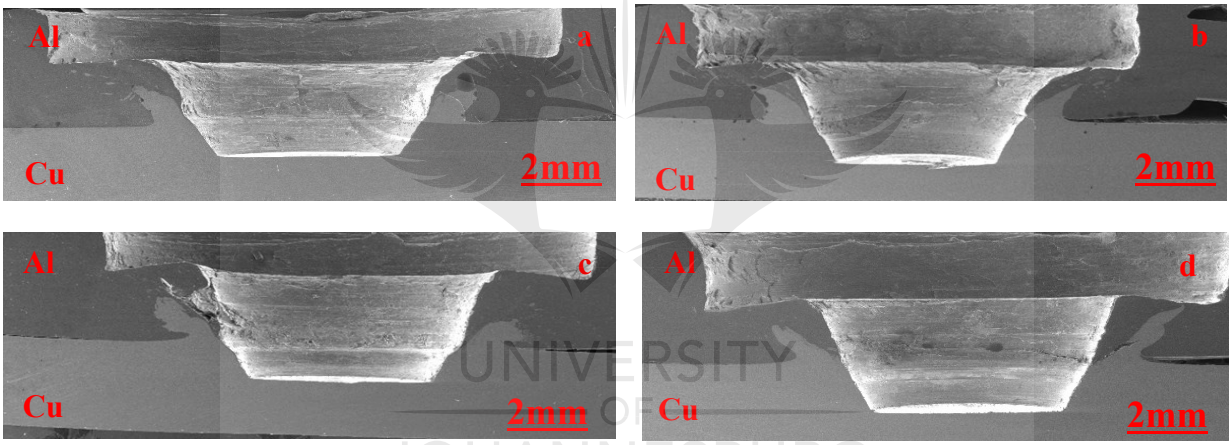

Figure 4-8 Micrographs of the cross sections of friction stir spot welds produced by using a flat pin and shoulder tool (a: CCS_800_0.5, b: CCS_800_1, c: CCS_1200_0.5 and d: CCS_1200_1)

It was observed in Figures 4-7 and 4-8, that the shapes of the pin and the shoulder in the cross sections of the produced spot welds, namely flat pin/flat shoulder and conical pin/concave shoulder, were visible.

The colour contrast between the two plates welded, namely: aluminium and copper could be seen; and the copper sheet has a lighter colour than the aluminium. The presence of a keyhole was also observed; and on both sides of the welds, there was a presence of copper rings [8] also known as hooks [31], which are a deformed part of the copper material (lower sheet) penetrating into the aluminium (top sheet). This was in agreement with the results obtained by Ozdemir *et al.* [9].

Figures 4-9 and 4-10 show the copper rings and the corresponding lengths, which were measured using the scanning electron microscope measuring tool, as presented in Figures 4-9 and 4-10.

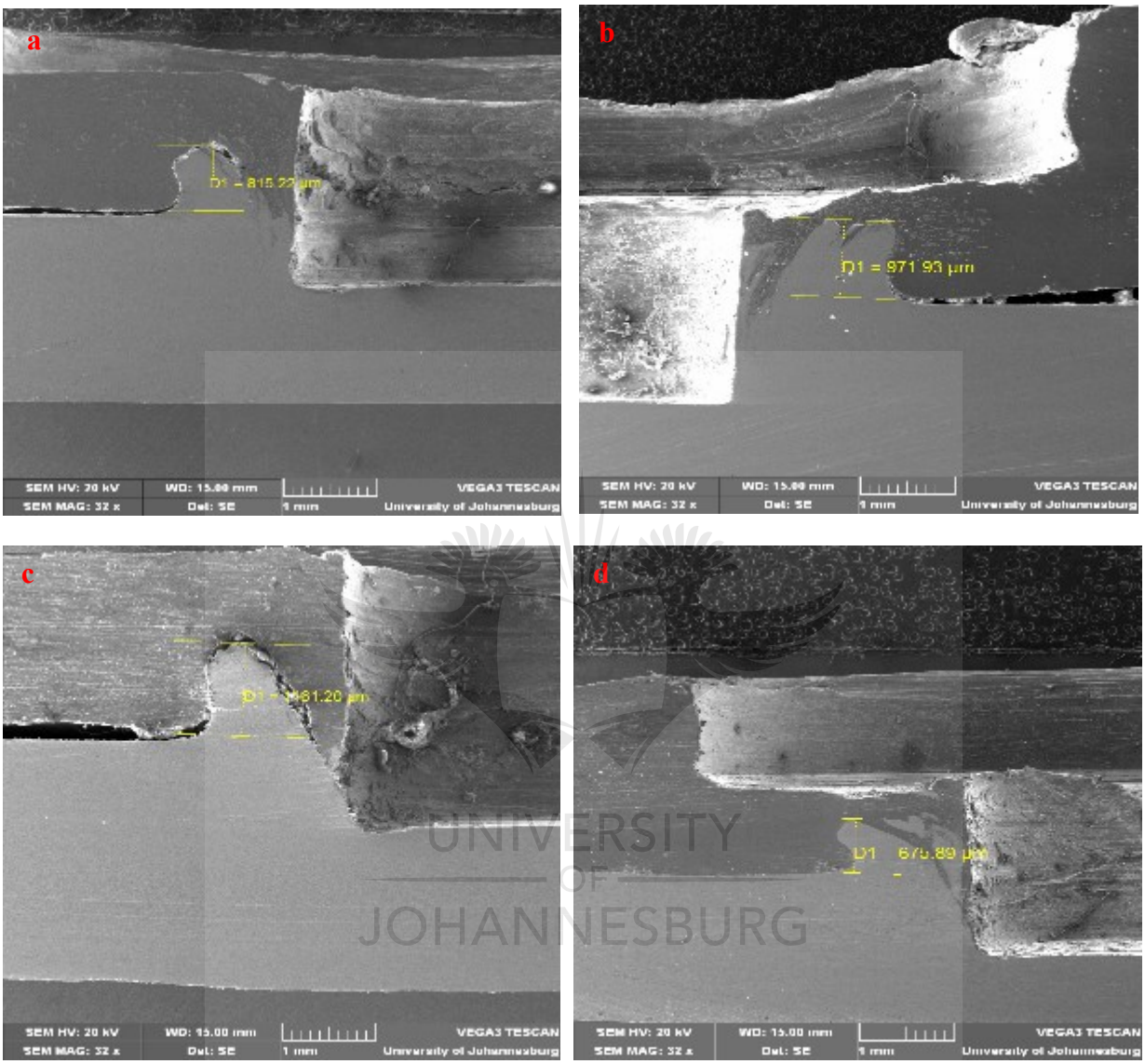

Figure 4-9 Copper ring length of the spot weld produced: (a) 800 rpm, 0.5 mm, (b) 800 rpm, 1 mm , (c) 1200 rpm, 0.5 mm and (d) 1200 rpm, 1mm using flat pin and shoulder tool

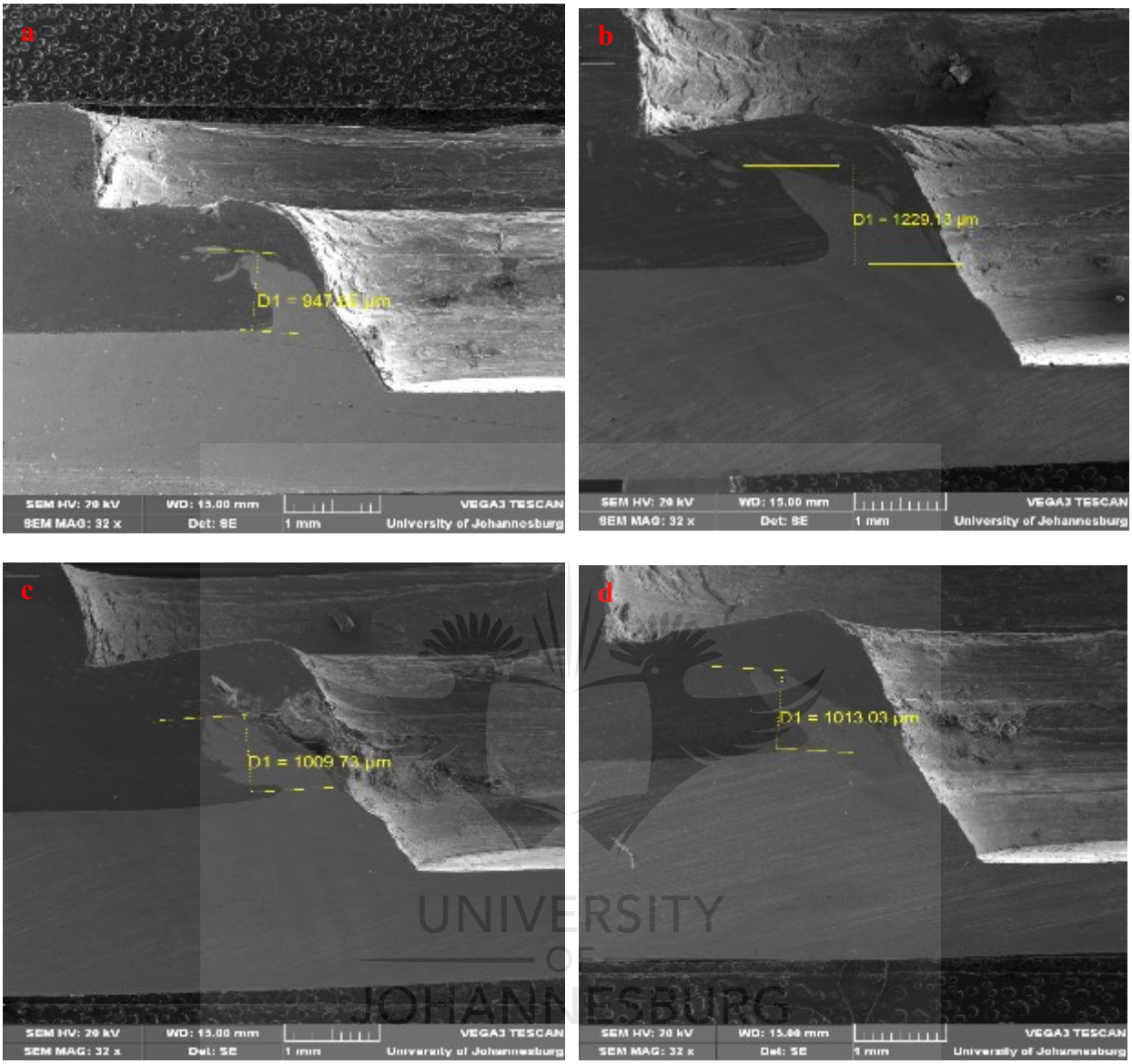

Figure 4-10 Copper ring length of the spot weld produced: (a) 800 rpm, 0.5 mm, (b) 800 rpm, 1 mm , (c) 1200 rpm, 0.5 mm and (d) 1200 rpm, 1mm using a conical pin and concave shoulder tool

The presence of the copper ring was also observed by Heideman *et al.* [8] with different lengths in all the spot welds. The copper ring lengths of the spot welds produced at different process parameters using a flat pin / flat shoulder and conical pin a/ concave shoulder, are depicted in Figures 4-9 and 4-10. The formation of the copper rings, which consists of the copper parent material extruded in the aluminium plate, was observed in the current study. This suggests that while the copper material was moving and diffusing into the aluminium, the aluminium was not

diffusing or being pushed into the copper ring [8]. There was also a reduction in the workpiece thicknesses in all the produced spot welds. Ozdemir *et al.* [9] observed that the penetration length of the copper into the aluminium was about half of the thickness of the aluminium sheet; but this was not the case in the current study.

In our study, the penetration length of the copper into the aluminium was also studied. The formed copper rings were measured; and results are shown in Figures 4-11 and 4-12 for the flat pin / shoulder and the conical pin and concave shoulder, respectively.

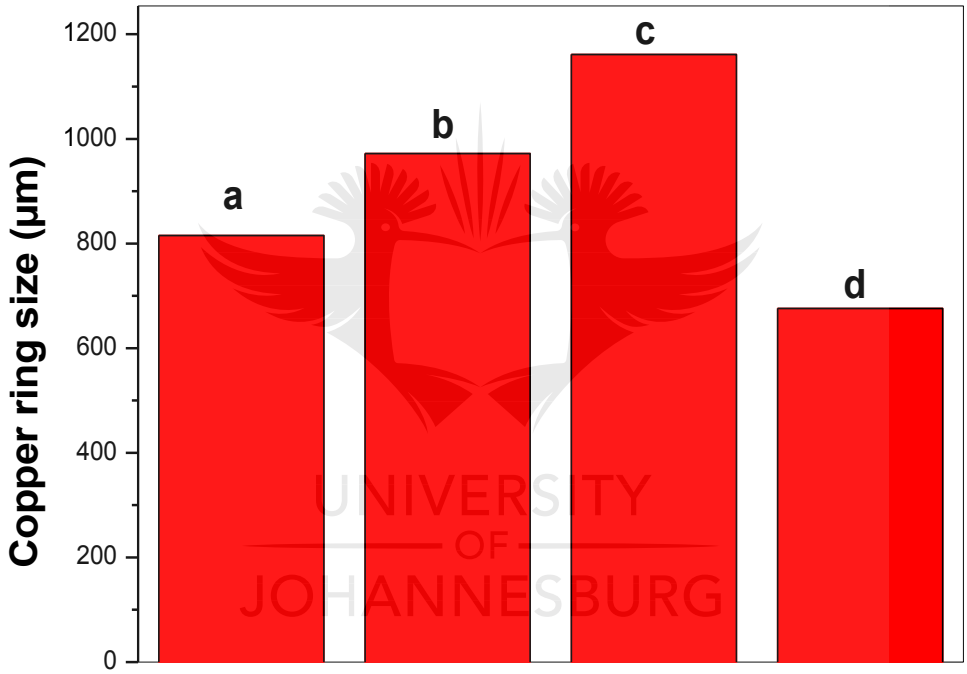

Figure 4-11 The copper ring lengths obtained using a flat pin and concave shoulder tool at different process parameters, a (FPS_800_0.5), b (FPS_800_1), c (FPS_1200_0.5) and d (FPS_1200_1)

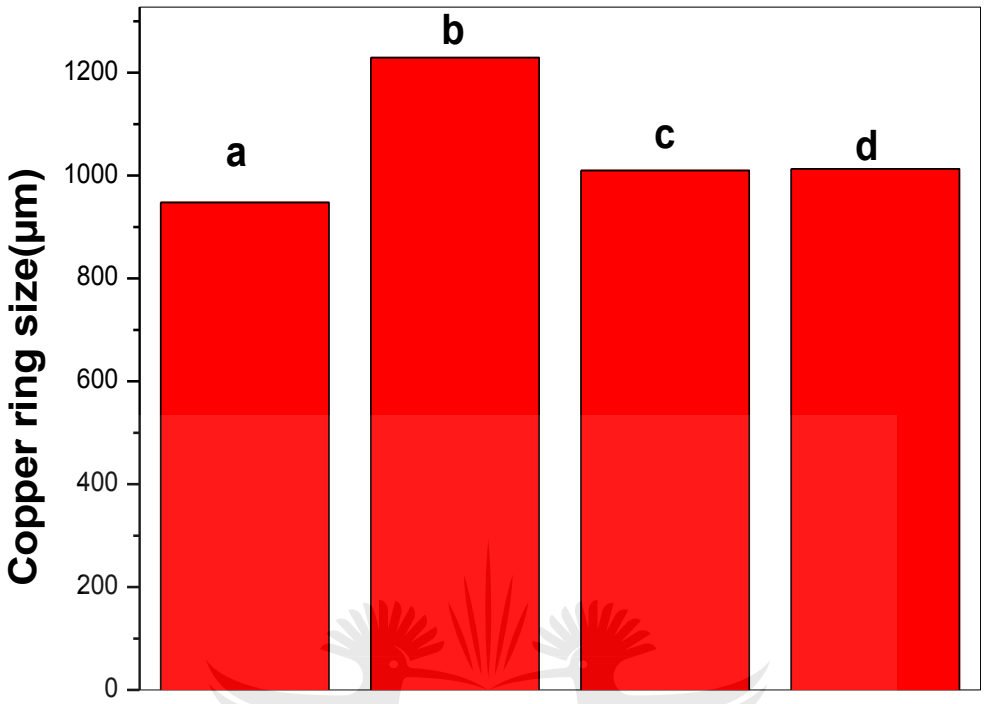

Figure 4-12 The copper ring (hook) lengths obtained using a conical pin and concave shoulder tool at different process parameters, a (CCS_800_0.5), b (CCS_800-1), c (CCS_1200_0.5). d (CCS_1200_1)

It was observed that the copper ring length increases with the increase of the shoulder plunge depth, expect for the spot welds produced at 1200 rpm, using a flat pin and shoulder, where a decrease was observed. The copper ring lengths of the welds produced at 1200 rpm using a conical pin and concave shoulder also show a slight difference in the copper ring length. This shows that the welds produced at high rotational speed exhibit either a decrease or a slight increment in the copper ring length. It has been reported that, the copper ring caused interlocking between the two plates and help the plates adhere to each other during tensile testing and reach a high strength before failure [8].

The energy dispersive spectroscopy (EDS) mapping of a region of the keyhole and the copper ring area was conducted. Figures 4-13 to 4-16 show the EDS mapping of the spot welds produced at different process parameters, including the rotational speed and the shoulder plunge depth using a

flat pin /flat shoulder. The distribution of copper (red) and aluminium (black) can be seen from Figures 4-13 to 4-16.

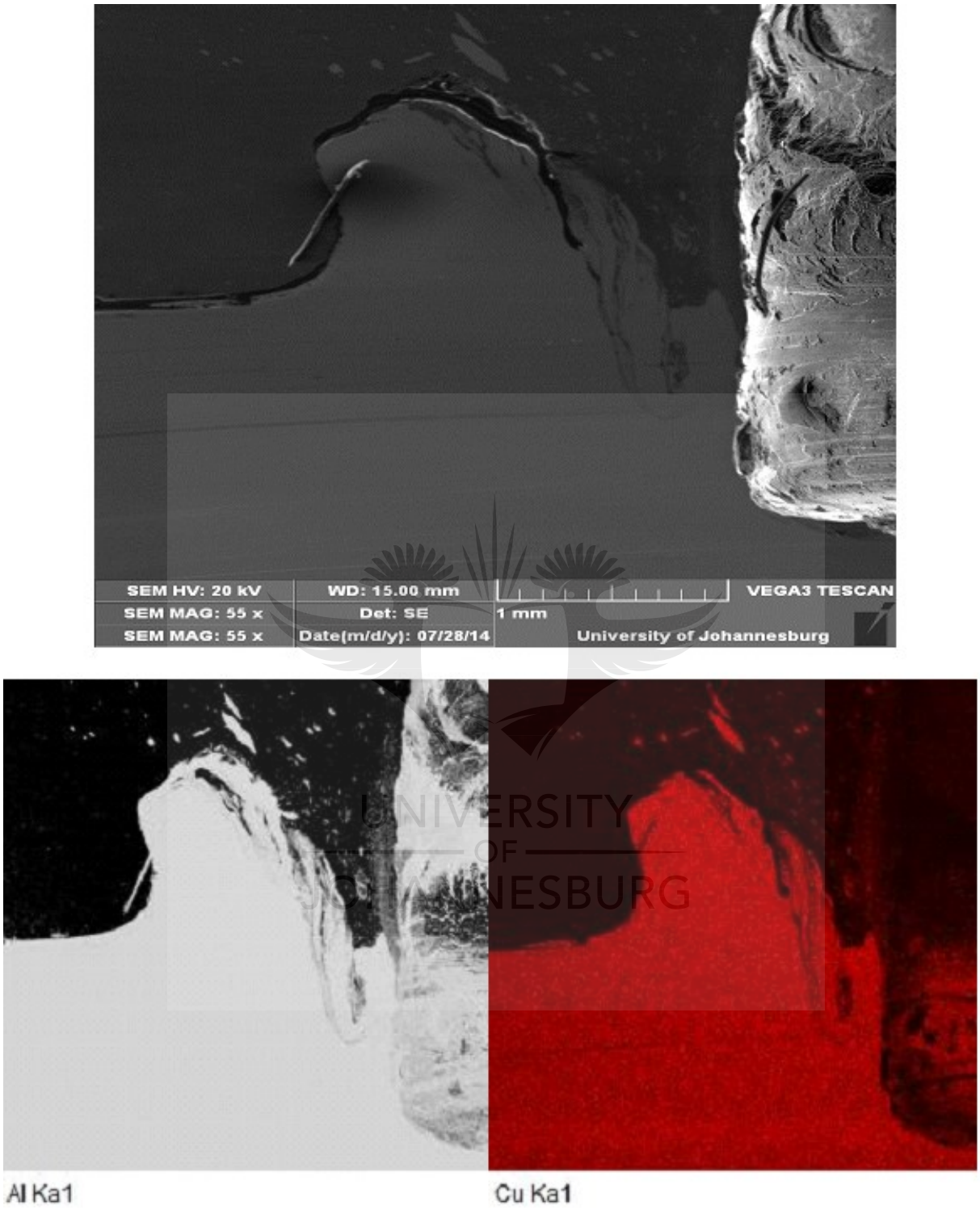

Figure 4-13 Mapping of spot weld produced using a flat pin and a flat shoulder tool at 800 rpm and 0.5 mm shoulder plunge depth, copper (red), aluminium (black)

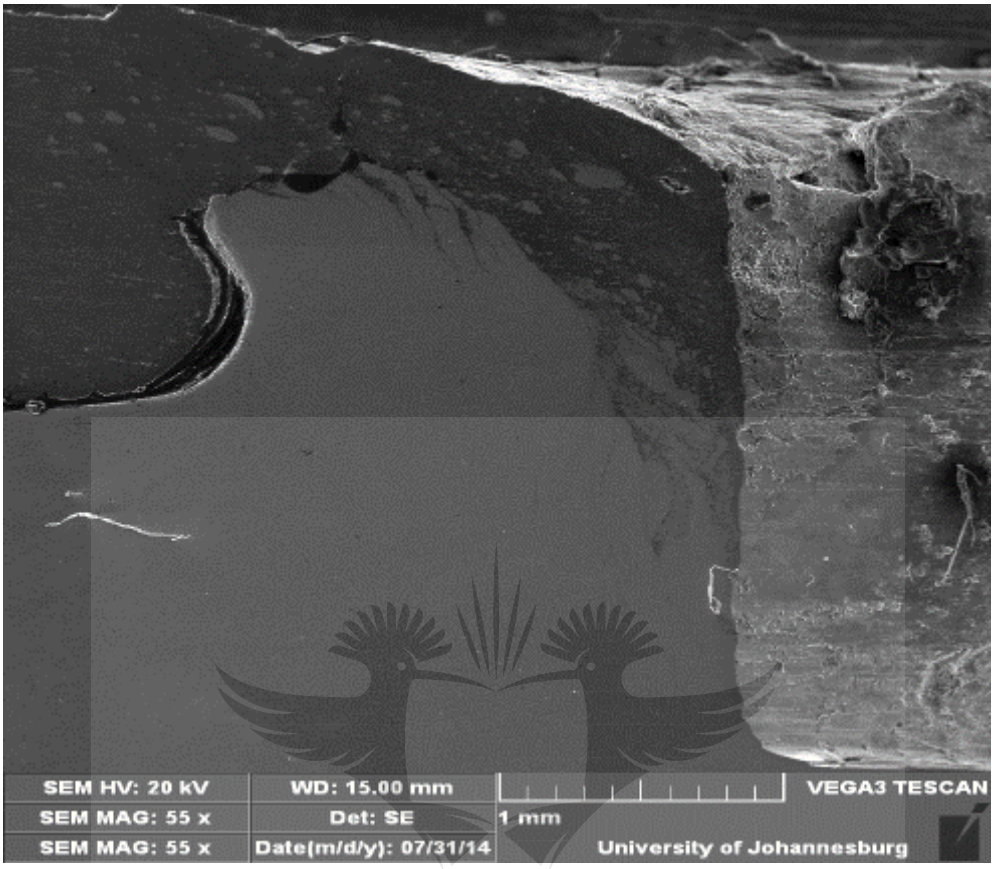

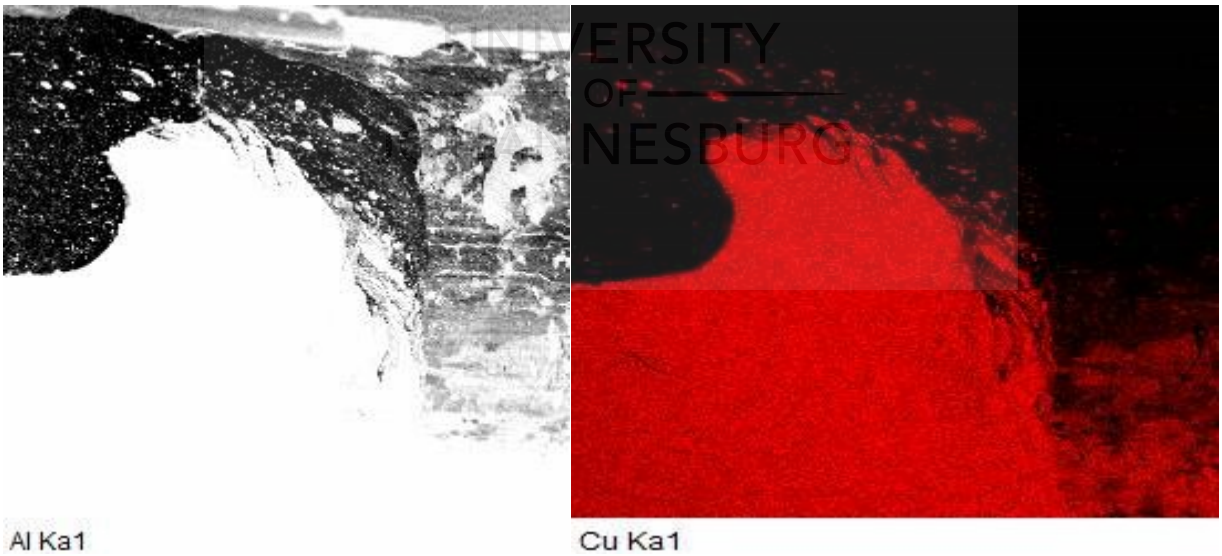

Figure 4-14 Mapping of spot weld produced using a flat pin and a flat shoulder tool at 800 rpm and 1 mm shoulder plunge depth, copper (red), aluminium (black)

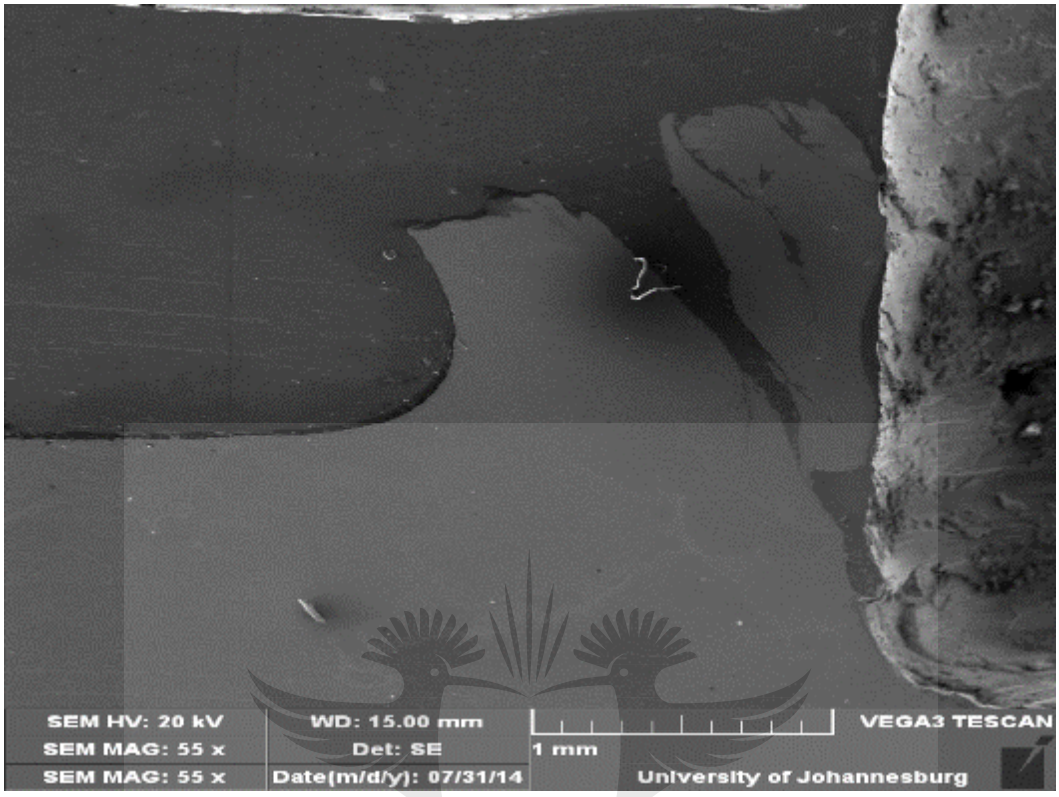

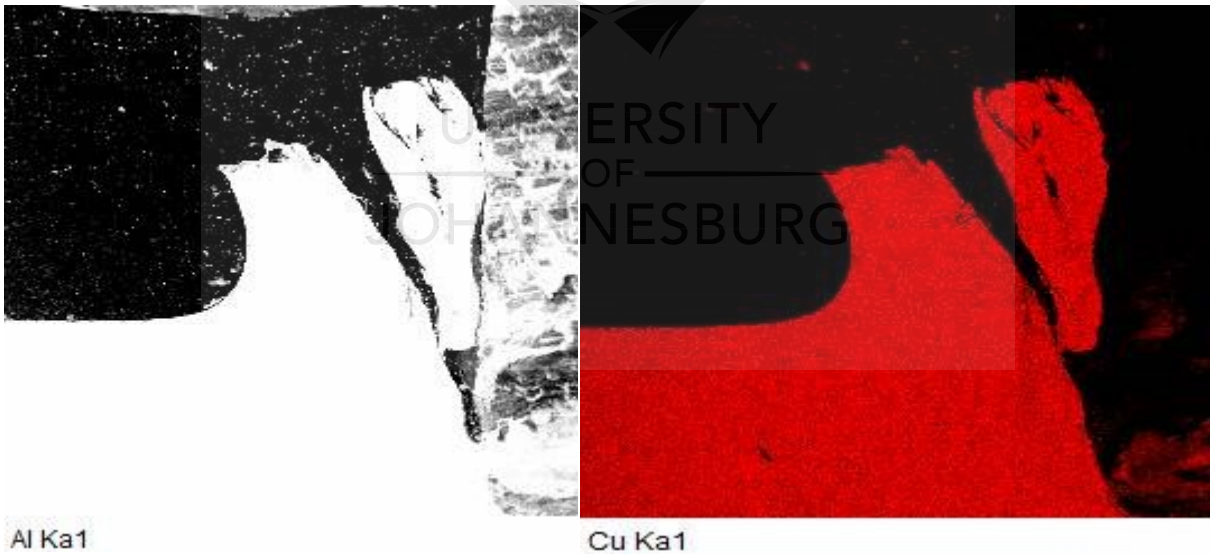

Figure 4-15 Mapping of spot weld produced using a flat pin and a flat shoulder tool at 1200 rpm and 0.5 mm shoulder plunge depth, copper (red), aluminium (black)

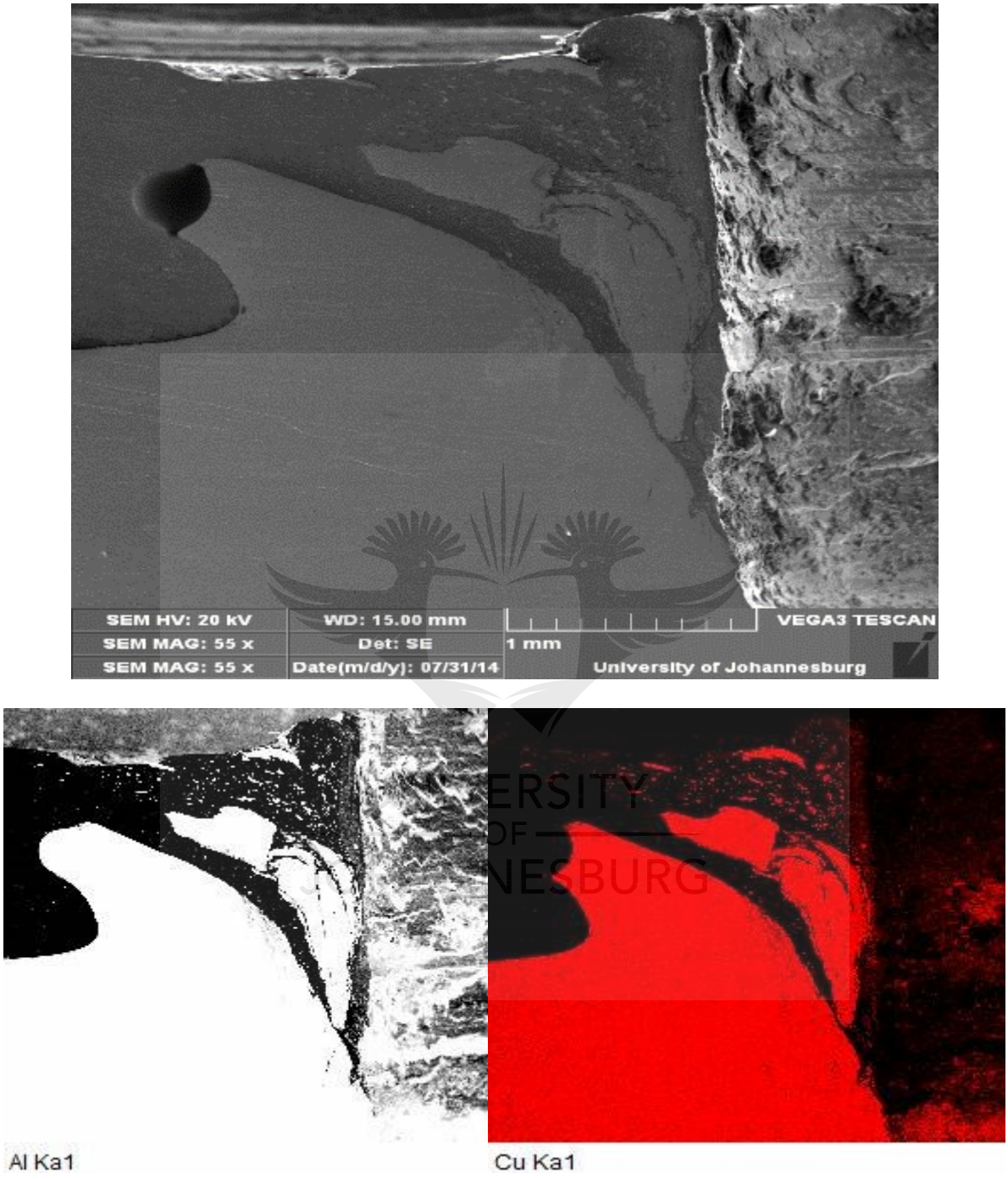

Figure 4-16 Mapping of spot weld produced using a flat pin and a flat shoulder tool at 1200 rpm and 1 mm shoulder plunge depth, copper (red), aluminium (black)

It was observed that there is a presence of copper particles and fragments in the aluminium matrix; but there was almost no presence of aluminium particles in the copper matrix. It was noticed in the EDS mapping of the spot welds produced at the rotational speed namely 800 rpm which was considered low in this current study; while at the two shoulder plunge depths, only the presence of a large deformed copper material (copper ring) with some small copper particles in its surroundings could be seen.

The EDS mapping of the welds produced at the rotational speed of 1200 rpm, which was considered to be high, and at both shoulder plunge depths, there was besides the presence of the copper ring another large piece of copper material next to the copper ring. This could be due to the effect of the rotational speed on the material flow, whereas at 1200 rpm, the copper rings were seen to be sectioned into two. This was observed by the change in the widths of the copper rings of the welds produced at 1200 rpm. This observation should be compared with the welds produced using a conical pin and a concave shoulder.

Additionally, it could be seen, from Figures 4-17 to 4-20, the EDS mapping of the spot weld produced at different process parameters using a conical pin and concave shoulder.

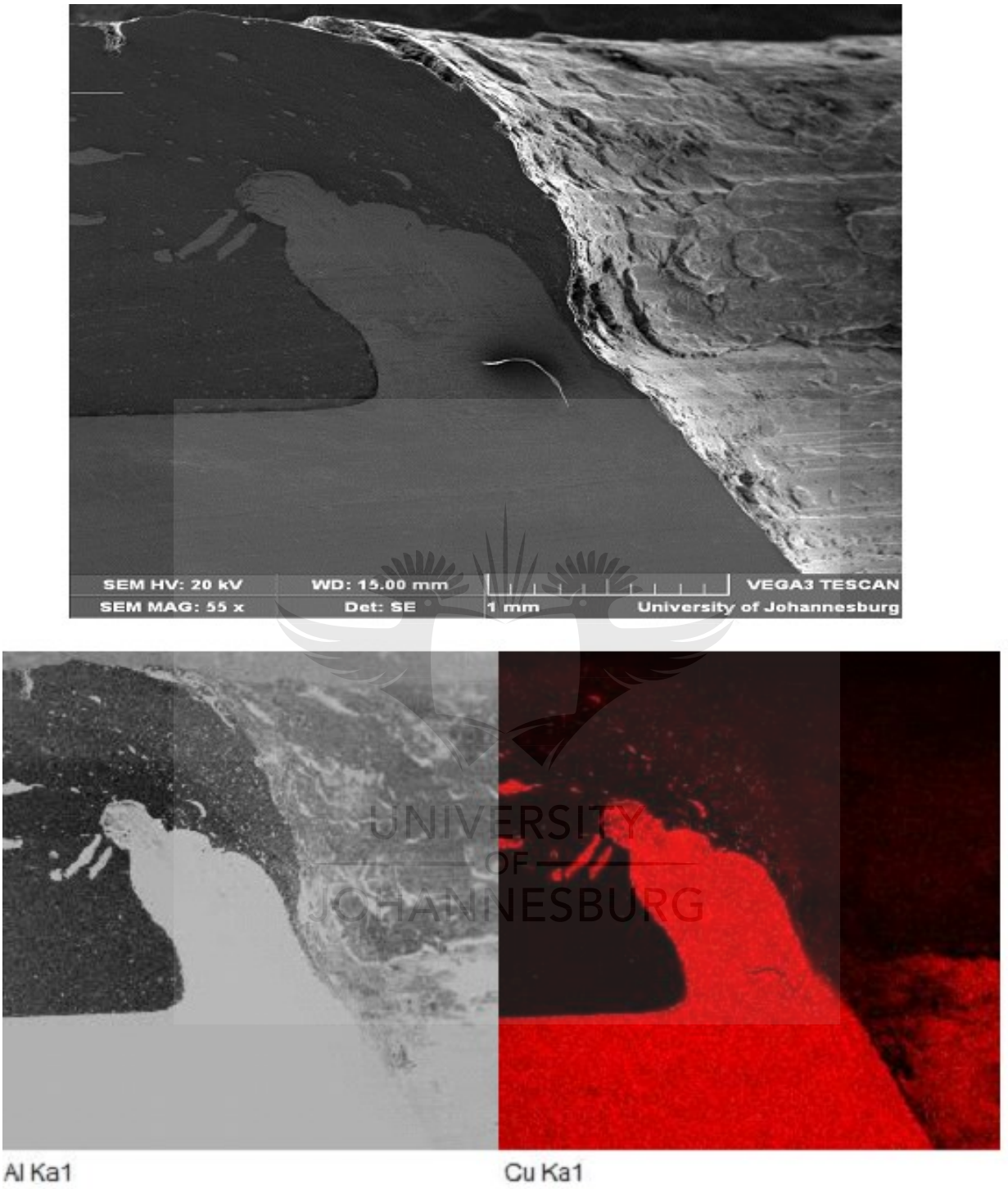

Figure 4-17 Mapping of spot weld produced using a conical pin and a concave shoulder tool at 800 rpm and 0.5 mm shoulder plunge depth, copper (red), aluminium (black)

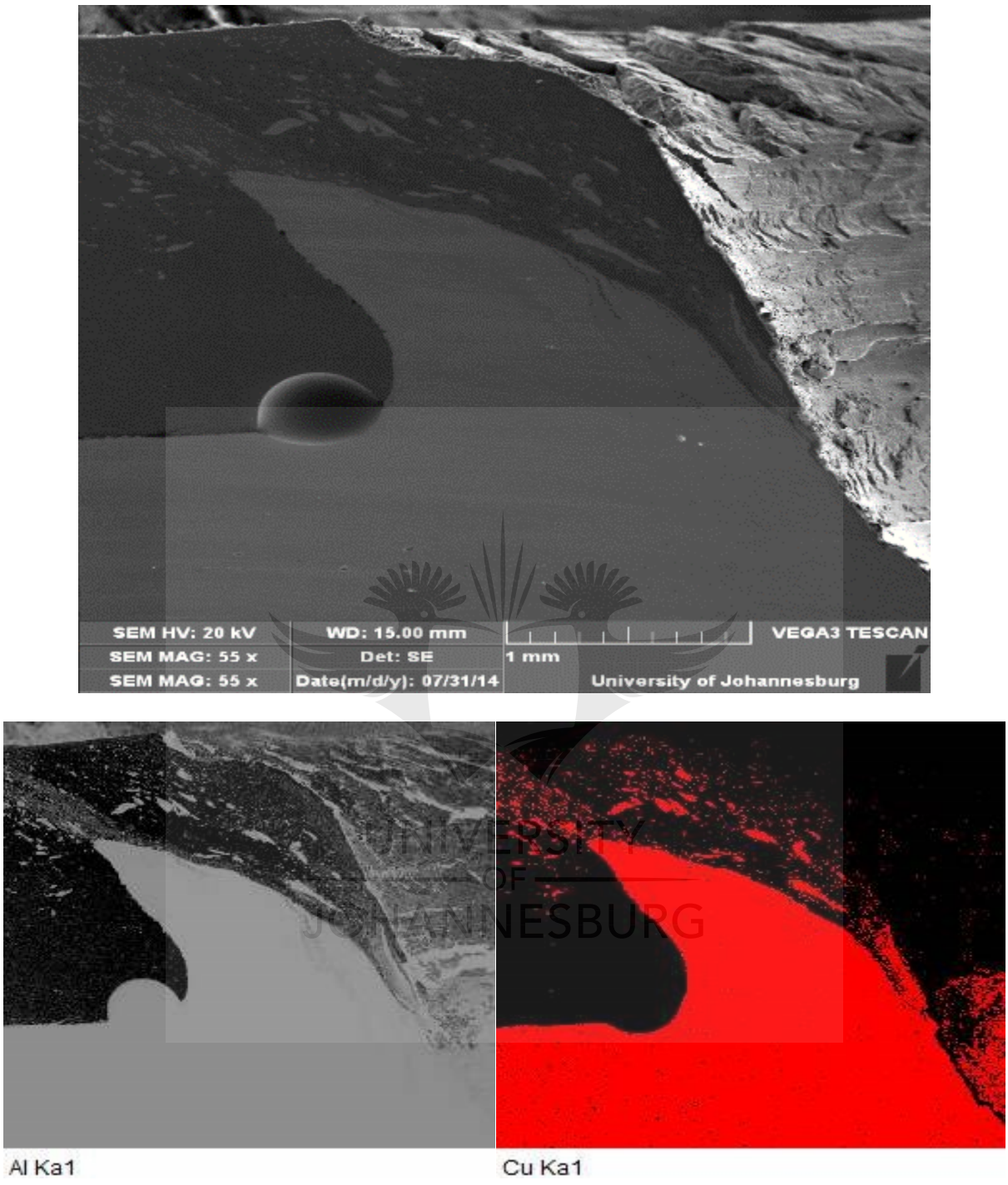

Figure 4-18 Mapping of spot weld produced using a conical pin and a concave shoulder tool at 800 rpm and 1 mm shoulder plunge depth, copper (red), aluminium (black)

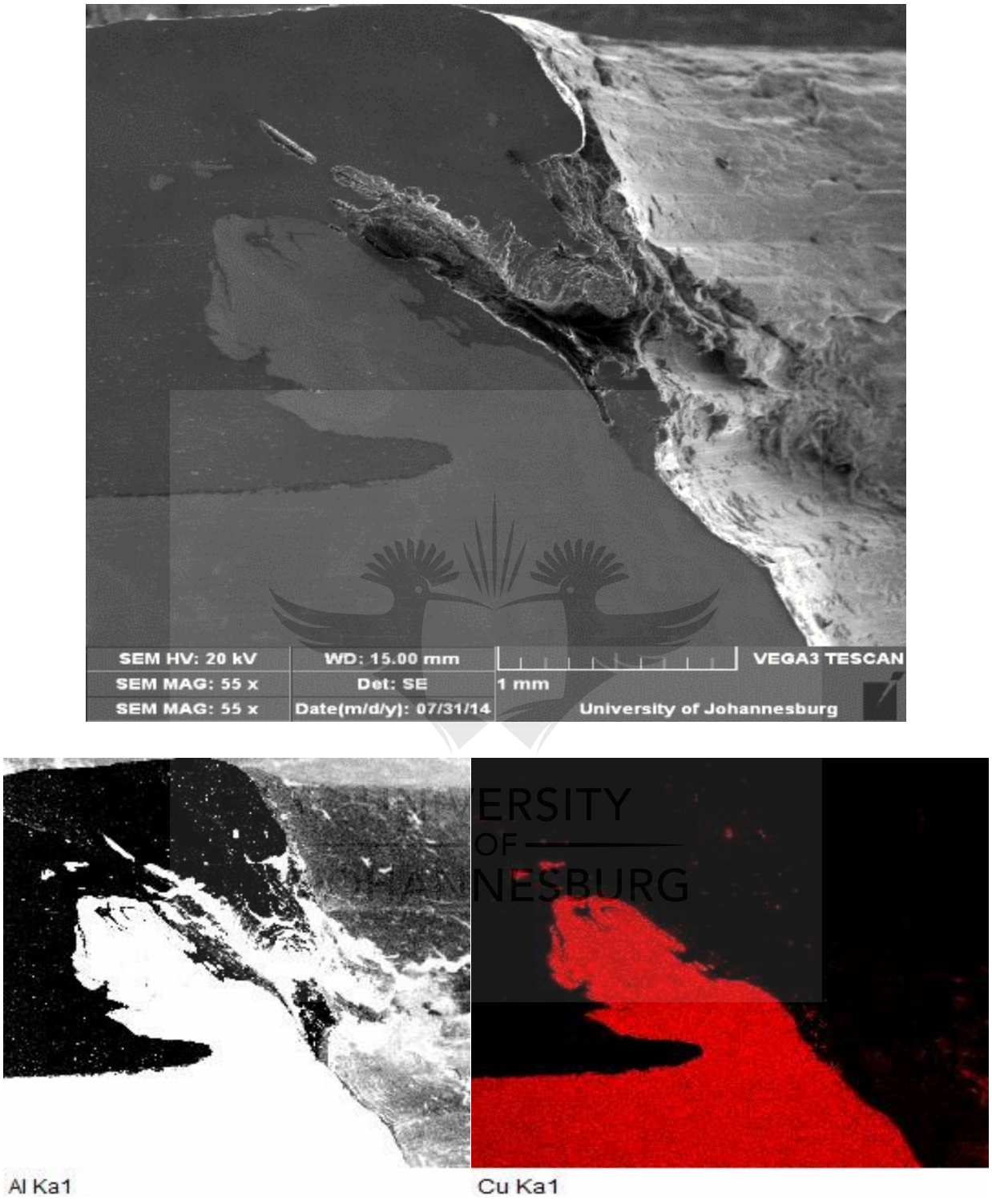

Figure 4-19 Mapping of spot weld produced using a conical pin and a concave shoulder tool at 1200 rpm and 0.5 mm shoulder plunge depth, copper (red), aluminium (black)

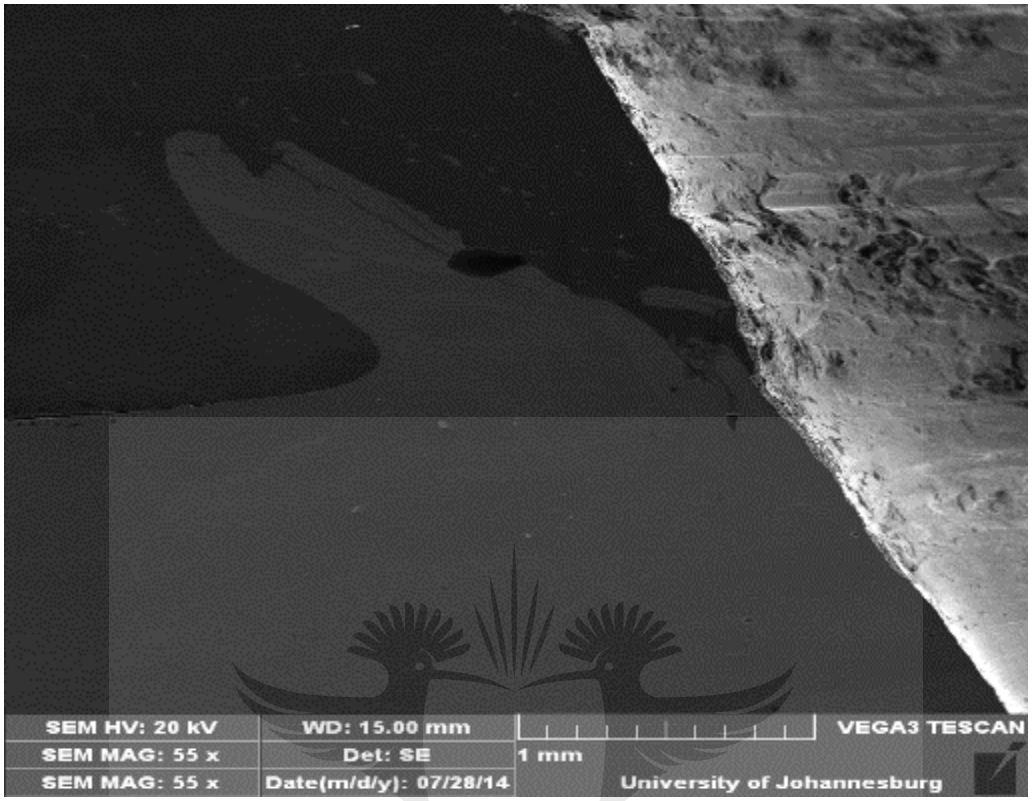

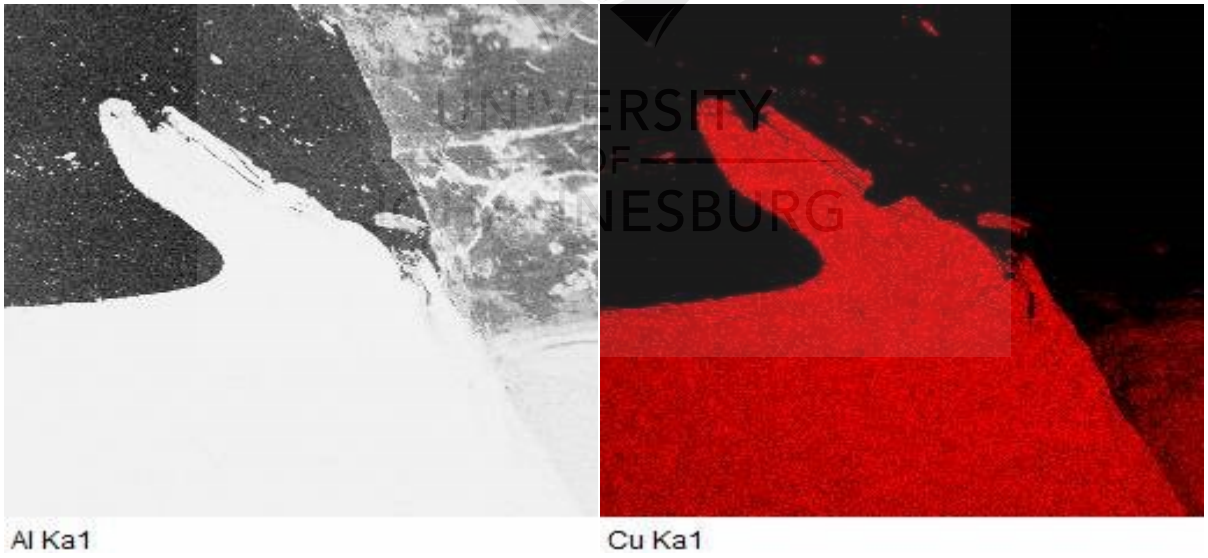

Figure 4-20 Mapping of a spot weld produced using a conical pin and a concave shoulder tool at 1200 rpm and 1 mm shoulder plunge depth, copper (red), aluminium (black)

The reduction of the widths of the copper rings was observed when the rotational speed increased. The presence of elongated small copper particles of different sizes can be seen from the EDS mapping of the welds produced when using a conical pin and concave shoulder tool. It was further observed that by increasing the rotational speed, the amount of small copper particles decreases.

Furthermore, the energy dispersive spectroscopy (EDS) mapping was also conducted for the SZ (stir zone) of the different welds. From Figures 4-21 to 4-23, one can see the EDS mapping of the SZ for the spot weld produced when using a flat pin and a flat shoulder.

Figure 4-21 shows the SZ mapping of the weld produced at 800 rpm, 0.5 mm shoulder plunge depth; while Figure 4-22 depicts the spot welds produced at 1200 rpm, 0.5 mm shoulder plunge depth. Moreover, Figure 4-23 shows the spot welds produced using 1200 rpm, and 1 mm shoulder plunge depth.

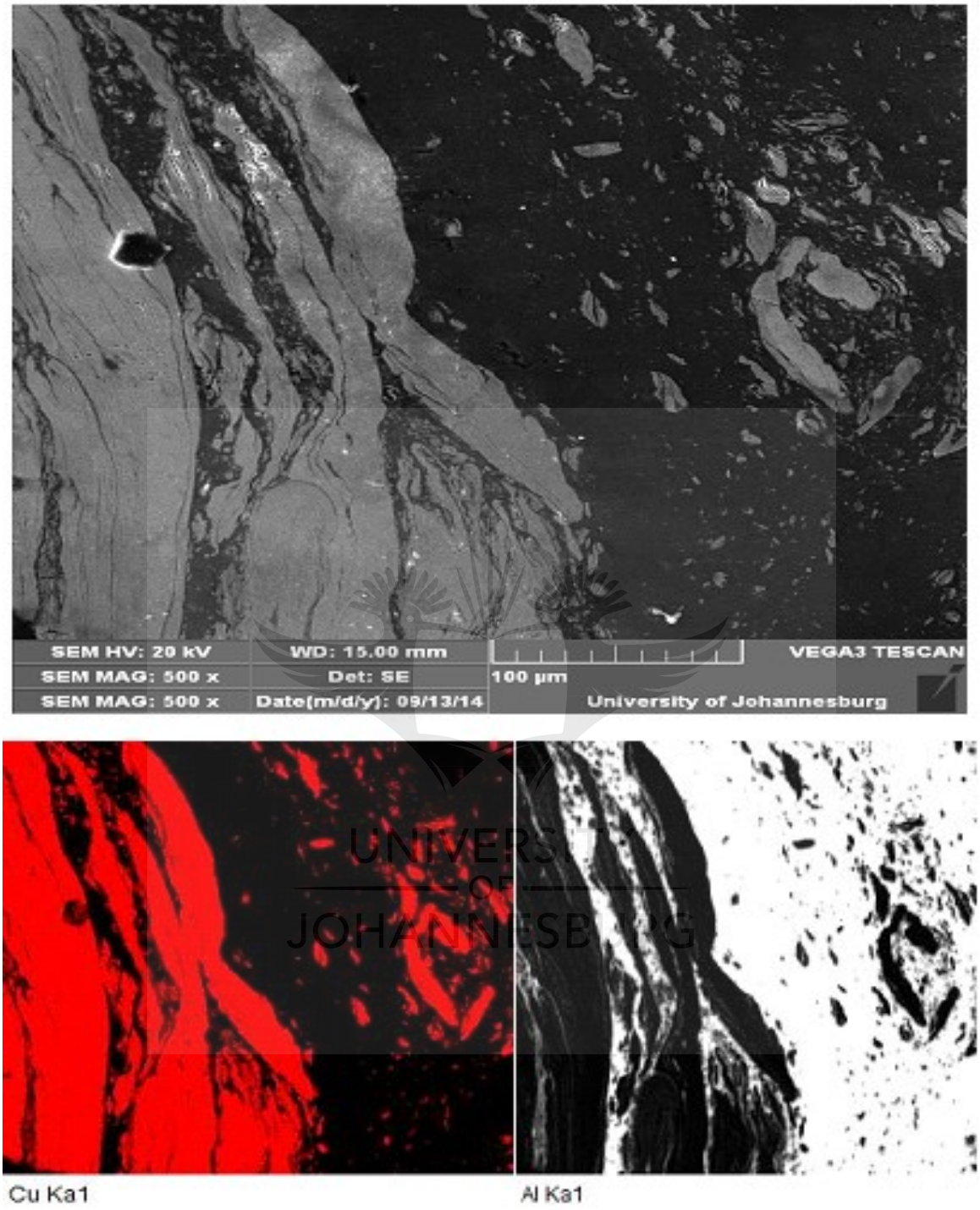

Figure 4-21 Mapping of the stir zone (SZ) for the spot weld produced using a flat pin and a flat shoulder tool at 800 rpm and 0.5 mm shoulder plunge depth, copper (red), aluminium (black)

Figure 4-22 Mapping of the stir zone (SZ) for the spot weld produced using a flat pin and a flat shoulder tool at 1200 rpm and 0.5 mm shoulder plunge depth, copper (red), aluminium (black)

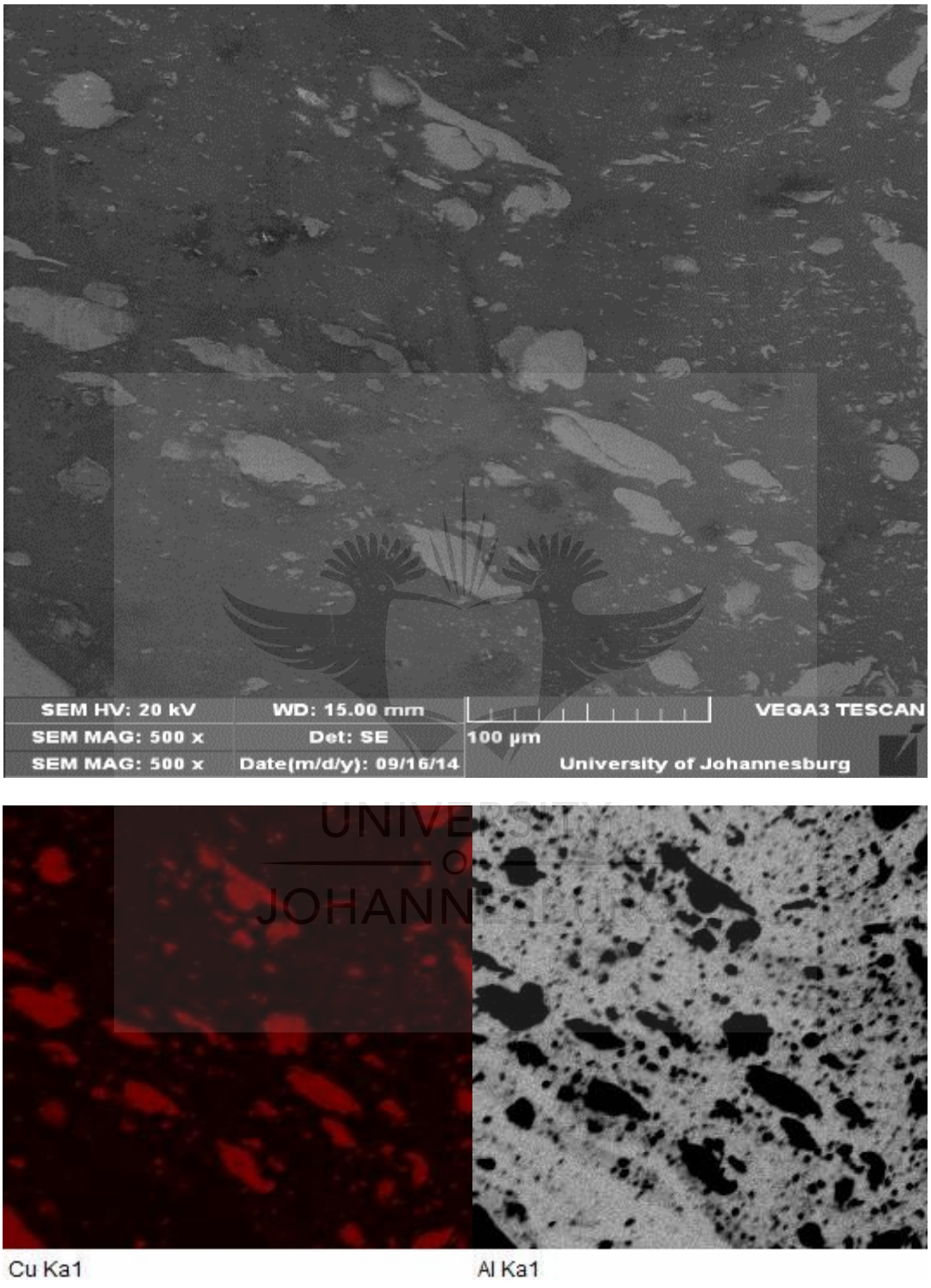

Figure 4-23 Mapping of the stir zone (SZ) for the spot weld produced using a flat pin and a flat shoulder tool at 1200 rpm and 1 mm shoulder plunge depth, copper (red), aluminium (black)

It can be observed that the element distribution shows a mixing of copper and aluminium, which was expected; since the SZ is in the vicinity of the keyhole, where the material is expected to move around the tool pin to produce good mixing of the materials. A large number of copper particles can be seen in the aluminium matrix (Figures 4-21 and 4-23) compared with the number of copper particles found in the aluminium matrix in Figure 4-22. The presence of the copper particles mixed in the aluminium matrix, and the aluminium particles mixed in the copper matrix could possibly favour the formation of hard and brittle intermetallic compounds (Figure 4-23). This will be analysed and discussed in the sections to follow.

Figure 4-24 shows the SZ mapping of the weld produced at 800 rpm, 0.5 mm shoulder plunge depth; whereas Figure 4-25 depicts the spot welds produced at 800 rpm, 1 mm shoulder plunge depth. Furthermore, Figures 4-26 and 4-27 show the spot welds produced using 1200 rpm, 0.5 mm shoulder plunge depth and 1200 rpm, 1 mm shoulder plunge depth, respectively**.**

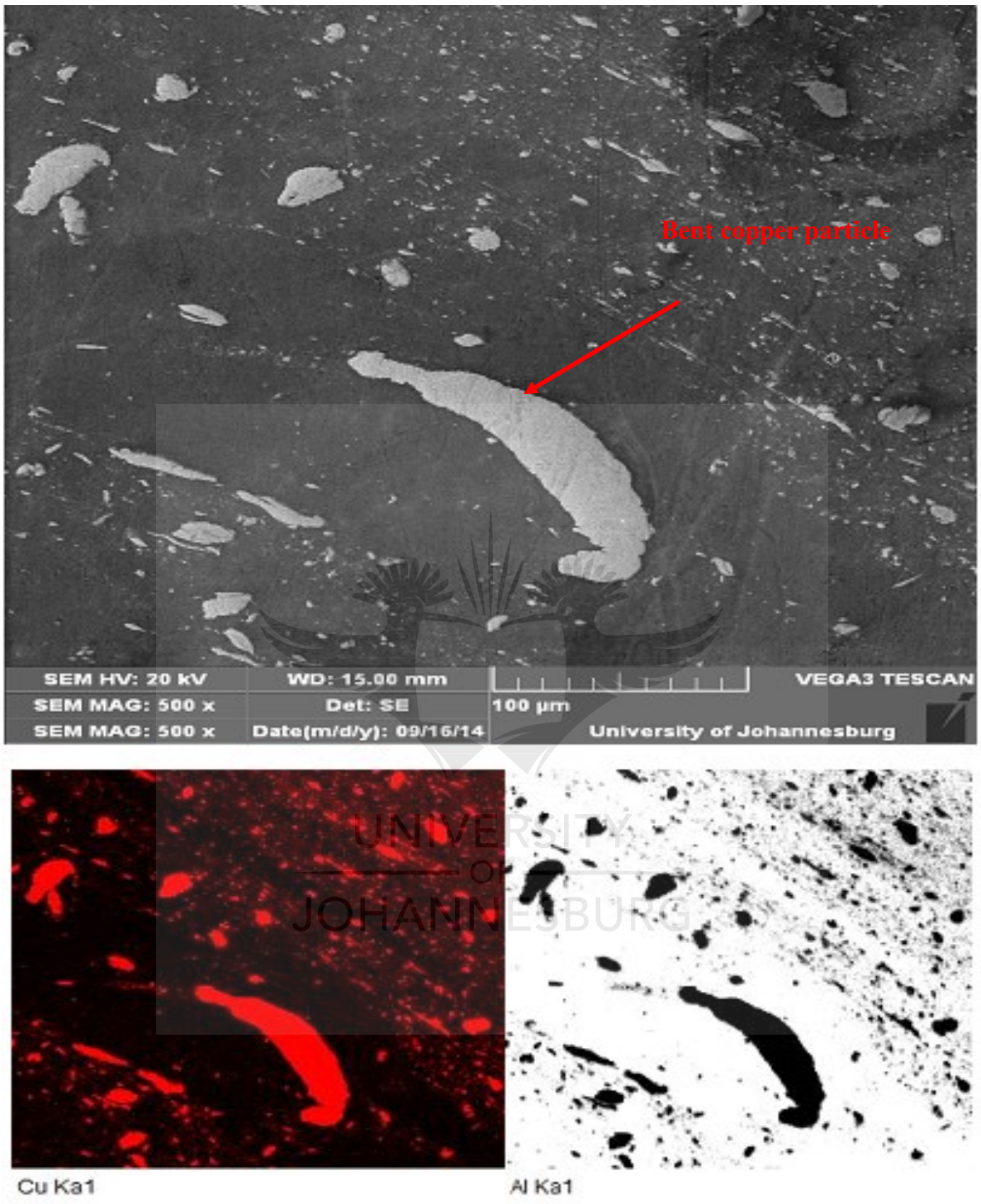

Figure 4-24 Mapping of the stir zone (SZ) for the spot weld produced using a conical pin and a concave shoulder tool at 800 rpm and 0.5 mm shoulder plunge depth, copper (red), aluminium (black)

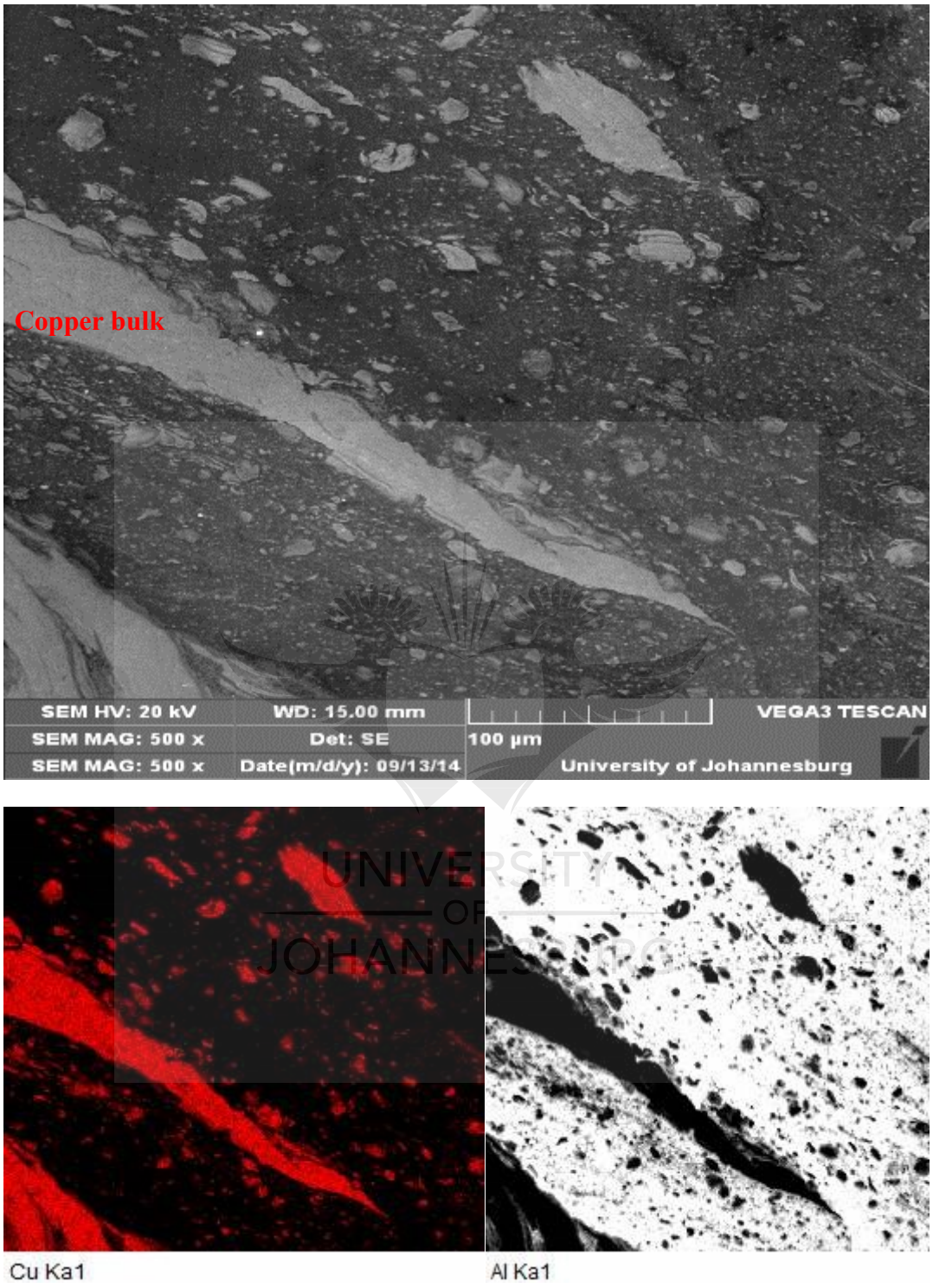

Figure 4-25 Mapping of the stir zone (SZ) for the spot weld produced using a conical pin and a concave shoulder tool at 800 rpm and 1 mm shoulder plunge depth, copper (red), aluminium (black)

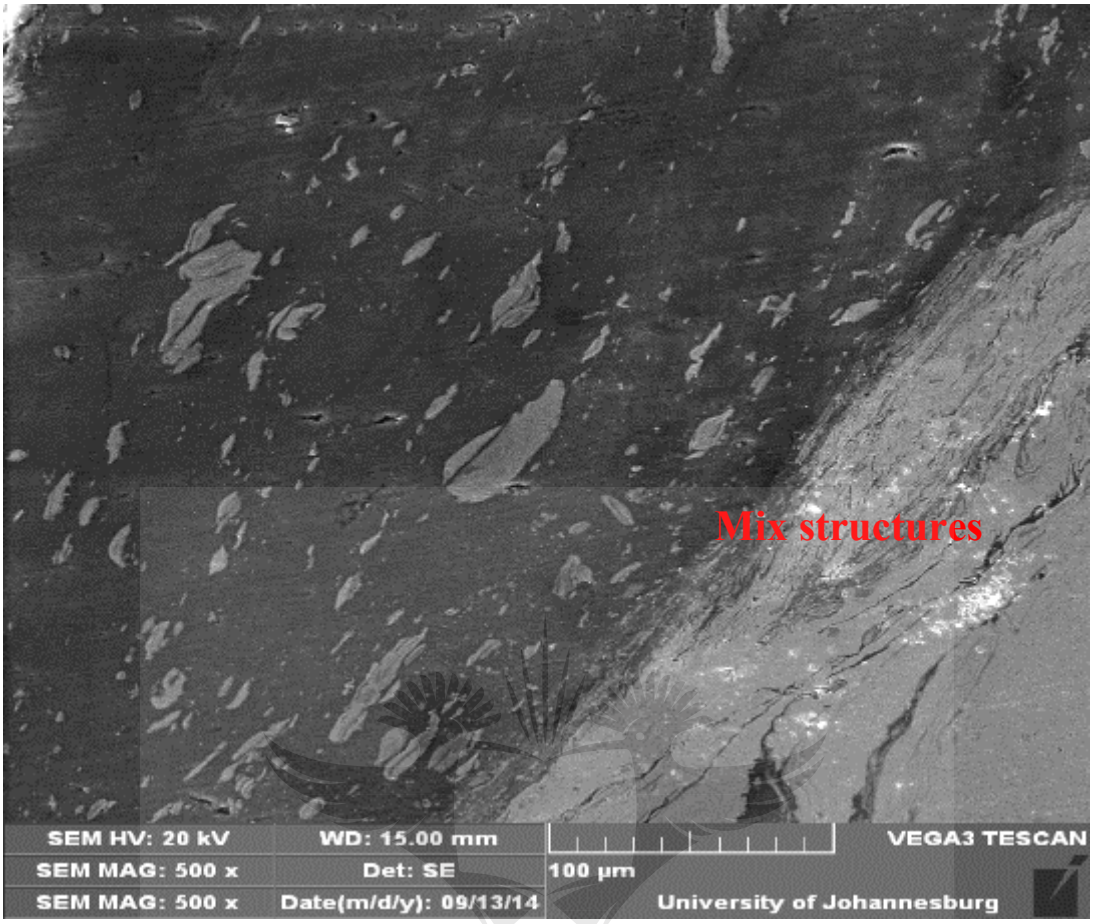

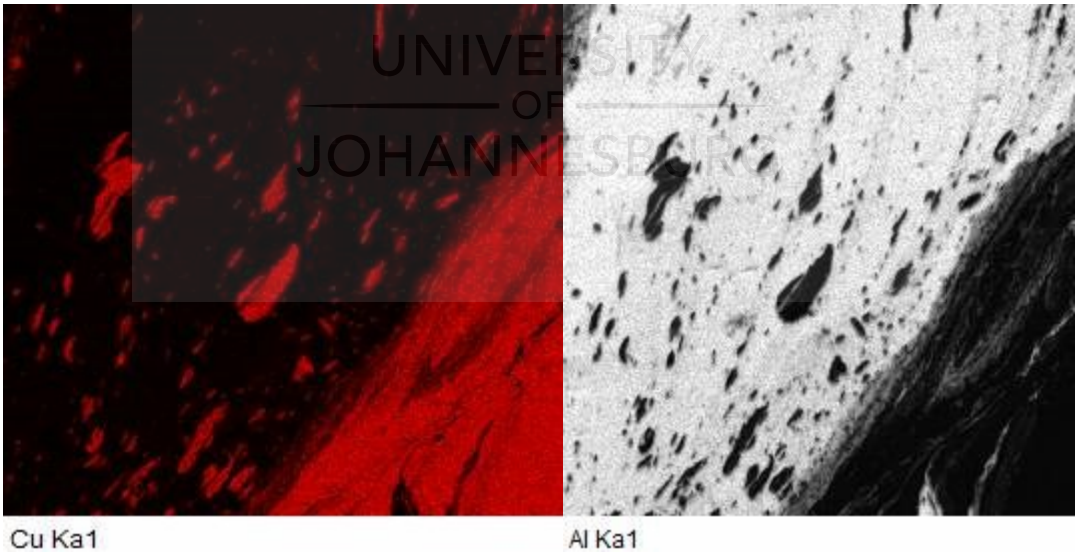

Figure 4-26 Mapping of the stir zone (SZ) for the spot weld produced using a conical pin and a concave shoulder tool at 1200 rpm and 0.5 mm shoulder plunge depth, copper (red), aluminium (black)

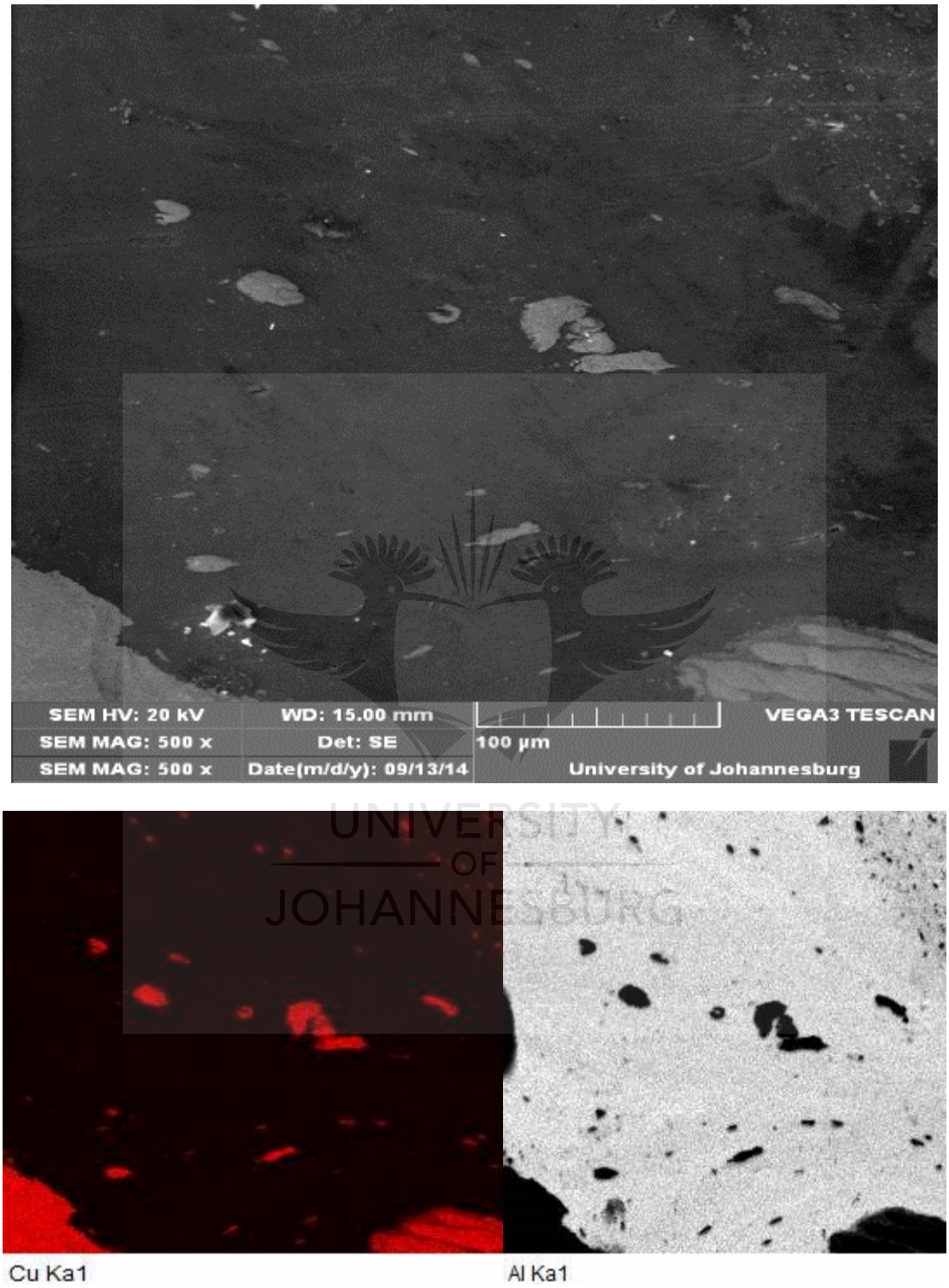

Figure 4-27 Mapping of the stir zone (SZ) for the spot weld produced using a conical pin and a concave shoulder tool at 1200 rpm and 1 mm shoulder plunge depth, copper (red), aluminium (black)

It was observed in Figure 4-24 the presence of large copper particles surrounded by small copper particles in the aluminium matrix, that the large copper particle has a curved like microstructure (bent copper particle). This weld was produced using 800 rpm and 0.5 shoulder plunge depth.

The mapping of the weld produced using 1200 rpm and 1 mm shoulder plunge depth shows fewer copper particles in the aluminium matrix (Figure 4-27). The mapping of the spot weld produced using 800 rpm, 1 mm shoulder plunge depth (Figure 4-25) shows the presence of a number of larger particles of copper mixed with small copper particles in the aluminium matrix.

Furthermore, in Figure 4-26 shows the EDS mapping of the welds produced at 1200 rpm and 0.5 mm shoulder plunge depth, where the presence of more uniform copper particles of more or less same size in the aluminium matrix and a mixture structure could also be observed.

The morphology of the micrographs showing different features of the spot welds produced in the current research study; and these are hereby discussed. Figures 4-28 (a) and (b) present the microstructure of the stir zone of the spot welds produced using 800 and 1200 rpm at 0.5 mm shoulder plunge depth. The tool used was a flat pin and a flat shoulder. It was observed that a good material mixing, showing a distribution of Cu particles and fragments with irregular shapes and various sizes, was seen in the spot welds produced when using a rotational speed of 800 rpm; whereas at a rotational speed of 1200 rpm, large copper fragments were present.

The microstructures shown in Figures 4-29 (a) and (b) depict the spot welds produced when using a conical pin and a concave tool. The rotational speeds were 800 rpm and 1200 rpm for Figures 4-29 (a) and (b), respectively.

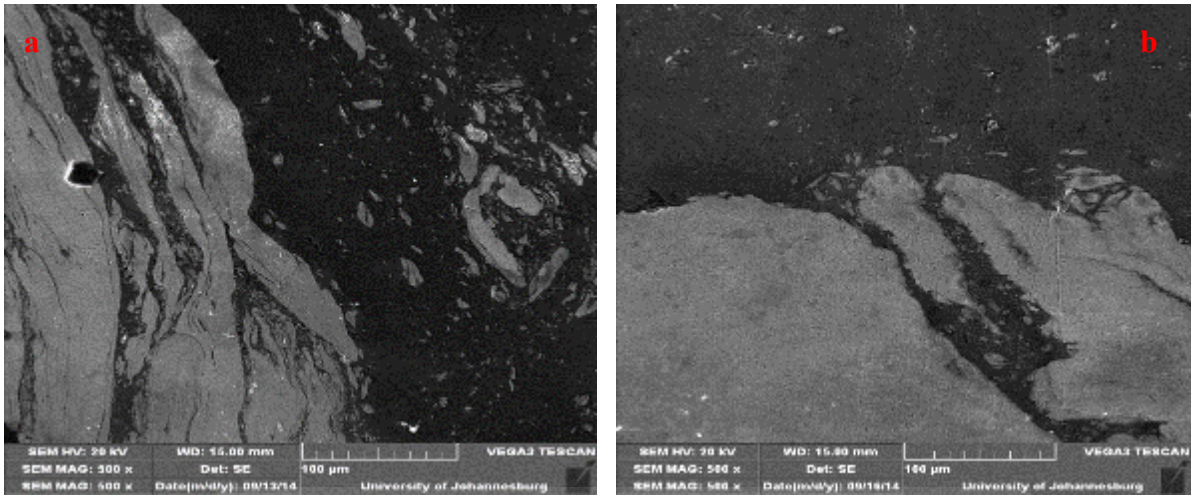

Figure 4-28 Microstructure of the stir zone (SZ) of the spot weld produced at 800 (a) and 1200 rpm (b) , 0.5 mm shoulder plunge depth using a flat pin and a flat shoulder

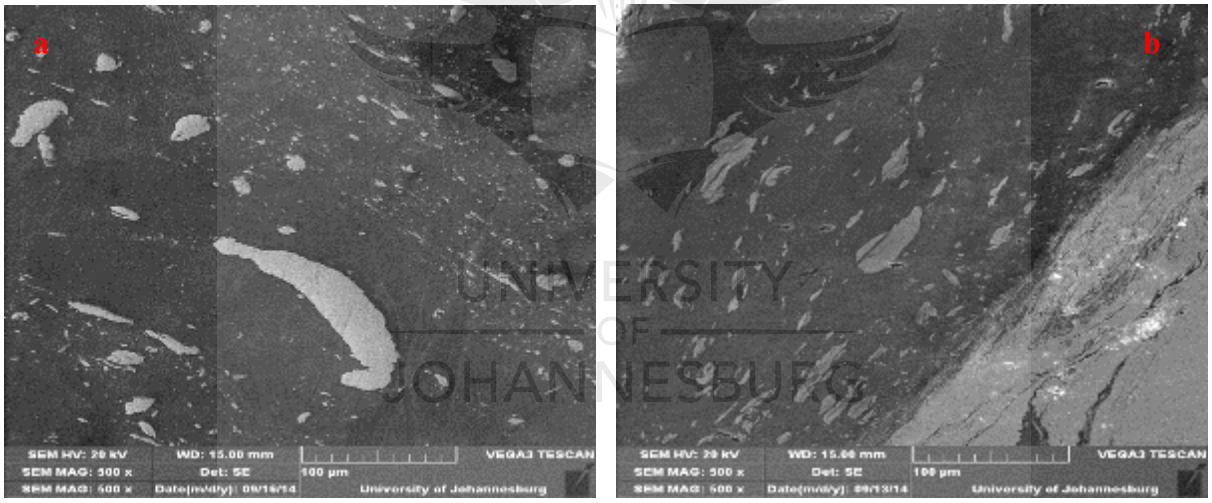

Figure 4-29 Microstructure of the stir zone (SZ) of the spot weld produced at 800 (a) and 1200 rpm (b), 0.5 mm shoulder plunge depth using a conic pin and concave shoulder tool

It was observed that there was a good mixing in both welds with Cu particles present in the aluminium matrix. The presence of the copper particles in the aluminium matrix is attributed to the stir action of the tool pin, which has worn out copper pieces from the copper parent material, breaking them up and dispersing them into the aluminium parent material. Furthermore, the dispersion of the fine copper fragments and particles was seen in the zone close to the aluminium parent material, as shown in Figures 4-28 (a), (b) and Figures 4-29 (a), (b).

Interlayers of aluminium and copper were also observed in the stir zone, as shown in Figure 4-29(b), which is an indication of a good dissimilar joint.

4.5 Optical Microscope analyses

The micrograph of the microstructure of the parent materials is presented in Figure 4-30, showing the grains morphology of the aluminium (Figure 4-30 a) and the copper (Figure 4-30 b).

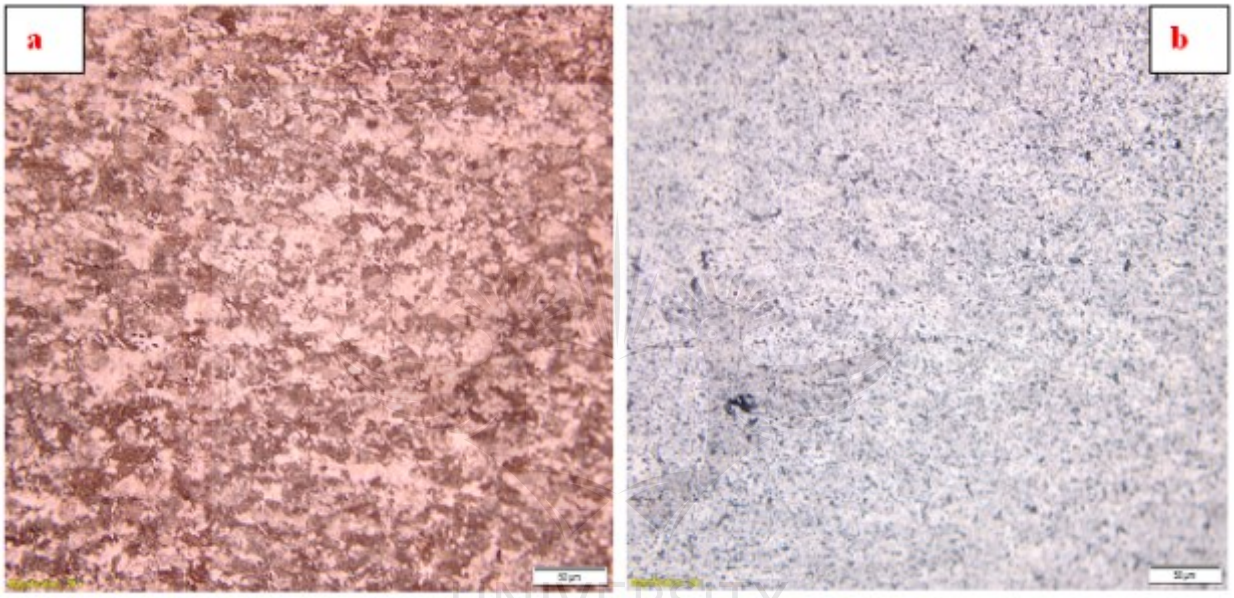

Figure 4-30 Microstructure of the parent materials (a) C11000 and (b) AA1060

The microstructure of the friction stir spot welds was examined using an optical microscope; and the results are shown in Figures 4-31 and 4-32. Figure 4-31 depicts the microstructure of the spot weld produced at 800 rpm (a) and 1200 rpm (b), 1mm shoulder plunge depth using a flat pin and a flat shoulder tool. In addition, Figure 4-32 shows the microstructure of the spot weld produced at 800 rpm (a) and 1200 rpm (b), 0.5 mm shoulder plunge depth using a conical pin and a concave shoulder tool.

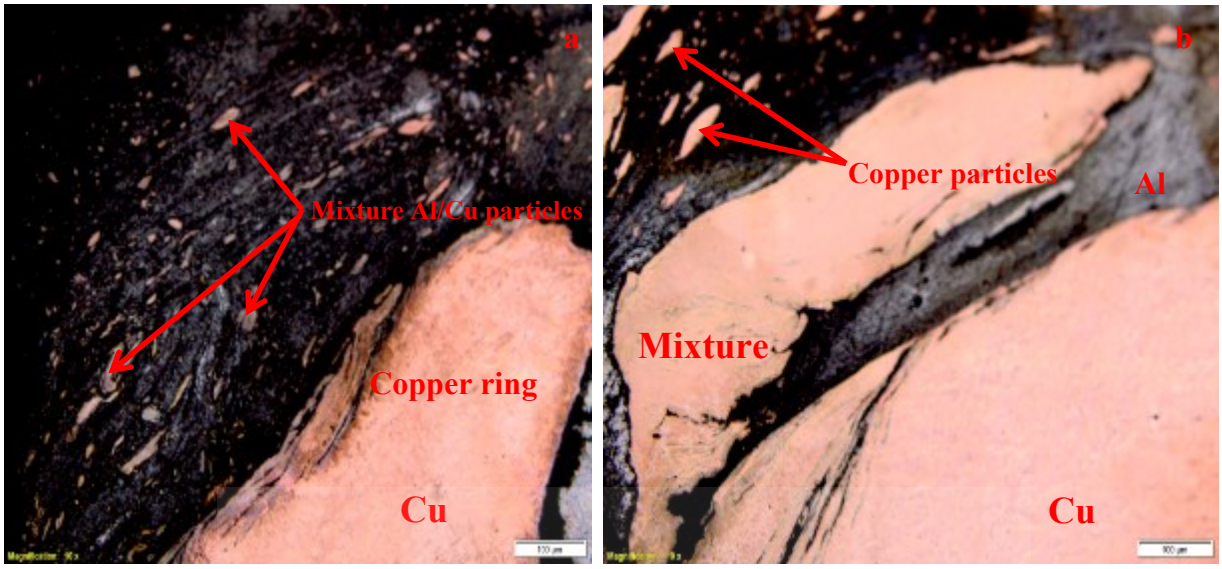

Figure 4-31 Optical microscope images showing the macrostructure of the joints at 800 rpm (a) and 1200 rpm (b), 1 mm shoulder plunge depth using a flat pin and flat shoulder tool

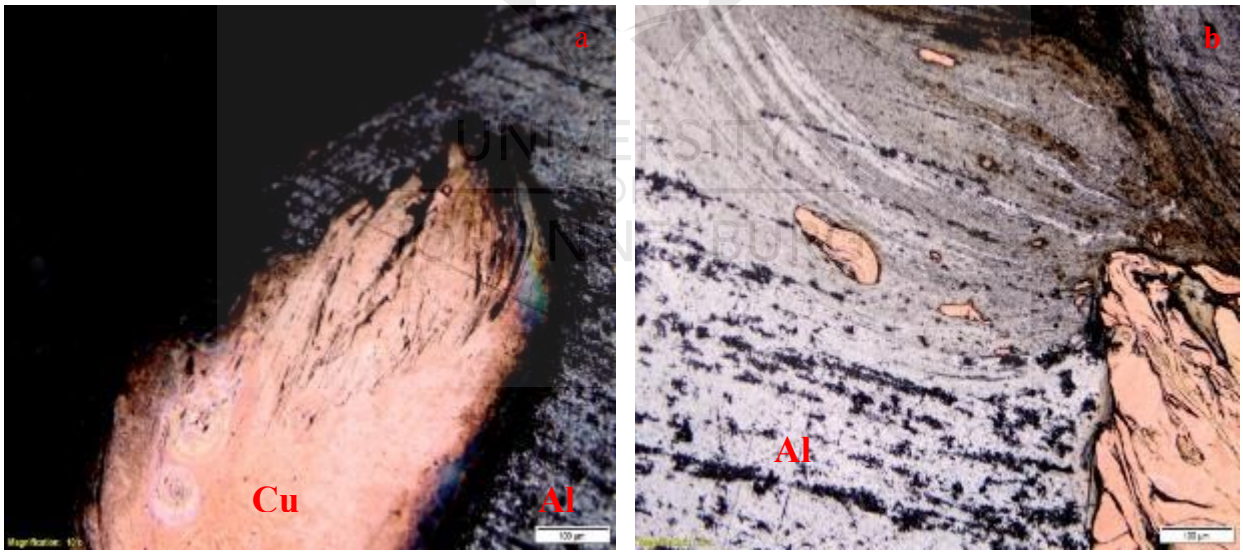

Figure 4-32 Optical microscope images showing the macrostructure of the joints at 800 rpm (a) and 1200 rpm (b), 0.5 mm shoulder plunge depth using a conical pin and concave shoulder tool

It can be seen in Figure 4-31 (a) that there is a presence of a copper ring and a mixture of Al/Cu particles present in the SZ. There is no obvious welding defect in the joint; and the copper is

distributed in this zone with different shapes. In the upper part of the joint, the large bulk of copper with irregular shapes can be observed (Figure 4-31 (a)). The tool pin was inserted in the aluminium plate and the copper ring extruded upward from the lower copper plate in the aluminium plate was observed. This was in agreement with previous work [8].

Additionally, the intermixing of copper and aluminium is not homogenous for the different produced spot welds; and different microstructures are formed in different regions of the welds. It has been reported that the FSW of dissimilar materials is distinguished from those of similar materials by the formation of a complex, intercalated vortex-like and related flow pattern [141].

In Figure 4-32 (b), a good interlaced structure can be seen. This is formed by aluminium and copper, thereby indicating that the two plates are bonded together firmly in this region; and it is composed of a lamellae structure of copper particles with a streamlined shape of aluminium strips. In that region, it was also observed that there were a few disseminated copper particles. The microstructures of the different spot welds produced when using different process parameters and tool geometries are presented in Appendix I.

4.6 Scanning Electron Microscope combined with Energy Dispersive Spectroscopy (SEM/EDS)

Figures 4-33 to 4-40 depict the SEM secondary electron (SE) (a) and A backscattered electron (BSE) (b) micrographs of the copper ring and part of the keyhole of the welds produced using different process parameters and tool geometries, namely, a flat pin/ flat shoulder and conical pin/ concave shoulder tools. This was conducted to show the contrast between the two different materials, namely copper and aluminium.

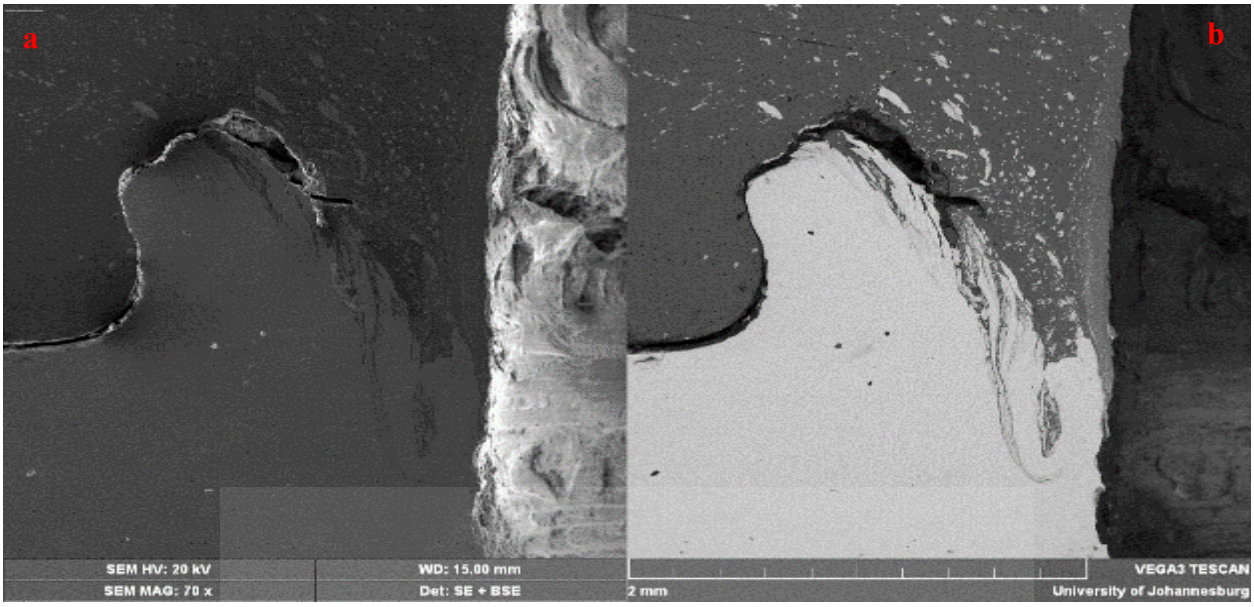

Figure 4-33 Showing a secondary electron (a) and a backscattered electron (b) images of the spot weld produced at 800 rpm and 0.5 mm plunge depth using a flat pin and a flat shoulder tool

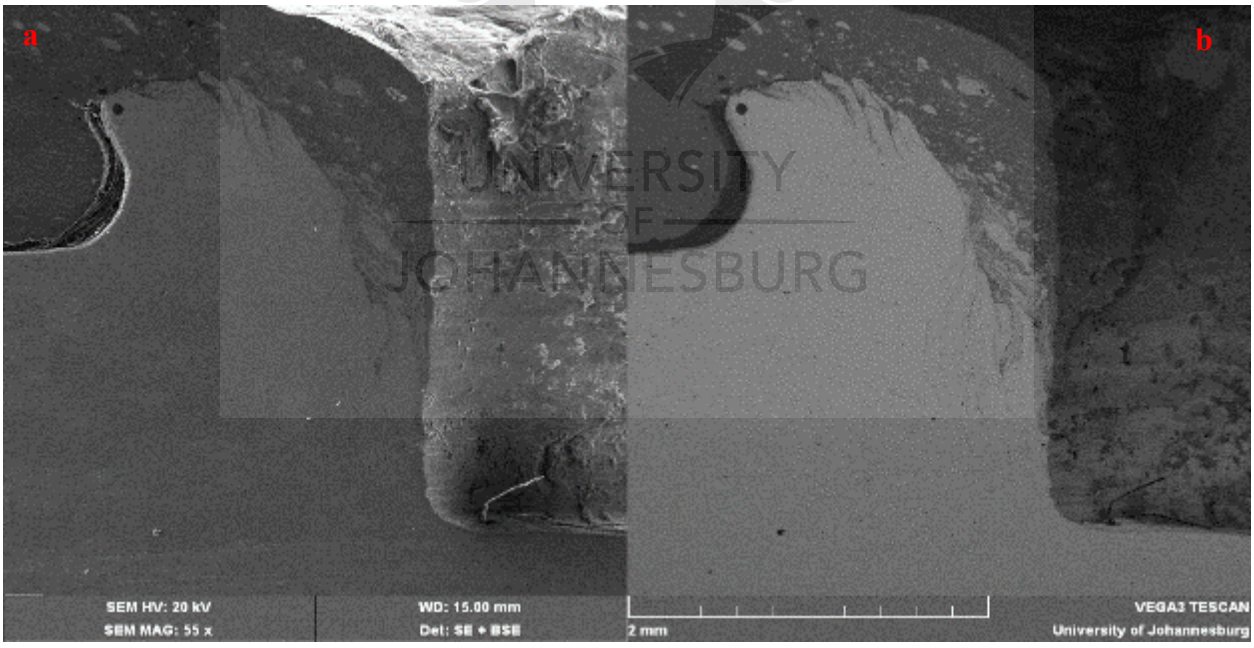

Figure 4-34 Showing a secondary electron (a) and a backscattered electron (b) images of the spot weld produced at 800 rpm and 1 mm plunge depth using a flat pin and a flat shoulder tool

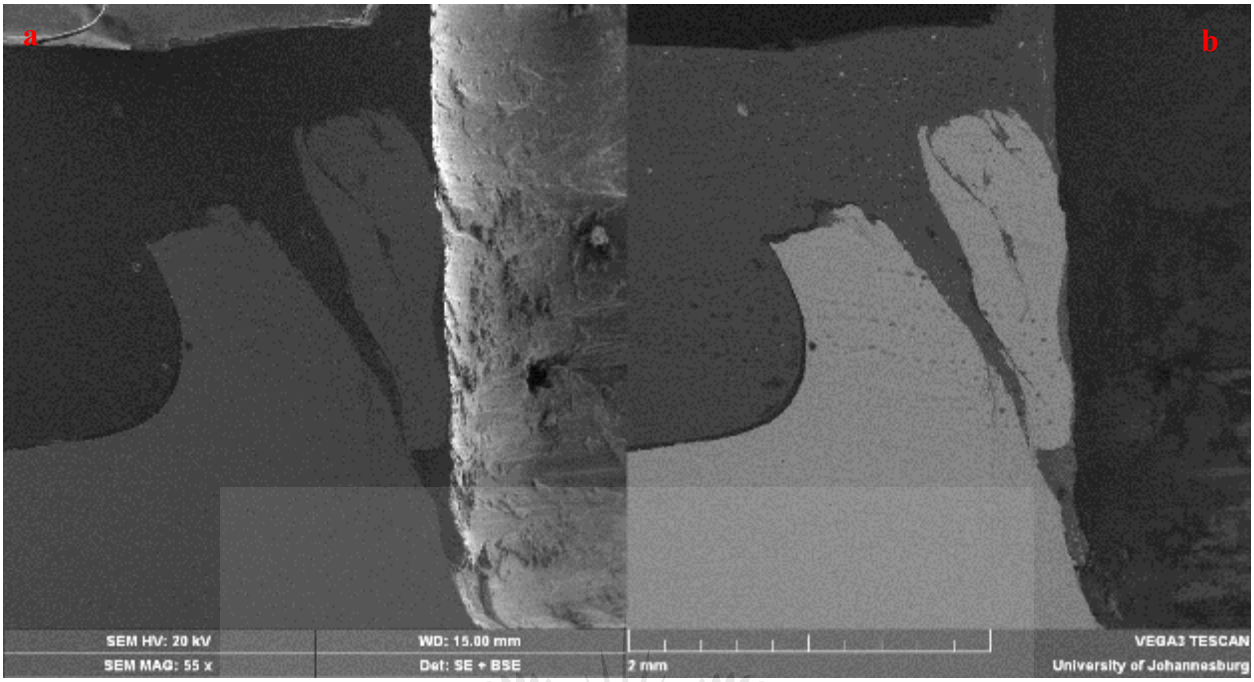

Figure 4-35 Showing a secondary electron (a) and a backscattered electron (b) images of the spot weld produced at 1200 rpm and 0.5 mm plunge depth using a flat pin and a flat shoulder tool

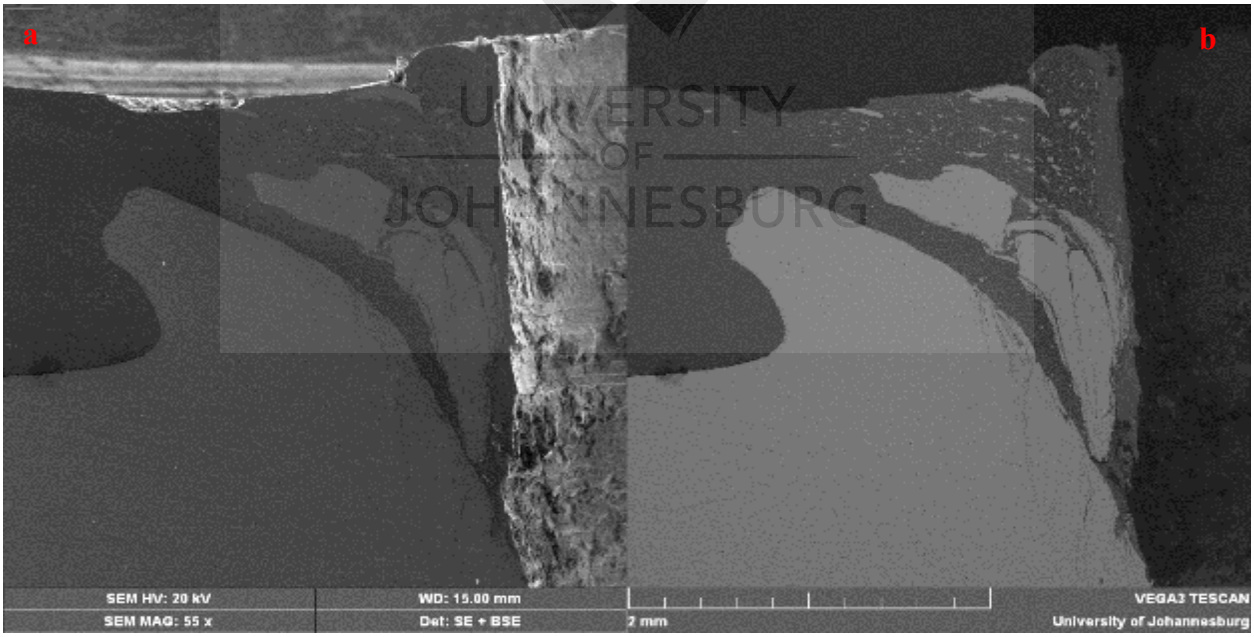

Figure 4-36 Showing a secondary electron (a) and a backscattered electron (b) images of the spot weld produced at 1200 rpm and 1 mm plunge depth using a flat pin and a flat shoulder tool

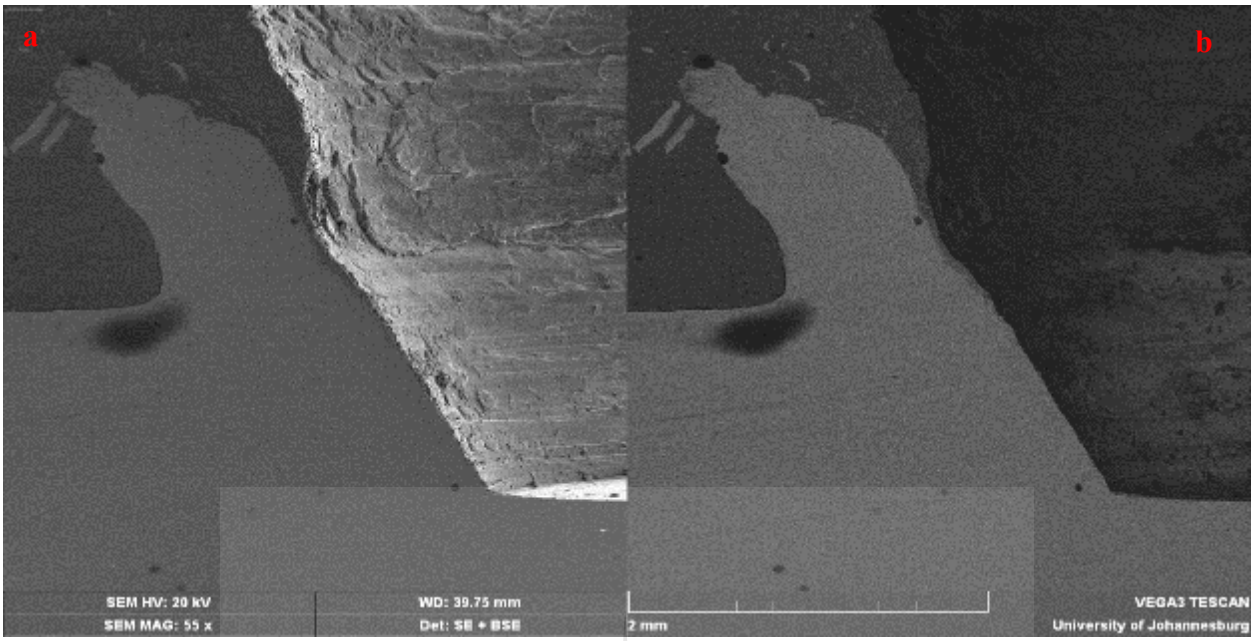

Figure 4-37 Showing a secondary electron (a) and a backscattered electron (b) images of the spot weld produced at 800 rpm and 0.5 mm plunge depth using a conical pin and a concave shoulder tool

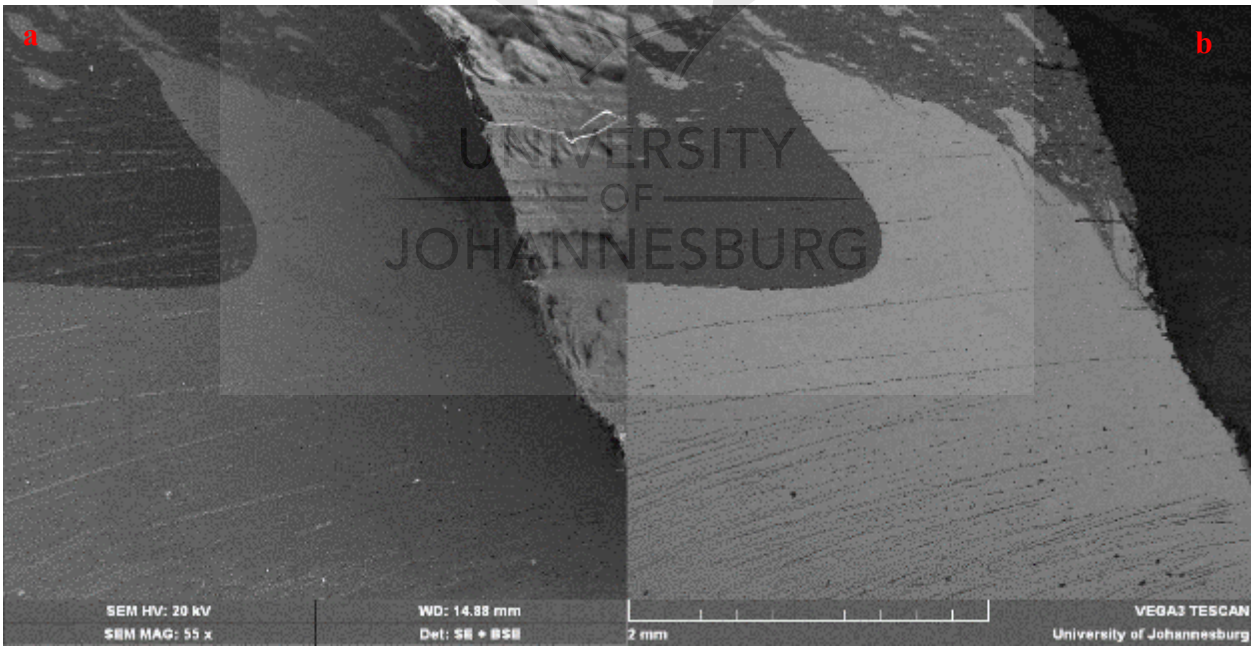

Figure 4-38 Showing a secondary electron (a) and a backscattered electron (b) images of the spot weld produced at 800 rpm and 1 mm plunge depth using a conical pin and a concave shoulder tool

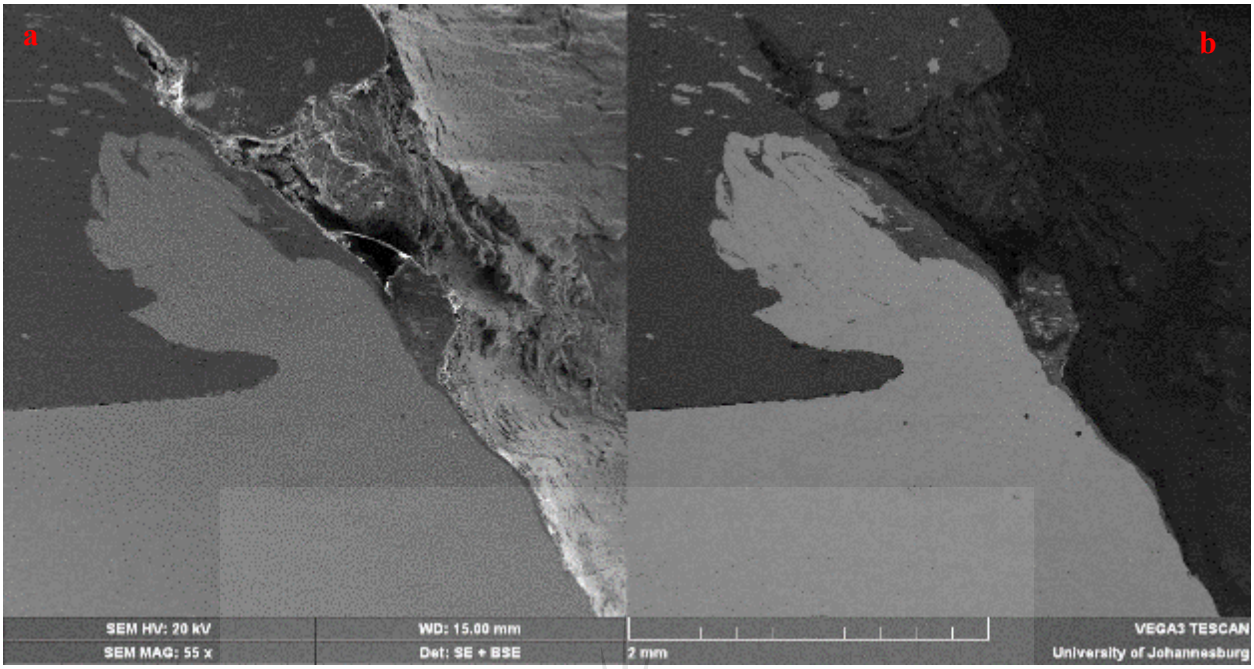

Figure 4-39 Showing a secondary electron (a) and a backscattered electron (b) images of the spot weld produced at 1200 rpm and 0.5 mm plunge depth, using a conical pin and a concave shoulder tool

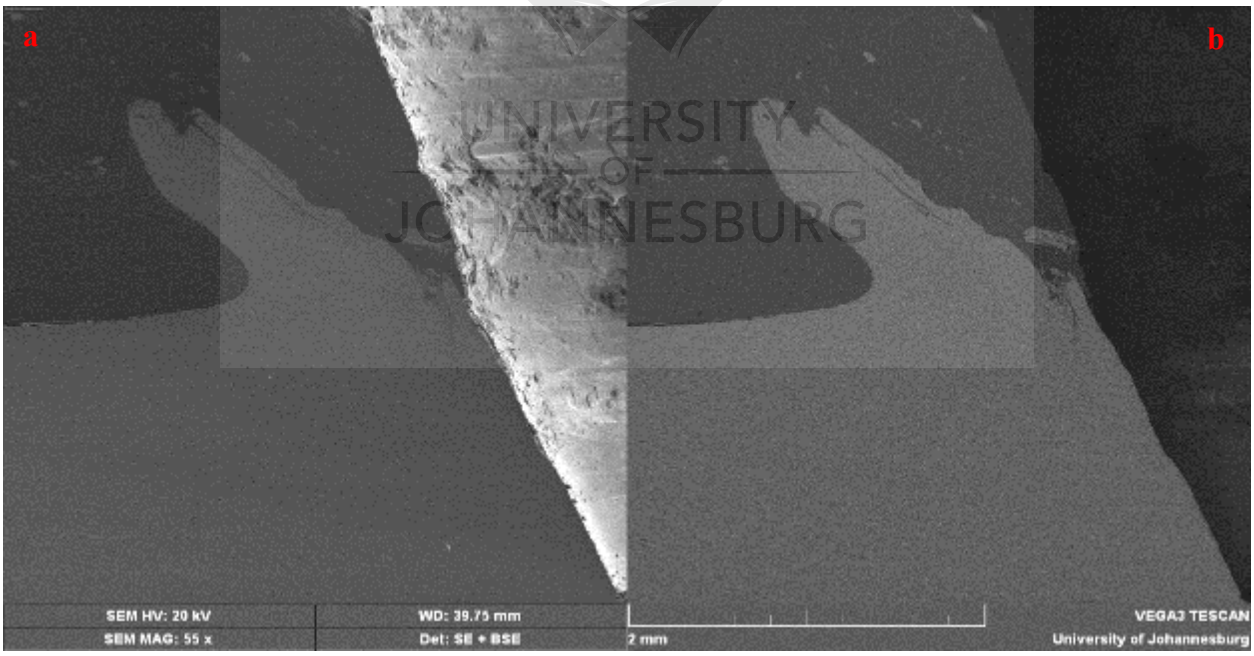

Figure 4-40 Showing a secondary electron (a) and a backscattered electron (b) images of the spot weld produced at 1200 rpm and 1 mm plunge depth using a conical pin and a concave shoulder tool

The contrast between the two materials and the presence of Cu particles in the aluminium matrix can be clearly seen. This difference could lead to the formation of hard and brittle intermetallic compounds. To investigate the presence of intermetallic compounds in the spot welds, energy dispersive spectroscopy (EDS) analysis was carried out in the keyhole and stir zone (SZ) of the produced spot welds using the two tool geometries.

The EDS results indicate the formation of hard and brittle intermetallic compounds. From Figures 4-41 to 4-44 the SEM micrographs can be seen, and the EDS analysis of selected points of the keyhole of the welds produced when using a flat pin and a flat shoulder, using different process parameters. Furthermore, from Figures 4-45 to 4-48 the SEM and EDS analyses of the selected points of the keyhole are presented.

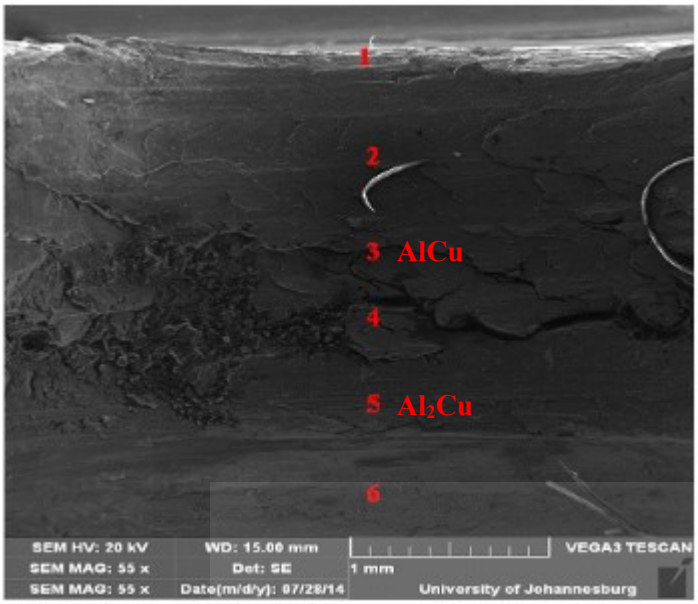

	Points					
Elements	**1**	**2**	**3**	**4**	**5**	**6**
Al	99	89	32	86	58	7
Cu	0.09	11	67	13	41	93

Figure 4-41 Scanning electron microscopy image and energy dispersive spectroscopy spectrums and the chemical percentages of the weld produced at 800 rpm, 0.5 mm shoulder plunge depth using a flat pin and a flat shoulder of the keyhole

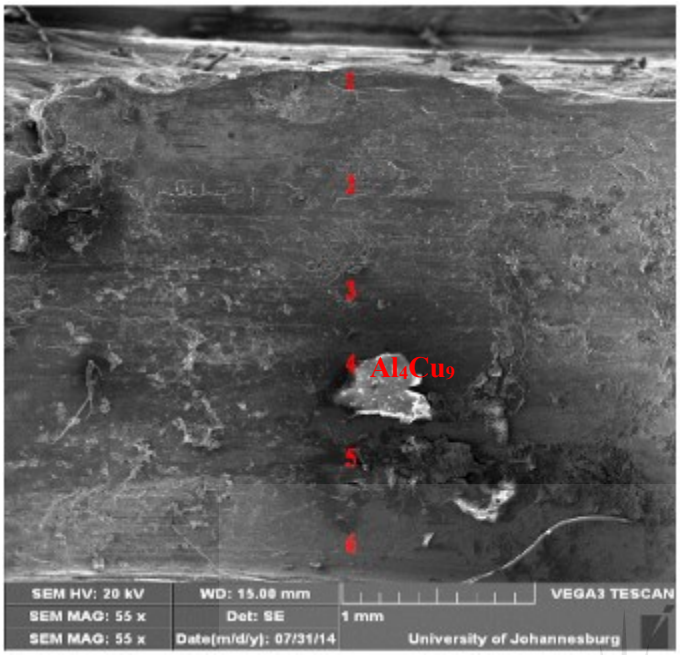

	Points					
Elements	**1**	**2**	**3**	**4**	**5**	**6**
Al	92	93	81	19	9	7
Cu	8	7	18	80	90	93

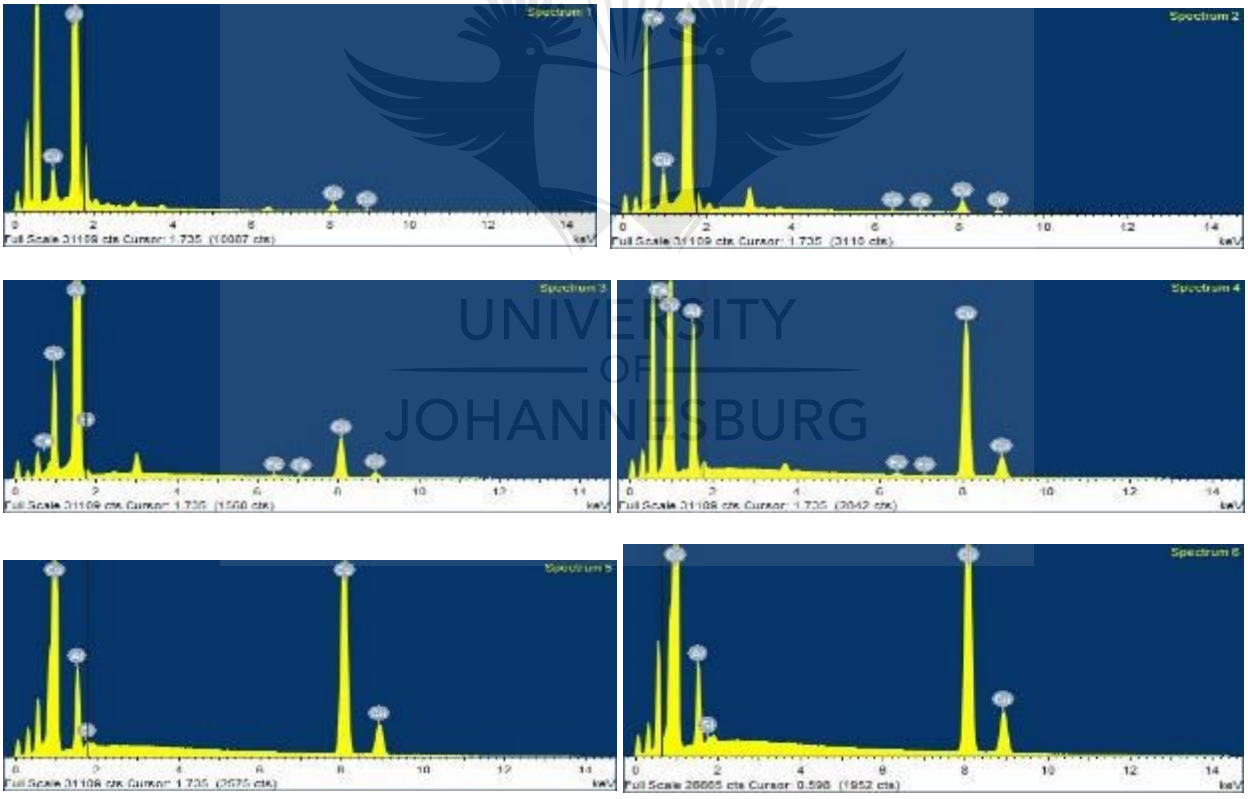

Figure 4-42 Scanning electron microscopy image and energy dispersive spectroscopy spectrums and chemical percentages of the weld produced at 800 rpm, 1 mm shoulder plunge depth using a flat pin and a flat shoulder of the keyhole

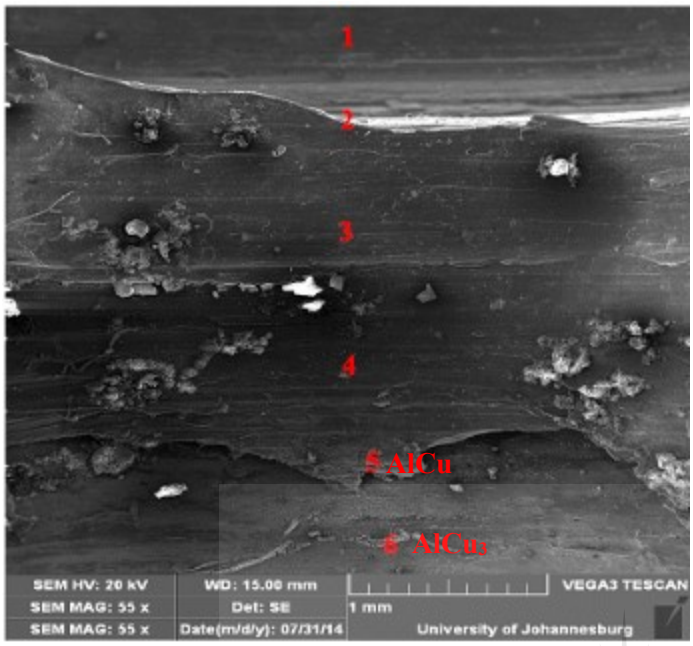

	Points					
Elements	**1**	**2**	**3**	**4**	**5**	**6**
Al	98	97	97	98	37	13
Cu	1	3	2	1	62	86

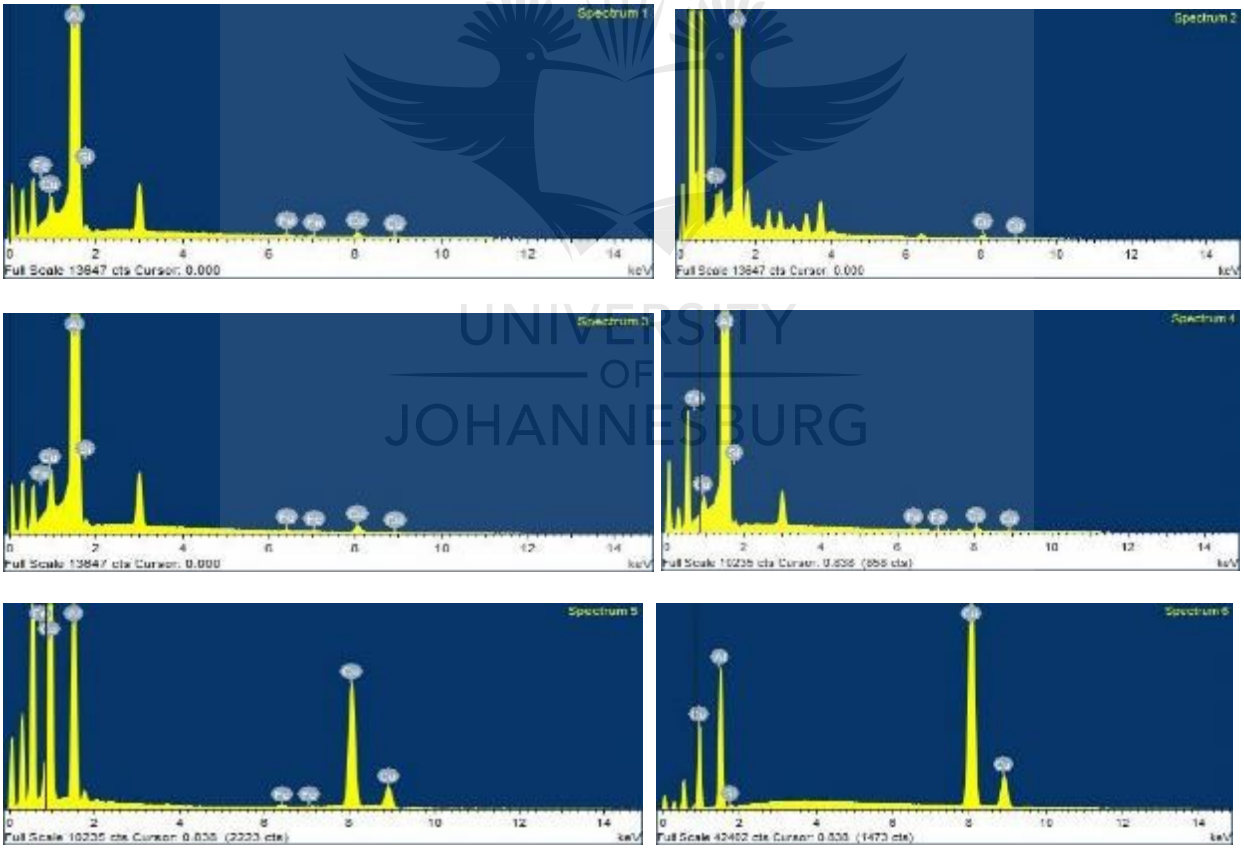

Figure 4-43 Scanning electron microscopy image and energy dispersive spectroscopy spectrums and chemical percentages of the weld produced at 1200 rpm, 0.5 mm shoulder plunge depth using a flat pin and a flat shoulder of the keyhole

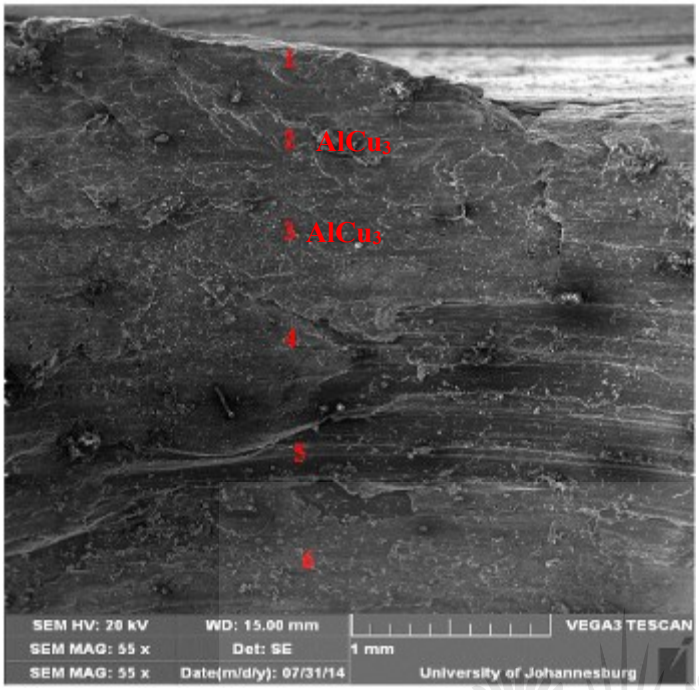

Elements	Points					
	1	**2**	**3**	**4**	**5**	**6**
Al	89	15	12	96	98	68
Cu	11	84	87	2	2	31

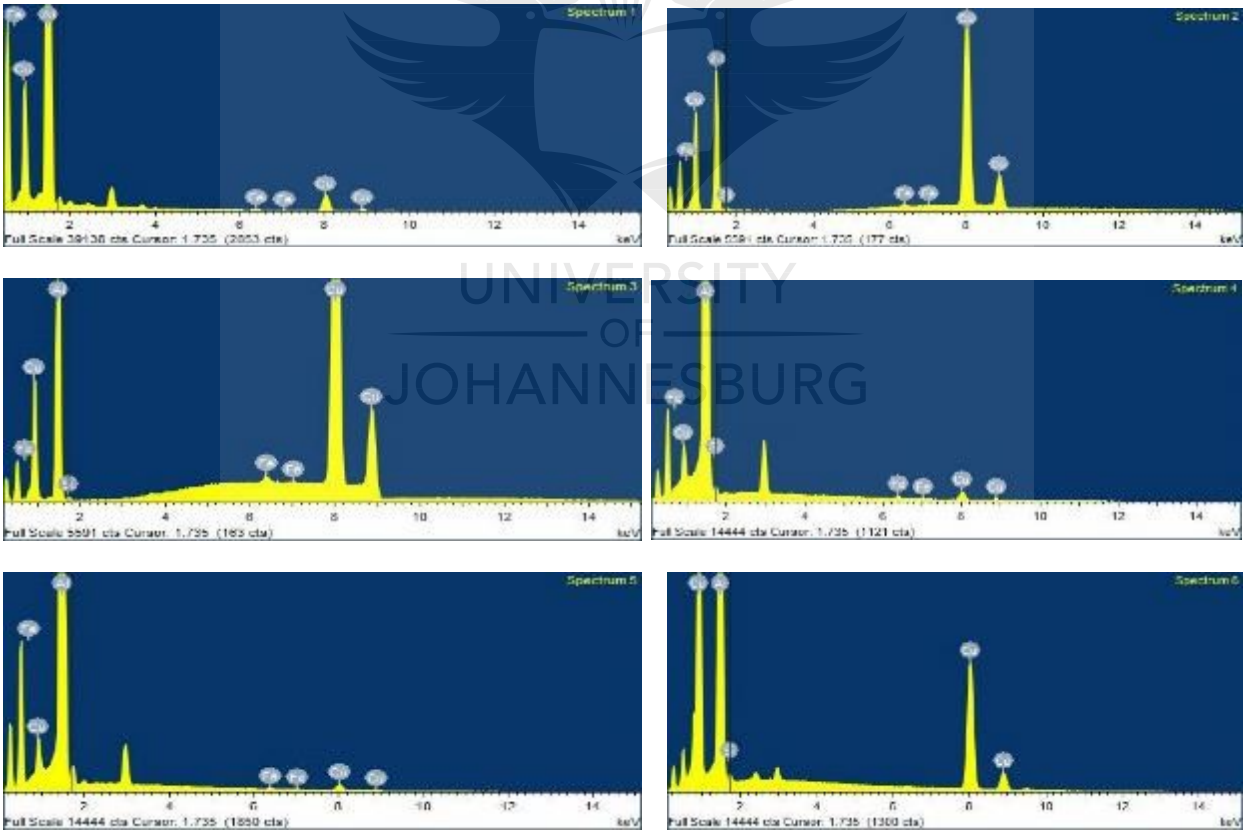

Figure 4-44 Scanning electron microscopy image and energy dispersive spectroscopy spectrums and chemical percentages of the weld produced at 1200 rpm, 1 mm shoulder plunge depth using a flat pin and a flat shoulder of the keyhole

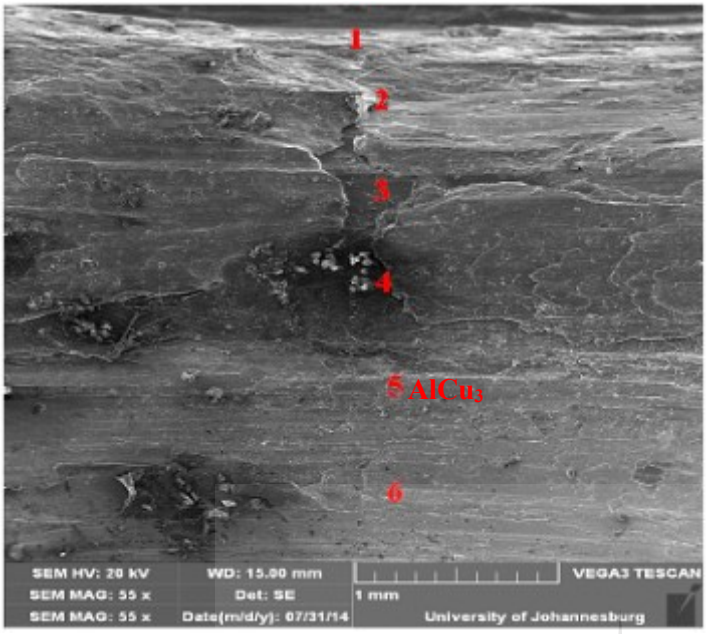

	Points					
Elements	**1**	**2**	**3**	**4**	**5**	**6**
Al	92	96	89	68	12	5
Cu	7	4	10	32	88	95

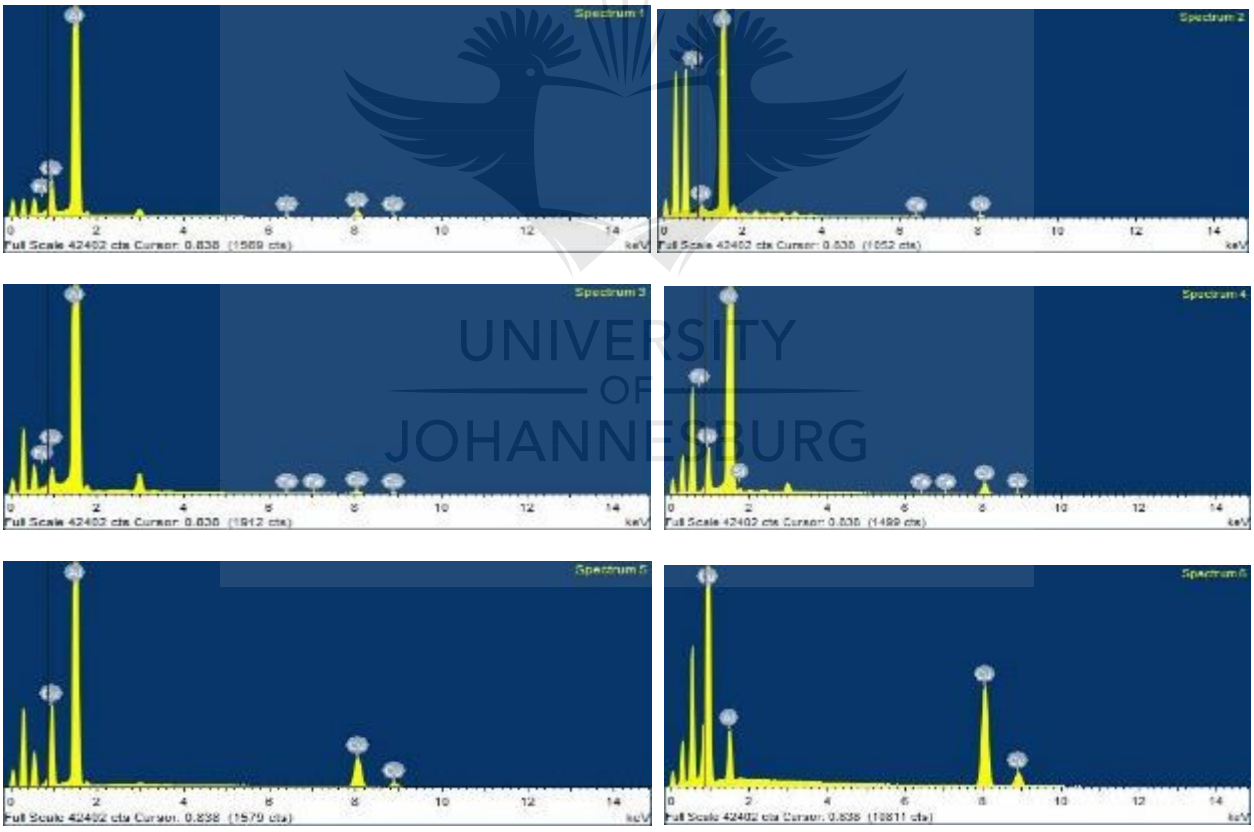

Figure 4-45 Scanning electron microscopy image and energy dispersive spectroscopy spectrums and chemical percentages of the weld produced at 800 rpm, 0.5 mm shoulder plunge depth using a conical pin and a concave shoulder of the keyhole

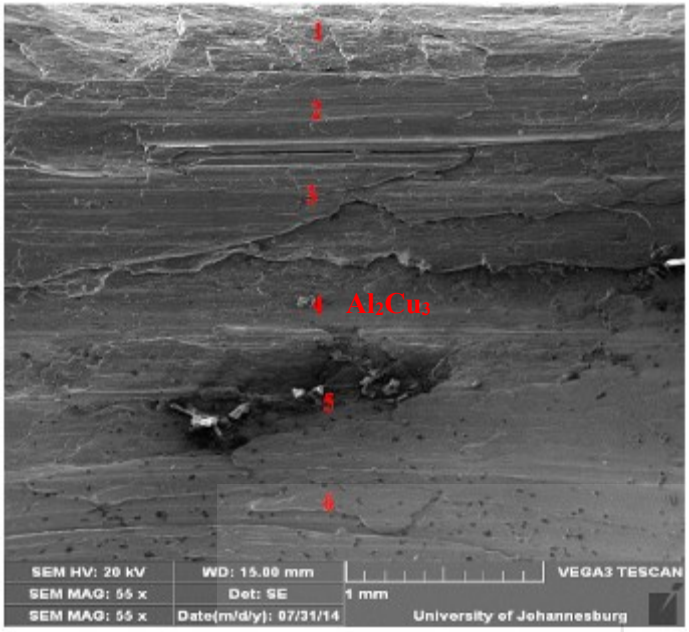

Elements	Points					
	1	**2**	**3**	**4**	**5**	**6**
Al	92	84	83	77	71	4
Cu	7	15	17	23	29	96

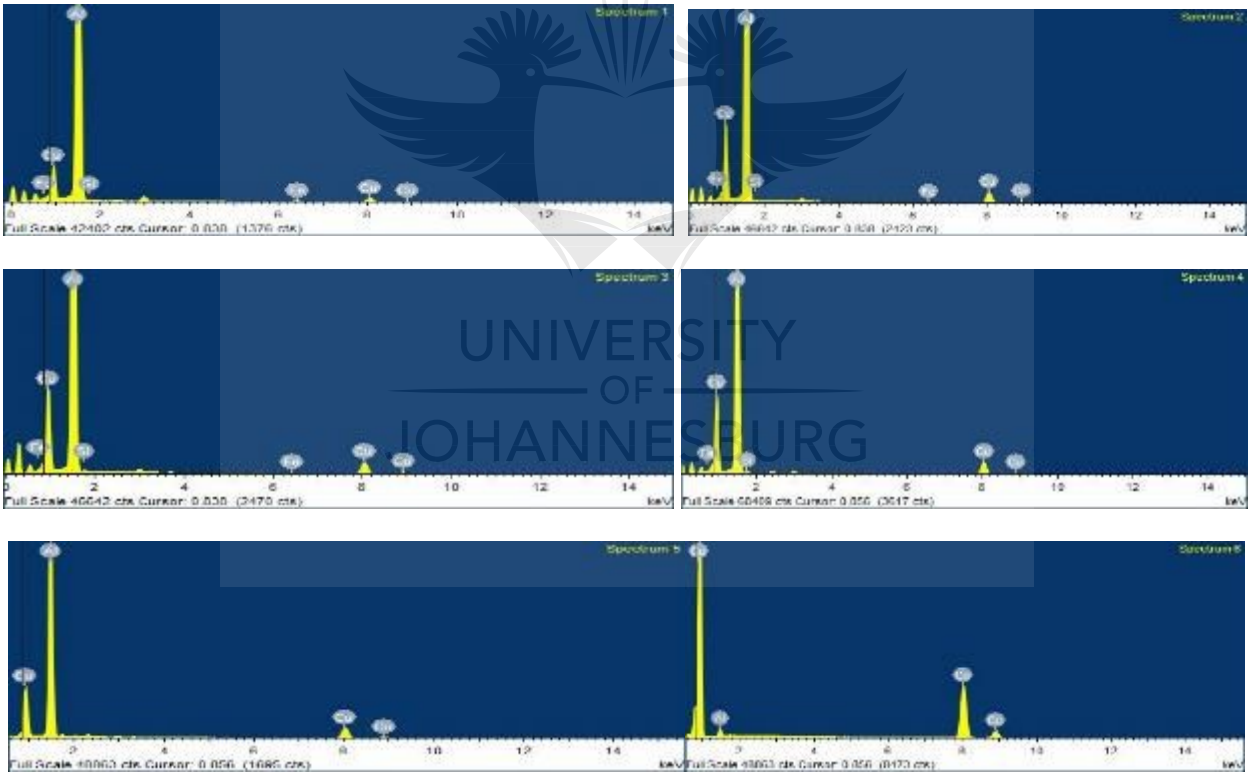

Figure 4-46 Scanning electron microscopy image and energy dispersive spectroscopy spectrums and chemical percentages of the weld produced at 800 rpm, 1 mm shoulder plunge depth using a conical pin and a concave shoulder of the keyhole

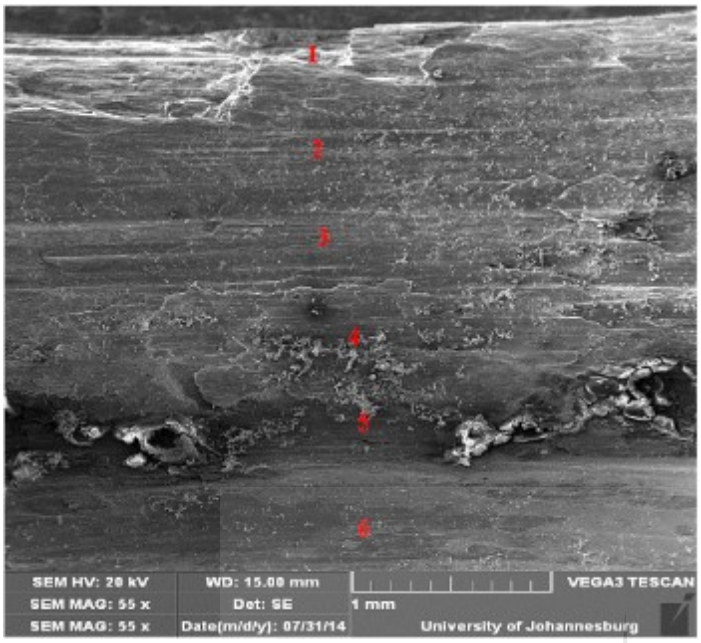

	Points					
Elements	**1**	**2**	**3**	**4**	**5**	**6**
Al	96	97	94	72	90	78
Cu	3	3	6	27	9	21

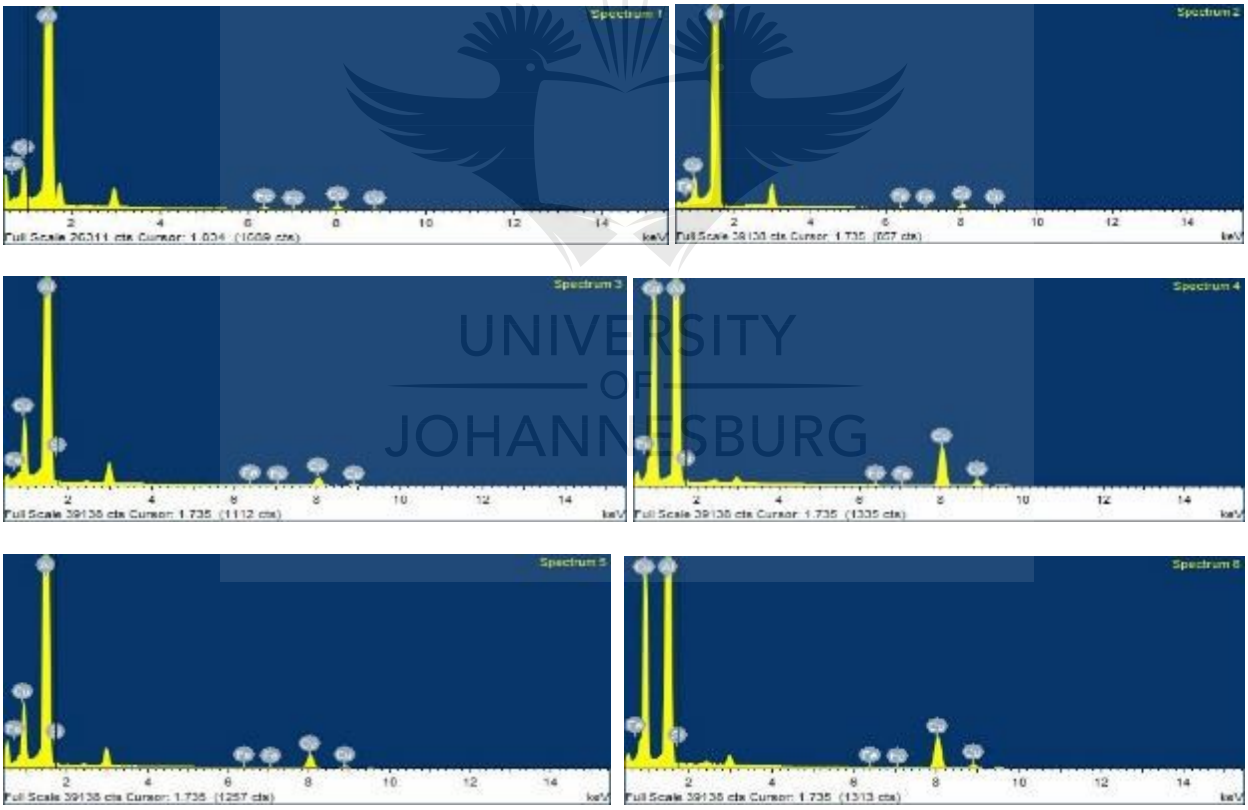

Figure 4-47 Scanning electron microscopy image and energy dispersive spectroscopy spectrums and chemical percentages of the weld produced at 1200 rpm, 0.5 mm shoulder plunge depth using a conical pin and a concave shoulder of the keyhole

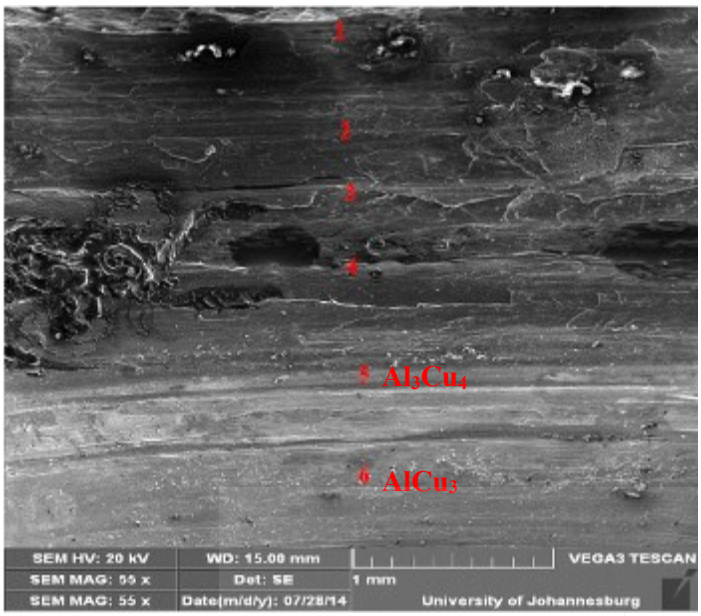

	Points					
Elements	**1**	**2**	**3**	**4**	**5**	**6**
Al	92	95	93	92	24	14
Cu	8	5	6	8	76	86

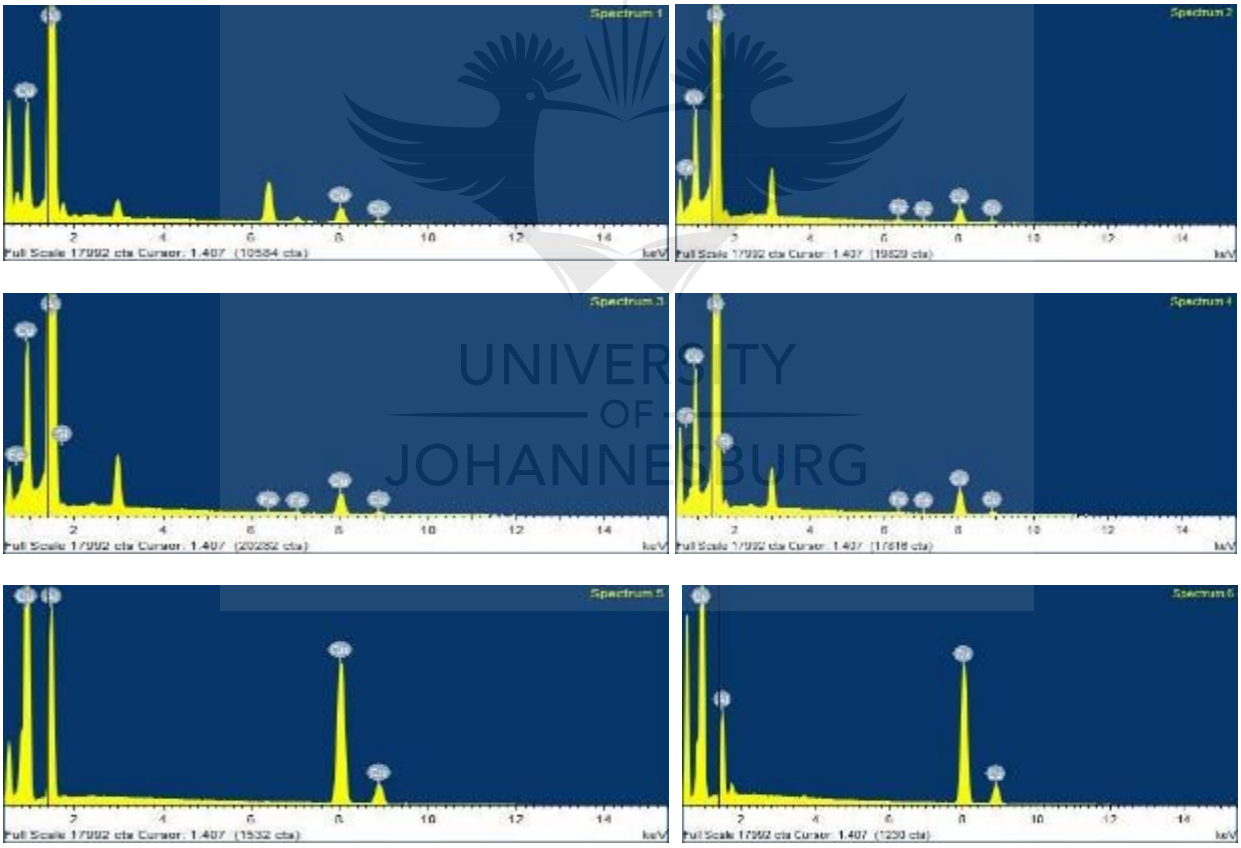

Figure 4-48 Scanning electron microscopy image and energy dispersive spectroscopy spectrums and chemical percentages of the weld produced at 1200 rpm, 1 mm shoulder plunge depth using a conical pin and a concave shoulder of the keyhole

The low peaks of the intermetallic compounds of AlCu, Al_2Cu, $AlCu_3$, Al_2Cu, Al_3Cu_4, Al_2Cu_3 and Al_4Cu_9 were present in the weld samples. The sample produced at 800 rpm, 0.5 mm shoulder plunge depth using a flat pin and a flat shoulder has the presence of AlCu and Al_2Cu in its keyhole; whereas Al_2Cu, Al_4Cu_9 and Al Cu intermetallics were found in the stir zone. On the other hand, the welds produced with the same process parameters, but using a conical pin and a concave shoulder showed the presence of $AlCu_3$ only.

Furthermore, the stir zone of the same welds showed the presence of Al_2Cu, Al_4Cu_9 and AlCu intermetallics; while using a flat pin and a flat shoulder only Al_4Cu_9 intermetallic was found for the weld produced when using a conical pin and a concave shoulder. It has been reported that the presence of the intermetallic compounds in the joint interface could preferentially favour the development of a crack during the shear tensile analysis [9]. In various samples, it was noticed that there was region rich in aluminium, especially in the upper zone (aluminium sheet) of the keyhole, with a lower percentage of copper. This could have been caused by the stirring of the tool pin, which took the copper particles from the bottom plate upward, and favoured the presence of either rich aluminium regions or the presence of intermetallics.

This was observed by the decrease in the percentage of aluminium from the first analysed point to the last (eventually in the copper, where the percentage of copper increases considerably). This was observed in all the welds, except for the weld produced at 1200 rpm, 0.5 mm shoulder plunge depth using a conical pin and a concave shoulder.

Figures 4-49 – 4-51 show the SEM/EDS analyses of stir zone for the spot welds produced when using a flat pin and a flat shoulder tool, using 800 and 1200 rpm and using two shoulder plunge depths namely 0.5 and 1mm.

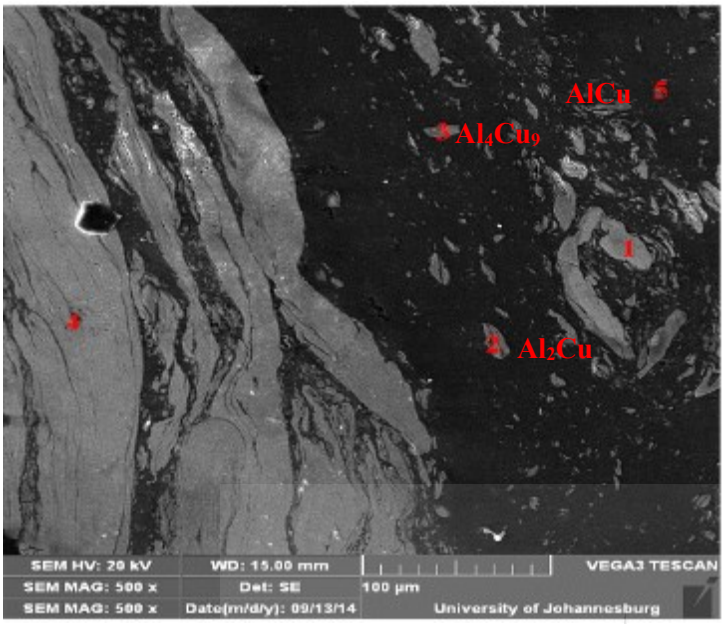

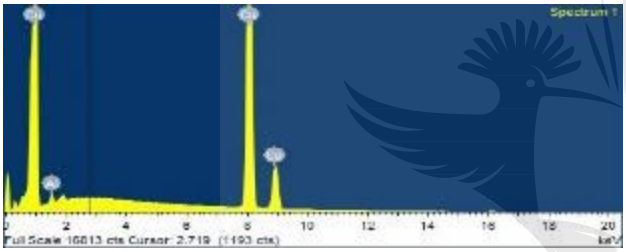

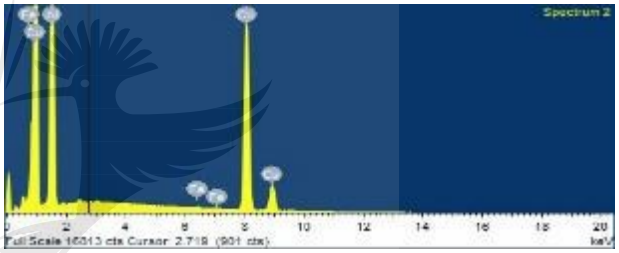

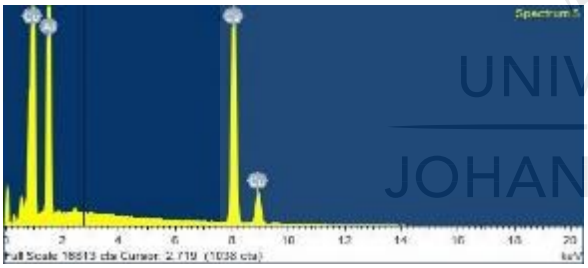

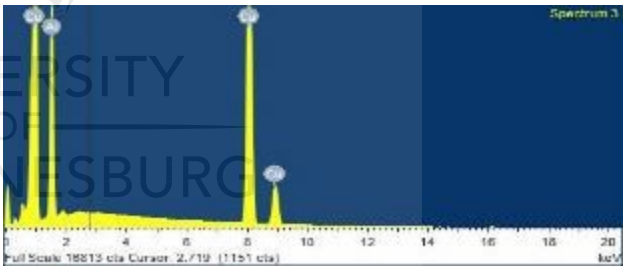

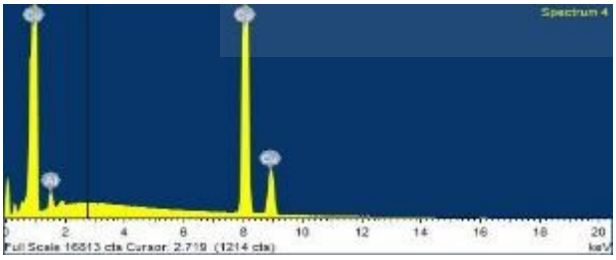

	Points				
Elements	1	2	3	4	5
Al	0.72	40.88	16.4	1.49	35.51
Cu	99.28	58.91	83.6	98.51	64.49

Figure 4-49 Scanning electron microscopy image and energy dispersive spectroscopy spectrums and chemical percentages of the weld produced at 800 rpm, 0.5 mm shoulder plunge depth using a flat pin and a flat shoulder of the stir zone

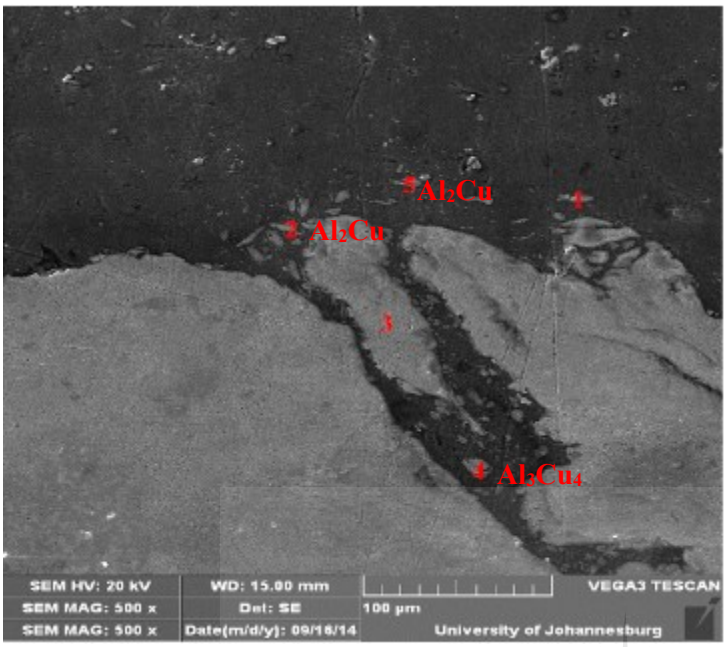

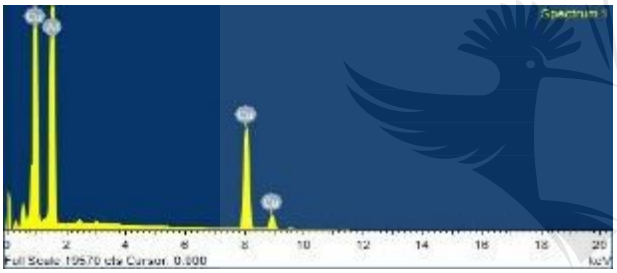

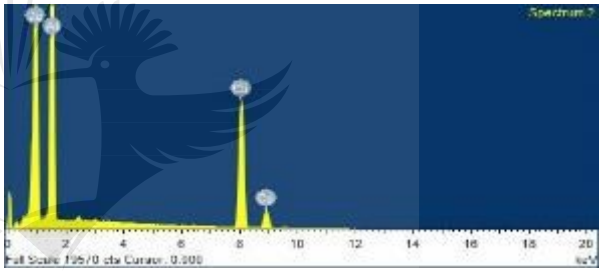

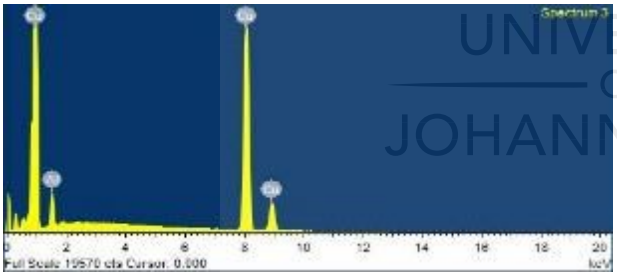

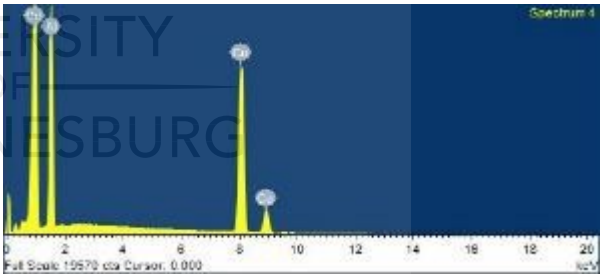

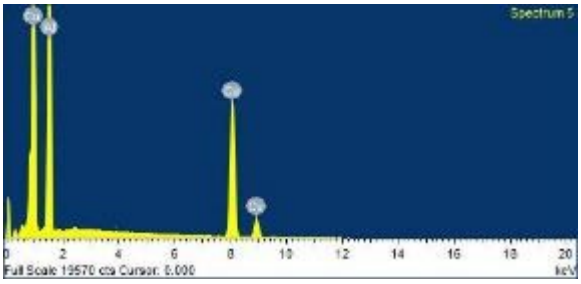

	Points				
Elements	1	2	3	4	5
Al	54.94	48.5	4.34	24.55	41.98
Cu	45.06	51.5	95.66	75.45	58.02

Figure 4-50 Scanning electron microscopy image and energy dispersive spectroscopy spectrums and chemical percentages of the weld produced at 1200 rpm, 0.5 mm shoulder plunge depth using a flat pin and a flat shoulder of the stir zone

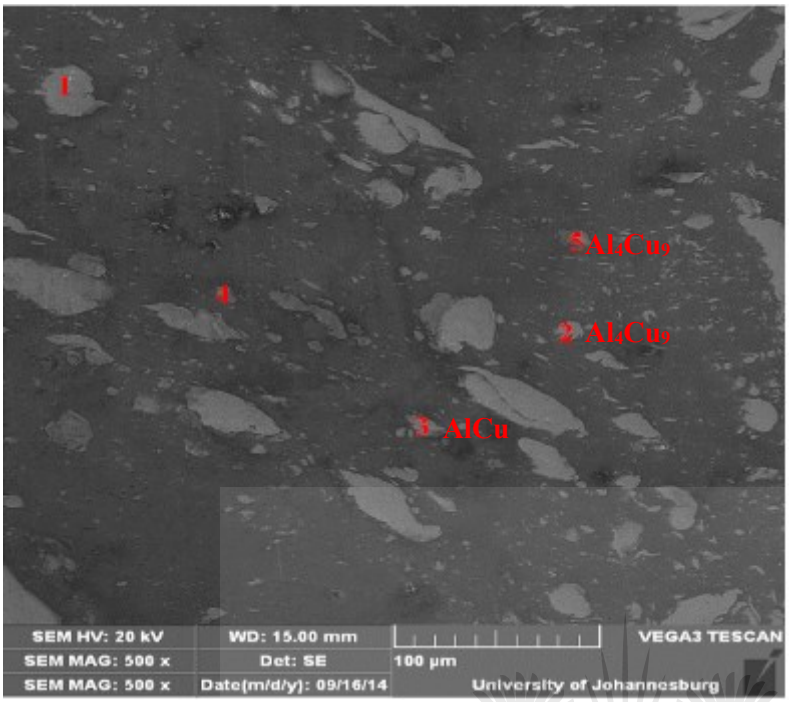

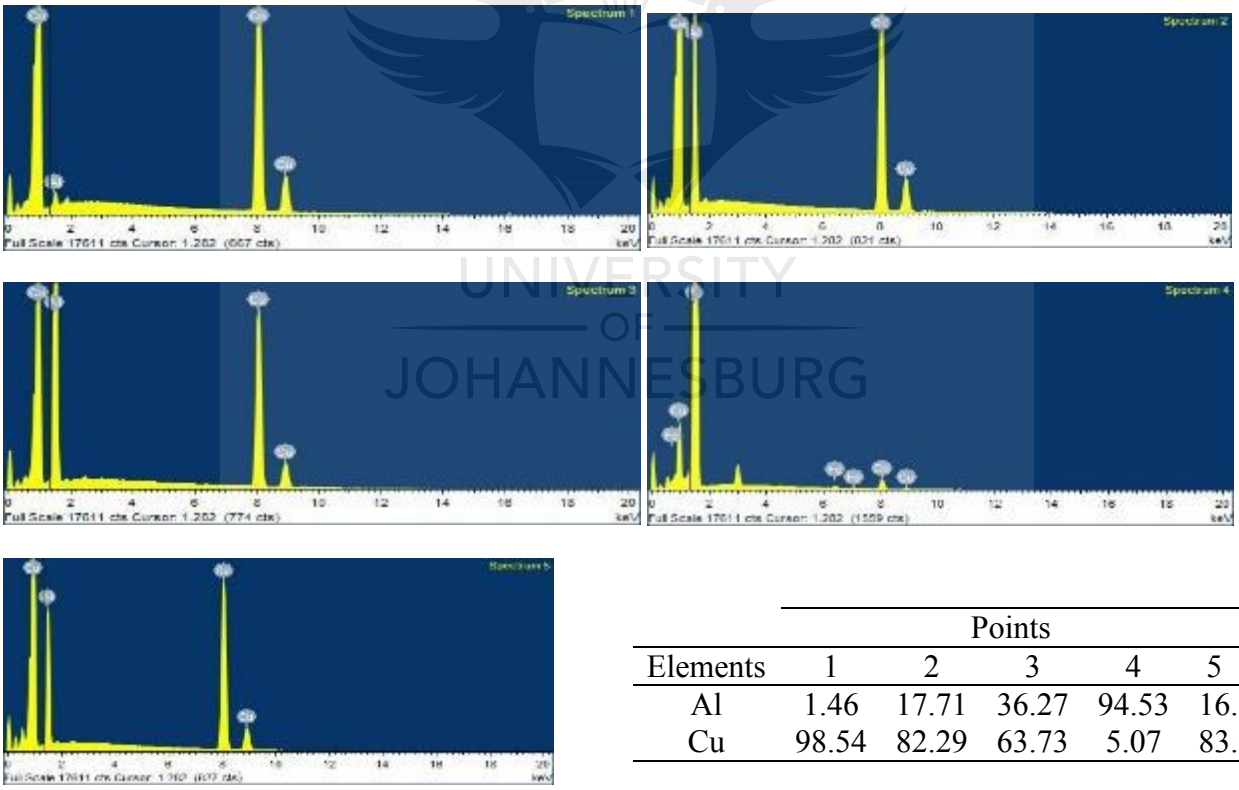

	Points				
Elements	1	2	3	4	5
Al	1.46	17.71	36.27	94.53	16.98
Cu	98.54	82.29	63.73	5.07	83.02

Figure 4-51 Scanning electron microscopy image and energy dispersive spectroscopy spectrums and chemical percentages of the weld produced at 1200 rpm, 1 mm shoulder plunge depth using a flat pin and a flat shoulder of the stir zone

Three intermetallic compounds, namely: AlCu, Al_4Cu_9 and Al_2Cu were found in the stir zone of the weld produced at 800 rpm, 0.5 mm shoulder plunge depth, as shown in Figure 4-49; whereas the weld produced at 1200 rpm and 0.5 mm shoulder plunge depth contained Al_2Cu and Al_3Cu_4 intermetallic compounds (Figure 4-50). On the other hand, the Al_4Cu_9 and AlCu intermetallics were found in the weld produced at 1200 rpm and 1 mm shoulder plunge depth (Figure 4-51).

From Figure 4-52 to Figure 4-55, the SEM/EDS results of the stir zone for the spot welds produced when using a conical pin and a concave shoulder tool, are shown. These welds were produced using different process parameters. Only Al_4Cu_9 intermetallic was found in the weld produced at 800 rpm and 0.5 shoulder depth (Figure 4-52); whereas Al_4Cu_9 and AlCu were present in the weld produced at the same rotational speed, but with a 1 mm shoulder plunge depth (Figure 4-53). Three intermetallics, namely: Al_2Cu, AlCu and $AlCu_3$ were present in the weld produced at 1200 rpm and 0.5 shoulder plunge depth (Figure 4-54); while only AlCu was found in the weld produced at 1200 rpm and 1 mm shoulder plunge depth (Figure 4-55).

The presence of intermetallics in the produced welds were further investigated by using the XRD technique in three different zones, namely: the stir zone (SZ); the thermo mechanically affected zone (TMAZ); and the heat- affected zone (HAZ). The above cited investigation will be presented in the section to follow.

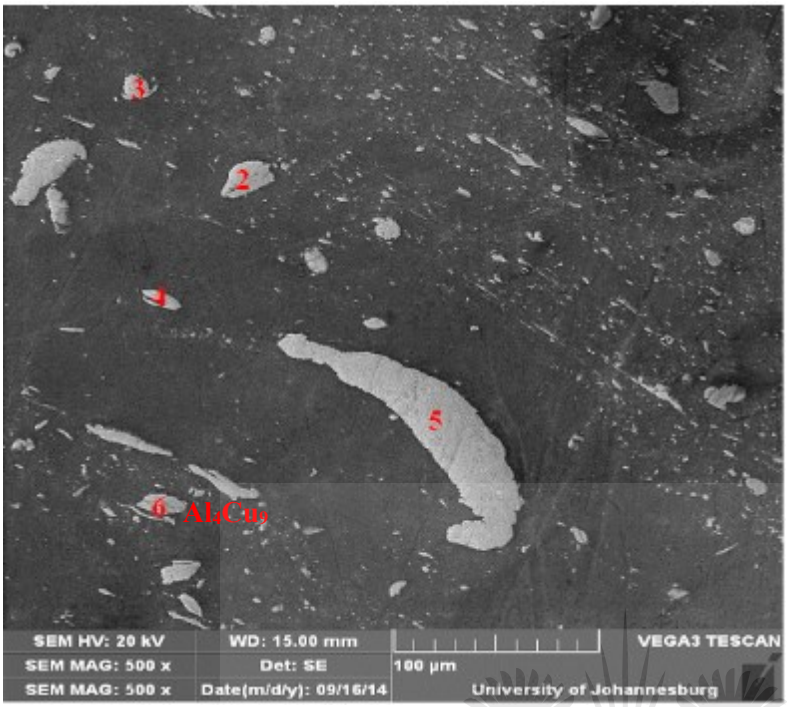

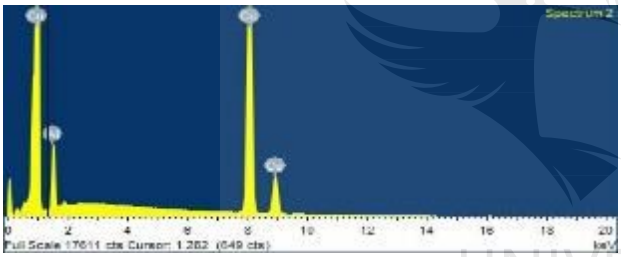

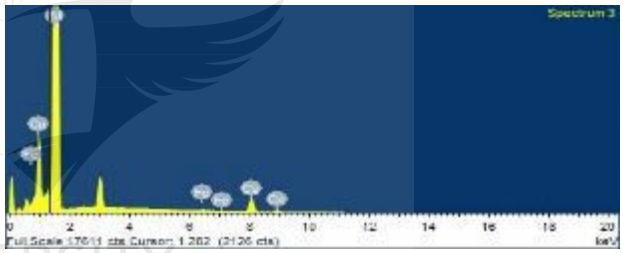

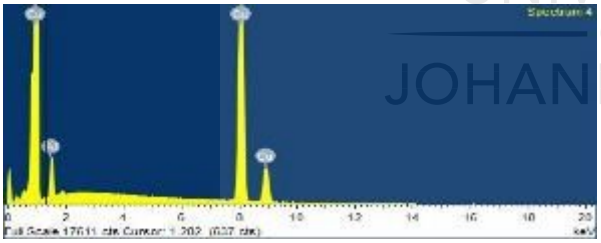

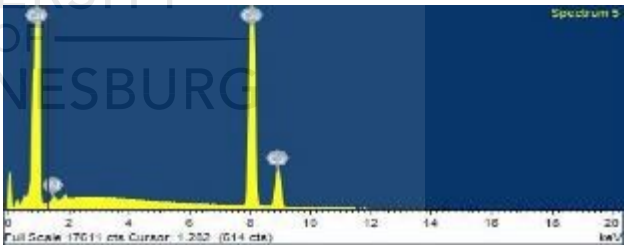

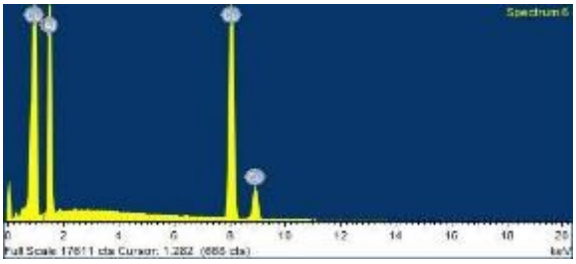

	Points				
Elements	2	3	4	5	6
Al	6.21	94.79	4.17	0.55	20.45
Cu	93.79	5.01	95.83	99.45	79.55

Figure 4-52 Scanning electron microscopy image and energy dispersive spectroscopy spectrums and chemical percentages of the weld produced at 800 rpm, 0.5 mm shoulder plunge depth using a conical pin and a concave shoulder of the stir zone

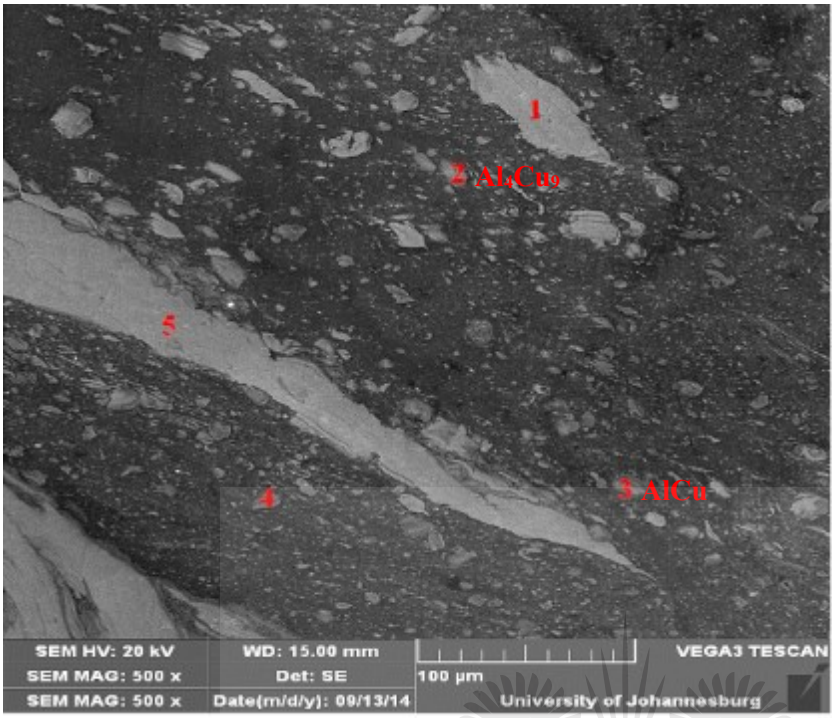

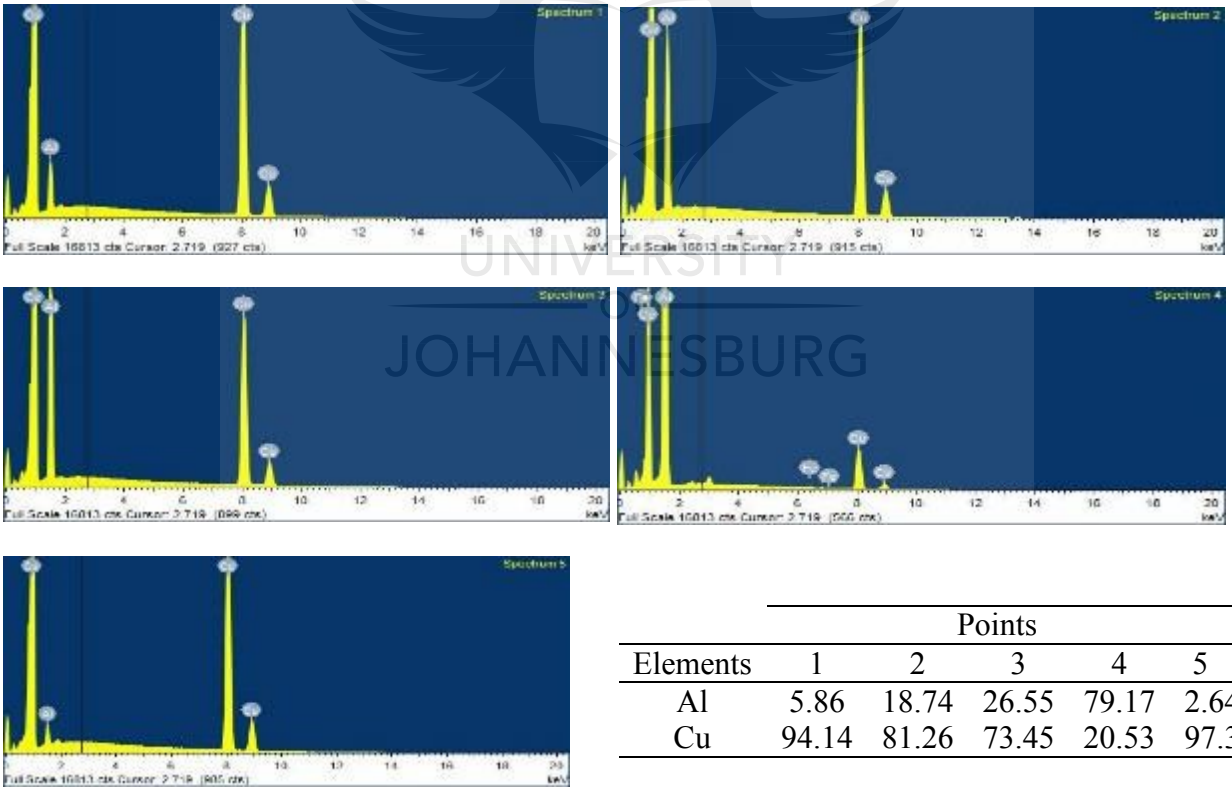

	Points				
Elements	1	2	3	4	5
Al	5.86	18.74	26.55	79.17	2.64
Cu	94.14	81.26	73.45	20.53	97.36

Figure 4-53 Scanning electron microscopy image and energy dispersive spectroscopy spectrums and chemical percentages of the weld produced at 800 rpm, 1 mm shoulder plunge depth using a conical pin and a concave shoulder of the stir zone

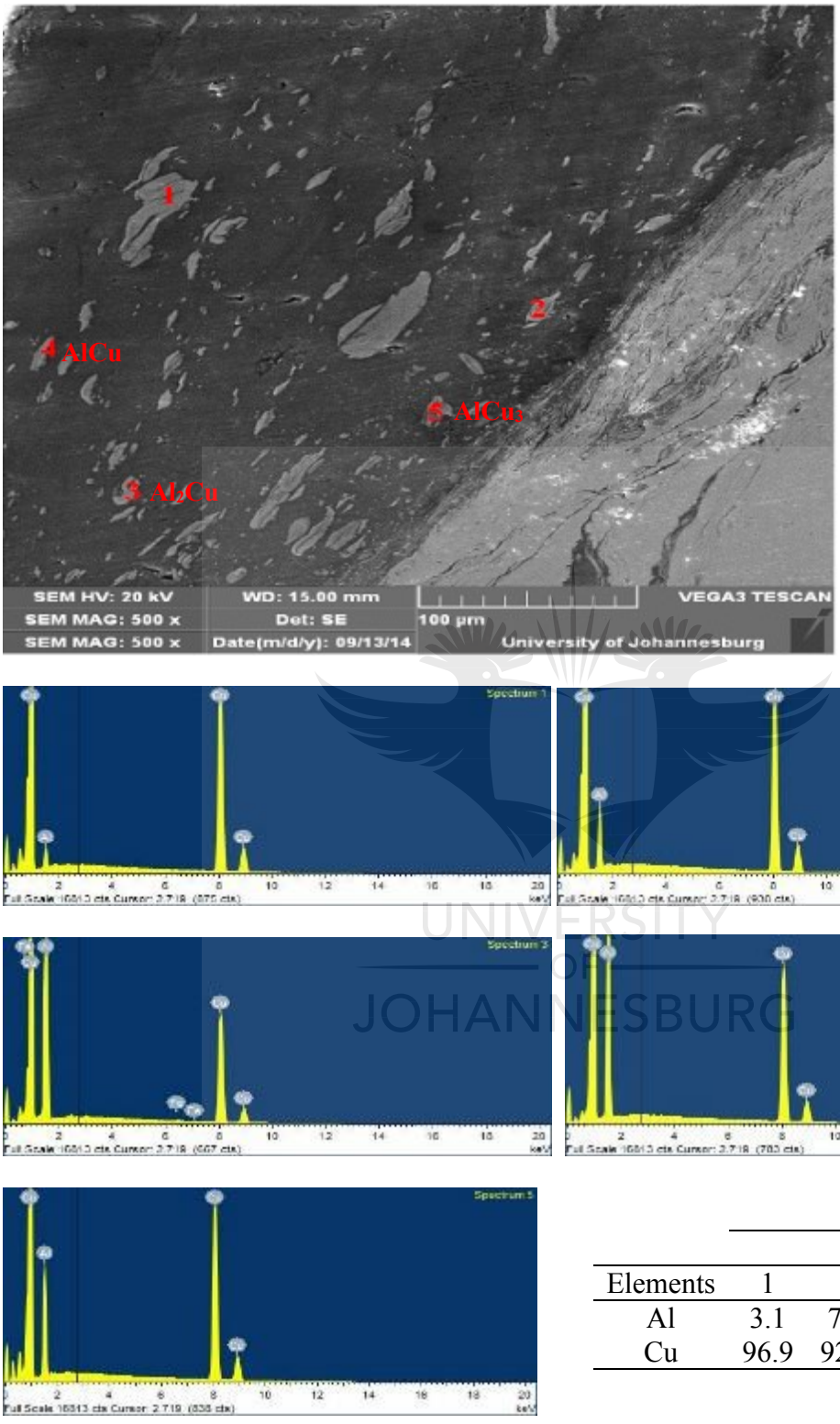

	Points				
Elements	1	2	3	4	5
Al	3.1	7.82	49.49	29.22	13.77
Cu	96.9	92.18	50.27	70.78	86.23

Figure 4-54 Scanning electron microscopy image and energy dispersive spectroscopy spectrums and chemical percentages of the weld produced at 1200 rpm, 0.5 mm shoulder plunge depth using a conical pin and a concave shoulder of the stir zone

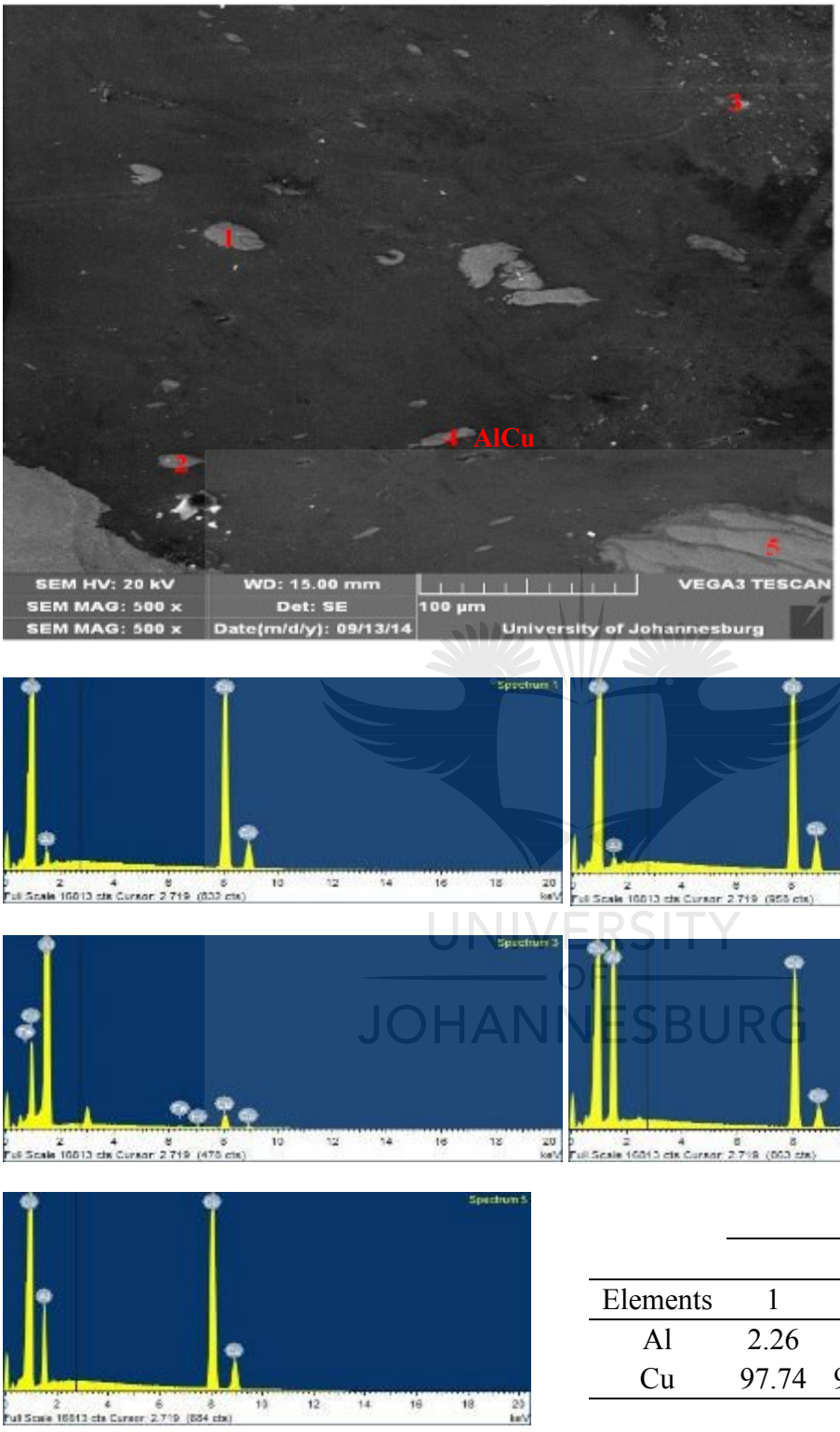

	Points				
Elements	1	2	3	4	5
Al	2.26	1.33	92.77	37.35	9.15
Cu	97.74	98.67	6.97	62.65	90.85

Figure 4-55 Scanning electron microscopy image and energy dispersive spectroscopy spectrums and chemical percentages of the weld produced at 1200 rpm, 1 mm shoulder plunge depth using a conical pin and a concave shoulder of the stir zone

4.7 Lap shear tensile tests

In dissimilar-metal friction stir spot welding (FSSW), the formation of intermetallic compounds, especially in the SZ, can significantly reduce the joint strength. The results in Tables 4.7 and 4.8 reveal the failure loads results of FSSW between aluminium and copper when using different tools and process parameters. The shear load / displacement results for individual welds can be found in Appendix J.

Table 4.7: Failure load results for the welds produced with a flat pin and a flat shoulder

Rotation speed (rpm)	Tool shoulder plunge depth (mm)	Failure load (N)			Mean Failure load (N)
		Weld 1	Weld 2	Weld 3	
800	0.5	761	2547	2697	2622
800	1	5225	1281	4498	3668
1200	0.5	245	4459	1271	4459
1200	1	3207	4289	4844	4113

Table 4.8: Failure load results for the welds produced using a conical pin and a concave shoulder

Rotation speed (rpm)	Tool shoulder plunge depth (mm)	Failure load (N)			Mean Failure load (N)
		W 1	W2	W3	
800	0.5	1173	1833	2991	2412
800	1	1373	1077	2739	2056
1200	0.5	3454	3978	4086	3839
1200	1	4609	202	2380	3495

High failure loads of 5225 N and 4844 N were obtained when using a flat pin and a flat shoulder at 800 rpm, 1 mm shoulder plunge depth and 1200 rpm and 1 mm shoulder plunge depth, respectively. It was observed that by increasing the plunge depth, strong welds were obtained; this was in agreement with the results obtained by Heideman *et al.* [8]. Furthermore, the two highest failure loads obtained using a conical pin and a concave shoulder were 2991 N and 4606 N; the

parameters used were 800 rpm, 0.5mm shoulder plunge depth and 1200 rpm, 1 mm shoulder plunge depth, respectively.

It was observed that, a strong weld was obtained by using 800 rpm and 0.5 mm shoulder plunge depth; and the welds using the same rotation speed and 1 mm shoulder plunge depth gave a slightly lower failure load. Figures 4-56 and 4-57 show the test results, representing the highest shear loads and displacements curves of the friction stir spot welds when using different tool geometries and process parameters.

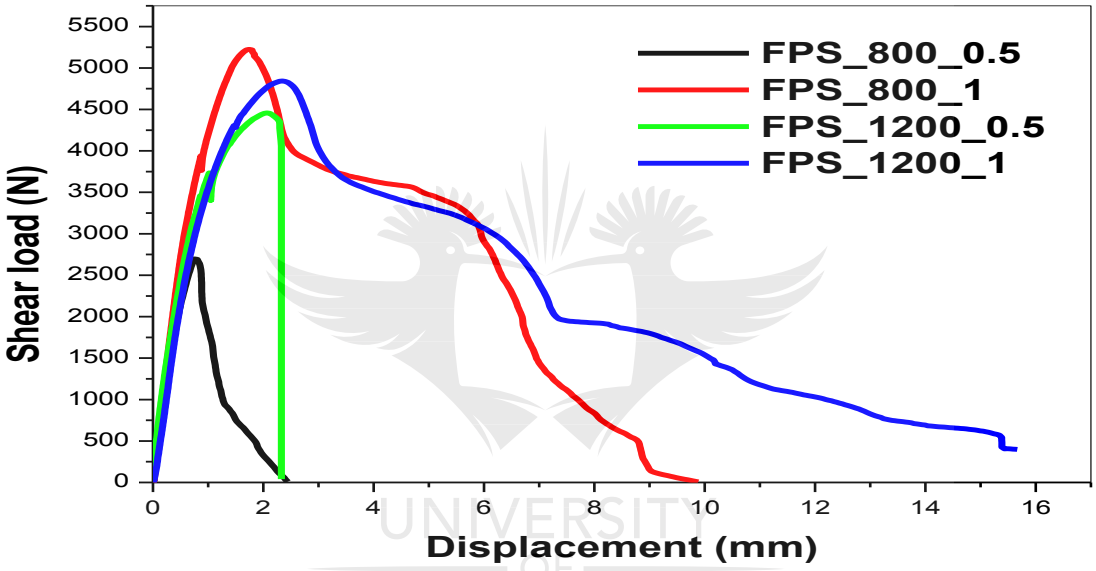

Figure 4-56 Load- displacement curves of friction stir spot welds, using a flat pin and shoulder

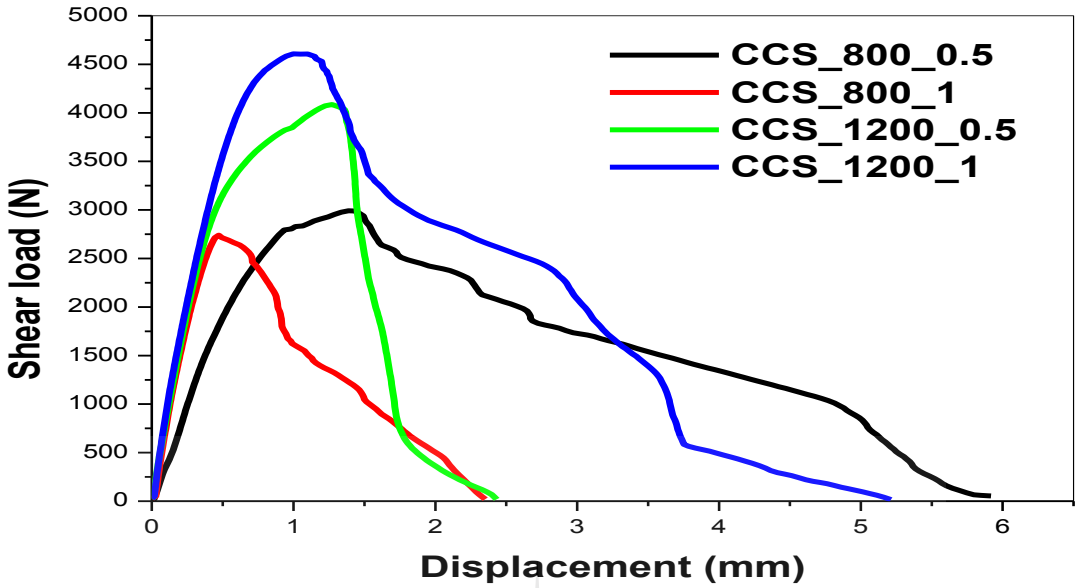

Figure 4-57 Load- displacement curves of friction stir spot welds when using a conical pin and a concave shoulder

It was observed that all the fractures were ductile. Furthermore, the presence of the copper ring extruded upward on both side of the keyhole from the lower copper plate. This was suspected to influence the fracture mode. The copper ring caused interlocking between the two sheets and helped the sheets adhere to each other during the tensile testing, and to reach a high strength before failure [8]. The effect of the process parameters on the maximum failure load is depicted in Figures 4-58 and 4-59, respectively for the welds produced when using a flat pin/ flat shoulder and conical pin and concave shoulder. It was observed that as the shoulder plunge depth increases, the failure load increases, except for the weld produced at 800 rpm when using a conical pin and a concave shoulder.

Figures 4-60 and 4-61 show the fractured samples of the welds produced at 1200 rpm, 0.5 mm shoulder plunge depth using a flat pin and a flat shoulder tool, and at 800 rpm, 0.5 mm shoulder plunge depth when using a conical pin and a concave shoulder tool, respectively.

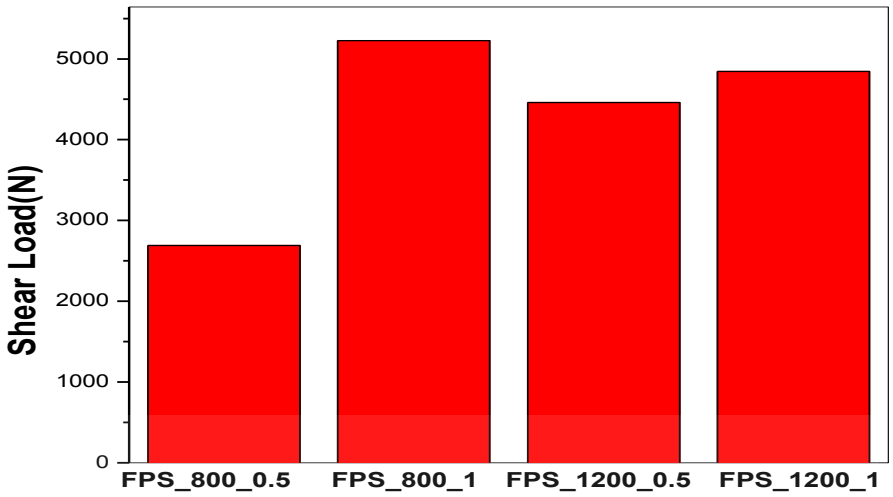

Figure 4-58 Showing the effect of process parameters on the maximum failure load of the welds produced using a flat pin and a flat shoulder tool at 800 rpm and 1200 rpm.

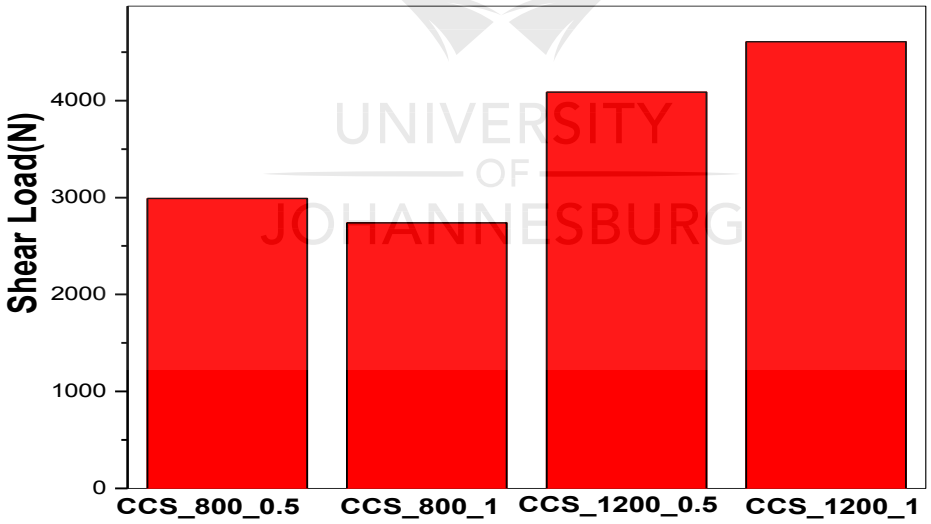

Figure 4-59 Showing the effect of process parameters on the maximum failure load of the welds produced using a conical pin and a concave shoulder tool at 800 rpm and 1200 rpm.

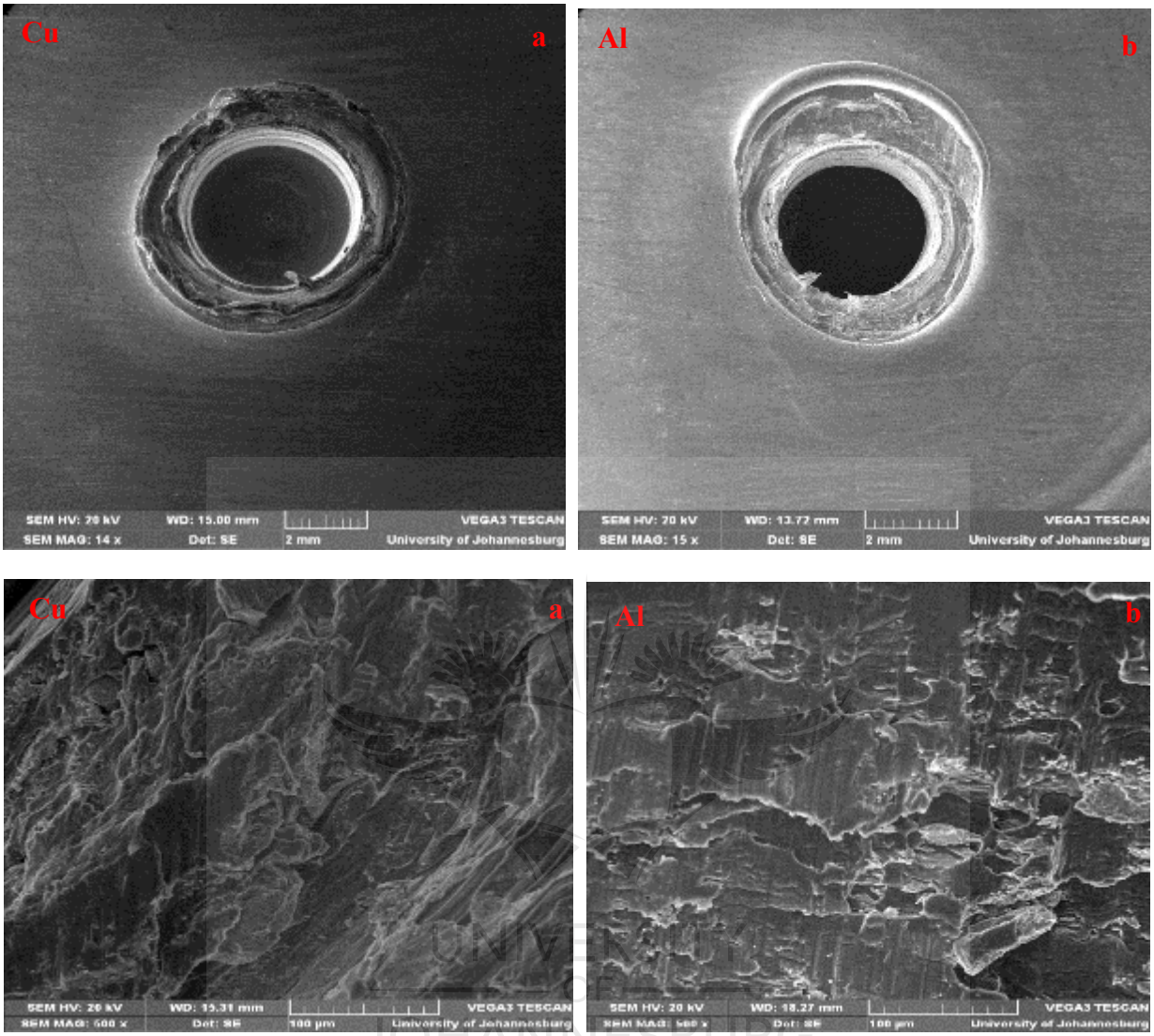

Figure 4-60 SEM images of spot weld produced using a flat pin and a flat shoulder tool; the rotation speed was 1200 rpm and the shoulder plunge depth of 0.5mm, (a) failed nugget upper sheet (Cu), (b) the lower sheet (Al), (c) and (d) fractured surface on the copper and aluminium side, respectively

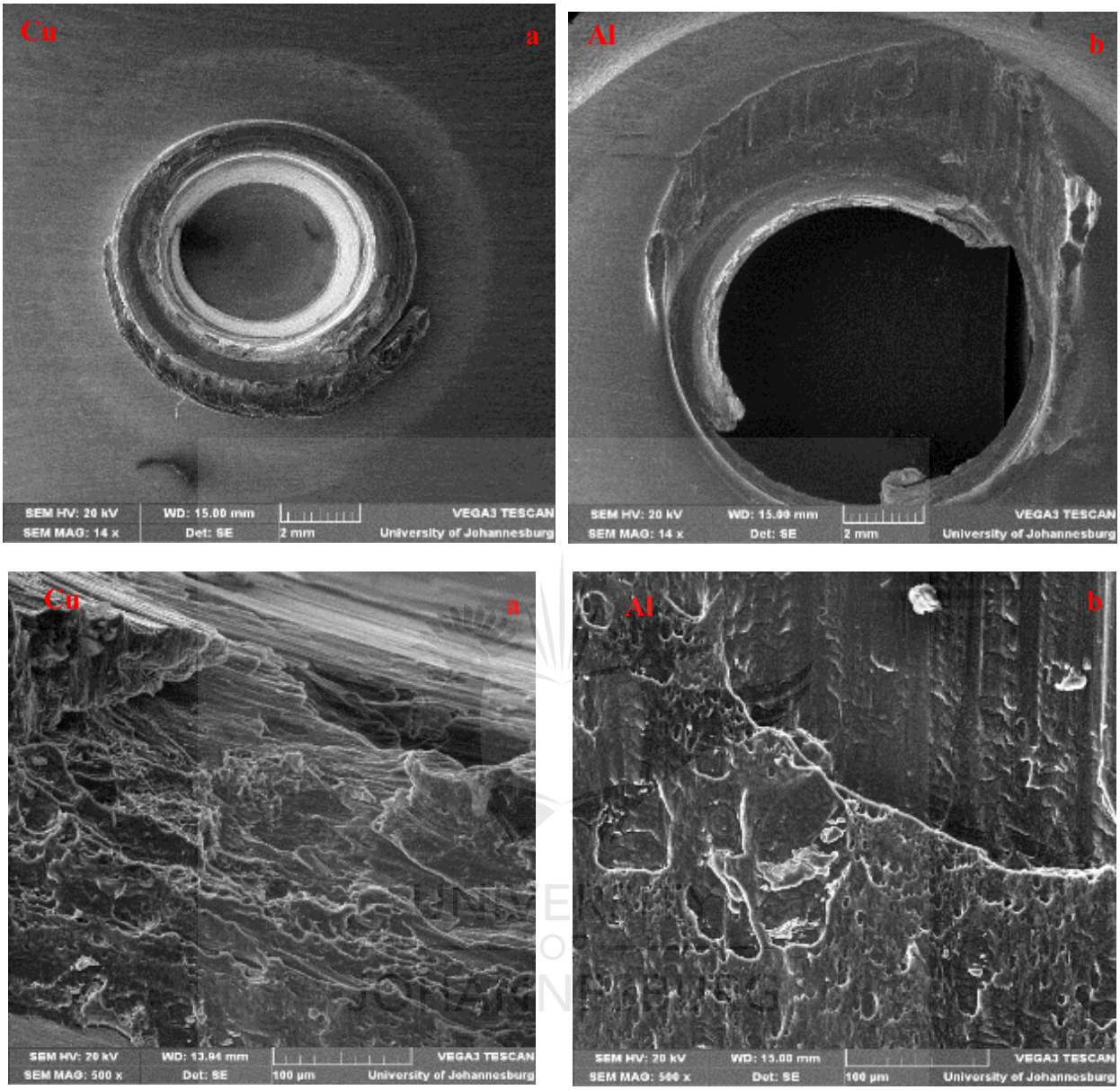

Figure 4-61 SEM images of spot weld produced using a conical pin and a concave shoulder tool; the rotation speed was 800 rpm and the shoulder plunge depth of 0.5mm, (a) failed nugget upper sheet (Cu), (b) the lower sheet (Al), (c) and (d) fractured surface on the copper and aluminium side, respectively

Based on a study conducted by Lin *et al.* [148], the shear failure mechanism is the principal failure initiation mechanism of the nugget pull out failure mode in lap-shear specimens from the mechanical point of view. Only one fracture mode was observed in all the analysed samples, as is shown in Figures 4-60 and 4-61 (a and b). Only the pull nugget failure mode was observed; and

this was due to the difference in properties of the parent materials. The fracture surface of the spot weld made when using a flat pin / flat shoulder tool and a conical pin/concave shoulder tool at a the rotation speed of 1200 rpm / 0.5 mm shoulder plunge depth and 800 rpm / 0.5 mm shoulder plunge depth, respectively, observed using SEM, is shown in Figures 4-60 and 4-61 (c and d), which reveals a ductile morphology. It can also be seen that the prominent fracture surface includes the presence of small dimples, which can be attributed to the homogeneous microstructure of the small grains at the failure location [149]. The dimples were in different sizes, which can be attributed to the different process parameters and the tool geometries used.

The presence of a cavity defect in some of the fractured samples was observed; this could be the cause of the low shear tensile load results (Tables 4.7 and 4.8). This was in agreement with the results obtained by Tan *et al.* [150].

4.7.1 Effect of varying shoulder plunge depths

The shear tensile results showed in some cases that there is a big difference in the results of the spot welds produced when using the same process parameters and tool geometry. In this section, the effect of the variation in plunge depth using the same process parameters and tool geometry will be investigated. Measurements were taken from the bottom of the pin hole to the original bottom of the bottom plate (copper); and the results are shown in Tables 4.9 and 4.10.

Table 4.9: Measurement from the bottom of the tool pin hole to the bottom of the second plate (copper) for the flat pin and the flat shoulder tool

Sample ID	FPS_800_0.5	FPS_800_1	FPS_1200_0.5	FPS_1200_1
Measurement	0.998 mm	0.815 mm	1.133 mm	0.839 mm

Table 4.10: Measurement from the bottom of the tool pin hole to the bottom of the second plate (copper) for the concave pin and the conical shoulder

Sample ID	CCS_800_0.5	CCS_800_1	CCS_1200_0.5	CCS_1200_1
Measurement	0.784 mm	0.711 mm	0.916 mm	0.629 mm

It is clear that the length of the plunge depth differs significantly, despite the use of the same welding parameters and tool geometry. The variation in the plunge depth is the responsible factor

for these differences in shear tensile results. It should be noted that the welding machine used in the current research project was position controlled machine, and not force controlled. Subsequently, a repeatable and exact plunge depth was difficult to obtain, which leads to a large variation of the plunge depths and differences in the shear tensile stress results. For repeatability reasons, it is recommended to use force controlled machines to produce good quality friction stir spot welds.

4.8 Microhardness profiles results of the spot welds

As indicated and illustrated in Chapter 3 (Figure 3-6). The Vickers microhardness measurements ($HV_{0.1}$) were conducted at the top (in the middle of the copper ring penetrating into the aluminium sheet) and the bottom (middle of the copper plate) of the samples. Figure 4-62 (a and b) and Figure 4-63 (a and b) show the microhardness values of the spot weld produced by using a flat pin and a flat shoulder tool, and a conical pin and a concave shoulder, respectively, at different process parameters. The measurements were taken at the top and bottom, as illustrated in Figure 3-6.

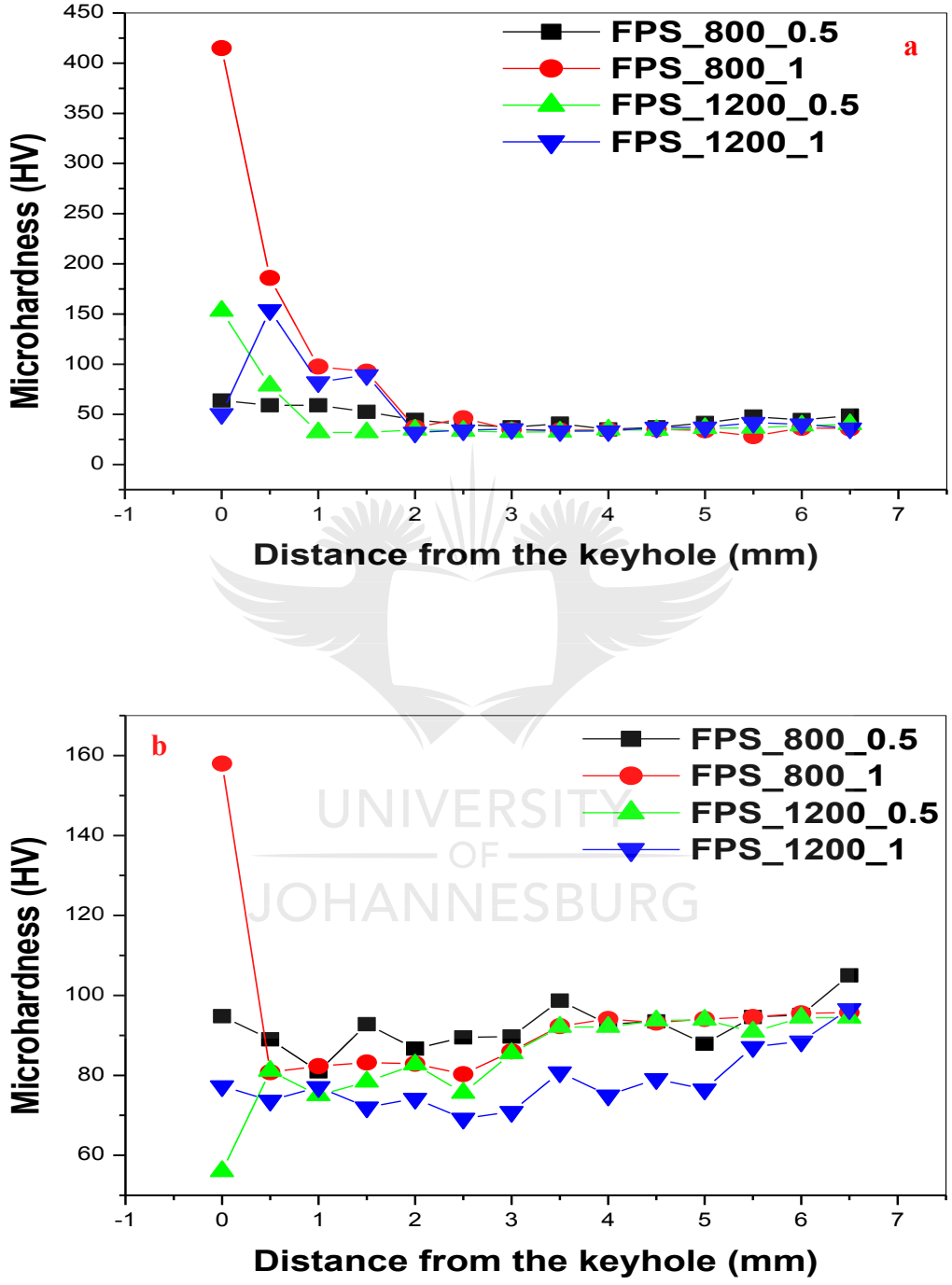

Figure 4-62 Microhardness distributions along the welds produced using a flat pin and a flat shoulder tool at different process parameters, (a) top and (b) the bottom

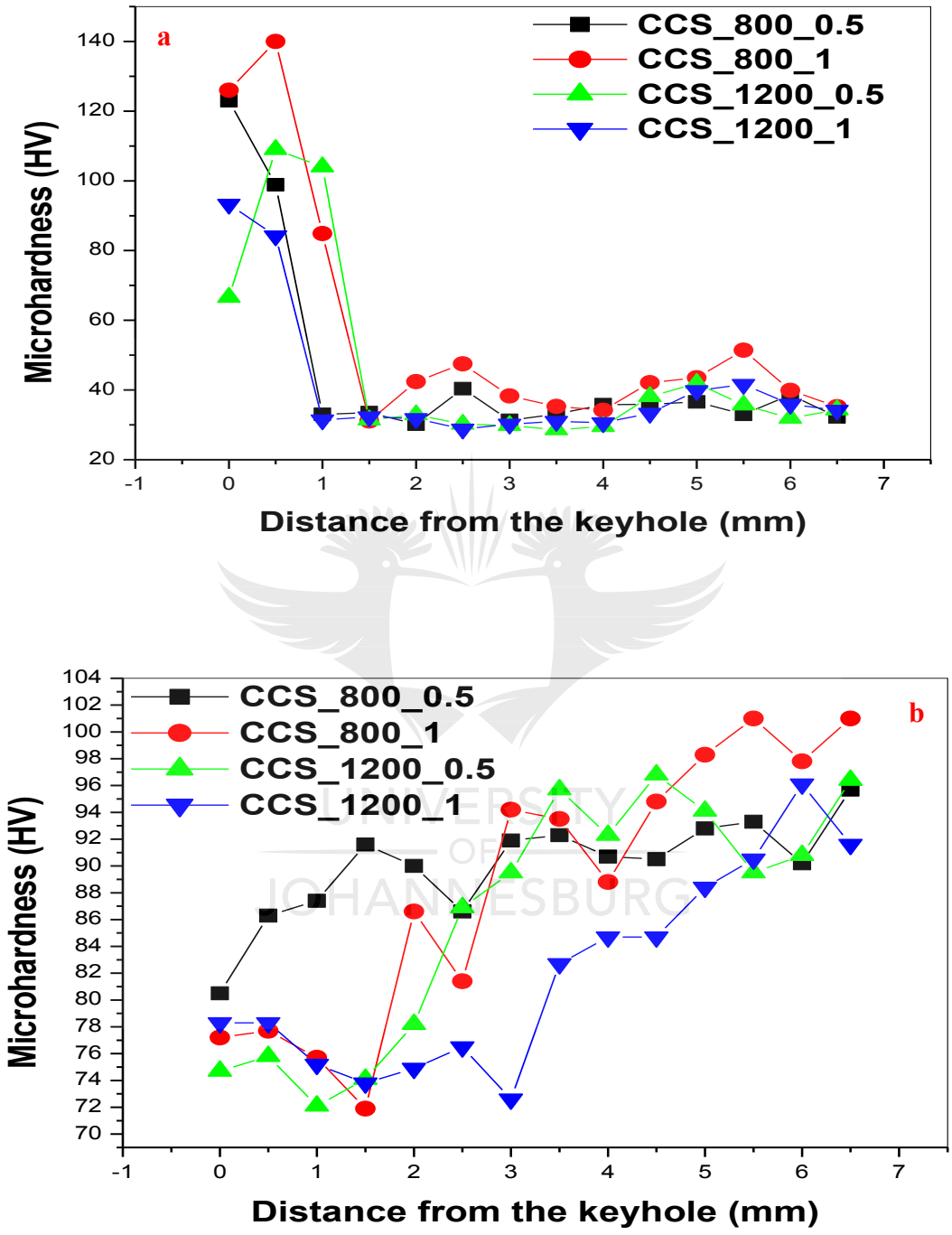

Figure 4-63 Microhardness distributions along the welds produced using a conical pin and a concave shoulder at different process parameters, (a) top and (b) the bottom

The base material microhardness values are in the range of 86.7- 96.3 HV for Cu; whereas for Al, the range is between 34.6- 40.3 HV. In all the samples, high microhardness values were recorded in the region close to the keyhole. It has been reported that the presence of hard and brittle intermetallic compounds could have caused the sudden increase of microhardness in the stir zone [10]. Furthermore, Shiraley [10] stated that the higher microhardness values around the keyhole have good consistency with the Cu layers severely broken up into fine particles that are randomly dispersed. However, the high microhardness values were possibly due to the presence of the intermetallic compounds [10].

These statements were in agreement with the results obtained in the current research study. The XRD analyses of the SZ revealed the presence of hard and brittle intermetallic compounds, including Al_2Cu, Al_3Cu_2, $AlCu_3$, Al_4Cu_9 and AlCu. This was further confirmed with the Energy Dispersive Spectroscopy conducted in the SZ. The highest microhardness values of 63.8 HV, 415 HV, 153 HV and 154 HV were obtained at the top side of the samples for FPS_800_0.5, FPS_800_1, FPS_1200_0.5 and FPS_1200_1, respectively (Figure 4-62 (a)). While, 105 HV, 158 HV, 94.4 HV, and 96 HV microhardness values were found at the bottom measurements of the same samples, as illustrated in Figure 4-62 (b).

On the other hand, the maximum microhardness values of 123 HV, 140 HV, 109 HV, and 93.3 HV were obtained at the top for CCS_800_0.5, CCS_800_1, CCS_1200_0.5 and CCS_1200_1, respectively (Figure 4-63 (a)). Whereas, 95. 7 HV, 101 HV, 96 HV and 96.1 HV microhardness values were obtained in the bottom measurements of the same samples, as shown in Figure 4-63 (b). Furthermore, all the microhardness values recorded in the regions close to the keyhole for all the spot welds produced using a conical pin and a concave shoulder (bottom) have the lower values, which were close to the average value of the copper base material; the microhardness values increase with the increase of the distance from the keyhole. This was possibly due to the presence of the aluminium particles mixed in with the copper particles in that region close to the copper plate.

The aluminium particles were pushed down into the vicinity of the copper plate during the tool rotation movement.

Figures 4-64 (a and b) and 4-65 (a and b) depict the variation of the maximum obtained microhardness values when using different process parameters and tool geometries.

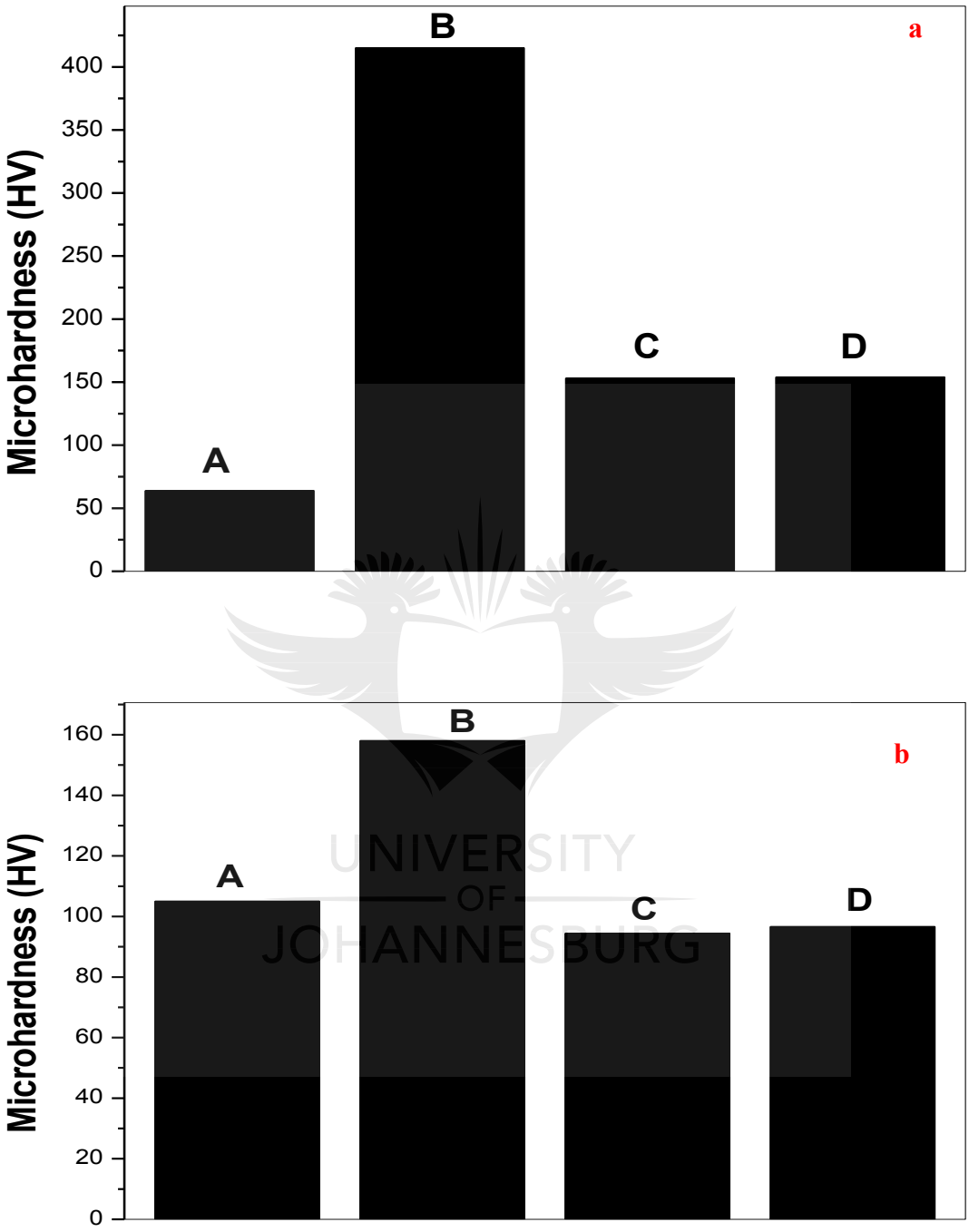

Figure 4-64 Variation of maximum obtained microhardness values using different process parameters and locations a (top), b (bottom), A (FPS_800_0.5), B (FPS_800_1), C (FPS_1200_0.5), and D (FPS_1200_1)

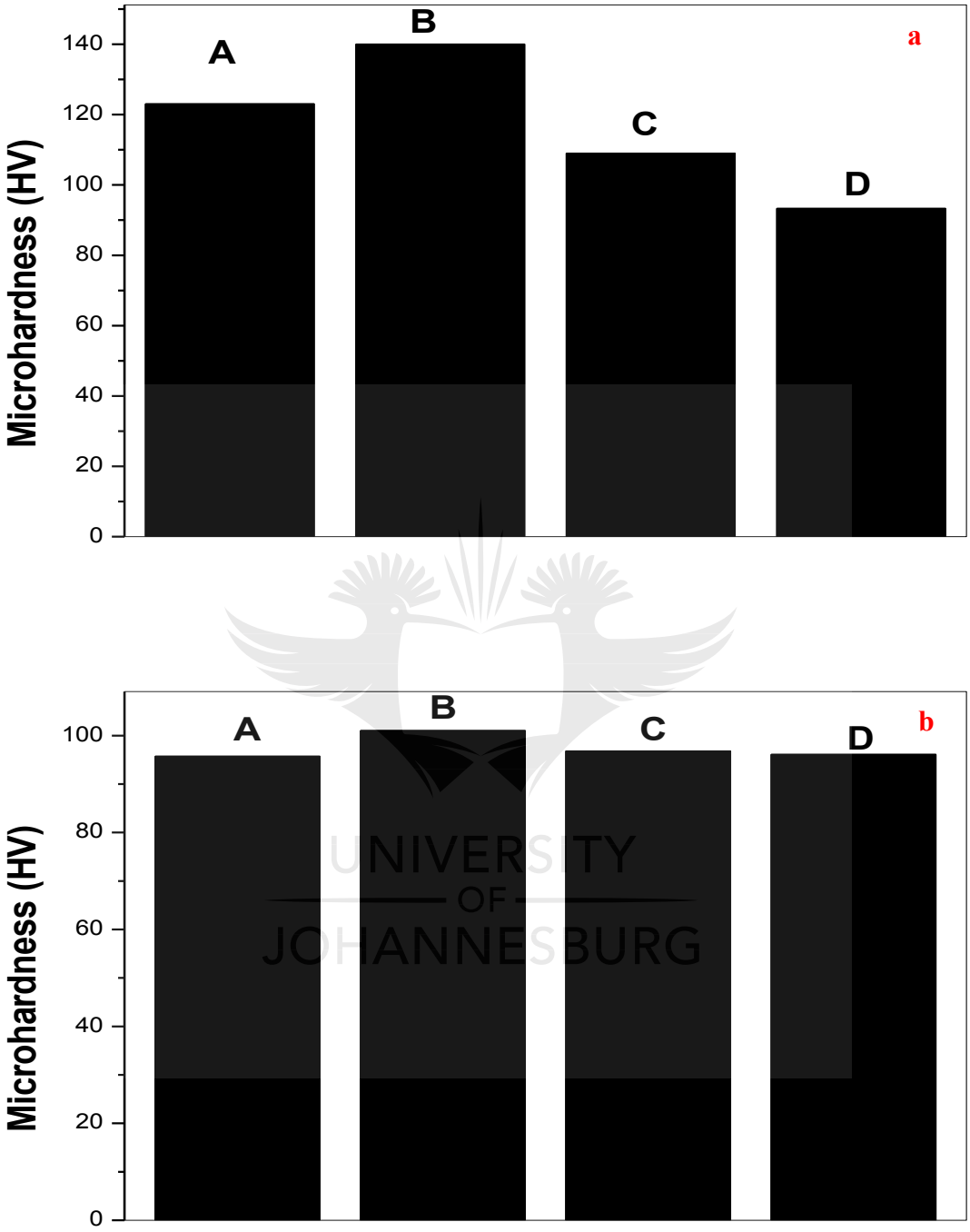

Figure 4-65 Variation of maximum obtained microhardness values using different process parameters and locations a (top), b (bottom), A (CCS_800_0.5), B (CCS_800_1), C (CCS_1200_0.5), and D (CCS_1200_1)

Additionally, it was observed that the shoulder plunge depth had an effect on the microhardness values of all the samples, except the spot weld produced at 1200 rpm and 1 mm shoulder plunge depth; where a decrease was observed for the measurement carried out at the top the samples. As for the bottom measurements, a similar observation was noticed (Figure 4-64 (a and b) and 4-65 (a and b).

4.9 X-Ray Diffraction analysis

The X-ray diffraction pattern of the aluminium and copper is shown in Figures 4-66 and 4-67 respectively.

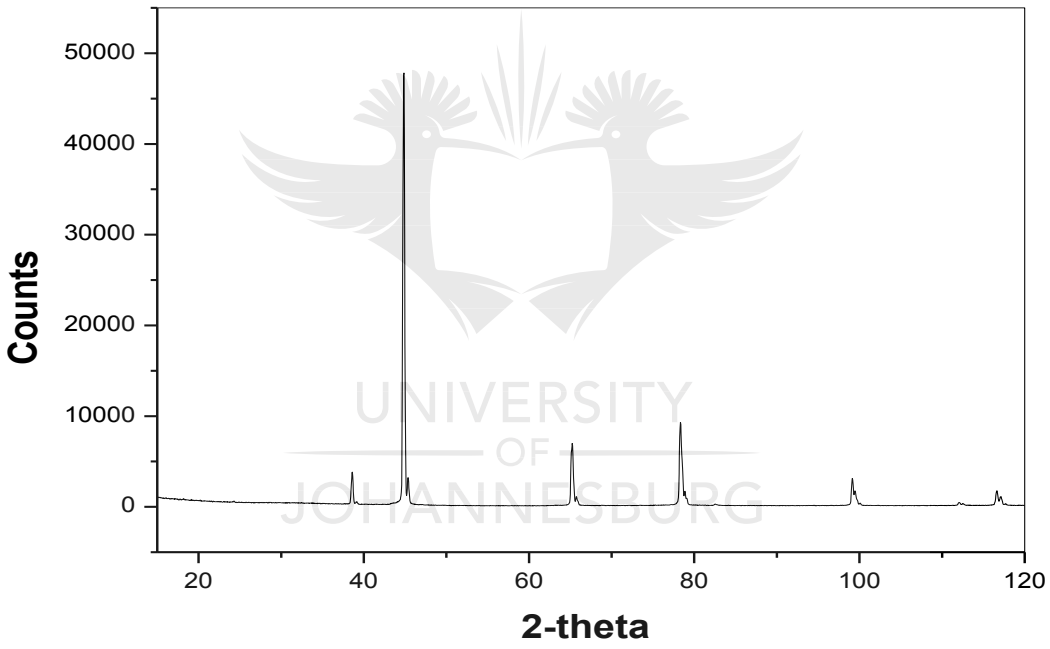

Figure 4-66 XRD diffraction pattern of the aluminium parent material (AA1060)

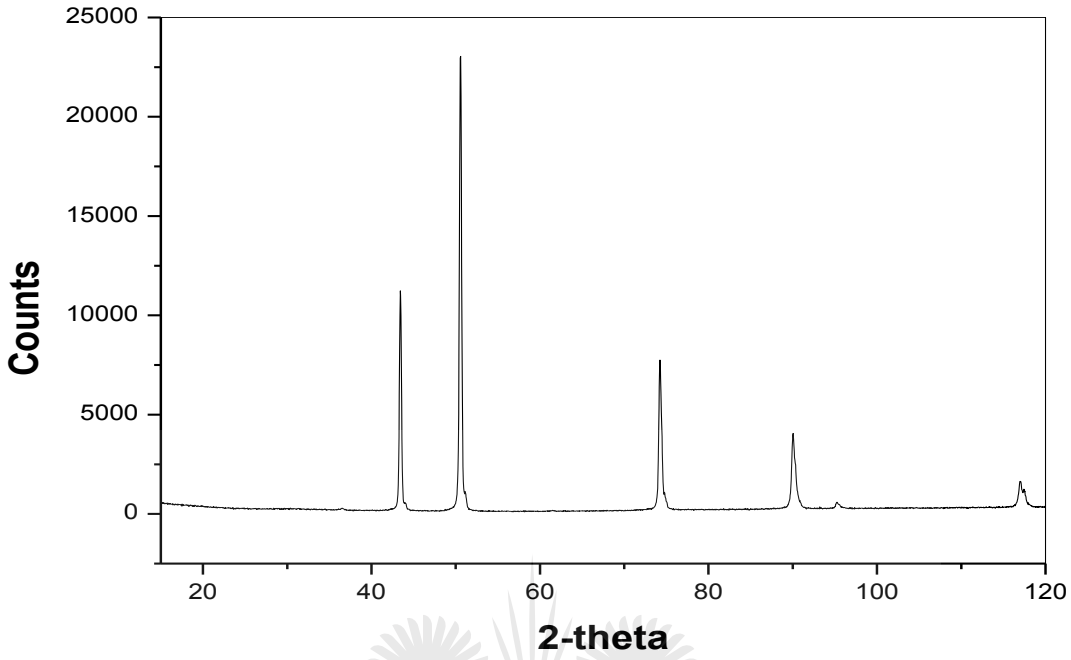

Figure 4-67 XRD diffraction pattern of the copper parent material (C11000)

The results of the XRD analysis performed in three different locations of the spot weld samples, namely, the stir zone, the thermo-mechanically affected zone and the heat-affected zone. This was done by using a 0.8 mm collimator, as shown in Tables 4.11 and 4.12 for the samples produced using a flat pin/ flat shoulder and conical pin / concave shoulder tool, respectively. The XRD patterns obtained in the three different zones show intense aluminium and copper peaks; while low intensity XRD peaks depict the intermetallic compounds. Several authors in friction stir welding and friction stir spot welding between aluminium and copper found the presence of intermetallic compounds in different zones of the welds [10, 87, 89, 95, 101, and 105].

Because of their low concentrations in the different samples, the intermetallics could not be well identified. Similar results were obtained by Akinlabi [105]. Furthermore, intermetallics were found in all the analysed spot samples. This could be due to the fact that welds were produced at one spot; where the amount of heat generated was high, which could lead to the formation of intermetallic compounds; since they are thermally activated phases [91]. Furthermore, a study conducted by Galvao *et al.* [95] confirmed and justified the presence of a high melting point for

intermetallic compounds, such as Cu_9Al_4 (1030°C) in the characterised samples when using XRD. They further justified that this was due to the occurrence of the thermo mechanically induced solid state diffusion.

XRD analyses conducted by using a 2 mm collimator revealed the presence of intermetallics (Al_2Cu, Cu_3Al) in only the samples produced at 800 rpm, 1mm shoulder plunge depth and 1200 rpm, 0.5 mm shoulder plunge depth using a conical pin and concave shoulder. It was also noticed that some of the intermetallic compounds' peaks overlapped with the peaks of the base materials. Figure 4-68 shows the XRD diffractogram of the FPS_800_1 sample for the stir zone. While Figure 4-69 depicts the XRD diffractogram for the stir zone of the CCS_800_0.5 sample.

Table 4.11: List of intermetallic compounds found in different zones of the spot weld samples produced using a flat pin and a flat shoulder

Weld ID	Zone	Intermetallic compounds
FPS_800_0.5	Stir zone	Al Cu_3, Al_4Cu_9, Al_2Cu, Al_3Cu_2, Al_2Cu_3, AlCu
	Thermo-mechanically affected zone	$AlCu_4$
	Heat-affected zone	$AlCu_4$
FPS_800_1	Stir zone	Al_2Cu, Al_3Cu_2, Al Cu_3
	Thermo-mechanically affected zone	Al Cu_3, Al_2 Cu_3, Al_2Cu
	Heat-affected zone	Al_4Cu_9, Al_2 Cu_3, Al_2Cu
FPS_1200_0.5	Stir zone	Al Cu_3, Al_4Cu_9, Al_2Cu, AlCu
	Thermo-mechanically affected zone	Al_4Cu_9, Al_2Cu, Al_2Cu_3, Al_4Cu, AlCu
	Heat-affected zone	Al Cu_3, Al_4Cu_9, Al_2Cu_3, AlCu
FPS_1200_1	Stir zone	Al Cu_3, Al_4Cu_9, Al_2Cu, Al_2Cu_3 , AlCu
	Thermo-mechanically affected zone	Al_4Cu_9, Al_2Cu, Al_2Cu_3 , Al_4Cu
	Heat-affected zone	Al Cu_3, Al_4Cu_9, Al_2Cu, Al_3Cu_2, Al_2 Cu_3, Al_4Cu

Table 4.12: List of intermetallic compounds found in different zones of the spot welds samples produced using a conical pin and a concave shoulder

Weld ID	Zone	Intermetallic compounds
CCS_800_0.5	Stir zone	$AlCu_3$, Al_4Cu_9, Al_2Cu, Al_3Cu_2
	Thermo-mechanically affected zone	Al Cu_3, Al_2Cu, Al_2 Cu_3
	Heat-affected zone	Al_2Cu, Al_2Cu_3, Cu_3Al, Al_4Cu_9, Al_3Cu_2
CCS_800_1	Stir zone	Al_2Cu, Al_4Cu_9, Cu_3Al, Al_3Cu_2, AlCu, Al_2Cu_3
	Thermo-mechanically affected zone	Al Cu_3, Al_4Cu_9, Al_2Cu, Al_3Cu_2, AlCu
	Heat-affected zone	Al Cu_3, Al_4Cu_9, Al_2Cu, Al_3Cu_2, AlCu, Al_2 Cu_3
CCS_1200_0.5	Stir zone	$AlCu_3$, Al_4Cu_9, Al_2Cu, Al_3Cu_2
	Thermo-mechanically affected zone	Al Cu_3, Al_4Cu_9, Al_2Cu, Al_2 Cu_3
	Heat-affected zone	Al_2 Cu_3, Al_2Cu
CCS_1200_1	Stir zone	Al Cu_3, Al_4Cu_9, Al_2Cu, Al_3Cu_2, AlCu
	Thermo-mechanically affected zone	Al Cu_3, Al_4Cu_9, Al_2Cu, Al_3Cu_2, Al_2Cu_3 , Al_4Cu
	Heat-affected zone	$AlCu_3$, Al_4Cu_9, Al_2Cu_3, Al_2Cu

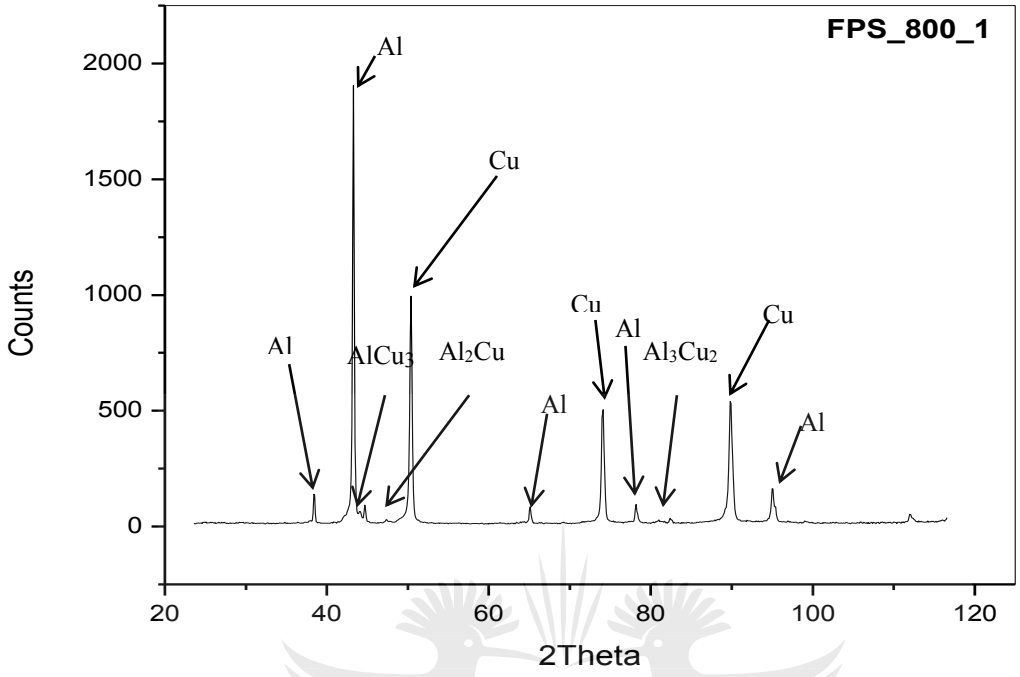

Figure 4-68 X-ray diffractogram of the stir zone of the weld produced at 800 rpm, 1 mm shoulder plunge depth using a flat pin and a flat shoulder tool.

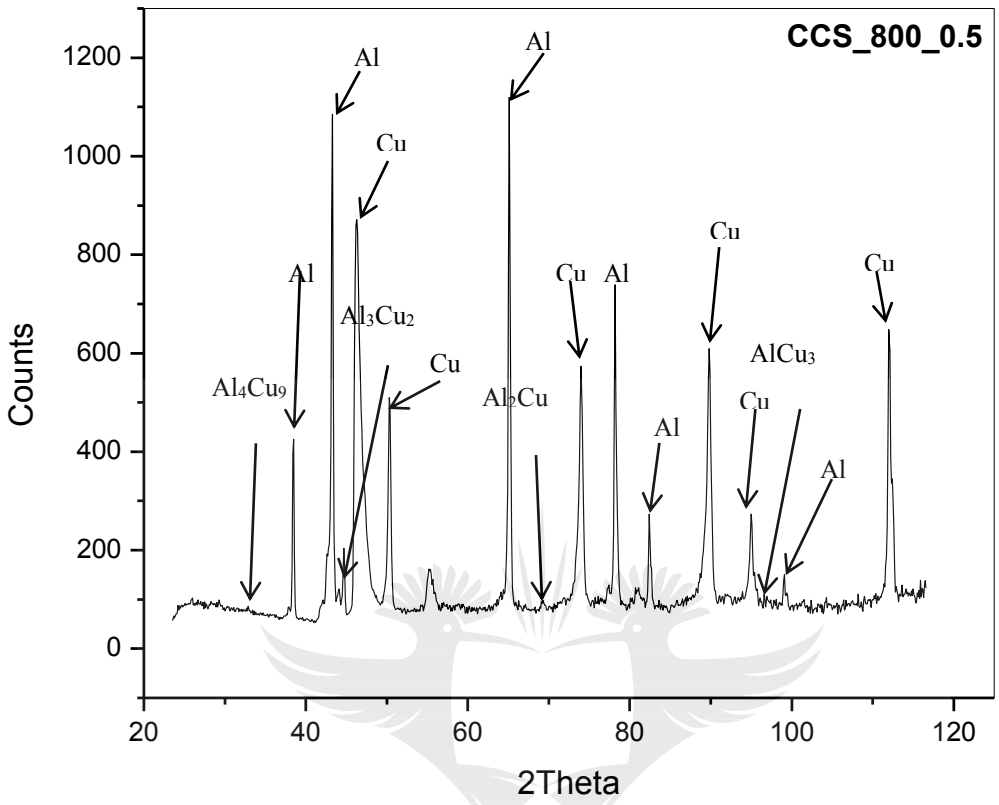

Figure 4-69 X-ray diffractogram of the stir zone of the weld produced at 800 rpm, 0.5 mm shoulder plunge depth using a conical pin and a concave shoulder tool

A number of different intermetallics were found in the samples of the spot welds. Intermetallics of Al Cu_3, Al_4Cu_9, Al_2Cu, Al_3Cu_2, Al_2Cu_3, AlCu were found in the SZ of the weld produced at 800 rpm, 0.5 mm shoulder plunge depth using a flat pin and a flat shoulder tool; whereas $AlCu_3$, Al_4Cu_9, Al_2Cu, Al_3Cu_2 were found in the SZ of the weld produced at the same process parameters, but when using a conical pin and a concave shoulder tool. On the other hand, in the TMAZ of the welds produced at the same process parameters, as indicated above, only the $AlCu_4$ intermetallic compound was found, while using a flat pin and a flat shoulder; while $AlCu_3$, Al_2Cu, Al_2Cu_3 intermetallics were found in the TMAZ of the weld produced when using a conical pin and a concave shoulder tool. This could be linked to the generation of low heat input which would generate less heat.

It has been reported that, low heats in FSW can disfavour the formation of intermetallics [91]. The most common intermetallic compounds formed in the spot weld samples are: Al_4Cu_9, $AlCu_3$, Al_2Cu_3 and Al_2Cu.

The XRD results showing the presence of intermetallic compound in the samples were confirmed with the energy dispersive spectroscopy (EDS) analyses. The EDS results were discussed in the Section 4.6. The diffractograms of the XRD analysis are shown in Appendix K.

4.9.1 Effect of process parameters on the FHWM of the spot welds

The full width at half maximum (FWHM) acquired from the diffraction peak widths provides a measure of the microstrain and plastic deformation in materials (Hutchings *et al.* cited by Lombard) [22].

The FWHM of an X-ray diffraction peak also contains valuable information density; since the broadening of the peak shows an accumulation of plastic damage including damage caused by dislocation generation during the deformation of the workpiece surface [142]. A diffraction peak from both parent materials was chosen, namely: 44.83 ^{o} (200) and 50.57 ^{o} (200) (2 Theta) for aluminium and copper, respectively. Those peaks were used to investigate the effects of process parameters and tool geometry on the FWHM. A 2 mm collimator was used to produce the XRD spectrums of the different weld samples produced when using different process parameters and tool geometries.

Table 4.13 shows the variation of FWHM and the shift in peak position of the weld produced at different process parameters and tool geometries; while Figure 4-70 depicts the X ray diffraction peaks used to measure the FWHM of different spot weld samples.

Table 4.13: The variation FWHM and the shift in peak position of the weld produced at different process parameters and tool geometries

Sample Name	2 Theta	FWHM
Copper PM	50.56656	0.29271
FPS_800_0.5	50.48321	0.36551
FPS_800_1	50.46155	0.32128
FPS_1200_0.5	50.6059	0.33443
FPS_1200_1	50.15458	0.33662
CCS_800_0.5	50.64972	0.3749
CCS_800_1	50.27259	0.27384
CCS_1200_0.5	50.47013	0.27202
CCS_1200_1	50.49228	0.29128

Sample Name	2 Theta	FWHM
Aluminium PM	44.83307	0.24875
FPS_800_0.5	43.38238	0.3594
FPS_800_1	43.34289	0.26731
FPS_1200_0.5	43.45799	0.31654
FPS_1200_1	43.01861	0.29351
CCS_800_0.5	43.54	0.3517
CCS_800_1	43.15948	0.23817
CCS_1200_0.5	43.34772	0.23237
CCS_1200_1	43.3729	0.28471

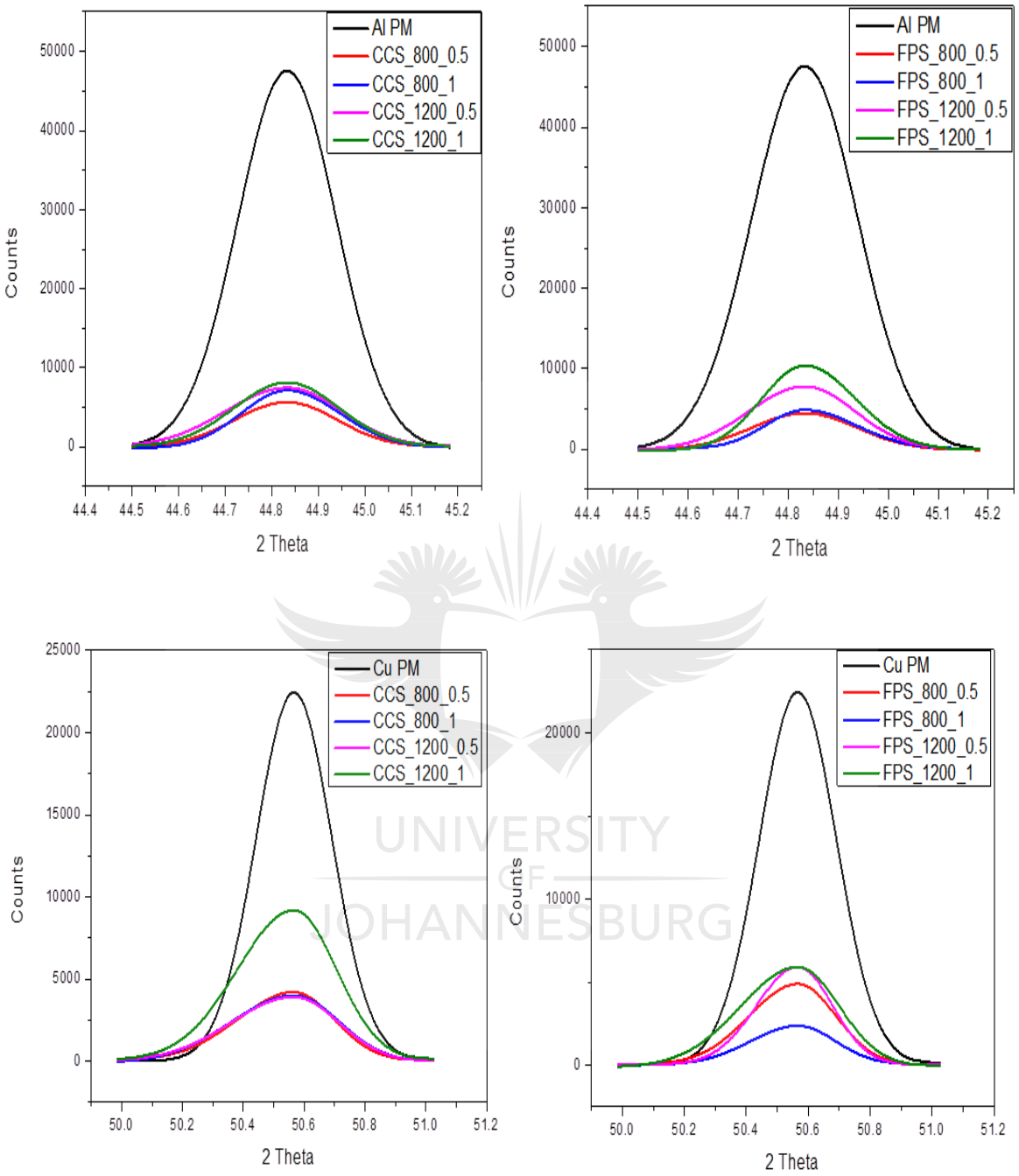

Figure 4-70 X- ray diffraction peaks used to measure the FWHM of the produced spot welds, showing the variation in peak intensity and widths

It can be seen that the intensity of all the peaks decreases in comparison to the peaks generated by the parent materials at the same position and those peaks that were broadened (Figure 4-70). This shows that the welding parameters generated stress in the produced spot welds. It has been reported that not only microstrains, but also small grains (microstructure), can broaden the peaks [139]. It was observed that welding parameters affect the position of the peaks compared to the peaks generated from the parent materials (Table 4.13).

The aluminium diffraction peaks had a higher shift when compared with the copper diffraction peaks; this can be attributed to their different properties, such as the melting point. The variations of the FWHM for all the welds can be found in Figure 4-71.

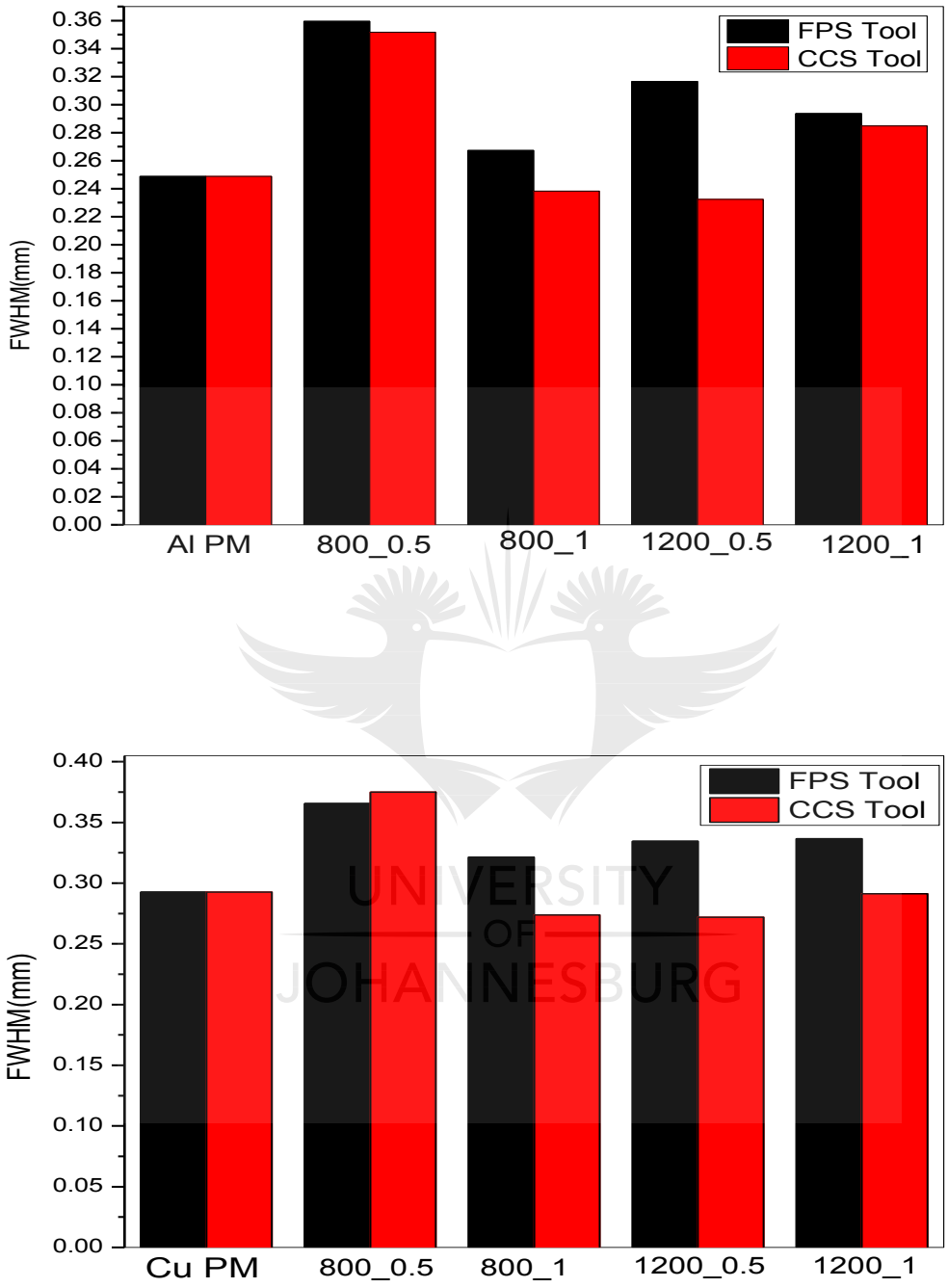

Figure 4-71 Variation in FWHM of the X-ray Diffraction peaks of the Al and Cu using different parameters and tool geometries

It can be seen that the FWHM increases at 800 rpm, 0.5 mm shoulder plunge depth; and then it decreases when the shoulder plunge is changed at 1mm. When the rotation speed is increased, the FWHM of the flat pin /flat shoulder also increases; while a decrease is observed for the conical pin and concave shoulder when using a 0.5 mm shoulder plunge depth. Furthermore, when the shoulder plunge depth is increased to 1 mm, the FWHM decreases for the flat pin/flat shoulder tool; whereas an increase is observed for the conical pin/ concave shoulder tool. This shows that the shoulder plunge depth has an effect on the FWHM.

4.10 Electrical resistivity measurements

The presence of hard and brittle intermetallic compounds in the produced samples using X-ray diffraction and energy dispersive spectroscopy techniques was observed. It has been reported that intermetallic compounds at the joint interface of aluminium and copper are known to exhibit high electrical resistivity [143].

The electrical resistivity of the aluminium/ copper dissimilar material Friction Stir Spot Welds was measured at the joint interface and then studied. The electrical resistivity measurement results are shown in Tables 4.14 and 4.15 for the flat pin and the flat shoulder, and for the conical pin and the concave shoulder, respectively.

Table 4.14: Electrical resistivity results using a flat pin and a flat shoulder tool

Spot welds ID	Resistivity ρ(μΩ)
Parent material_Al	0.014
Parent material_Cu	0.025
Average ρ	0.02
FPS_800_0.5_1	0.064
FPS_800_0.5_2	0.064
FPS_800_0.5_3	0.063
FPS_800_1_1	0.035
FPS_800_1_2	0.033
FPS_800_1_3	0.033
FPS_1200_0.5_1	0.034
FPS_1200_0.5_2	0.032
FPS_1200_0.5_3	0.032
FPS_1200_1_1	0.032
FPS_1200_1_2	0.031
FPS_1200_1_3	0.03

Table 4.15: Electrical resistivity results using a conical pin and a concave shoulder tool

Spot welds ID	Resistivity ρ(μΩ)
Parent material_Al	0.014
Parent material_Cu	0.025
Average ρ	0.02
CCS_800_0.5_1	0.035
CCS_800_0.5_2	0.032
CCS_800_0.5_3	0.033
CCS_800_1_1	0.011
CCS_800_1_2	0.009
CCS_800_1_3	0.011
CCS_1200_0.5_1	0.033
CCS_1200_0.5_2	0.033
CCS_1200_0.5_3	0.034
CCS_1200_1_1	0.034
CCS_1200_1_2	0.032
CCS_1200_1_3	0.029

The results show that by increasing the rotational speed and the shoulder plunge depths, the electrical resistivity decreases when using the flat pin and a flat shoulder tool (Table 4.14). It was further noticed that there is a big difference between the values of the electrical resistivity of the parent materials compared to most of the spot welded samples. This could be due to the presence of defects in the SZ, such as micro cracks. The highest electrical resistivity value of 0.064 μΩ was found for the sample produced at 800 rpm, 0.5 mm shoulder plunge depth, using a flat pin and flat shoulder. It was also observed that most of the welds had an electrical resistivity of between 0.029 μΩ and 0.035 μΩ; but when compared with the average of the parent materials showed a depreciation between 0.009 μΩ (45 %) and 0.015 μΩ (75 %), respectively, for 0.029 μΩ and 0.035 μΩ. On the other hand, a depreciation of 220% was found for the sample produced at 800 rpm, 0.5 mm shoulder plunge depth using a flat pin and a flat shoulder tool.

The electrical resistivity results for the welds produced with a conical pin and a concave shoulder (Table 4.15) showed different trends. A low resistivity value of 0.009 μΩ was found when using 800 rpm and 1 mm shoulder plunge depth, which shows an appreciation of 0.011 μΩ (55 %). However, the results obtained using the other parameters showed values varying from 0.029 to 0.035 μΩ. This result was obtained for the sample at 800 rpm, 1 mm shoulder plunge using a conical pin and a concave shoulder; and it has low electrical resistivity compared to the other spot welds and could be an attractive option for electrical conductivity purposes.

Figures 4-72 and 4-73 depict the effects of process parameters and tool geometry on the electrical resistivity of the produced spot welds.

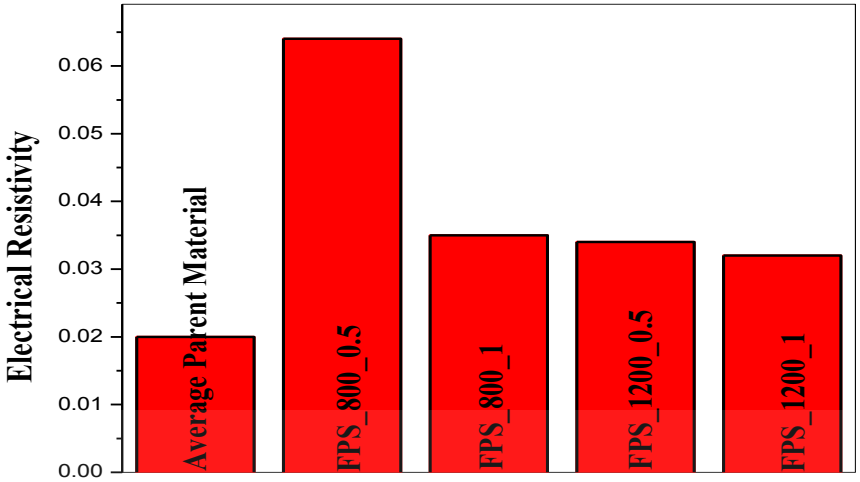

Figure 4-72 The effect of process parameters on the electrical resistivity of the spot welds when compared to the average resistivity of the parent materials produced using a flat pin and a flat shoulder tool

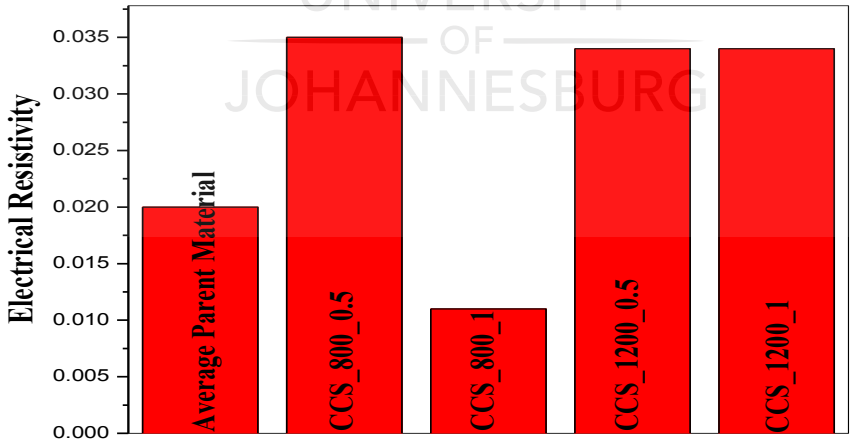

Figure 4-73 Effect of the process parameters on the electrical resistivity of the spot welds compared to the average resistivity of the parent materials produced when using a conical pin and a concave shoulder tool

It can be seen that the electrical resistivity of all the welds is higher than those of the average parent materials. Akinlabi [105] calculated the electrical resistivity of the friction stir welding between commercially pure copper to AA5754. She concluded that the presence of intermetallics affect the electrical resistivity. This was seen in the welds, where intermetallics were not found [105]. The high values of the electrical resistivity obtained except for the welds produced at 800 rpm and 1 mm shoulder plunge depth in the current research work could be due to the presence of intermetallics in the vicinity of the keyhole. This was confirmed with XRD and EDS analyses, and also with the high values of the microhardness in the vicinity of the keyhole.

4.11 Residual stress analyses using the XRD technique

Figure 4-74 depicts a two dimensional image of the residual stress measurement and texture conducted in the current study. It can be seen that the weld had a strong texture. Figure 4-75 shows the residual stress measurement location (SZ) for the welds produced at 800 rpm, 05 mm shoulder plunge depth when using a flat pin and a flat shoulder and 800 rpm, 0.5 shoulder plunge depth when using a conical pin and a concave shoulder.

Figure 4-76 presents a typical $\sin^2\psi$ diagram for the (331) diffraction plane of the welds produced at 1200 rpm, 0.5 mm shoulder plunge depth using a flat pin and a flat shoulder tool. The solid line represents the linear least-square fit to a set of data points. Even though the data were slightly scattered, the lattice strain decrease almost linearly with the increase of the $\sin^2\psi$. It was observed that all the residual stresses are compressive (Tables 4.16 and 4.17)

The residual stresses of the welds are shown in Figures 4-77 and 4-78, respectively, for the welds produced using a flat pin/ flat shoulder and conical pin/ concave shoulder. The residual stresses were measured in the SZ (stir zone) and on the copper ring.

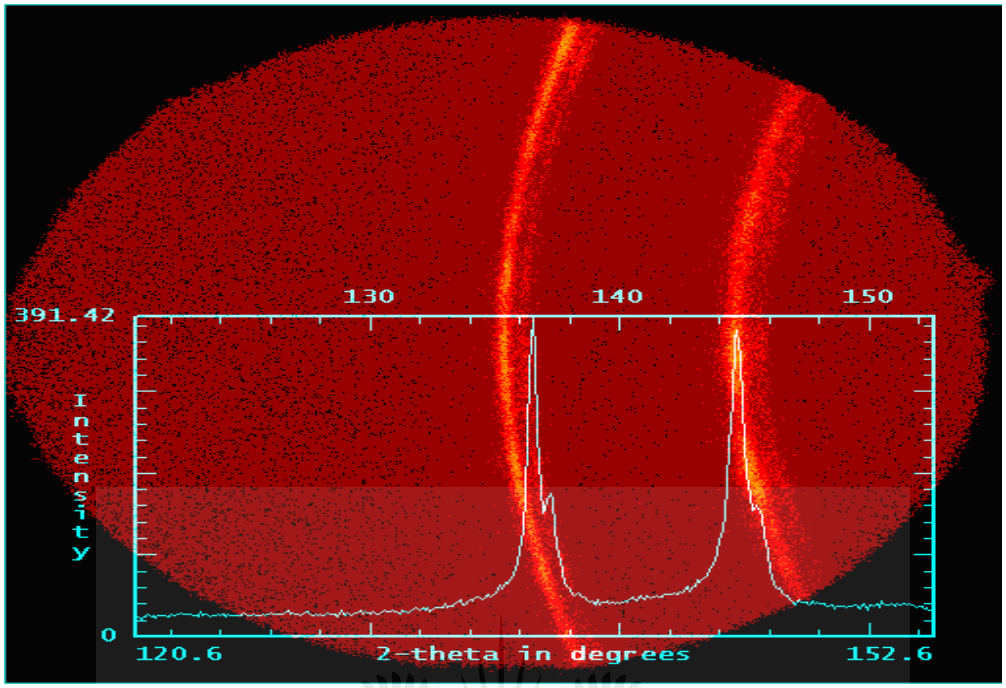

Figure 4-74 The representative two-dimensional image of one of the welds used in the current study

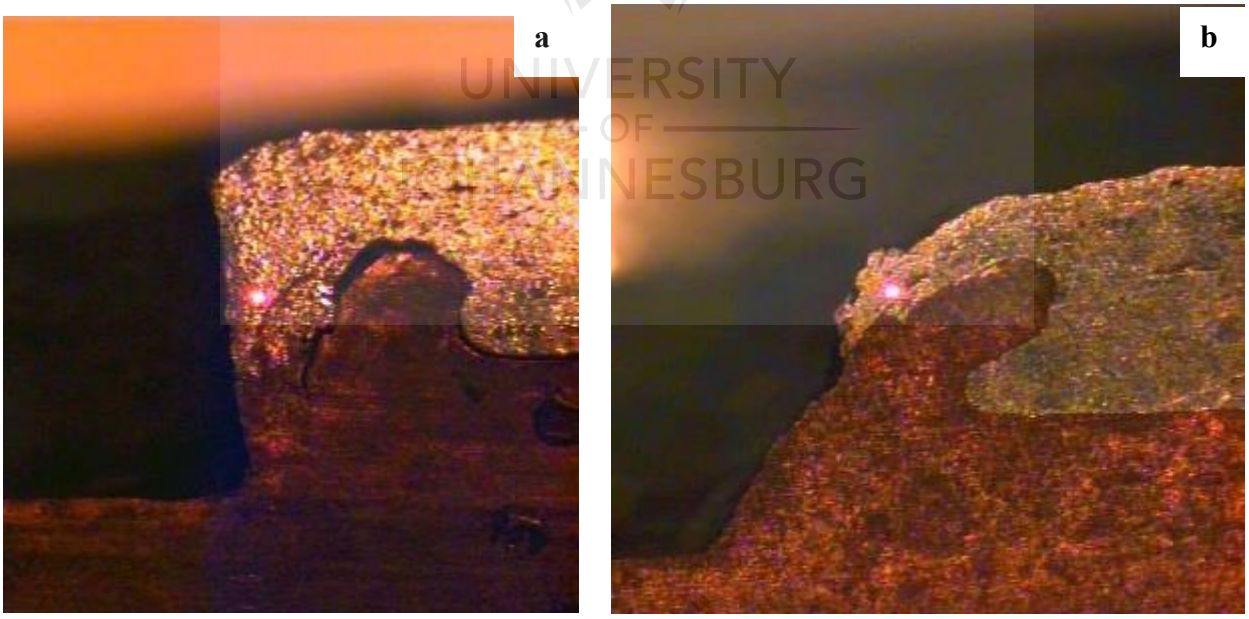

Figure 4-75 The residual stress measurement position (SZ) of the welds, (a) 800 rpm, 05 mm shoulder plunge depth using a flat pin and flat shoulder, (b) 800 rpm, 0.5 shoulder plunge depth using a conical pin and a concave shoulder

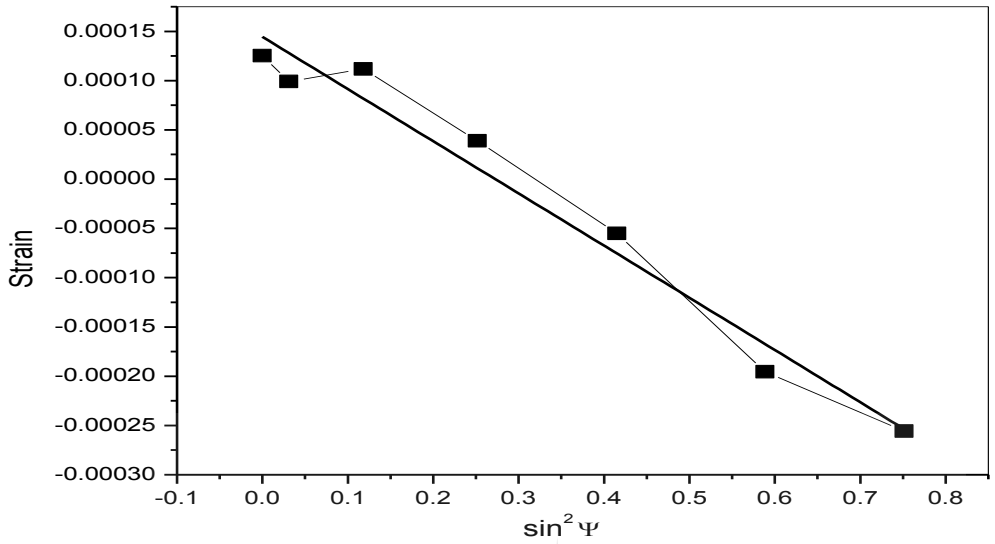

Figure 4-76 The $\sin^2 \Psi$ diagram for the (331) diffraction plane of the weld at 1200 rpm and 0.5 shoulder plunge depth using a flat pin and flat shoulder tool, where the solid line represents the linear least square fit to the data

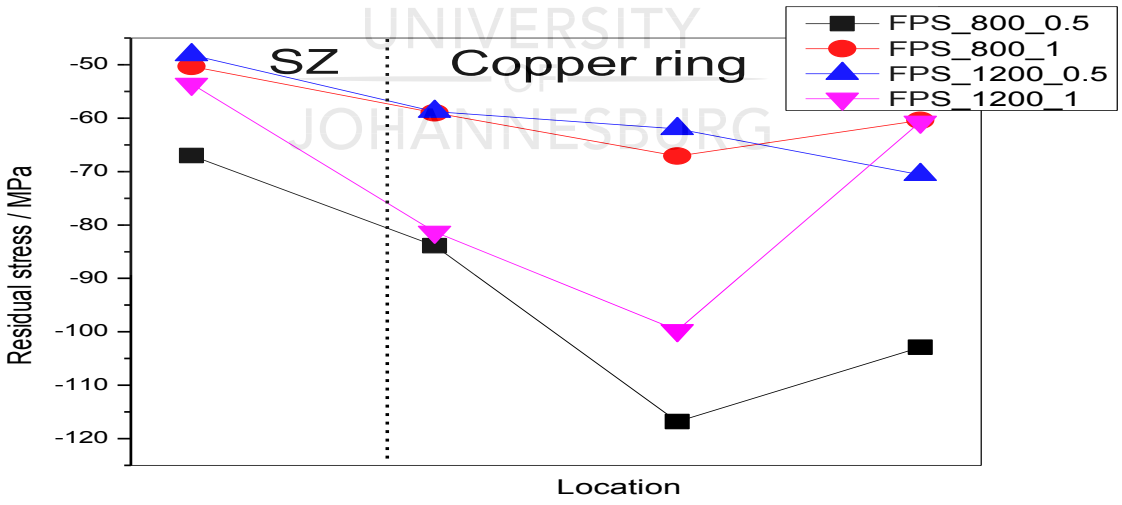

Figure 4-77 Residual stress distribution of the stir zone (SZ) and on the copper ring of the spot welds produced at different process parameters using a flat pin and a flat shoulder

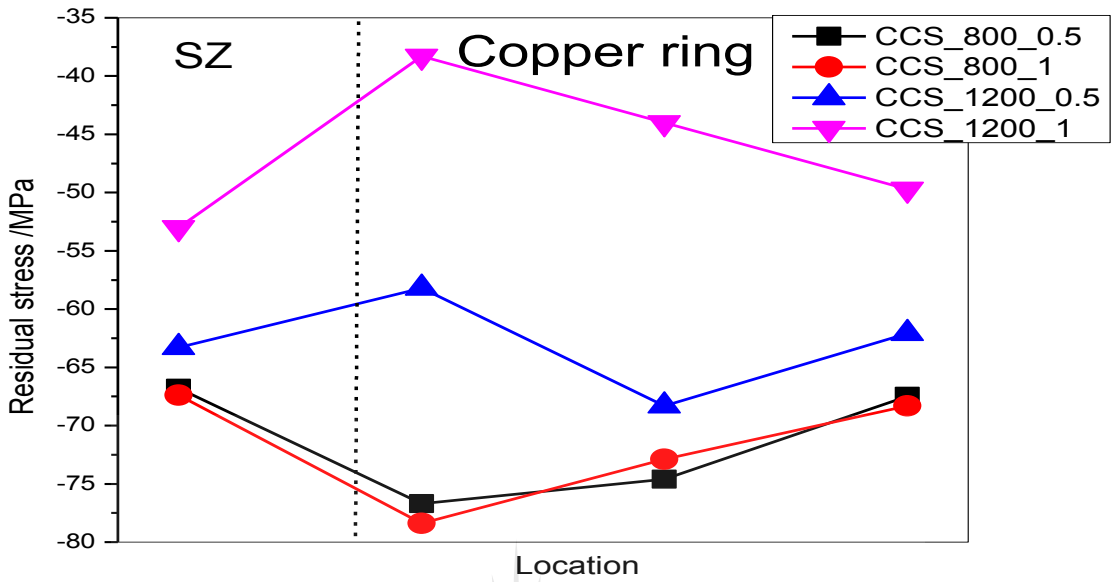

Figure 4-78 Residual stress distribution of the stir zone (SZ) and on the copper ring of the spot welds produced at different process parameters using a conical pin and a concave shoulder

It was observed a residual stress of -67 and -50.3 MPa were obtained in the SZ of the weld produced at 800 rpm using a flat pin and a flat shoulder when using 0.5 and 1 mm shoulder plunge depths, respectively; while the weld produced at 1200 rpm exhibited an increase. This shows that the shoulder plunge depth has an effect on the residual stress values obtained. As for the weld produced using a conical pin and a concave shoulder, the residual stresses of -66.8 and -67.4 MPa were obtained in the SZ, respectively. Those welds (800 rpm/0.5 mm shoulder plunge depth and 800 rpm / 1 mm shoulder plunge depth) showed that the two values were similar. A decrease was observed for the weld produced at the high rotation speed of 1200 rpm. Residual stress values of -63.3 and -53 MPa were obtained using 1200 rpm/0.5 shoulder plunge depth and 1200 rpm/ 1 mm shoulder plunge depth, respectively.

It was further observed that there was no trend in the effect of the shoulder plunge depth on the variations in the residuals stresses in the stir zone. The maximum residual stress measurement was found on the copper ring of the welds. A maximum of -116.8 MPa was obtained on the copper

ring of the weld produced at 800 rpm, 0.5 mm shoulder plunge depth using a flat pin and a flat shoulder tool. The high values of the residual stresses found in the copper ring are due to the stress generated by the extrusion of the copper (bottom sheet) into the aluminium plate (top sheet). Tables 4.16 and 4.17 present the residual stress results obtained at different process parameters and when using different tool geometries.

Table 4.16: Residual stresses obtained at different locations of the welds at different process parameters using a flat pin and a flat shoulder tool

	Residual stress (MPa)			
Location	FPS_800_0.5	FPS_800_1	FPS_1200_0.5	FPS_1200_1
SZ	-67	-50.3	-48.2	-53.6
Copper ring	-83.9	-59	-58.8	-81.3
Copper ring	-116.8	-67.1	-62	-99.7
Copper ring	-102.9	-60.4	-70.6	-60.7

Table 4.17: Residual stresses obtained at different location of the welds at different process parameters when using a conical pin and a concave shoulder tool

	Residual stress (MPa)			
Location	CCS_800_0.5	CCS_800_1	CCS_1200_0.5	CCS_1200_1
SZ	-66.8	-67.4	-63.3	-53
Copper ring	-76.7	-78.4	-58.2	-38.3
Copper ring	-74.6	-72.9	-68.3	-44
Copper ring	-67.5	-68.3	-62.1	-49.7

4.12 Statistical analysis of the selected properties of the spot welds

4.12.1 Probability Density Function (PDF) of the microhardness results

The current section depicts the statistical analyses of the microhardness results obtained by using different process parameters and tool geometries. It has been reported that all the mechanical tests are subject to large statistical fluctuations, which should be evaluated [144].

The probability distribution function (PDF) of the Vickers hardness was reported in the literature to correspond to a Gaussian (or Normal law) [145] and a log normal [146]. Hassan *et al.* [147]

studied the significance of the process parameters in FSW of aluminium matrix composites (AMCs), to set the optimal level for each of these parameters, and further to predict which responses are affected when using the analyses of variance (ANOVA) [147]. The present study used a statistical toolbox Matlab2014a. This latter was used to analyse the probability density function (PDF) of the obtained microhardness results. This was done to establish an understanding on how different parameters and tool geometries can affect the probability of obtaining specific microhardness values.

The microhardness data were collected after measuring them using a Vickers microhardness a Diamond pyramid indenter EMCO Test DuraScan tester (Section 3.2.4.4). They were then analysed by using the Matlab software. Two locations on the spot welds were used, namely, the top and the bottom, as shown in Figure 3-6. Measurements were taken from the keyhole for all the different parameters and tool geometries, in order to find the probability density function (PDF) of each one. A probability density function (PDF) is a function that describes the relative possibility for a random variable to take on a given value. The probability of the random variable falling within a particular range [a, b] of values is given by a finite integral of the pdf within that range [a, b].

$$p(x) = \int_b^a f(x, \mu, \sigma) = \int_b^a \frac{1}{\sqrt{2\pi\sigma^2}} e^{-\frac{(x-\mu)^2}{2\sigma^2}} \quad 4.2$$

That is given by the area under the density function, but above the horizontal axis, and between the lowest and highest values of the range. The probability density function is non negative everywhere; and its integral over the entire space is equal to one.

The PDF histograms of the microhardness and their fits of the parent materials, namely, aluminium and copper, are depicted in Figures 4-79 a and b, respectively. The PDF of the top and bottom hardness measurements were investigated, Figures 4-80 a and b depict the PDF histograms of the microhardness for the weld produced at 800 rpm, 0.5 mm shoulder plunge depth when using a flat pin and a flat shoulder tool.

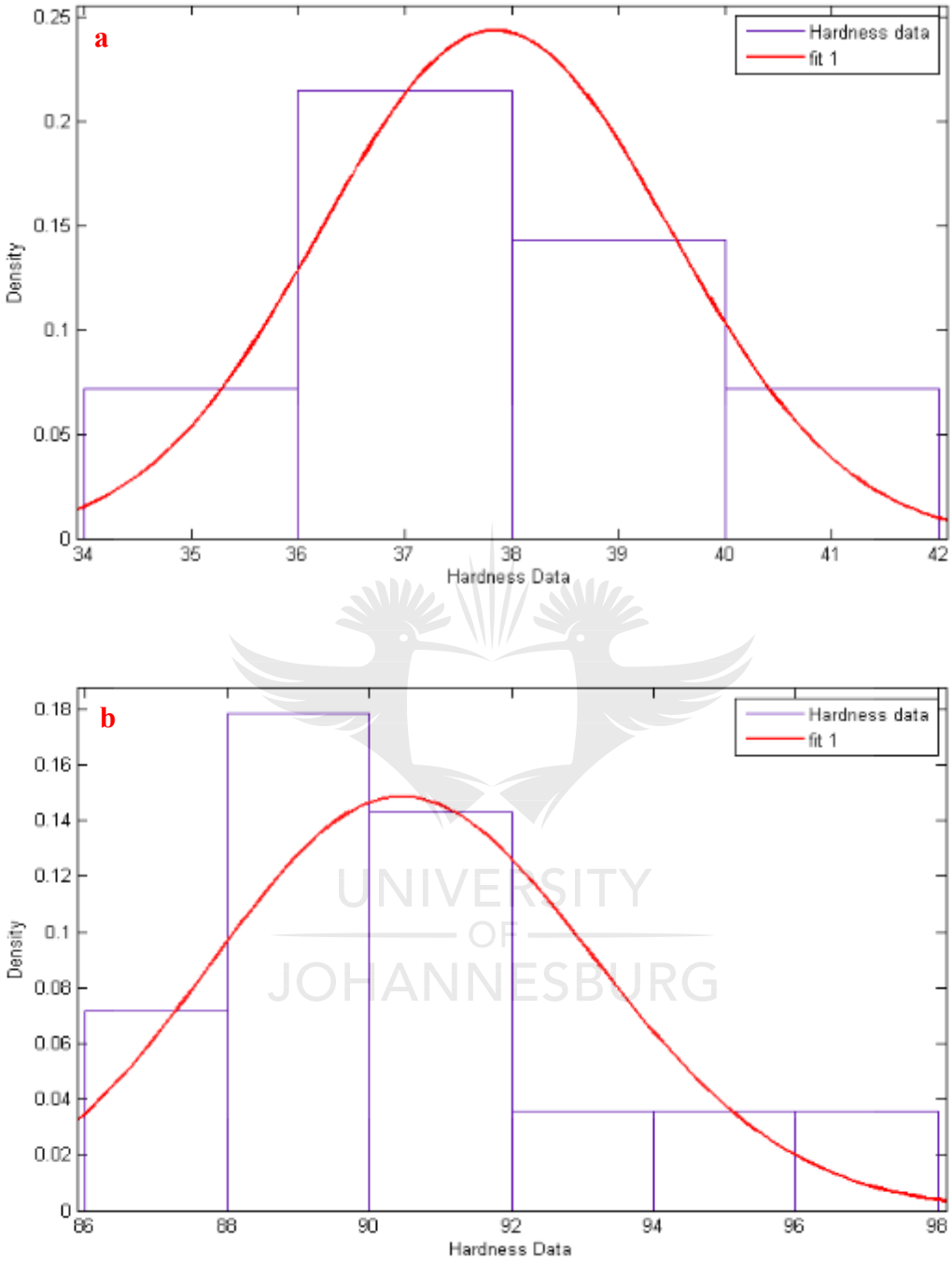

Figure 4-79 Depicting the microhardness PDF histograms of the parent materials, (a) aluminium, (b) copper

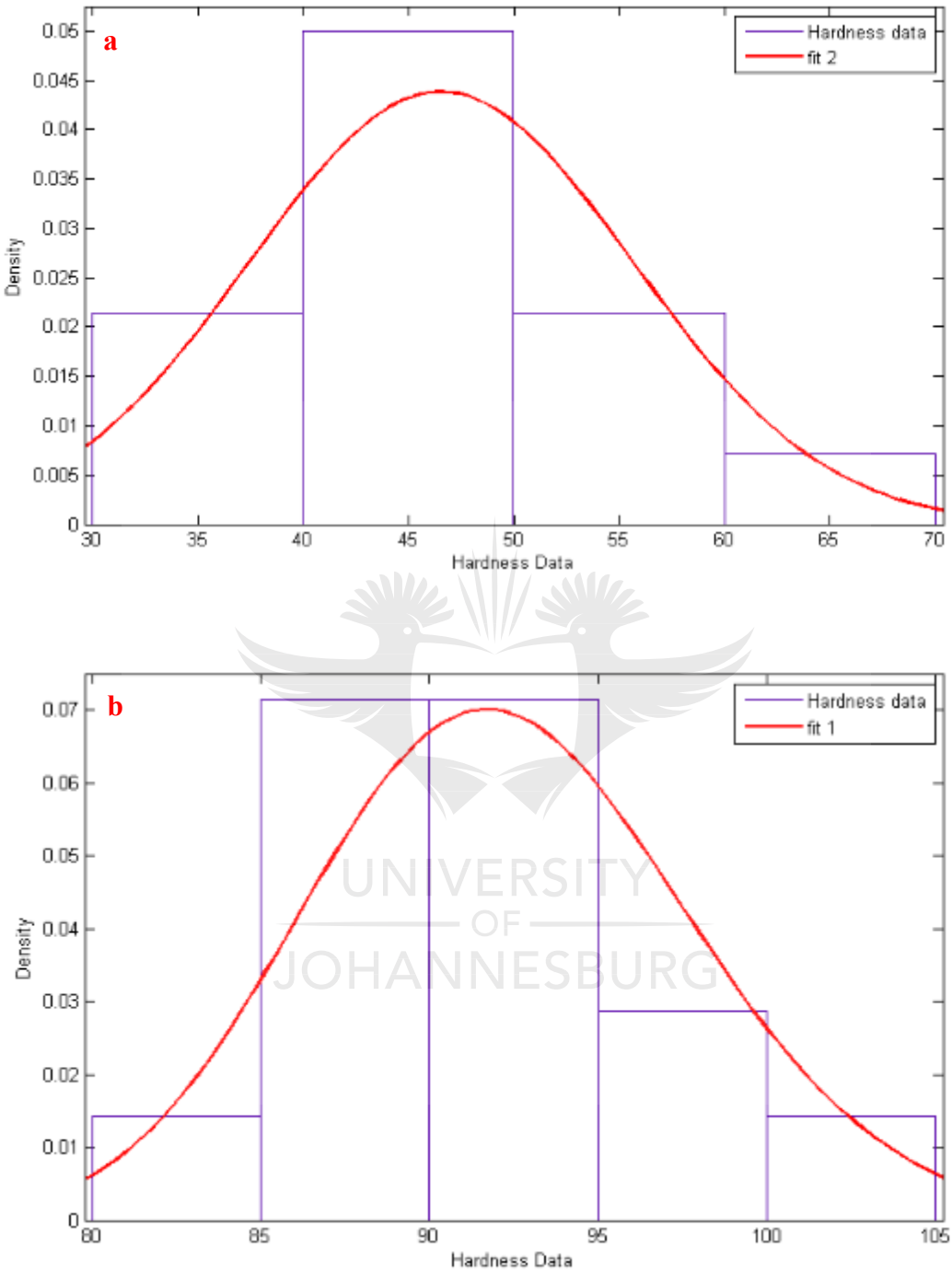

Figure 4-80 PDF histograms of the microhardness of FPS_800_0.5 spot weld, (a) top and (b) bottom

It can be seen that the probability of having microhardness values between 40 and 45 HV is high in the histogram, as shown in Figure 4-80 (a), which represents the microhardness measured at the top of the spot weld. This corresponds mostly to the microhardness of the aluminium parent material; whereas, the possibility of getting high microhardness values between 50 and 60 HV is low.

On the other hand, the PDF of bottom measurement (Figure 4-80 (b)) shows that there is a high possibility of getting microhardness values between 85 and 95 HV. This corresponds with the microhardness of the copper parent materials plates; while the microhardness values between 100 and 105 HV are likely to show a lower possibility of being obtained when using the same process parameters as those used in this research work. The possibility of having higher microhardness values compared to the values of the parent materials in the two different sheets (copper and aluminium) was observed to be due to the presence of a mixture of copper and aluminium in the vicinity of the keyhole.

Additionally, Figure 4-81 depicts the PDF histogram of the microhardness (top (a) and bottom (b) measurements) for the weld produced at 800 rpm, 0.5 mm shoulder plunge depth when using a conical pin and a concave shoulder.

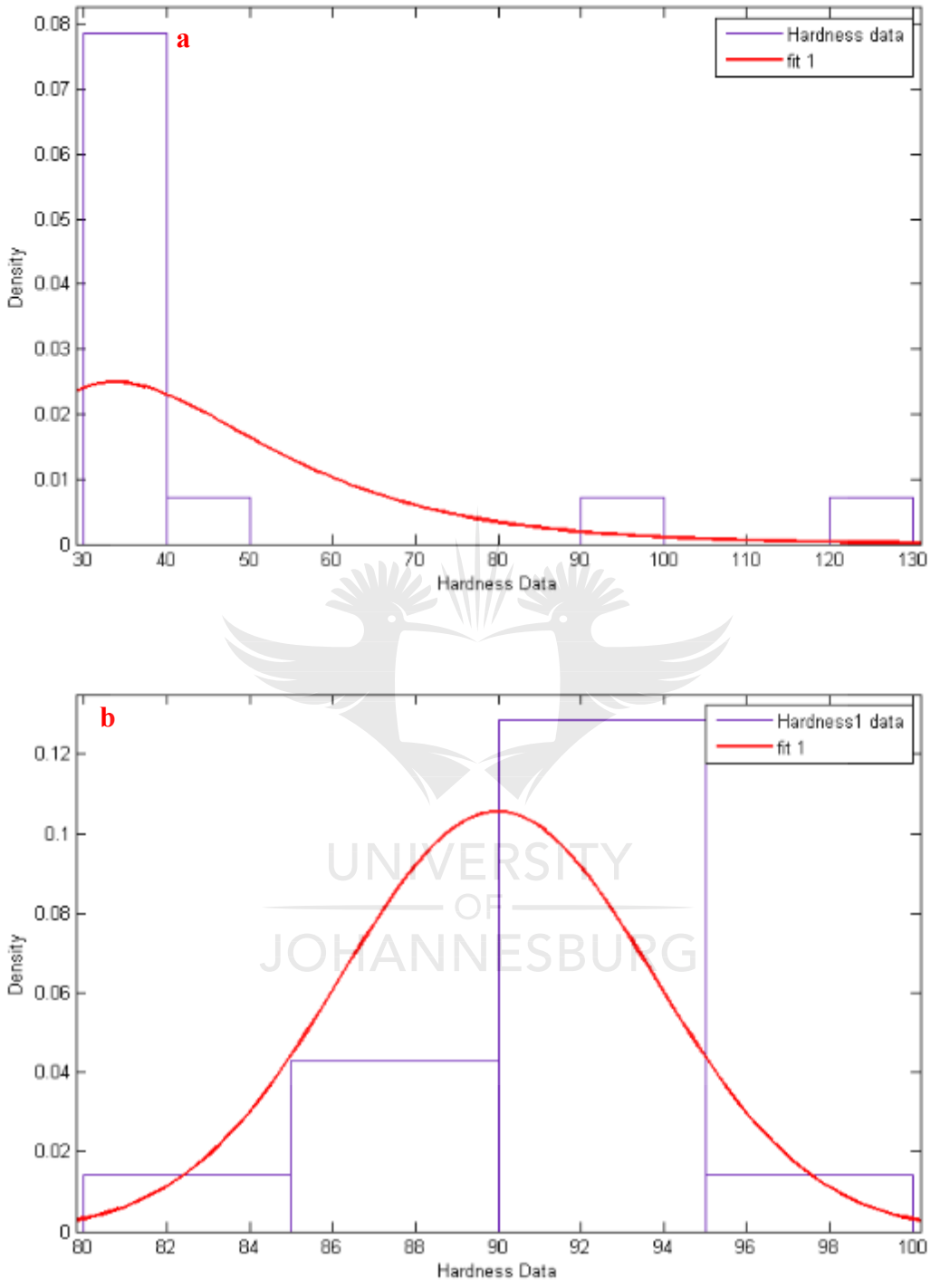

Figure 4-81 PDF histogram of the microhardness of CCS_800_0.5 spot weld, (a) top and (b) bottom

The results show that there is a higher possibility of microhardness values between 30 and 50 HV; whereas the high values between 120 and 130 HV can be obtained at a low possibility (Figure 4-81 a). The trend is the similar for the bottom (Figure 4-81 b), as discussed above for the PDF of the bottom microhardness measurement using a flat pin and a flat shoulder.

Moreover, when the rotational speed at 1200 rpm is increased, the possibility of getting high microhardness values between 100 to 110 HV and 90 to 100 HV increases for the spot weld produced using a conical pin and a concave shoulder for the top measurement, and for the top and bottom microhardness values, respectively. It can be seen that the rotational speed and the tool geometry can influence the possibility of different probability distributions.

The PDF of the two different measurement positions for all the produced spot welds and the two parent materials can be found in Appendix L.

The model shows that in order to get the probability in a certain region, we need to compute the integral of the PDF in the region of interest. The pdf found in the current research work is a normal distribution (called a Gaussian distribution) as well. In order to get any probability, we can compute the finite integral of the normal distribution equation below:

$$f(x,\mu,\sigma) = \frac{1}{\sqrt{2\pi\sigma^2}} e^{-\frac{(x-\mu)^2}{2\sigma^2}} \quad 4.3$$

Where, σ is the standard deviation, σ^2 the variance and μ the mean.

The goodness of the fit and the residuals were also analysed. The results show that most of the values of the R^2 ranged between 0.8842 and 0.9999, which is an indication on how well the model fits with the produced experimental data (Tables 4.18 to 4.21).

Table 4.18: R^2 and adjusted R^2 of the welds produced using a flat pin and a flat shoulder tool for the microhardness measured on top

Sample ID	*R* square	*R* square adjusted
FPS_800_0.5	0.9896	0.9322
FPS_800_1	0.9996	na
FPS_1200_0.5	0.9999	0.9995
FPS_1200_1	0.9993	0.9952

Table 4.19: R^2 and adjusted R^2 of the welds produced using a conical pin and a concave shoulder tool for the microhardness measured on top

Sample ID	*R* square	*R* square adjusted
CCS_800_0.5	0.9924	0.9505
CCS_800_1	0.9976	0.9843
CCS_1200_0.5	0.9893	0.9303
CCS_1200_1	0.9997	0.9978

Table 4.20: R^2 and adjusted R^2 of the welds produced using a flat pin and a flat shoulder tool for the microhardness measured at the bottom

Sample ID	*R* square	*R* square adjusted
FPS_800_0.5	0.8842	0.2475
FPS_800_1	0.9999	na
FPS_1200_0.5	0.9937	0.9589
FPS_1200_1	0.9298	0.5439

Table 4.21: R^2 and adjusted R^2 of the welds produced using a conical pin and a concave shoulder tool for the microhardness measured at the bottom

Sample ID	*R* square	*R* square adjusted
CCS_800_0.5	0.9818	0.8819
CCS_800_1	0.9424	0.6258
CCS_1200_0.5	0.987	0.9157
CCS_1200_1	0.9866	0.9126

Figures 4-82 (a and b) present the goodness of the fit and the residuals for the weld produced at 1200 rpm, 1 mm shoulder plunge depth using a flat pin and a flat shoulder tool (top microhardness measurement). In addition, Figures 4-83 (a and b) depict the goodness of the fit and the residuals for the weld produced at 1200 rpm, 1 mm shoulder plunge depth when using a conical pin and a concave shoulder (top microhardness measurement). The Tables showing the R^2 and the Figures of the goodness of the fits are found in Appendix I. Apart from the R^2 values, the residual analysis has also been employed in the study, in order to check the adequacy of the models. Figure 4-82 (b) and Figure 4-83 (b) show the residual plots for the microhardness values obtained at the top using a flat pin / flat shoulder and a conical pin/ concave shoulder when using a 1200 rpm and 1 mm plunge shoulder plunge depth, respectively.

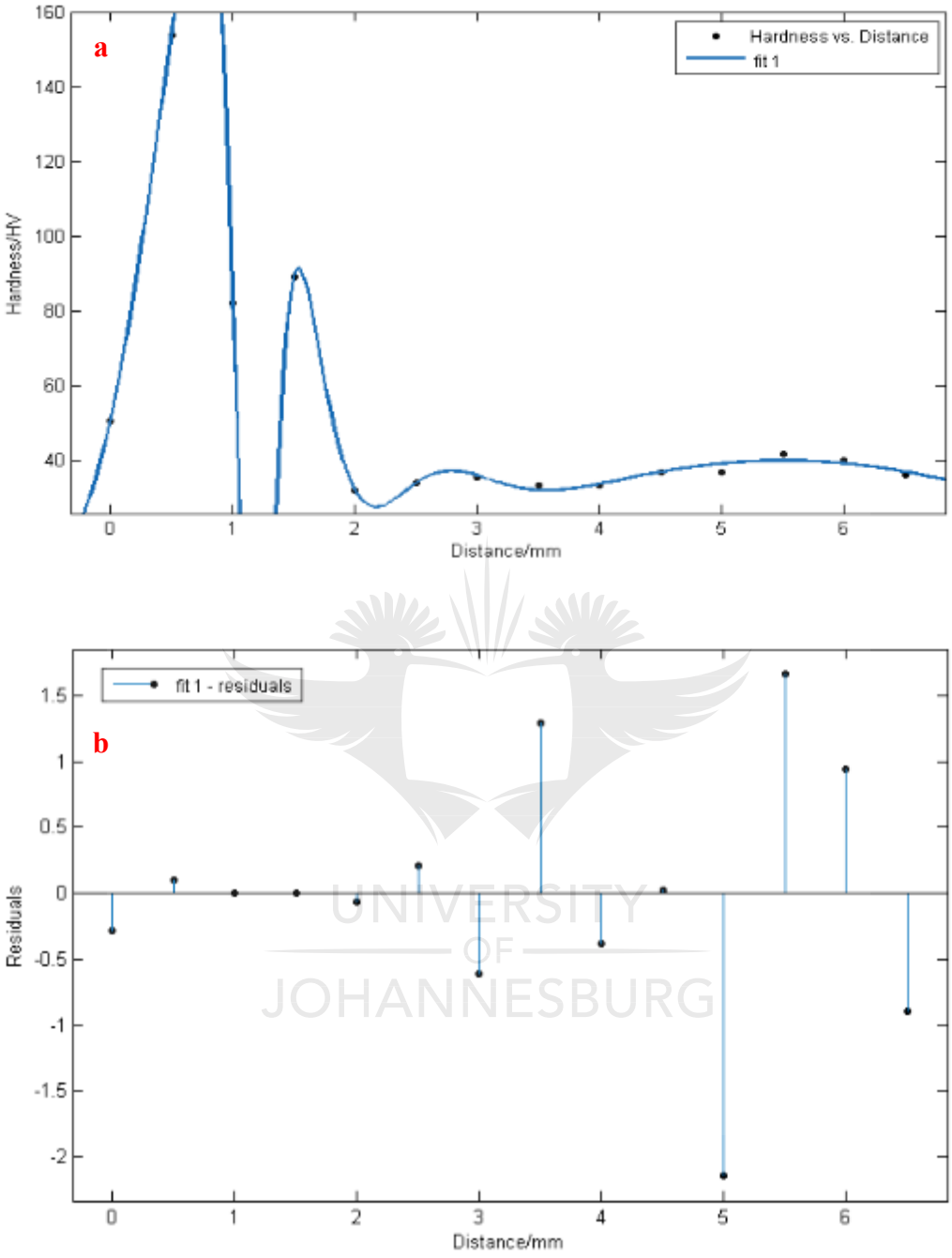

Figure 4-82 Goodness of the fit (a) and the residuals (b) for the spot weld produced at 1200 rpm, 1 mm shoulder plunge depth using a flat pin and a flat shoulder (top microhardness measurements)

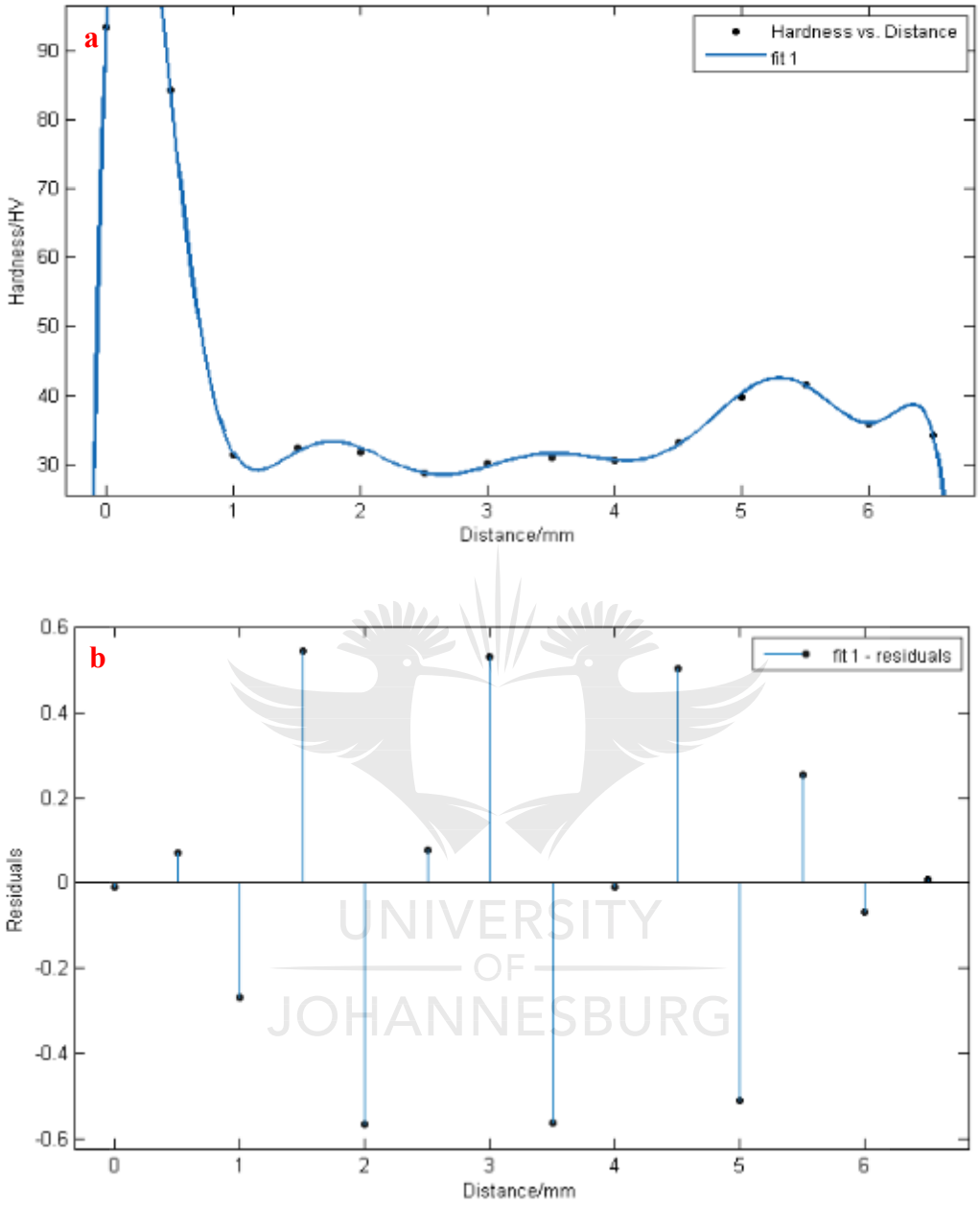

Figure 4-83 Goodness of the fit (a) and the residuals (b) for the spot weld produced at 1200 rpm, 1 mm shoulder plunge depth when using a conical pin and a concave shoulder (top microhardness measurements)

Tables 4.22 to 4.25 present the standard deviation, the variance and the mean obtained from the statistical analyses of the measured microhardness values of the two different positions, namely, the top and bottom of the spot weld produced from the different tools when using different process parameters.

Table 4.22: Mean, variance, mu and sigma of the spot samples produced when using a flat pin and a flat shoulder tool for the microhardness taken on top

Sample name	Mean	σ^2	μ	σ
FPS_800_0.5	46.5429	82.8442	46.5429	9.10188
FPS_800_1	75.0992	4994.97	4.00167	0.79641
FPS_1200_0.5	45.1208	441.806	3.71115	0.44317
FPS_1200_1	51.7308	672.845	3.83391	0.47359

Table 4.23: Mean, variance, mu and sigma of the spot samples produced when using a conical pin and a concave shoulder tool for the microhardness taken on top

Sample name	Mean	σ^2	μ	σ
CCS_800_0.5	44.5748	409.802	3.70341	0.43303
CCS_800_1	55.8872	813.763	3.90757	0.48119
CCS_1200_0.5	45.4532	482.889	3.71166	0.45831
CCS_1200_1	40.9416	248.04	3.64315	0.37148

Table 4.24: Mean, variance, mu and sigma of the spot samples produced using a flat pin and a flat shoulder tool for the microhardness taken at the bottom

Sample name	Mean	σ^2	μ	σ
FPS_800_0.5	92.2338	32.7196	4.52241	0.06196
FPS_800_1	84.7	119.974	84.7	10.9533
FPS_1200_0.5	84.7	119.974	84.7	10.9533
FPS_1200_1	78.4286	58.0637	78.4286	7.61996

Table 4.25: Mean, variance, mu and sigma of the spot samples produced using a conical pin and a concave shoulder tool for the microhardness taken at the bottom

Sample name	Mean	σ^2	μ	σ
CCS_800_0.5	89.9857	14.2859	89.9857	3.77967
CCS_800_1	88.5643	102.307	88.5643	10.1147
CCS_1200_0.5	86.2521	89.6604	4.45128	0.10945
CCS_1200_1	82.0425	54.8519	4.40318	0.09009

It should be noted that the mean is equal to μ if the distribution is normal. It can be seen that in some cases in the current work μ and the mean have different values, which shows that the distributions in some of the analyses were not normal. The standard deviation σ should be close to zero; but in the current work, the value of the standard deviation is not close to zero in some of the cases. This shows that the microhardness values are not close to the expected values; and this could be due to the presence of very far apart measured microhardness values in the different locations of the weld samples.

This was further suspected due to the presence of intermetallics, which could have been the cause of the high microhardness values; since intermetallics are invariably hard and brittle.
Each figure contains residual versus the distance (distance from the keyhole) between the data and the constant variance of the residuals. In a plot of residual versus distance, it has been shown that the models are adequate to predict the responses in an acceptable manner. The figures showing the residuals of all the spot welds, including the two parent materials, can be found in Appendix I.

CHAPTER FIVE

5 CONCLUSIONS AND RECOMMENDATIONS

5.1 Introduction

The objective of this research project was to join pure aluminium (AA1060) and commercially pure copper (C11000), using the friction stir spot welding process. In this chapter, the summary of the results obtained in the previous chapter are presented. This include, the results on the microstructure evolution, chemical element analyses, and phase' identification, shear tensile test and microhardness profile, electrical resistivity and the residual stresses. Additionally, the summary on probability density distribution (PDF) results of the microhardness profile is presented. Recommendations for further investigation are also presented.

5.2 Conclusions

The present research study has shown that pure AA 1060 and commercially pure copper C11000 can be successfully joined with friction stir spot welding technique. The produced spot welds were characterised and reported in this thesis. Investigations of the effects of the welding parameters, such as the shoulder plunge depth and the tool geometry on the evolving microstructure, as well as the mechanical and chemical properties, were conducted.

A comprehensive literature review was conducted and discussed (Chapter Two) on friction stir welding (FSW) and friction stir spot welding (FSSW) of similar and dissimilar materials. In the existing literature, there are very few published papers on friction stir spot welding between aluminium and copper. This was the main motivation of the current study, which was to characterise the evolving properties of friction stir spot welds between aluminium and copper, and to generate results to enhance the application of friction stir spot welding (FSSW) between aluminium and copper.

Dissimilar metal joining techniques are of interest in the manufacturing industries; where a number of structures and parts need to be produced. Aluminium and copper are generally used in

engineering, due to their unique properties, including high electrical conductivity, heat conductivity, corrosion resistance and good mechanical properties. Joining aluminium and copper to meet the requirements of the electrical industry have been conducted by using different joining techniques, such as ultrasonic welding, friction welding and laser welding; but their major challenge is the occurrence of brittle intermetallic compounds in the joint zone. FSSW has been successfully used to join copper and aluminium by very few researchers; and more research is needed to investigate the evolving properties of FSSW between aluminium and copper.

The microstructural evolution of the welds was investigated using an optical light microscopy and the scanning electron microscopy. The presence of intermetallic compounds was carried out using two different collimators for the X-ray diffraction and the energy dispersive spectroscopy. Additionally, microhardness measurements, lap-shear tensile and electrical resistivity analyses were conducted to complete the investigations on the produced spot welded samples, and to allow for the evaluation of the quality of these spot welds. Residual stresses in the stir zone and on the copper ring were measured. Forge forces on the tool and the torque were measured continuously during the spot welding.

The presence of a copper ring (hook) was observed in all the produced spot welds and the length increases with the shoulder plunge depth; while the spot welds produced at 1200 rpm for the two tool geometries exhibited a decrease and a minor increase in the length of the copper ring using a flat pin/flat shoulder and a conical pin/ concave shoulder, respectively.

The mapping of a region of the keyhole/copper ring and the stir zone of the spot weld showed different microstructures with copper particles and fragments in the aluminium matrix. A good material mixing was achieved in most of the produced spot welds.

The X-ray diffraction analyses were conducted by using a 2 mm collimator; and this revealed the presence of the Al_2Cu, Cu_3Al intermetallic compounds in the joints produced when using a conical pin/concave shoulder at 800 rpm (1mm shoulder plunge depth) and 1200 rpm (0.5mm shoulder plunge depth). While using a 0.8 mm collimator in three different locations of the spot welds samples, namely, the stir zone (SZ), the thermo-mechanically affected zone (TMAZ) and the heat-

affected zone (HAZ), the most common intermetallic compounds formed in the spot weld samples were found to be Al_4Cu_9, Al Cu_3, Al_2Cu_3 and Al_2Cu. However, the peaks for all the intermetallics were very low indicating low volume concentrations.

The X-ray diffraction results were in correlation with the energy dispersive spectroscopy (EDS) analysis, which also revealed the presence of intermetallics compounds in the keyhole and the interfacial regions. High failure loads of 5225 N and 4844 N were obtained when using a flat pin/flat shoulder using 800 rpm, 1 mm shoulder plunge depth and 1200 rpm and 1 mm shoulder plunge depth, respectively. By increasing the shoulder plunge depth, strong welds were obtained. Furthermore, the two highest failure loads obtained using a conical pin/concave shoulder were 2991 N and 4606 N, where the parameters used were 800 rpm, 0.5mm pin plunge depth and 1200 rpm, 1 mm shoulder plunge depth, respectively. The above mentioned process parameters combinations are recommended. In addition, the higher microhardness values were obtained in the stir zone for all the welds. There was no apparent trend linking the process parameters and the tool geometries to the microhardness results.

The electrical resistivity results revealed high values for all the spot welds compared to the parent materials; but the electrical resistivity of the spot welds produced at 800 rpm, 1 mm shoulder plunge depth when using a conical pin and a concave shoulder exhibited lower values compared with those of the parent materials. For electrical application, these above mentioned process parameters are recommended.

The maximum forge forces recorded showed that there was an increase with the increase of the shoulder plunge depth; whereas a decrease was noticed when the rotational speed was increased for the flat pin/flat shoulder tool. A similar trend was also noticed for the conical pin/concave shoulder. The residual stresses were measured in the SZ (stir zone) and on the copper ring. All the obtained residual stress results were compressive. The maximum residual stress of -116.8 MPa was measured on the copper ring of the welds produced at 800 rpm, 0.5 mm shoulder plunge depth using a flat pin and a flat shoulder tool. The process parameters and tool geometries happened to have an effect on the distribution of the microhardness values in different locations of the produced spot welds. This was conducted using the probability distribution function (PDF).

Additionally, the goodness of the fit values were also analysed; and these showed that most of the values of the R^2 ranged between 0.8842 and 0.9999, which is an indication of how well the model fits with the produced experimental data.

Different process parameters and tool geometries were used in the current research work. This research has been able to provide valuable information on the joining between aluminium and copper when using the friction stir spot welding technique. It was noticed that the welds produced at 800 rpm and 1 mm shoulder plunge depth using a conical pin and a concave shoulder tool exhibited a low electrical resistivity which was more appropriate for use in the electrical industry. However, high strength welds were obtained for the welds produced using a flat pin and a flat shoulder tool. The produced welds were characterised; and the obtained results showed that the tools geometries and process parameters used in this research work can be recommended. The current research work has also provided valuable information to be used for the development and the usage of friction stir spot welding between aluminium and copper. This information can be used in various industries, including the manufacturing and the electrical.

5.3 Recommendations for future work

This thesis focused on some of the key issues in understanding the evolving properties of friction stir spot welding between aluminium and copper. As a result of some of the findings, there are additional areas that need to be addressed in more detail in future research. These can be summarised in the following:

- A study of different tool geometries and dimensions needs to be used, in order to further explain the correlation between the size of the copper ring and the shear tensile properties, which were found to affect the strength of the spot welds in the current study.
- The temperature measurements during the friction stir welding process need to be conducted to investigate the link between the formation of intermetallic compounds associated with the process parameters, as well as the tool geometries and dimensions.
- Further studies need to be conducted on the optimisation of the process parameters used to produce friction stir spot welds with limited amounts of these intermetallic compounds.

- The mode of the FSW machine employed in the current investigation was set at position control. Subsequently, a repeatable and exact plunge depth was difficult to attain, which leads to some variations of the plunge depths. It is recommended to use force control mode, in order to obtain replicate welds and to optimise the parameters.

REFERENCES

[1] Thomas W.M., Nicholas E.D., Needham J.C., Murch M.G. Temple-Smith P. and Dawes C.J., "Friction stir Butt Welding". 1991, International Patent No. PCT/GB92/02203, GB patent application No. 9125978.8.

[2] Mai T.A. and Spowage A.C., "Characterisation of dissimilar joints in laser welding of steel kovar, copper–steel and copper–aluminium". Materials Science and Engineering A, 2004, 374(1−2), pp 224-233.

[3] Badarinarayan H., "Fundamentals of Friction Stir Spot Welding" PhD Thesis, Missouri University of Science and Technology, 2009.

[4] Song X., Ke L., Xing L., Liu F., Huang C., "Effect of plunge speeds on hook geometries and mechanical properties in friction stir spot welding of A6061-T6 sheets" Int J Adv Manuf Technol (2014) 71, pp. 2003-2010.

[5] Yilba B.S., Sahin A.Z., Kahraman N., Al-Garni A.Z., "Friction stir welding of St-Al and Al-Cu materials" J. Mater. Process. Technol., 49, (1995), pp. 431-443.

[6] Ouyang J., Yarrapareddy E., Kovacevic R., " Microstructural evolution in the friction stir welded 6061 aluminum alloy (T6-temper condition) to copper" Journal of Materials Processing Technology, 2006, **172**, pp 110-122.

[7] Galvao I., Leal R.M., Rodrigues D.M. and Loureiro A., "Dissimilar welding of very thin aluminium and copper plates" Proceedings, 8th International Friction Stir Welding Symposium, 18-20 May 2010, Timmendorfer Strand, Germany.

[8] Heideman R., Johnson C., Kou S., "Metallurgical analysis of Al/Cu friction stir spot welding" Science and Technology of Welding and Joining Vol. 15 , No 7 (2010), pp. 597-604.

[9] Özdemir U., Sayer S., Yeni Ç., Bornova-Izmir., "Effect of Pin Penetration Depth on the Mechanical Properties of Friction Stir Spot Welded Aluminum and Copper" Materials Testing IN Joining Technology, 54(2012) 4, pp. 233-239.

[10] Shiraly M., Shamanian M., Toroghinejad M.R. and Ahmadi Jazani M., "Effect of Tool Rotation Rate on Microstructure and Mechanical Behavior of Friction Stir Spot-Welded Al/Cu Composite" Journal of Materials Engineering and Performance, Volume 23(2) February 2014, pp. 413-420.

[11] Di Paola M., Falchero A. and Spigarelli S., "Mechanical and microstructural characterisation of an aluminium friction stir welded butt joint", Metallurgical Science and Technology (2013), pp. 18-21.

[12] Hua T., "Monitoring and intelligent control for complex curvature friction stir welding" Doctoral thesis, Faculty of Engineering, The Built Environment and Information Technology, Nelson Mandela Metropolitan University. 2006.

[13] Blignault C., "Design, Development and Analysis of the Friction Stir Welding Process" Master's Degree dissertation, Faculty: Electrical, Industrial & Mechanical Engineering Port Elizabeth Technikon (South Africa), 2002.

[14] Tyler A. D, Yung C.S, and Yao B., "Observer-Based Adaptive Robust Control of Friction Stir Welding Axial Force' IEEE/ASME International Conference on Advanced Intelligent Mechatronics Montréal, Canada, July 6-9, 2010

[15] Akinlabi E.T. and Akinlabi S.A., "Effect of Shoulder Diameter on The Resulting Interfacial Regions of Friction Stir Welds Between Aluminium And Copper". Journal of Advanced Material Research, Vols. 299-300, (2011) pp. 1146-1150.

[16] Akinlabi E.T., "Effect of Shoulder Size on Weld Properties of Dissimilar Metal Friction Stir Welds" Journal of Materials Engineering and Performance, 2012, Vol **21**, No 7, pp. 1514-1519.

[17] Babu S., Sankar V.S., Janaki Ram G.D., Venkitakrishnan P.V., Madhusudhan Reddy G., and Prasad Rao K., "Microstructures and Mechanical Properties of Friction Stir Spot Welded Aluminum Alloy AA2014" Journal of Materials Engineering and Performance Vol. 22(1), (2013), pp. 71-84.

[18] Lienert T.J., Stellwag W.L., Grimmett B.B. and Warke R.W., "Friction stir welding studies on mild steel" Welding research, American Welding Society and The Welding Research Council, 2003.

[19] Kahl S. and Osikowish W., "Composite Aluminum-Copper sheet material by Friction Stir Welding and Cold Rolling" Journal of Materials Engineering and Performance, Vol. 22(8), (2013), pp. 2176-2184.

[20] Mathers G., "The welding of aluminium and its alloys" Woodhead Publishing Limited, Abington Hall, Abington Cambridge CB1 6AH, England, www.woodhead-publishing.com, 2002.

[21] Rossini N.S., Dassisti M., Benyounis K.Y., Olabi A.G., "Methods of measuring residual stresses in components" Materials and Design 35 (2012), pp 572-588.

[22] Lombard H., "optimized fatigue and fracture performance of friction stir welded aluminium plate: a study of the inter-relationship between process parameters, TMAZ, microstructure, defect population and performance" 2007, PhD thesis, Faculty of Technology University of Plymouth (England) in collaboration with Nelson Mandela Metropolitan University (South Africa).

[23] Mishra R.S. and Mahoney M.W., "Friction Stir Welding and Processing" ASM International, DOI: 10.1361/fswp2007p001, www.asminternational.org, 2007.

[24] Timothy J.M., "Friction Stir Welding of Commercially available Superplastic Aluminium", PhD thesis, Department of Engineering and Design, Brunel University, 2008.

[25] Thomas W.M., Nicholas E.D., Smith S.D., "Friction Stir Welding - Tool Developments" Aluminium joining symposium, New Orleans USA, 2001. http://www.twi.co.uk/j32k/protected/band_8/spwmtfeb2001.html.

[26] Merzoug M., Mazari M., Berrahal L., Imad A., "Parametric studies of the process of friction spot stir welding of aluminium 6060-T5 alloys" Materials and Design 31 (2010), pp. 3023-3028.

[27] Mijajlović M. and Milčić D., "Analytical Model for Estimating the Amount of Heat Generated During Friction Stir Welding: Application on Plates Made of Aluminium Alloy 2024 T351" Welding Processes, Edited by Radovan Kovačević, 11/2012: chapter Chapter 11, pp247-274; InTech., ISBN: 978-953-51-0854-2.

[28] Klobčar D., Tušek J., Skumavc A., Smolej A., "parametric study of friction stir spot welding of aluminium alloy 5754" METALURGIJA 53 (2014) 1, pp21-24.

[29] Yang Y.K., Dong H., Cao H., Chang Y.A., Kou S., "Liquation of Mg Alloys in Friction Stir Spot Welding" Welding Journal, July 2008, Vol. 87, pp 167-177.

[30] Zhang Y.N., Cao X., Larose S. and Wanjara P., "Review of tools for friction stir welding and processing" Canadian Metallurgical Quarterly 2012, Vol 51 No 3, pp 255-261.

[31] Badarinarayan H., Yang Q., and Zhu S., "Effect of tool geometry on static strength of friction stir spot-welded aluminum alloy", International Journal of Machine Tools and Manufacture, 2009. **49**(2): p.p 142-148.

[32] MA Z.Y., "Friction Stir Processing Technology: A Review", Metallurgical and Materials Transactions A, 2008, 39A, pp. 642-658.

[33] DebRoy T. and Bhadeshia H.K.D.H., "Friction stir welding of dissimilar alloys – a Perspective", Science and Technology of Welding and Joining 2010, 15, No 4, pp. 266- 270.

[34] Sivashanmugam M., Ravikumar S., Kumar T., Seshagiri Rao V., Muruganandam D., "A Review on Friction Stir Welding for Aluminium Alloys", 978-1-4244-9082-0/10/$26.00 ©2010 IEEE, pp. 216-221.

[35] Kumar A. and Jadoun R.S., "Friction Stir Welding of dissimilar materials/alloys: A review" int.J. Mech. Eng. & Rob. Res., ISSN: 2278-0149, special issue, vol. 1, No. 1, January 2014.

[36] Li B., Shen Y., "A feasibility research on friction stir welding of a new-typed lap–butt joint of dissimilar Al alloys" Materials and Design 34 (2012) , pp. 725-731.

[37] Leitão C., Louro R., Rodrigues D.M., " Analysis of high temperature plastic behaviour and its relation with weldability in friction stir welding for aluminium alloys AA5083-H111 and AA6082-T6 Materials and Design 37 (2012), pp. 402-409.

[38] Guo J., Gougeon P., Chen X.G., "Microstructure evolution and mechanical properties of dissimilar friction stir welded joints between AA1100-B4C MMC and AA6063 alloy", Materials Science and Engineering A 553 (2012) 149-156.

[39] Koilraj M., Sundareswaran V., Vijayan S., Koteswara Rao S.R., "Friction stir welding of dissimilar aluminum alloys AA2219 to AA5083 – Optimization of process parameters using Taguchi technique" Materials and Design 42 (2012), pp. 1-7.

[40] Palanivel R., Mathews P.K., Murugan N., Dinaharan I., "Effect of tool rotational speed and pin profile on microstructure and tensile strength of dissimilar friction stir welded AA5083-H111 and AA6351-T6 aluminum alloys", Materials and Design 40 (2012) , pp. 7-16.

[41] Palanivel R., Mathews P.K., "Mechanical and microstructural behaviour of friction stir welded dissimilar aluminium alloy", IEEE-International Conference on Advances in Engineering, Science and Management (ICAESM -2012) March 30, 31, 2012, pp. 7- 11.

[42] Da Silva A.A.M., Arruti E., Janeiro G., Aldanondo E., Alvarez P., Echeverria A., "Material flow and mechanical *behaviour* of dissimilar AA2024-T3 and AA7075-T6 aluminium alloys friction stir welds", Materials and Design 32 (2011) , pp. 2021-2027.

[43] Jamshidi Aval H., Serajzadeh S., Kokabi A.H., "Evolution of microstructures and mechanical properties in similar and dissimilar friction stir welding of AA5086 and AA6061", Materials Science and Engineering A 528 (2011), pp. 8071-80853.

[44] Shen C., Zhang J., Ge J., "Microstructures and electrochemical behaviors of the friction stir welding dissimilar weld", Journal of Environmental Sciences, 2011, 23(Supplement) S32-S35.

[45] Tran V.X., Pan J., Pan T., "Fatigue behavior of spot friction welds in lap-shear and cross-tension specimens of dissimilar aluminum sheets", International Journal of Fatigue 32 (2010), pp. 1022-1041.

[46] Jun T.S., Dragnevski K., Korsunsky A.M., "Microstructure, residual strain, and eigenstrain analysis of dissimilar friction stir welds", Materials and Design 31 (2010), pp. S121-S125.

[47] Ghosh M., Kumar K., Kailas S.V., Ray A.K., "Optimization of friction stir welding parameters for dissimilar aluminum alloys" Materials and Design 31 (2010) , pp. 3033-3037.

[48] Sundaram N.S, Murugan N., "Tensile behavior of dissimilar friction stir welded joints of aluminium alloys" Materials and Design 31 (2010) , pp. 4184-4193.

[49] Muruganandam D., Ravikumar S., Das S.L., "Mechanical and micro structural behavior of 2024–7075 Aluminium Alloy Plates joined by Friction Stir Welding", 978-1-4244-9082-0/10/$26.00 ©2010 IEEE, pp. 247- 251.

[50] Moreira P.M.G.P., Santos T., Tavares S.M.O., Richter-Trummer V., Vilaça P., de Castro P.M.S.T., "Mechanical and metallurgical characterization of friction stir welding joints of AA6061-T6 with AA6082-T6" Materials and Design 30 (2009), pp. 180-187.

[51] Leitao C., Leal R.M., Rodrigues D.M., Loureiro A., Vilaca P., "Mechanical behaviour of similar and dissimilar AA5182-H111 and AA6016-T4 thin friction stir welds" Materials and Design 30 (2009) , pp. 101-108.

[52] Cavaliere P., De Santis A., Panella F., Squillace A., "Effect of welding parameters on mechanical and microstructural properties of dissimilar AA6082–AA2024 joints produced by friction stir welding" Materials and Design 30 (2009), pp. 609-616.

[53] Leitão C., Emílio B., Chaparro B.M., Rodrigues D.M., "Formability of similar and dissimilar friction stir welded AA 5182-H111 and AA 6016-T4 tailored blanks" Materials and Design 30 (2009) , pp. 3235-3242.

[54] Hatamleh O., DeWald A., "An investigation of the peening effects on the residual stresses in friction stir welded 2195 and 7075 aluminum alloy joints", Journal of Materials Processing Technology 209 (2009), pp. 4822-4829.

[55] Mofid M.A., Abdollah-Zadeh A., Malek Ghaini F., "The effect of water cooling during dissimilar friction stir welding of Al alloy to Mg alloy" , Materials and Design 36 (2012), pp. 161-167.

[56] Malarvizhi S., Balasubramanian V., "Influences of tool shoulder diameter to plate thickness ratio (D/T) on stir zone formation and tensile properties of friction stir welded dissimilar joints of AA6061 aluminium–AZ31B magnesium alloys", Materials and Design 40 (2012) , pp. 453-460.

[57] Simoncini M., Forcellese A., "Effect of the welding parameters and tool configuration on micro- and macro-mechanical properties of similar and dissimilar FSWed joints in AA5754 and AZ31 thin sheets" , Materials and Design 41 (2012), pp. 50-60.

[58] Venkateswaran P., Reynolds A.P., "Factors affecting the properties of Friction Stir Welds between aluminium and magnesium alloys" Materials Science and Engineering A 545 (2012), pp.26-37.

[59] Sharifitabar M., Nami H., "Microstructures of dissimilar friction stir welded joints between 2024-T4 aluminium alloy and Al/Mg2Si metal matrix cast composite, Composites: Part B 42 (2011), pp. 2004-2012.

[60] Yan Y., Zhang D., Qiu C., Zhang W., "Dissimilar friction stir welding between 5052 aluminium alloy and AZ31 magnesium alloy", Trans. Nonferrous Met. Soc. China 20 (2010), pp. s619-s623.

[61] Liu C., Chen D.L., Bhole S., Cao X., Jahazi M., "Polishing-assisted galvanic corrosion in the dissimilar friction stir welded joint of AZ31 magnesium alloy to 2024 aluminium alloy" , Materials Characterization 60 (2009) , pp. 3 7 0 -3 7 6.

[62] Kostka A., Coelho R.S., dos Santos J., Pyzalla A.R., "Microstructure of friction stir welding of aluminium alloy to magnesium alloy", Scripta Materialia 60 (2009), pp. 953-956.

[63] Chen Y.C., Gholinia A., Prangnell P.B., "Interface structure and bonding in abrasion circle friction stir spot welding: A novel approach for rapid welding aluminium alloy to steel automotive sheet" Materials Chemistry and Physics 134 (2012), pp. 459-463.

[64] Ogura T., Saito Y., Nishida T., Nishida H., Yoshida T., Omichi N., Fujimoto M., Hirose A., "Partitioning evaluation of mechanical properties and the interfacial microstructure in a friction stir welded aluminum alloy/stainless steel lap joint", Scripta Materialia 66 (2012) , pp. 531-534.

[65] Coelho R.S., Kostka A., Dos Santos J.F., Kaysser-Pyzalla A., "Friction-stir dissimilar welding of aluminium alloy to high strength steels: Mechanical properties and their relation to microstructure", Materials Science & Engineering A 556 (2012), pp. 175-183.

[66] Bang H.S, Jeon G.H, Oh I.H, Ro C.S., "Gas tungsten arc welding assisted hybrid friction stir welding of dissimilar materials Al6061-T6 aluminum alloy and STS304 stainless steel" Materials and Design 37 (2012), pp. 48-55.

[67] Mashiko Y., Hatsukade Y., Yasui T., Takenaka H., Todaka Y., Fukumoto M., Tanaka S., "Evaluation of joint interface of friction stir welding between dissimilar metals using HTS-SQUID gradiometer", Physica C 470 (2010), pp. 1524-1528.

[68] Tanaka T., Morishige T. and Hirata T., "Comprehensive analysis of joint strength for dissimilar friction stir welds of mild steel to aluminum alloys" Scripta Materialia 61 (2009), pp. 756-759.

[69] Uematsu Y., Tokaji K., Tozaki Y., Nakashima Y., "Fatigue behaviour of dissimilar friction stir spot weld between A6061 and SPCC welded by a scrolled groove shoulder tool" , Procedia Engineering 2 (2010), pp. 193-201.

[70] Chen Y., Ni Q., Ke L., "Interface characteristic of friction stir welding lap joints of Ti/Al dissimilar alloys", Trans. Nonferrous Met. Soc. China 22(2012), pp. 299-304.

[71] Wei Y., Li J., Xiong J., Huang F., Zhang F., Raza S.H., "Joining aluminum to titanium alloy by friction stir lap welding with cutting pin" , Materials Characterization 71, (2012), pp. 1-5.

[72] Aonuma M., Nakata K., "Effect of calcium on intermetallic compound layer at interface of calcium added magnesium–aluminum alloy and titanium joint by friction stir welding, Materials Science and Engineering B 173 (2010), pp. 135-138.

[73] Chen Y.C., Nakata K., "Microstructural characterization and mechanical properties in friction stir welding of aluminum and titanium dissimilar alloys", Materials and Design 30 (2009), pp. 469-474.

[74] Dressler U., Biallas G., Mercado U.A., "Friction stir welding of titanium alloy TiAl6V4 to aluminium alloy AA2024-T3" , Materials Science and Engineering A 526 (2009) , pp. 113-117.

[75] Pfeiffer W., Reisacher E., Windisch M., Kahnert M., "The effect of specimen size on residual stresses in friction stir welded aluminum components" Advanced Materials Research Vol. 996, (2014), pp. 445-450

[76] Bach M., Merati A., Gharghouri M., "effects of fatigue on the integrity of a friction stir welded lap joint containing residual stresses" Advanced Materials Research Vol. 996 (2014) pp 794-800.

[77] Fratini L., Pasta S., Reynolds A.P., "Fatigue crack growth in 2024-T351 friction stir welded joints: Longitudinal residual stress and microstructural effects" International Journal of Fatigue 31 (2009), pp. 495-500.

[78] Ma Yu E., Staron P., Fischer T., Irving P.E., "Size effects on residual stress and fatigue crack growth in friction stir welded 2195-T8 aluminium – Part I: Experiments" International Journal of Fatigue 33 (2011), pp. 1417-1425.

[79] Ni D.R., Chen D.L., Xiao B.L., Wanga D., Ma Z.Y., " Residual stresses and high cycle fatigue properties of friction stir welded SiCp/AA2009 composites" International Journal of Fatigue 55 (2013) , pp. 64-73.

[80] Steuwer A., Peel M.J., Withers P.J., "Dissimilar friction stir welds in AA5083–AA6082: The effect of process parameters on residual stress" Materials Science and Engineering A 441 (2006), pp. 187-196.

[81] Altenkirch J., Steuwer A., Peel M., Richards D.G., Withers P.J., "The effect of tensioning and sectioning on residual stresses in aluminium AA7749 friction stir welds" Materials Science and Engineering A 488 (2008) , pp. 16-24.

[82] Lombard H., Hattingh D.G., Steuwera A., James M.N., "Effect of process parameters on the residual stresses in AA5083-H321 friction stir welds" Materials Science and Engineering A 501 (2009), pp. 119-124.

[83] Peel M., Steuwer A., Preuss M., Withers P.J., "Microstructure, mechanical properties and residual stresses as a function of welding speed in aluminium AA5083 friction stir welds" Acta Materialia 51 (2003), pp. 4791-4801.

[84] Prime M.B., Gna¨upel-Herold T., Baumann J.A., Lederich R.J., Bowden D.M., Sebring R.J., "Residual stress measurements in a thick, dissimilar aluminum alloy friction stir weld" Acta Materialia 54 (2006), pp. 4013-4021.

[85] Linton V.M., Ripley M.I., "Influence of time on residual stresses in friction stir welds in age hardenable 7xxx aluminium alloys" Acta Materialia 56 (2008), pp. 4319-4327.

[86] Liu P., Shi Q., Wang W., Wang X., Zhang Z., "Microstructure and XRD analysis of FSW joints for copper T2/aluminium 5A06 dissimilar materials" Materials Letters, (2008), **62** , pp 4106-4108.

[87] Xue P., Xiao B.L. , Ni D.R., Ma Z.Y., "Enhanced mechanical properties of friction stir welded dissimilar Al–Cu joint by intermetallic compounds" Materials Science and Engineering A, (2010), **527**, pp 5723-5727.

[88] Bisadi H., Tavakoli A., Tour Sangsaraki M., Tour Sangsaraki K., "The influences of rotational and welding speeds on microstructures and mechanical properties of friction stir welded Al5083 and commercially pure copper sheets lap joints" Materials and Design (2013), **43**, pp 80-88.

[89] Xue P., Ni D.R., Wang D., Xiao B.L., Ma Z.Y., "Effect of friction stir welding parameters on the microstructure and mechanical properties of the dissimilar Al–Cu joints" Materials Science and Engineering A, 2011, **528**, pp 4683-4689.

[90] Esmaeili A., Besharati Givi M.K., Zareie Rajani H.R., "A metallurgical and mechanical study on dissimilar Friction Stir welding of aluminum 1050 to brass (CuZn30)" Materials Science and Engineering, (2011), **A 528**, pp. 7093-7102.

[91] Abdollah-Zadeh A., Saeid T., Sazgari B., "Microstructural and mechanical properties of friction stir welded aluminum/copper lap joints" Journal of Alloys and Compounds, (2008), **460**, pp. 535-538.

[92] Saeid T., Abdollah-Zadeh A., Sazgari B., " Weldability and mechanical properties of dissimilar aluminum–copper lap joints made by friction stir welding" Journal of Alloys and Compounds, 2010, **490**, pp 652-655.

[93] Akinlabi E.T., Madyira D. M., Akinlabi S.A., "Effect of Heat Input on the Electrical Resistivity of Dissimilar Friction Stir Welded Joints of Aluminium and Copper" IEEE Africon (2011) - The Falls Resort and Conference Centre, Livingstone, Zambia, 13 - 15 September 2011.

[94] Akinlabi E.T., Reddy R.D., Akinlabi S.A., "Microstructural Characterizations of Dissimilar Friction Stir Welds" Proceedings of the World Congress on Engineering (WCE), 2012, ISBN: 978-988-19252-2-0, **III**, pp. 4-6.

[95] Galvao I., Oliveira J. C., Loureiro A. and Rodrigues D.M., "Formation and distribution of brittle structures in friction stir welding of aluminium and copper: influence of process parameters" Science and Technology of Welding and Joining, (2011), **16**, No 8, pp. 681- 689.

[96] Galvao I., Leal R. M., Loureiro A. and Rodrigues D. M., "Material flow in heterogeneous friction stir welding of aluminium and copper thin sheets" Science and Technology of Welding and Joining, (2010), **15**, No 8, pp. 654-660.

[97] Pratik A.S., Nageswaran P., Arivazhagan N., Devendranath Ramkumar K., "Development of Friction Stir Welded Butt Joints of AA 6063 Aluminium Alloy and Pure Copper" International Conference on Advanced Research in Mechanical Engineering, (2012), (ICARM), pp. 46-50.

[98] Singh R.K.R., Prasad R., Pandey S., "Mechanical Properties of Friction Stir Welded Dissimilar Metals" Proceedings of the National Conference on Trends and Advances in Mechanical Engineering, (2012), pp. 579-583.

[99] Shukla R.K., Shah P.K.," Investigation of Joint Properties of Friction Stir Welding of Aluminum 6061 Alloy to Copper" International Journal of Engineering Research and Technology, 2010, **3**, Number 3, pp. 613-620.

[100] Guerra M., Schmidt C. , McClure J.C., Murr L.E., Nunes A.C., "Flow patterns during friction stir welding" Materials Characterization , 2003, **49** , pp. 95-101.

[101] Xue P., Xiao B.L., Wang D. and Ma Z.Y., "Achieving high property friction stir welded aluminium/copper lap joint at low heat input" Science and Technology of Welding and Joining, 2011, **16**, No 8, pp. 657-661.

[102] Akinlabi E.T., Akinlabi S.A., "Effect of Heat Input on the Properties of Dissimilar Friction Stir Welds of Aluminium and Copper" American Journal of Materials Science, (2012), 2(5), pp. 147-15.

[103] Li X., Zhang D., Qiu C., Zhang W., "Microstructure and mechanical properties of dissimilar pure copper/1350 aluminum alloy butt joints by friction stir welding" Trans. Nonferrous Met. Soc. China 22, (2012), pp. 1298-1306.

[104] Esmaeili A., Zareie Rajani H.R, Sharbati M., Besharati Givi M.K., Shamanian M., "The role of rotation speed on intermetallic compounds formation and mechanical behavior of friction stir welded brass/aluminum 1050 couple" ,2011, Intermetallics 19 , pp. 1711-1719.

[105] Akinlabi E.T., "Characterisation of Dissimilar Friction Stir Welds between 5754 Aluminium Alloy and C11000 Copper" D-Tech thesis, (2010), Nelson Mandela Metropolitan University, South Africa.

[106] Avettand-Fenoel M.N., Taillard R., Ji G. and Goran D., "Multiscale Study of Interfacial Intermetallic Compounds in a Dissimilar Al 6082-T6/Cu Friction-Stir Weld", 2012, Metallurgical and Materials Transactions A, pp 4655-4666.

[107] Al-Roubaiy A.O., Nabat S.M., Batako A.D.L., "Experimental and theoretical analysis of friction stir welding of Al–Cu joints" Int J Adv Manuf Technol (2014) 71, pp 1631-1642.

[108] Muthu M.F.X, Jayabalan V., "Tool Travel Speed Effects on The Microstructure of Friction Stir Welded Aluminium - Copper Joints", Journal of Materials Processing Technology 217 (2015), pp 105-113.

[109] Rai R., De A., Badeshia H.K.D.H and DebRoy T., "Review: Friction Stir Welding tools" Science and Technology of Welding and Joining, (2011), vol 16, No 4, pp 325-341.

[110] Uematsu Y., Tokaji K., Tozaki Y., Kurita T., Murata S., "Effect of re-filling probe hole on tensile failure and fatigue behaviour of friction stir spot welded joints in Al–Mg–Si alloy" International Journal of Fatigue 30 (2008), pp. 1956-1966.

[111] Zhang Z., Yang X., Zhang J., Zhou G., Xu X., Zou B., "Effect of welding parameters on microstructure and mechanical properties of friction stir spot welded 5052 aluminum alloy" Materials and Design 32 (2011), pp 4461-4470.

[112] Shen Z., Yang X., Zhang Z., Cui L., Li T., "Microstructure and failure mechanisms of refill friction stir spot welded 7075-T6 aluminum alloy joints" Materials and Design 44 (2013), pp 476-486.

[113] Shen Z., Yang X., Zhang Z., Cui L., Yin Y., " Mechanical properties and failure mechanisms of friction stir spot welds of AA 6061-T4 sheets" Materials and Design 49 (2013), pp 181–191.

[114] Tozaki Y., Uematsu Y., Tokaji K., "Effect of tool geometry on microstructure and static strength in friction stir spot welded aluminium alloys" International Journal of Machine Tools & Manufacture 47 (2007), pp 2230-2236.

[115] Mitlin D., Radmilovic V., Panc T., Chen J., Feng Z., Santella M.L. "Structure–properties relations in spot friction welded (also known as friction stir spot welded) 6111 aluminum" Materials Science and Engineering A 441 (2006) , pp 79-96.

[116] Wang D.A., Lee S.C., "Microstructures and failure mechanisms of friction stir spot welds of aluminum 6061-T6 sheets" Journal of Materials Processing Technology 186 (2007), pp 291-297.

[117] Buffa G., Fratini L., Piacentini M., "On the influence of tool path in friction stir spot welding of aluminum alloys" journal of materials processing technology 208 (2008), pp. 309-317.

[118] Wang D., Chao C., Lin P., Uan J., "Mechanical characterization of friction stir spot microwelds" Journal of Materials Processing Technology 210 (2010), pp 1942-1948.

[119] Yuan W., Mishra R.S., Webb S., Chen Y.L., Carlson B., Herling D.R., Grant G.J., "Effect of tool design and process parameters on properties of Al alloy 6016 friction stir spot welds" Journal of Materials Processing Technology 211 (2011), pp 972-977.

[120] Jeon C., Hong S., Kwon Y., Cho H., Han H., "Material properties of friction stir spot welded joints of dissimilar aluminum alloys" Trans. Nonferrous Met. Soc. China 22(2012) s605-s613.

[121] Thoppul S.D and Gibson R.F., "Mechanical characterization of spot friction stir welded joints in aluminum alloys by combined experimental/numerical approaches Part I: Micromechanical studies" Materials Characterization 60 (2009), pp 1342-1351.

[122] Gerlich A., Su P., Yamamoto M., North T.H., "Effect of welding parameters on the strain rate and microstructure of friction stir spot welded 2024 aluminum alloy" J Mater Sci (2007) 42, pp 5589-5601.

[123] Su P., Gerlich A., North T.H., and Bendzsak G.J., "Intermixing in Dissimilar Friction Stir Spot Welds" Metallurgical and Materials Transactions A 38 (3) (2007), pp 584-295.

[124] Pathak N., Bandyopadhyay K., Sarangi M., and Panda S.K., "Microstructure and Mechanical Performance of Friction Stir Spot-Welded Aluminum-5754 Sheets" Journal of Materials Engineering and Performance 22 (1), pp131-144.

[125] Suhuddin U.F.H., Fischer V. and dos Santos J.F., "The thermal cycle during the dissimilar friction spot welding of aluminum and magnesium alloy" Scripta Materialia 68 (2013), pp 87-90.

[126] Chowdhury S.H., Chen D.L., Bhole S.D., Cao X., Wanjara P., "Lap shear strength and fatigue life of friction stir spot welded AZ31 magnesium and 5754 aluminum alloys" Materials Science & Engineering A 556 (2012), pp 500-509.

[127] Chowdhury S.H., Chen D.L., Bhole S.D., Cao X., Wanjara P., "Lap shear strength and fatigue behaviour of friction stir spot welded dissimilar magnesium-to-aluminum joints with adhesive" Materials Science & Engineering A 562 (2013), pp 53-60.

[128] Choi D., Ahn B., Lee C., Yeon Y., Song K., Jung S., "Formation of intermetallic compounds in Al and Mg alloy interface during friction stir spot welding" Intermetallics 19 (2011), pp 125-130.

[129] Gerlich A., Su P., North T.H., "Tool penetration during friction stir spot welding of Al and Mg alloys" Journal of Materials Science 40 (2005), pp 6473-6481.

[130] Chen Y.C., Gholinia A., Prangnell P.B., "Interface structure and bonding in abrasion circle friction stir spot welding: A novel approach for rapid welding aluminium alloy to steel automotive sheet" Materials Chemistry and Physics 134 (2012), pp 459-463

[131]Sun Y.F., Fujii H., Takaki N., Okitsu Y., "Microstructure and mechanical properties of dissimilar Al alloy/steel joints prepared by a flat spot friction stir welding technique" Materials and Design 47 (2013), pp 350-357

[132] Bozzi S., Helbert-Etter A.L., Baudin T., Criqui B., Kerbiguet J.G., "Intermetallic compounds in Al 6016/IF-steel friction stir spot welds" Materials Science and Engineering A 527 (2010) , pp 4505-4509.

[133] Figner G., Vallant R., Weinberger T., Schrottner H., Pasic H., Enzinger N., "Friction Stir Spot Welds between aluminium and steel automotive sheets: influence of welding parameters on mechanical properties and microstructure" Welding in the World, 53(2009), 1/2 R13-R23.

[134] Metallographic preparation of copper and copper alloys. Struers Application notes. Available from www.struers.com [Accessed August 2013].

[135] Metallographic preparation of aluminium and aluminium alloys. Struers Application notes. Available from www.struers.com [Accessed August 2013].

[136] ASTM Standard E3-11, 2011 "Standard guide for preparation of metallographic specimens", ASTM International, West Conshohocken, PA, 2011, DOI: 10.1520/E0003-11, www.astm.org.

[137] Herguth W.R., Nadeau G., "Application of Scanning Electron Microscopy and energy Dispersive Spectroscopy (SEM/EDS) to Practical Tribology Problems" Herguth Laboratories, INC. (website).

[138] ASTM Standard E384-11$^{\varepsilon 1}$, 2012, "Standard Test Method for Knoop and Vickers Hardness of Materials", ASTM International, West Conshohocken, PA, 2012, DOI: 10.1520/E0384-11E01, www.astm.org.

[139] Lomholt T.C., 'Microstructure Evolution during Friction Stir Spot Welding of TRIP steel', PhD thesis, Technical University of Denmark, Department of Mechanical Engineering, (2011).

[140] Fitzpatrick M.E., Fry A.T., Holdway P., Kandil F.A., Shackleton J. and Suominen L., "Determination of Residual Stresses by X-ray Diffraction" Measurement Good Practice Guide No. 52 Issue 2, ISSN: 1744-3911.

[141] Murr L.E., "A Review of FSW Research on Dissimilar Metal and Alloy Systems" Journal of Materials Engineering and Performance (2010), Volume 19(8), pp 1071-108.

[142] Vashista M. and Paul S., (2012) "Correlation between full width at half maximum (FWHM) of XRD peak with residual stress on ground surfaces", Philosophical Magazine, 92:33, pp 4194-4204, DOI: 10.1080/14786435.2012.704429.

[143] Kim H.J, Lee Y.J, Paik K.W., Koh K.W., Won J., Choe S., Lee J., Moon J.T, Park Y.T., "Effects of Cu/Al intermetallic compound (IMC) on Copper Wire and aluminum pad bondability" IEEE transactions on components and packaging technologies, vol. 26, Nº. 2, June 2003.

[144] Schneider J.M, Bigerelle M. and Iost A., "Statistical analysis of the Vickers hardness" Materials Science and Engineering A262 (1999), pp 256-263.

[145] Yurkov A. L., Jhuravleva N. V., Lukin E. S., "Kinetic microhardness measurements of sialon-based ceramics" Journal of Materials Science 29 (1994) , pp. 6551 6560.

[146] Yanchev I. Y, Trifonova E. P., "Analysis of microhardness data in Tl_x ln $_{l-x}$ Se" Journal of Materials Science 30 (1995), pp 5576-5580.

[147] Hassan A.M., Almomani M., Qasim T. and Ghaithan A., "Statistical analysis of some mechanical properties of friction stir welded aluminium matrix composite", Int. J. Experimental Design and Process Optimisation, Vol. 3, No. 1, (2012), pp 91-109.

[148] Lin P.C., Lin S.H and Pan J., "modeling of plastic deformation and failure near spot welds in lap shear specimens" SAE Technical paper No 2004-01-0817, Society of Automotive Engineering, Warrendale, PA.,(2004).

[149] Lina Yu ., Kazuhiro Nakata., Jinsun Liao., "Microstructural modification and mechanical property improvement in friction stir zone of thixo-molded AE42 Mg alloy" Journal of Alloys and Compounds , Vol. 480, Issue 2, 8 July 2009, pp 340-346.

[150] Tan C.W., Jiang Z.G., Li L.Q., Chen Y.B., Chen X.Y., "Microstructural evolution and mechanical properties of dissimilar Al–Cu joints produced by friction stir welding" Materials & Design , Vol. 51, (October 2013), pp. 466-473.

APPENDIX A

Appendix A.1 X-ray Fluorescence spectrometer (XRF) results of AA1060

AA1060						
Bulk	Metal					
Al	99.317	mass%	0.02151	Al-KA	3176.514	88.9656
Si	0.1777	mass%	0.00317	Si-KA	1.3222	0.1592
P	0.0054	mass%	0.00178	P -KA	0.1007	0.0049
S	0.0044	mass%	0.00091	S -KA	0.0709	0.0039
K	0.0066	mass%	0.00275	K -KA	0.1424	0.0059
V	0.0133	mass%	0.00439	V -KA	0.1524	0.0119
Fe	0.4544	mass%	0.00391	Fe-KA	19.9808	0.407
Ni	0.0066	mass%	0.00251	Ni-KA	0.539	0.0059
Ga	0.0147	mass%	0.00188	Ga-KA	2.3921	0.0132

Appendix A.2 X-ray Fluorescence spectrometer (XRF) results of C11000

C11000						
Bulk	Metal					
Mg	0.0132	mass%	0.01772	Mg-KA	0.0318	0.0137
Al	0.0379	mass%	0.0022	Al-KA	0.3173	0.0394
Si	0.0909	mass%	0.00232	Si-KA	0.8259	0.0945
P	0.0254	mass%	0.00064	P -KA	0.7651	0.0264
S	0.0145	mass%	0.00076	S -KA	0.2912	0.0151
Cl	0.0506	mass%	0.00367	Cl-KA	0.227	0.0526
K	0.0184	mass%	0.00362	K -KA	0.5174	0.0191
Ca	0.0089	mass%	0.00496	Ca-KA	0.2378	0.0092
Fe	0.0094	mass%	0.00382	Fe-KA	0.6072	0.0098
Cu	99.7307	mass%	0.01477	Cu-KA	5790.81	103.6866

APPENDIX B

Table showing the number of spot welds produced

Welds Nº	RPM	Shoulder diameter	Shoulder plunge depth	Tool Geometry
W1	800	15	0.5	Flat pin and shoulder
W2	800	15	0.5	
W3	800	15	0.5	
W4	800	15	1.0	
W5	800	15	1.0	
W6	800	15	1.0	
W7	1200	15	0.5	
W8	1200	15	0.5	
W9	1200	15	0.5	
W10	1200	15	1.0	
W11	1200	15	1.0	
W12	1200	15	1.0	
W25	800	15	0.5	Conical pin and concave shoulder
W26	800	15	0.5	
W27	800	15	0.5	
W28	800	15	1.0	
W29	800	15	1.0	
W30	800	15	1.0	
W31	1200	15	0.5	
W32	1200	15	0.5	
W33	1200	15	0.5	
W34	1200	15	1.0	
W35	1200	15	1.0	
W36	1200	15	1.0	
W49	800	15	0.5	Flat pin and shoulder
W50	800	15	0.5	
W51	800	15	0.5	
W52	800	15	1.0	
W53	800	15	1.0	
W54	800	15	1.0	
W55	1200	15	0.5	
W56	1200	15	0.5	
W57	1200	15	0.5	
W58	1200	15	1.0	
W59	1200	15	1.0	
W60	1200	15	1.0	
W73	800	15	0.5	Conical pin and concave shoulder
W74	800	15	0.5	
W75	800	15	0.5	
W76	800	15	1.0	
W77	800	15	1.0	
W78	800	15	1.0	
W79	1200	15	0.5	
W80	1200	15	0.5	
W81	1200	15	0.5	
W82	1200	15	1.0	
W83	1200	15	1.0	
W84	1200	15	1.0	

APPENDIX C

XRD spectrums of the parent materials using X-ray Diffractometer Rigaku Ultima IV

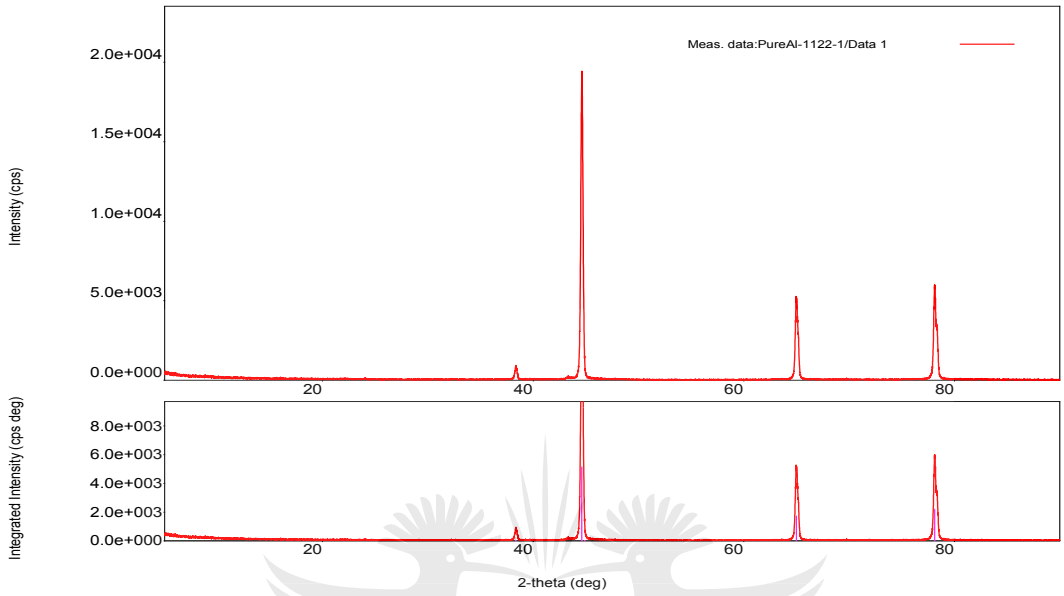

Appendix C.1 XRD diffraction pattern of the aluminium parent material (AA1060)

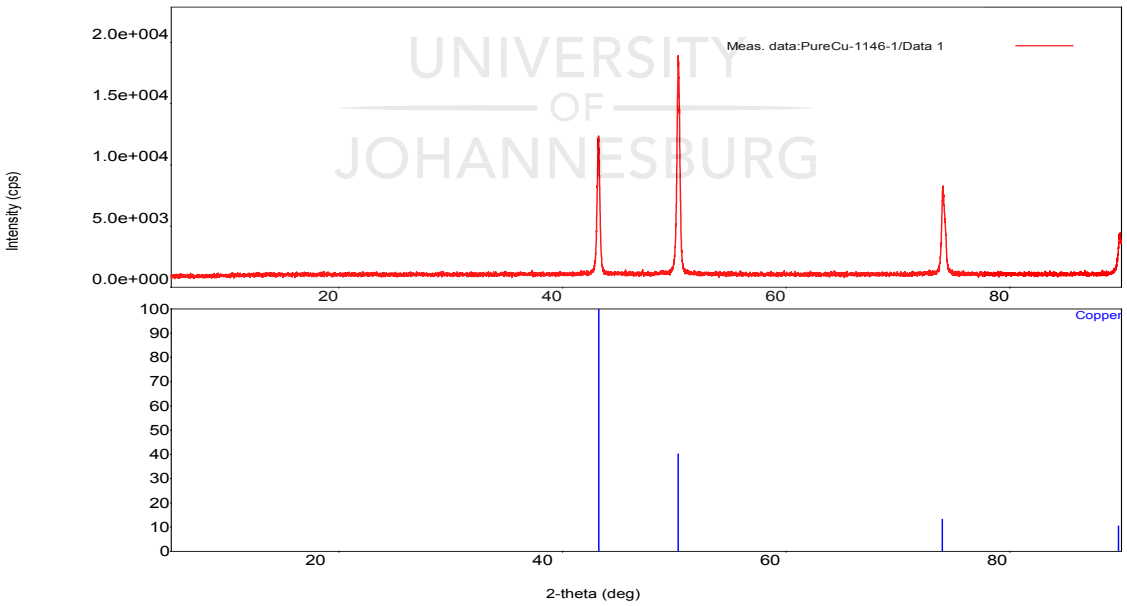

Appendix C.1 XRD diffraction pattern of the copper parent material (C11000)

APPENDIX D

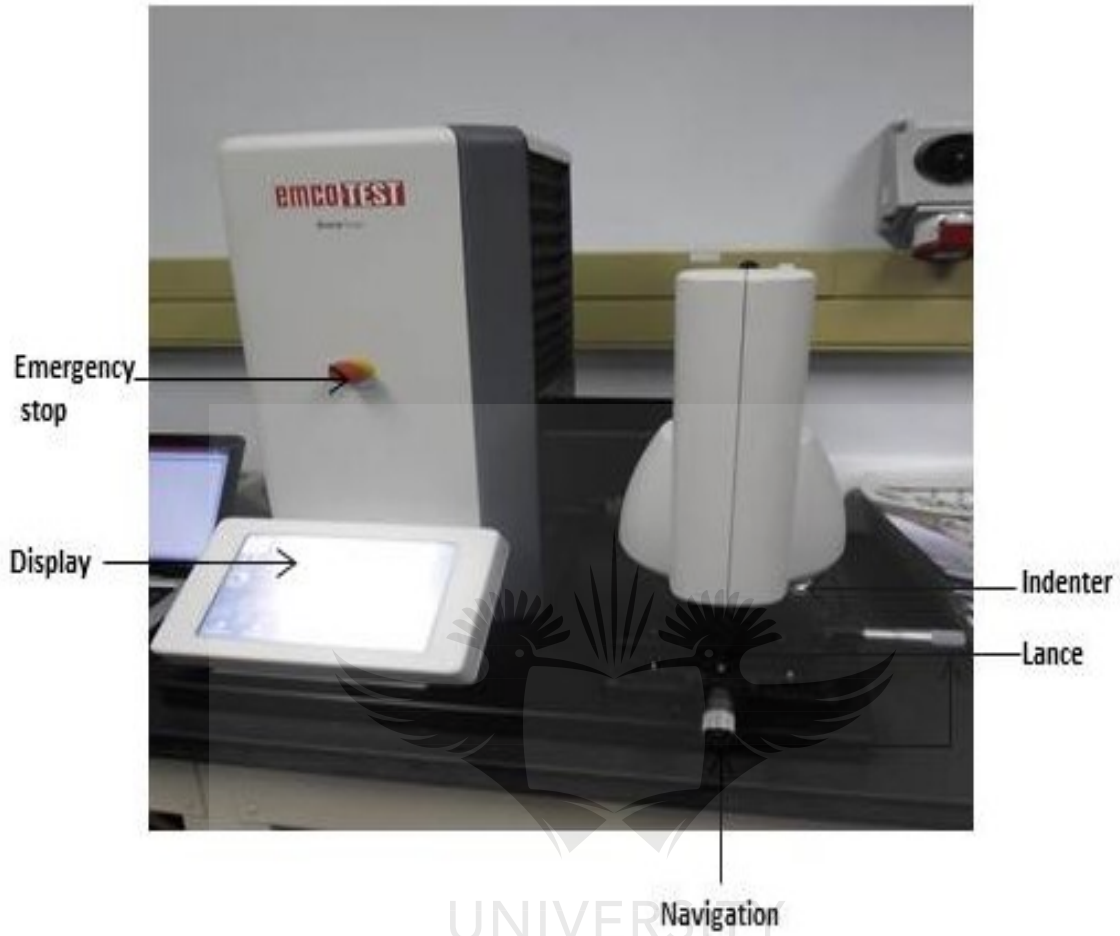

Microhardness machine used in the current study

APPENDIX E

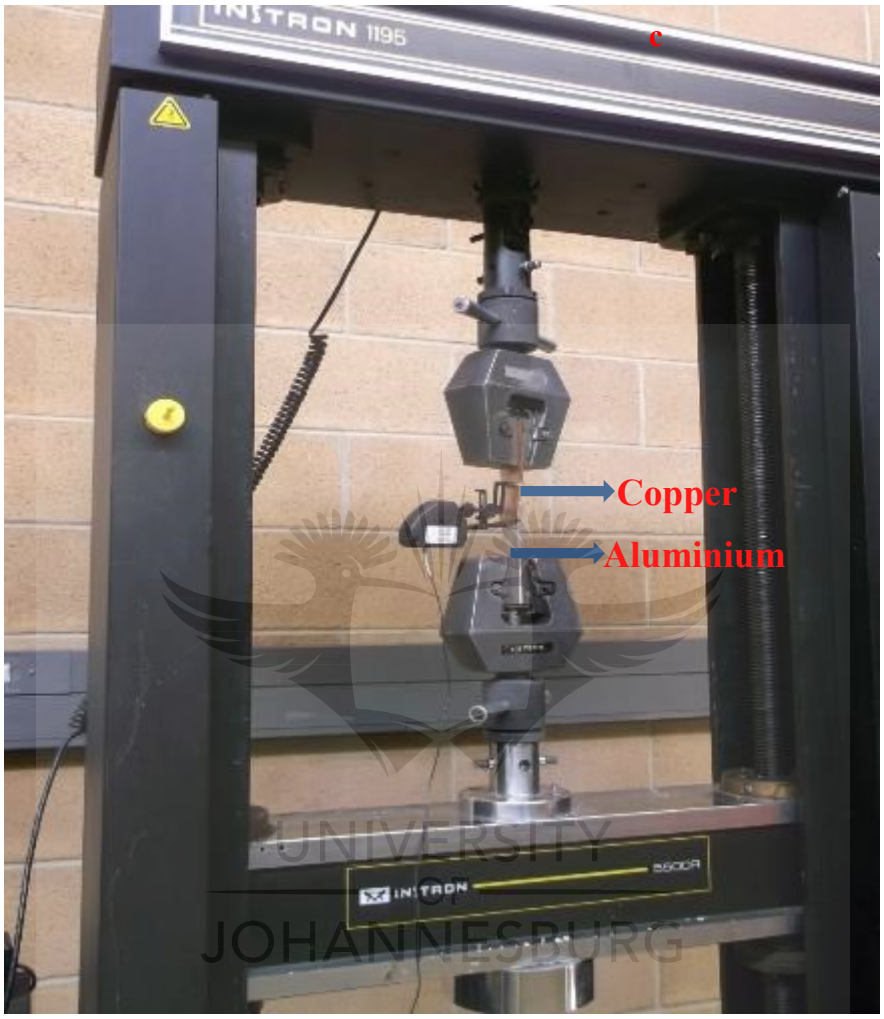

Tensile test machine and specimen of FSSW

APPENDIX F

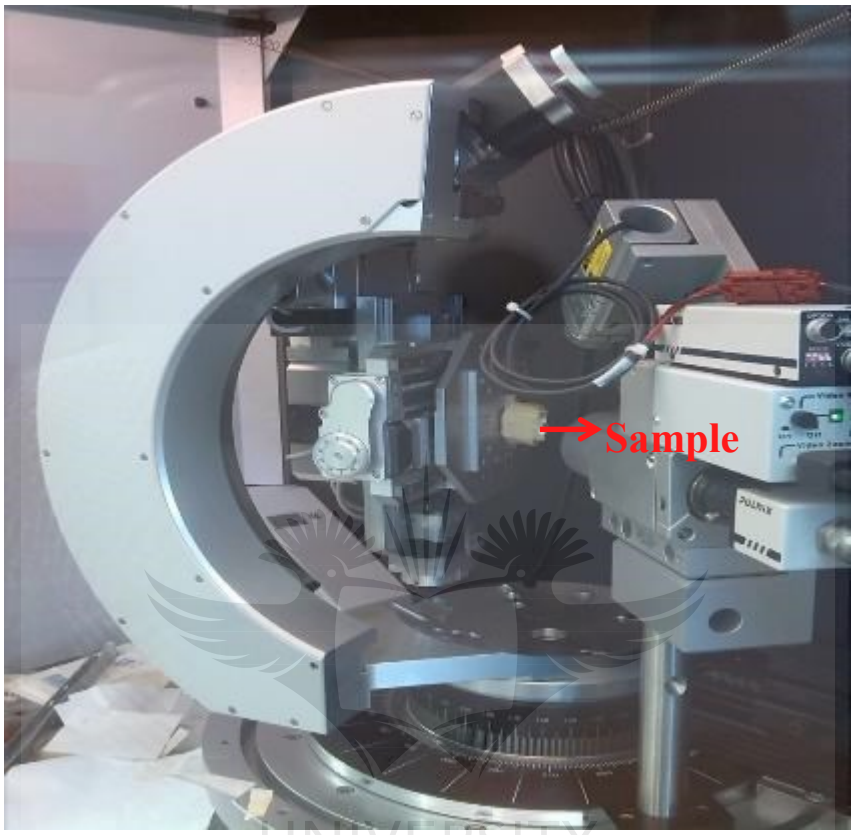

Showing the BRUKER D8 Discover diffractometer used for the measurement of the residual stresses

APPENDIX G

Forge forces generated during the production of the welds using a flat pin and flat shoulder tool

FPS_800_0.5_1

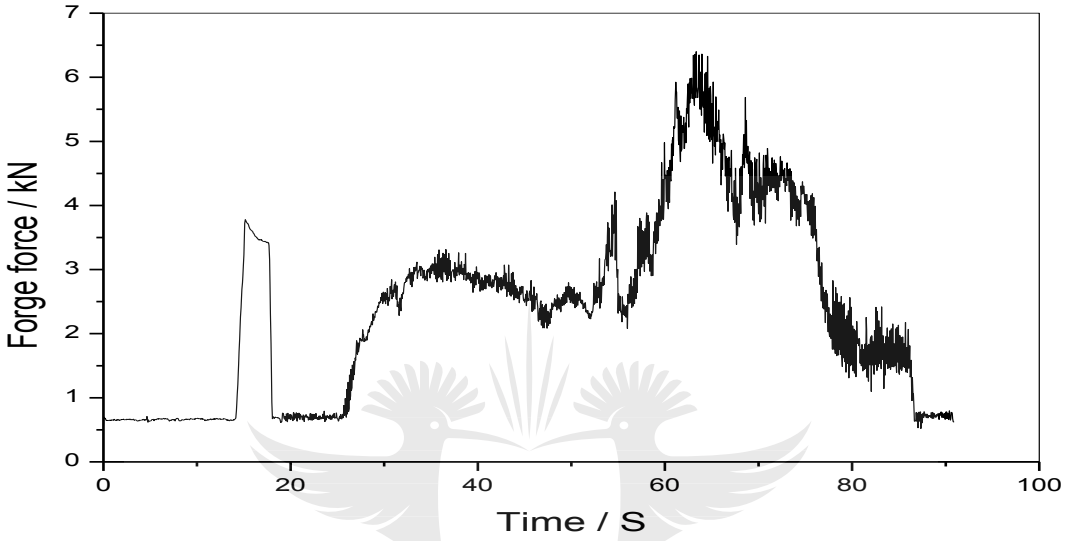

FPS_800_0.5_2

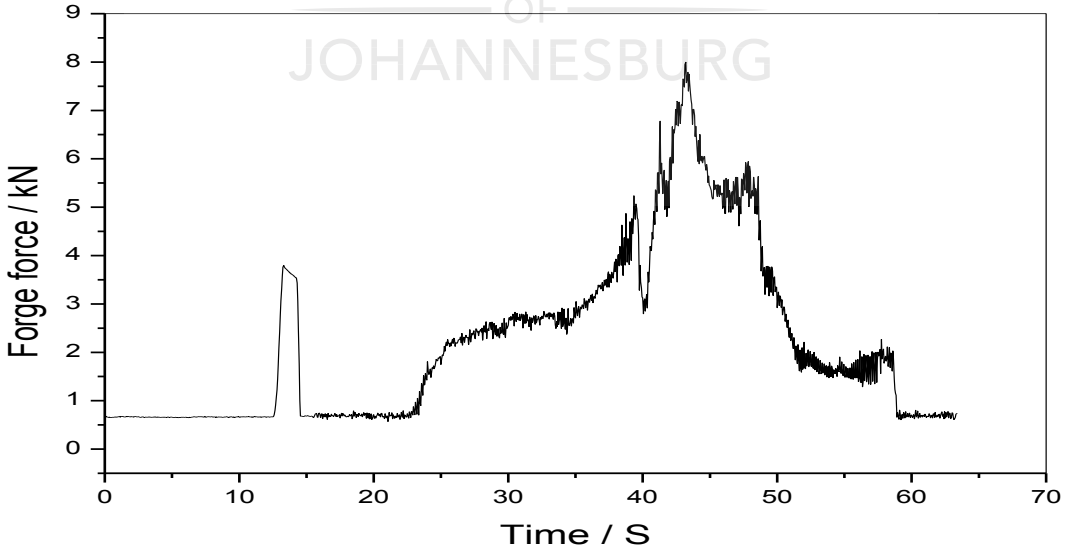

FPS_800_800_3

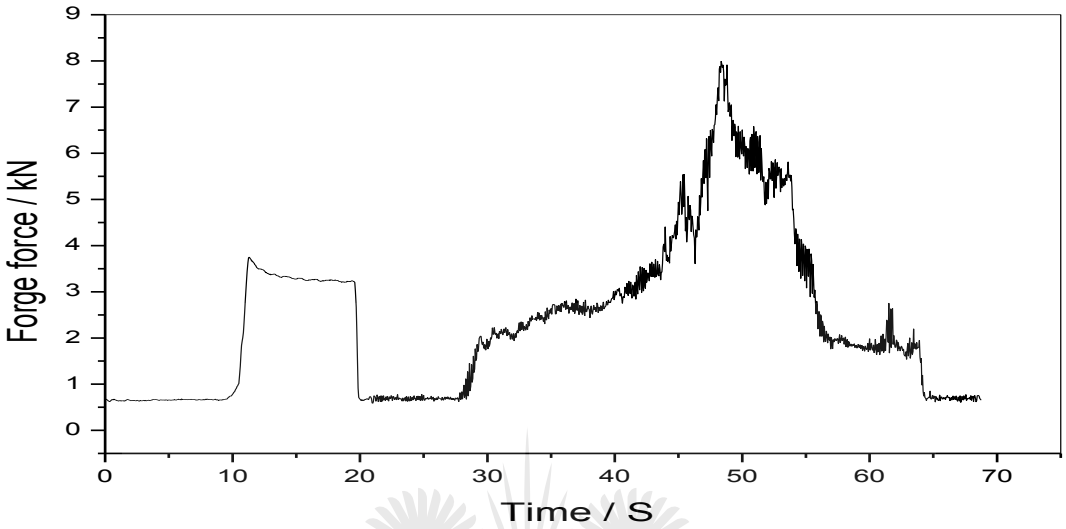

FPS_800_1_1

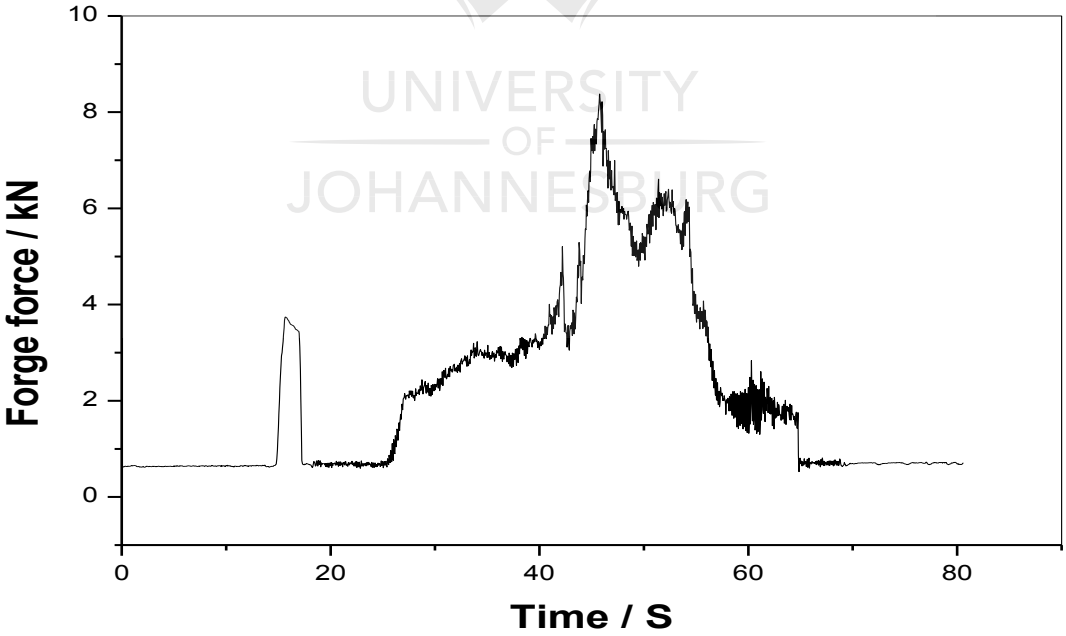

FPS_800_1_2

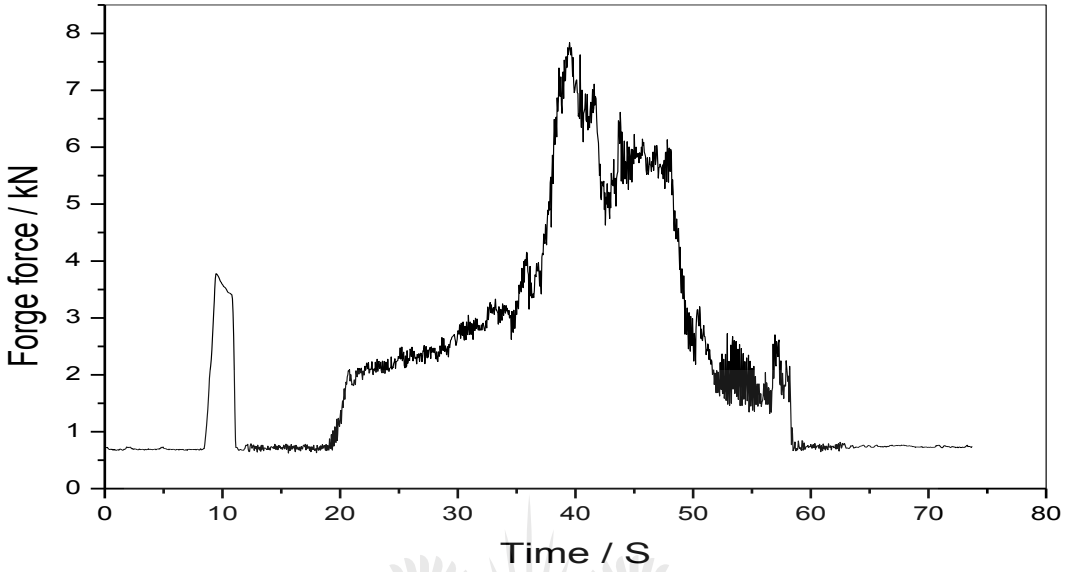

FPS_800_1_3

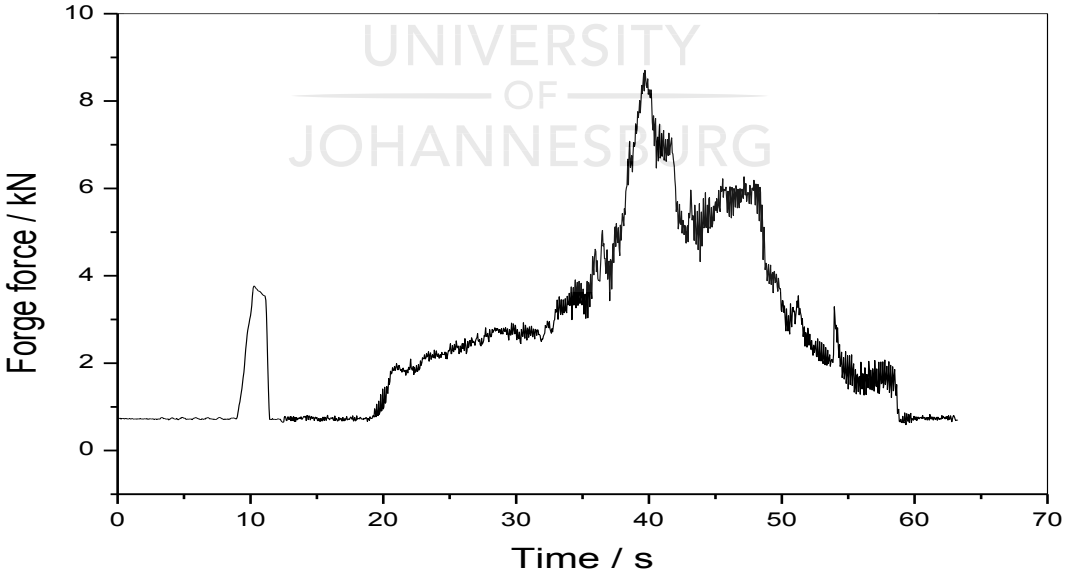

FPS_1200_0.5_1

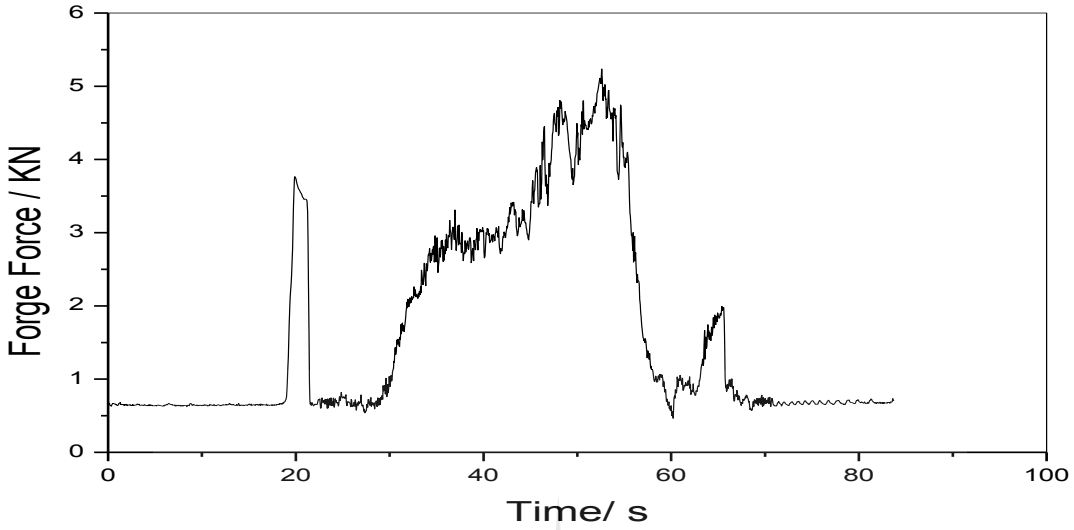

FPS_1200_0.5_2

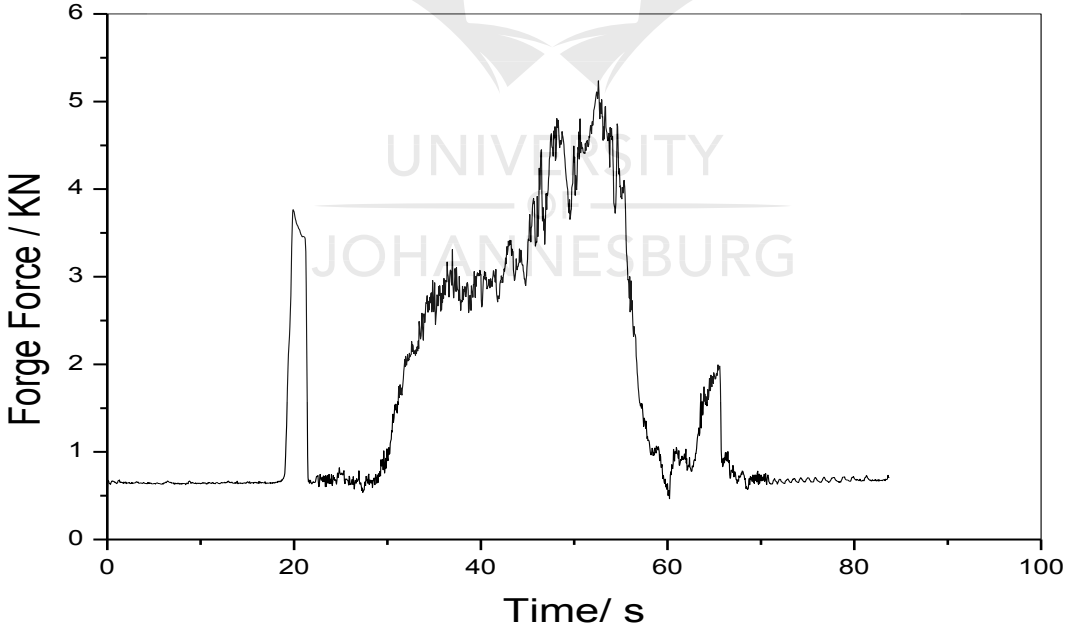

FPS_1200_0.5_3

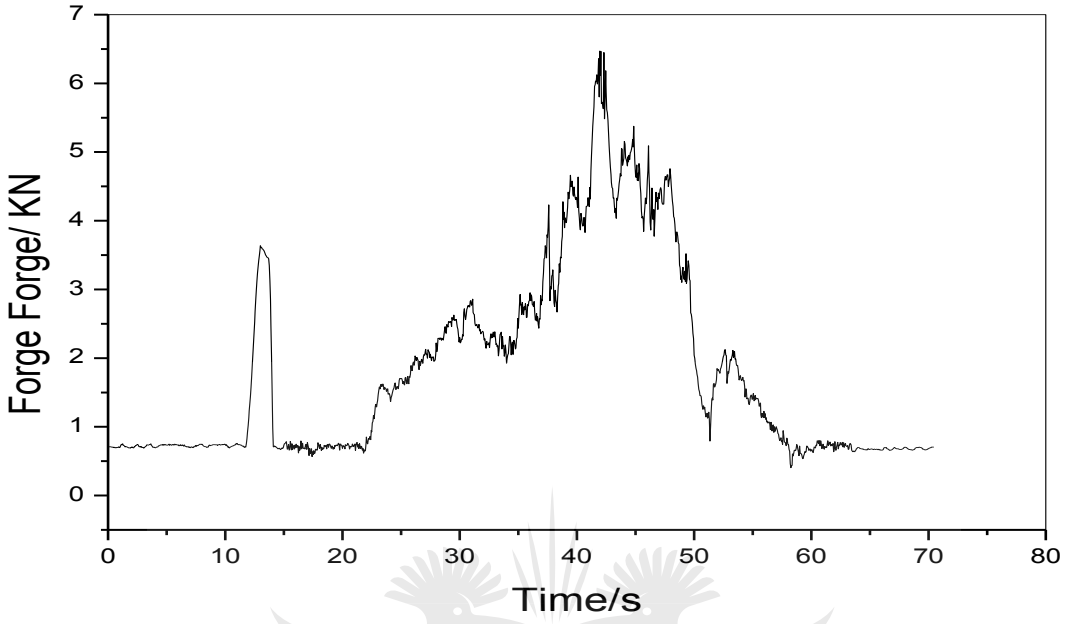

FPS_1200_1_1

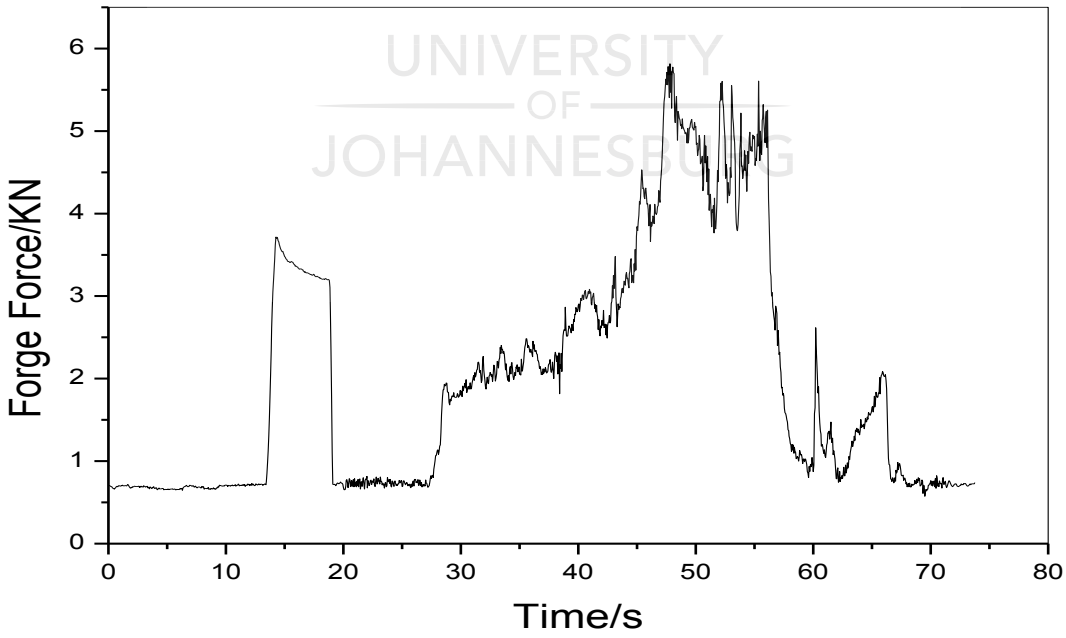

FPS_1200_1_2

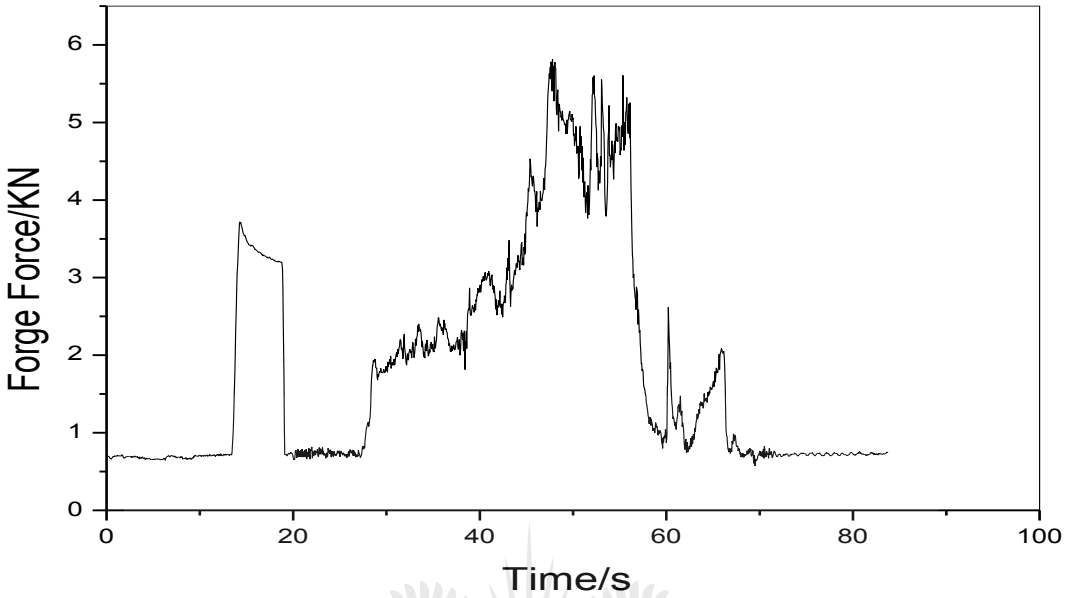

FPS_1200_1_3

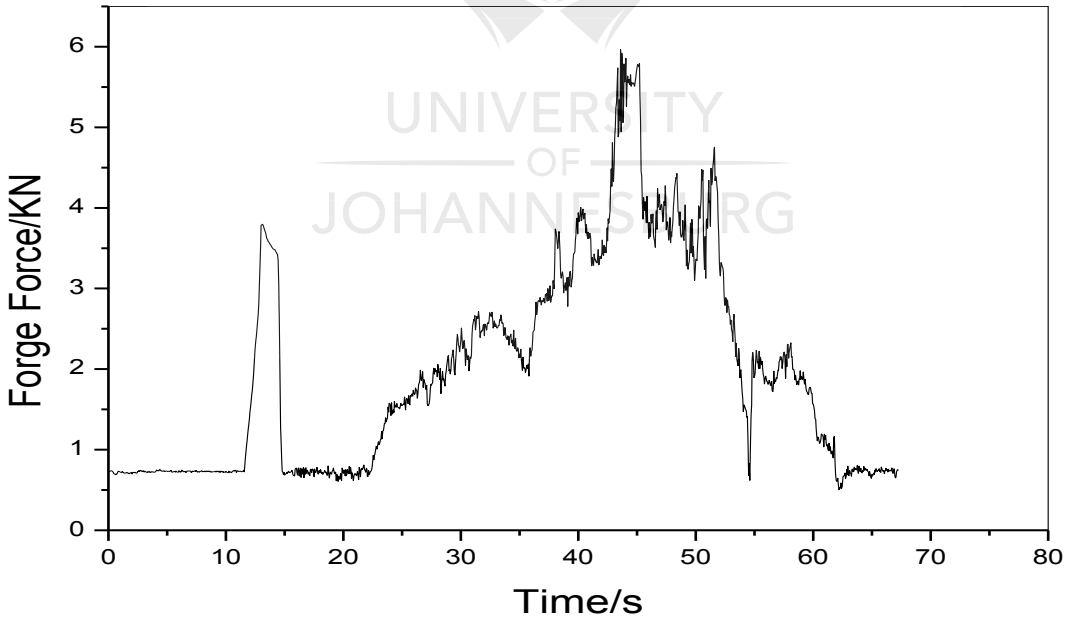

APPENDIX H

FPS_800_0.5_2

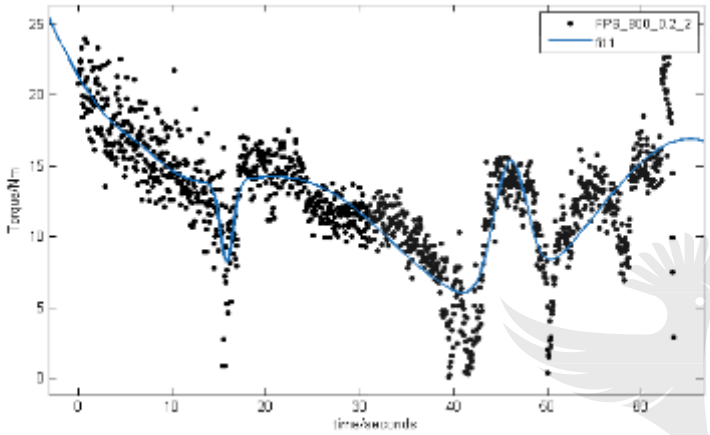

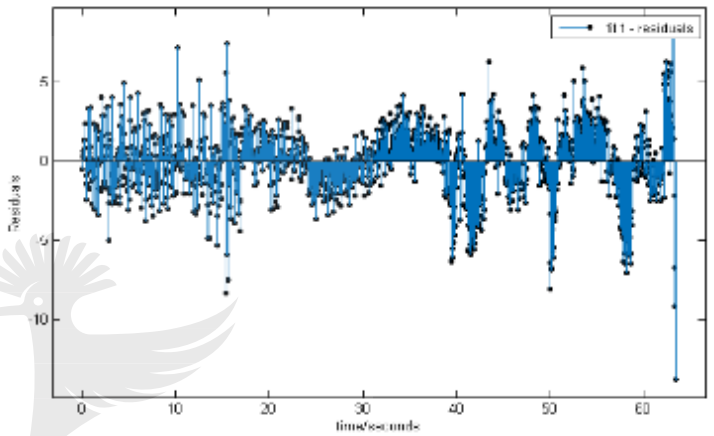

FPS_800_0.5_3

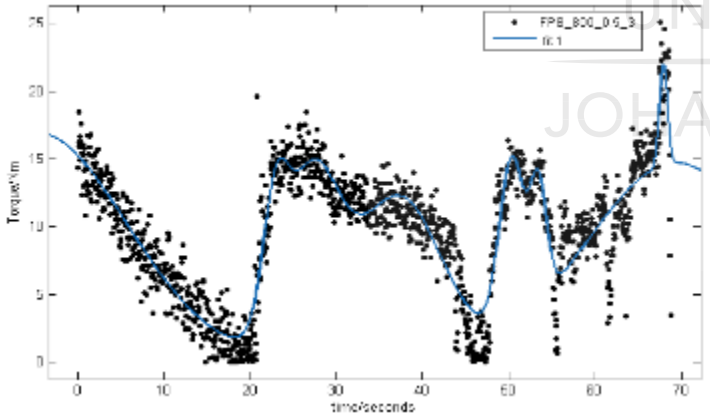

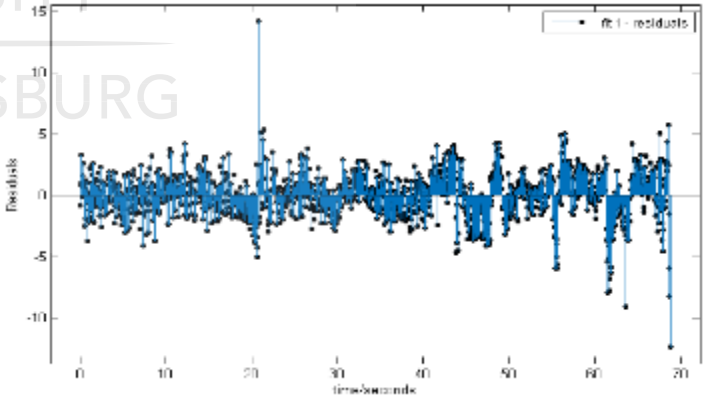

FPS_800_1_1

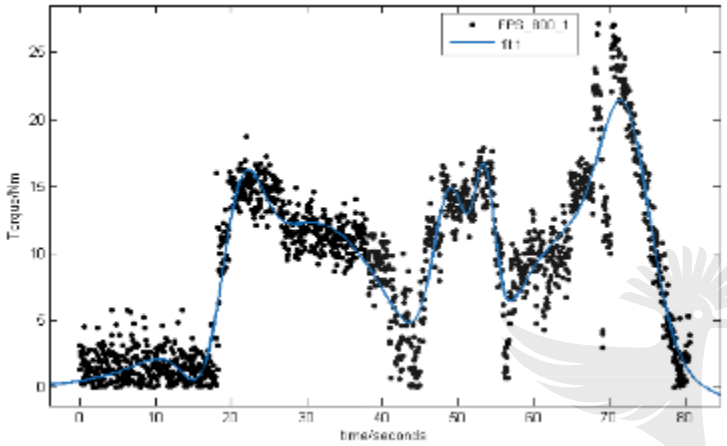

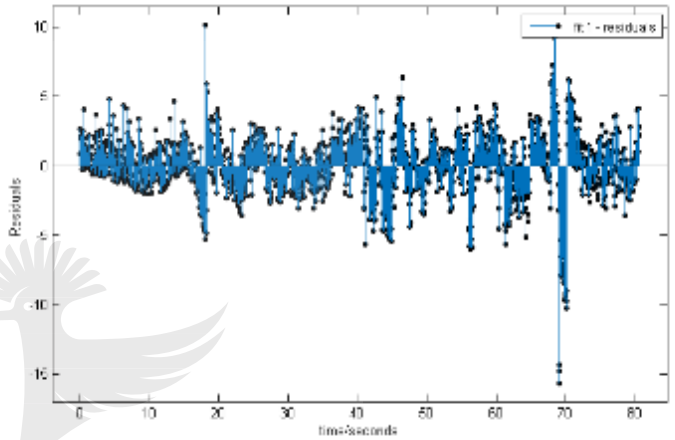

FPS_800_1_2

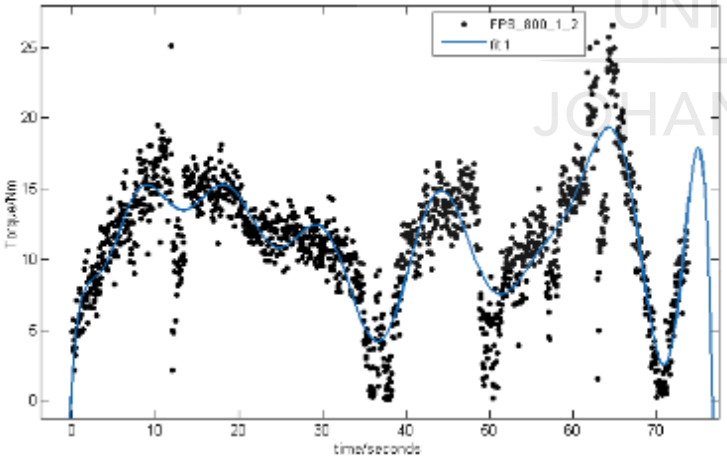

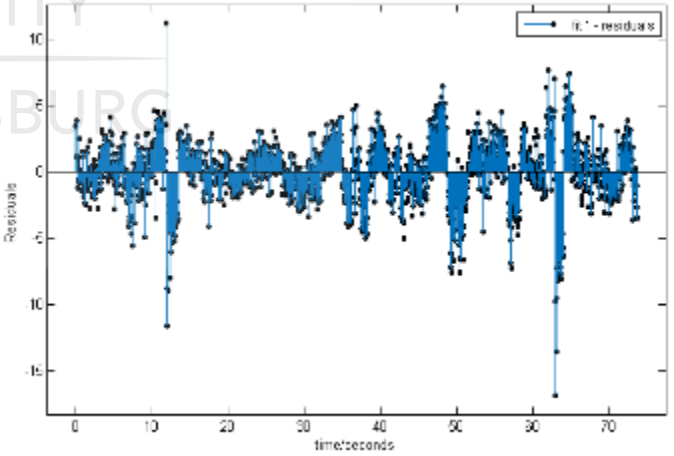

FPS_800_1_3

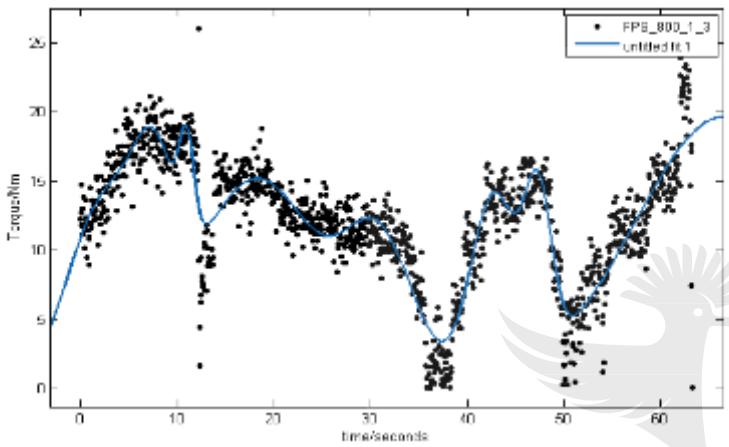

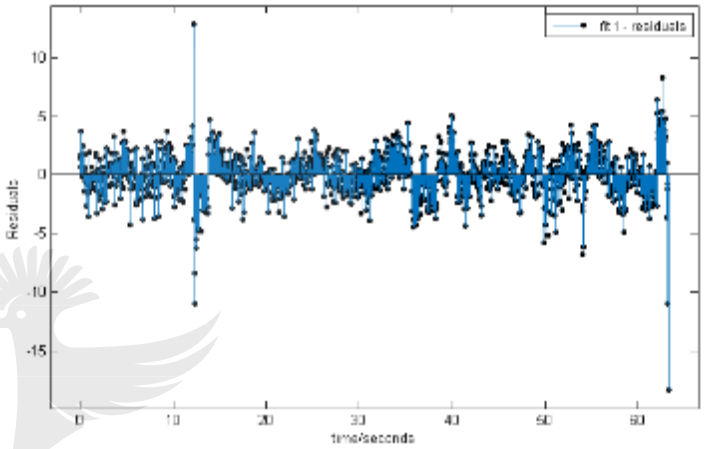

FPS_1200_0.5_1

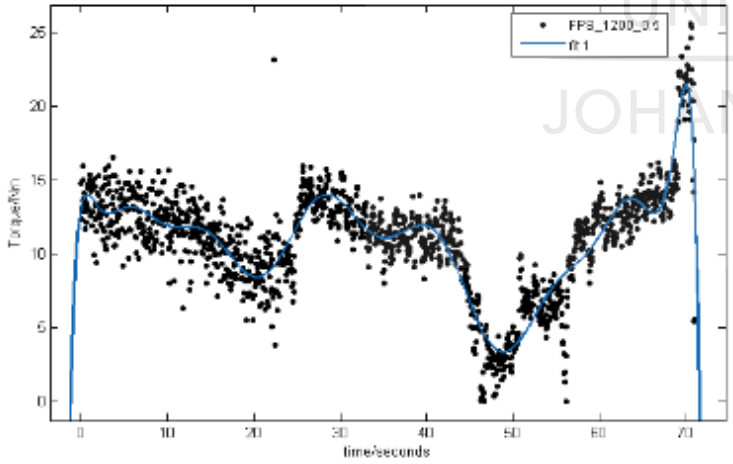

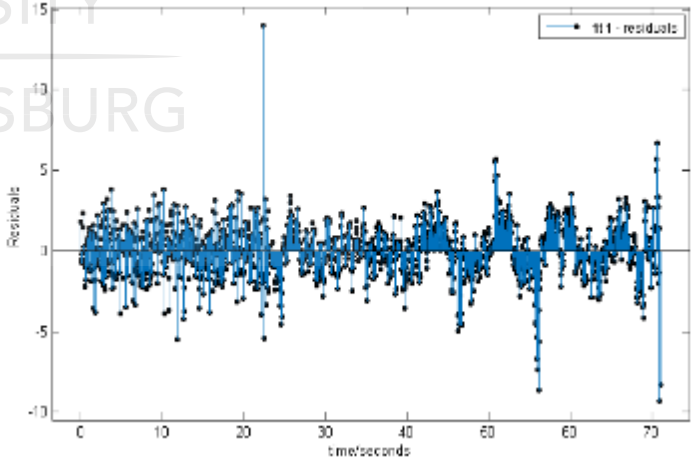

FPS_1200_0.5_2

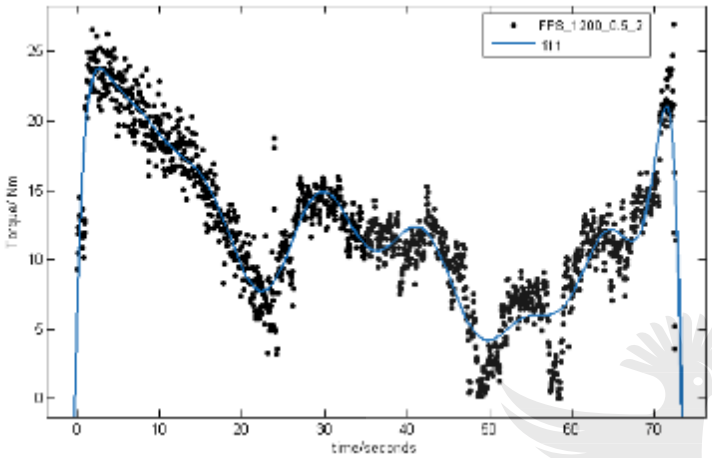

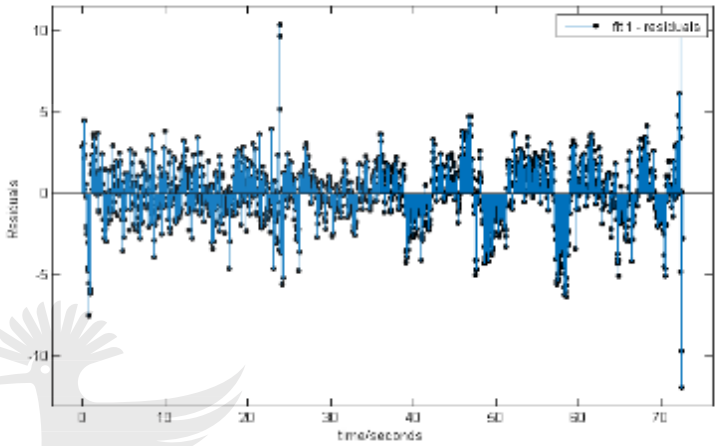

FPS_1200_0.5_3

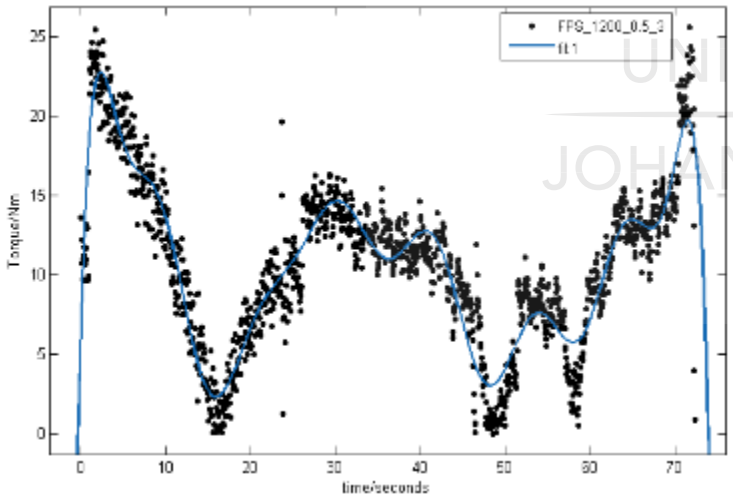

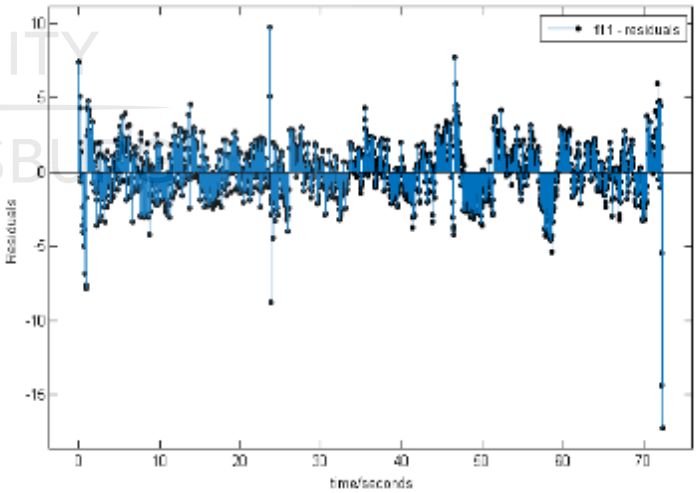

FPS_1200_1_1

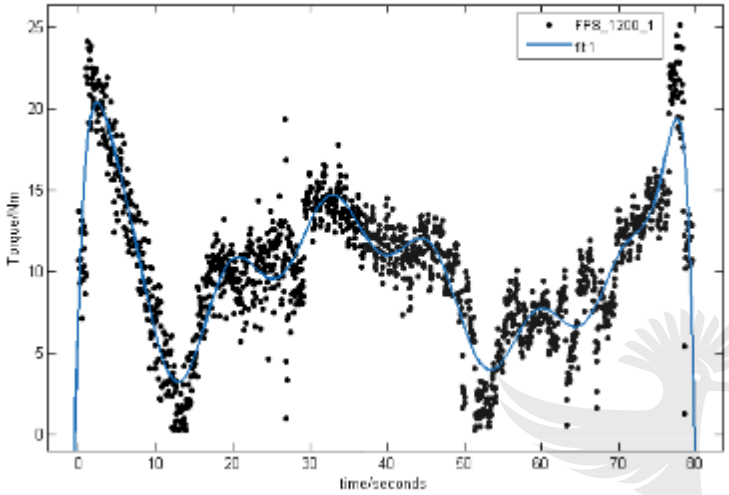

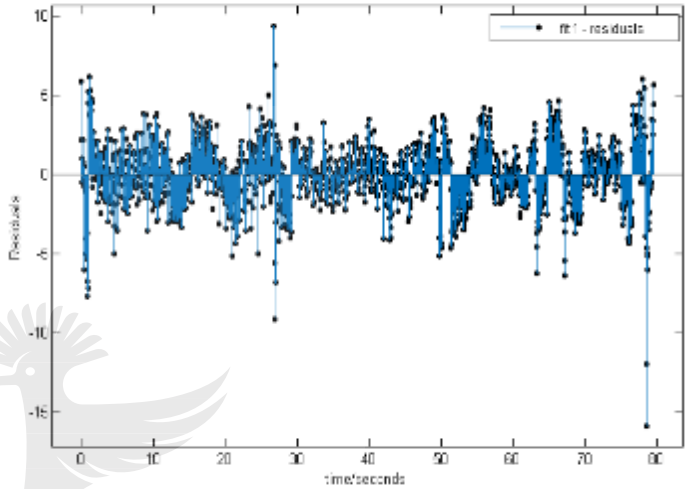

FPS_1200_1_2

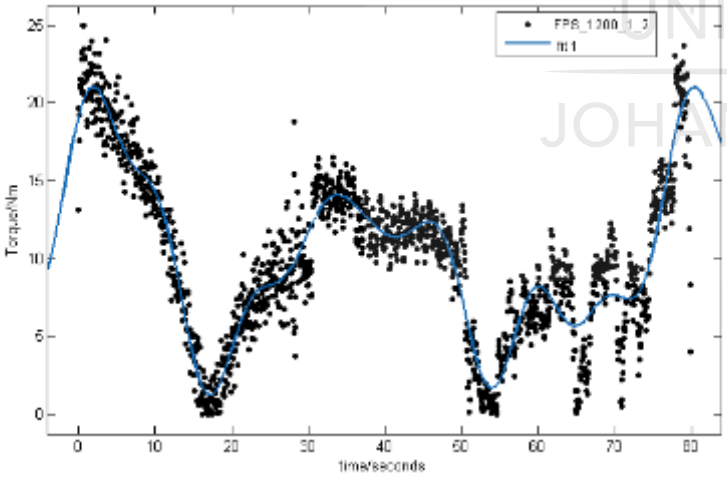

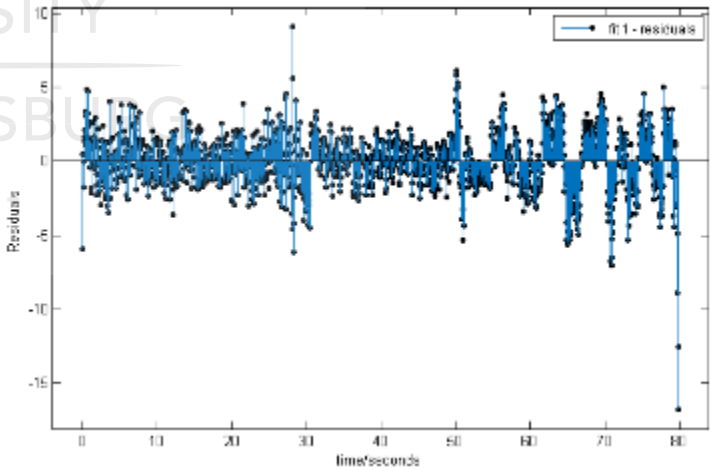

FPS_1200_1_3

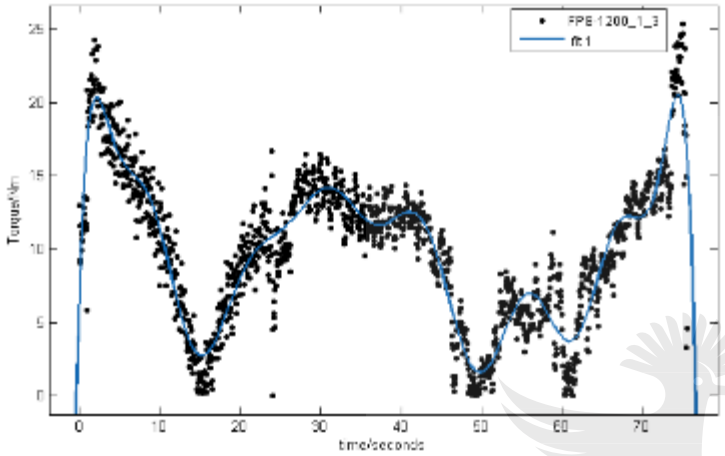

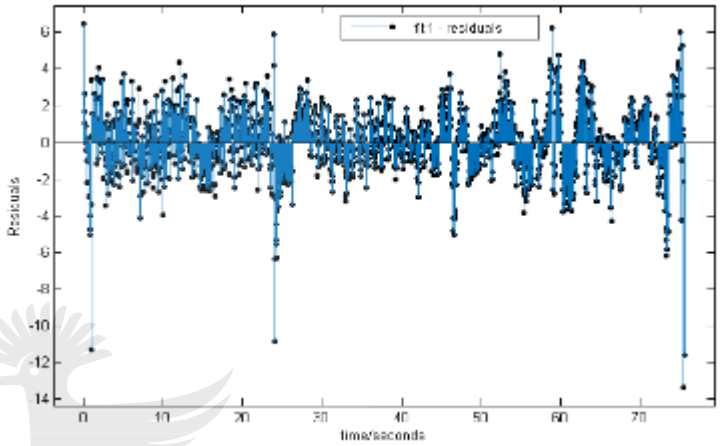

CCS_800_0.5_2

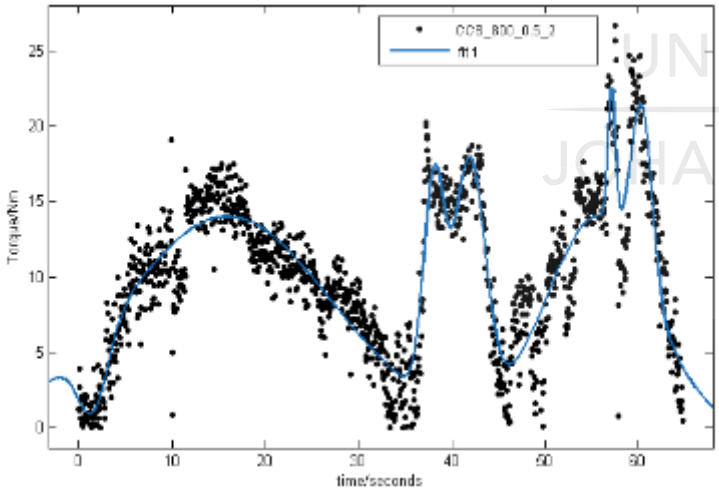

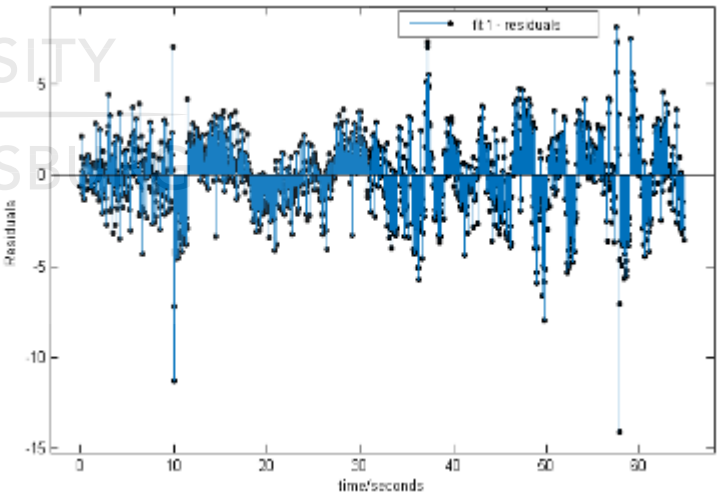

CCS_800_0.5_3

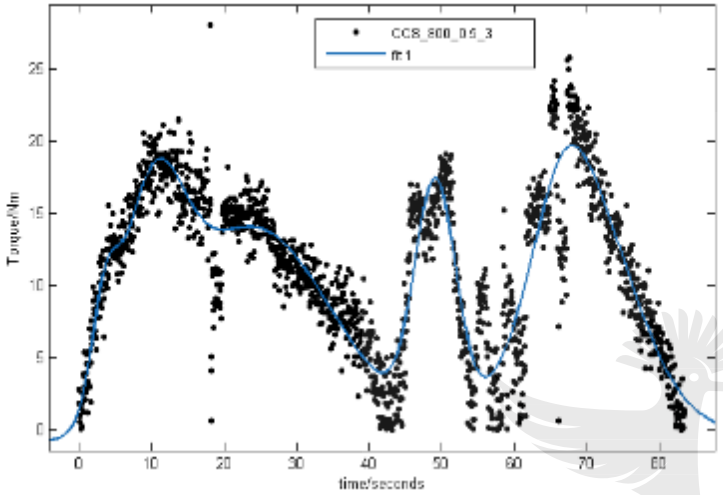

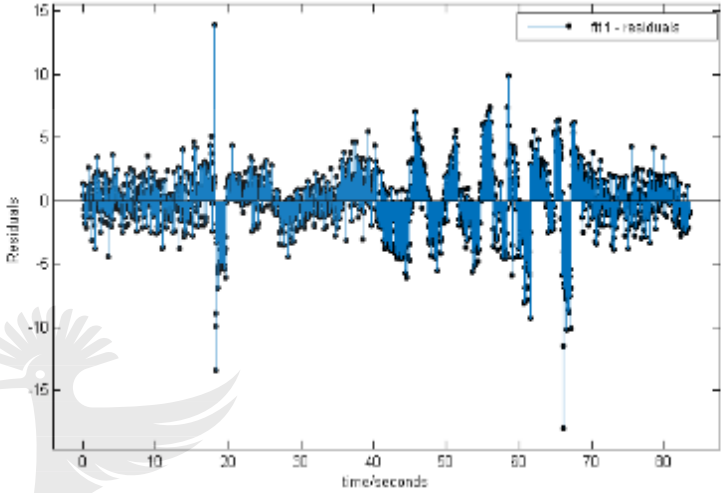

CCS_800_1_1

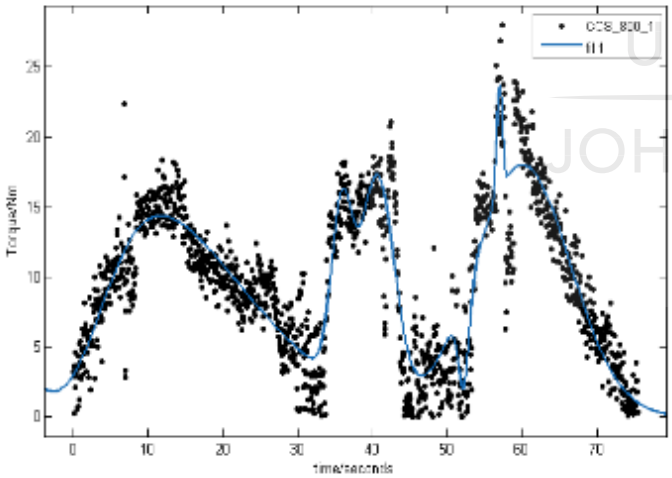

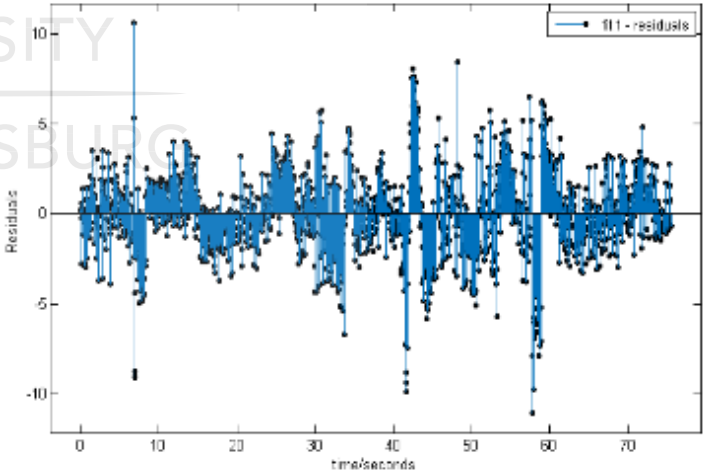

CCS_800_1_2

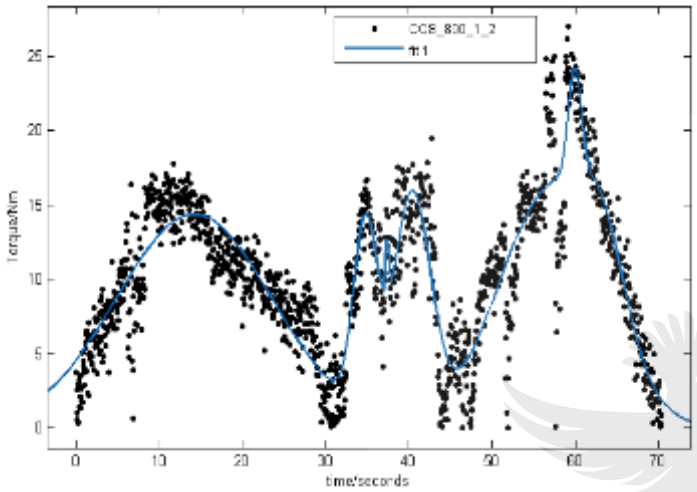

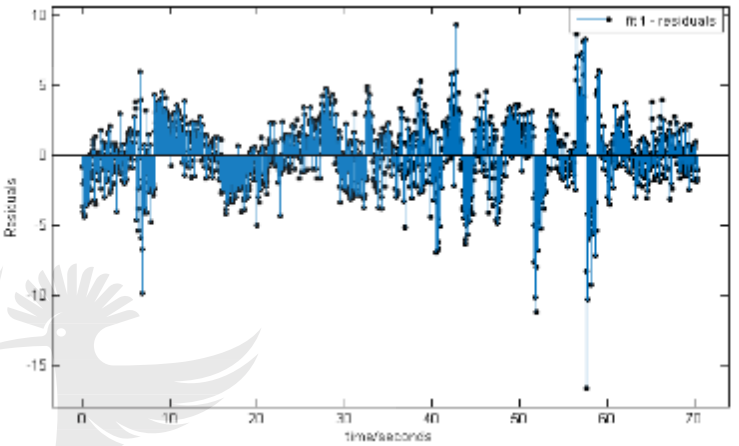

CCS_800_1_3

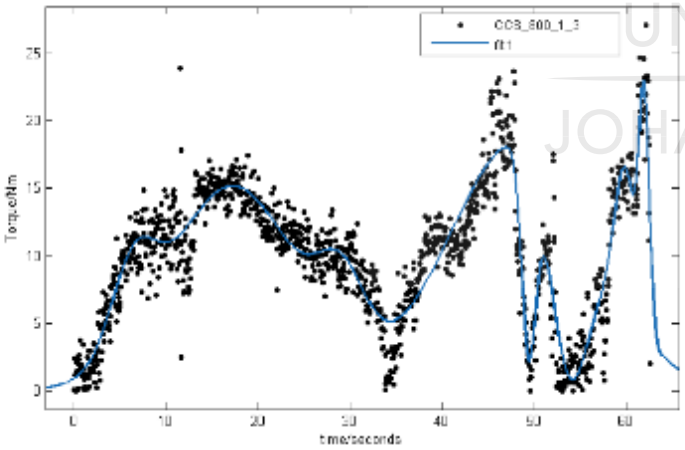

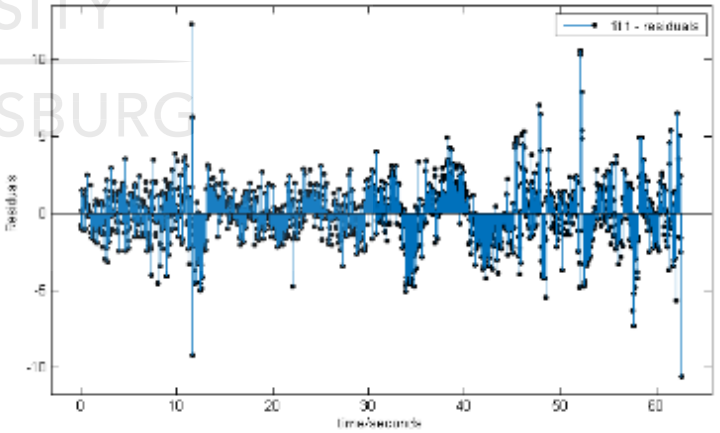

CCS_1200_0.5_1

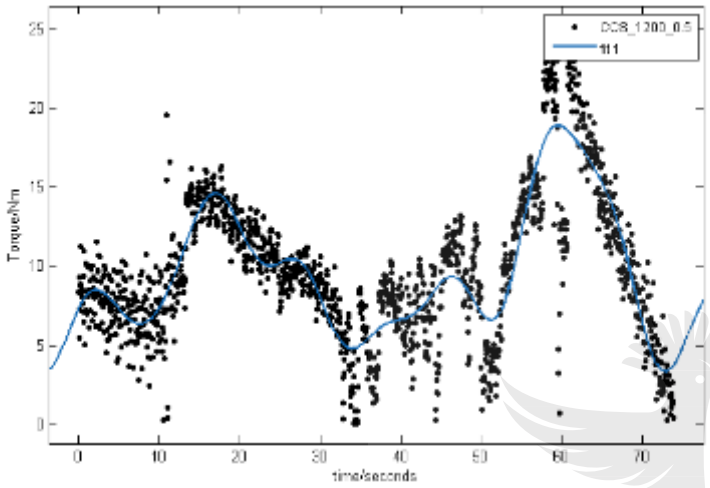

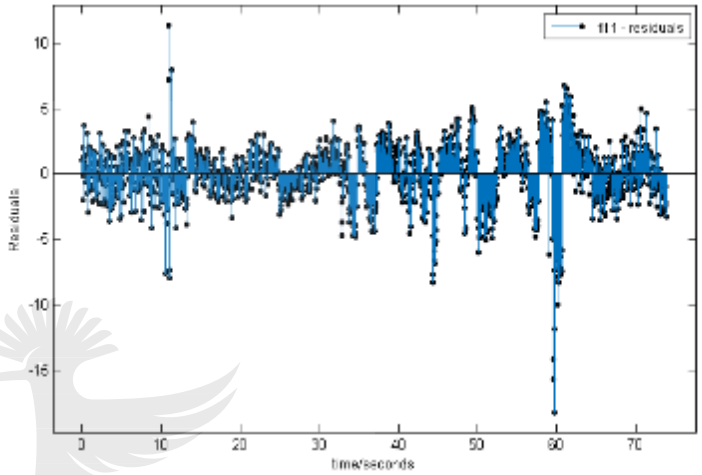

CCS_1200_0.5_2

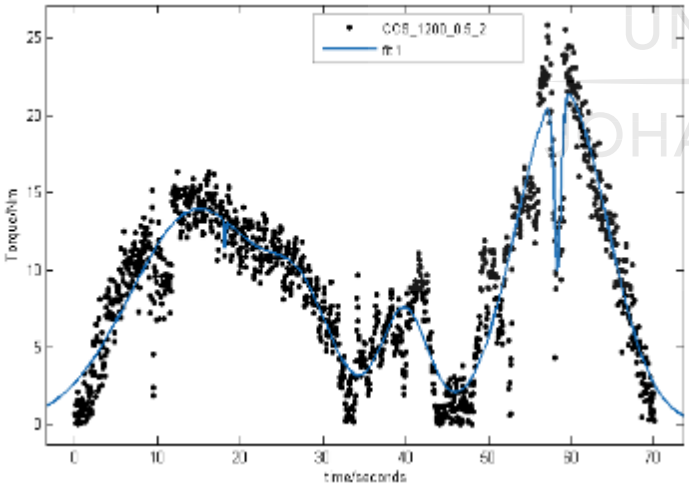

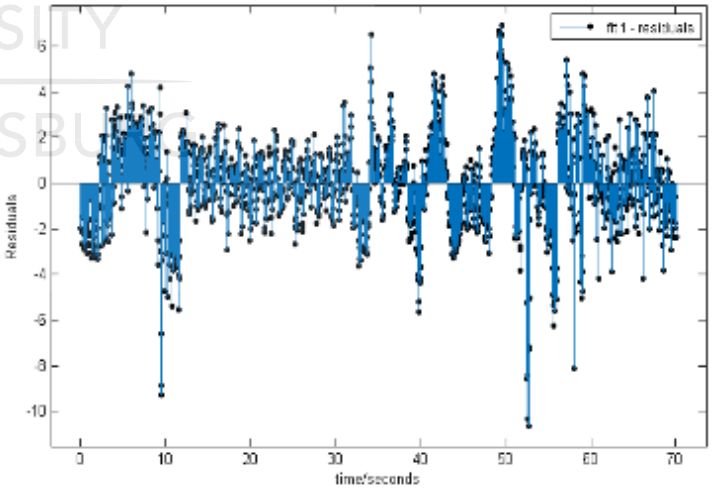

CCS_1200_0.5_3

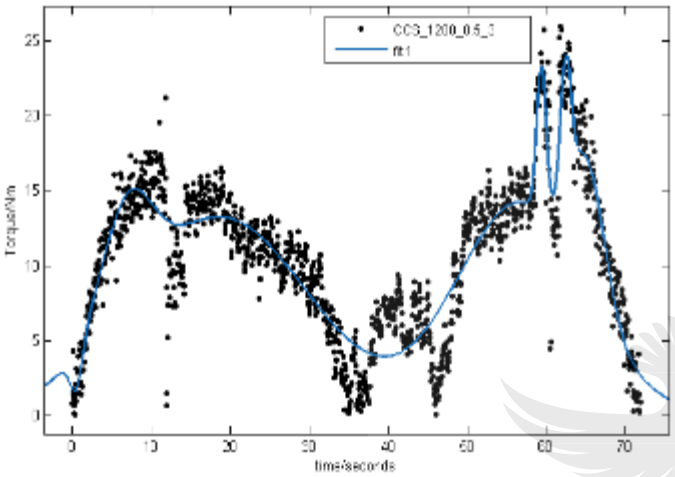

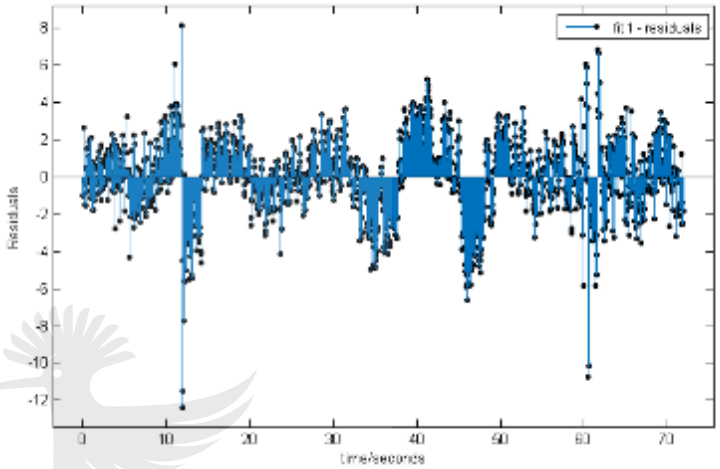

CCS_1200_1_1

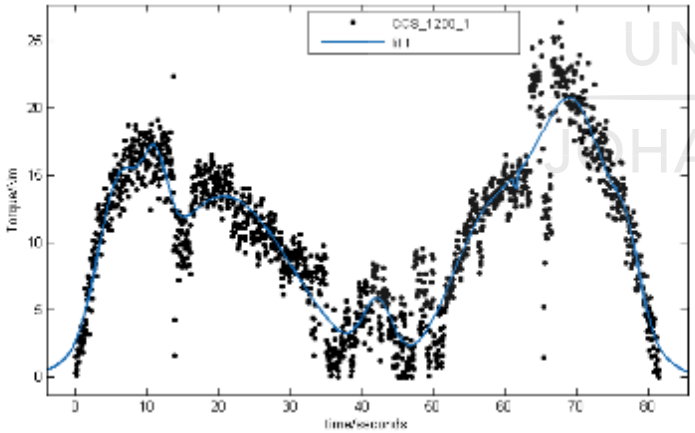

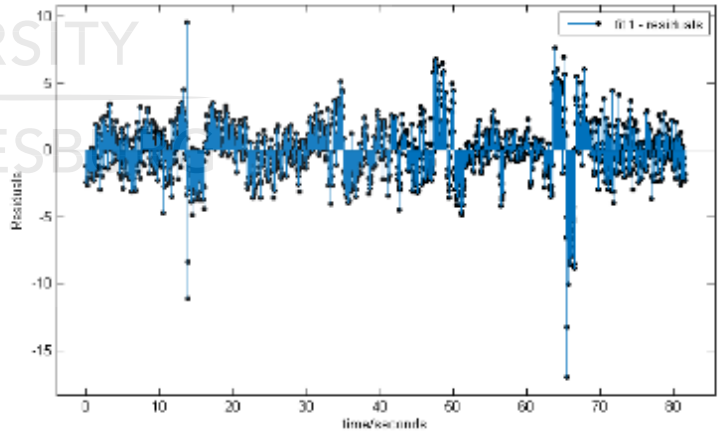

CCS_1200_1_2

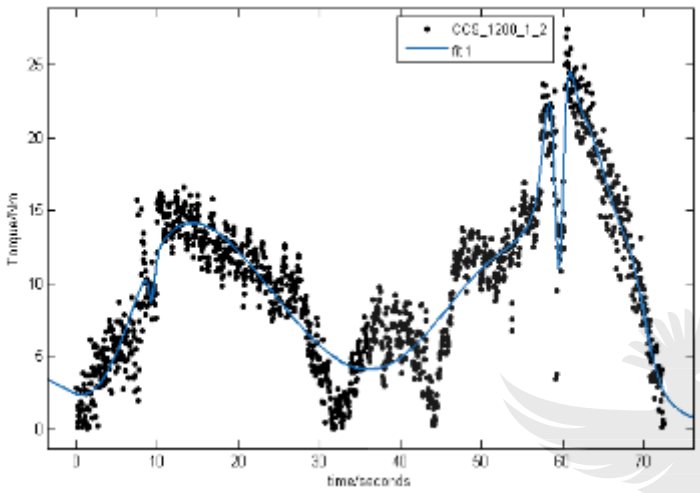

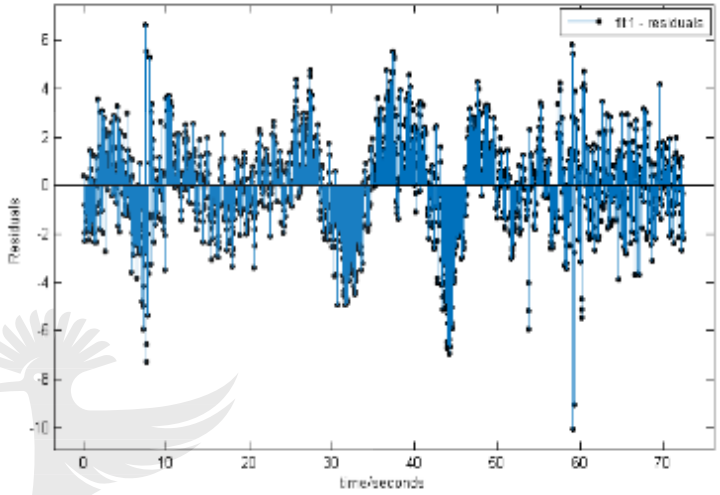

CCS_1200_1_3

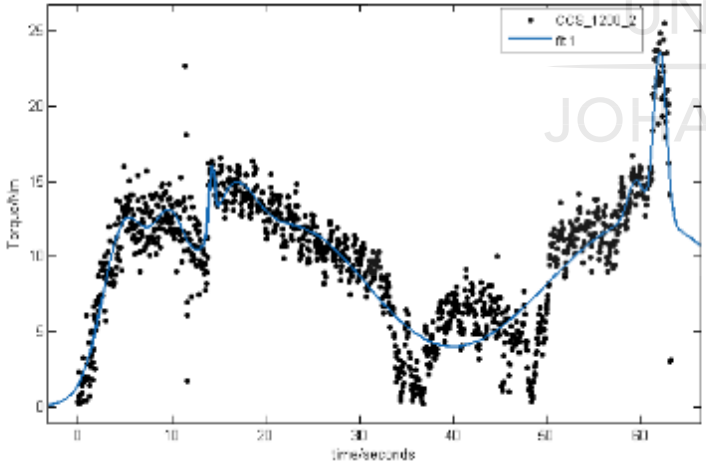

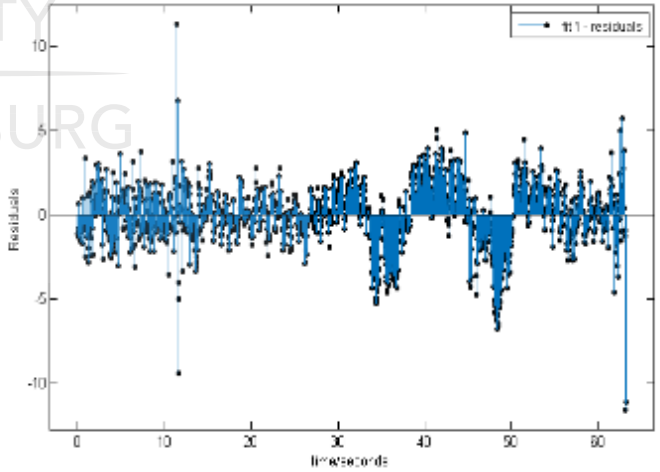

APPENDIX I

Welds produced at 800 rpm, 0.5 mm shoulder plunge depth using a flat pin and flat shoulder tool

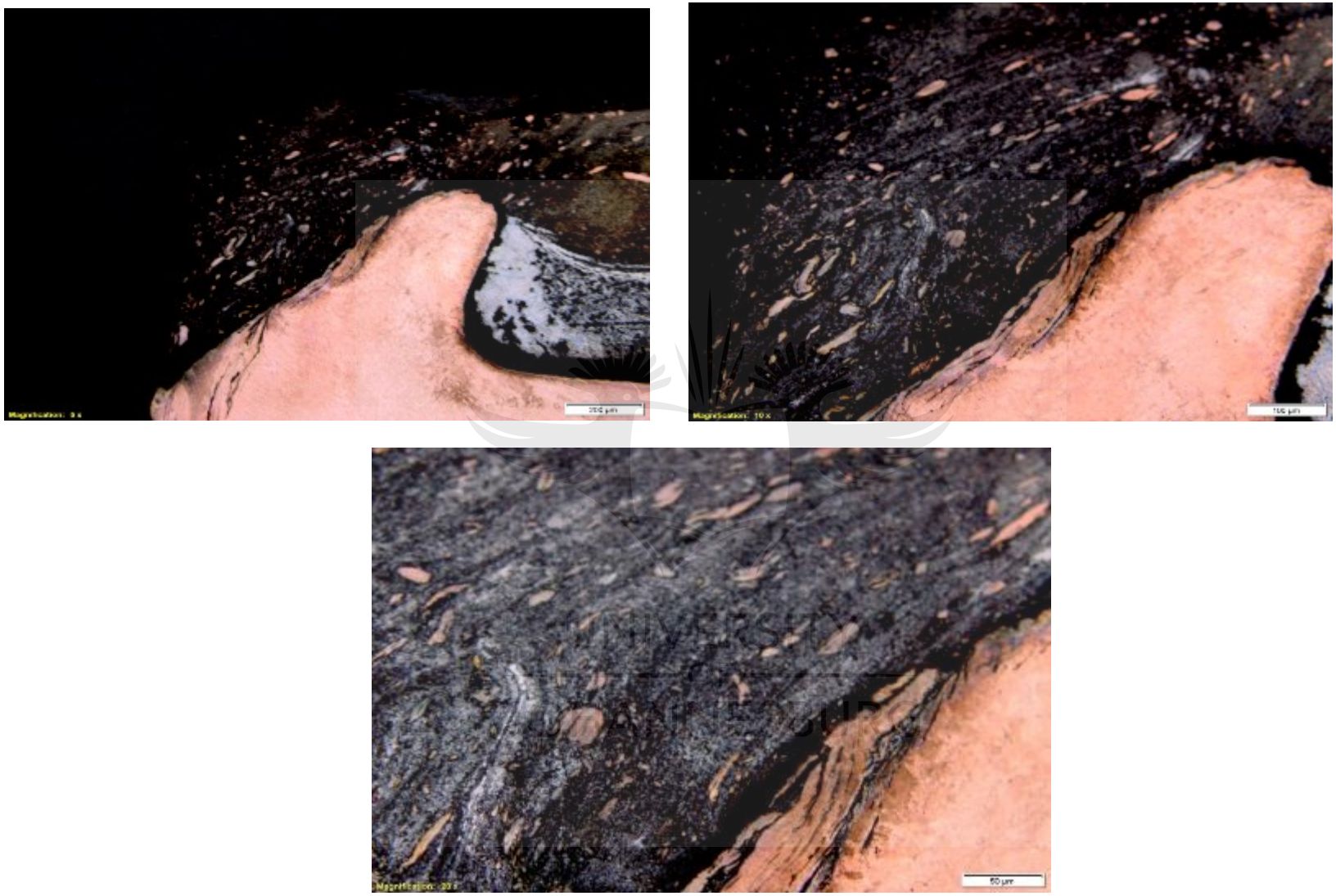

Welds produced at 800 rpm, 1 mm shoulder plunge depth using a flat pin and flat shoulder tool

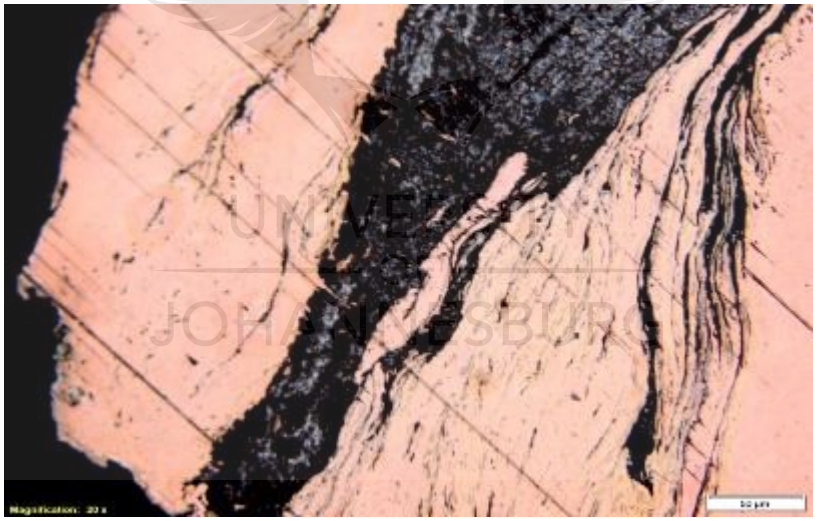

Welds produced at 1200 rpm, 0.5 mm shoulder plunge depth using a flat pin and flat shoulder tool

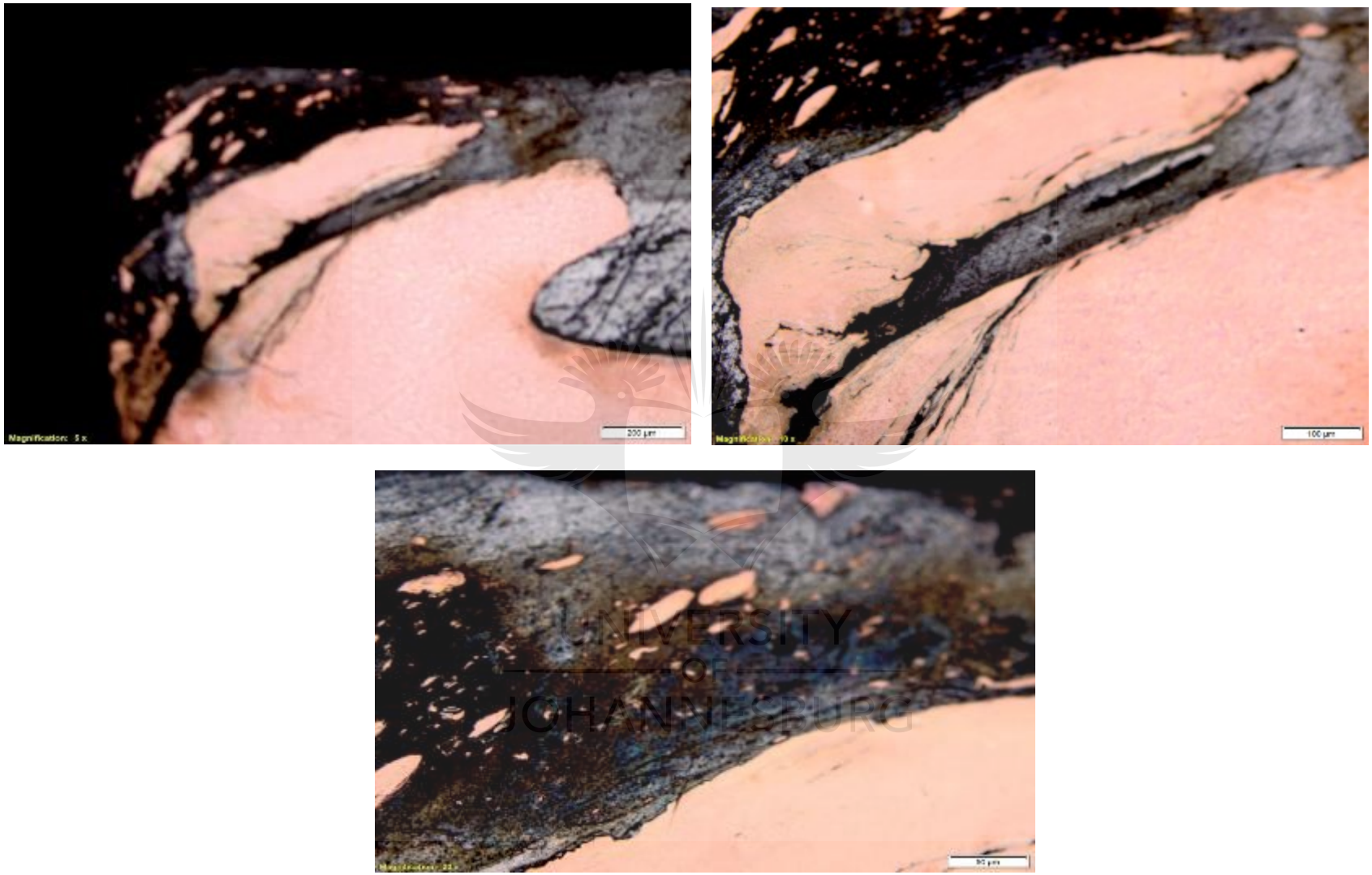

Welds produced at 1200 rpm, 1 mm shoulder plunge depth using a flat pin and flat shoulder tool

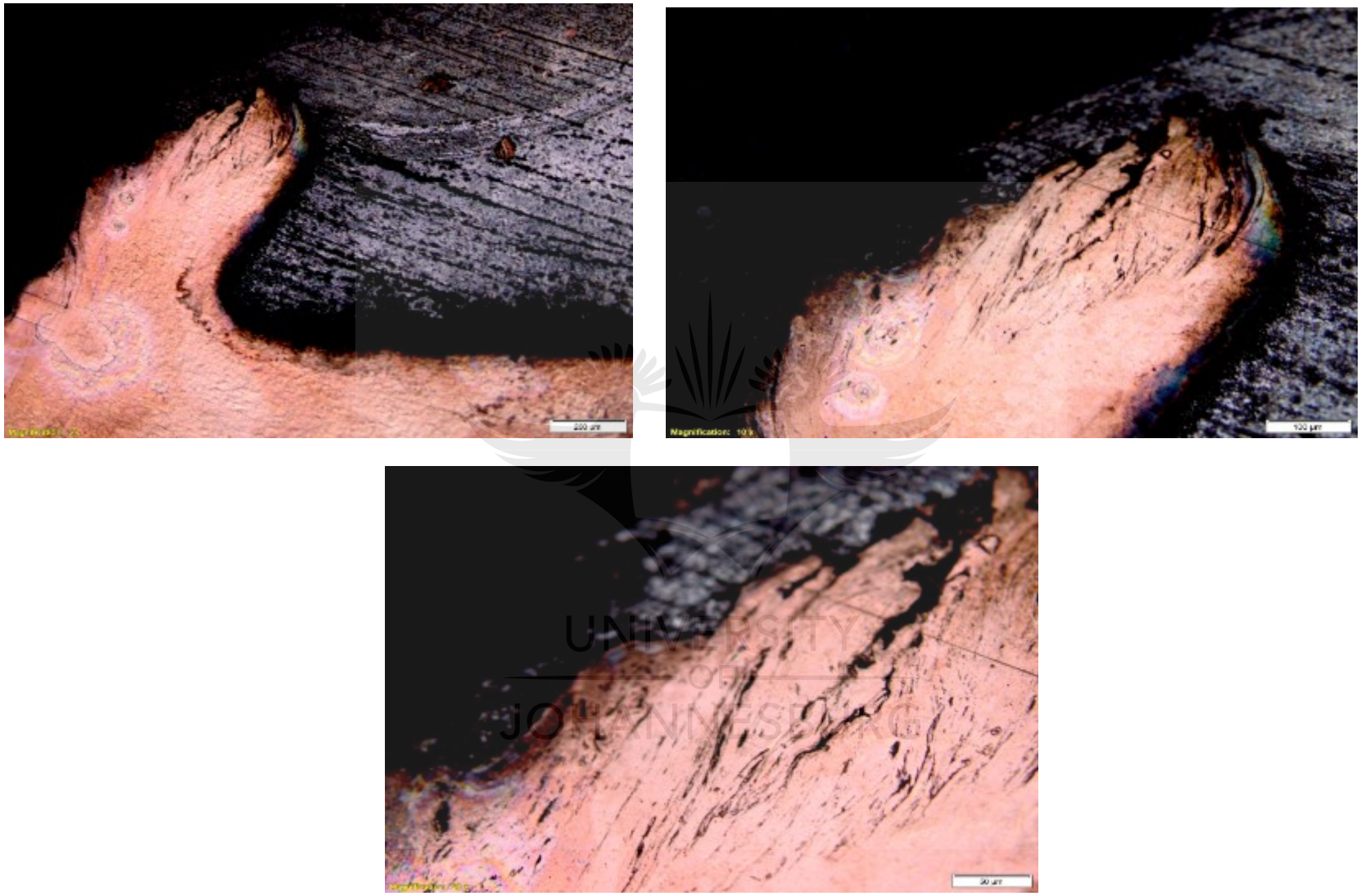

Welds produced at 800 rpm, 0.5 mm shoulder plunge depth using a conical pin and concave shoulder tool

W29 (CCS_800_1)

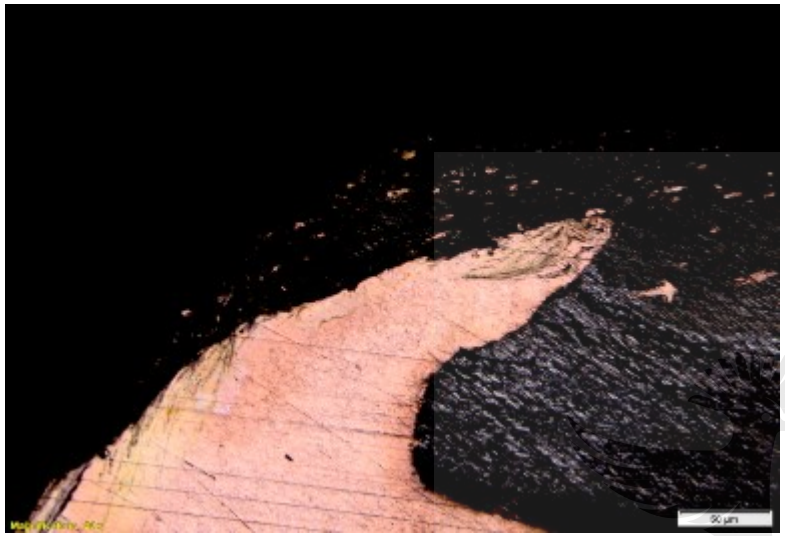

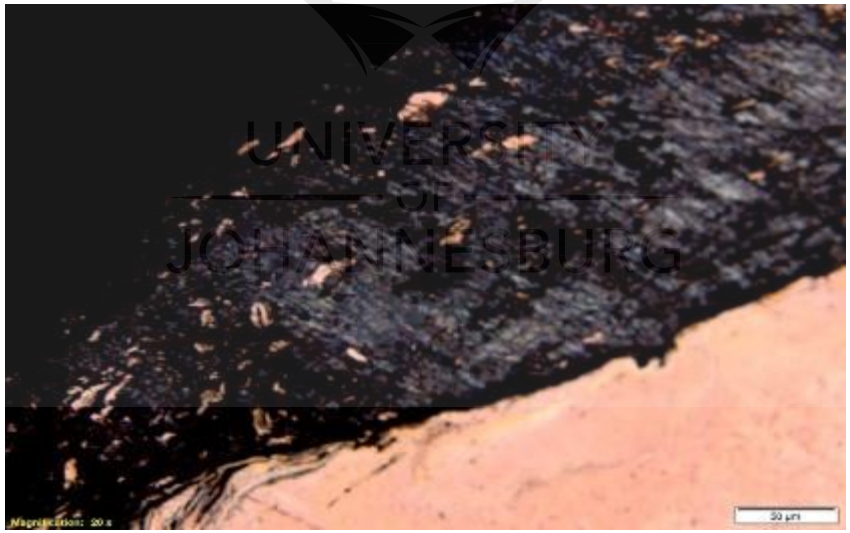

Welds produced at 800 rpm, 1 mm shoulder plunge depth using a conical pin and concave shoulder tool

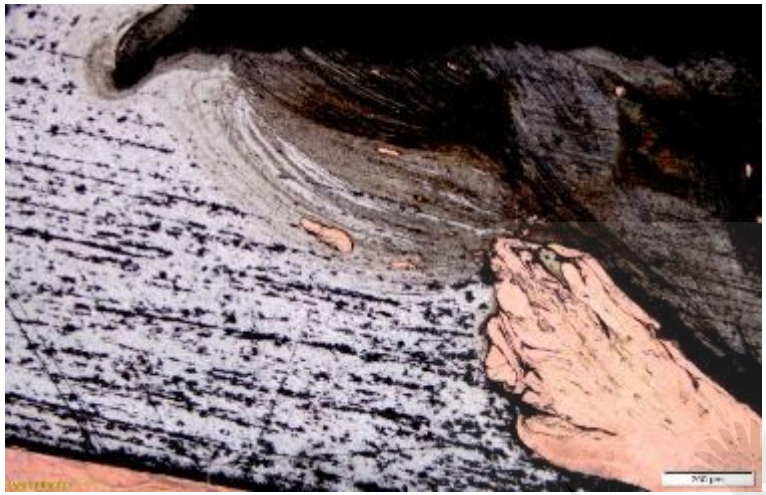

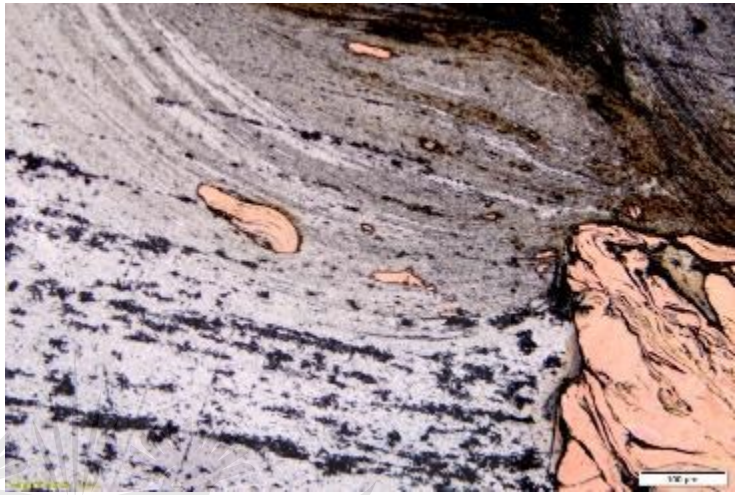

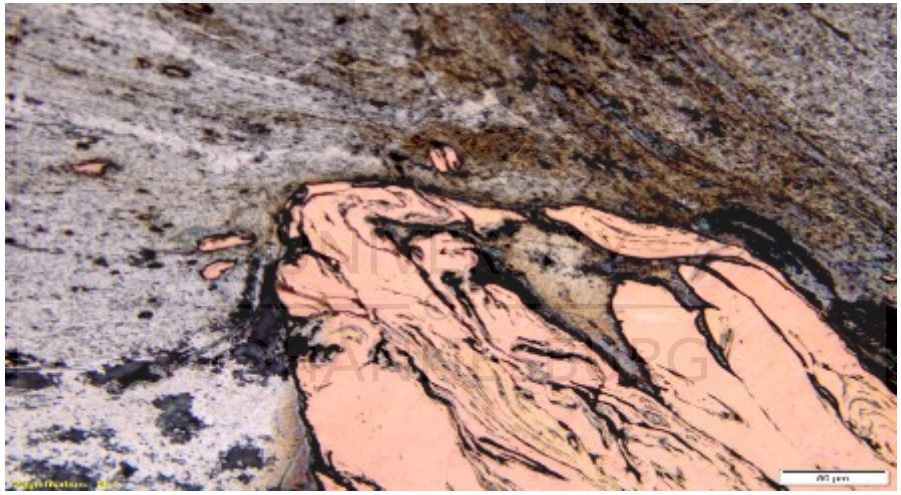

Welds produced at 1200 rpm, 0.5 mm shoulder plunge depth using a conical pin and concave shoulder tool

Welds produced at 1200 rpm, 1 mm shoulder plunge depth using a conical pin and concave shoulder tool

APPENDIX J

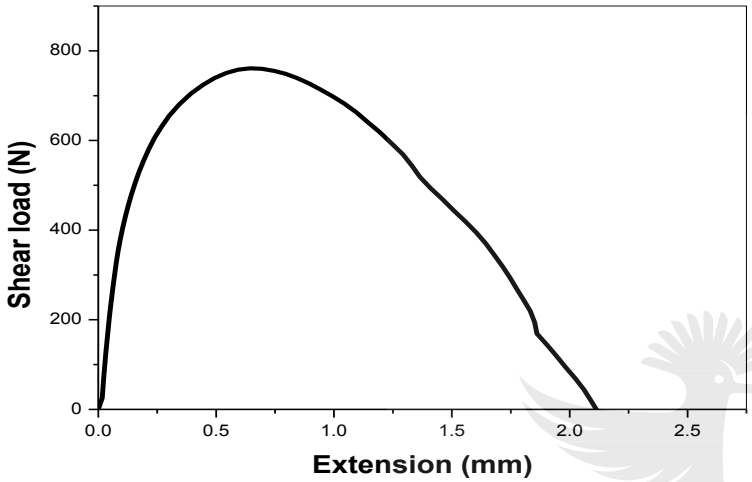

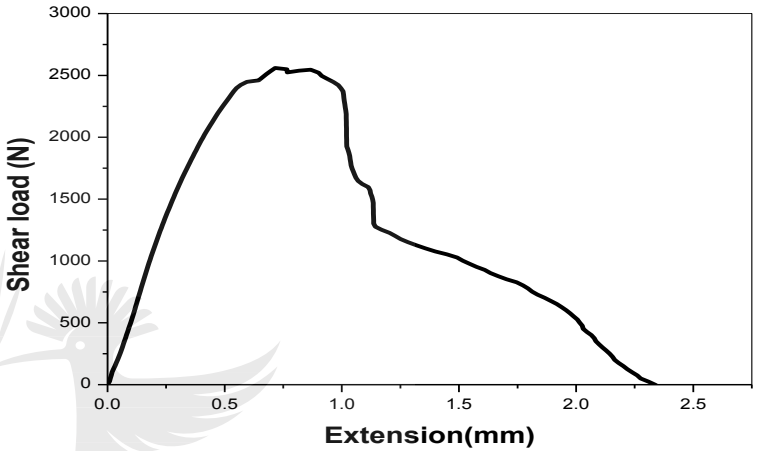

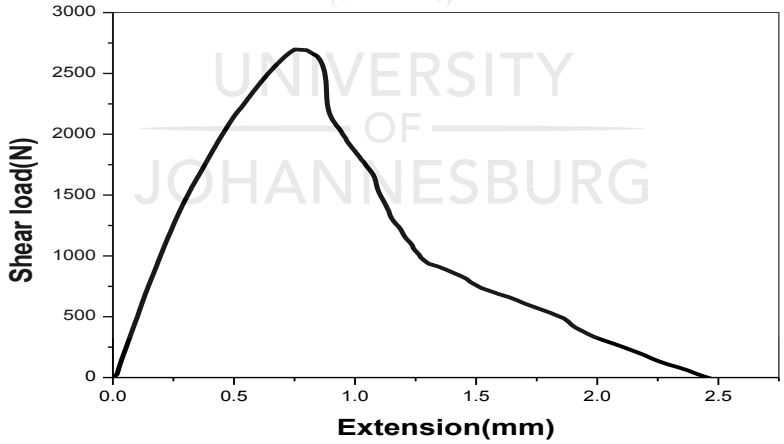

Shear tensile behaviour of weld produced at 800 rpm and 0.5 mm shoulder plunge depth using a flat pin and flat shoulder

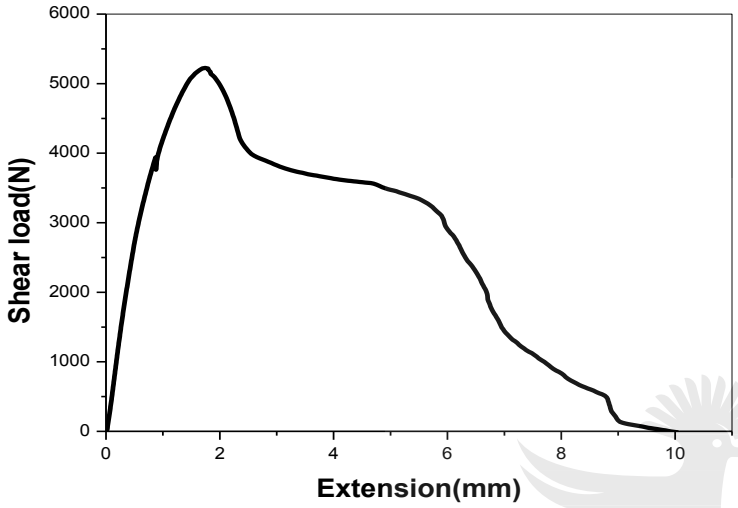

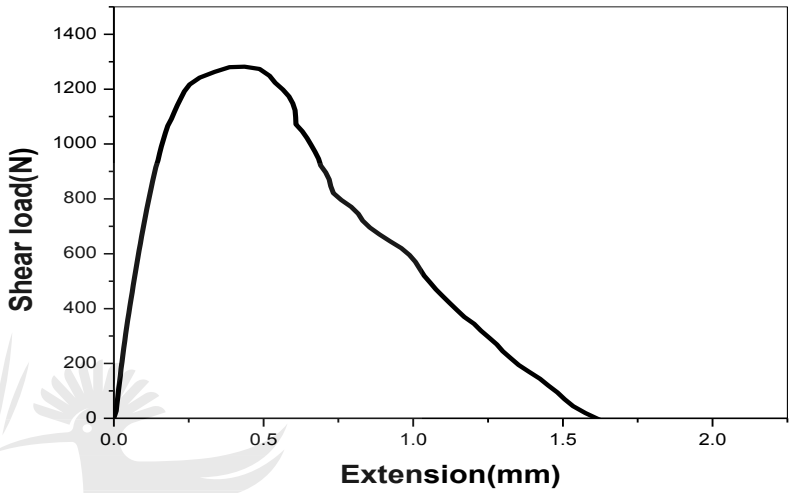

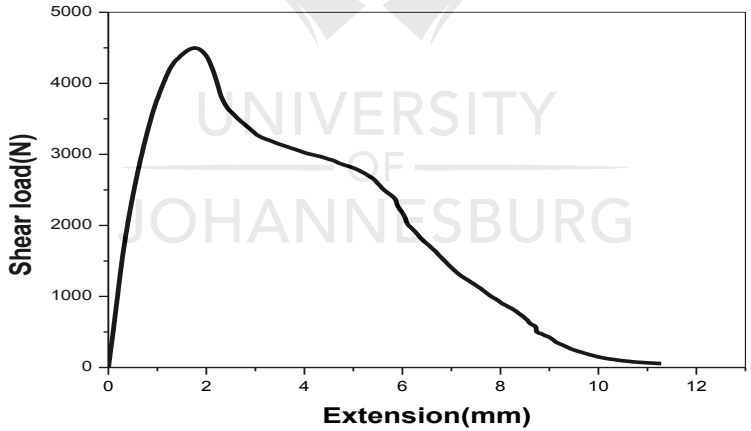

Shear tensile behaviour of weld produced at 800 rpm and 1mm shoulder plunge depth using a flat pin and flat shoulder

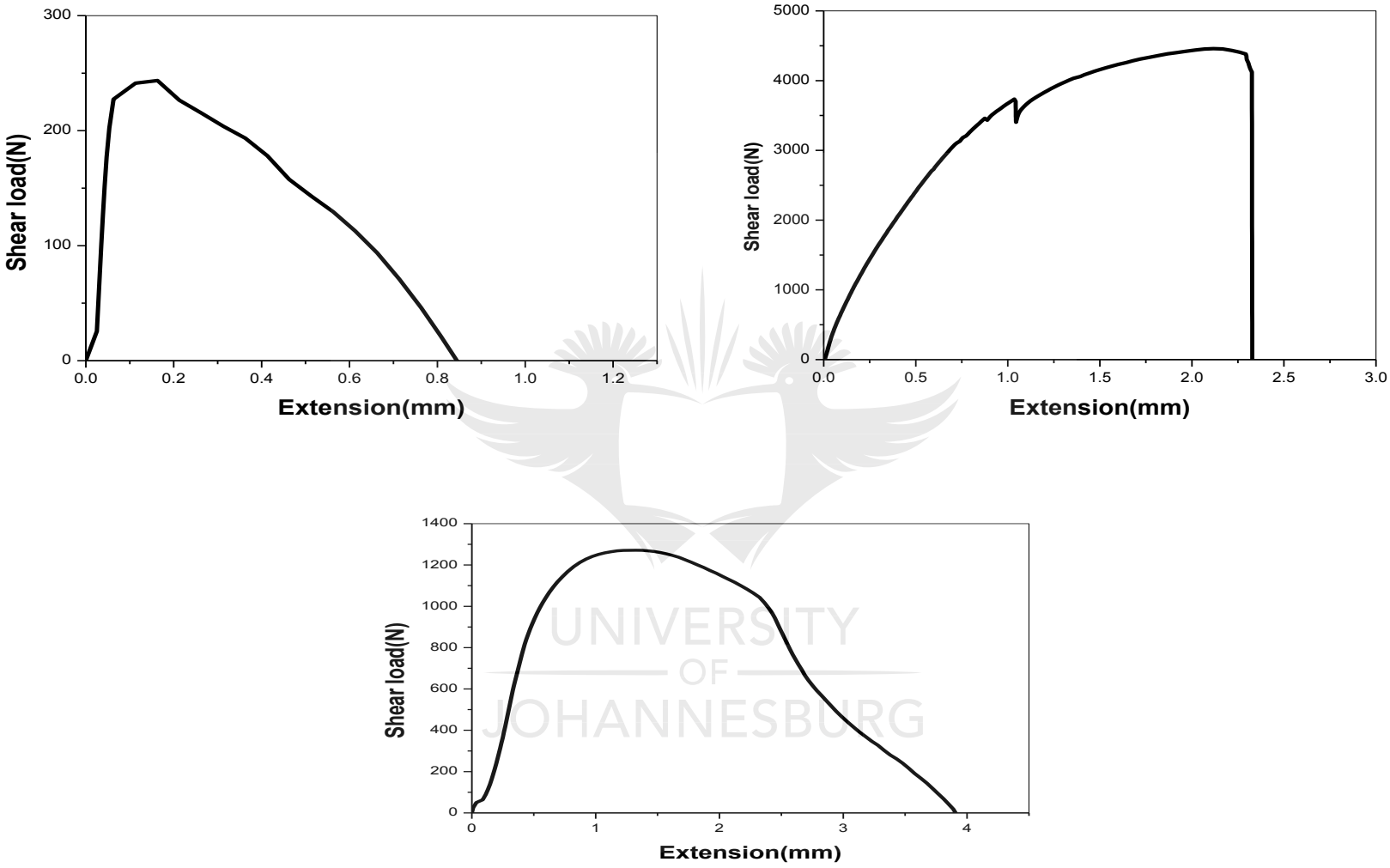

Shear tensile behaviour of weld produced at 1200 rpm and 0.5 mm shoulder plunge depth using a flat pin and flat shoulder

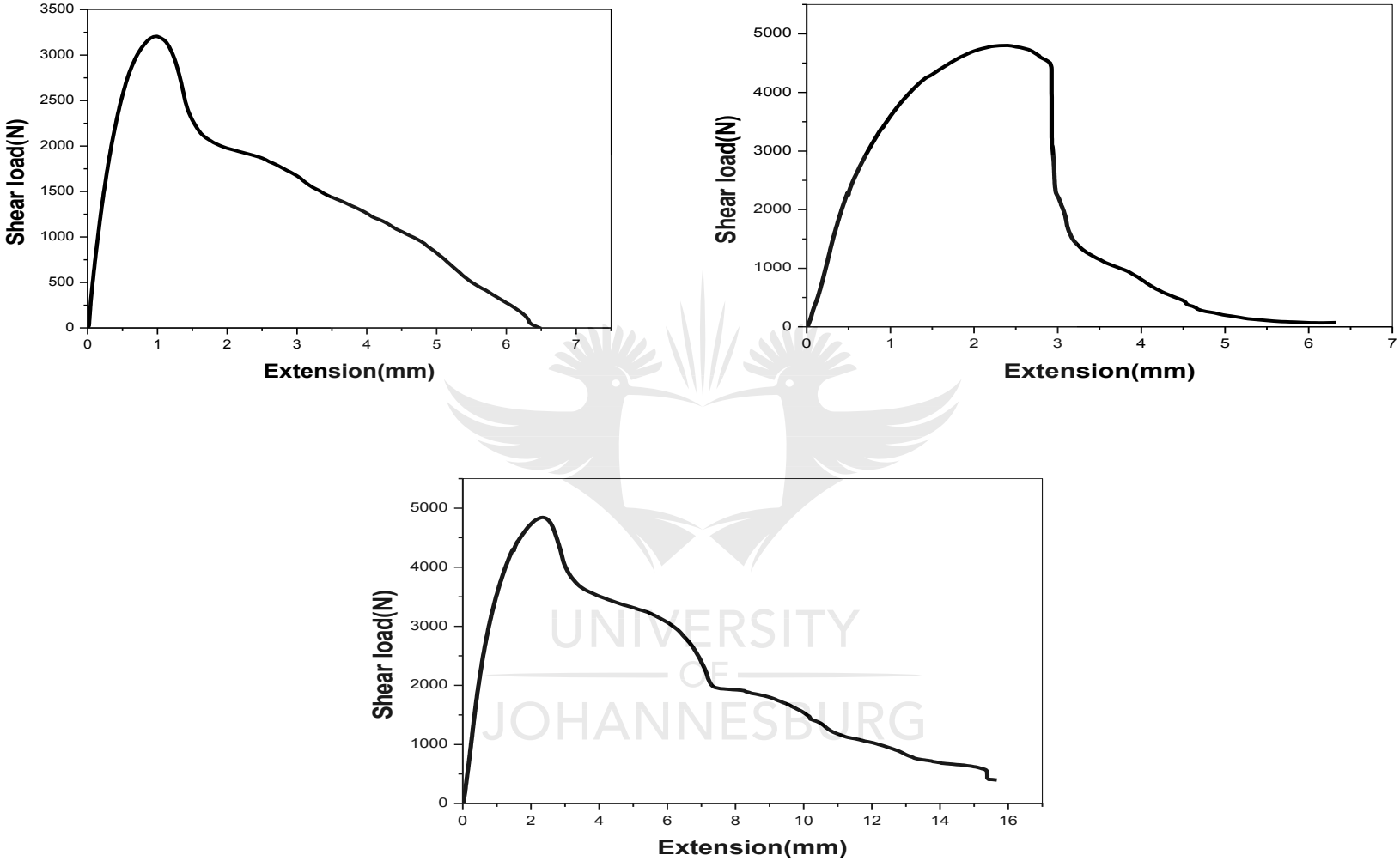

Shear tensile behaviour of weld produced at 1200 rpm and 1 mm shoulder plunge depth using a flat pin and flat shoulder

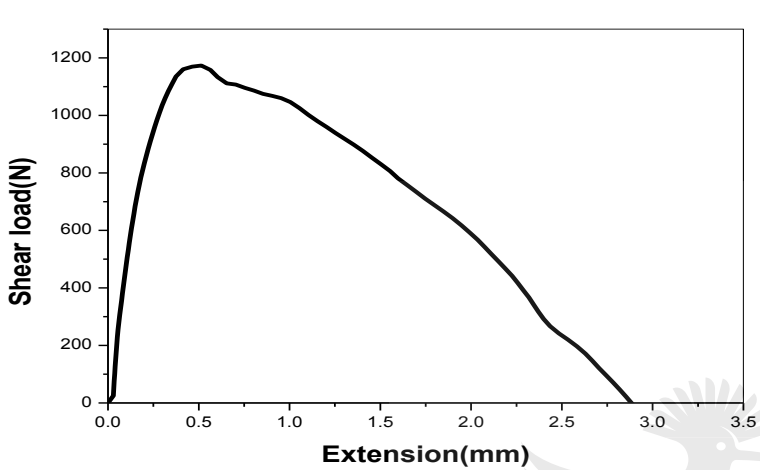

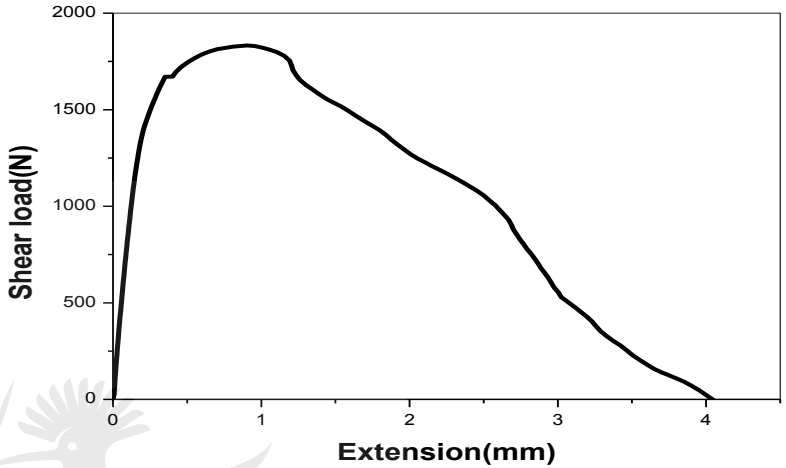

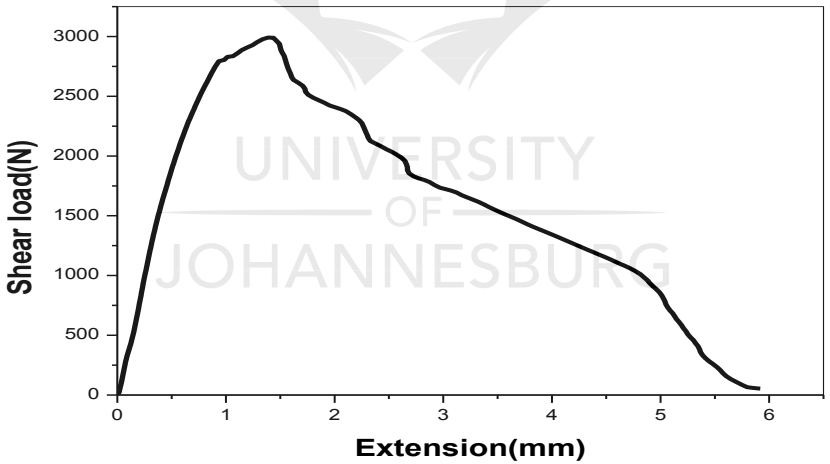

Shear tensile behaviour of weld produced at 800 rpm and 0.5 mm shoulder plunge depth using a conical pin and concave shoulder

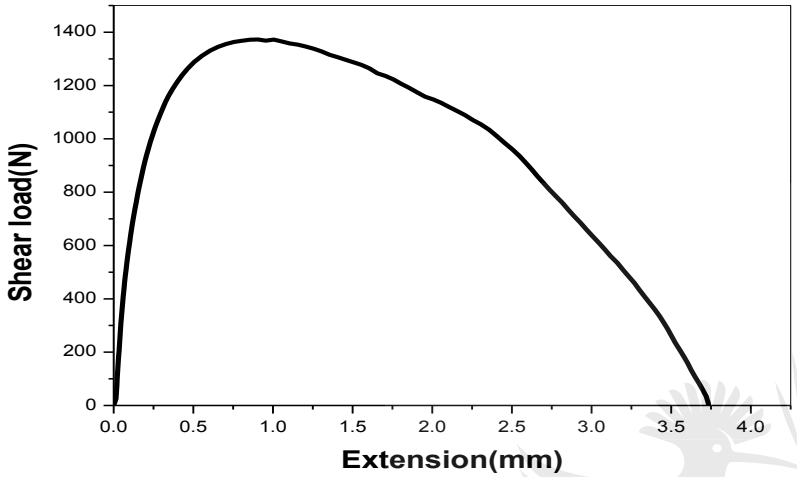

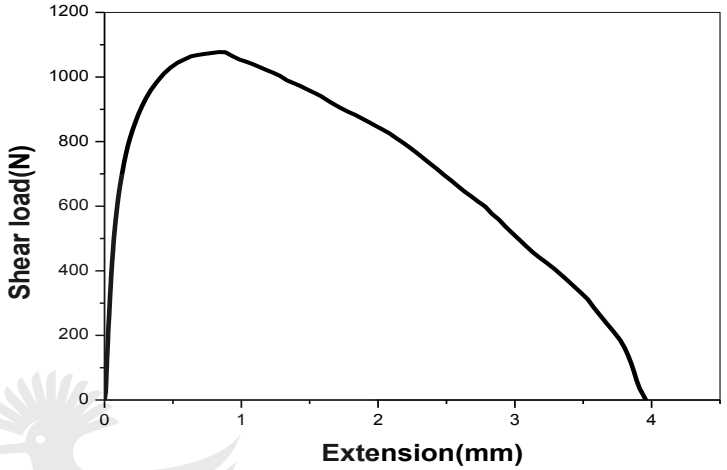

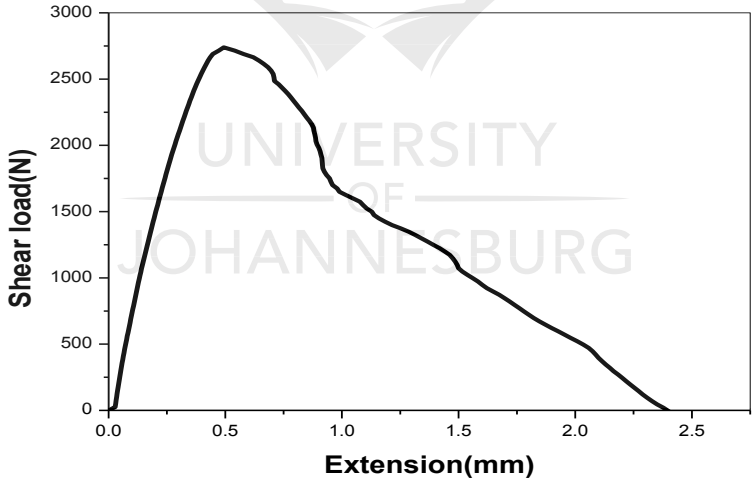

Shear tensile behaviour of weld produced at 800 rpm and 1 mm shoulder plunge depth using a conical pin and concave shoulder

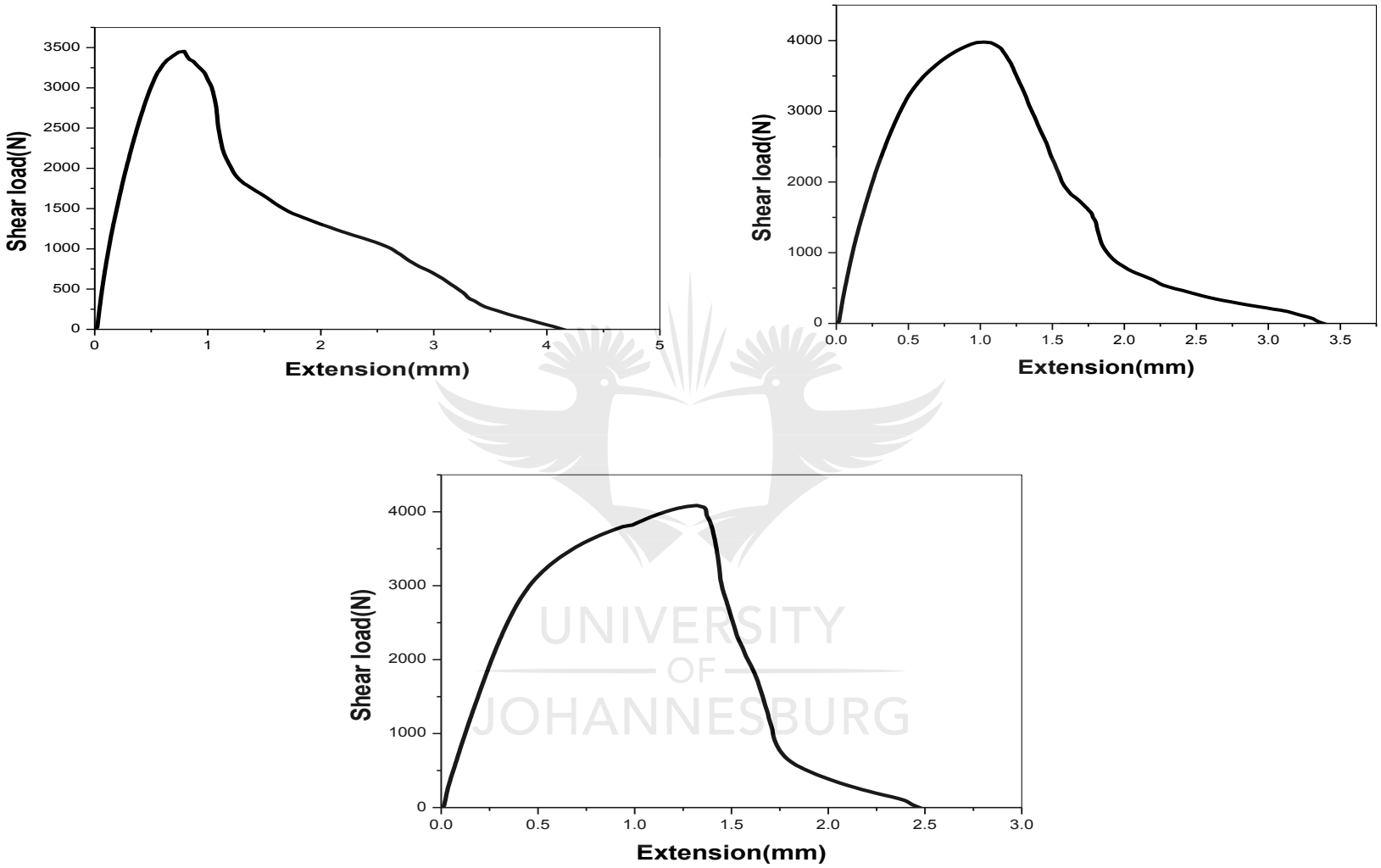

Shear tensile behaviour of weld produced at 1200 rpm and 0.5 mm shoulder plunge depth using a conical pin and concave shoulder

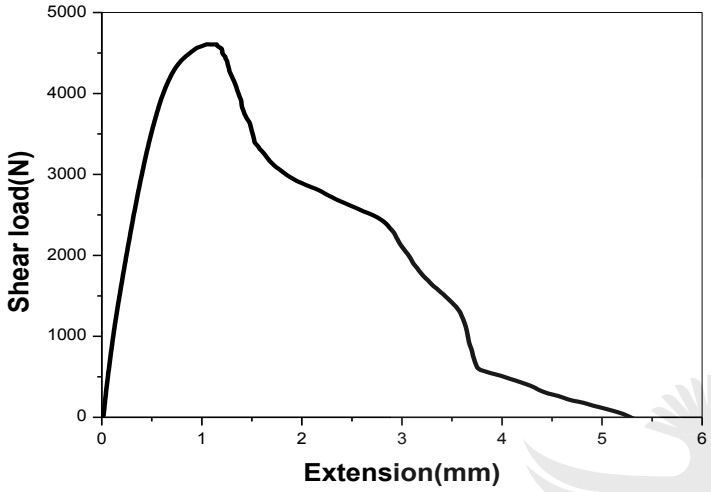

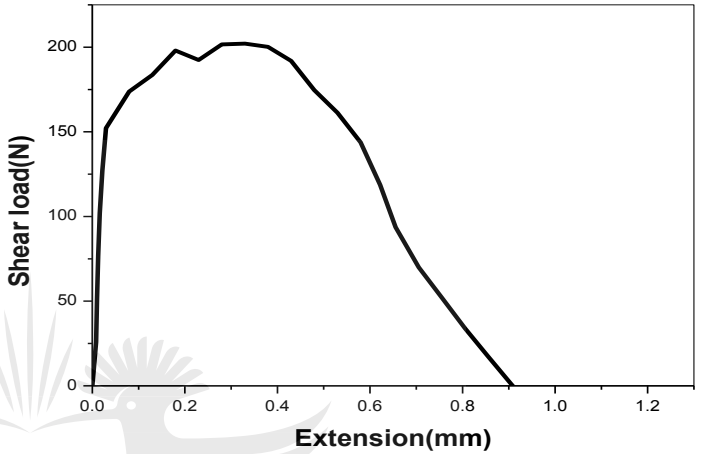

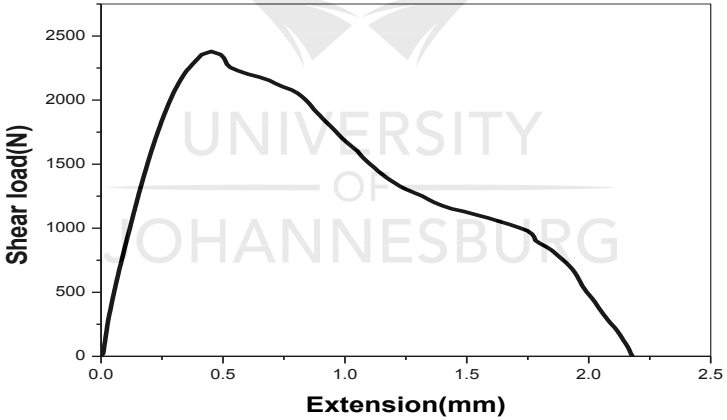

Shear tensile behaviour of weld produced at 1200 rpm and 1 mm shoulder plunge depth using a conical pin and concave shoulder

APPENDIX K

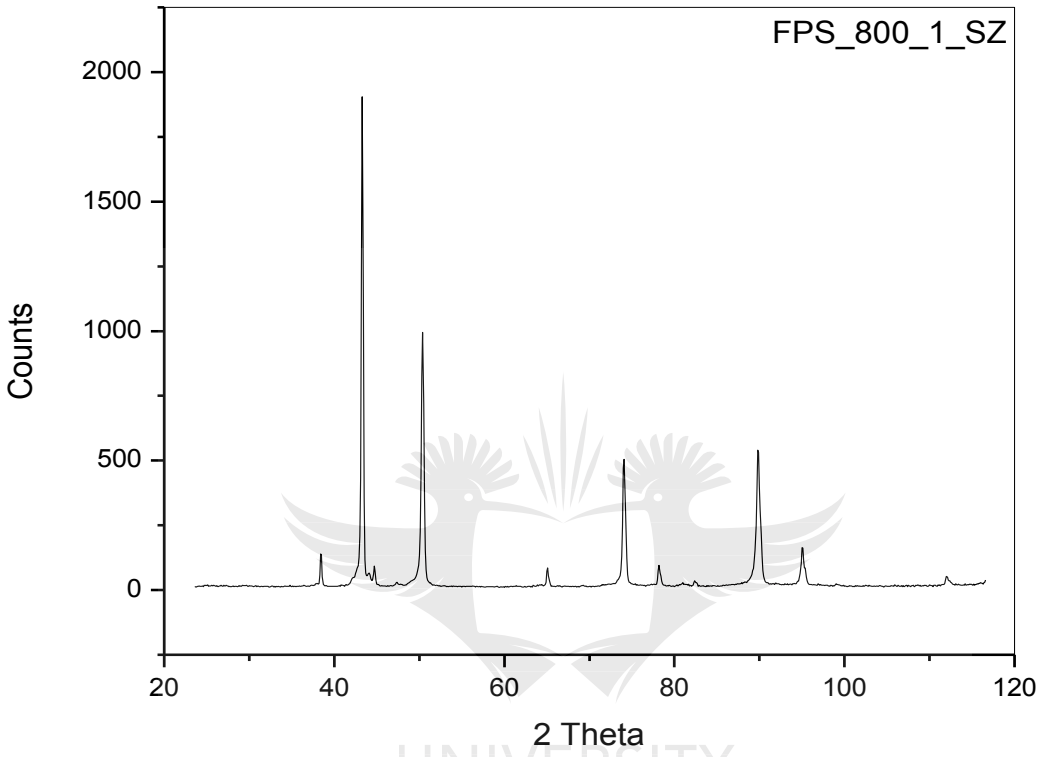

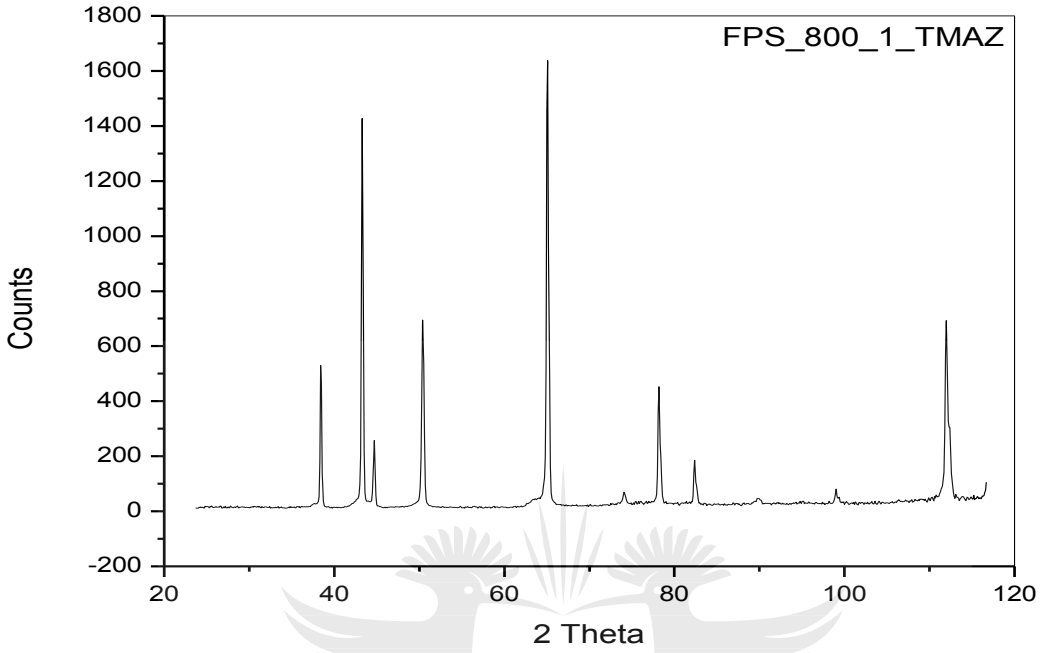

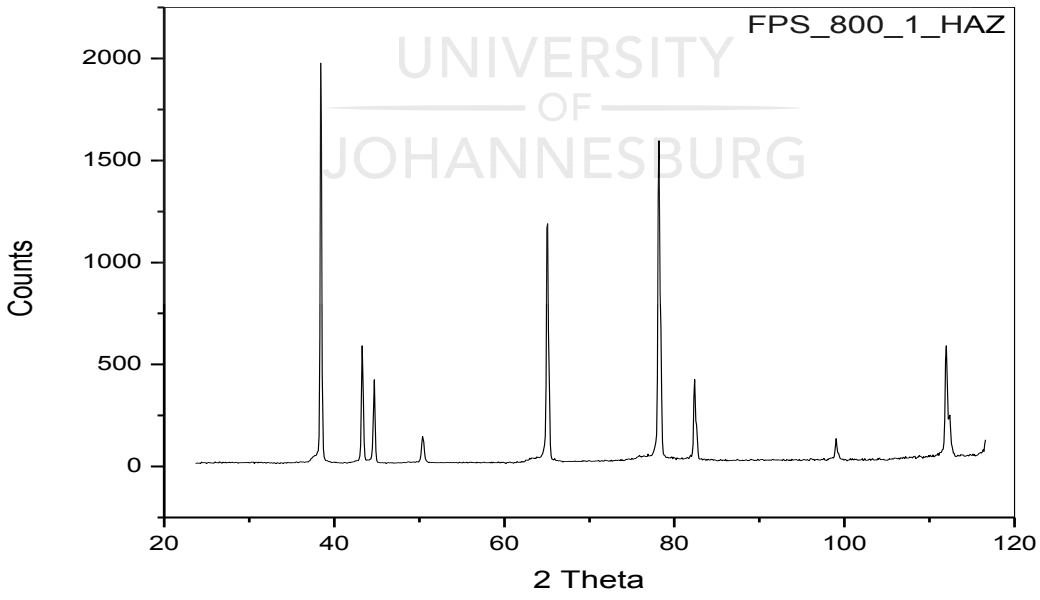

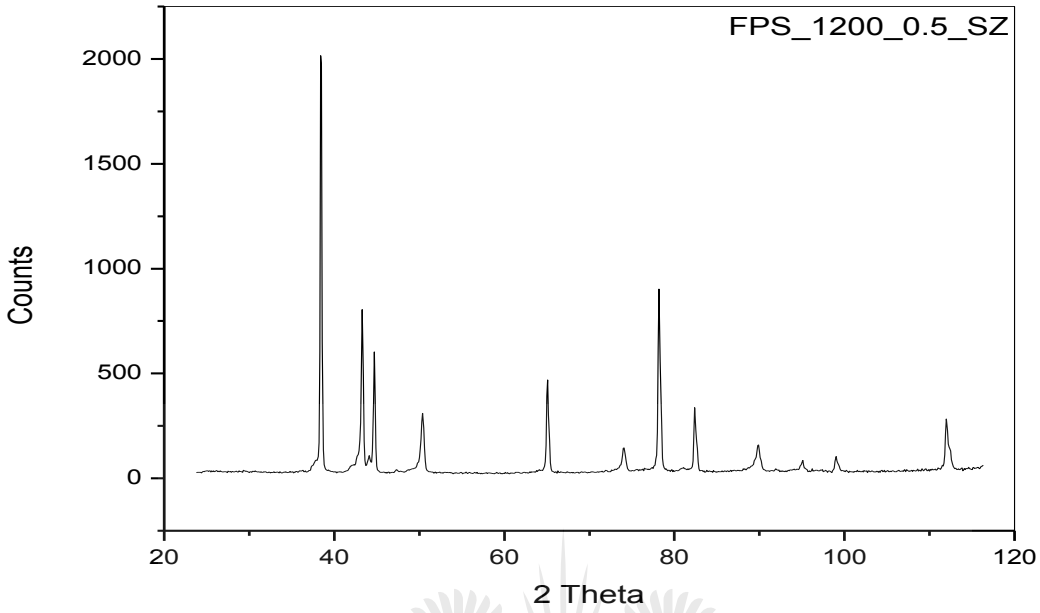

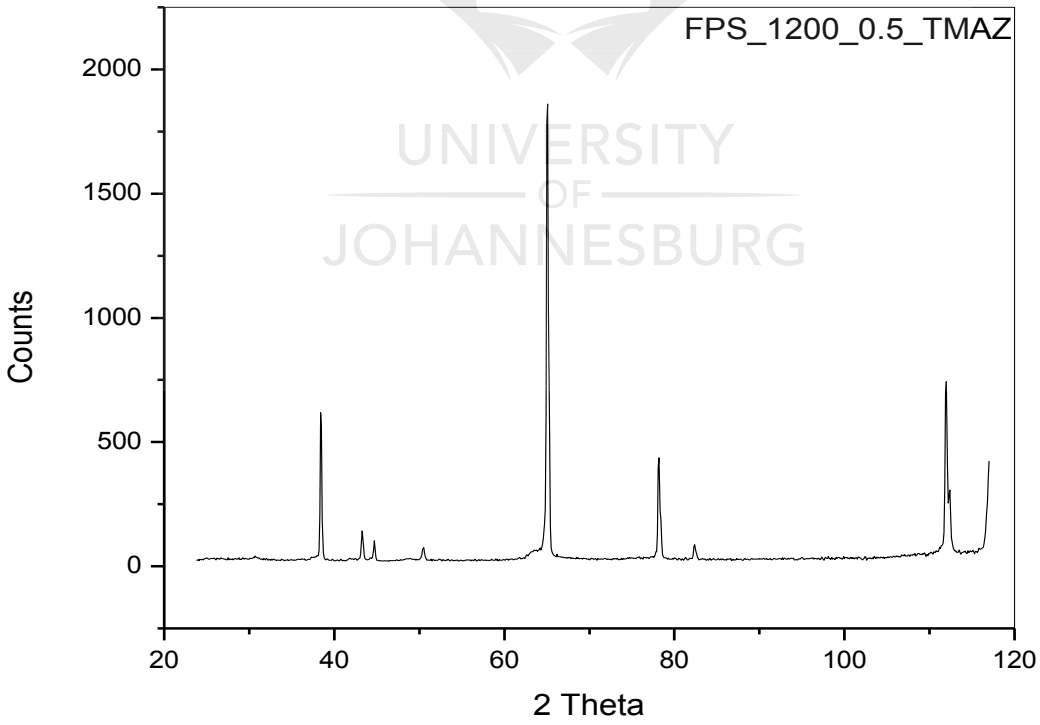

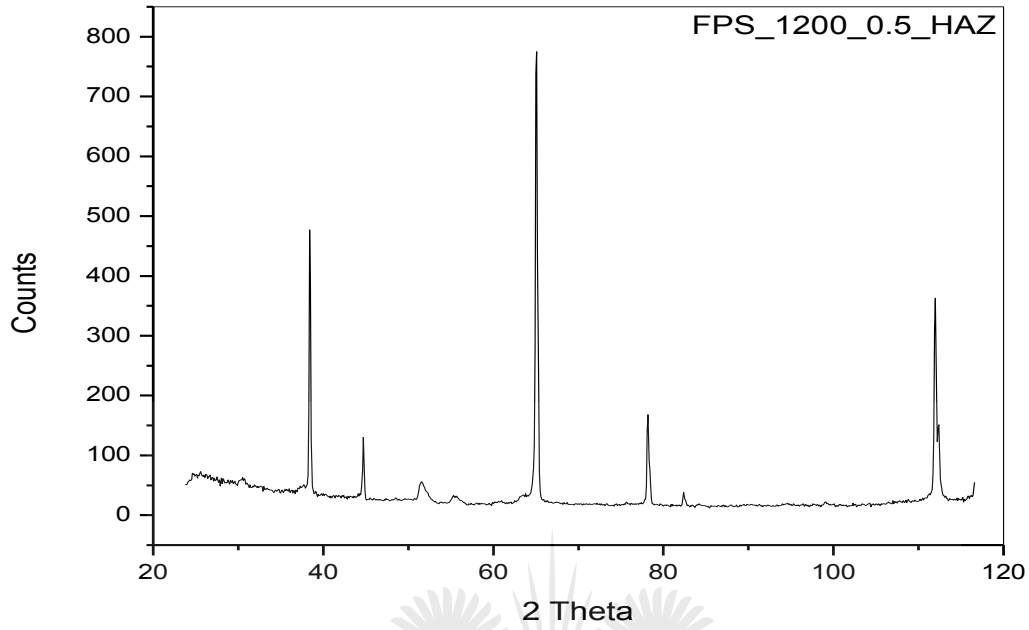

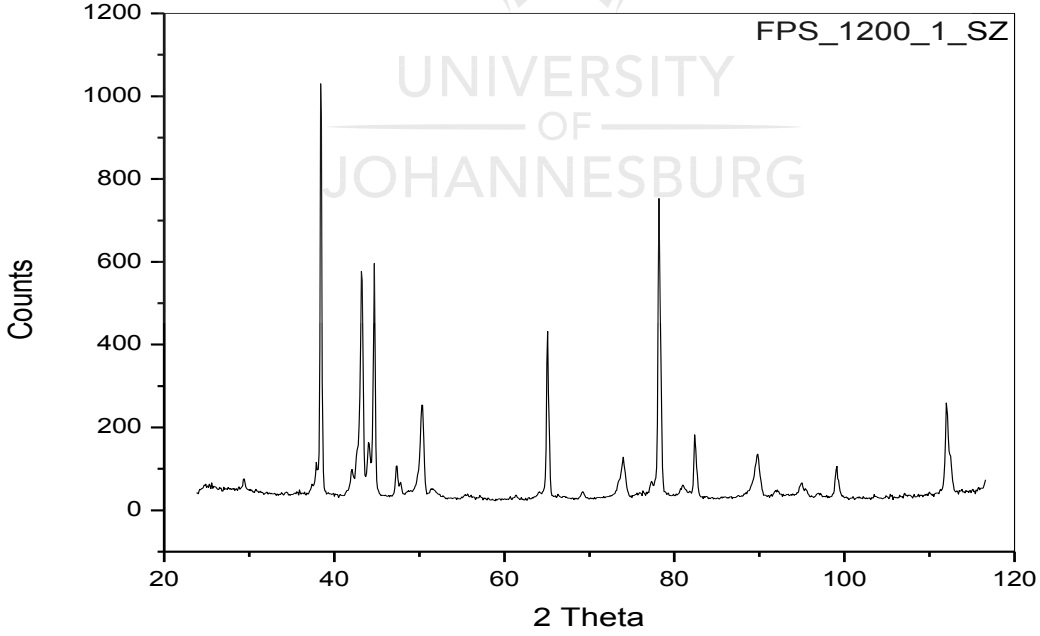

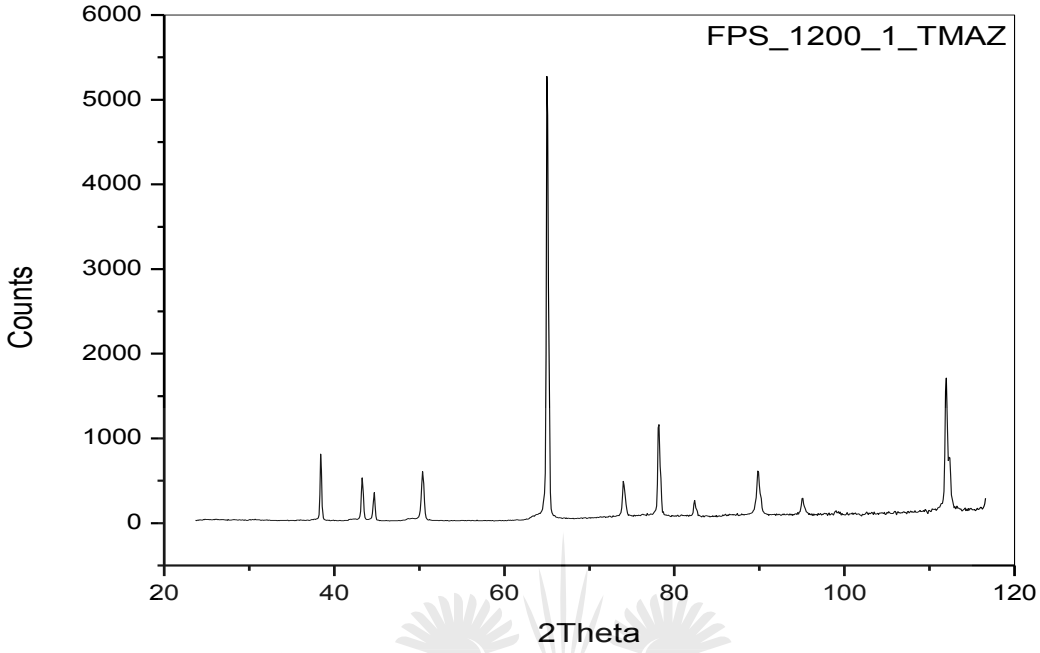

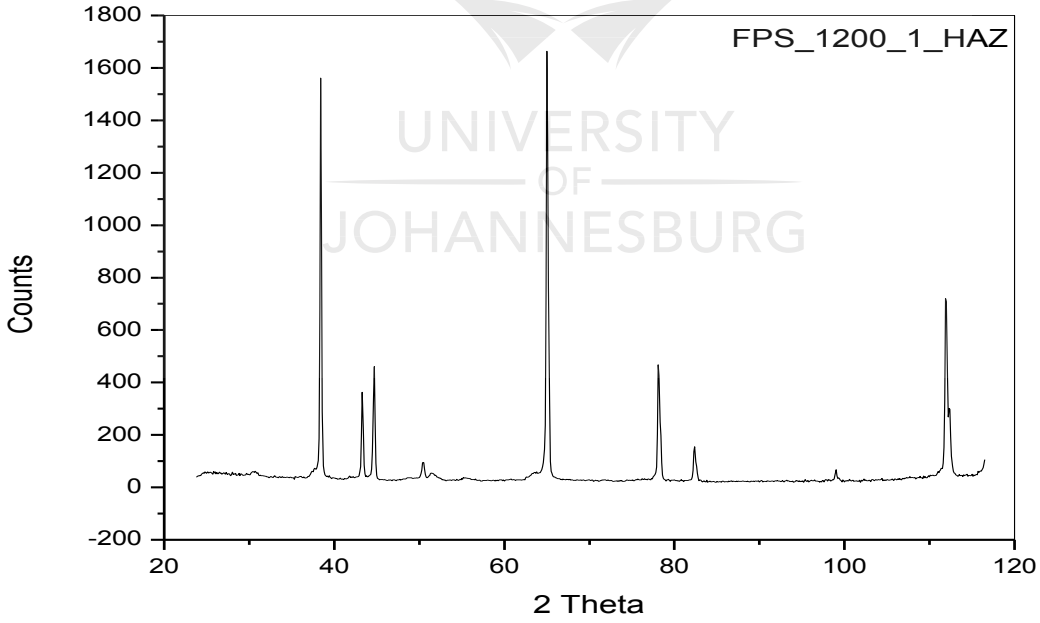

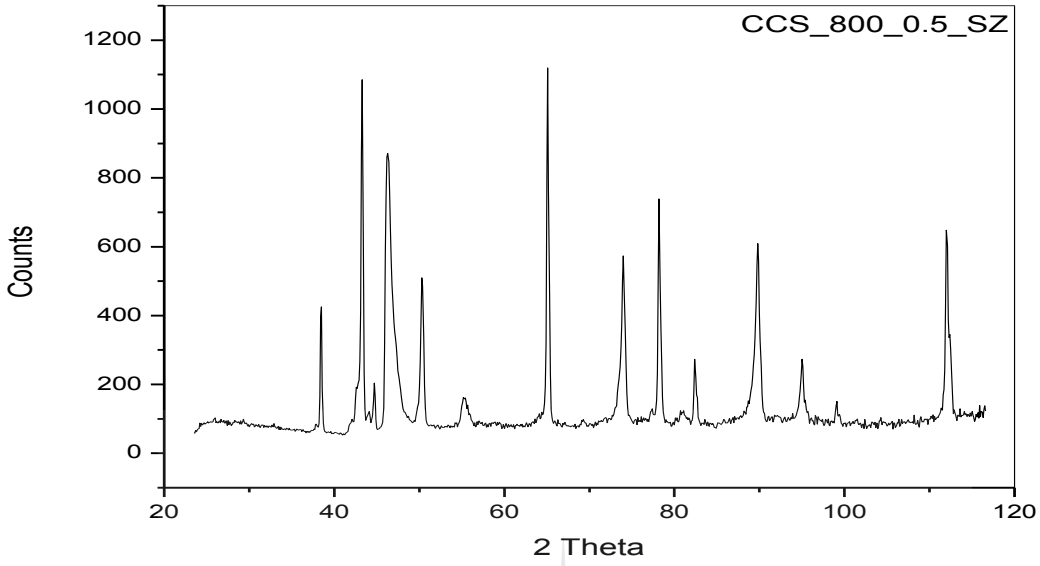

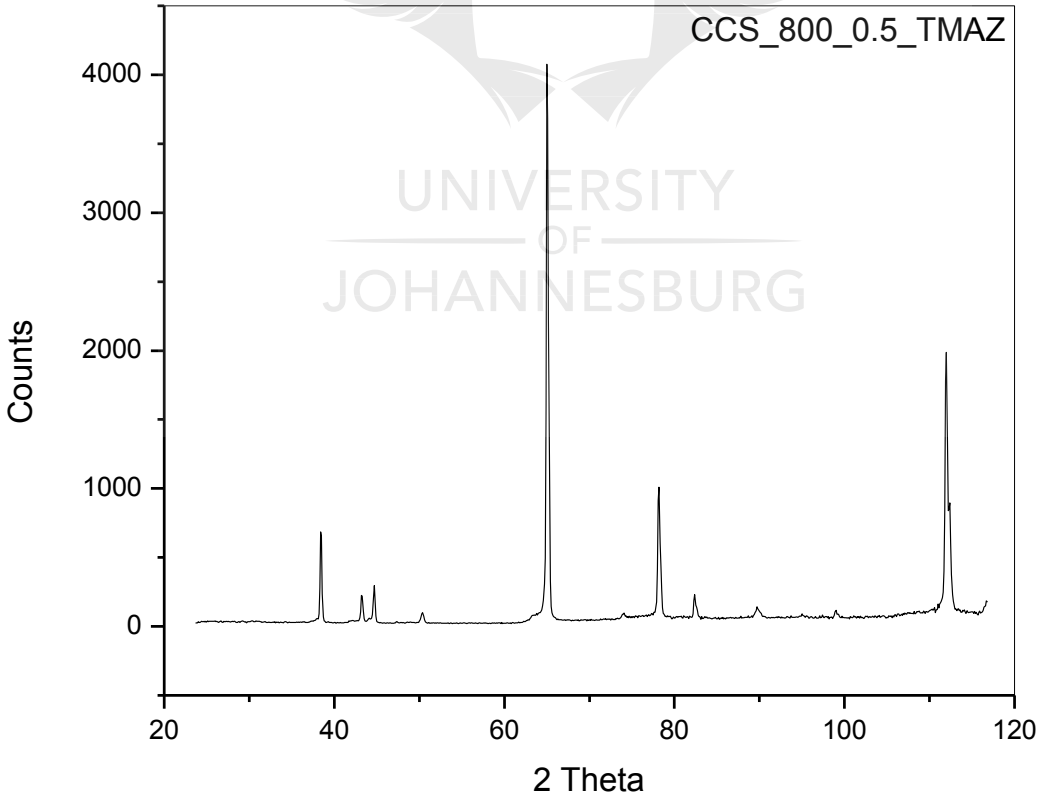

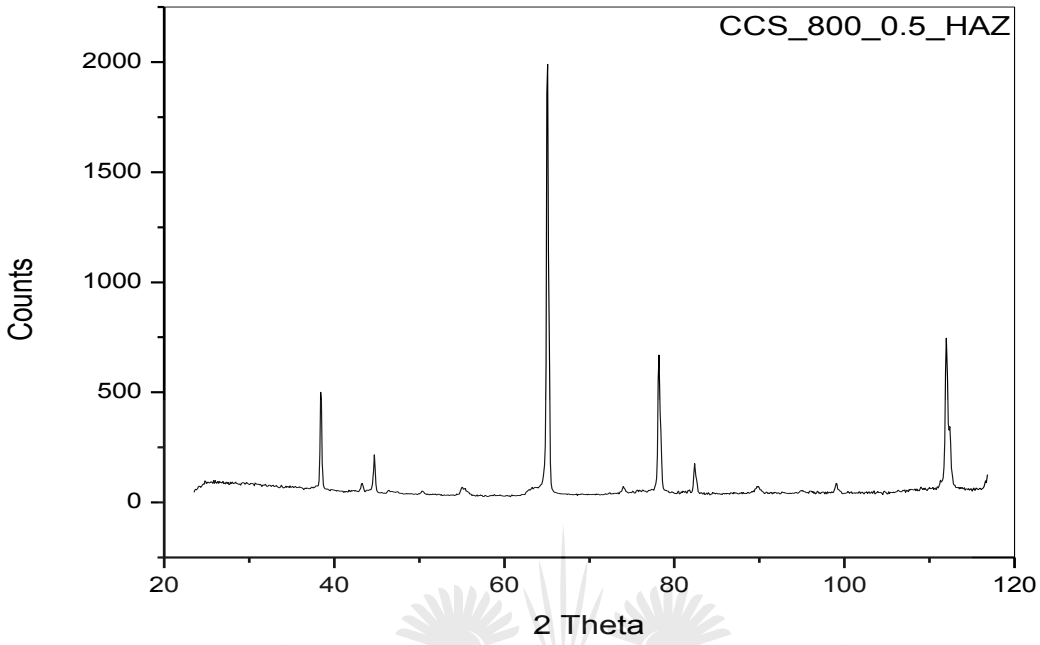

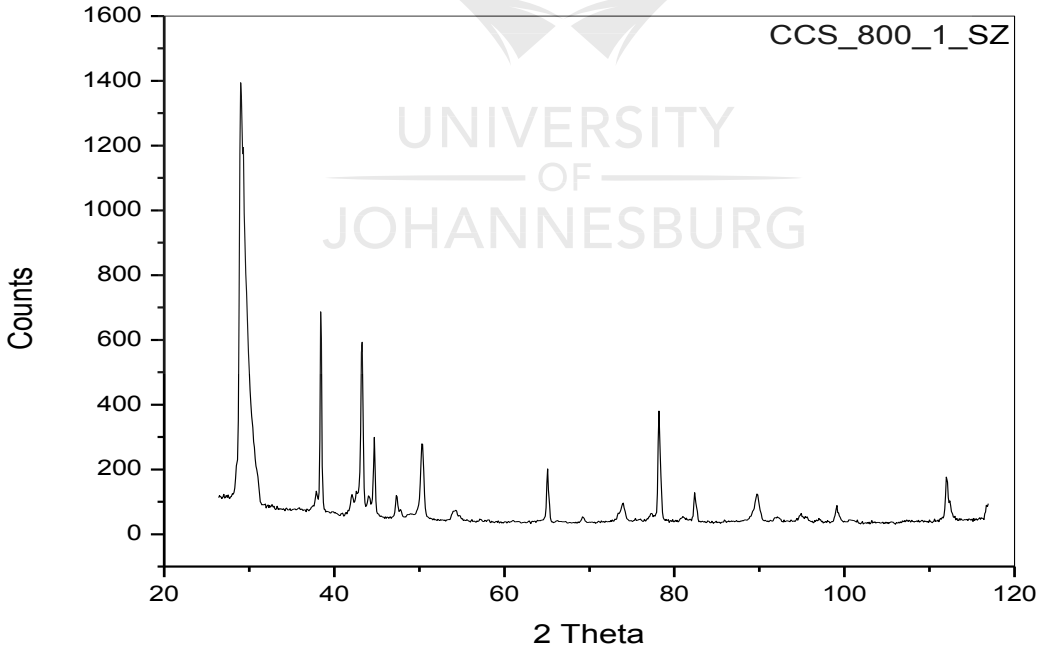

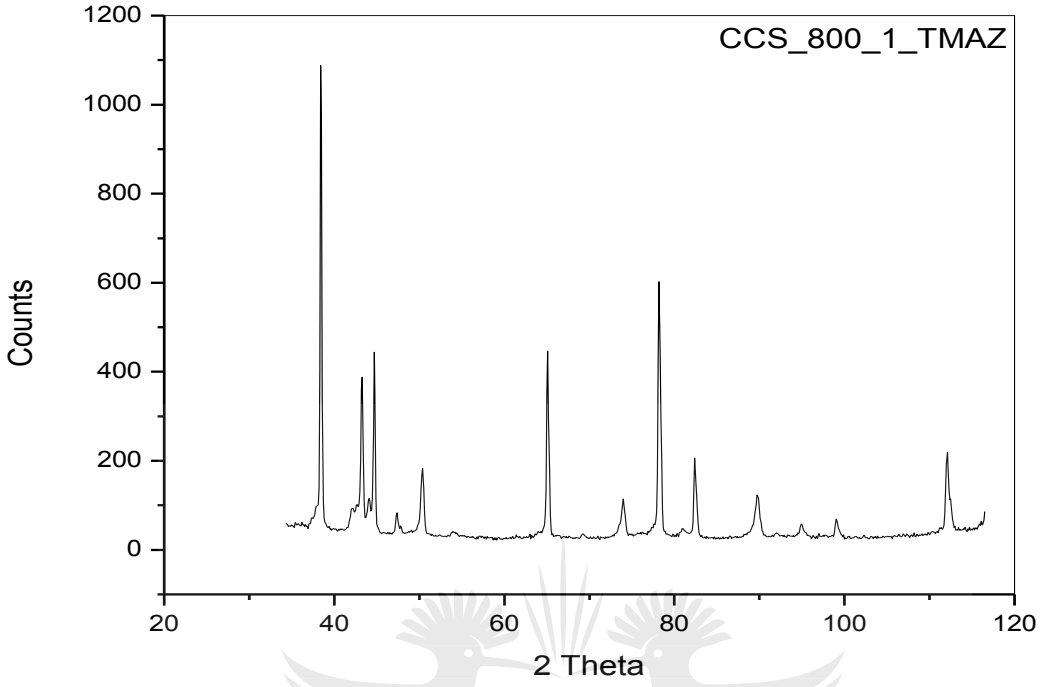

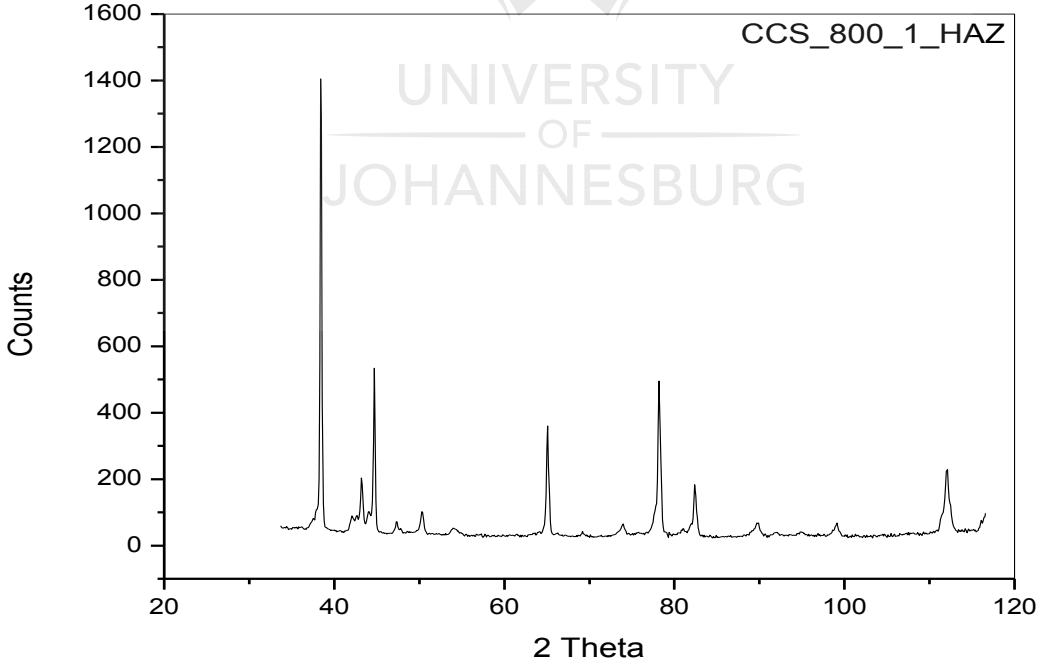

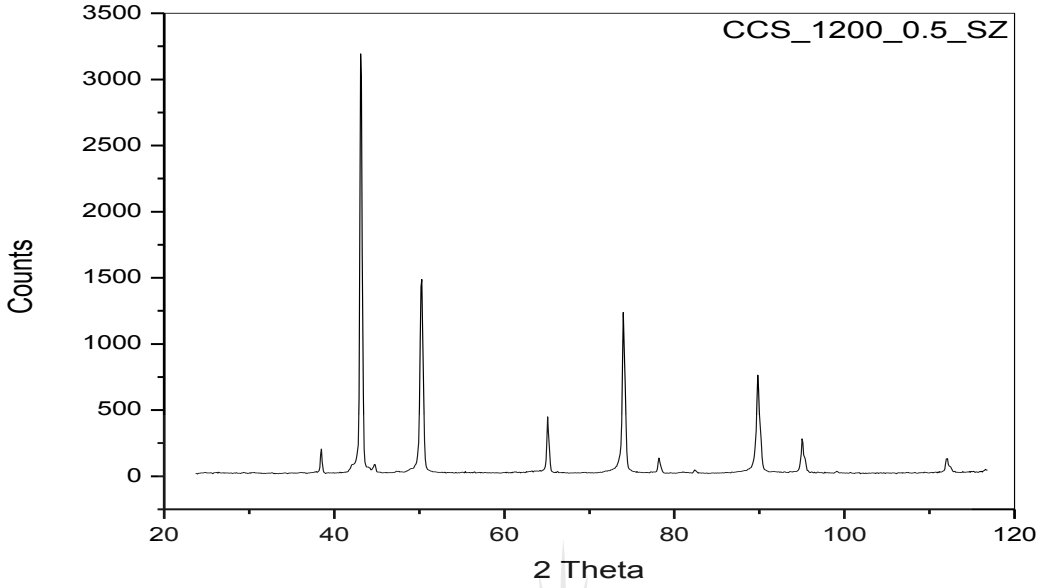

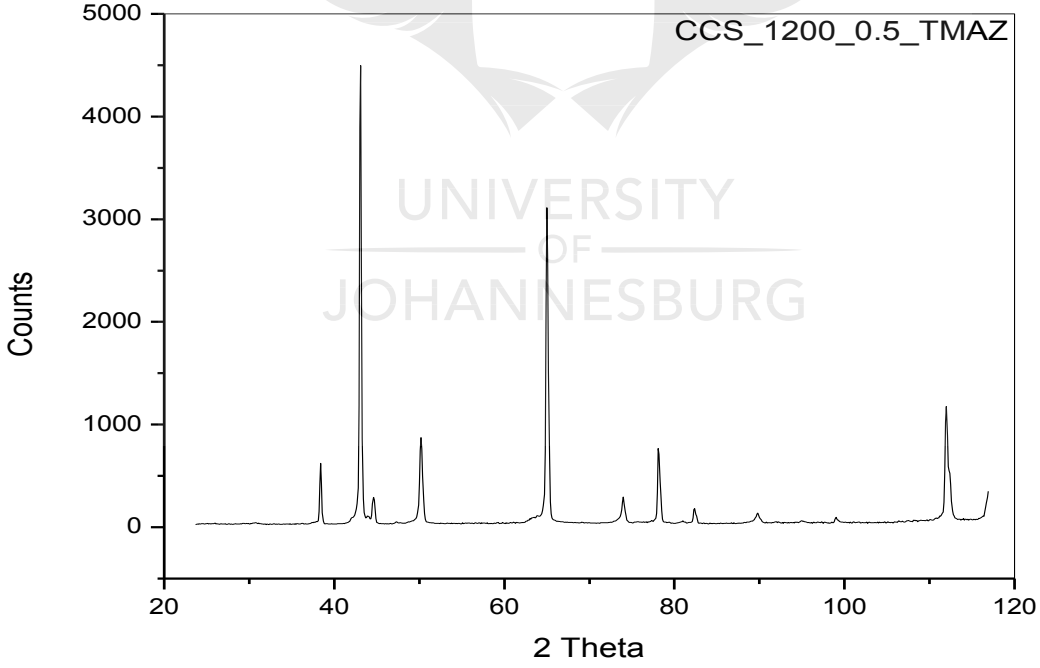

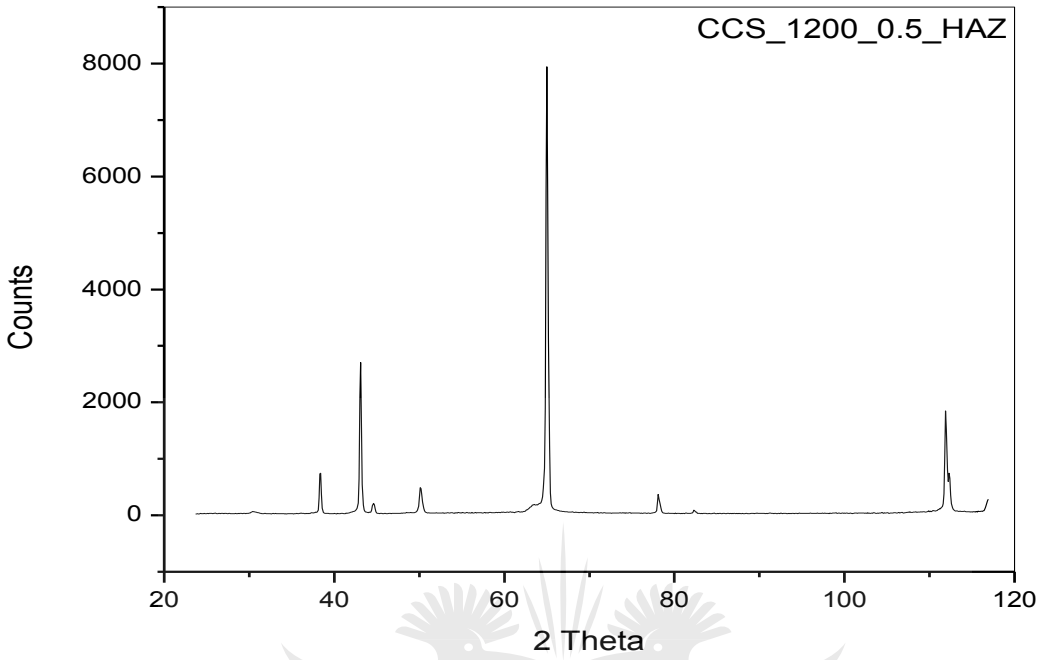

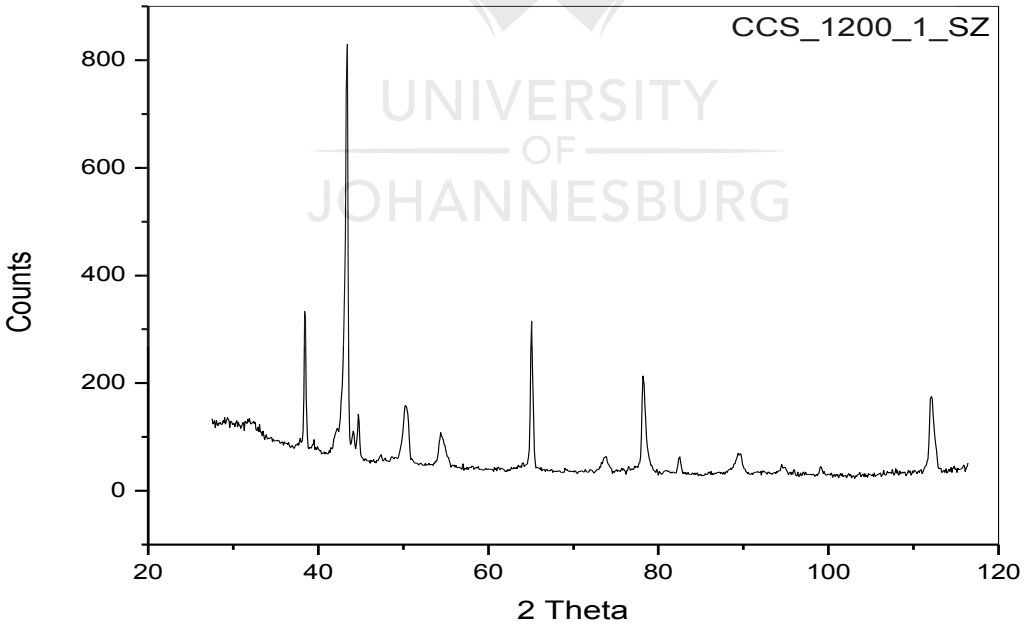

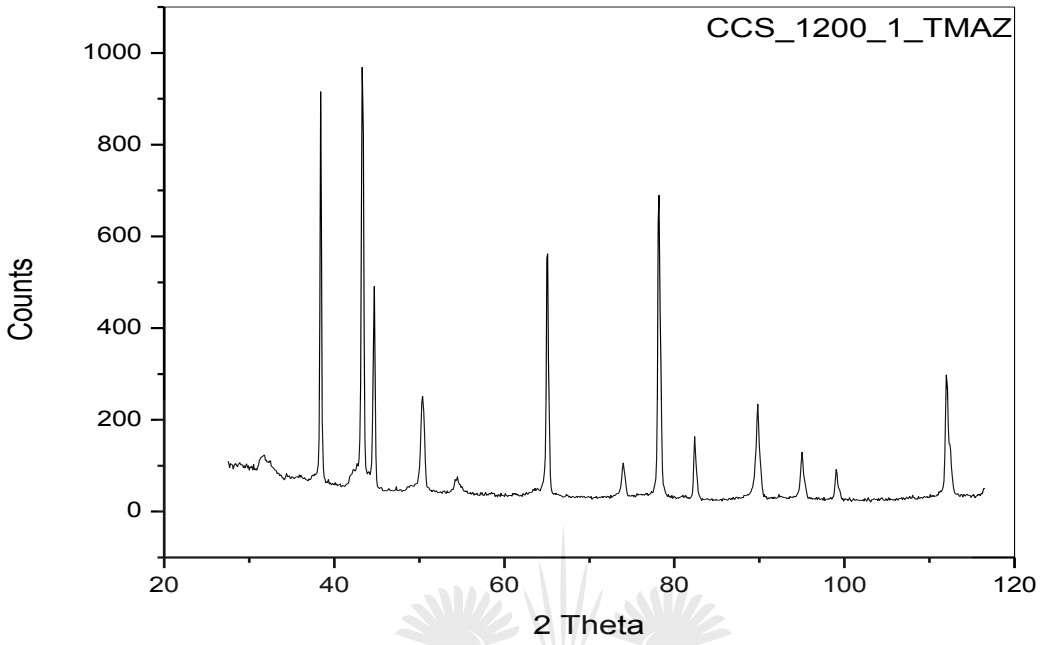

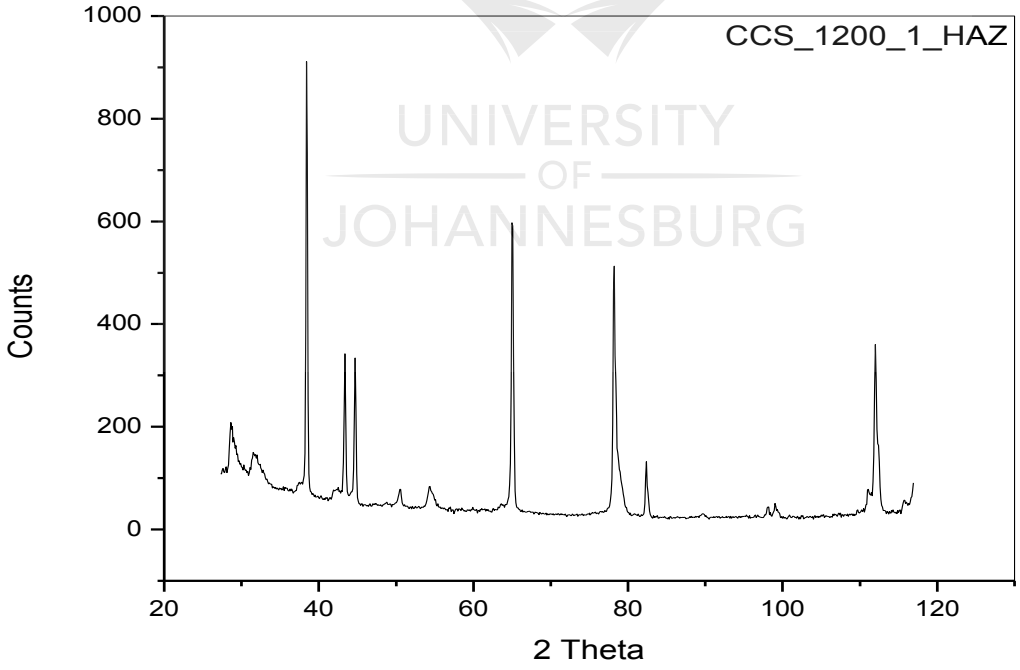

APPENDIX L

FPS_800_0.5

TOP

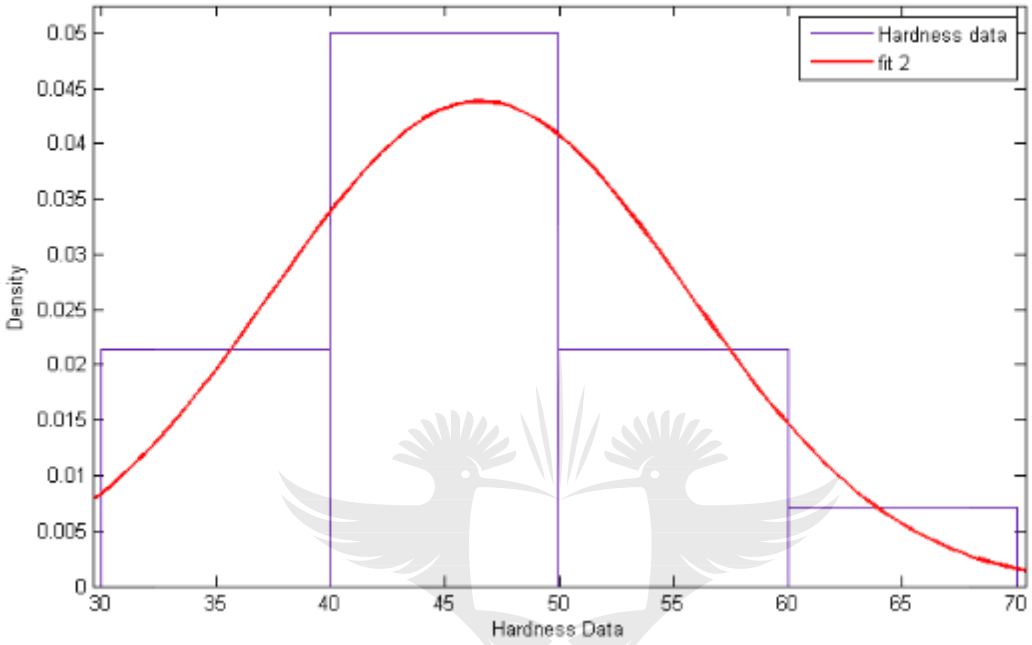

BOTOM

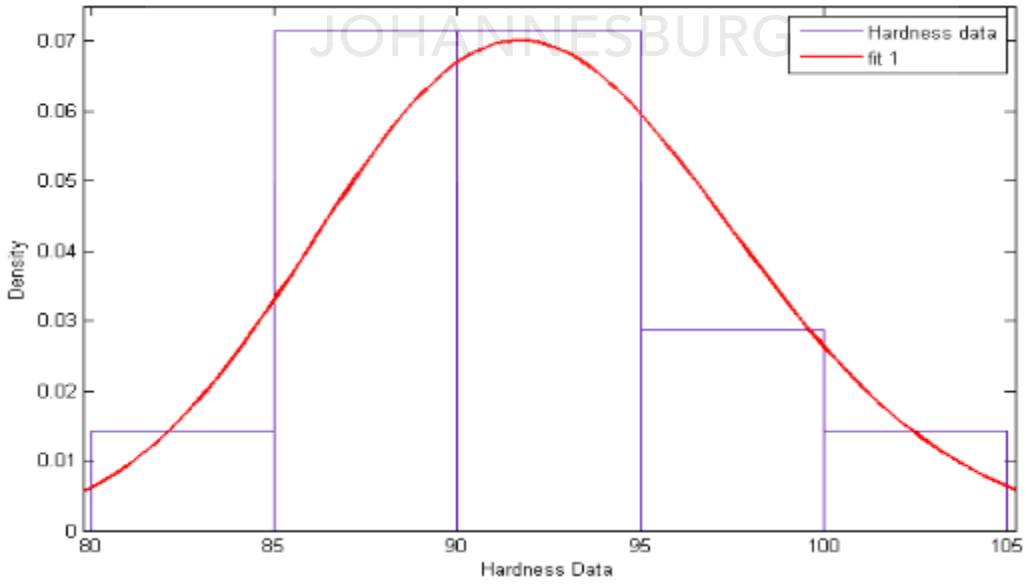

FPS_800_1

TOP

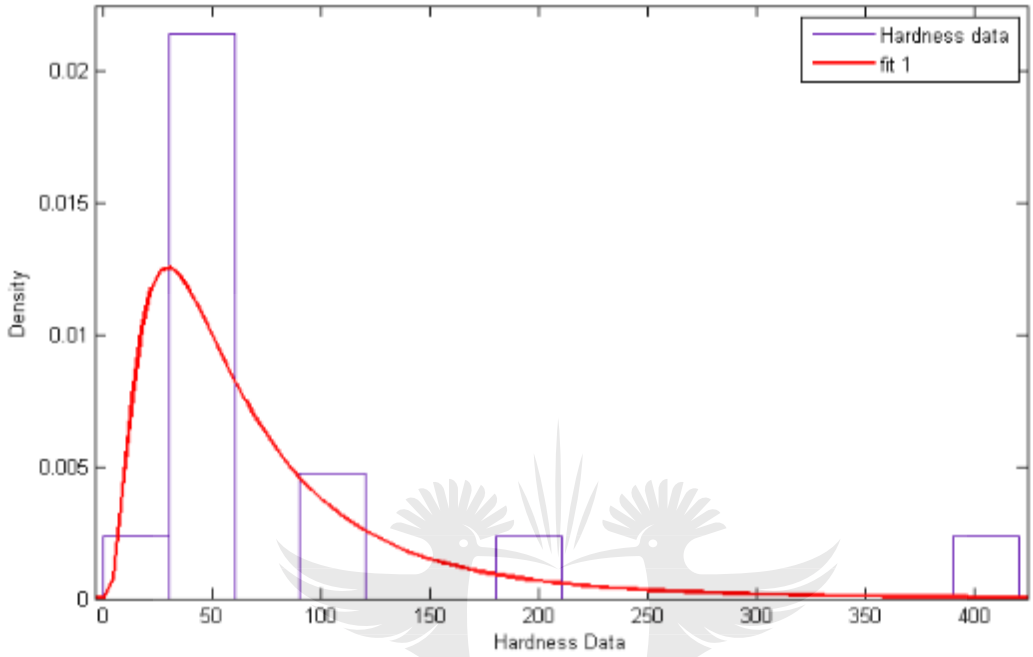

BOTTOM

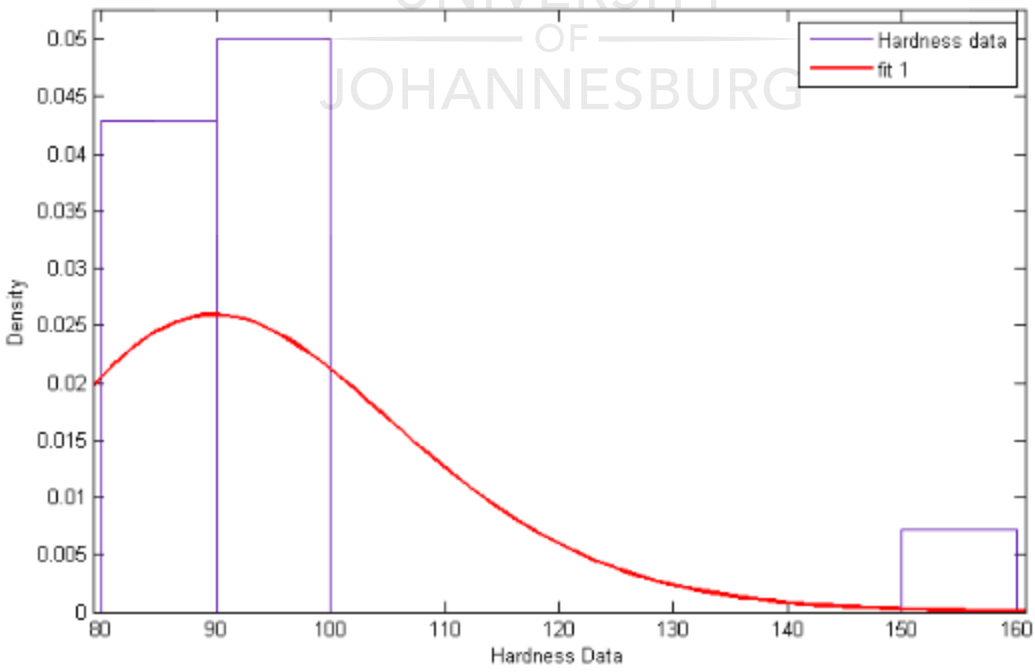

FPS_1200_0.5

TOP

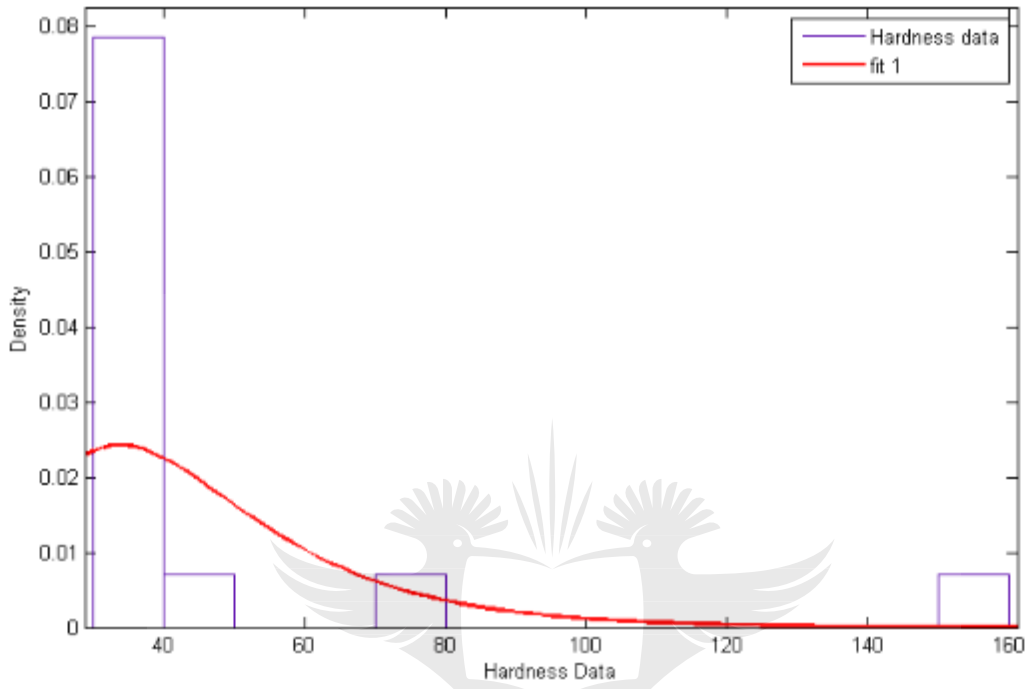

BOTTOM

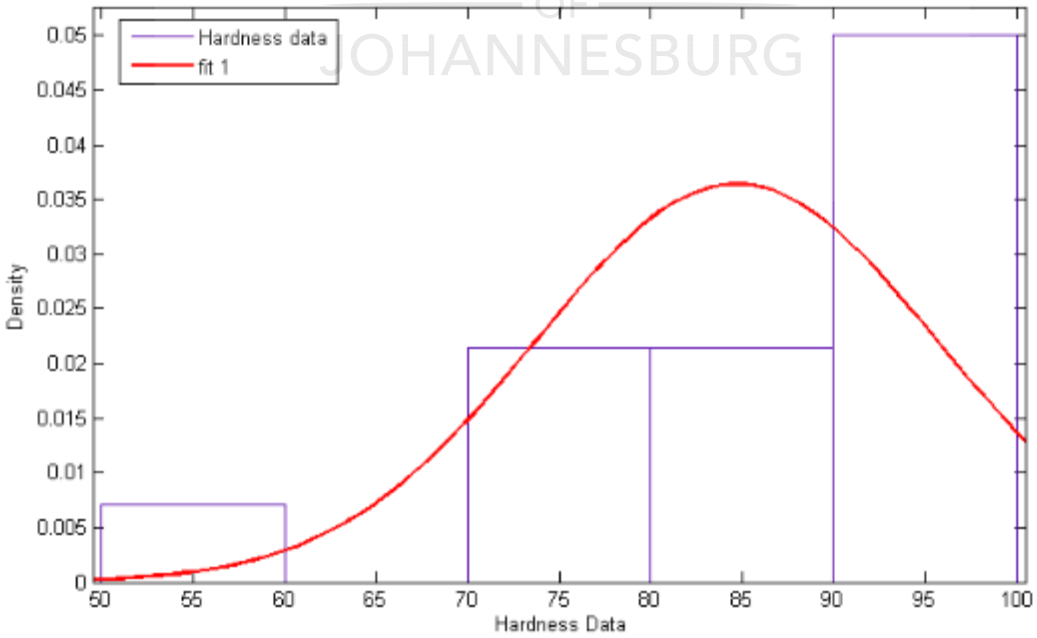

FPS_1200_1

TOP

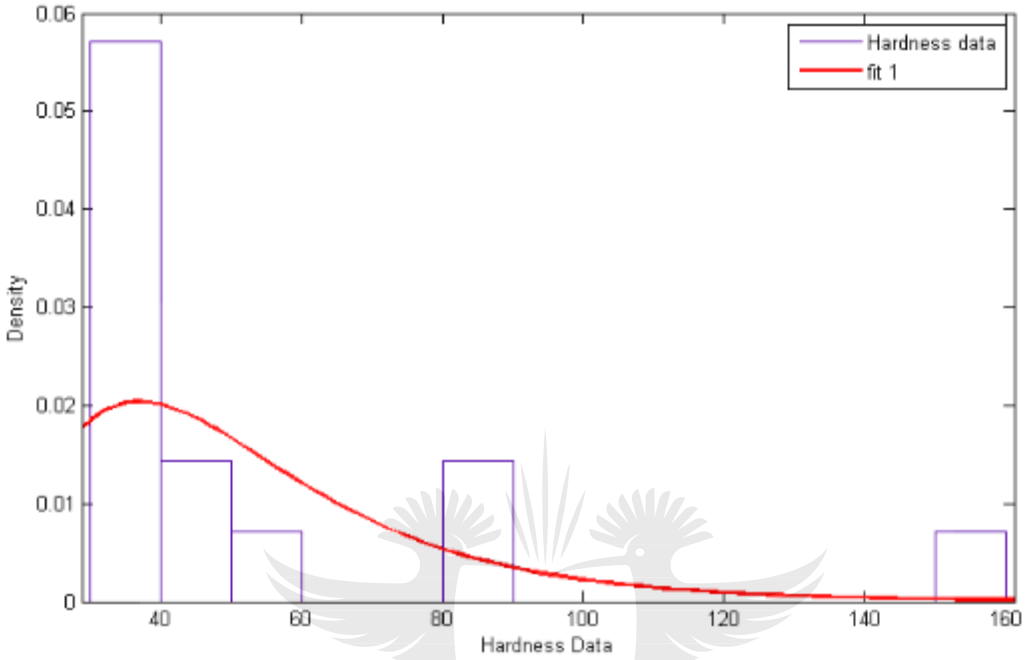

BOTTOM

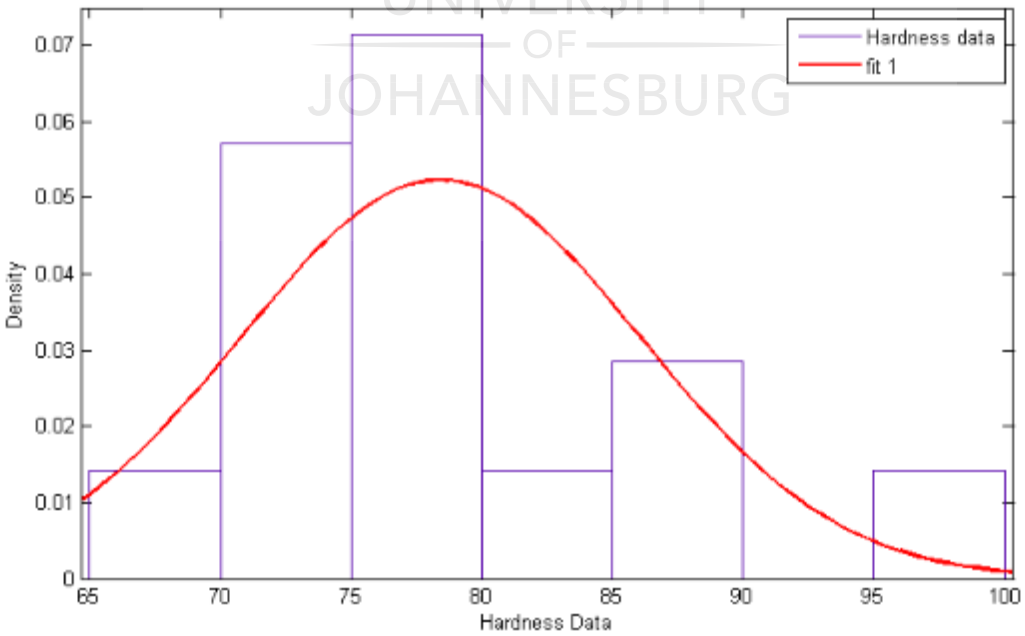

CCS_800_0.5

TOP

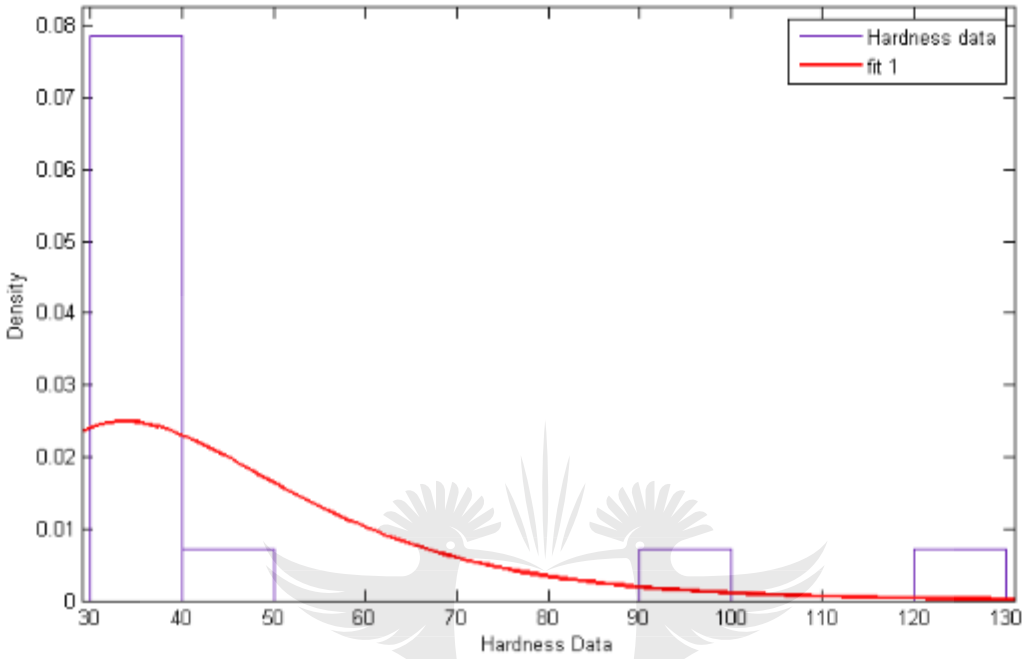

BOTTOM

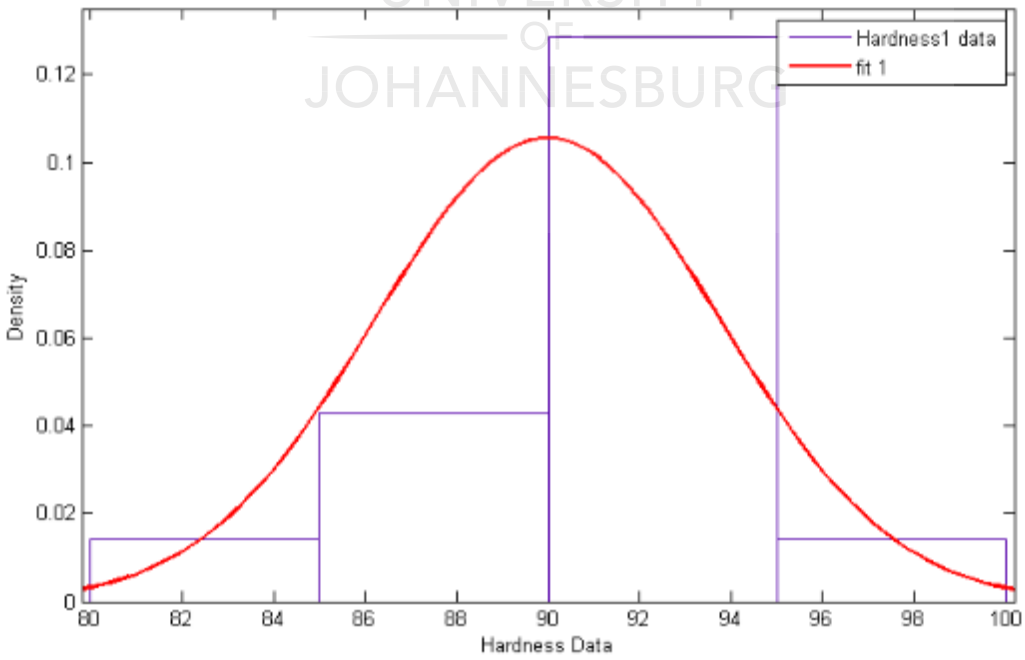

CCS_800_1

TOP

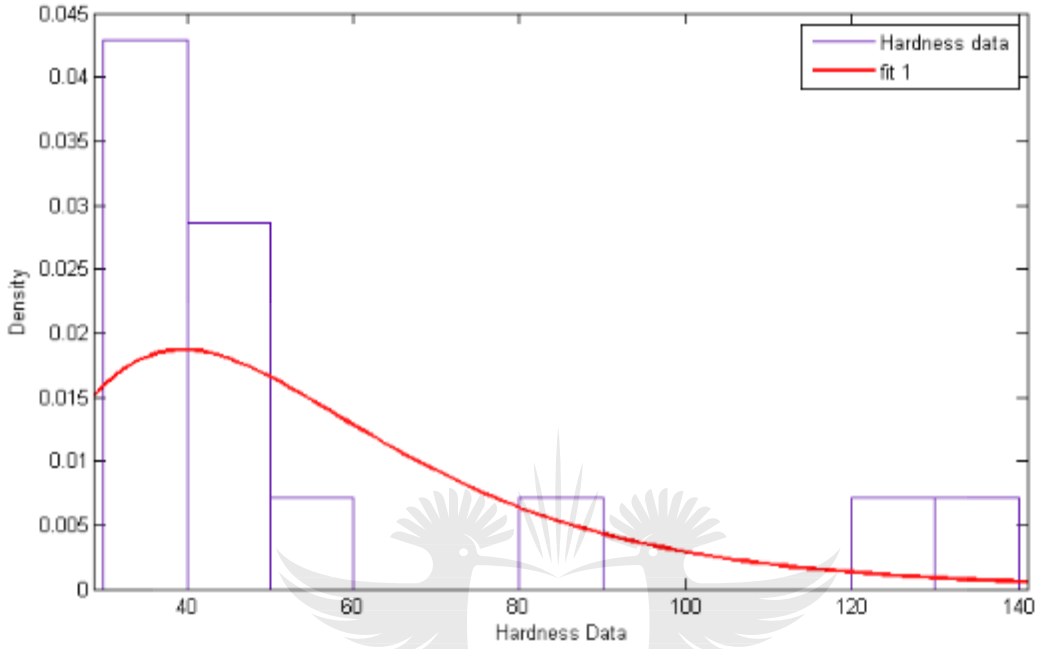

BOTTOM

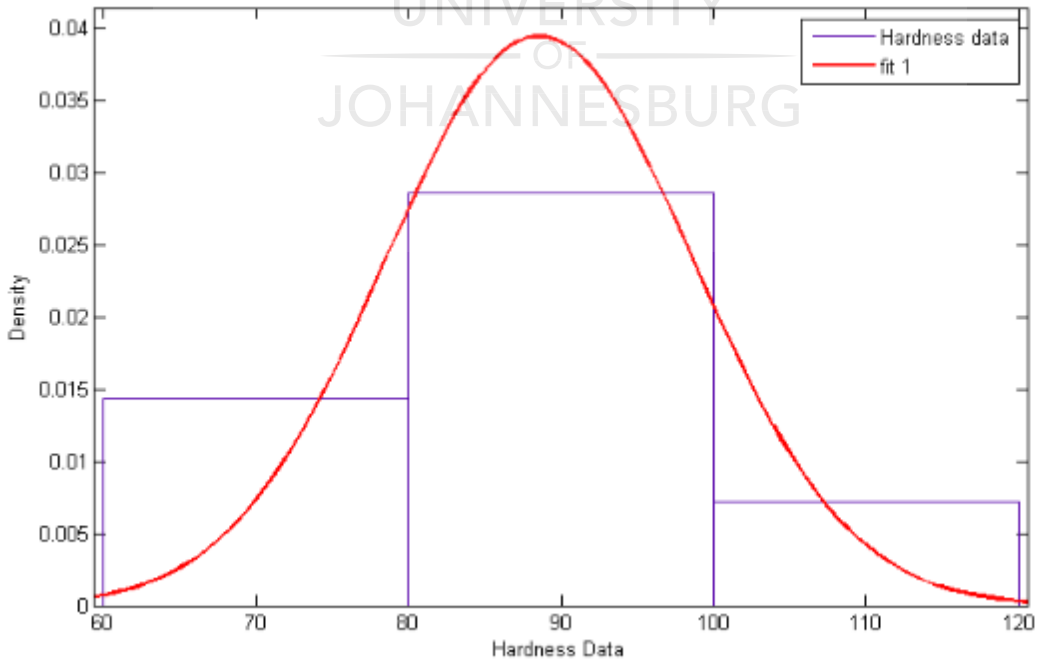

CCS_1200_0.5

TOP

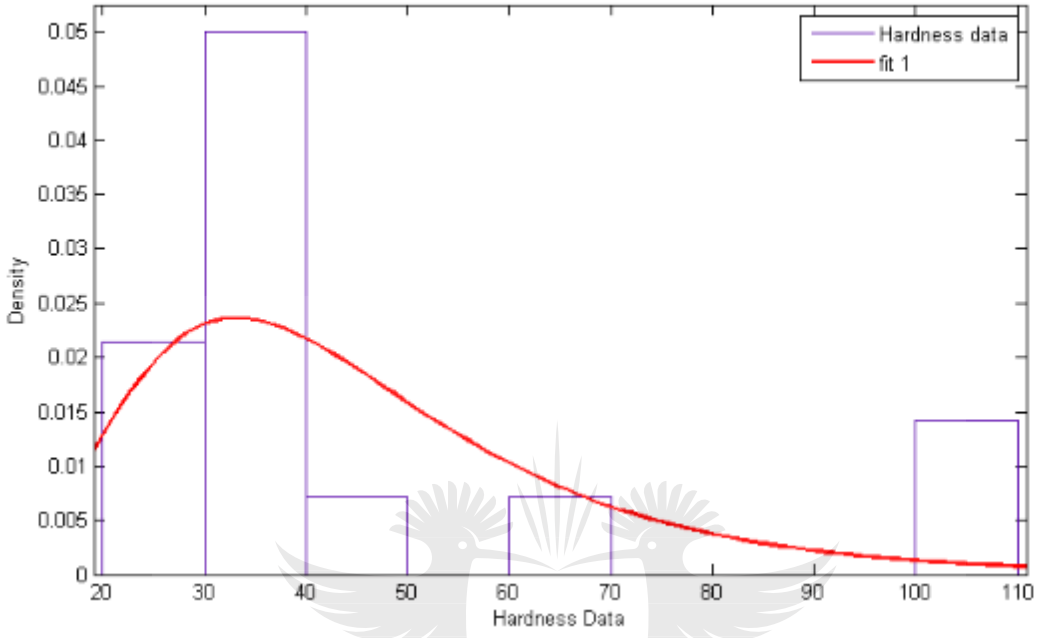

BOTTOM

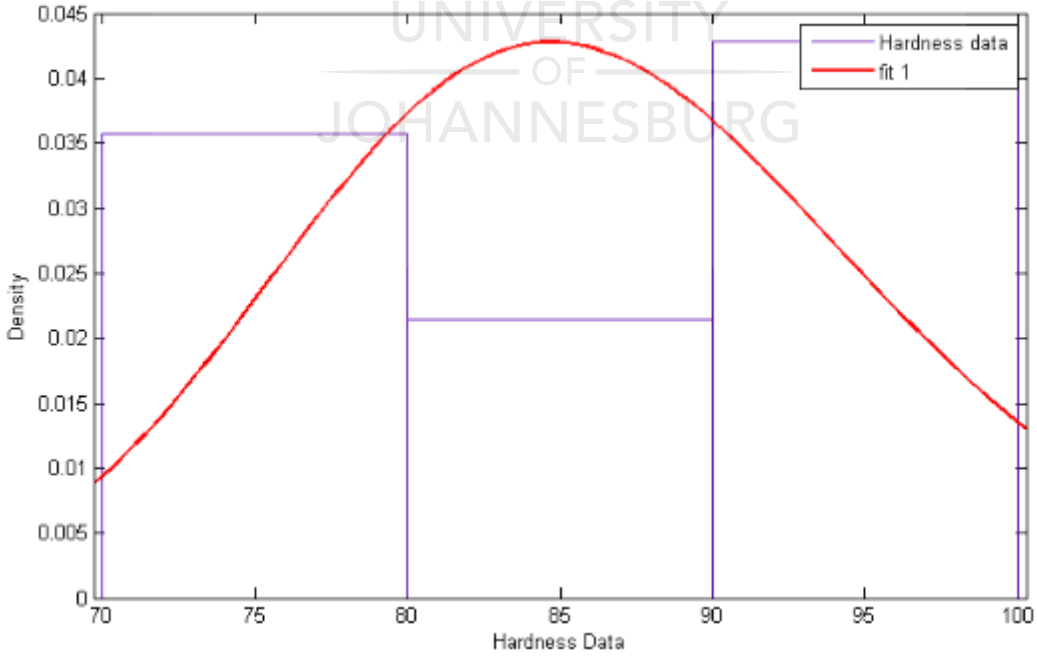

CCS_1200_1

TOP

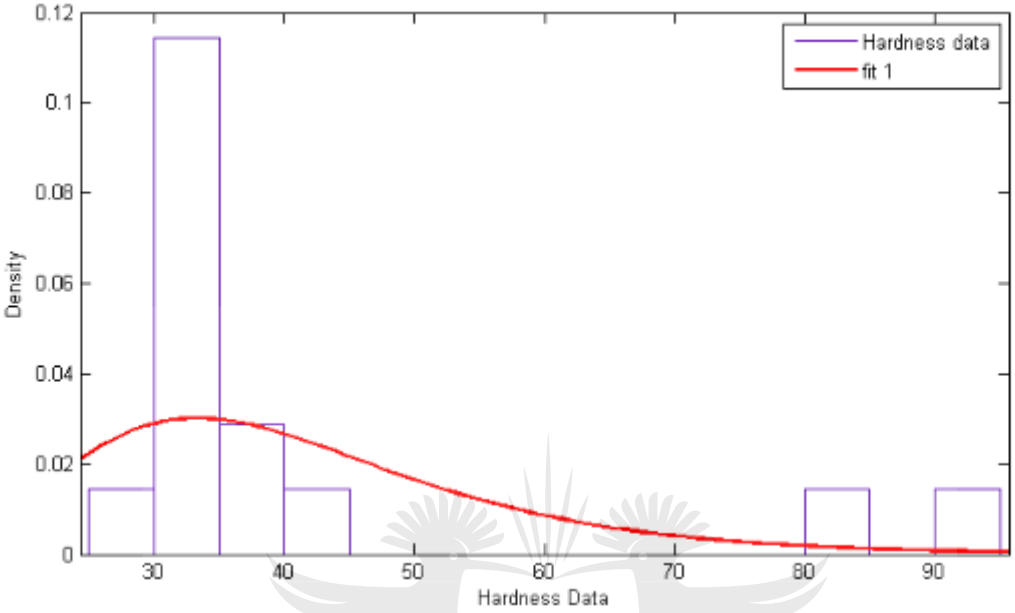

BOTTOM

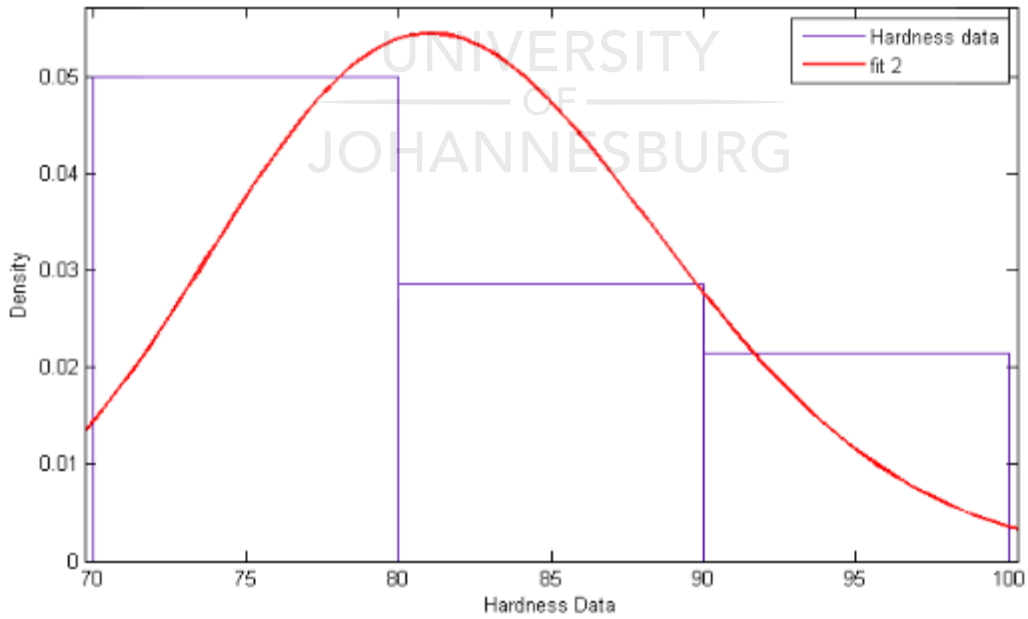

FIT

Al PM

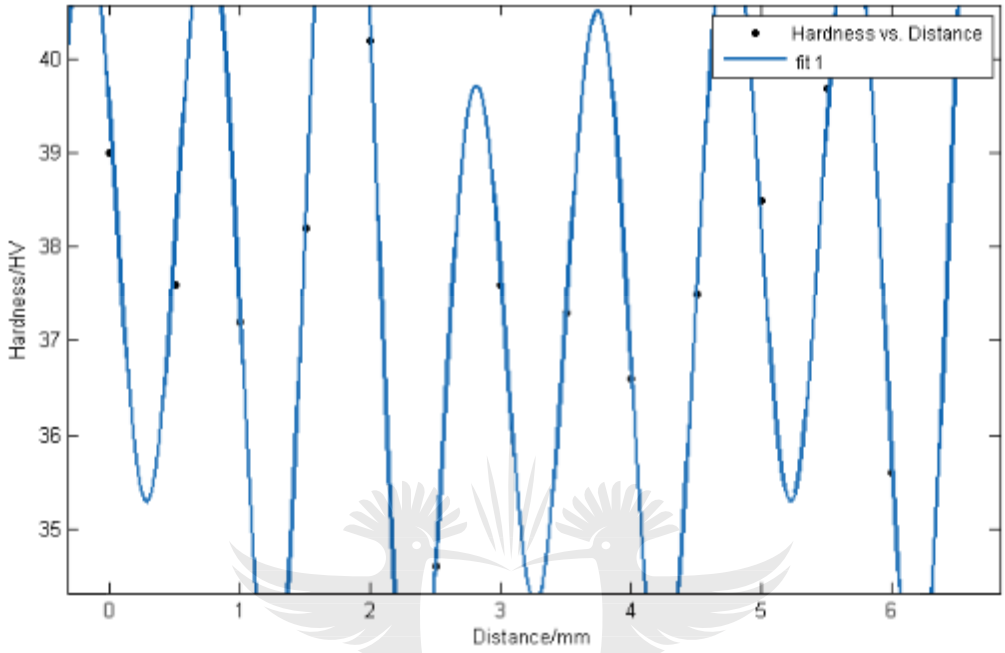

Cu PM

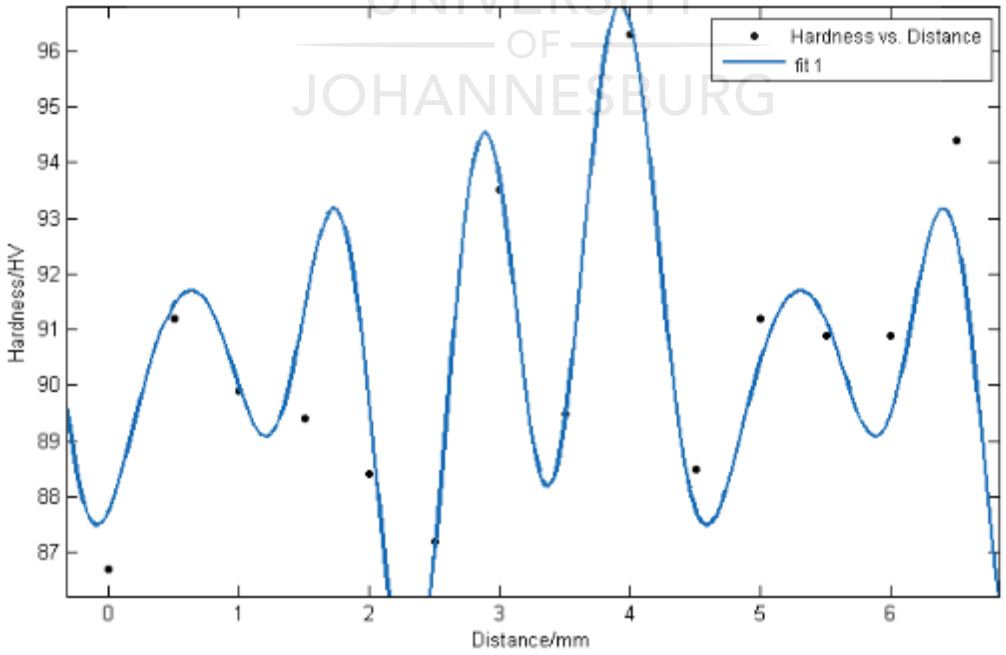

FPS_800_0.5

TOP

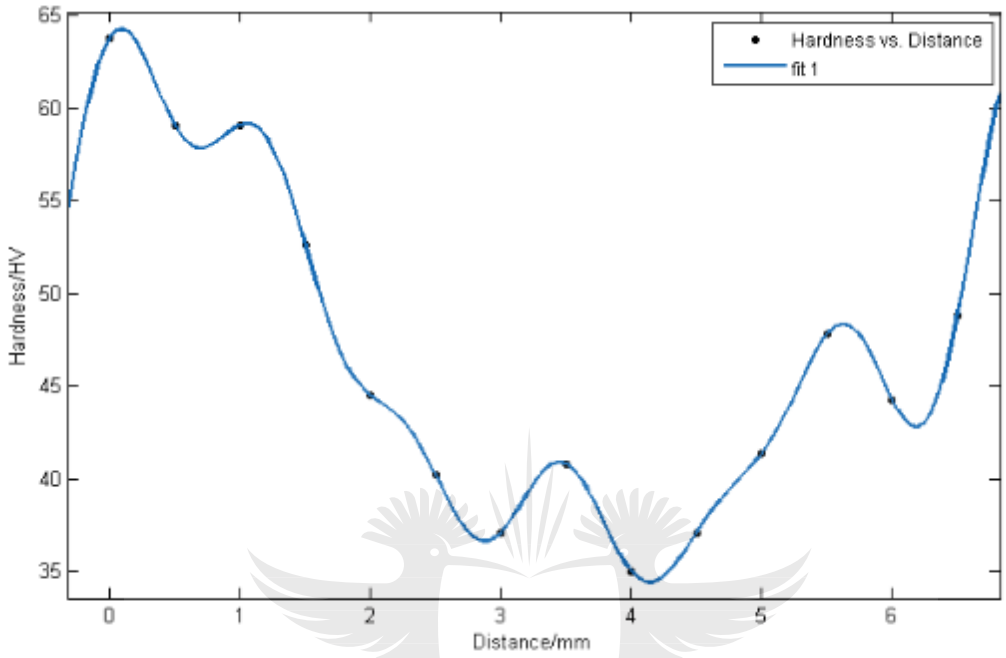

BOTTOM

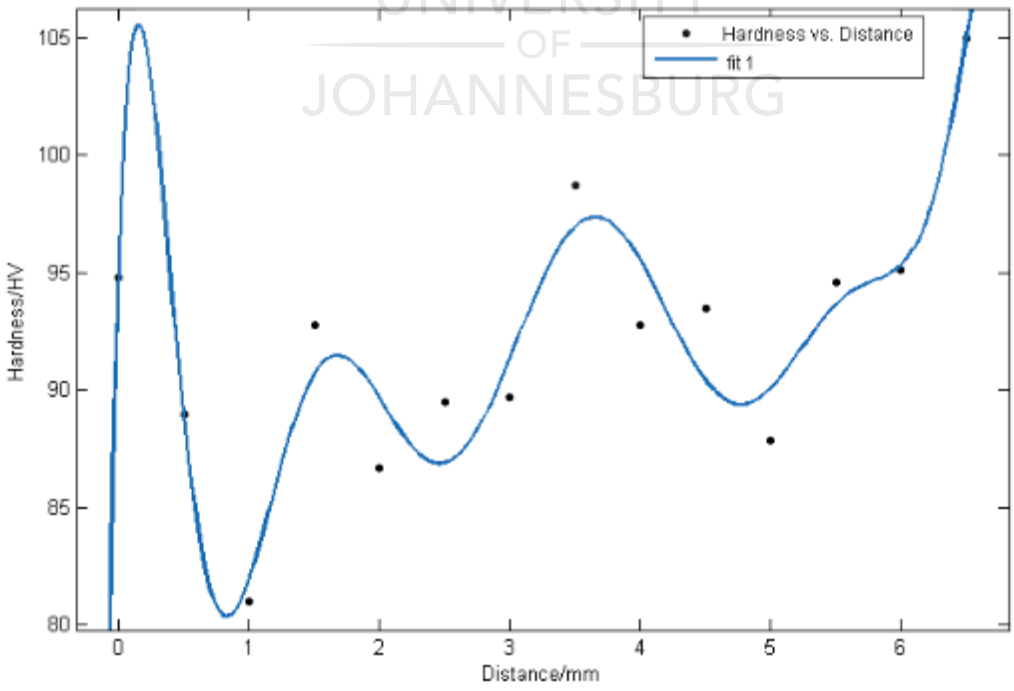

FPS_800_1

TOP

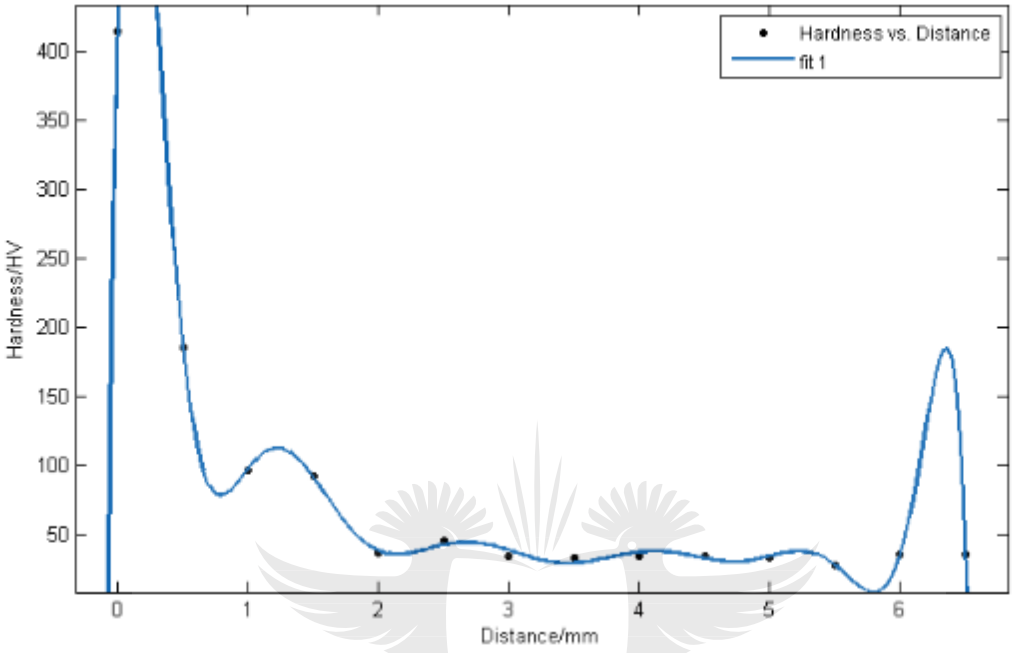

BOTTOM

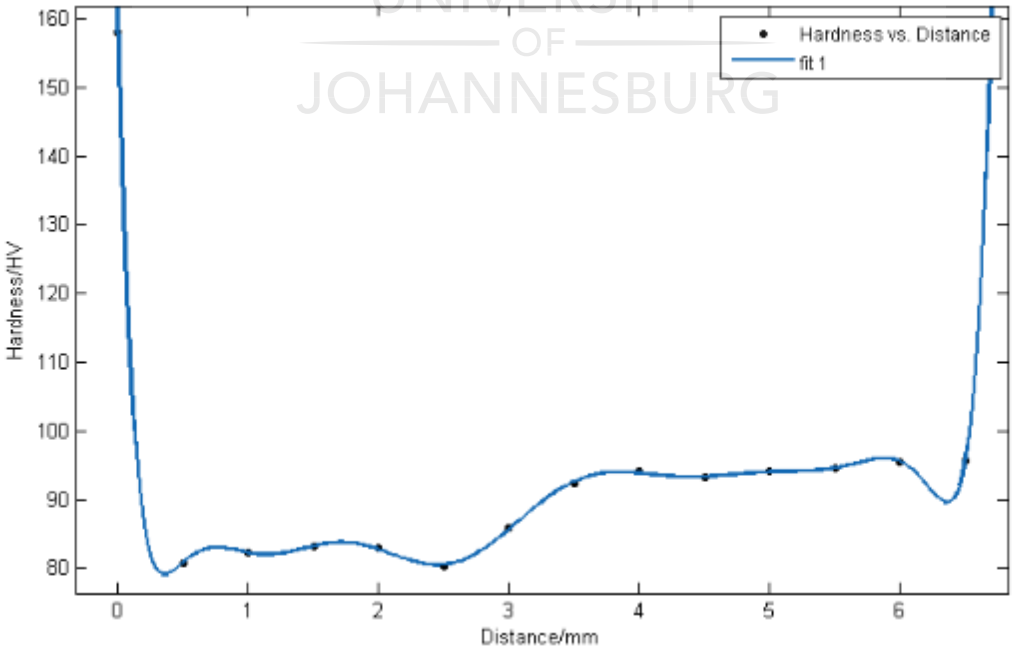

FPS_1200_0.5

TOP

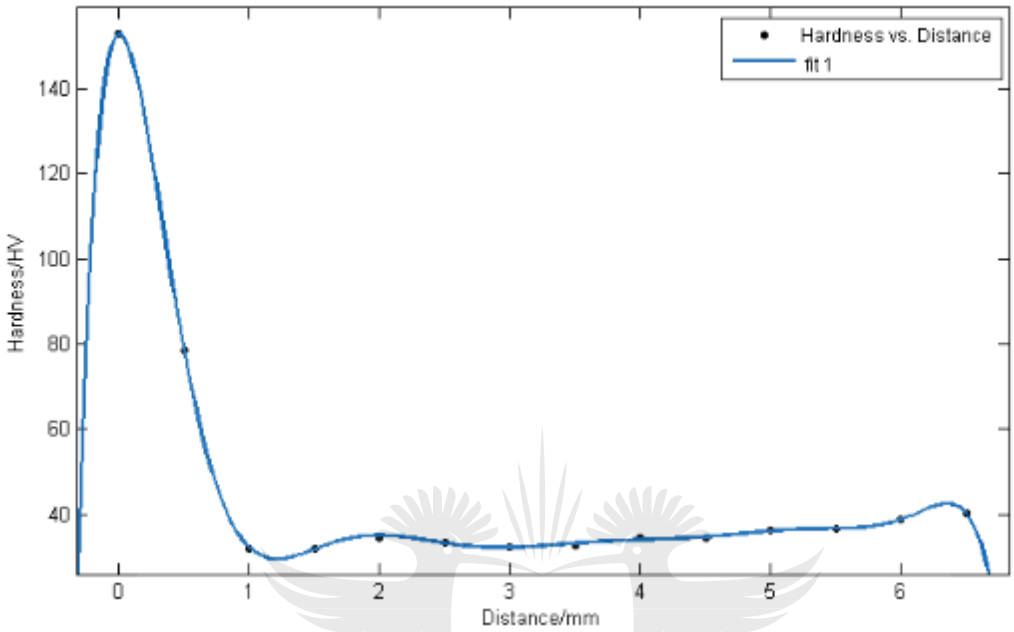

BOTTOM

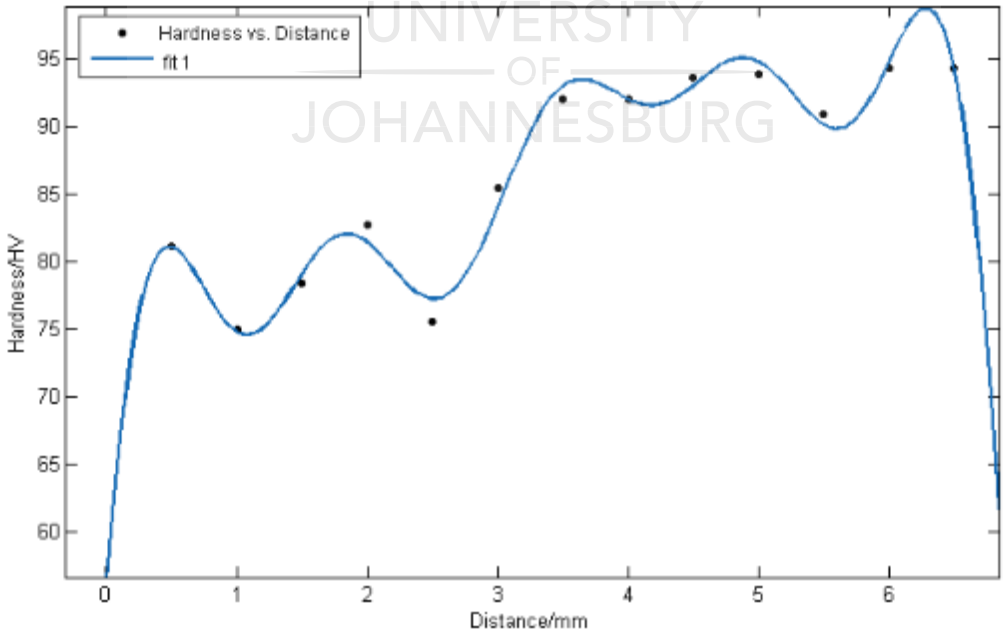

FPS_1200_1

TOP

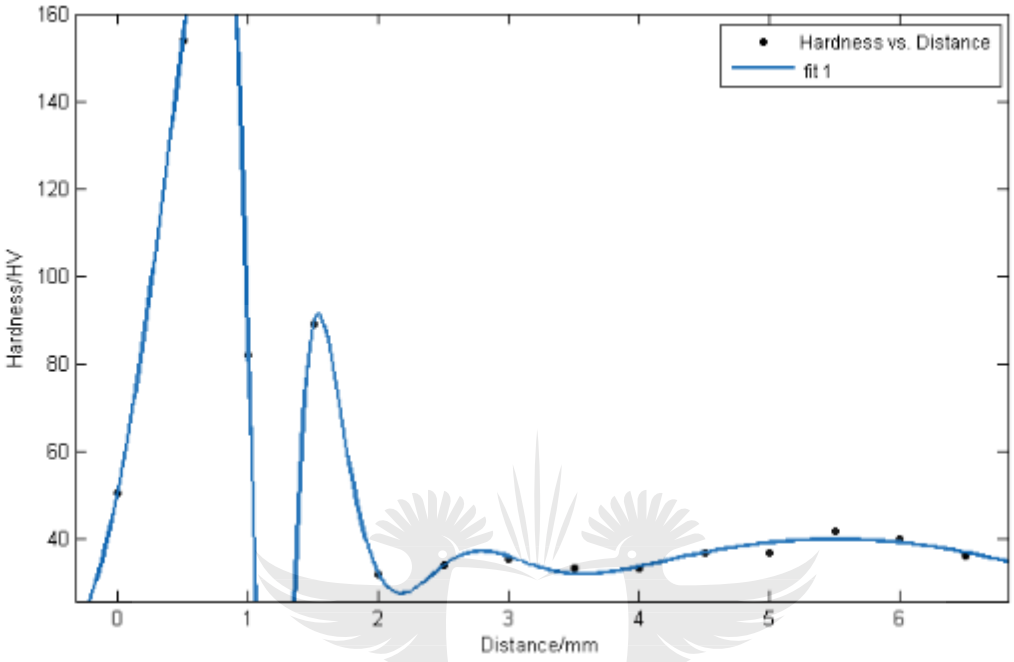

BOTTOM

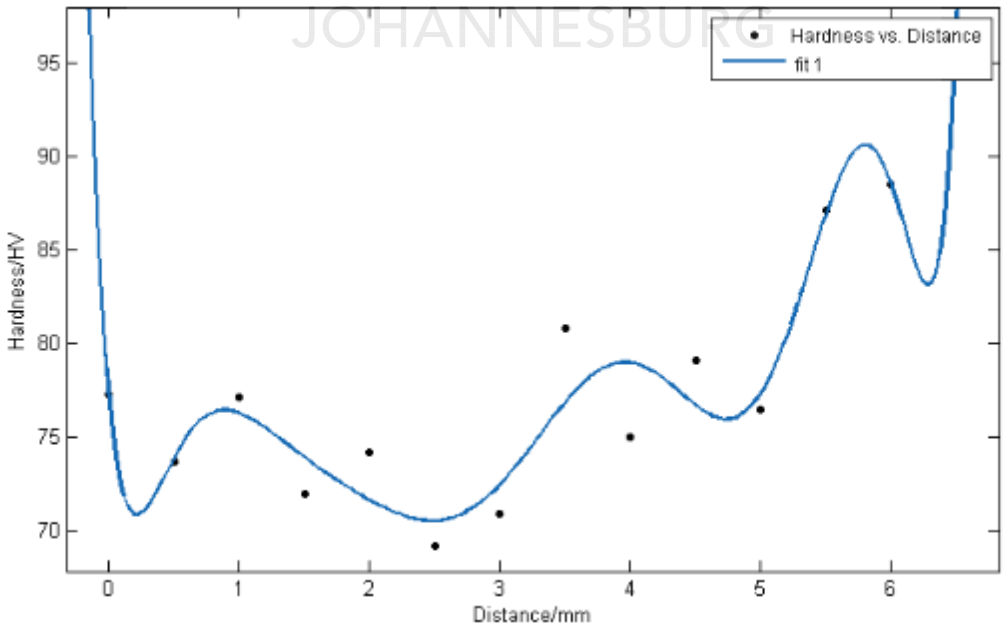

CCS_800_0.5

TOP

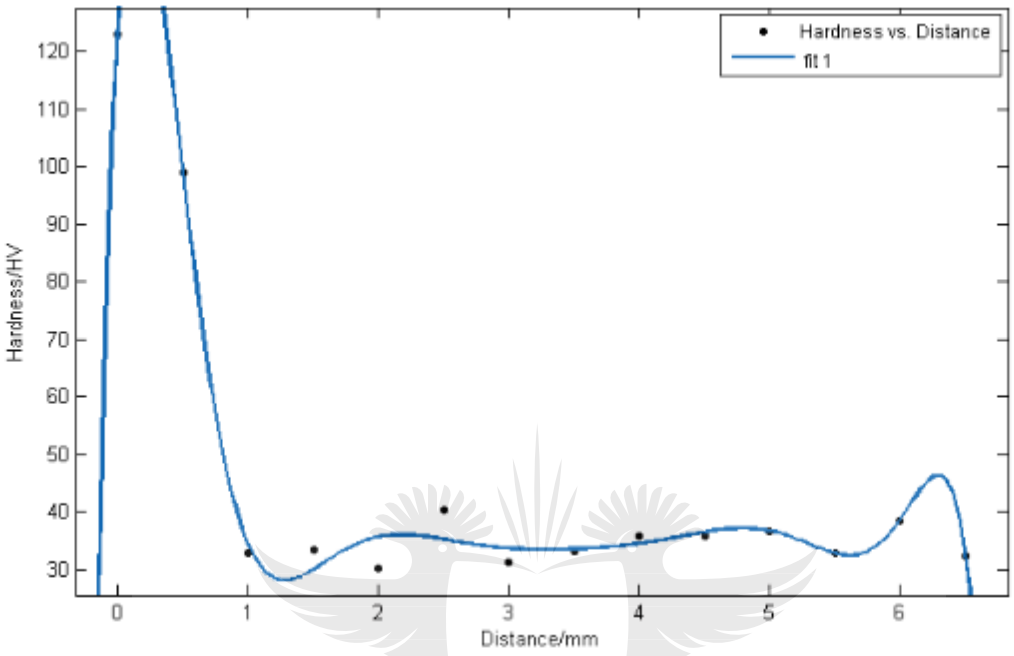

BOTTOM

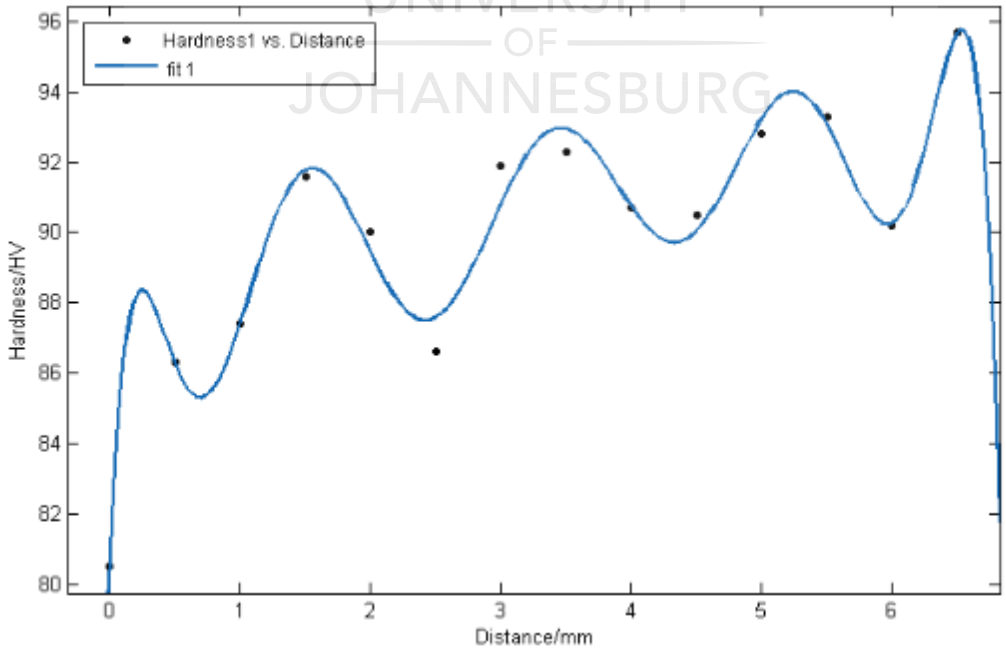

CCS_800_1

TOP

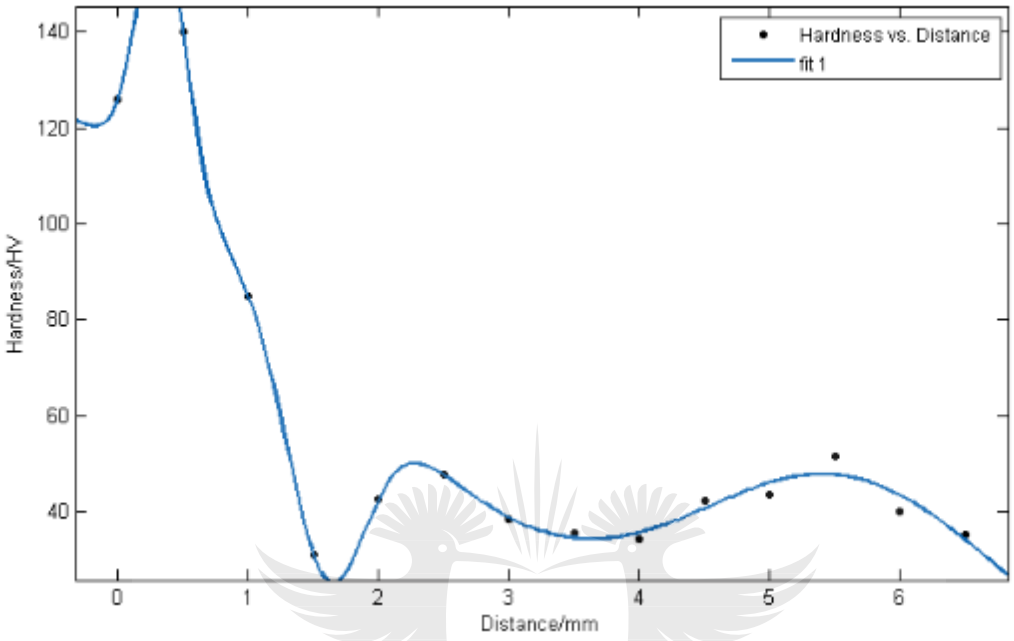

BOTTOM

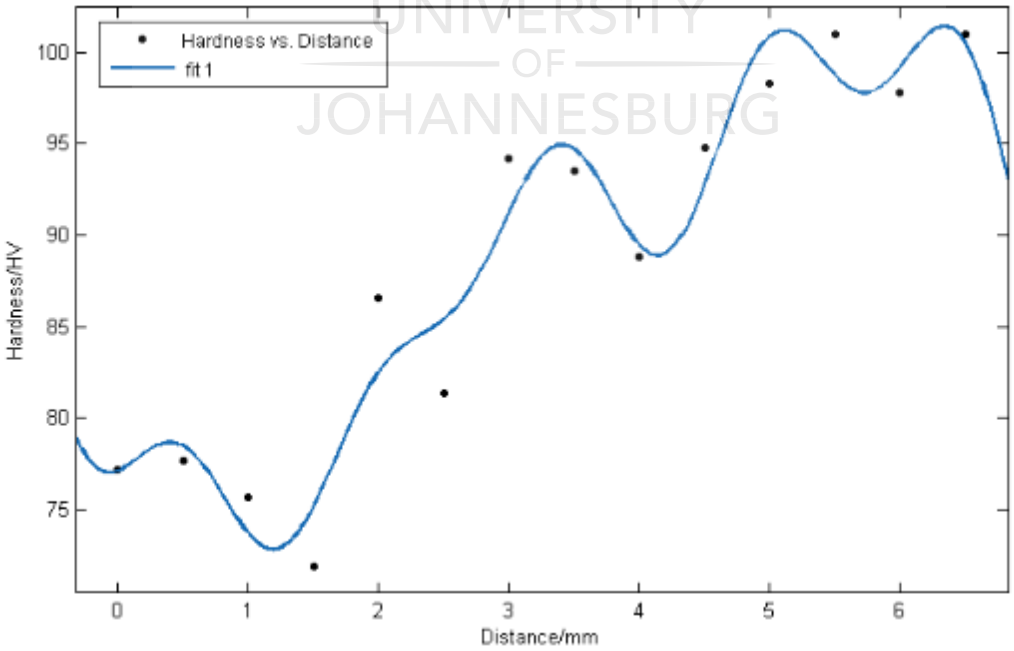

CCS_1200_0.5

TOP

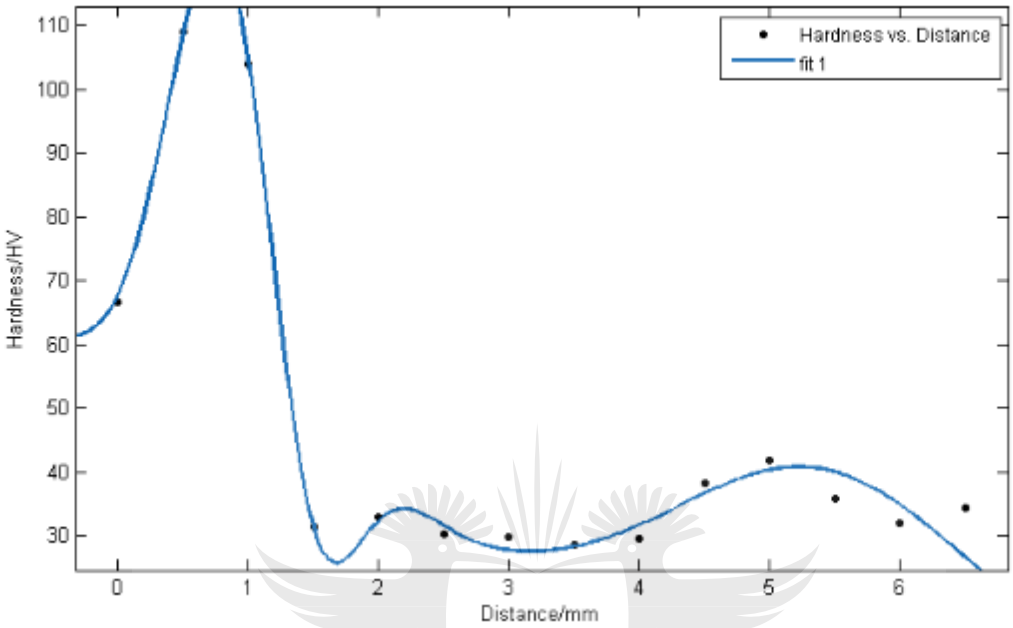

BOTTOM

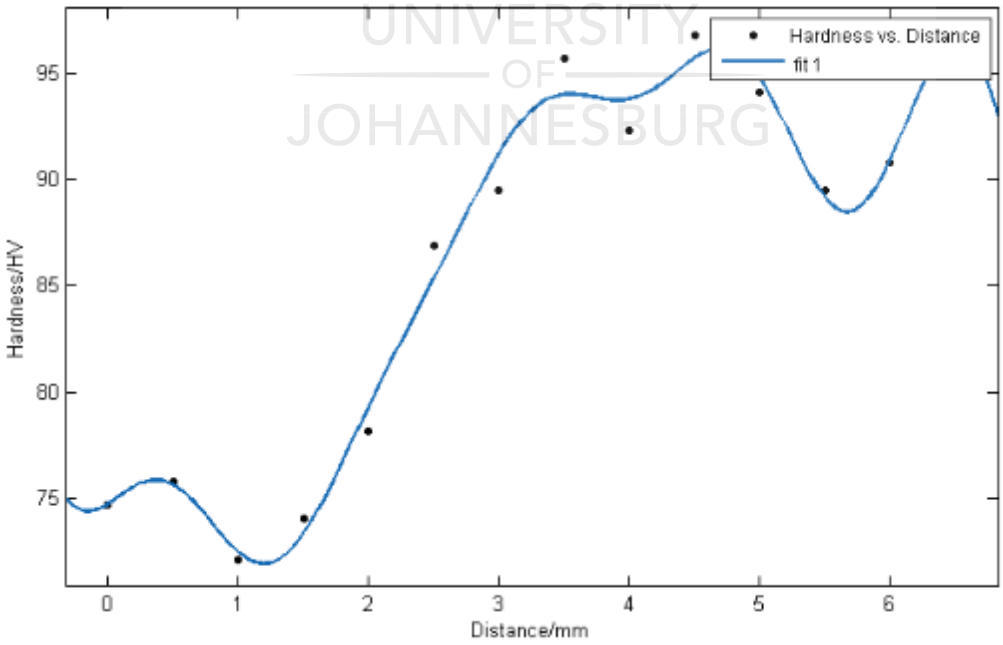

CCS_1200_1

TOP

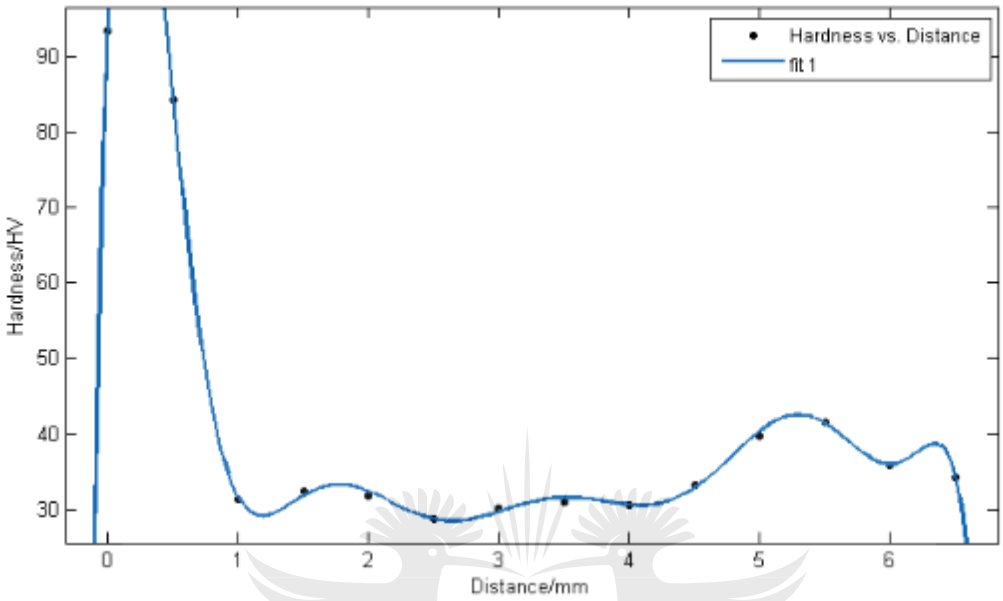

BOTTOM

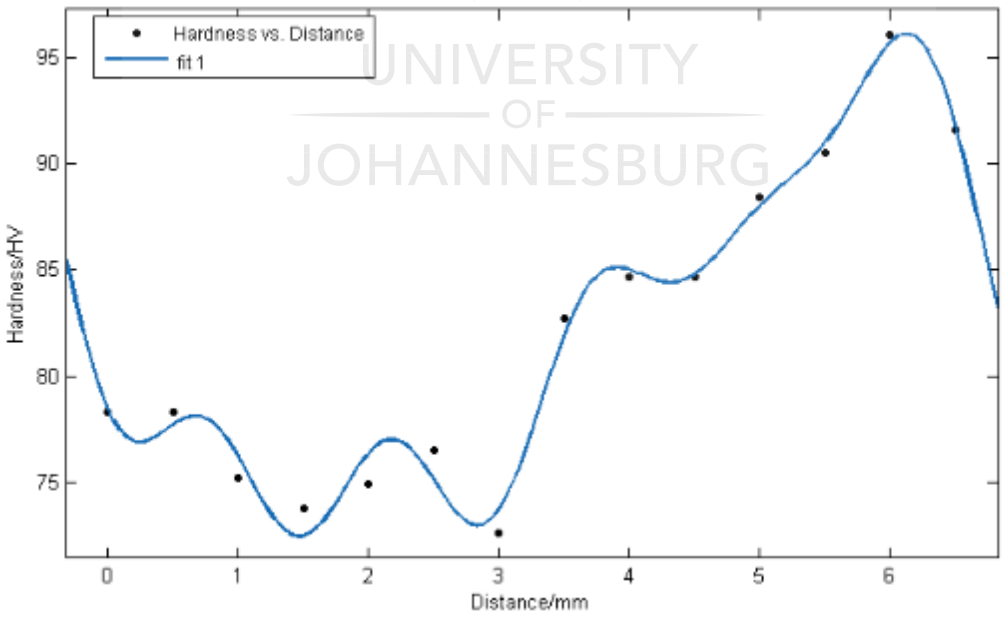

RESIDUALS

Al PM

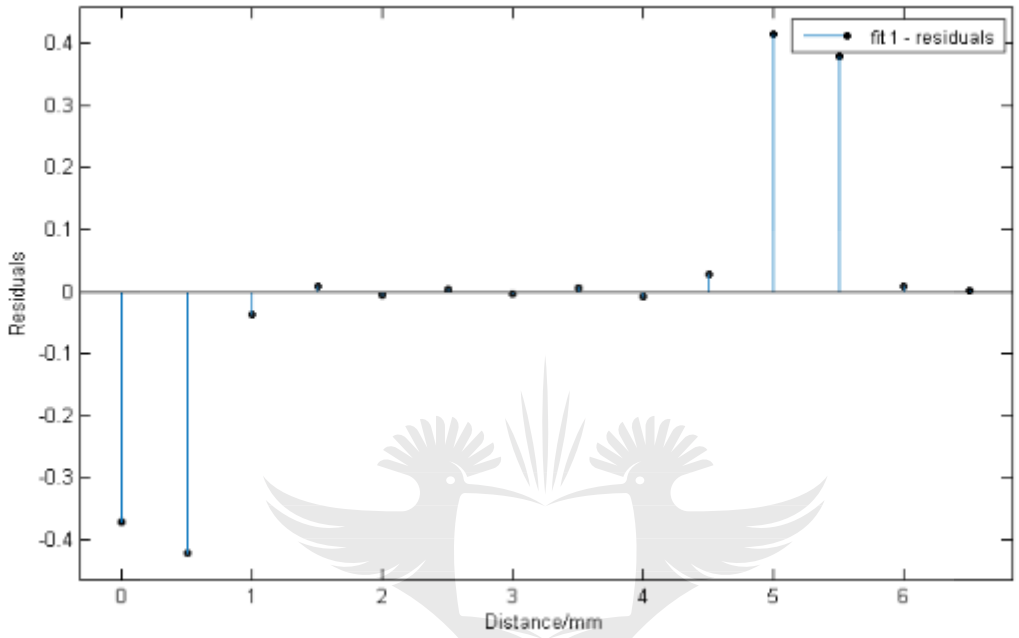

Cu PM

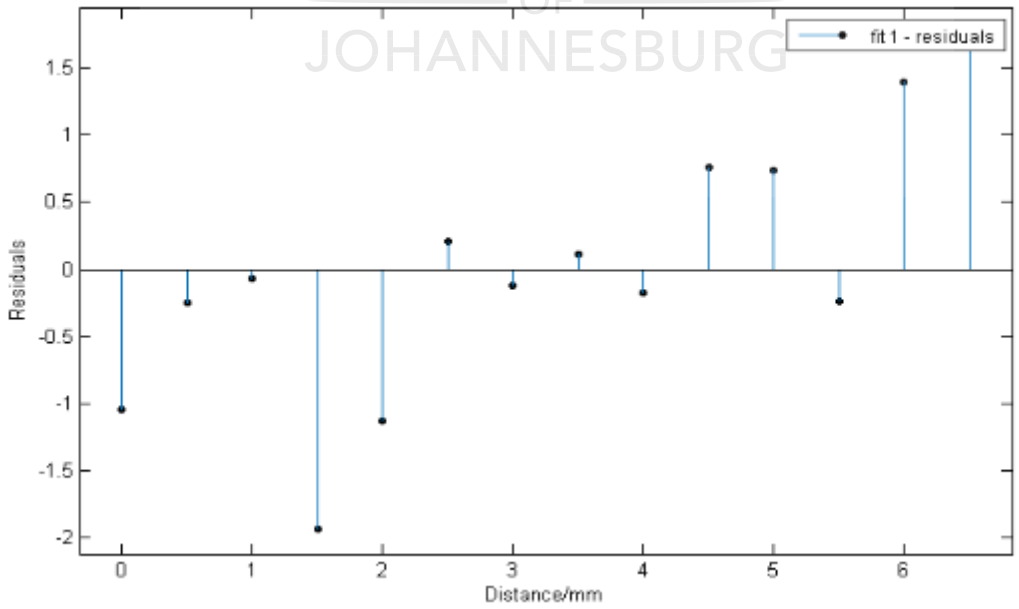

FPS_800_0.5

TOP

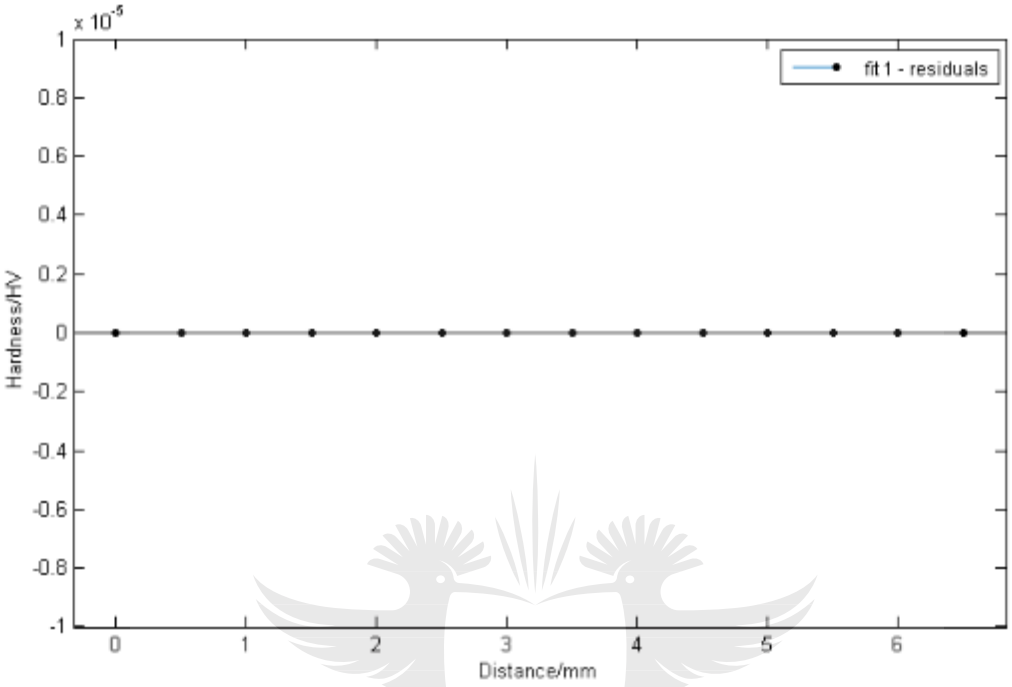

BOTTOM

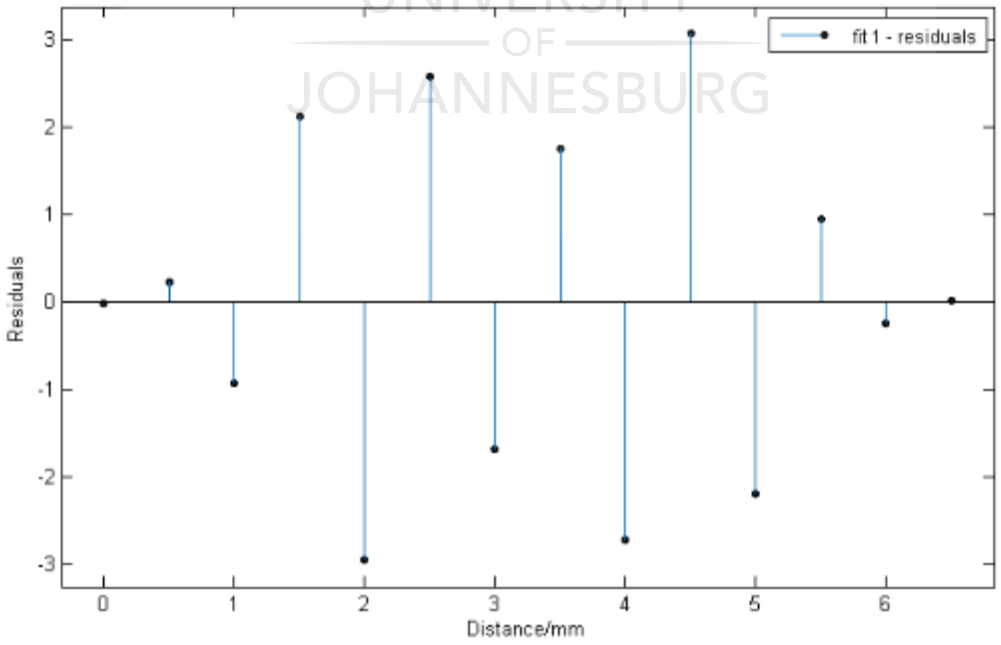

FPS_800_1

TOP

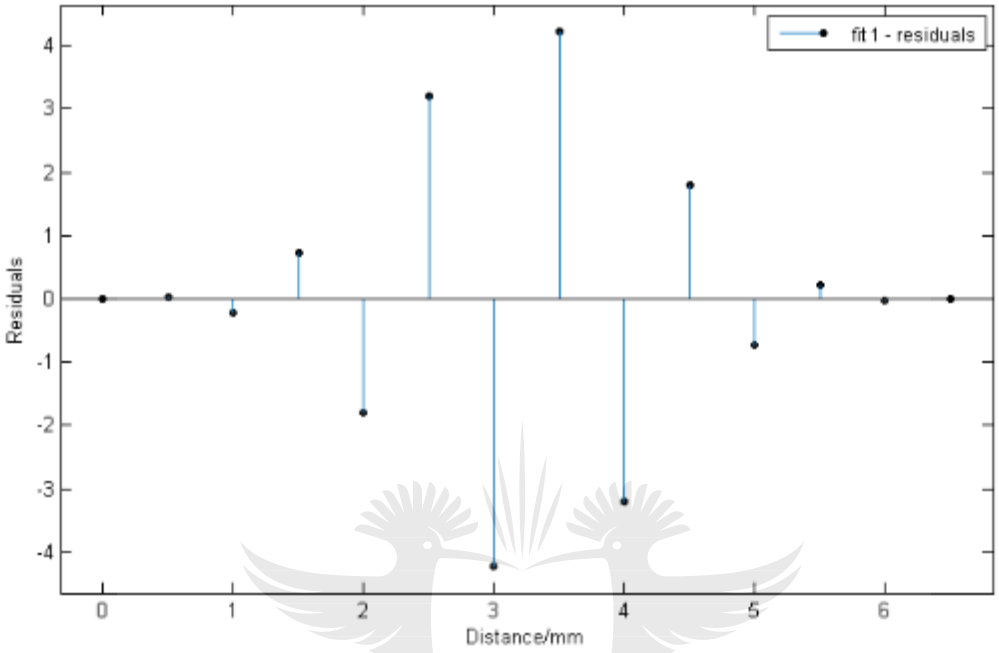

BOTTOM

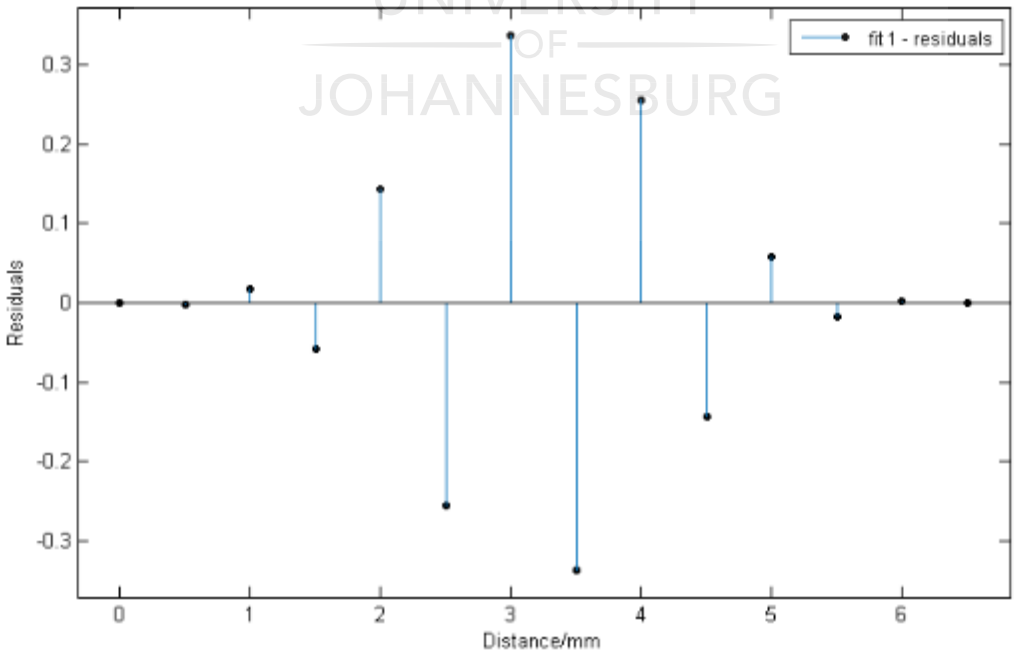

FPS_1200_0.5

TOP

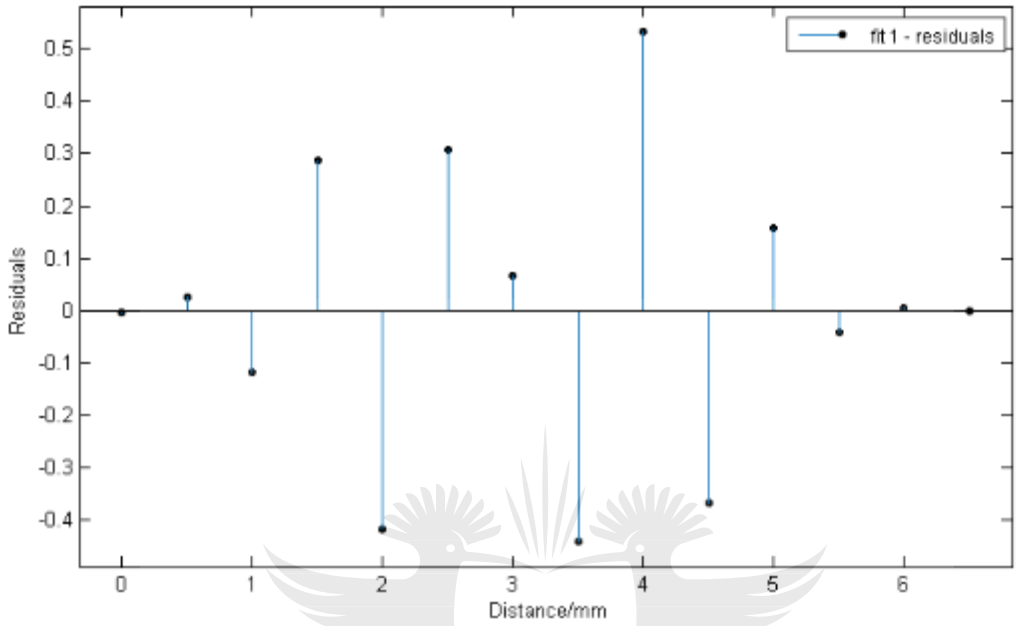

BOTTOM

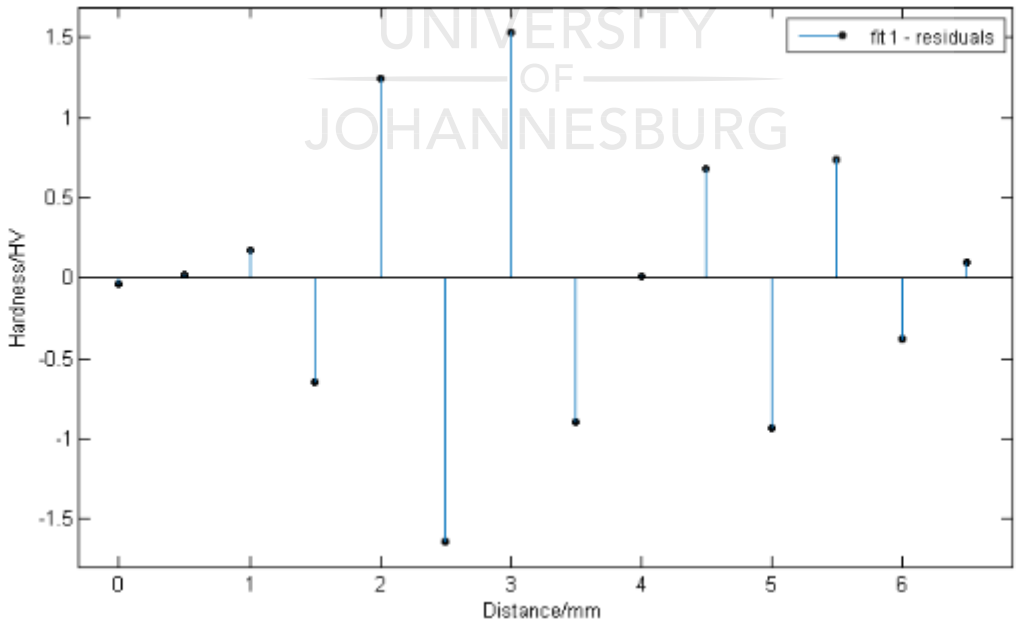

FPS_1200_1

TOP

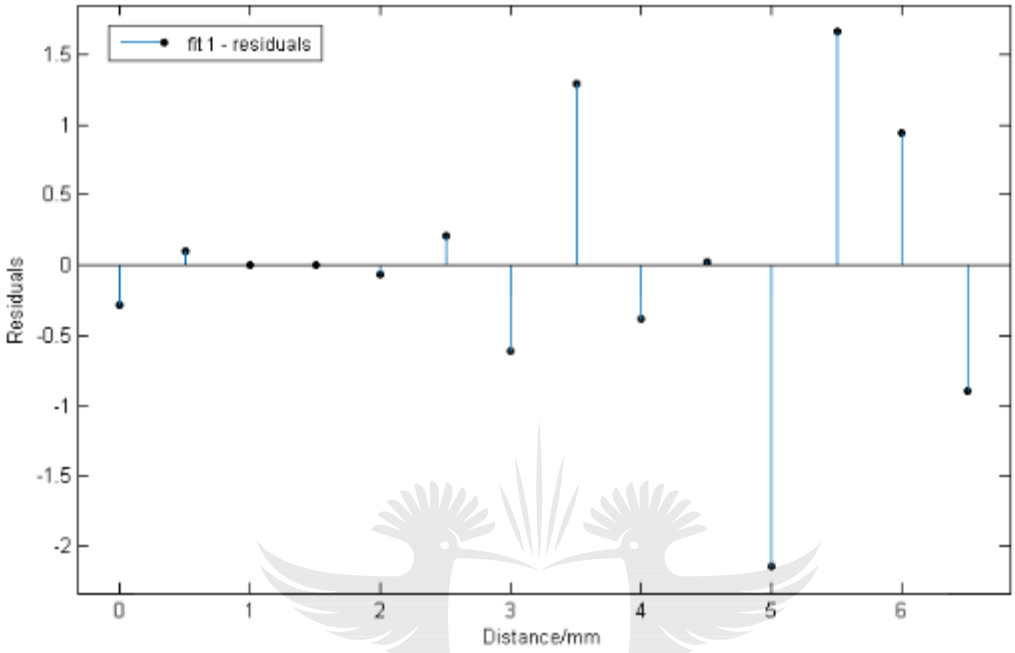

BOTTOM

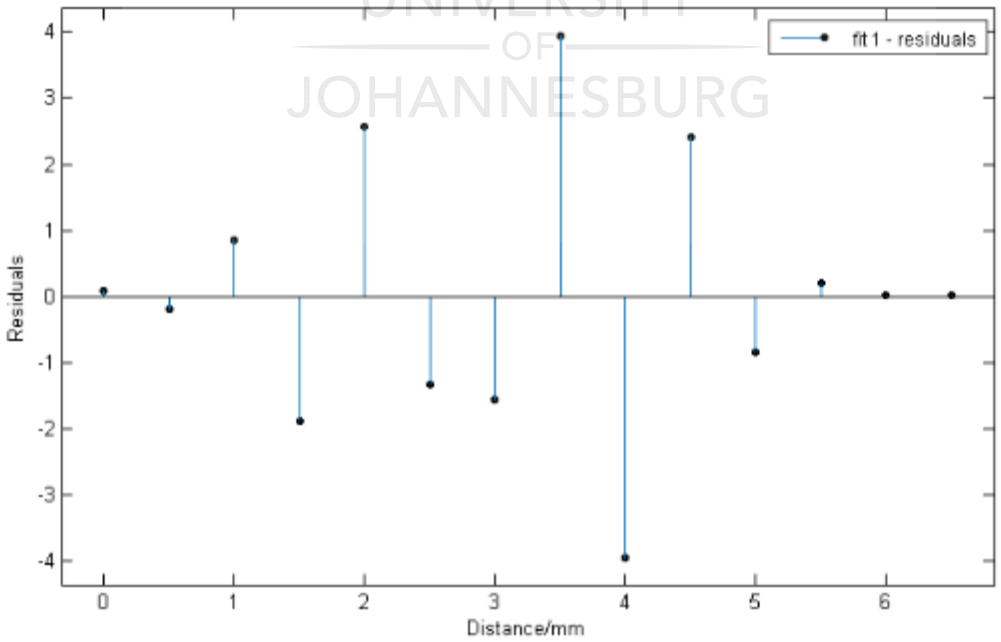

CCS_800_0.5

TOP

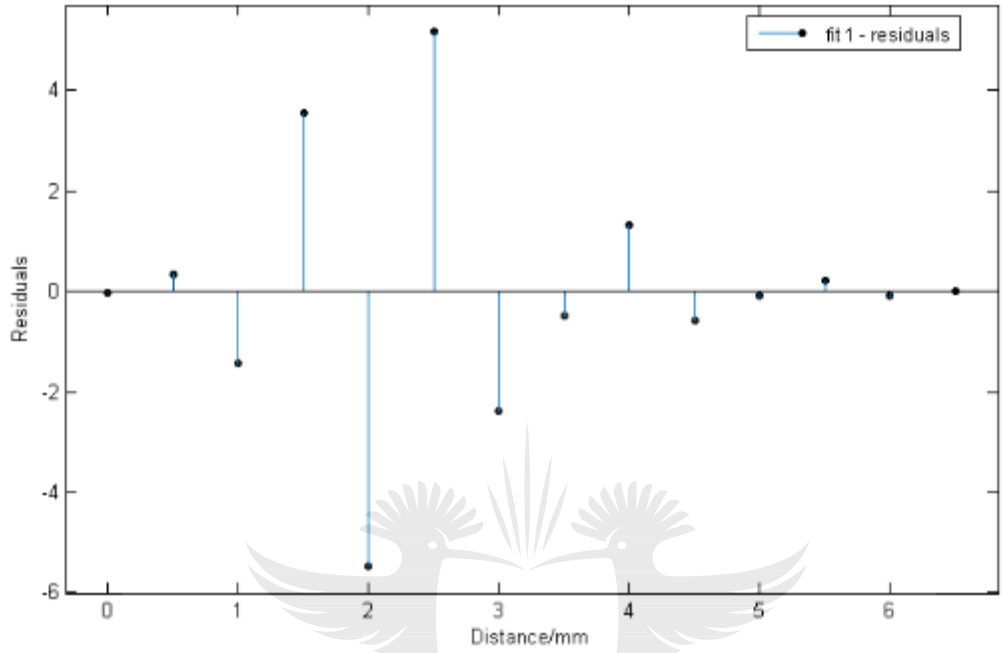

BOTTOM

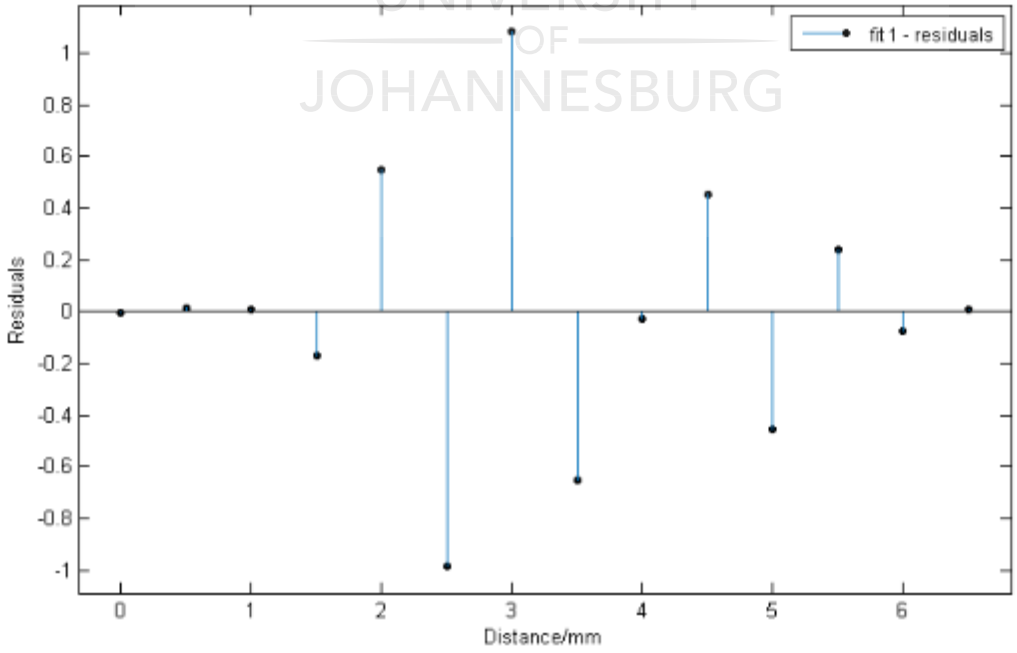

CCS_800_1

TOP

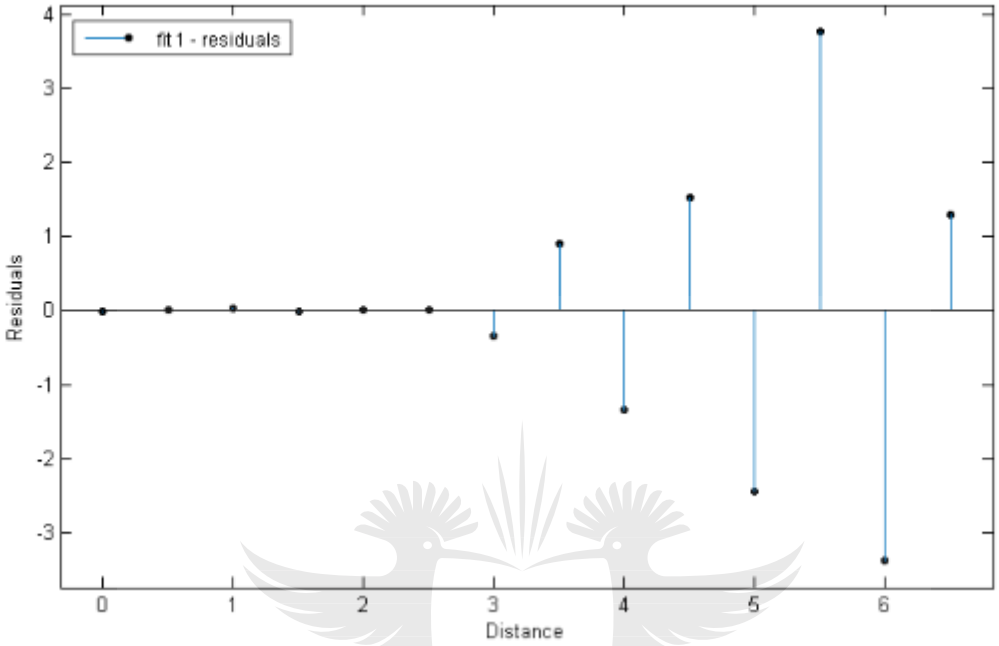

BOTTOM

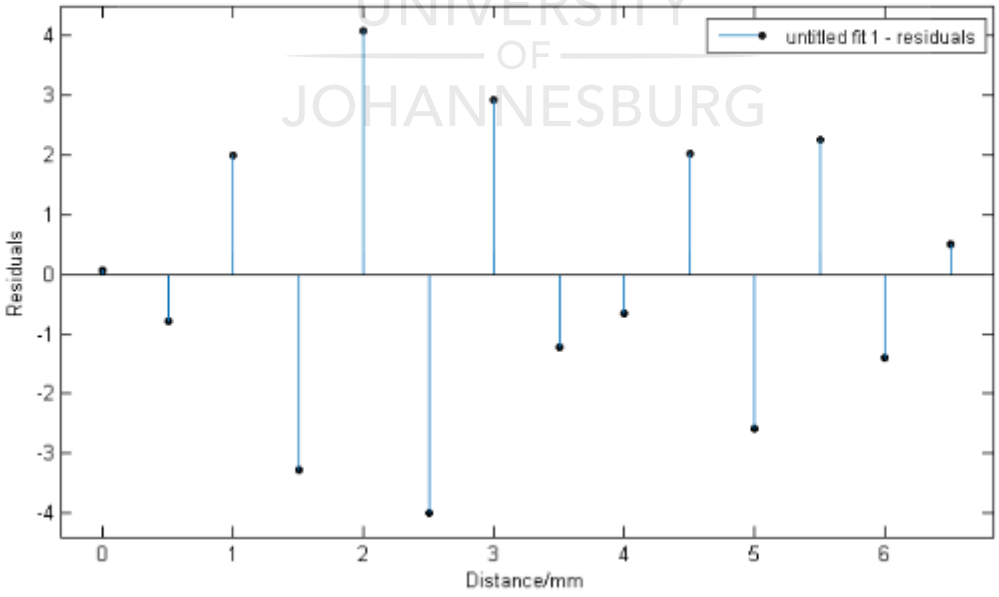

CCS_1200_0.5

TOP

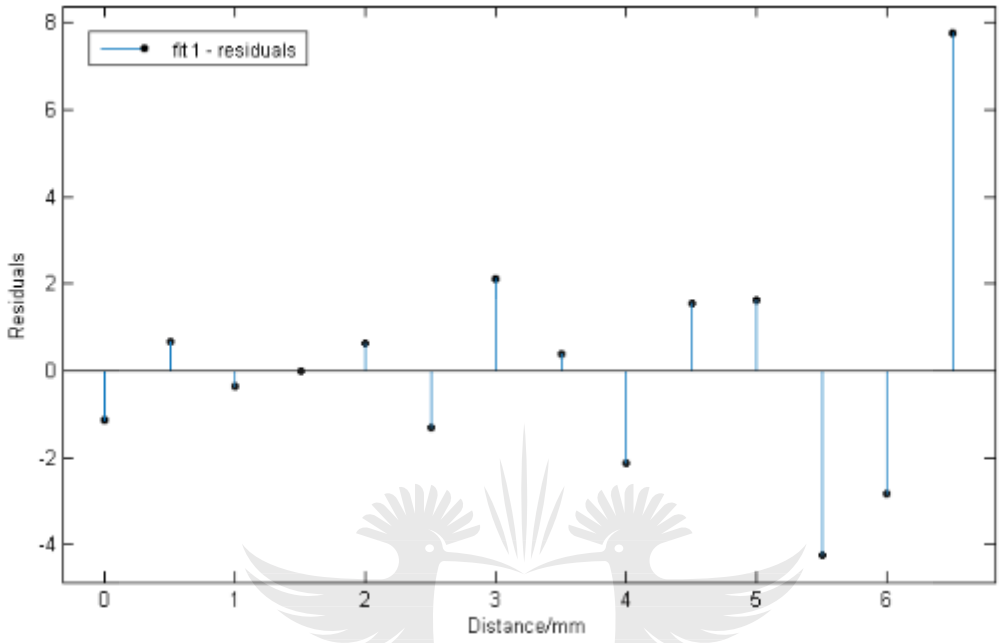

BOTTOM

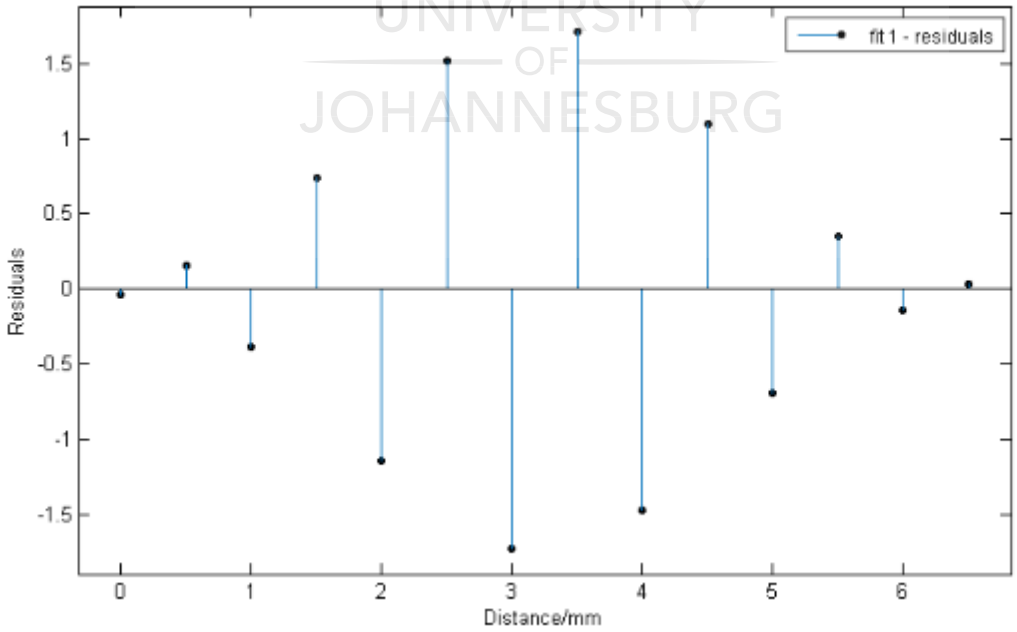

CCS_1200_1

TOP

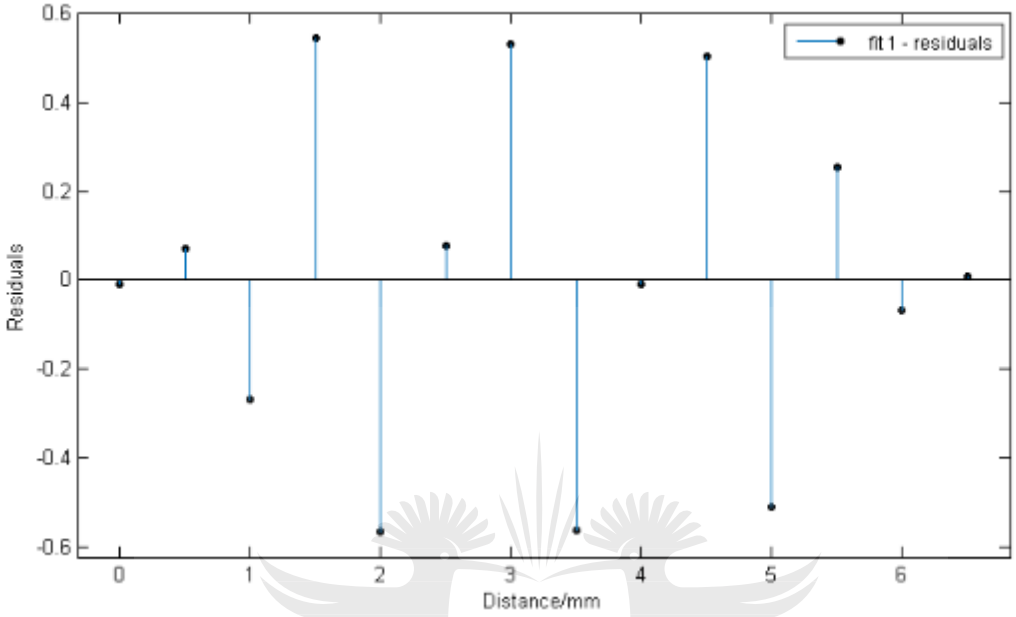

BOTTOM

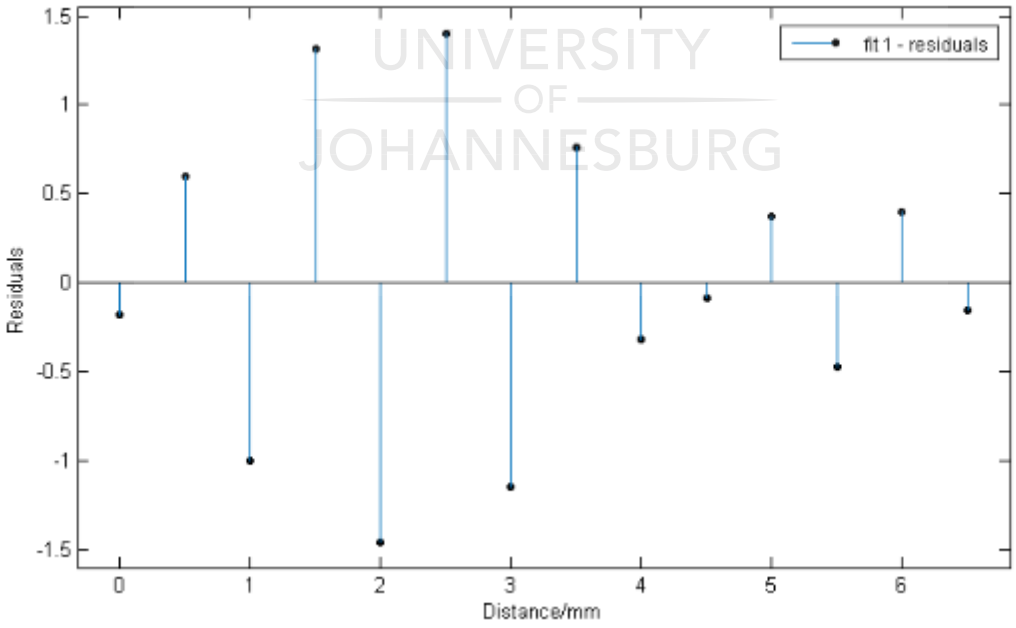

PDF TABLES

TOP

Sample name	Mean	Variance	mu	Sigma
FPS_800_0.5	46.5429	82.8442	46.5429	9.10188
FPS_800_1	75.0992	4994.97	4.00167	0.79641
FPS_1200_0.5	45.1208	441.806	3.71115	0.44317
FPS_1200_1	51.7308	672.845	3.83391	0.47359

Sample name	Mean	Variance	mu	Sigma
CCS_800_0.5	44.5748	409.802	3.70341	0.43303
CCS_800_1	55.8872	813.763	3.90757	0.48119
CCS_1200_0.5	45.4532	482.889	3.71166	0.45831
CCS_1200_1	40.9416	248.04	3.64315	0.37148

BOTTOM

Sample name	Mean	Variance	mu	Sigma
FPS_800_0.5	92.2338	32.7196	4.52241	0.06196
FPS_800_1	84.7	119.974	84.7	10.9533
FPS_1200_0.5	84.7	119.974	84.7	10.9533
FPS_1200_1	78.4286	58.0637	78.4286	7.61996

Sample name	Mean	Variance	mu	Sigma
CCS_800_0.5	89.9857	14.2859	89.9857	3.77967
CCS_800_1	88.5643	102.307	88.5643	10.1147
CCS_1200_0.5	86.2521	89.6604	4.45128	0.10945
CCS_1200_1	82.0425	54.8519	4.40318	0.09009

FITS

TOP

Sample ID	*R* square	*R* square adjusted
FPS_800_0.5	0.9896	0.9322
FPS_800_1	0.9996	na
FPS_1200_0.5	0.9999	0.9995
FPS_1200_1	0.9993	0.9952

Sample ID	*R* square	*R* square adjusted
CCS_800_0.5	0.9924	0.9505
CCS_800_1	0.9976	0.9843
CCS_1200_0.5	0.9893	0.9303
CCS_1200_1	0.9997	0.9978

BOTTOM

Sample ID	*R* square	*R* square adjusted
FPS_800_0.5	0.8842	0.2475
FPS_800_1	0.9999	na
FPS_1200_0.5	0.9937	0.9589
FPS_1200_1	0.9298	0.5439

Sample ID	*R* square	*R* square adjusted
CCS_800_0.5	0.9818	0.8819
CCS_800_1	0.9424	0.6258
CCS_1200_0.5	0.987	0.9157
CCS_1200_1	0.9866	0.9126